NATIONAL ADVISORY COMMITTEE FOR AERONAUTICS

TECHNICAL NOTE 4201

COLLECTION OF ZERO-LIFT DRAG DATA ON BODIES OF REVOLUTION FROM FREE-FLIGHT INVESTIGATIONS

By William E. Stoney, Jr.

SUMMARY

This report presents a compilation of most of the zero-lift drag results obtained from free-flight measurements made by the Langley Pilotless Aircraft Research Division on fin-stabilized bodies of revolution. The data are arranged on standard forms, which also contain the significant geometrical factors. Supplementary data have been provided to facilitate the determination of the body pressure drags from the measured total drags. Summary plots and discussions have been included to provide a unified and broad picture of the effects of body geometry on zero-lift drag.

The Mach number range of the tests extends from 0.6 to approximately 2.0 and the Reynolds numbers based on body length from 2×10^6 to 100×10^6.

INTRODUCTION

At the present time, the most accurate method of obtaining the zero-lift drag at transonic and low supersonic Mach numbers of an arbitrarily shaped body of revolution is measurement by means of wind-tunnel or free-flight tests. The importance of accurate knowledge of zero lift has been increased by the usefulness of the "area rule" concept in the design of complete aircraft configurations, since this concept states that the drag of a complete aircraft configuration can be determined from its equivalent body of revolution.

The Langley Pilotless Aircraft Research Division has flown nearly 200 bodies of revolution of different sizes and shapes for the purpose of measuring their drag at zero lift. The results of many of these tests have been published in reports dealing with the systematic variations which they explored. However, many of these models were designed as equivalent bodies of revolution, and their drags have been published in the widely scattered reports dealing with the airplane configurations they represented. In view of the large amount of data available and of the comparative obscurity of a large part of it, it was felt that a collection of such data presented in a standard form would be of aid to the aircraft and missile designers.

It is hoped that this collection will be useful in several ways. The large number of shapes presented herein may allow the designer to estimate easily the drag of a desired shape by a simple comparison. Supplementary data and theoretical estimates have been provided to facilitate the determination of the body pressure drags from the measured total drags. Summary plots and discussions have been included to provide the user with a unified and broad picture of the effects of body geometry on zero lift drag.

SYMBOLS

l	length
d	maximum diameter
l/d	fineness ratio
r/R	ratio of body radius at any station to maximum body radius
x/l	ratio of distance measured from apex of nose to total body length
S_b/A	ratio of body wetted area to body frontal area (actual values calculated from expression $\frac{C_{D_f}}{C_f} = 4l/d \int_0^1 \frac{r}{R}\, d\frac{x}{l}$ which is correct relationship between friction coefficient C_f based on wetted area and friction drag coefficient C_{D_f} based on body frontal area)
S_f/A	ratio of fin wetted area to body frontal area
A_b/A	ratio of body base area to body frontal area
θ_b	body slope at $x/l = 1$ (slope is always negative but is expressed as positive)
R	Reynolds number based on body length, $\frac{\rho U l}{\mu}$

ρ free-stream density

U free-stream velocity

μ free-stream viscosity

M free-stream Mach number

C_D drag coefficient based on body frontal area, $\dfrac{\text{Drag}}{\frac{\rho}{2}U^2\pi\frac{d^2}{4}}$

C_p pressure coefficient, $\dfrac{\text{Pressure - Free-stream pressure}}{\frac{\rho}{2}U^2}$

C_f friction drag coefficient based on wetted area

$r' = r/R$ where R is maximum body radius

$x' = x/l_{nose}$ or $x/l_{afterbody}$

$r_b' = r_{base}/R$

TESTS

Most data of this report were obtained by the following procedure: A fin-stabilized model flying at or near zero lift was tracked with a CW Doppler radar unit as it decelerated through a speed range from supersonic Mach numbers to high subsonic Mach numbers. The resulting velocity time history was arithmetically differentiated to give a deceleration time history. Shortly before or after the flight, a record of the atmospheric properties (density, temperature, and wind velocity) was obtained from the flight of a radiosonde balloon. This record, together with a space-position time record of the flight, permitted the zero-lift drag coefficient to be calculated. The tests differ only in the method of launching the models into free flight and in the method of obtaining the altitude time history.

Rocket Model Tests

The rocket-test method is the propulsion of the models by rockets located in the model, or behind the model in the form of booster rockets which dropped away after burnout. In these tests the models were also tracked by an NACA modified SCR-584 position radar tracking unit, the data of which were used to obtain the space-position time records used in the data reduction. In general, the rocket models were of a fair size: 5 to 8 inches in diameter and up to 12 feet in length. The data were obtained with the models at all altitudes up to over 50,000 feet and Mach numbers over 4. A few carried telemetering equipment and from these the total drag was also obtained from decelerometers and the base drag from pressure cells.

Helium-Gun Tests

The second technique, the helium-gun test, was the launching of small models (roughly 2 inches in diameter and 12 inches long) from a helium gun. The helium gun used to launch these models was a 24-foot smooth-bore barrel 6 inches in diameter attached by valves to a 100-cubic-foot tank of helium under a pressure of 200 pounds per square inch absolute. The models were ejected at Mach numbers up to 1.4. The space time histories of these models were calculated from the velocity-time data, and the data were reduced as before. A satisfactory check of the flight-path calculation method was made by tracking several models with the SCR-584 unit. The models were fired at an angle of 20° to the horizontal and never rose over an altitude of 2,000 feet.

Accuracy

Inasmuch as the tests have been made over a period of several years with continually varying techniques, it is difficult to assign a general figure for their accuracy. The velocimeter record is accurate to within 0.2 percent, and the derived accelerations, although the result of a short-time averaging process, are accurate to within 1 percent except in the region of the drag rise where it is possible for abrupt changes to be somewhat softened by the averaging process.

One approach to a value of accuracy is the comparison of the drag of identical models, since all the variable factors, inaccuracies in body ordinates, velocity measurement, atmospheric conditions, wind velocity, and data reduction are included.

From the variations shown by the models of configurations 8, 22, 27 to 30, 75 to 77, 106 to 109, 128, 139, and 151 reasonable limits of error for C_D and Mach number appear to be

$$\Delta C_D = \pm 0.01$$

$$\Delta M = \pm 0.01$$

Another check on the accuracy is given by a comparison of the data of model 109 with a wind-tunnel test of an identical configuration. This comparison is shown in figure 1 and is quite good.

A third indication of the accuracy of the tests is given by a comparison of the nose pressure drags obtained from eight helium-gun models with values measured in a wind tunnel and calculated by second-order theory. The comparisons are quite close and indicate accuracy at least to the values quoted (see the discussion on nose drags in the section "Summary Curves").

PRESENTATION OF DATA

General Organization

With the thought in mind that the important product of these tests is the body pressure drag, the configurations are divided into two types - "smooth" and "bumpy" - and are presented in order of increasing fineness ratio. A smooth body is defined as one whose meridian increases without inflection points to a maximum and stays constant or decreases without inflection points to a minimum. All other bodies are considered to be bumpy. Since only the nose and afterbody[1] contribute to the pressure drag, the significant fineness ratio of the smooth bodies has been assumed to be that of the sum of the nose and afterbody. Such grouping assumes that the effects of the nose on the afterbody drag are of second order. Since such a division cannot, in general, be made for the bumpy bodies, they are presented in the order of their total fineness ratios. This classification by fineness ratio has the advantage of simplicity, and its usefulness is based on the general fact that this parameter is the most important single factor affecting body pressure drag.

The shape of the parts of the body is the other variable and since the assumption that the effect of shape is independent of fineness ratio appears to be useful, the body ordinates have been nondimensionalized and are presented in graphical form for each of the configurations. In order to utilize this assumption strictly, the individual parts should have been presented individually; however, this manner of presentation would have posed great problems for the bumpy bodies and was abandoned in favor of the simpler method used. This method has the advantage of enabling comparisons of bumpy and smooth bodies to be made by matching

---

[1]The nose is herein defined as that part of the body up to the maximum diameter and the afterbody as that part from the maximum diameter to the base. Cylindrical sections of maximum diameter are considered as separate units and thus the sum of the values of l/d of the nose and afterbody can be less than the total value of l/d of the body.

their nondimensional ordinate curves and their total fineness ratios. Comparisons of the drag curves of such bodies allow estimates of the bumpiness of a bumpy body, that is, insofar as drag is concerned.

The basic data are supplemented by curves of friction, base, step, and fin drag (figs. 2 to 5). Summary curves of data from various systematic investigations are presented in figures 6 to 10. Some curves showing the general effect of body shape on drag appear in figures 11 to 15. The basic data are presented in figures 16 to 183 and are separated into two main groups. Figures 16 to 120 present the data for all the smooth bodies and the data for the bumpy bodies are presented in figures 121 to 138. (These data were compiled from refs. 1 to 16.) A particular configuration may be found quickly by reference to table I where the configurations are listed together with their distinguishing geometrical properties.

Presentation of Model Characteristics

Enough information appears in the drawing and graphical presentation of the ordinates to allow reconstruction of the model with reasonable accuracy. Many of the smooth bodies had analytical meridians of parabolic form or mixed parabolic and hemispherical form; this notation has been made in the figure. The following equations were used for parabolic noses and afterbodies, respectively,

$$r' = 2x' - x'^2$$

$$r' = 1 - (1 - r_b')x'^2$$

Pertinent fineness ratios, area ratios, and angles are given to allow quick comparisons of configurations. The type of test, rocket or helium gun, is also noted. All dimensions given in these figures are in inches.

Presentation of Data

Total zero-lift drag coefficients based on body frontal area and Reynolds number based on body length are presented for each model. The total-drag curves are curves faired through the original data points by the present author and thus may in some cases differ slightly from values previously published. For those configurations for which more than one model were flown the individual curves are labeled a, b, and so forth. For the models on which base pressures were measured, the base pressures are also presented.

For convenience, the friction drag calculated by the method of Van Driest (ref. 17) has been presented for each model. For cases in which the Reynolds numbers and the data appeared such that the flow over both the body and fins was turbulent, the points calculated were indicated by a square symbol ⊡ and connected with a dashed line. If the data appeared to be in the range in which the fin boundary layer may have been either laminar or turbulent, calculations were made for both conditions, and the points for both conditions were presented and left unconnected; thus, the circled points ⊙ represent the calculation for turbulent body flow plus laminar fin flow.

A word of warning is in order here: In the figures in which both symbols appear at the subsonic end of the Mach number scale and only the fully turbulent symbol ⊡ appears at the supersonic value, the Reynolds numbers are such that it is possible that transition from laminar to turbulent flow has occurred at some Mach number between the two extremes. This means that any pressure or wave drags derived by subtracting base, fin, and friction drag from the total drag can be in error by the amount of the difference between the turbulent and laminar fin friction drags. Configuration 158 (fig. 164) presents a case in point, although for this model the transition appears rather dramatically in the total-drag curve. This is unusual, and the change would not be at all apparent if the transition had occurred in the rapidly rising section of the drag curve.

Further discussion of friction drag is presented in the "Supplementary Data" section.

SUPPLEMENTARY DATA

This report presents a collection of total-drag curves for various bodies of revolution stabilized by fins. The usefulness of the data is largely determined by the information which can be obtained from these total drags concerning the values of the pressure or wave drags of the bodies alone (i.e., not influenced by the fins), since it is the value of this component of the supersonic drag that is always difficult and often impossible to calculate from theoretical considerations in the low supersonic speed ranges considered. In order to obtain the wave drag of the body alone from the test results, the friction, base, and fin pressure drags must be known or assumed.

The friction drag can be calculated accurately for most bodies. For many bodies, the base drag is negligible and the base drag for most of the remaining bodies can be estimated accurately from empirical curves. The fin affects the drag in three ways - fin pressure drag due to fin induced pressures, pressure drag of the fin due to the body, and pressure drag on the body due to the fins. The value of the first component has in this report been either measured or calculated for most of the fins used. Values of the interference terms are, in general, not calculable. For the models of the present report, it appears reasonable to assume that the interference terms are negligible for most cases since the fins are extremely thin[2].

The following sections provide the data necessary in the breakdown of the total-drag curves into their component parts.

Friction Drag

Figure 2 presents average flat-plate friction coefficients based on wetted area as functions of total Reynolds number for various Mach numbers. All values are for an insulated wall (no heat flow), which is correct for the wooden-surface models and is nearly correct for the models with metal surfaces and Mach numbers near 1. These values were used in the calculation of the friction drags shown on the data plots. The use of flat-plate values for bodies of revolution is not exactly correct because of at least two factors - first, the difference between two- and three-dimensional flow, and, second, the existence of velocities higher than free-stream velocity on the surface of the bodies. Both of these effects are functions of body fineness ratio, the effects being most in evidence at lower values of l/d. Reference 18 gives an approximate correction factor for the higher average velocities existing on bodies of revolution as $\frac{\left(C_{D_f}\right)_{\text{body of rev}}}{\left(C_{D_f}\right)_{\text{flat plate}}} = 1 + \frac{0.5}{l/d}$ which is supposedly valid at Mach numbers as high as 1. Both effects are apparently small for the bodies of this report.

---

[2]The interference has been shown to be essentially zero by wind-tunnel tests of configuration 109 (see fig. 1) since the fin drag obtained by subtracting finned and unfinned results agreed exactly (except at $M = 1$) with fin drags obtained on special free-flight models on which the interference drag was zero by virtue of the cylindrical shape of the body. Since model 109 is of high fineness ratio this result cannot be applied generally. An attempt to measure fin interference was made with configurations 48 and 49. Although these bodies had low-fineness-ratio afterbodies on which the fin interference was expected to be large, the measured differences were small and in the opposite sense to that expected.

Another assumption has been made in the calculation of the friction drag - namely, the bodies have been assumed to have either completely laminar or completely turbulent flow on the body and fins. This assumption may be erroneous for some of the models flying at Reynolds numbers from 1×10^6 to 5×10^6 and should be kept in mind in the analysis of such data. The only models for which this assumption is obviously wrong are models 104 and 105 (figs. 112 and 113), even though they flew at extremely high Reynolds numbers. These models are both models of the NACA RM-10 body, which has been extensively tested in wind tunnels (see refs. 13, 19, and 20). These models are more carefully finished than the majority and long runs of laminar flow (Reynolds numbers up to 40×10^6) have been detected on the body on some flights. Even more likely are long runs of laminar flow on the fins and since the fins of these models contribute nearly as much friction-drag area as the body, this would cause a large error in the calculations as made. With these considerations, if the pressure drag of this configuration is desired it would be best to obtain it from theory or the wind-tunnel results presented in references 13, 19, and 20. Note, however, that the base drags obtained from flight measurements should be the most accurate, since the tunnel measurements contain sting interference effects. References 13, 19, and 20 also give examples of the effects of Reynolds number, transition, and heat transfer on friction drag.

Base Pressure and Base Drag

Reference 21 contains excellent analysis and data on base pressure behind both two- and three-dimensional bodies when the boundary layer is turbulent ahead of the base and the Mach numbers are in the range considered in this report. The following discussion follows this reference.

Three-dimensional base drag.- Figure 3 presents the base-pressure drag coefficients as a function of Mach number for a cylindrical afterbody of infinite length (refs. 21 to 23). As mentioned in reference 21, the base pressure behind a cylindrical base can be influenced by flow conditions such as fin and nose pressure fields ahead of the base even when the boundary layer is turbulent well ahead of the base. For the bodies of the present report, such differences are believed to be small enough that the curve shown in figure 3 may be used, the possibility of such an error being always kept in mind, however, especially for subsonic speeds (see ref. 18, pp. 30 to 34).

Most of the bodies reported herein have afterbodies, that is, a base diameter which is smaller than the maximum diameter. The base drag of such bodies is discussed in reference 21; however, the method of evaluating such base pressures discussed therein is too complicated for the purposes of the present paper, since the value of the base drag is seldom a very large percentage of the total drag for boattailed bodies. Some published wind-tunnel data on the base drag of conical afterbodies suggest the empirical expression

$$C_{D,base} = C_{D,cylinder\ base}\left(\frac{r_{base}}{R}\right)^3$$

Care must be taken in applying this equation at subsonic Mach numbers since it does not account for the possibility of negative base drags which can exist (ref. 24).

Two-dimensional base pressures.- Figure 3 also presents base-pressure coefficients for a two-dimensional base from references 21 and 25. The data represent the base pressures behind slab wings. They are presented herein as an estimate of the pressures behind a rearward facing step on a body of revolution.

Pressures on a Forward Facing Step

Figure 23 presents the pressure coefficients required to separate the turbulent boundary layer in front of a step of several times the boundary-layer thickness. (See ref. 26.) It appears from page 52 of reference 18 that a pressure coefficient of $C_p = 0.41$ is valid at subsonic speeds as well as Mach 1. Again these essentially two-dimensional values are presented as estimates for the pressures ahead of forward facing steps on bodies of revolution.

Fin Pressure Drag

Figure 5 presents the pressure-drag coefficients based on the exposed plan-form area of the fin (note this is one-half the value of S_f/A given on model sheets) for most of the fins used in this report. Extreme accuracy has not been striven for or obtained, since in most cases the fin pressure drag is such a small part of the total drag that a 50-percent error in fin drag is of the order of the test accuracy.

The pressure drag of fin type A  , which is used by the majority of the models, was measured by means of special helium-gun models. The drag of fin type B 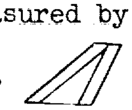 was measured by special rocket models, the data for which are presented in reference 27. The supersonic pressure drag thus obtained is so similar to that measured on type A that they have been shown as one curve. The pressure drag of fin type C  was estimated by reducing the drag rise of a 6-percent-thick delta wing of reference 27 (p. 47) by the square of the thickness ratios. The pressure drag of type D  is simply the two-dimensional base pressure of figure 3 referred now to the fin plan-form area.

SUMMARY CURVES

Systematic Investigations

A majority of the smooth bodies of this report were flown in programs designed to investigate the results of systematic geometrical changes in the body shapes on zero-lift drag. Figures 6 to 10 present summary plots of total-drag coefficients for the most important of these investigations. These figures give a broad picture of the effect of the most important variables on the total body drag; that is, fineness ratio and maximum diameter location (fig. 6), nose shape and fineness ratio (figs. 7 to 9); (see also configurations 1 to 8) and afterbody fineness ratio and shape (fig. 10). Various other methods of correlating the data will be immediately apparent to the reader, but it is suggested that the original references be consulted before too elaborate an analysis is attempted, since the various data have been handled in more detail in these reports than in the present report.

Drag Analysis

The data of this report, together with data from wind-tunnel tests and theoretical results allow some general conclusions useful to designers to be drawn. Some of these conclusions are presented in the following paragraphs. The effects of nose and afterbody shape are discussed separately, after which a brief discussion is given of the effects of the shapes of complete bodies.

Nose drag.- In the analysis of nose drag it is helpful to use one of the basic premises of this report, that is, that the effects of shape and fineness ratio may usefully be considered separately. The variation at $M = 1.4$ of the nose pressure drag with l/d is presented in figure 11. The lower curve represents near minimum nose pressure drags. At low values of l/d, the minimum curve was obtained by fairing through the flat-face value $\left(C_D = 0.8C_{p_{total}}\right)$ and hemisphere values (ref. 28). Above $l/d = 1.4$ it was determined from second-order calculations (by the method of Van Dyke, ref. 29) of bodies defined by $r' = x'^{3/4}$ and $r' = \dfrac{2x' - \frac{3}{4}x'^2}{1\frac{1}{4}}$. Note that neither of these bodies has zero slope at its maximum diameter. Since the calculations and experiment agree well for noses having $l/d = 3$ (see fig. 12) a fair amount of confidence may be placed in the values shown. Second-order calculations are also shown for the parabolic nose $r' = 2x' - x'^2$ used on so many of the models in this report. Taylor-McColl cone values are also shown for comparison.

Although l/d is shown to be a powerful parameter, the effects of shape can be important as can be seen in figure 12. The results shown in this figure are particularly gratifying in that the values from free-flight and wind-tunnel tests and several theories are in marked agreement. As can be seen from this figure, there is no one minimum-drag shape for the entire Mach number range but several do well over the entire range. (Refs. 30 and 31 present the drags of many shapes not shown here.) Note these results are for $l/d = 3$ and the relative drags may change with l/d. Data from reference 30 have been combined with the data of this report in part (b) of figure 12 to illustrate some general statements about the effect of nose geometry on drag. The drags of the $x^{1/4}$ and the ellipsoid show the high peak drag level and late peak drag Mach numbers characteristics of blunt nose bodies. The $x^{1/4}$ nose though not absolutely sharp (the cone could also have been used) shows the early drag rise and early sharp peak drag and the rapid decrease of drag with Mach number to be expected on sharp-nose bodies of revolution. The Von Kármán nose which has the $x^{3/4}$ profile at its apex but which is blunter immediately behind the apex produces a drag variation with Mach number which incorporates the desirable features of both types of nose, that is, late drag rise, soft peak and low peak drag level, and decreasing supersonic drag. This result is perhaps not so surprising since this nose was designed (from linearized theory) for minimum drag for a given l/d at low supersonic Mach numbers.

When these results are applied to the design of a complete body, it must be remembered that the interference drag of the nose on the after-body is also a function of nose shape. There are indications that the lowest drag shapes which do not have zero slope at their maximum diameter have higher interference drag potential than their smoother appearing brothers. (See the discussion entitled "Total body drag.")

Afterbody drag.- The data of figure 10 have been analyzed to give the drags of the afterbodies caused by the pressures acting over the afterbodies and bases. (For details of the drag breakdowns, see ref. 6.) The results are presented for $M = 1.2$ in figure 13. The data for the conical afterbodies are compared with the following semiempirical equation:

$$C_{D_{aft}} = \frac{0.001\theta + 0.00071\theta^2}{M}\left[1 - \left(\frac{r_b}{R}\right)^n\right] + C_{d_b}\left(\frac{r_b}{R}\right)^3 \tag{1}$$

where

$$n = 4 \qquad (M < 3.5)$$

$$n = 3 \qquad (M > 3.5)$$

θ is the slope of the afterbody in degrees (used as positive, although actually always negative; not applicable for positive values of θ) and C_{d_b} is the base pressure drag of the cylinder (fig. 3). The first term of the equation approximates the second-order theoretical values calculated by Jack (ref. 32) while the second term is a purely empirical approximation for the effect of base diameter ratio on the base pressure. In view of the inaccuracies inherent in both the experimental and the theoretical values (the theory, for instance, was calculated only for $M > 1.5$), the nearly exact agreement of the two shown in figure 13(a) is almost embarrassing and should be regarded as somewhat fortuitous. However, it is apparent, from the comparisons of this report with the second-order theory of reference 32 and from the comparisons of reference 6 with other theoretical calculations, that afterbody drags can be calculated reasonably accurately for afterbodies having maximum slopes of less than about 15°. At or above this degree of convergence large discrepancies may be expected (see ref. 6), theoretical calculations tending to overestimate the drag.

All the test results of both parabolic and conical afterbodies and the theoretical calculations lead to an extremely simple rule for selecting minimum drag afterbodies if a required value of l/d is given. The center line in figure 13(b) represent conical afterbodies with a slope of 4.5° (or parabolic meridians with a base slope of 9°). The data points represent the parabolic afterbodies of figure 10; note also that the tangent to the parabolic base angle is always exactly twice that of the inscribed conical body. The minimum drag bodies all fall on this line. The fact that for a given value of l/d the required ratio of base diameter to maximum diameter is much less important at the higher values of l/d can be noted in figure 13(a), and is shown more graphically by the shaded area on the lower figure which shows the limits of configurations whose drags lie within about 10 percent of the minimum. The range of optimum conical angles indicated (3.5° to 6.5°) is of the same order (5° to 7°) as that used for some time by ballisticians for the drag reduction of bullets.

Total body drag.- If the minimum afterbody drags at each value of l/d are taken, the resulting plot (fig. 14) may be said to represent a near minimum possible afterbody pressure drag for $M = 1.2$. A similar curve is presented for the nose drag and was obtained by fairing through the blunt nose values from configurations 1 to 7, through the minimum $l/d = 3$ nose drag $\left(r' = x'^{1/2}\ \text{(fig. 12)}\right)$ and through the $M = 1.4$ values for the higher values of l/d (fig. 11). These curves are presented to give some practical boundaries, admittedly empirical and rough, to the minimum drag problem.

If the nose and afterbody minimum drags are added for bodies with their maximum diameter at their midpoints, the solid curve on figure 15 is obtained. If the same drags are added with care taken to position the maximum diameter at the most favorable position the dashed curve is obtained. (This position moves rapidly rearward from $x/l = 0.55$ for $l/d = 7$ to $x/l = 1$ for $l/d = 3$ for the near minimum curves of figure 14; however, such values are extremely susceptible to small changes in level in either of the nose or afterbody drag curves and must only be considered as indicative of the trend.) Also, the drag rises $\left(\Delta C_D = C_{D_{total}} - C_{D_{friction}} - C_{D_{fin\ pressure}}\right)$ for the smooth bodies of this report are plotted at the fineness ratio representing the sum of their nose and afterbody fineness ratios. Most of the bodies at low values of l/d actually had cylindrical center sections and thus their interference drags were low. This must be kept in mind when the use of either of the empirical curves as minimum drag boundaries is contemplated. As an instance of this, compare the pressure drags of models 84 and 85 which are identical in shape $\left(r' = x'^{1/2}\right)$, and fineness ratio of nose and afterbody, and differ only in the cylindrical center section of model 85. The higher pressure drag of model 84 must be attributed to interference of the nose on the afterbody. This interference drag seems high in comparison with the drag produced by the interaction of nose and afterbodies of the parabolic bodies of figure 6 which are indicated to be of the order of model 85 (and essentially zero) by a breakdown of their drags into component parts and a comparison of the pressure components with second-order theoretical calculations (ref. 29). It seems reasonable to assume that at total fineness ratios below 6, the effect of nose induced pressures on afterbody drag and perhaps more significantly on base pressure (note large base diameter ratios of minimum drag afterbodies of fineness ratios less than 3 (fig. 13(b)), and see ref. 21 for some examples of such effects on base pressures) will be the important and perhaps the determining factors affecting both the shape of the body and the value of the drag of minimum drag designs.

While it is not a factor considered in the discussions of this report it must always be remembered that the dependence of drag on l/d is also a function of the friction coefficient, and that it is the increase of friction drag with l/d that limits the drag reduction due to increasing l/d.

Langley Aeronautical Laboratory,
National Advisory Committee for Aeronautics,
Langley Field, Va., September 3, 1957.

REFERENCES

1. Hopko, Russell N.: The Effect of Some Surface Roughness Elements on the Drag of a Body of Revolution at Supersonic Speeds. NACA RM L54I21, 1954.

2. Piland, Robert O., and Putland, Leonard W.: Zero-Lift Drag of Several Conical and Blunt Nose Shapes Obtained in Free Flight at Mach Numbers of 0.7 to 1.3. NACA RM L54A27, 1954.

3. Piland, Robert O.: Preliminary Free-Flight Investigation of the Zero-Lift Drag Penalties of Several Missile Nose Shapes for Infrared Seeking Devices. NACA RM L52F23, 1952.

4. Wallskog, Harvey A., and Hart, Roger G.: Investigation of the Drag of Blunt-Nosed Bodies of Revolution in Free Flight at Mach Numbers From 0.6 to 2.3. NACA RM L53D14a, 1953.

5. Hart, Roger G., and Katz, Ellis R.: Flight Investigations at High-Subsonic, Transonic, and Supersonic Speeds To Determine Zero-Lift Drag of Fin-Stabilized Bodies of Revolution Having Fineness Ratios of 12.5, 8.91, and 6.04 and Varying Positions of Maximum Diameter. NACA RM L9I30, 1949.

6. Stoney, William E., Jr.: Some Experimental Effects of Afterbody Shape on the Zero-Lift Drag of Bodies for Mach Numbers Between 0.8 and 1.3. NACA RM L53I01, 1953.

7. Stoney, William E., Jr.: Transonic Drag Measurements of Eight Body-Nose Shapes. NACA RM L53K17, 1954.

8. Walters, Richard E.: Application of Transonic Area Rule to a Sharp-Lipped Ducted Nacelle. NACA RM L53J09b, 1954.

9. Sears, R. I., and Merlet, C. F.: Flight Determination of the Drag and Pressure Recovery of an NACA 1-40-250 Nose Inlet at Mach Numbers From 0.9 to 1.8. NACA TN 3218, 1955. (Supersedes NACA RM L50L18.)

10. Sears, R. I., Merlet, C. F., and Putland, L. W.: Flight Determination of Drag of Normal-Shock Nose Inlets With Various Cowling Profiles at Mach Numbers From 0.9 to 1.5. NACA Rep. 1281, 1956. (Supersedes NACA RM L53I25a.)

11. Mason, Homer P., and Gardner, William N.: An Application of the Rocket-Propelled-Model Technique to the Investigation of Low-Lift Buffeting and the Results of Preliminary Tests. NACA RM L52C27, 1952.

12. Welsh, Clement J., and DeMoraes, Carlos A.: Results of Flight Tests To Determine Drag of Parabolic and Cone-Cylinder Bodies of Very Large Fineness Ratios at Supersonic Speeds. NACA RM L51E18, 1951.

13. Jackson, H. Herbert, Rumsey, Charles B., and Chauvin, Leo T.: Flight Measurements of Drag and Base Pressure of a Fin-Stabilized Parabolic Body of Revolution (NACA-RM 10) at Different Reynolds Numbers and at Mach Numbers From 0.9 to 3.3. NACA TN 3320, 1954. (Supersedes NACA RM L50G24.)

14. Hall, James Rudyard: Effect of Wing Size and Amount of Indentation on Applicability of Transonic Area Rule to Swept-Wing Configurations. NACA RM L55F03, 1956.

15. Stoney, William E., Jr., and Putland, Leonard W.: Some Effects of Body Cross-Sectional Shape, Including a Sunken-Canopy Design on Drag As Shown by Rocket-Powered-Model Tests at Mach Numbers From 0.8 to 1.5. NACA RM L52D07, 1952.

16. Hoffman, Sherwood: A Flight Investigation of the Transonic Area Rule for a 52.5° Sweptback Wing-Body Configuration at Mach Numbers Between 0.8 and 1.6. NACA RM L54H13a, 1954.

17. Van Driest, E. R.: The Turbulent Boundary Layer for Compressible Fluids on a Flat Plate With Heat Transfer. Rep. No. AL-997, North American Aviation, Inc., Jan. 27, 1950.

18. Heorner, Sighard F.: Aerodynamic Drag. Publ. by the author (148 Busteed, Midland Park, N. J.), 1951.

19. Evans, Albert J.: The Zero-Lift Drag of a Slender Body of Revolution (NACA RM-10 Research Model) As Determined From Tests in Several Wind Tunnels and in Flight at Supersonic Speeds. NACA Rep. 1160, 1954. (Supersedes NACA TN 2944.)

20. Carros, Robert J., and James, Carlton S.: Some New Drag Data on the NACA RM-10 Missile and a Correlation of the Existing Drag Measurements at $M = 1.6$ and 3.0. NACA TN 3171, 1954.

21. Love, Eugene S.: Base Pressure at Supersonic Speeds on Two-Dimensional Airfoils and on Bodies of Revolution With and Without Fins Having Turbulent Boundary Layers. NACA TN 3819, 1957. (Supersedes NACA RM L53C02.)

22. Hart, Roger G.: Effects of Stabilizing Fins and a Rear-Support Sting on the Base Pressures of a Body of Revolution in Free Flight at Mach Numbers From 0.7 to 1.3. NACA RM L52E06, 1952.

23. Peck, Robert F.: Flight Measurements of Base Pressure on Bodies of Revolution With and Without Simulated Rocket Chambers. NACA TN 3372, 1955. (Supersedes NACA RM L50I28a.)

24. Katz, Ellis, and Stoney, William E., Jr.: Base Pressures Measured on Several Parabolic-Arc Bodies of Revolution in Free Flight at Mach Numbers From 0.8 to 1.4 and at Large Reynolds Numbers. NACA RM L51F29, 1951.

25. Morrow, John D., and Katz, Ellis: Flight Investigation at Mach Numbers From 0.6 to 1.7 To Determine Drag and Base Pressures on a Blunt-Trailing-Edge Airfoil and Drag of Diamond and Circular-Arc Airfoils at Zero Lift. NACA TN 3548, 1955. (Supersedes NACA RM L50E19a.)

26. Love, Eugene S.: Pressure Rise Associated With Shock-Induced Boundary-Layer Separation. NACA TN 3601, 1955.

27. Morrow, John D., and Nelson, Robert L.: Large-Scale Flight Measurements of Zero-Lift Drag of 10 Wing-Body Configurations at Mach Numbers From 0.8 to 1.6. NACA RM L52D18a, 1953.

28. Sommer, Simon C., and Stark, James A.: The Effect of Bluntness on the Drag of Spherical-Tipped Truncated Cones of Fineness Ratio 3 at Mach Numbers 1.2 to 7.4. NACA RM A52B13, 1952.

29. Van Dyke, Milton D.: Practical Calculation of Second-Order Supersonic Flow Past Non-Lifting Bodies of Revolution. NACA TN 2744, 1952.

30. Perkins, Edward W., and Jorgensen, Leland H.: Investigation of the Drag of Various Axially Symmetric Nose Shapes of Fineness Ratio 3 for Mach Numbers From 1.24 to 3.67. NACA RM A52H28, 1952.

31. Eggers, A. J., Resnikoff, Meyer M., and Dennis, David H.: Bodies of Revolution Having Minimum Drag at High Supersonic Airspeeds. NACA TN 3666, 1956. (Supersedes NACA RM's A51K27 by Eggers, Dennis, and Resnikoff and A52D24 by Resnikoff.)

32. Jack, John R.: Theoretical Pressure Distributions and Wave Drags for Conical Boattails. NACA TN 2972, 1953.

TABLE I.- GEOMETRIC CHARACTERISTICS OF SMOOTH CONFIGURATIONS

Configuration	l/d_{N+A}	l/d_{total}	l/d_{nose}	l/d_{aft}	S_b/A	S_f/A	A_b/A	θ_b, deg	Test	Reference	Figure
1 - 8	0.50	12.00	0.50	0.00	49.00	6.36	1.00	0.00	Helium gun	--	16
9	3.71	8.57	1.38	2.33	28.30	11.00	.00	12.20	Helium gun	--	17
10	4.62	7.70	1.92	2.70	25.20	6.40	.00	68.00	Helium gun	--	18
11	4.64	11.20	3.50	1.14	39.30	11.00	.45	8.00	Rocket	1	19
12	4.85	7.15	2.02	2.83	22.40	11.00	.00	15.70	Helium gun	--	20
13	4.98	13.47	2.98	2.00	51.50	24.60	.52	4.02	Helium gun	2	21
14	4.98	13.47	2.98	2.00	51.30	24.60	.52	4.02	Helium gun	2	22
15	5.00	5.00	2.00	3.00	13.60	11.00	.00	18.80	Helium gun	--	23
16	5.00	5.00	2.00	3.00	13.30	11.00	.00	11.90	Helium gun	--	24
17	5.00	7.78	2.00	3.00	25.00	11.00	.00	12.70	Helium gun	--	25
18	5.10	5.10	1.92	3.18	14.60	11.00	.00	90.00	Helium gun	--	26
19	5.20	13.70	3.20	2.00	51.00	24.60	.52	4.02	Rocket	3	27
20	5.20	13.70	3.20	2.00	51.00	24.60	.52	4.02	Helium gun	2	28
21	5.34	9.51	2.67	2.67	30.60	11.00	.00	15.60	Helium gun	--	29
22	5.70	5.70	5.70	.00	11.40	.00	1.00	-5.00	Helium gun	--	30
23	5.79	14.29	3.79	2.00	51.90	24.60	.52	4.02	Helium gun	2	31
24	5.84	5.84	.50	5.34	19.00	11.00	.19	7.00	Rocket	4	32
25	5.84	12.90	3.10	2.74	51.80	12.40	.25	18.60	Rocket	--	33
26	6.00	8.78	3.00	3.00	26.20	11.00	.00	12.90	Helium gun	--	34
27	6.04	6.04	1.21	4.83	19.16	11.00	.19	9.20	Rocket	5	35
28	6.04	6.04	4.83	1.21	16.84	11.00	.19	25.00	Rocket	5	36
29	6.04	6.04	2.42	3.62	18.39	11.00	.19	8.80	Rocket	5	37
30	6.04	6.04	3.62	2.42	17.64	11.00	.19	13.00	Rocket	5	38
31	6.04	6.04	3.71	2.33	17.60	11.00	.37	6.10	Helium gun	--	39
32	6.08	9.60	5.01	1.07	31.60	12.30	.69	5.45	Helium gun	--	40
33	6.10	14.60	4.10	2.00	52.30	24.60	.52	4.02	Helium gun	3	41
34	6.10	14.60	4.10	2.00	52.30	24.60	.52	4.02	Rocket	3	42
35	6.42	9.32	2.98	3.44	30.20	11.00	.00	13.30	Helium gun	--	43
36	6.50	15.00	4.50	2.00	52.60	24.60	.52	4.02	Rocket	3	44
37	6.51	10.87	2.71	3.80	35.60	12.82	.00	60.00	Helium gun	--	45
38	6.52	13.90	3.80	2.72	49.60	12.40	.25	17.40	Rocket	--	46
39	7.00	7.00	2.80	4.20	19.00	11.00	.00	12.90	Helium gun	--	47
40	7.16	7.16	1.81	5.35	24.00	11.00	.19	7.00	Rocket	4	48
41	7.30	7.30	1.95	5.35	24.20	11.00	.19	7.00	Rocket	4	49
42	7.33	8.57	3.02	4.31	25.60	11.00	.00	90.00	Helium gun	--	50

TABLE I.- GEOMETRIC CHARACTERISTICS OF SMOOTH CONFIGURATIONS - Continued

Configuration	l/d_{N+A}	l/d_{total}	l/d_{nose}	l/d_{aft}	S_b/A	S_f/A	A_b/A	θ_b, deg	Test	Reference	Figure
43	7.35	7.35	2.00	5.35	22.70	11.00	0.19	6.00	Rocket	4	51
44	7.43	7.43	3.58	3.85	20.90	11.00	.00	15.00	Helium gun	--	52
45	7.47	7.47	2.12	5.35	24.30	11.00	.19	6.00	Rocket	4	53
46	7.60	7.60	2.25	5.35	25.10	11.00	.19	7.00	Rocket	4	54
47	7.66	7.66	2.33	5.33	25.30	11.00	.19	7.00	Rocket	4	55
48	7.72	10.90	6.00	1.72	32.60	11.00	.00	2.90	Helium gun	--	56
49	7.78	11.50	6.00	1.78	35.50	11.00	.00	29.30	Helium gun	6	57
50	7.78	11.50	6.00	1.78	35.50	11.00	.00	29.30	Helium gun	6	58
51	7.80	11.08	3.42	4.38	34.40	11.00	.00	9.80	Helium gun	--	59
52	7.90	7.90	2.57	5.33	25.70	11.00	.19	7.00	Rocket	4	60
53	8.00	8.00	3.20	4.80	21.90	11.00	.00	8.50	Helium gun	--	61
54	8.00	8.00	4.66	3.44	23.16	5.80	.17	9.50	Helium gun	--	62
55	8.00	8.00	4.00	4.00	26.30	4.43	.00	14.00	Helium gun	--	63
56	8.00	12.00	3.00	5.00	36.38	11.00	.19	3.20	Helium gun	7	64
57	8.00	12.00	3.00	5.00	37.05	11.00	.19	3.20	Helium gun	7	65
58	8.00	12.00	3.00	5.00	38.35	11.00	.19	3.20	Helium gun	7	66
59	8.00	12.00	3.00	5.00	38.40	11.00	.19	3.20	Helium gun	7	67
60	8.00	12.00	3.00	5.00	38.78	11.00	.19	3.20	Helium gun	7	68
61	8.00	12.00	3.00	5.00	37.24	11.00	.19	3.20	Helium gun	7	69
62	8.00	12.00	3.00	5.00	37.58	11.00	.19	3.20	Helium gun	7	70
63	8.00	12.00	3.00	5.00	38.40	11.00	.19	3.20	Helium gun	7	71
64	8.10	8.10	2.73	5.37	26.08	11.00	.19	7.00	Rocket	4	72
65	8.20	10.93	3.38	4.82	34.10	11.00	.00	9.00	Helium gun	--	73
66	8.30	8.30	2.96	5.34	26.50	11.00	.19	7.00	Rocket	4	74
67	8.33	9.02	3.27	5.06	26.60	9.20	.0384	23.00	Helium gun	8	75
68	8.44	8.44	3.20	5.24	24.90	5.45	.26	3.50	Rocket	--	76
69	8.50	8.50	3.60	4.90	26.30	9.74	.30	5.60	Rocket	9	77
70	8.50	8.50	3.16	5.34	26.80	11.00	.19	7.00	Rocket	4	78
71	8.60	8.60	5.59	3.01	25.70	5.20	.36	4.55	Rocket	--	79
72	8.65	8.65	3.28	5.37	27.30	11.00	.19	7.00	Rocket	4	80
73	8.81	8.81	4.04	4.77	28.80	11.00	.33	6.90	Helium gun	--	81
74	8.91	8.91	1.78	7.13	28.26	11.00	.19	6.50	Rocket	5	82
75	8.91	8.91	7.13	1.78	24.84	11.00	.19	18.30	Rocket	5	83
76	8.91	8.91	3.56	5.35	27.00	11.00	.19	6.00	Rocket	4 5	84
77	8.91	8.91	5.35	3.56	26.02	11.00	.19	10.20	Rocket	5	85
78	8.91	8.91	7.13	1.78	26.10	11.00	1.00	.00	Helium gun	6	86

TABLE I.- GEOMETRIC CHARACTERISTICS OF SMOOTH CONFIGURATIONS - Concluded

Configuration	l/d_{N+A}	l/d_{total}	l/d_{nose}	l/d_{aft}	S_b/A	S_f/A	A_b/A	θ_b, deg	Test	Reference	Figure
79	8.91	8.91	7.13	1.78	23.70	11.00	0.00	29.30	Helium gun	6	87
80	8.91	8.91	7.13	1.78	24.80	11.00	.19	17.50	Helium gun	6	88
81	8.91	8.91	7.13	1.78	25.40	11.00	.49	9.60	Helium gun	6	89
82	8.91	8.91	7.13	1.78	24.20	11.00	.19	9.00	Helium gun	6	90
83	8.91	8.91	7.13	1.78	25.10	11.00	.49	4.87	Helium gun	6	91
84	8.91	8.91	4.66	4.25	24.50	11.00	.09	9.70	Helium gun	--	92
85	8.91	12.50	4.66	4.25	38.80	11.00	.09	10.70	Helium gun	--	93
86	9.13	9.13	3.28	5.85	28.00	8.30	.008	30.00	Helium gun	8	94
87	9.38	9.38	3.63	5.75	28.00	6.40	.11	7.00	Rocket	10	95
88	9.54	9.54	4.20	5.34	28.60	6.40	.17	8.75	Rocket	10	96
89	10.00	10.00	4.00	6.00	30.88	11.40	.25	4.47	Rocket	--	97
90	10.00	10.00	4.73	5.27	29.60	17.76	.15	6.45	Rocket	11	98
91	10.54	10.54	5.38	5.16	34.40	11.00	.19	7.00	Rocket	4	99
92	10.63	10.63	7.13	3.50	33.00	11.00	1.00	.00	Helium gun	6	100
93	10.63	10.63	7.13	3.50	31.60	11.00	.49	5.40	Helium gun	6	101
94	10.63	10.63	7.13	3.50	30.06	11.00	.19	14.80	Helium gun	6	102
95	10.63	10.63	7.13	3.50	28.30	11.00	.00	15.80	Helium gun	6	103
96	11.19	21.20	7.16	4.03	62.50	11.00	.19	4.00	Rocket	12	104
97	11.19	17.20	7.16	4.03	48.80	11.00	.19	4.00	Rocket	12	105
98	12.13	12.13	7.13	5.00	38.90	11.00	1.00	.00	Helium gun	6	106
99	12.13	12.13	7.13	5.00	36.90	11.00	.49	3.42	Helium gun	6	107
100	12.13	12.13	7.13	5.00	35.80	11.00	.49	1.70	Helium gun	6	108
101	12.13	12.13	7.13	5.00	33.30	11.00	.19	3.20	Helium gun	6	109
102	12.13	12.13	7.13	5.00	35.20	11.00	.19	6.40	Helium gun	6	110
103	12.13	12.13	7.13	5.00	32.20	11.00	.00	11.70	Helium gun	6	111
104	12.20	12.20	7.50	4.70	36.30	30.80	.364	7.60	Rocket	--	112
105	12.20	12.20	7.50	4.70	36.30	30.80	.364	7.60	Rocket	--	113
106	12.50	12.50	2.50	10.00	39.65	11.00	.19	3.20	Rocket	5	114
107	12.50	12.50	10.00	2.50	34.85	11.00	.19	12.60	Rocket	5	115
108	12.50	12.50	5.00	7.50	38.10	11.00	.19	4.30	Rocket	5	116
109	12.50	12.50	7.50	5.00	36.50	11.00	.19	6.40	Rocket	5	117
110	12.50	12.50	6.25	6.25	33.40	11.00	.00	90.00	Helium gun	--	118
111	17.78	17.78	10.65	7.10	52.00	11.00	.19	4.60	Rocket	12	119
112	24.50	24.50	14.70	9.80	71.60	11.00	.19	3.30	Rocket	12	120

TABLE II.- GEOMETRIC CHARACTERISTICS OF BUMPY CONFIGURATIONS

Configuration	l/d_{total}	S_b/A	S_f/A	A_b/A	θ_b, deg	Test	Reference	Figure
113, 114, 115	3.67	12.40	0.00	1.00	-7.60	Helium gun	--	121
116	5.23	13.10	5.80	.04	5.50	Helium gun	--	122
117	5.26	24.79	11.64	.14	23.90	Helium gun	--	123
118	5.29	16.00	11.64	.23	17.30	Helium gun	--	124
119	5.36	15.60	11.28	.09	24.20	Helium gun	--	125
120	5.45	14.10	6.28	.04	5.50	Helium gun	--	126
121	5.68	16.60	11.60	.17	20.20	Helium gun	--	127
122	6.00	17.50	12.00	.00	13.60	Helium gun	--	128
123	6.66	17.19	9.22	.06	16.70	Helium gun	--	129
124	6.82	15.70	5.43	.0652	5.00	Helium gun	--	130
125	6.84	18.20	10.76	.00	90.00	Helium gun	--	131
126	6.86	21.15	12.20	.18	18.00	Helium gun	--	132
127	6.95	19.90	11.64	.20	8.80	Helium gun	--	133
128	6.98	21.16	11.80	.26	10.30	Helium gun	--	134
129	6.98	21.27	11.80	.29	9.70	Helium gun	--	135
130	7.08	19.40	13.00	.00	90.00	Helium gun	14	136
131	7.08	21.35	11.86	.20	11.30	Helium gun	--	137
132	7.08	19.60	3.56	.12	6.50	Helium gun	--	138
133	7.14	20.26	9.90	.00	90.00	Helium gun	--	139
134	7.33	21.70	11.70	.19	.00	Helium gun	--	140
135	7.42	19.00	11.50	.05	15.40	Helium gun	--	141
136	7.55	18.70	6.63	.08	5.00	Helium gun	--	142
137	7.70	18.80	11.95	.006	90.00	Helium gun	--	143
138	7.75	20.90	5.78	.20	26.50	Helium gun	--	144
139	7.76	21.54	11.00	.00	9.40	Helium gun	--	145
140	8.00	24.80	13.20	.18	33.20	Helium gun	--	146
141	8.03	20.70	9.00	.09	7.90	Helium gun	--	147
142	8.04	24.04	13.00	.23	12.60	Helium gun	--	148
143	8.07	23.75	4.12	.15	4.30	Helium gun	--	149
144	8.10	25.11	13.20	.18	21.50	Helium gun	--	150
145	8.10	25.08	13.20	.18	17.10	Helium gun	--	151
146	8.11	21.00	7.67	.09	5.00	Helium gun	--	152
147	8.12	25.40	13.20	.18	17.90	Helium gun	--	153
148	8.23	20.80	11.72	.00	16.80	Helium gun	--	154
149	8.27	24.00	10.90	.29	2.80	Helium gun	--	155
150	8.28	20.70	11.80	.06	15.00	Helium gun	--	156
151	8.40	23.00	7.88	.17	6.10	Helium gun	--	157
152	8.43	23.10	6.00	.17	6.80	Helium gun	--	158
153	8.48	23.76	12.62	.30	2.40	Helium gun	--	159
154	8.49	23.12	11.00	.00	7.40	Helium gun	--	160
155	8.52	23.40	11.50	.08	2.50	Helium gun	--	161
156	8.57	25.70	9.70	.00	90.00	Rocket	--	162
157	8.70	24.54	13.12	.20	12.10	Helium gun	--	163
158	8.84	25.64	6.64	.18	4.60	Helium gun	--	164
159	8.85	25.75	13.14	.21	12.30	Helium gun	--	165
160	8.91	25.00	11.00	.19	7.00	Rocket	15	166
161	8.92	24.10	11.50	.07	12.60	Helium gun	--	167
162	9.08	26.26	14.40	.16	9.10	Helium gun	--	168
163	9.09	24.40	11.60	.03	8.50	Helium gun	--	169
164	9.10	25.55	11.64	.04	10.00	Helium gun	--	170
165	9.22	26.17	7.14	.20	4.35	Helium gun	--	171
166	9.28	26.91	7.28	.20	4.06	Helium gun	--	172
167	9.31	28.19	10.00	.21	4.60	Helium gun	16	173
168	9.31	28.19	10.00	.21	4.60	Rocket	16	174
169	10.00	20.35	11.50	.00	90.00	Helium gun	--	175
170	10.00	27.40	11.00	.00	6.80	Helium gun	--	176
171	10.00	28.40	16.50	.25	4.15	Rocket	--	177
172	10.04	30.40	11.00	.00	90.00	Helium gun	--	178
173	10.46	27.40	15.35	.02	4.00	Helium gun	--	179
174	10.70	29.80	11.00	.00	6.80	Helium gun	--	180
175	11.02	32.40	17.04	.19	7.05	Helium gun	--	181
176	11.39	29.20	11.00	.00	18.90	Helium gun	--	182
177	12.05	31.90	15.00	.04	5.00	Helium gun	--	183

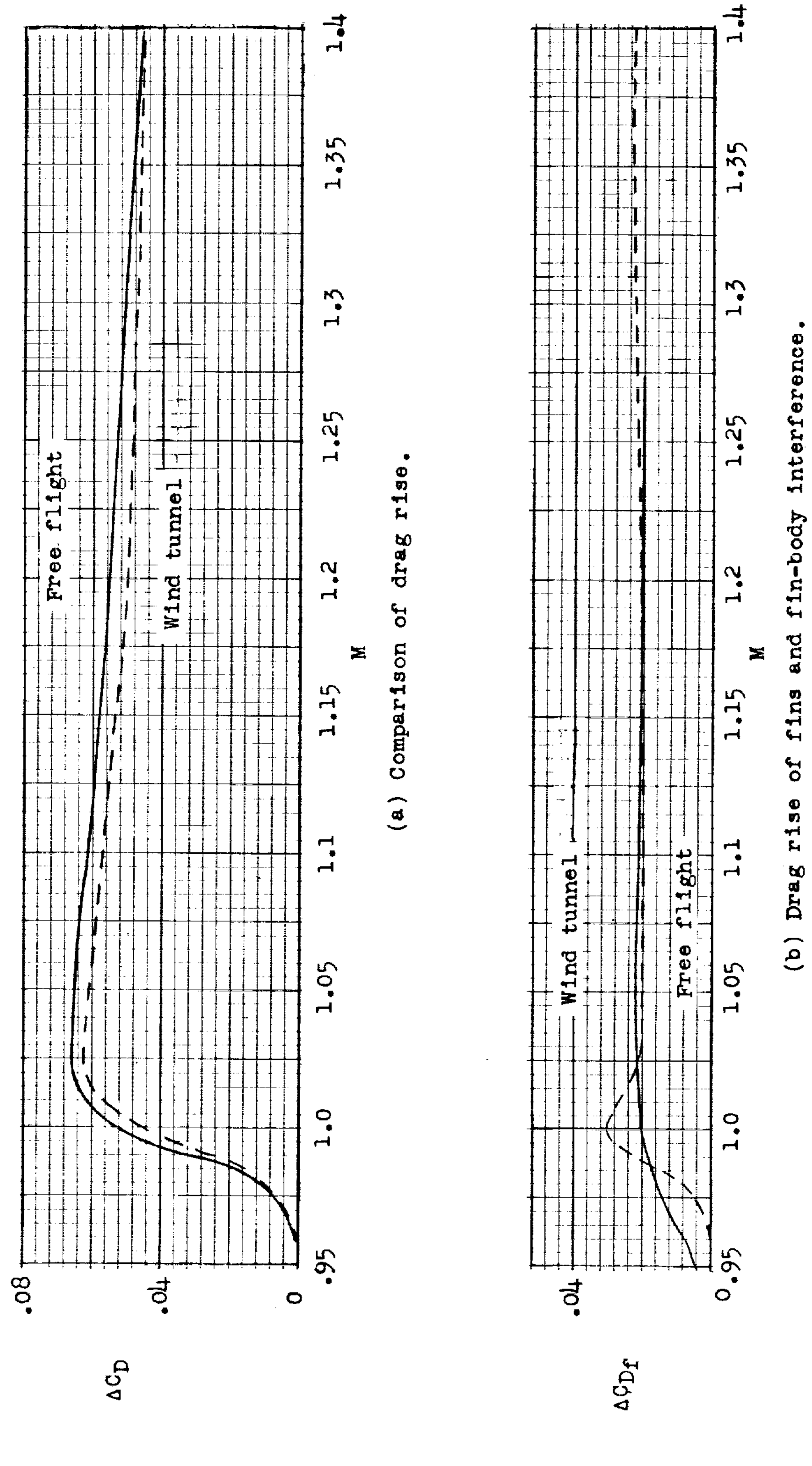

(a) Comparison of drag rise.

(b) Drag rise of fins and fin-body interference.

Figure 1.- Comparisons of data for model 109 obtained from wind-tunnel and free-flight tests.

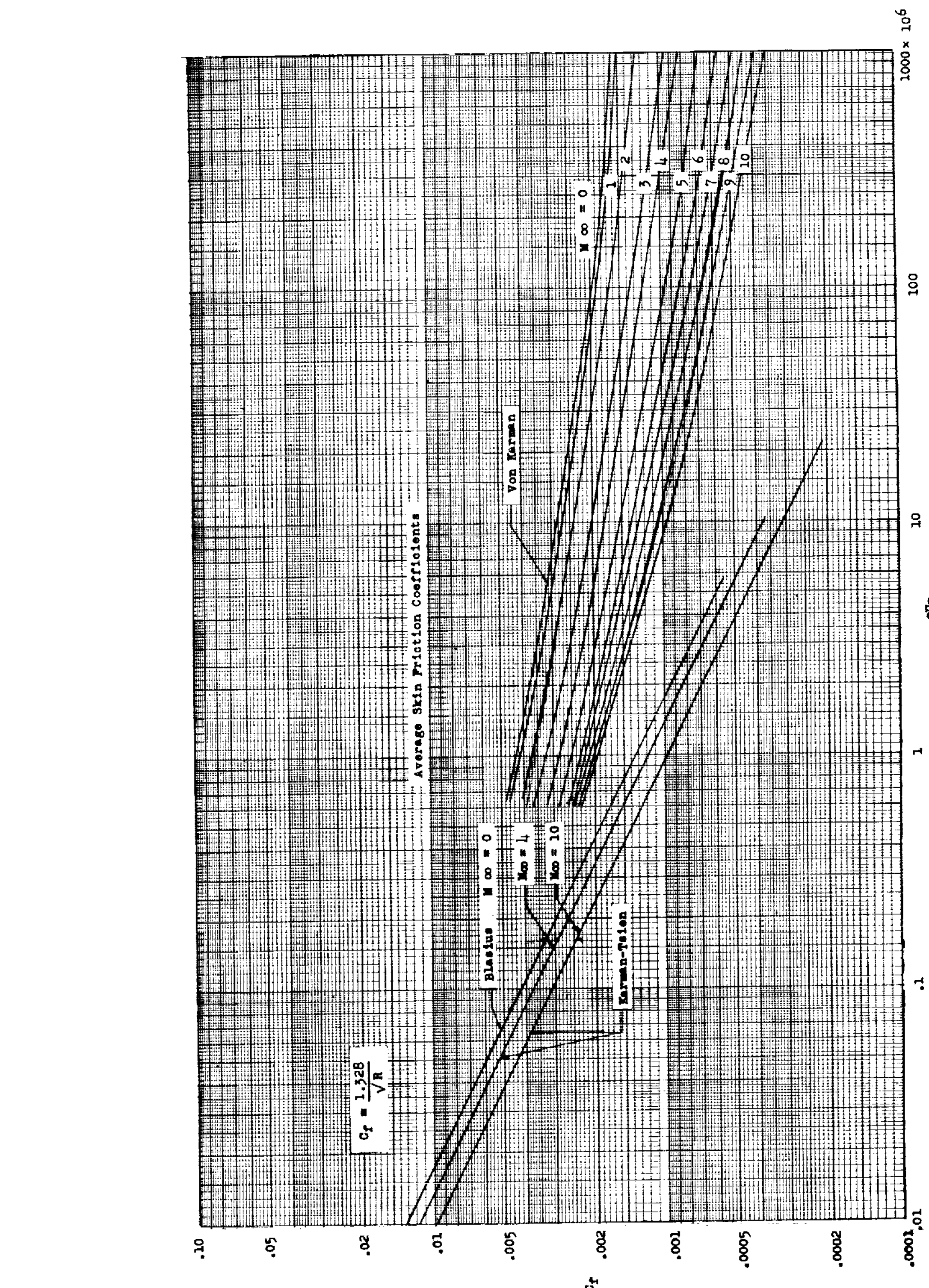

Figure 2.- Average skin-friction coefficients for flat plates based on wetted area.

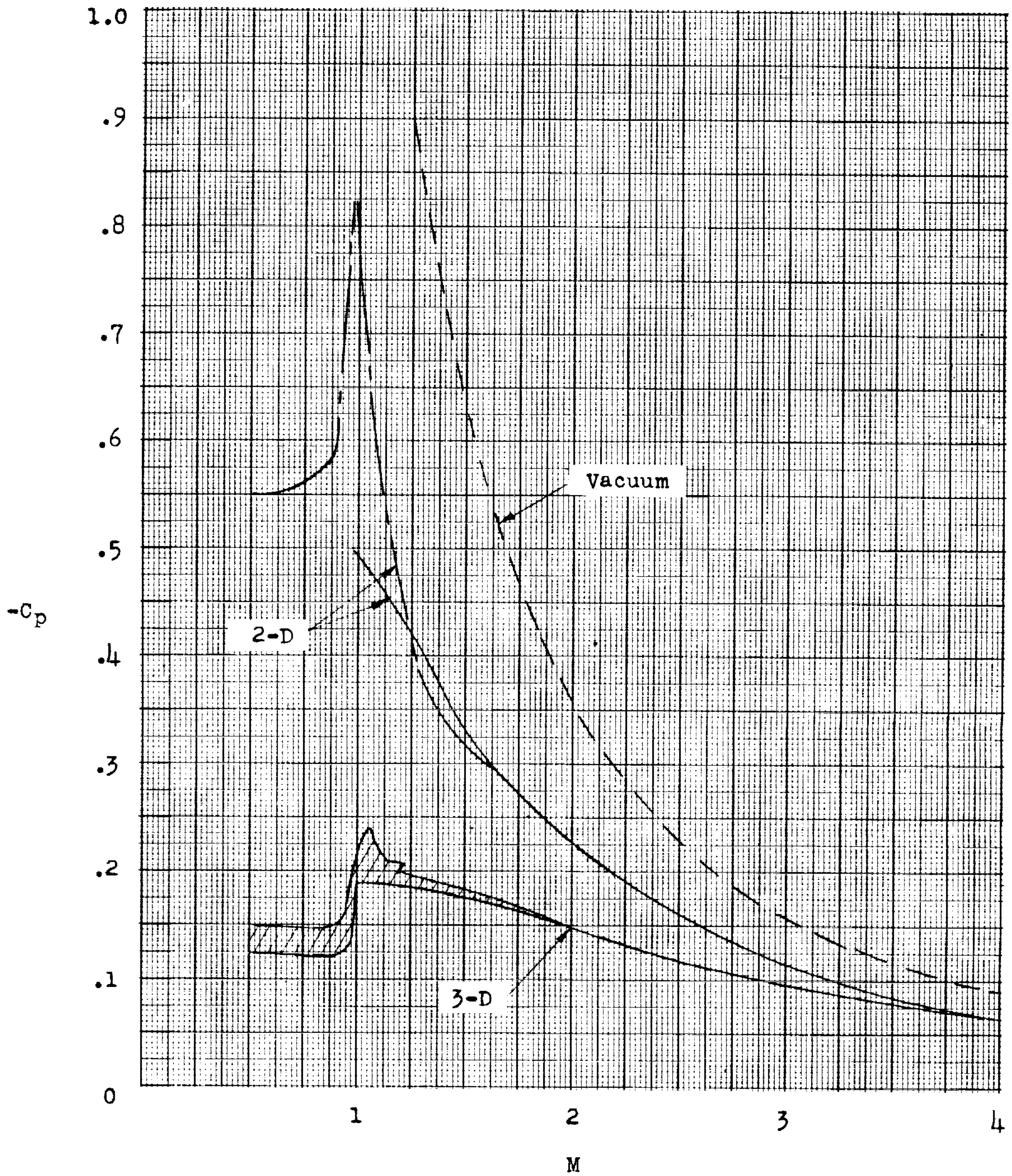

Figure 3.- Base-pressure coefficients behind two- and three-dimensional bodies for which flow is turbulent ahead of base.

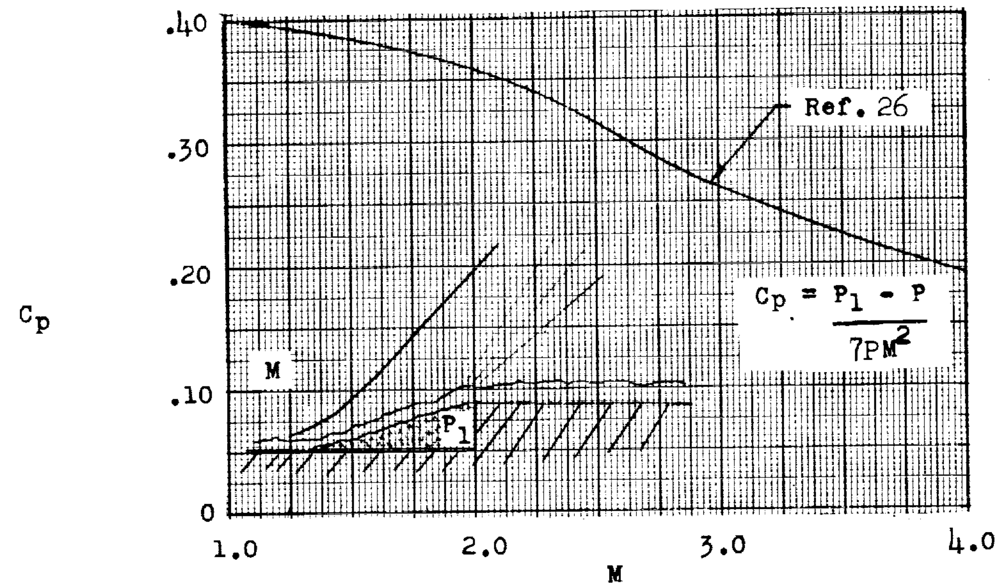

Figure 4.- Pressure coefficients on forward facing step for flow with turbulent boundary layer.

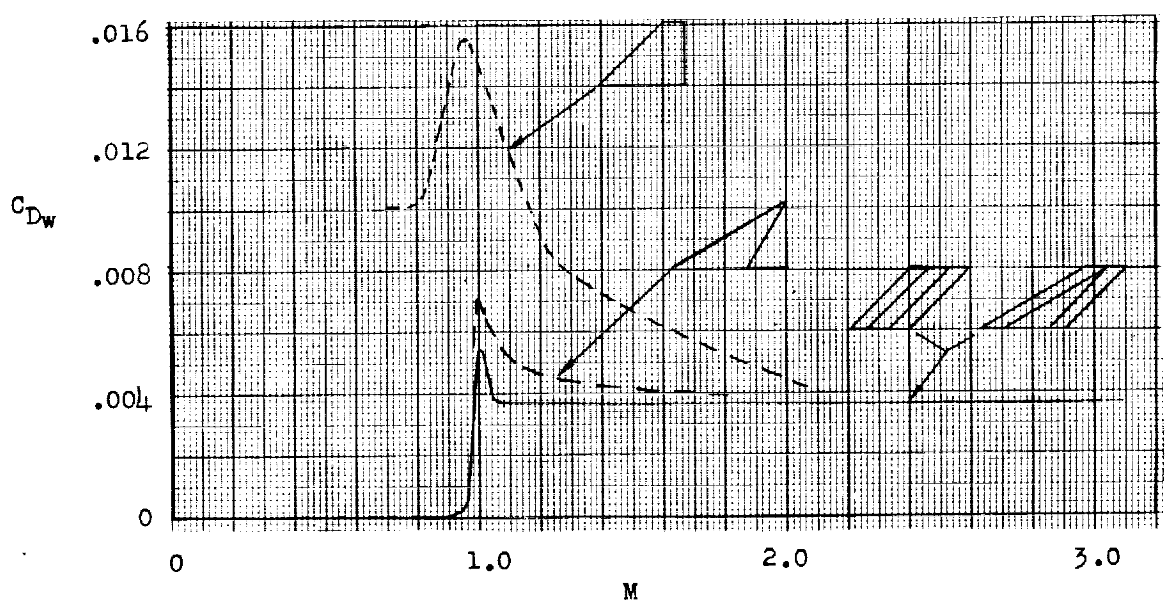

Figure 5.- Fin pressure drag coefficients (including base pressure) based on exposed fin area.

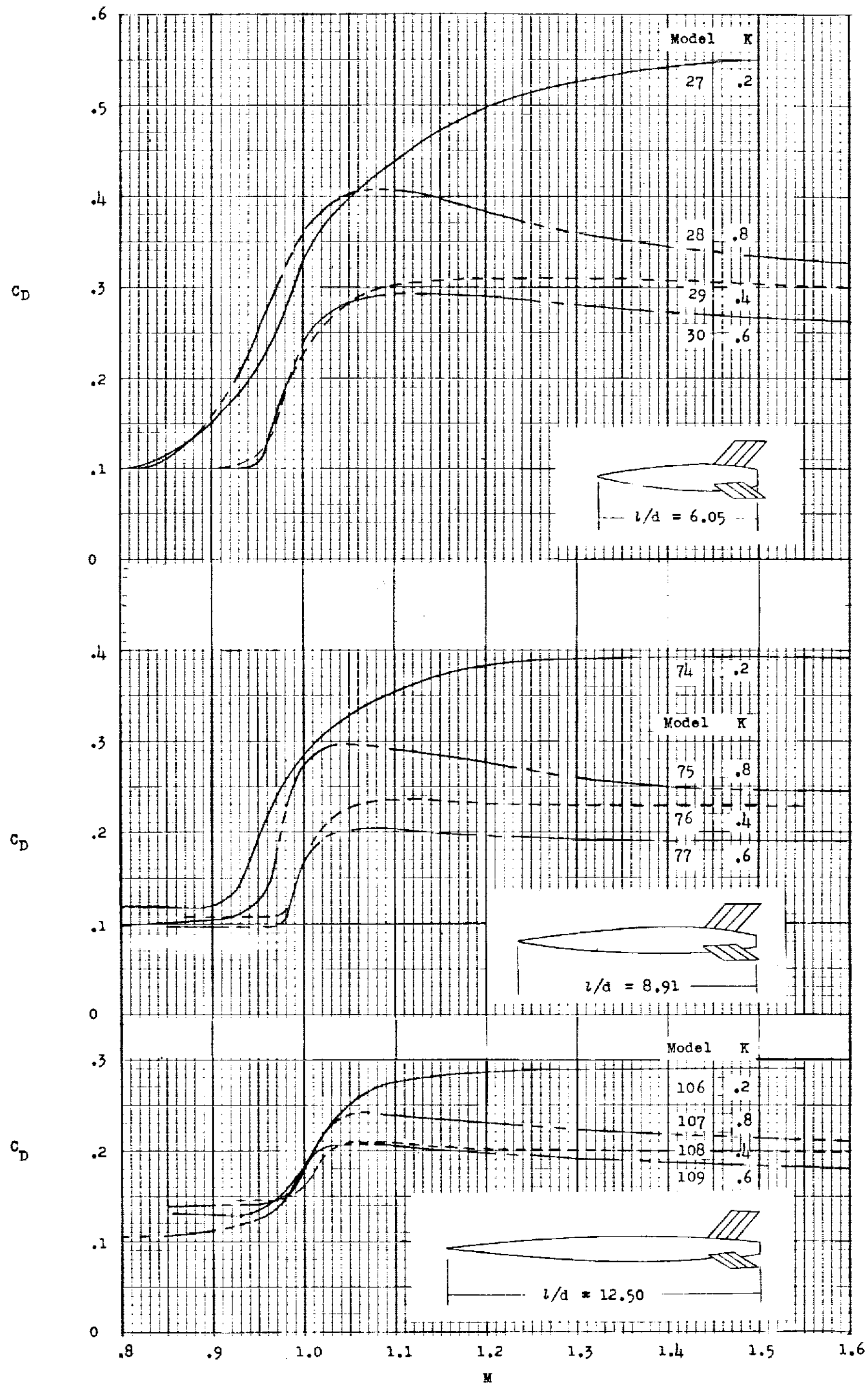

Figure 6.- Drag coefficients of parabolic bodies showing effects of fineness ratio and position of maximum diameter.

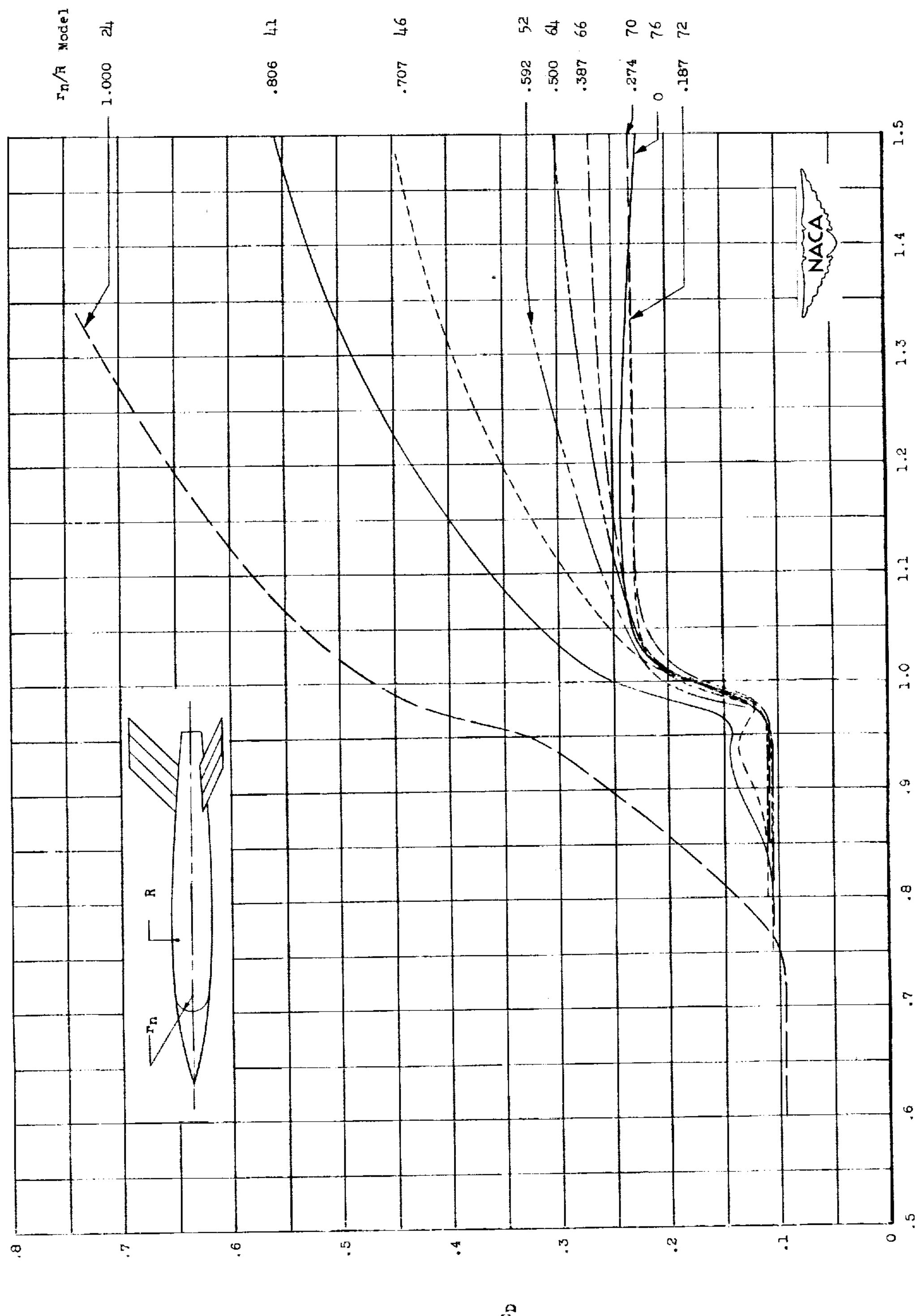

Figure 7.- Drag coefficient plotted against Mach number for configurations obtained by rounding off nose of parabolic body of fineness ratio 8.91.

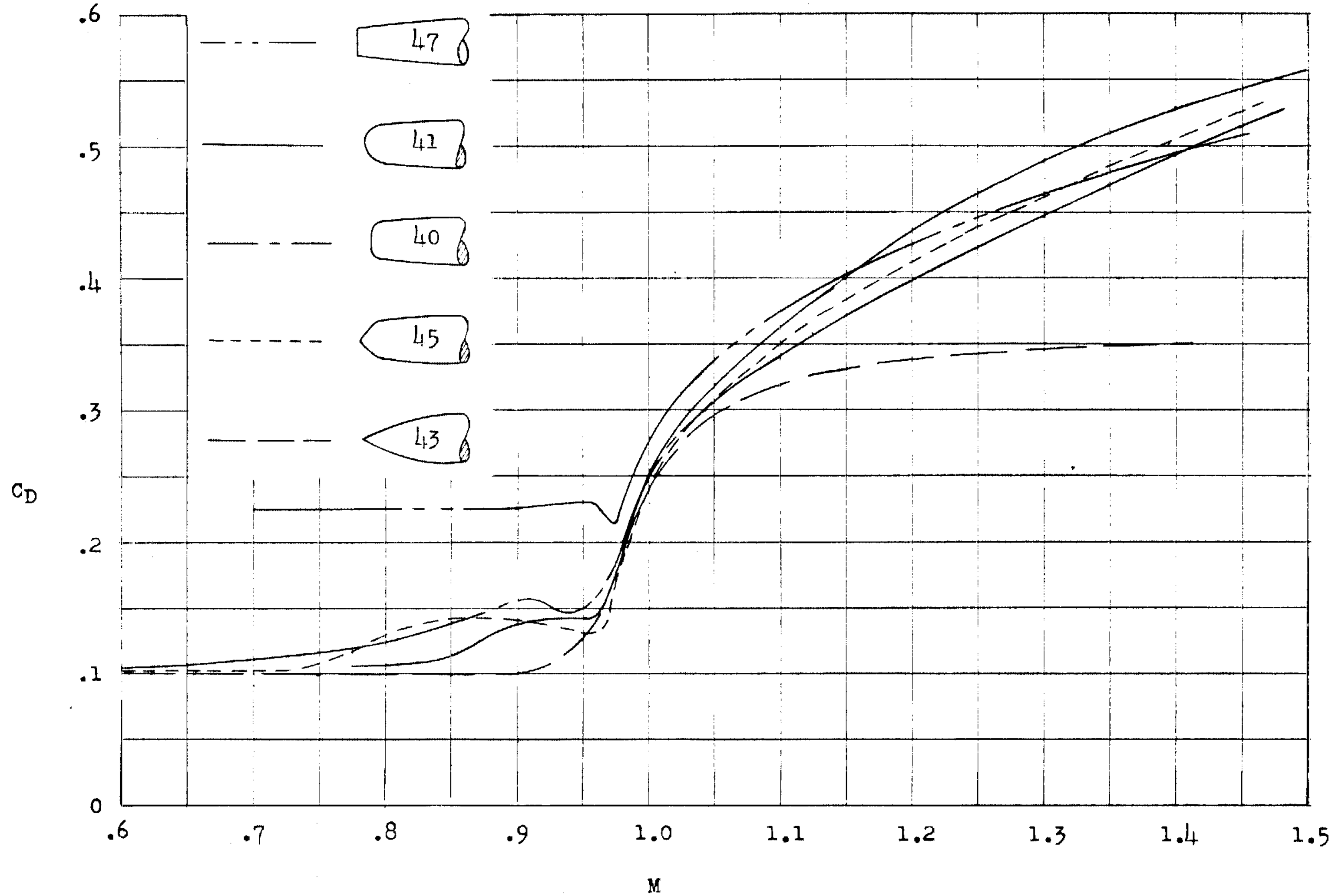

Figure 8.- Comparison of drag coefficients for five configurations having nose fineness ratios of about 2.

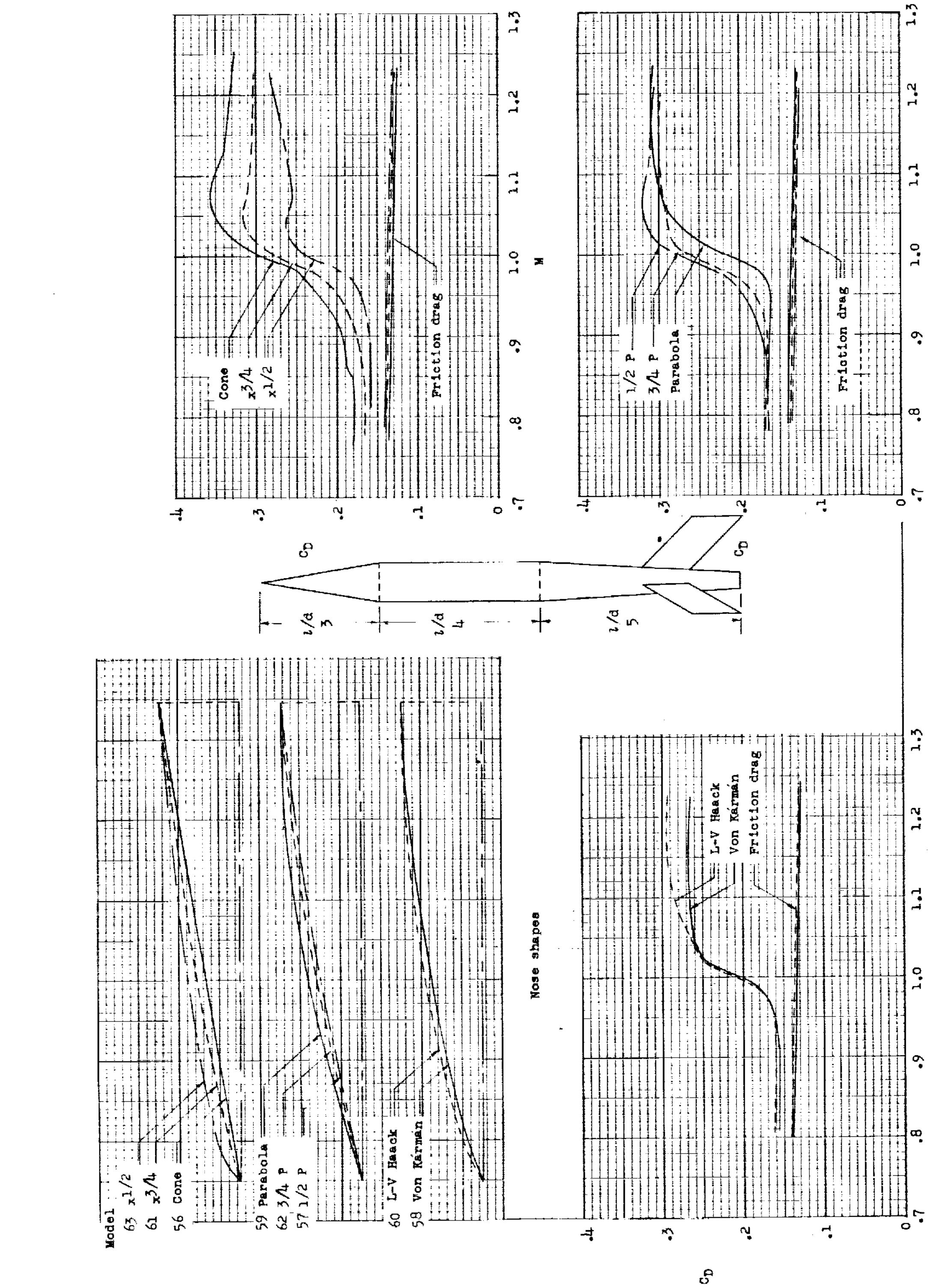

Figure 9.- Drag coefficients for eight bodies having fineness-ratio-3 noses of various shapes.

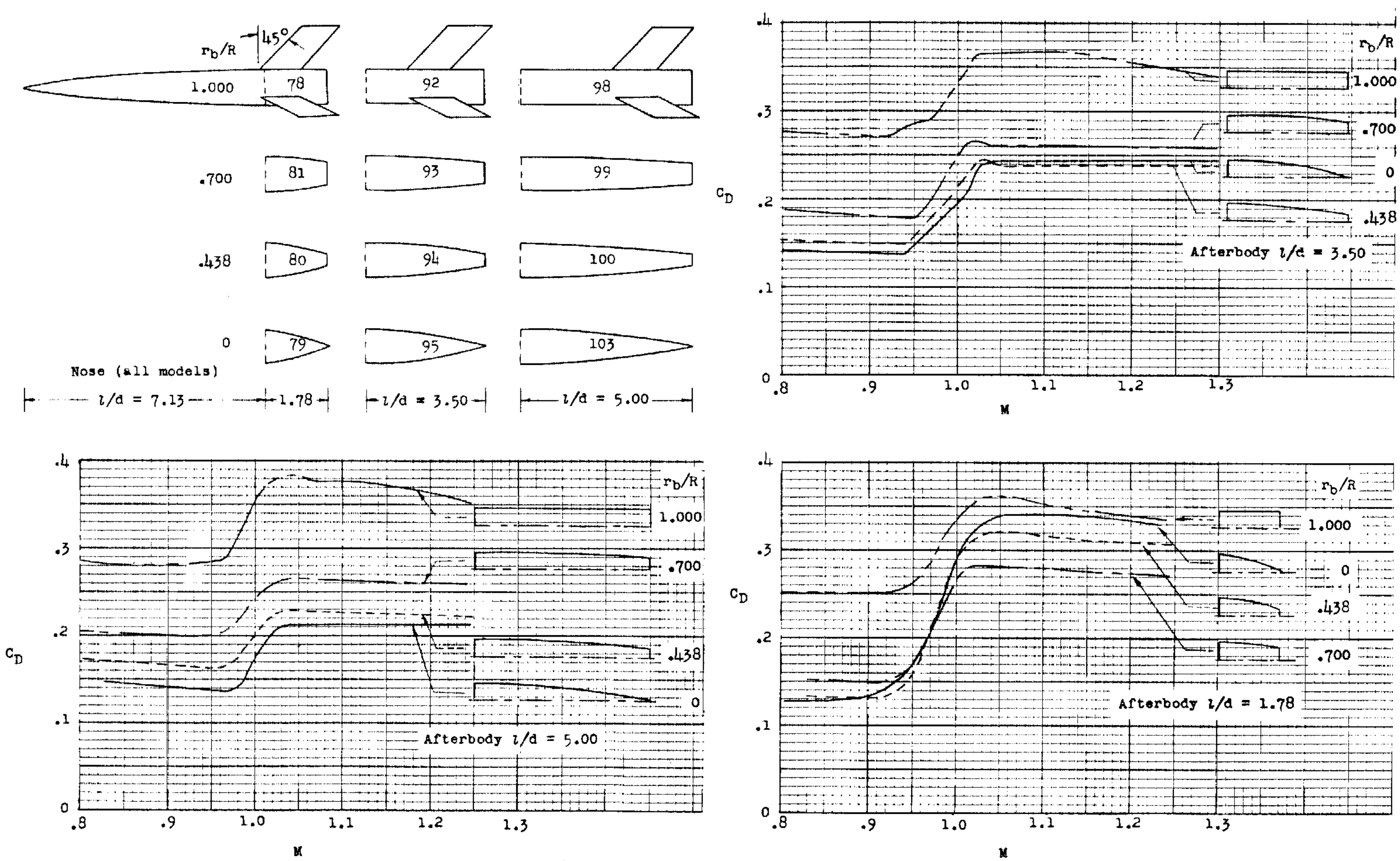

Figure 10.- Drag coefficients for 12 bodies having identical noses and different afterbodies.

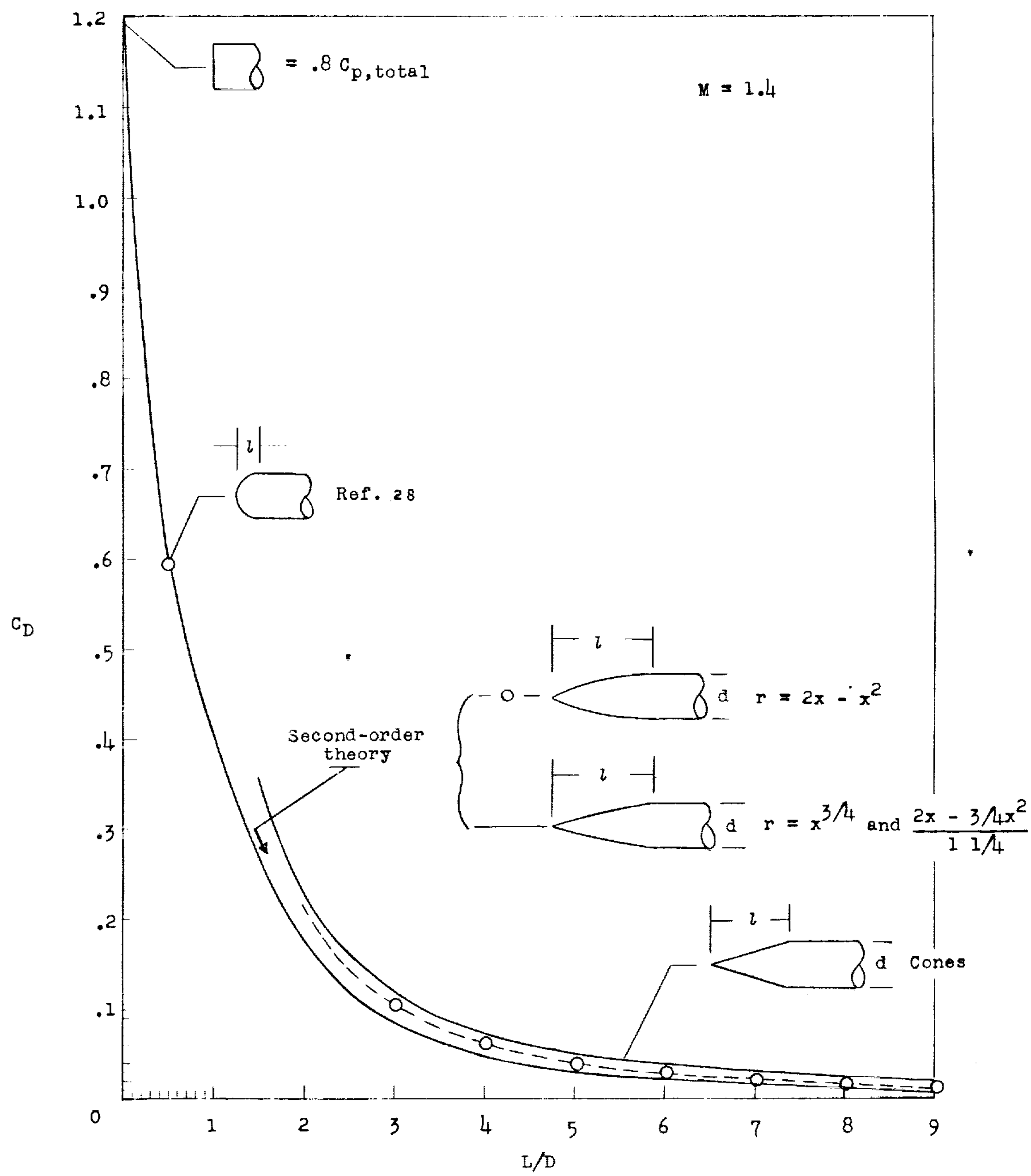

Figure 11.- Drag coefficients due to pressures on noses at M = 1.4.

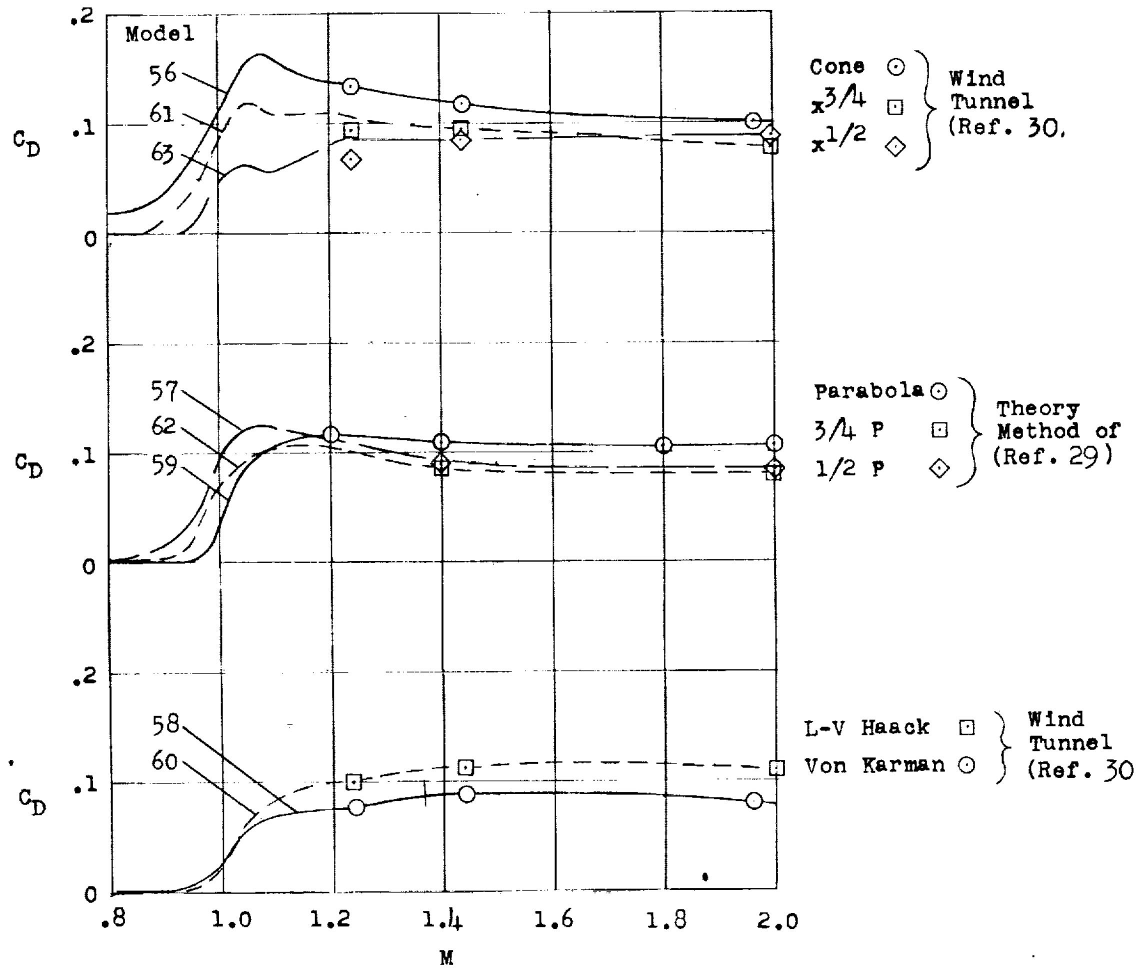

(a) Nose pressure drags of flight models compared with wind-tunnel results and theory.

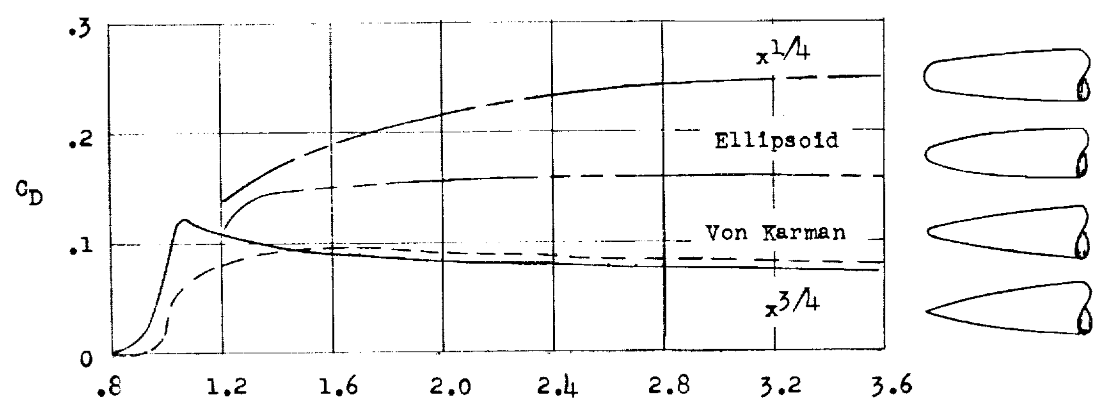

(b) Nose pressure drags from reference 30 showing general effects of nose shape on drag.

Figure 12.- Pressure drag of noses of fineness ratio 3.

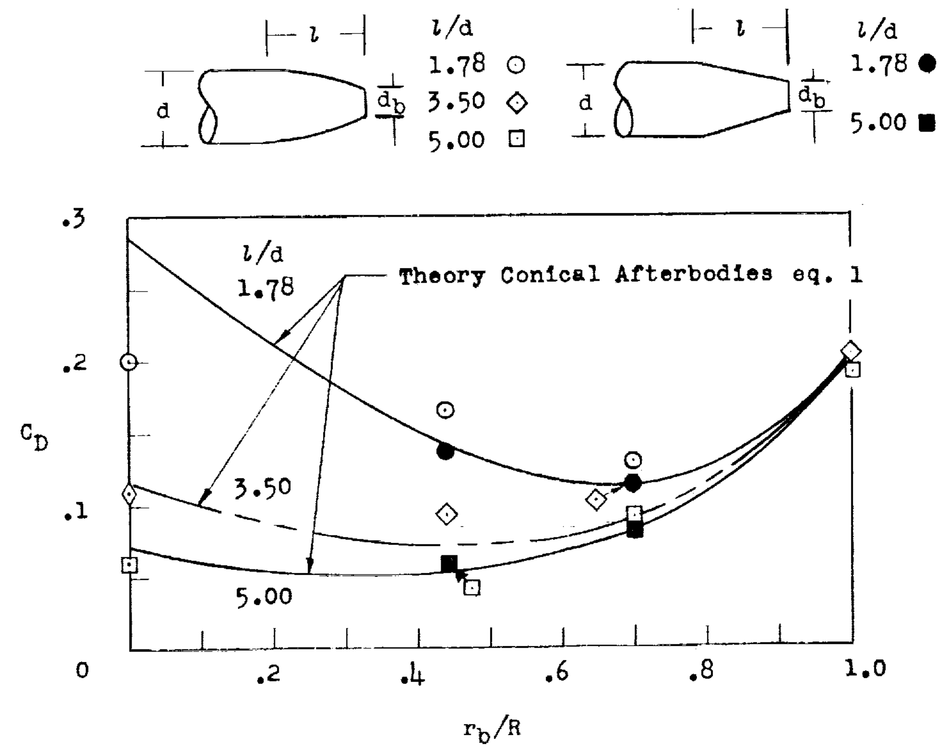

(a) Experimental and Theoretical Afterbody Pressure + Base Drag at M = 1.2.

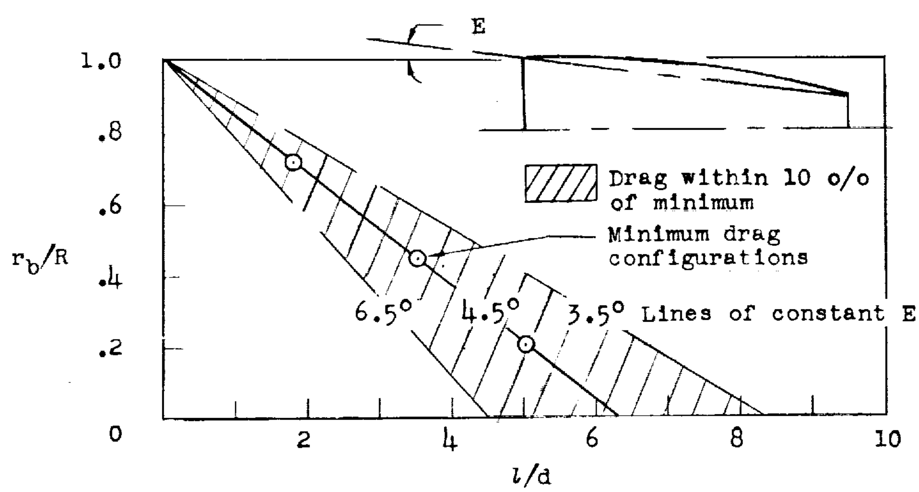

(b) Configurations for minimum afterbody drag at M = 1.2.

Figure 13.- Afterbody pressure drag at M = 1.2.

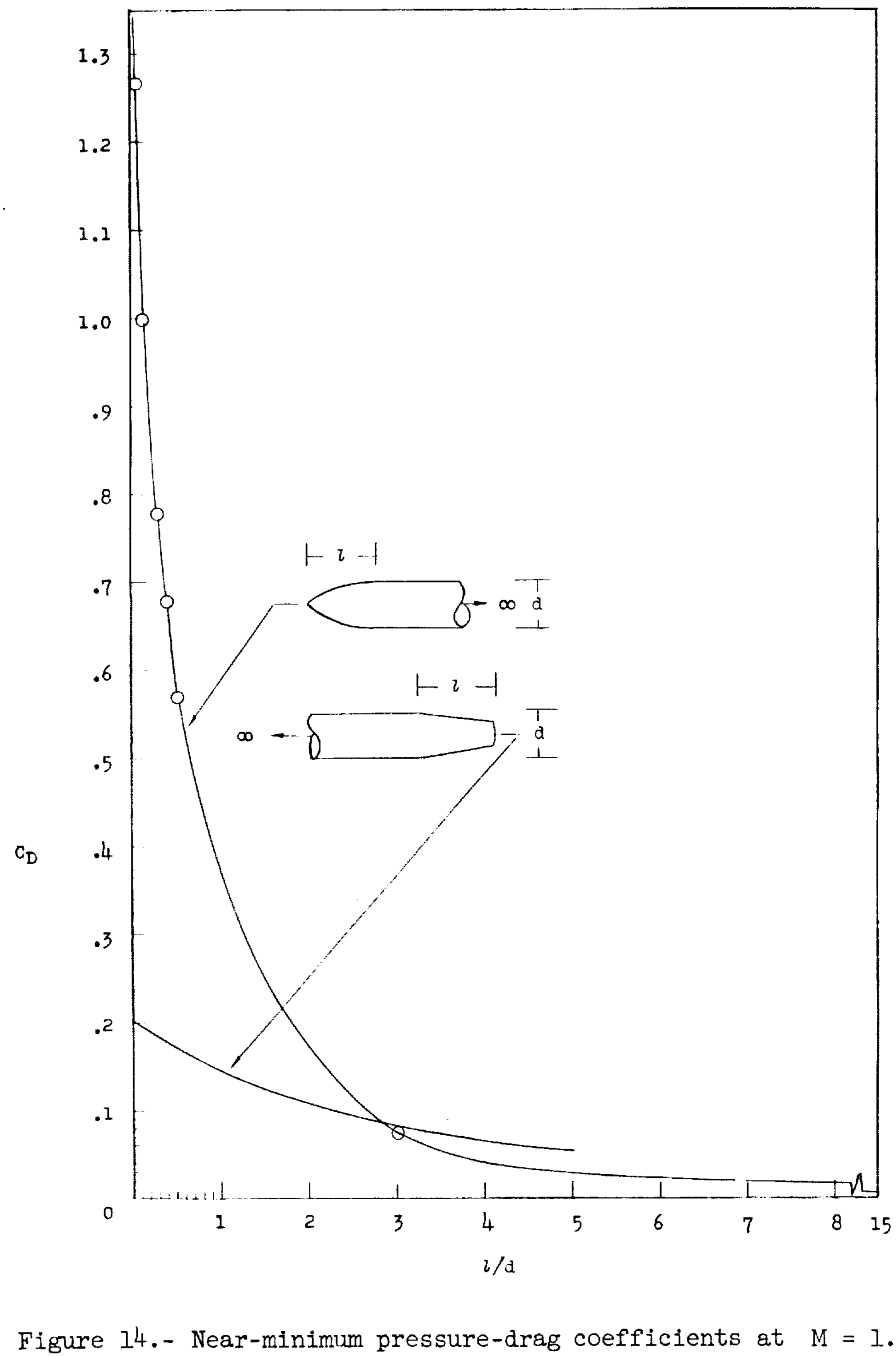

Figure 14.- Near-minimum pressure-drag coefficients at $M = 1.2$ for noses and afterbodies without interference.

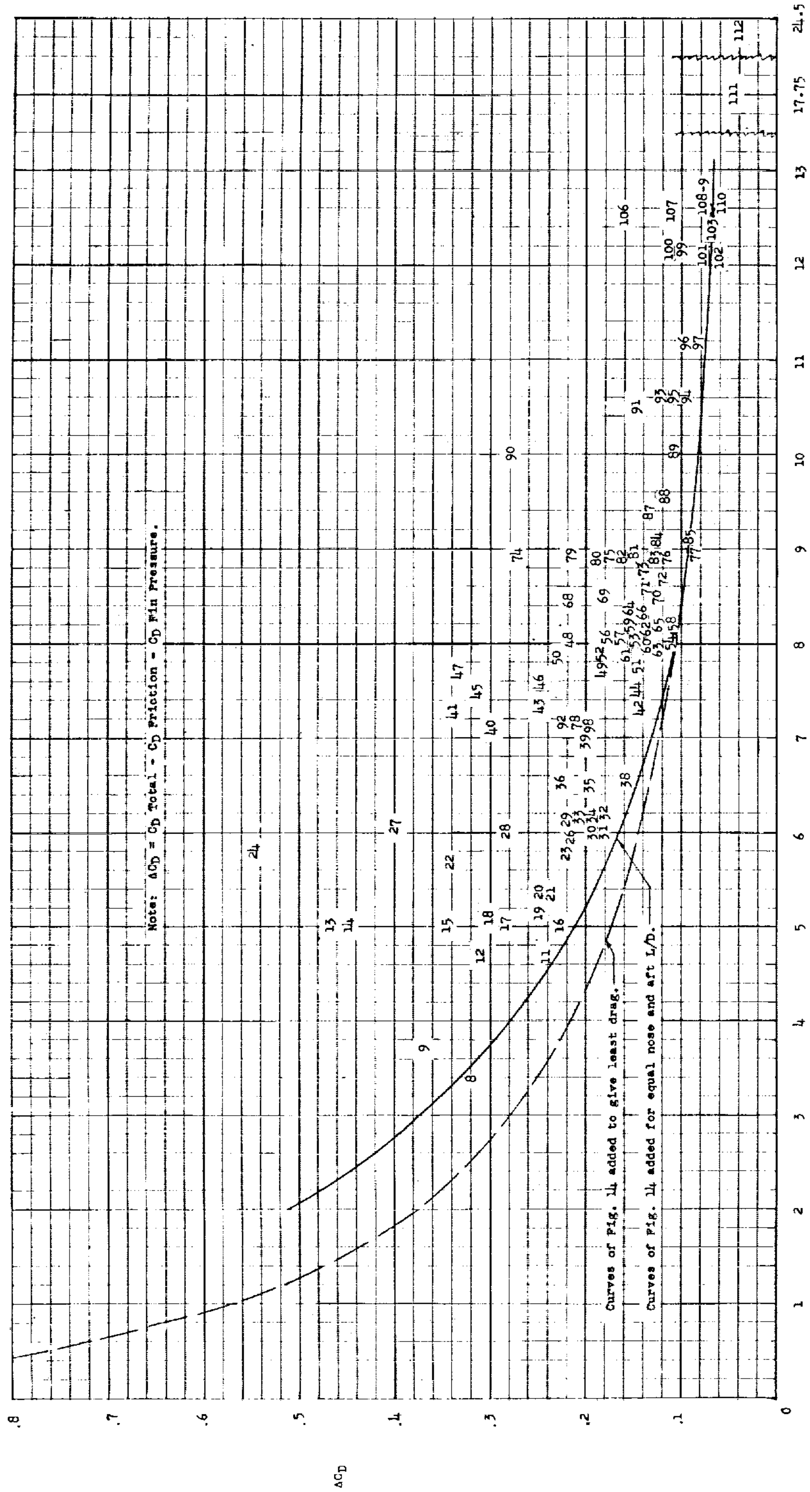

Figure 15.- M = 1.2 pressure drag coefficients.

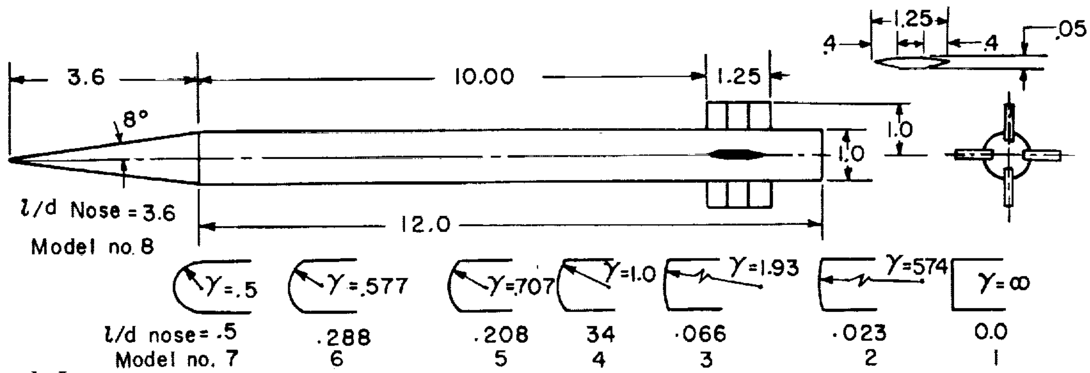

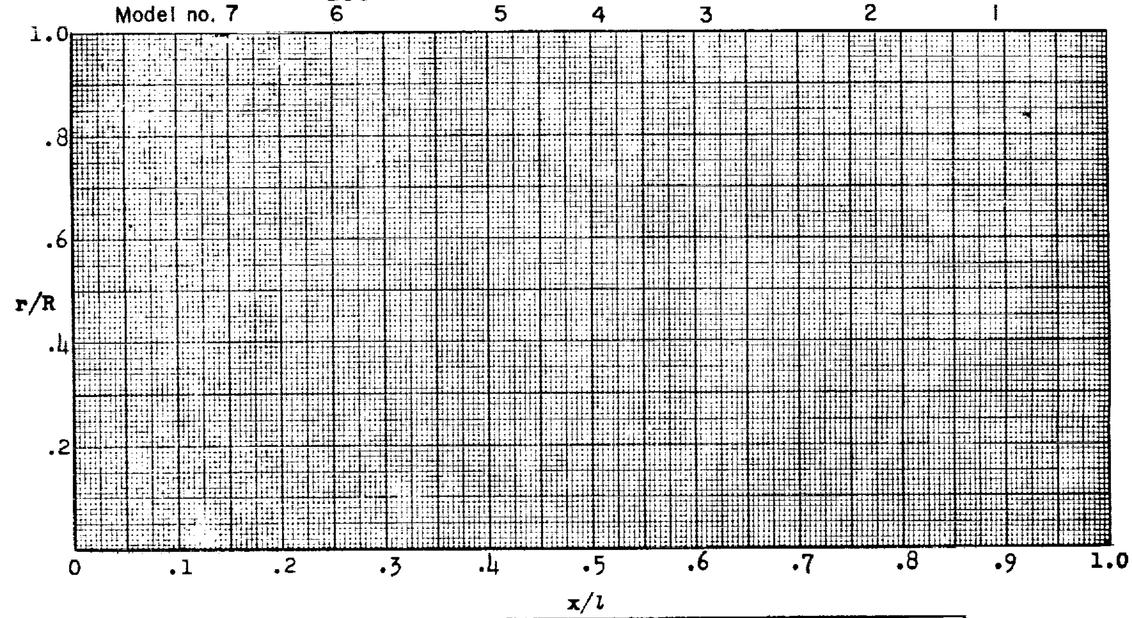

l/d_{Total}	12+	l/d_{Nose}	.5-	S_b/A	49.0	A_b/A	1.0
l/d_{N+A}	.5-	l/d_{Aft}	0	S_f/A	6.36	θ_b	0

Designation: 1 - 2 - 3 - 4 - 5 - 6 - 7 - 8

Test: Helium Gun

Remarks: The abrupt drag variations at subsonic speeds are undoubtedly somewhat distorted by the data-reduction process; however, they are real as evidenced by similar phenomena noted in reference 18 (pp. 200 and 210).

Figure 16.

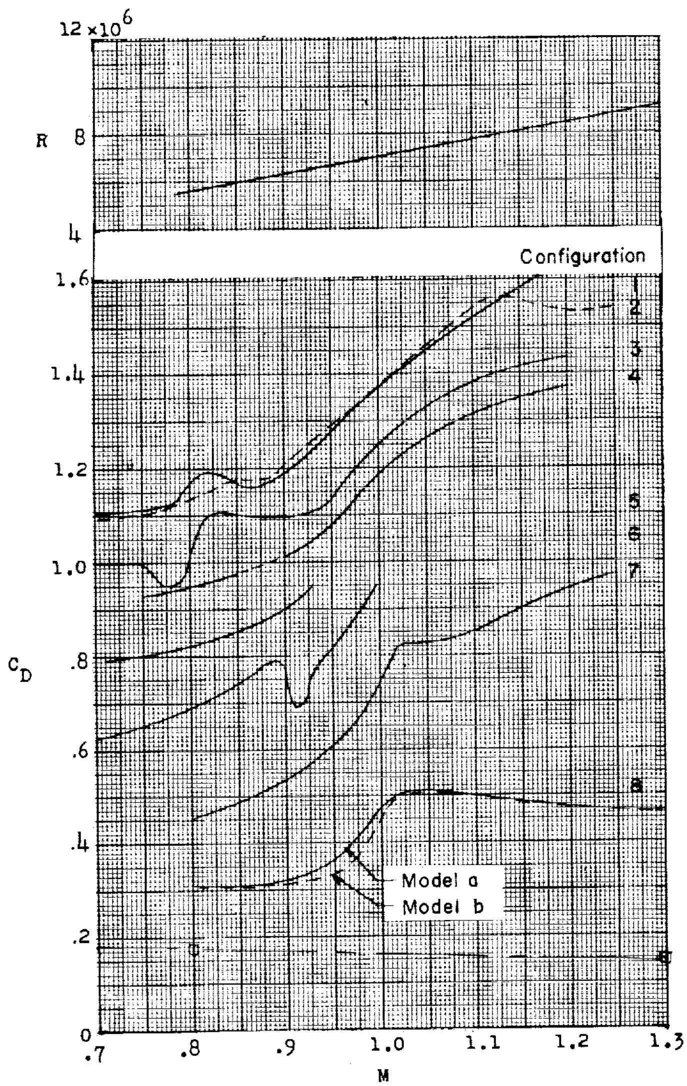

Figure 16.- Concluded.

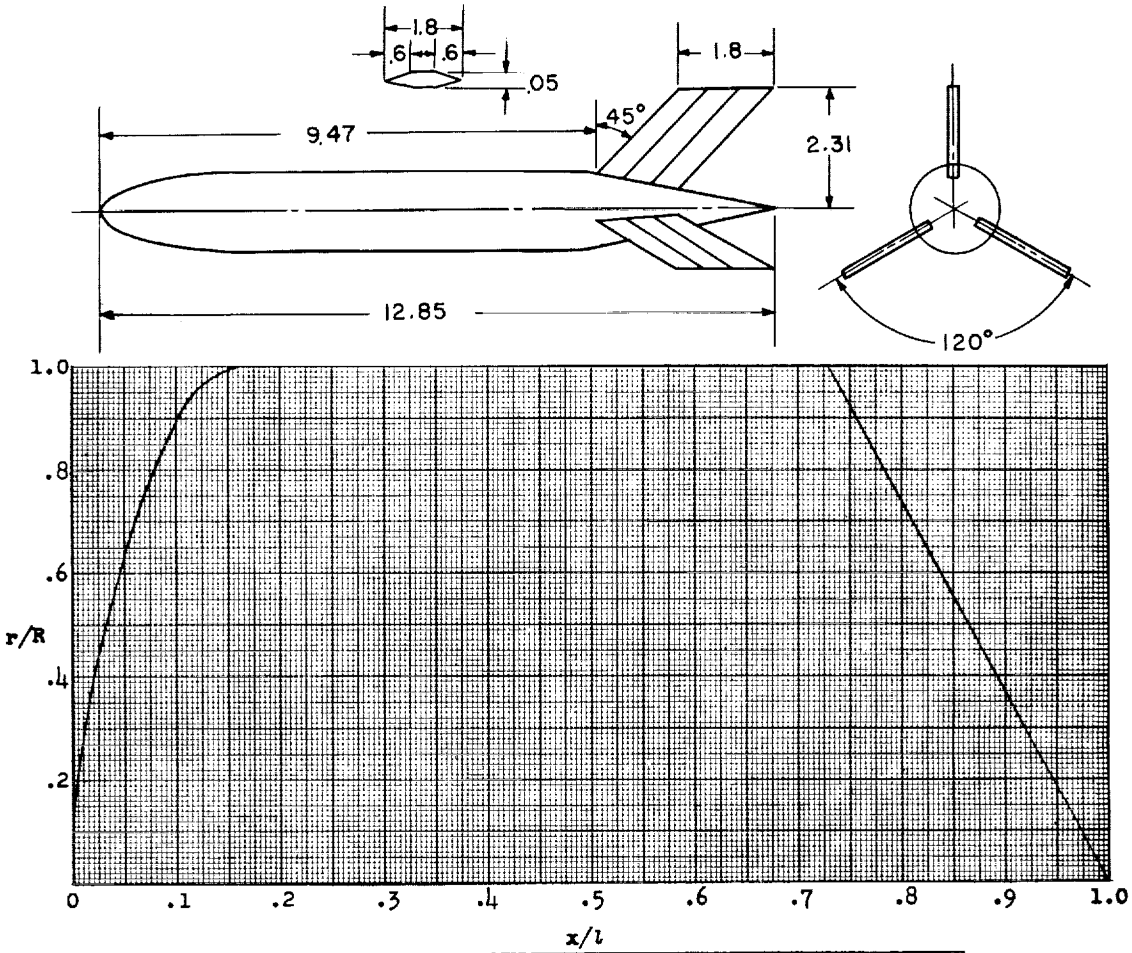

l/d_{Total}	8.57	l/d_{Nose}	1.38	S_b/A	28.30	A_b/A	0.0
l/d_{N+A}	3.71	l/d_{Aft}	2.33	S_f/A	11.0	θ_b	12.2°

Designation: 9

Test: **Helium Gun**

Figure 17.

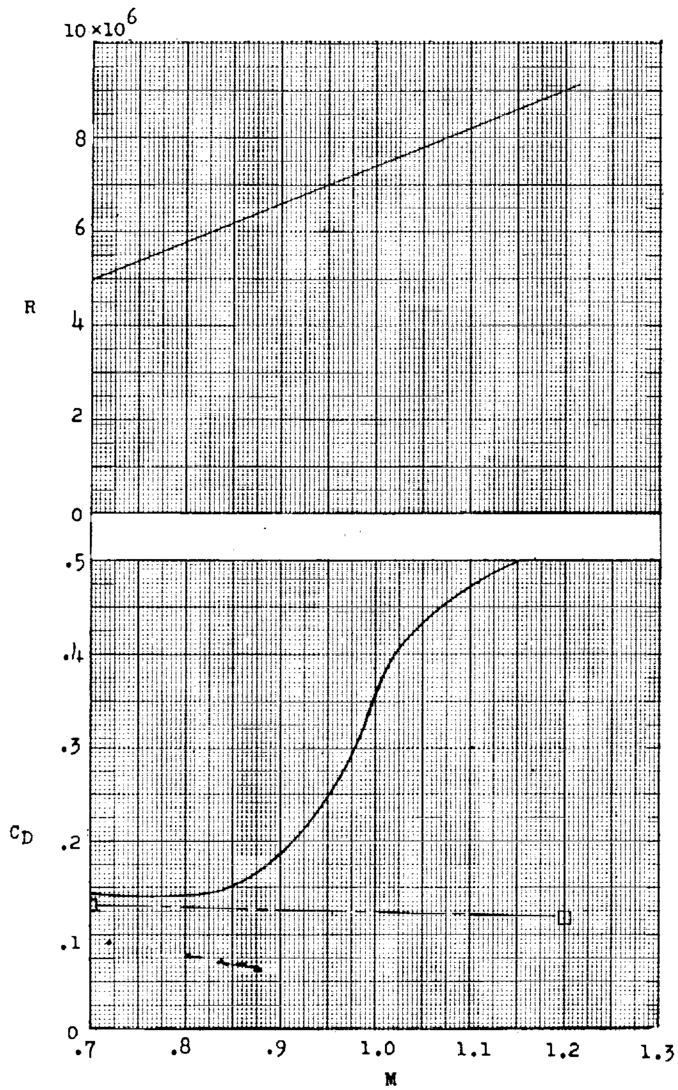

Figure 17.- Concluded.

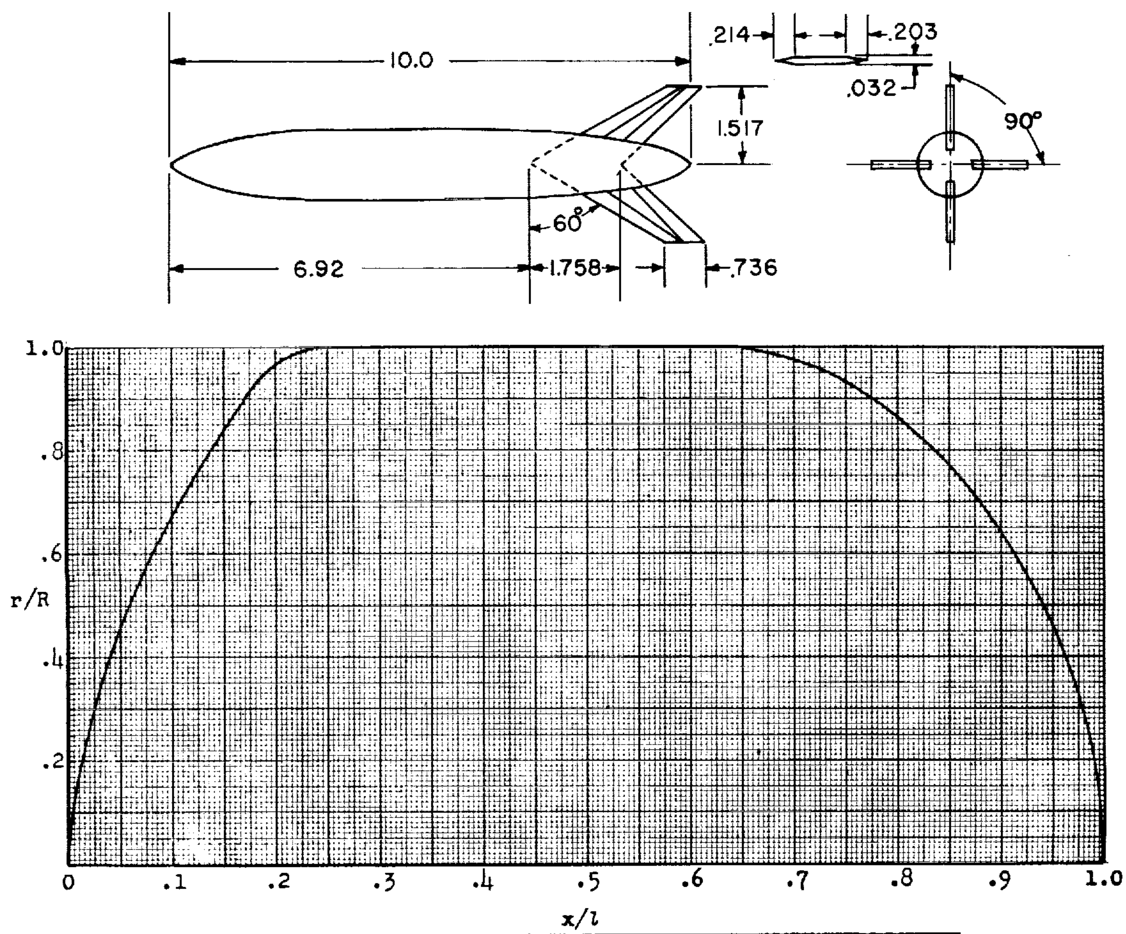

l/d_{Total}	7.7	l/d_{Nose}	1.92	S_b/A	25.2	A_b/A	0
l/d_{N+A}	4.62	l/d_{Aft}	2.7	S_f/A	6.4	θ_b	68°

Designation: 10

Test: **Helium Gun**

Remarks: Nondimensional ordinates same as configuration 37 (fig. 45).

Figure 18.

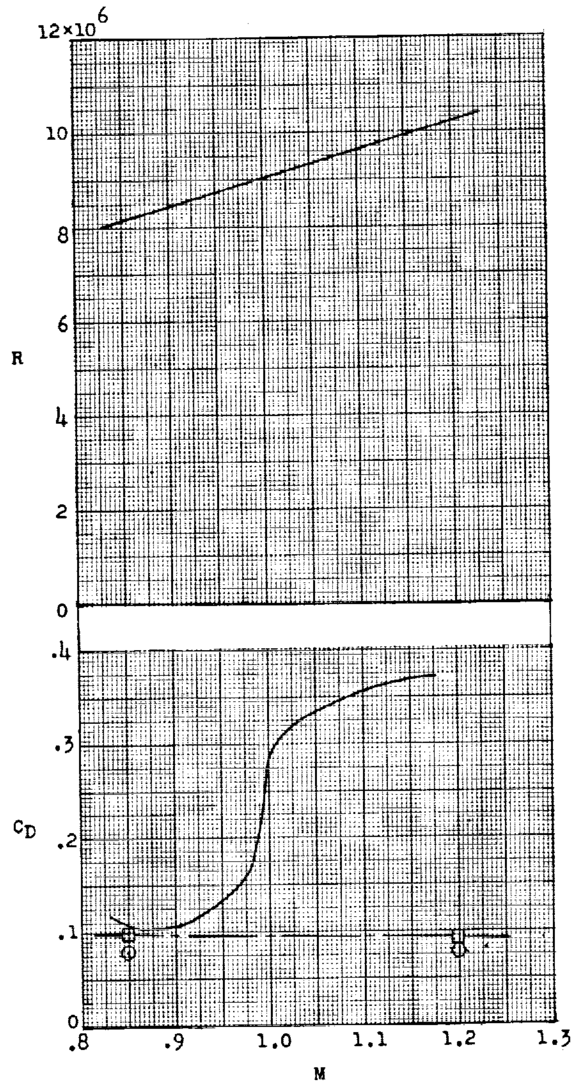

Figure 18.- Concluded.

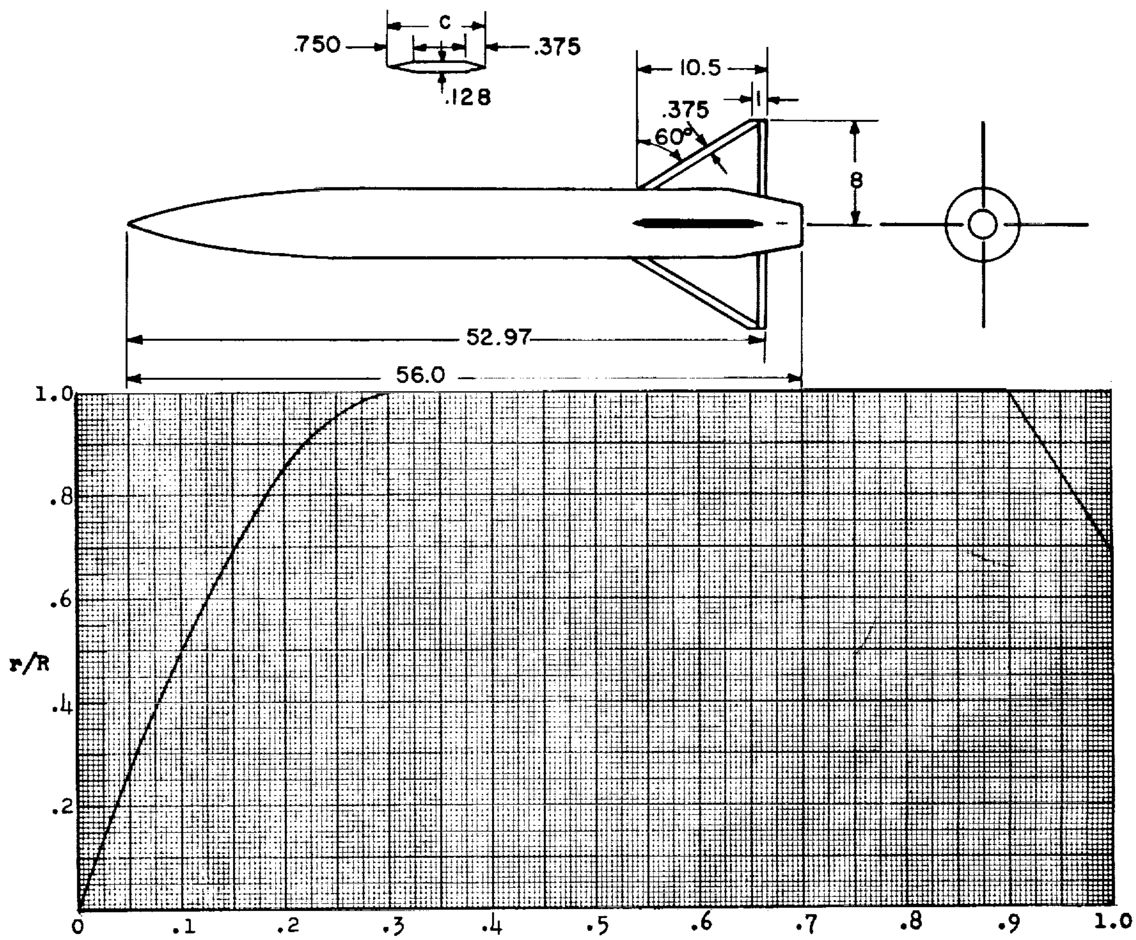

l/d_{Total}	11.2	l/d_{Nose}	3.5	S_b/A	39.3	A_b/A	.45
l/d_{N+A}	4.64	l/d_{Aft}	1.14	S_f/A	11.0	θ_b	8°

Designation: II

Test: Rocket

Figure 19.

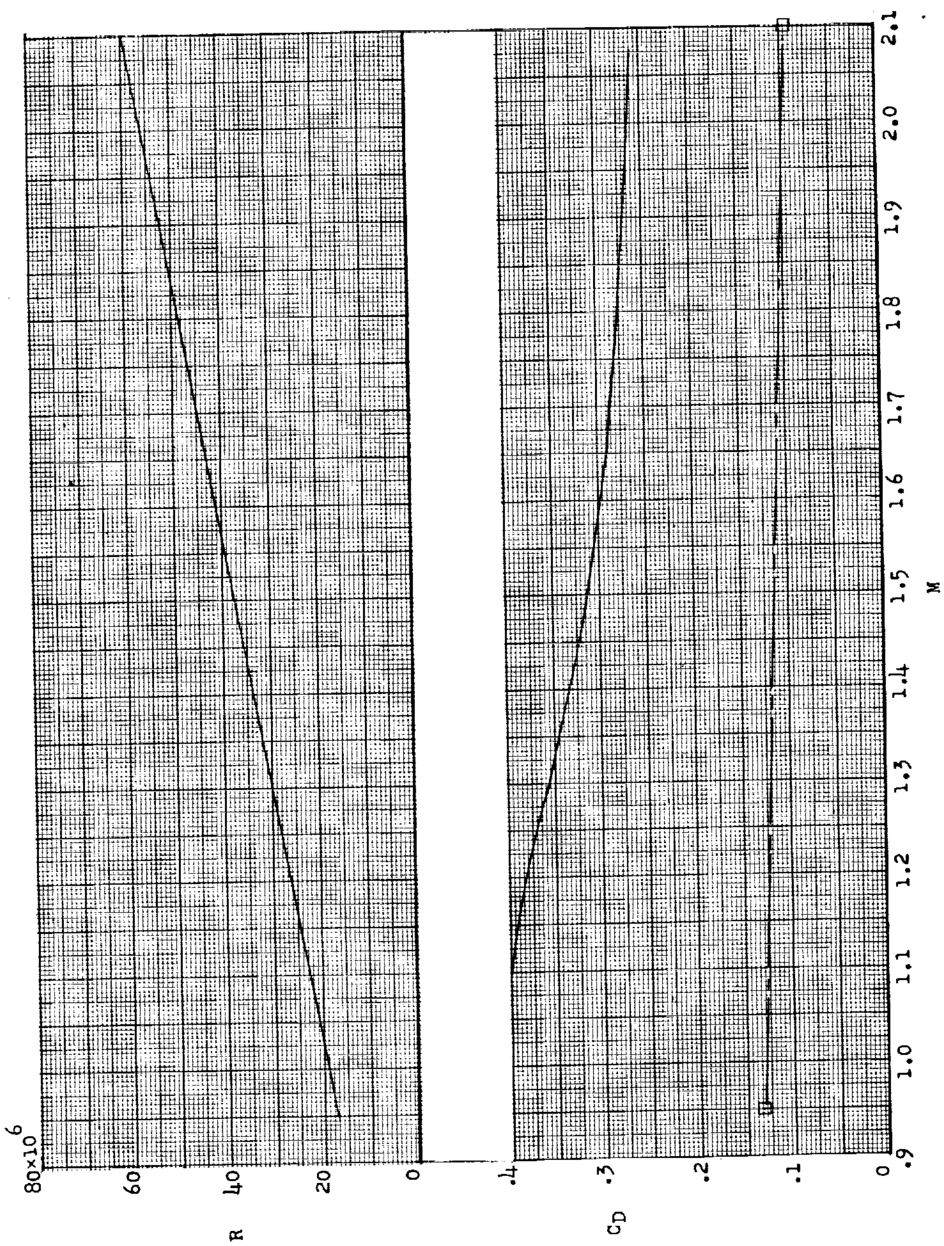

Figure 19.- Concluded.

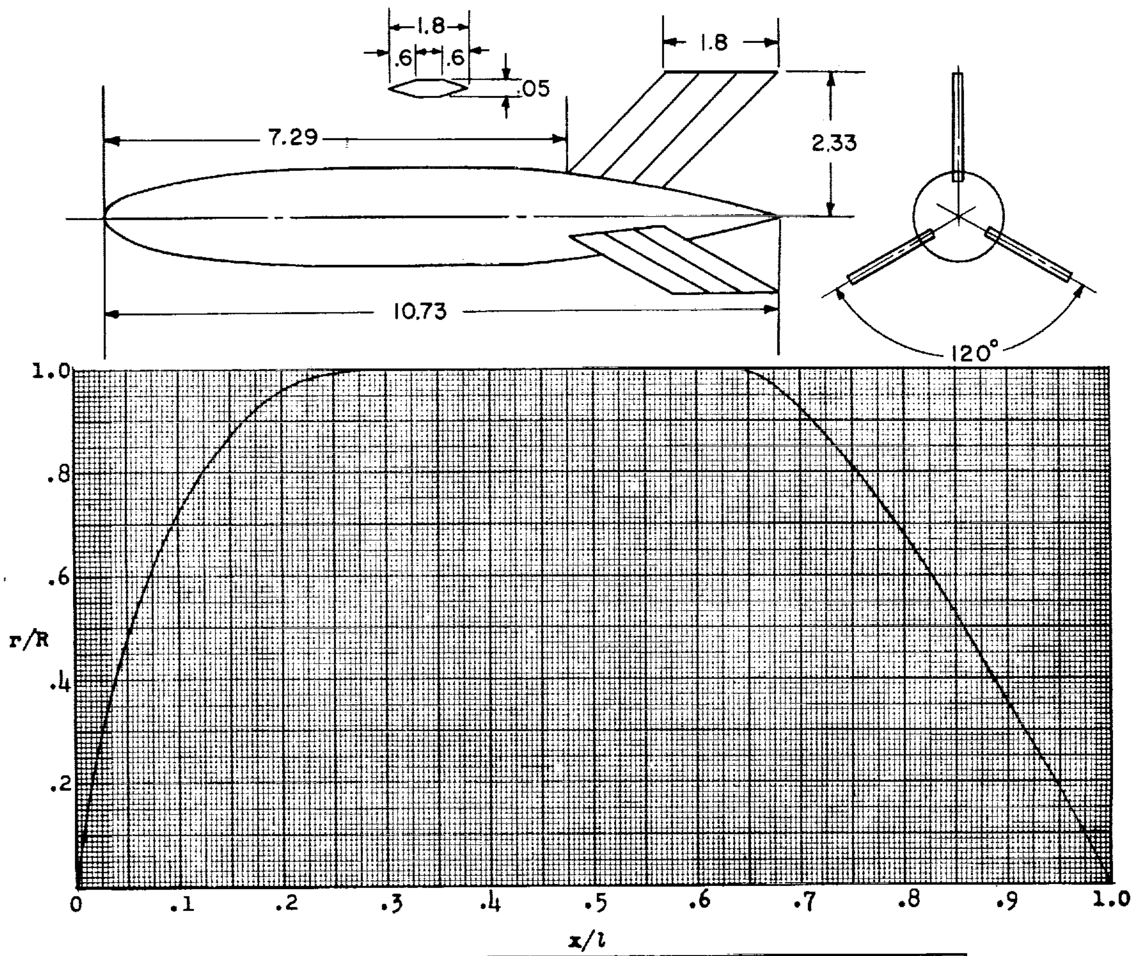

l/d_{Total}	7.15	l/d_{Nose}	2.02	S_b/A	22.40	A_b/A	0.0
l/d_{N+A}	4.85	l/d_{Aft}	2.83	S_f/A	11.0	θ_b	15.7°

Designation: 12

Test: **Helium Gun**

Figure 20.

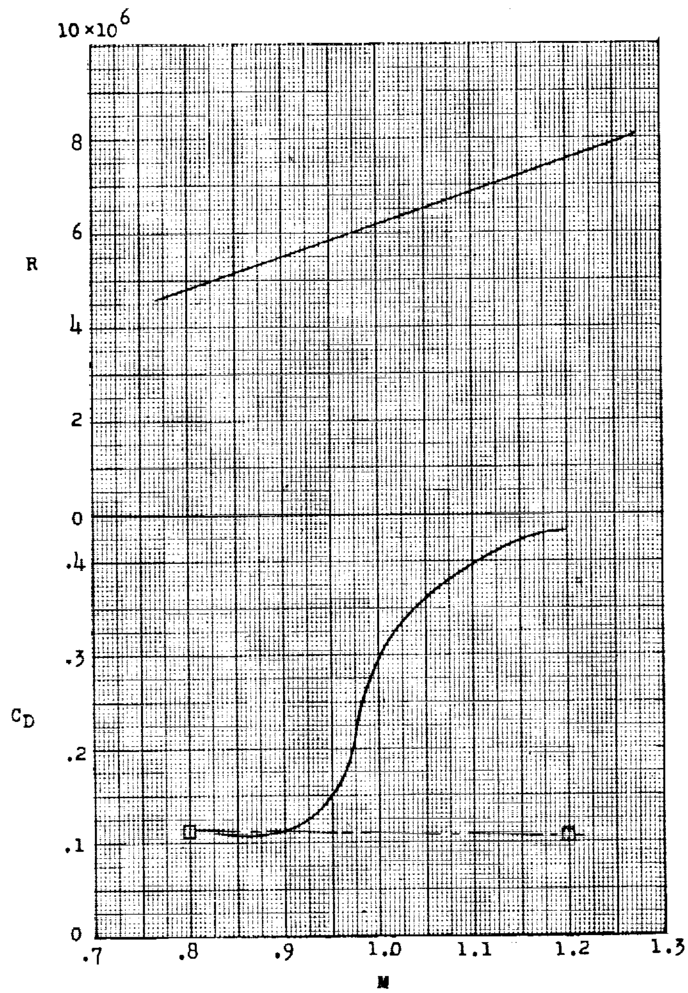

Figure 20.- Concluded.

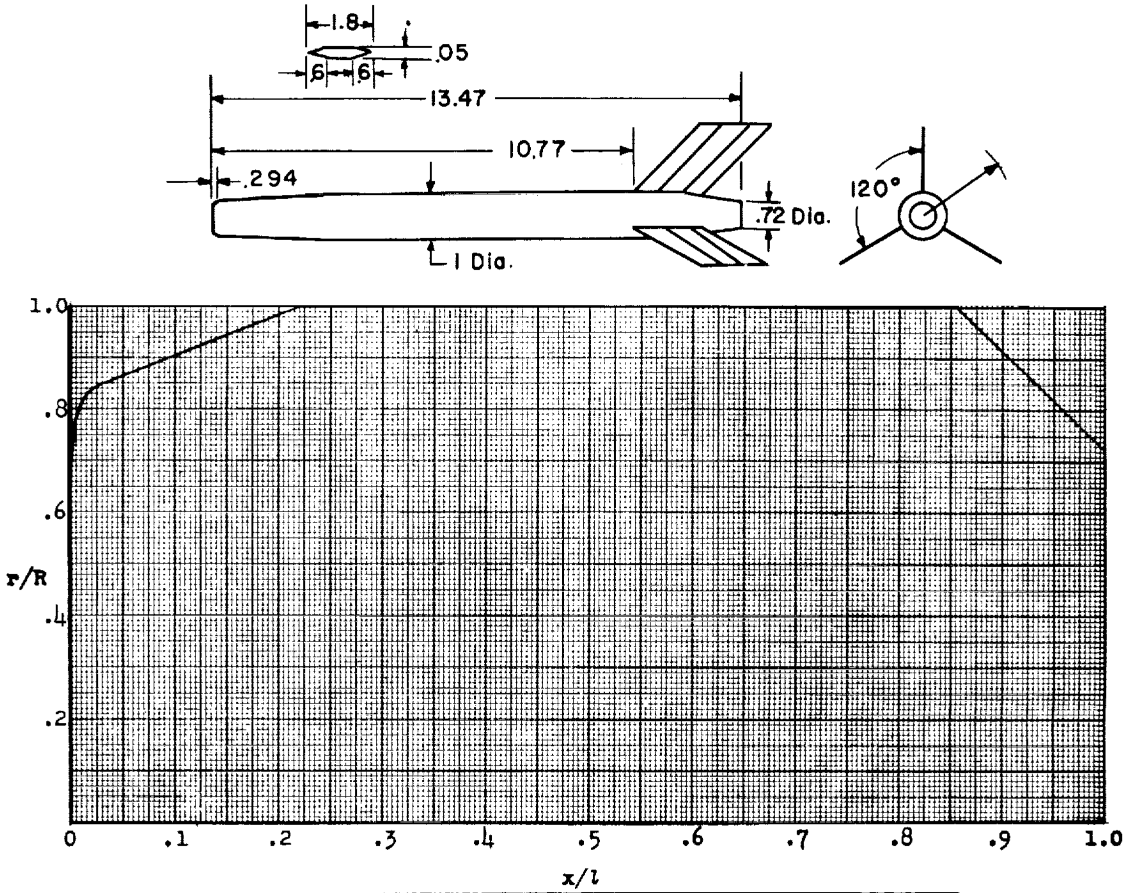

l/d_{Total}	13.47	l/d_{Nose}	2.98	S_b/A	51.5	A_b/A	.52
l/d_{N+A}	4.98	l/d_{Aft}	2.00	S_f/A	24.6	θ_b	4.02°

Designation: 13

Test: Helium Gun

Figure 21.

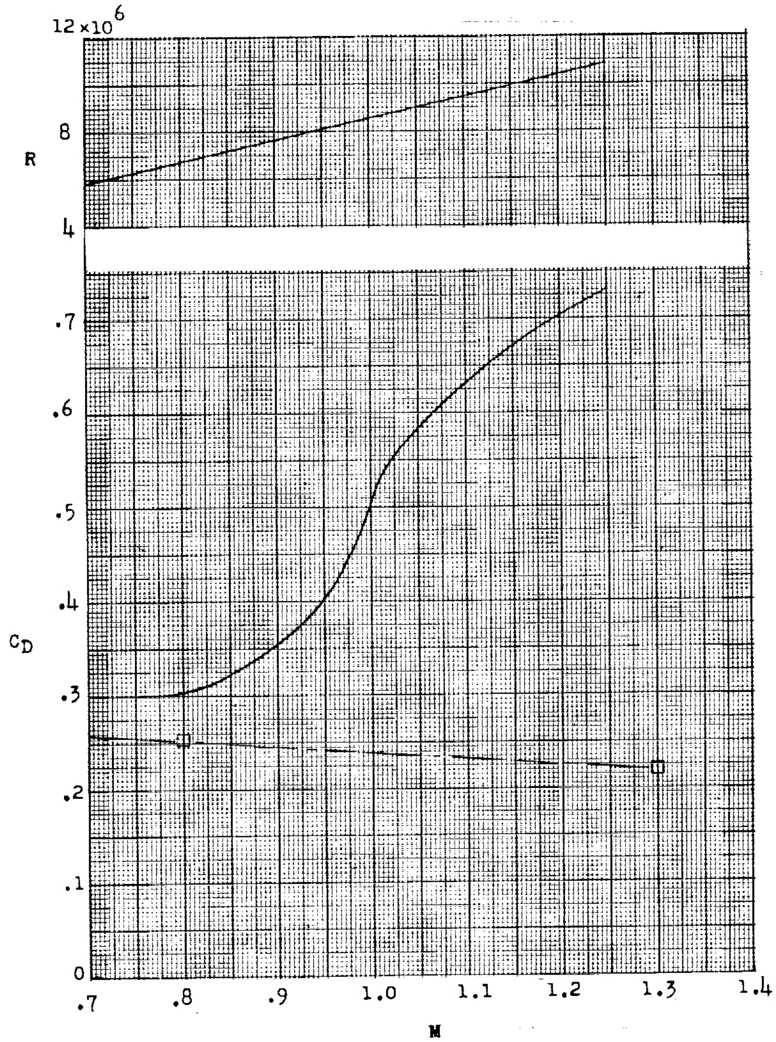

Figure 21.- Concluded.

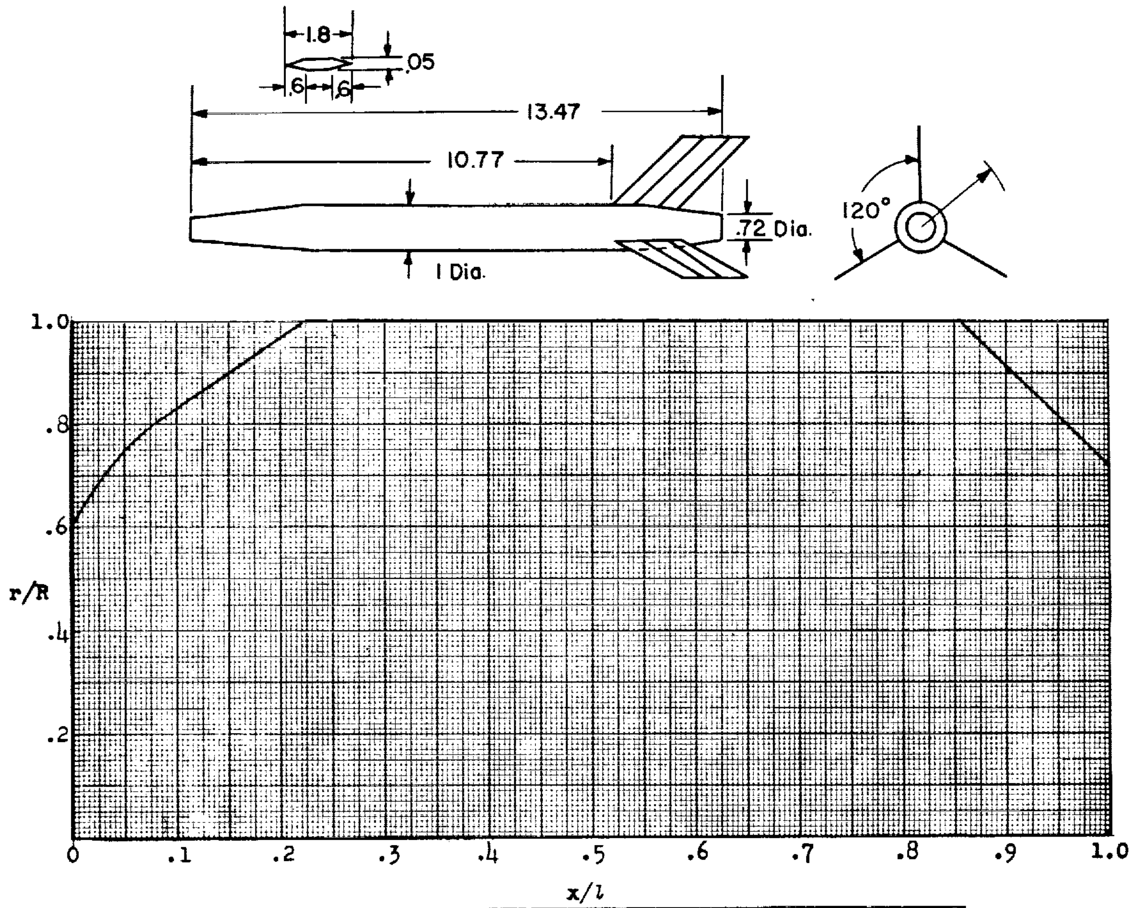

l/d_{Total}	13.47	l/d_{Nose}	2.98	S_b/A	51.3	A_b/A	.52
l/d_{N+A}	4.98	l/d_{Aft}	2.00	S_f/A	24.6	θ_b	4.02°

Designation: 14

Test: **Helium Gun**

Figure 22.

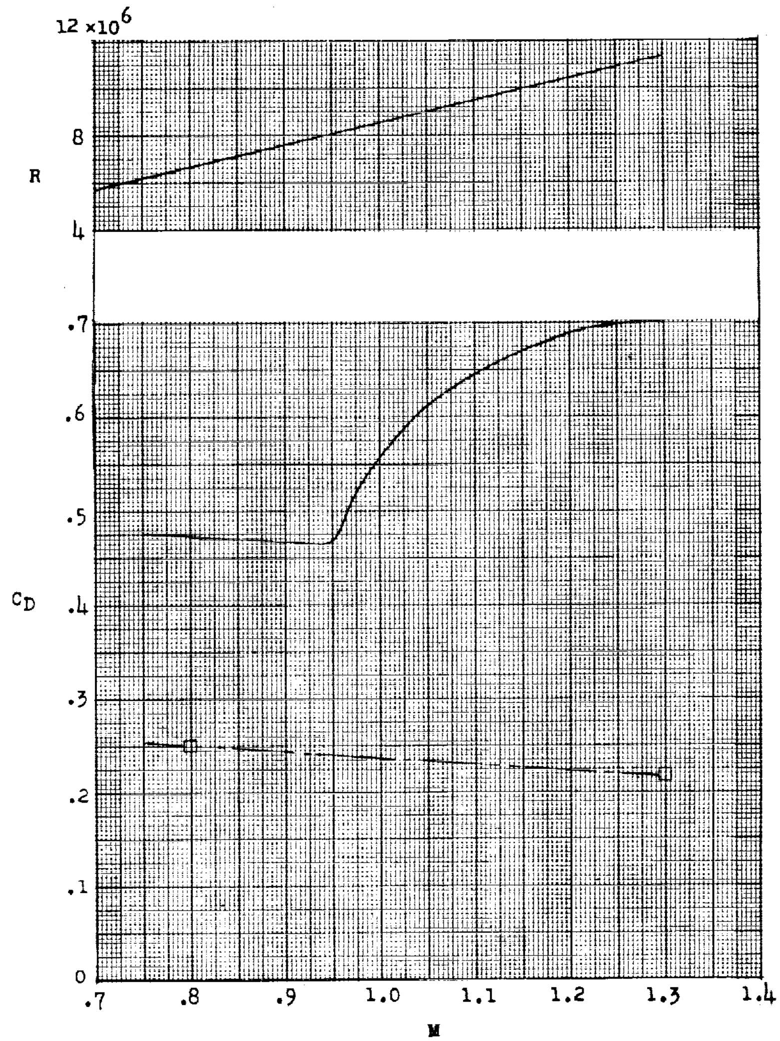

Figure 22.- Concluded.

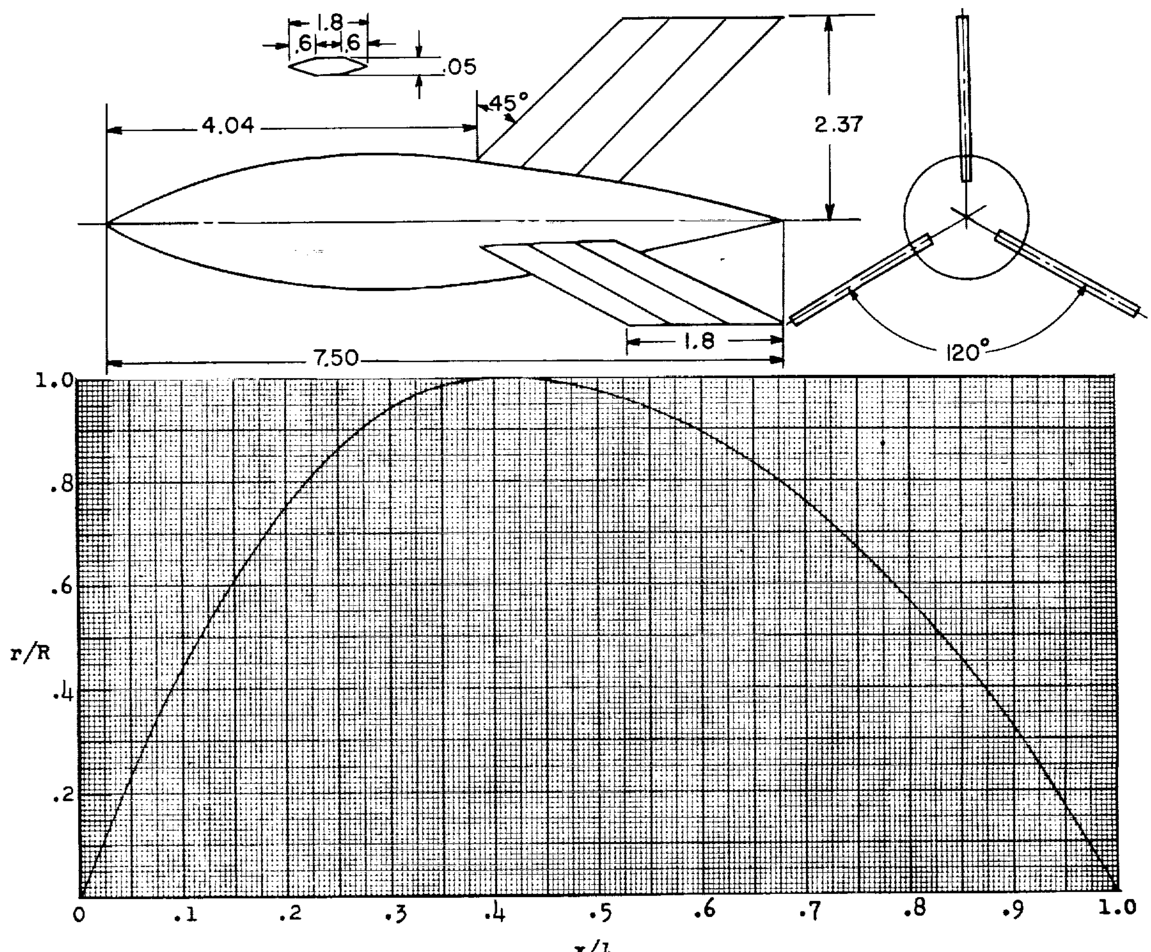

l/d_{Total}	5.00	l/d_{Nose}	2.00	S_b/A	13.60	A_b/A	0.0
l/d_{N+A}	5.00	l/d_{Aft}	3.00	S_f/A	11.0	θ_b	18.8°

Designation: 15

Test: Helium Gun

Figure 23.

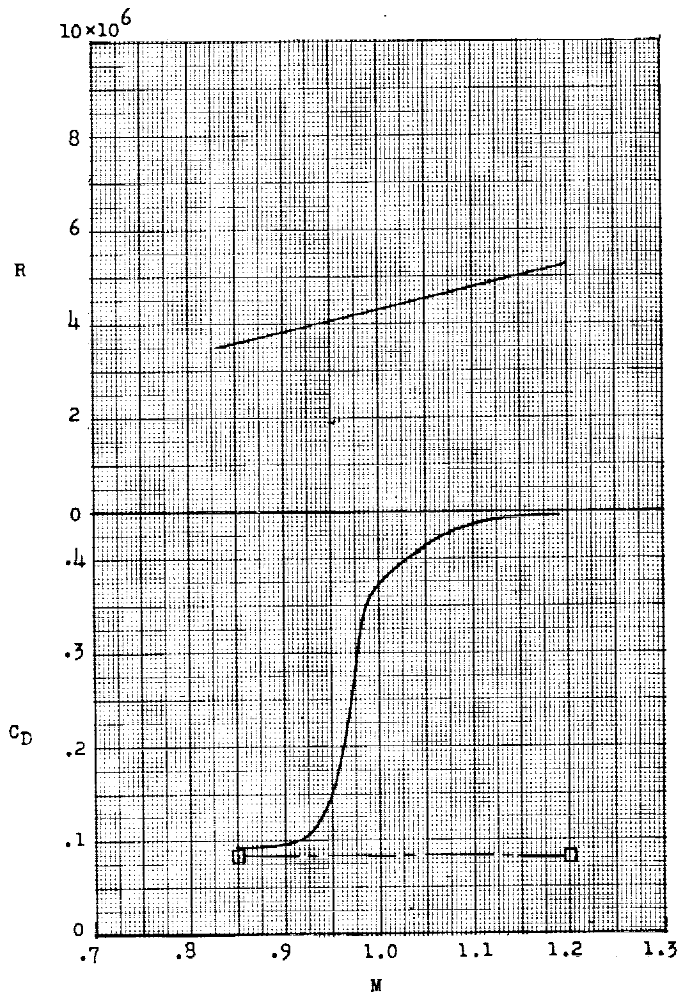

Figure 23.- Concluded.

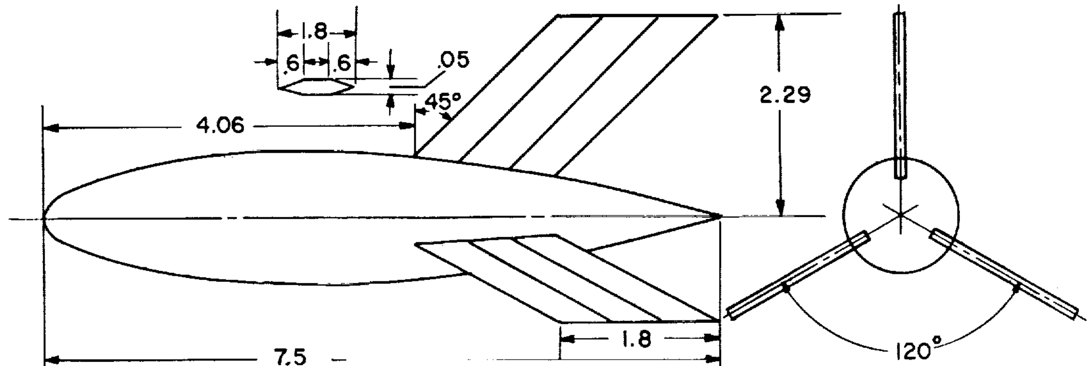

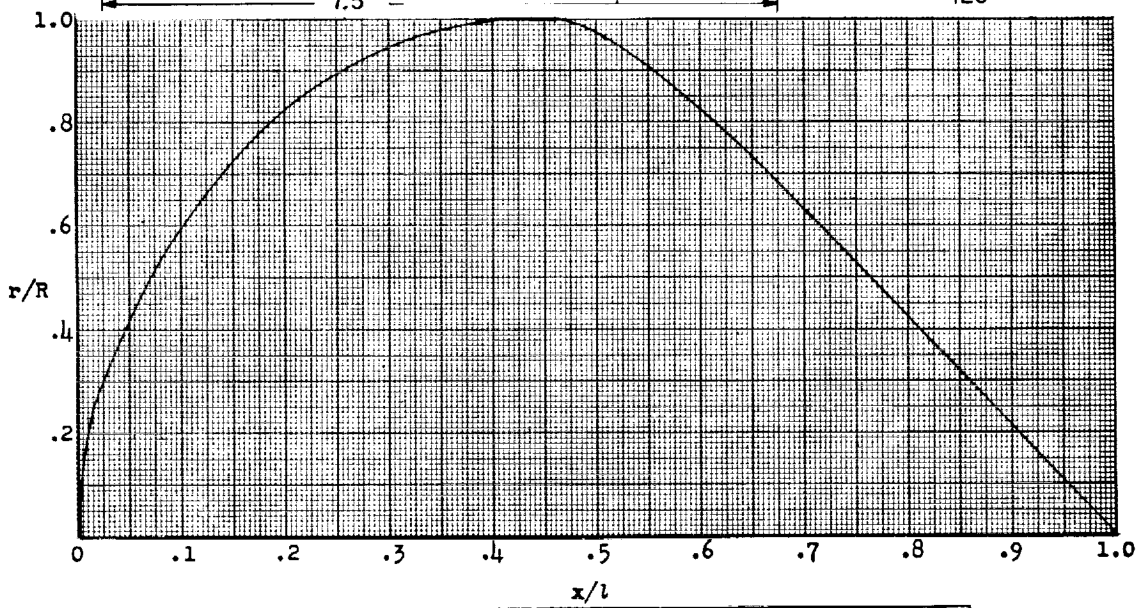

l/d_{Total}	5.00	l/d_{Nose}	2.00	S_b/A	13.30	A_b/A	0.0
l/d_{N+A}	5.00	l/d_{Aft}	3.00	S_f/A	11.0	θ_b	11.9°

Designation: 16

Test: Helium Gun

Figure 24.

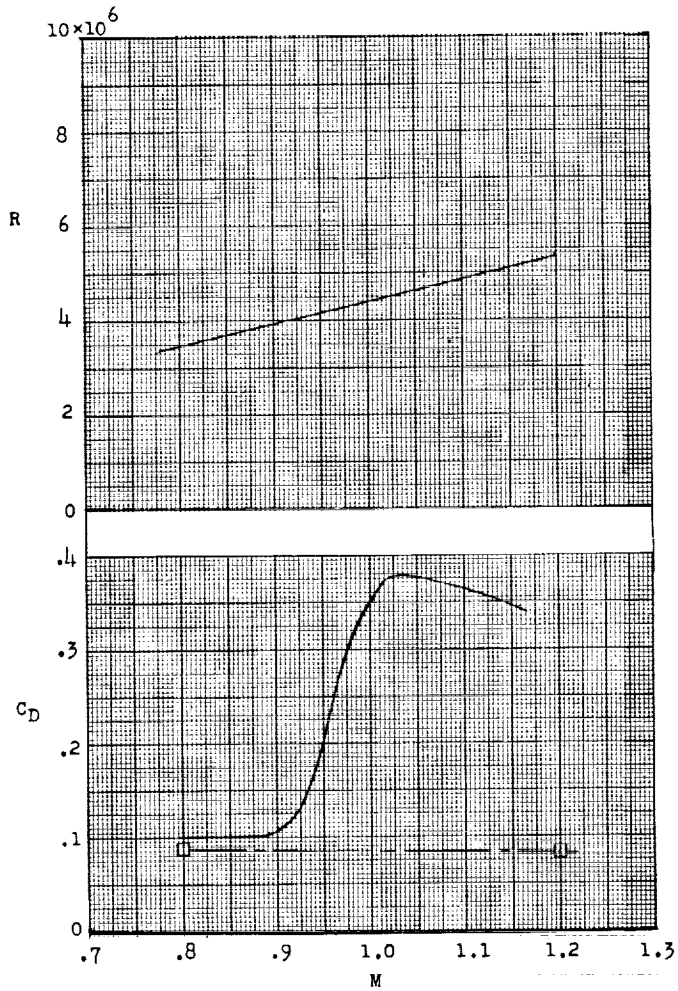

Figure 24.- Concluded.

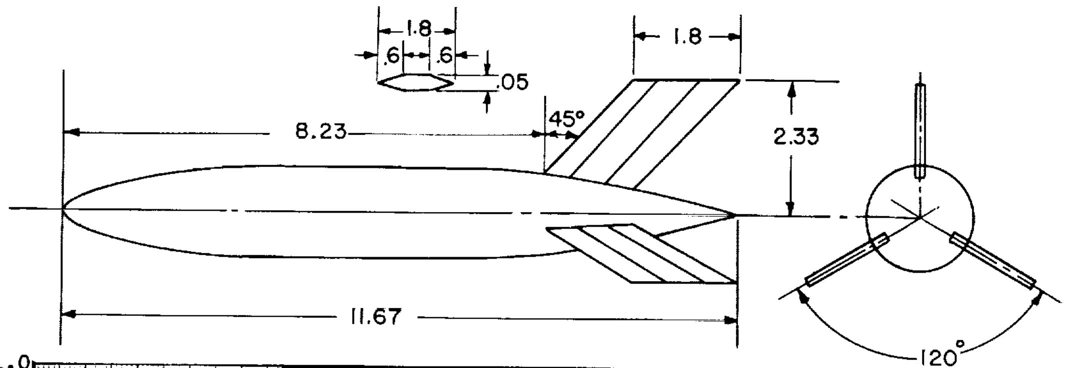

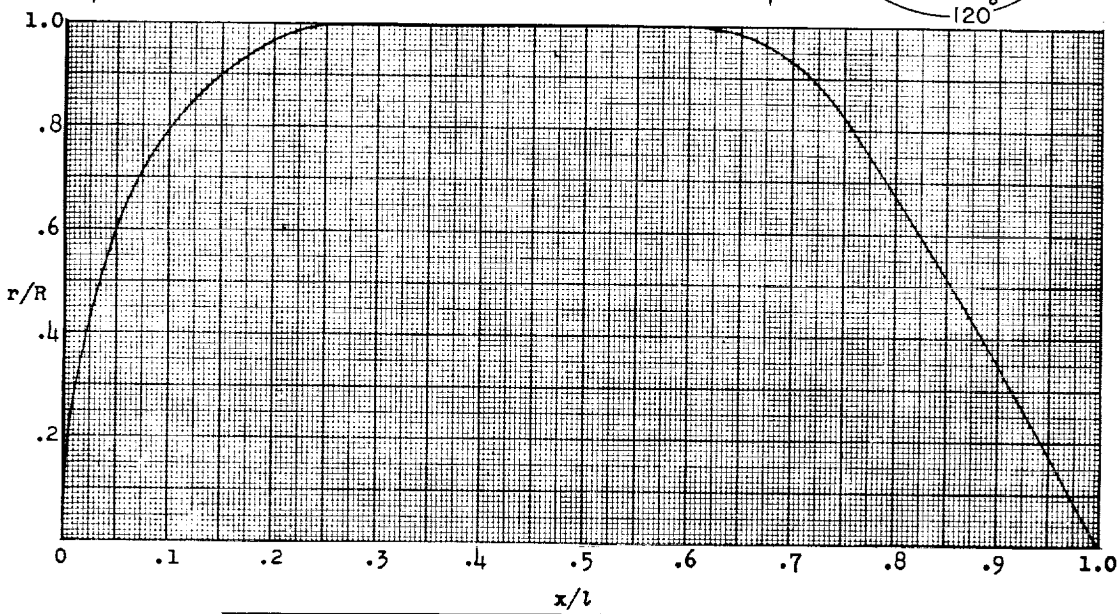

l/d_{Total}	7.78	l/d_{Nose}	2.00	S_b/A	25.00	A_b/A	0.0
l/d_{N+A}	5.00	l/d_{Aft}	3.00	S_f/A	11.0	θ_b	12.7°

Designation: 17

Test: Helium Gun

Figure 25.

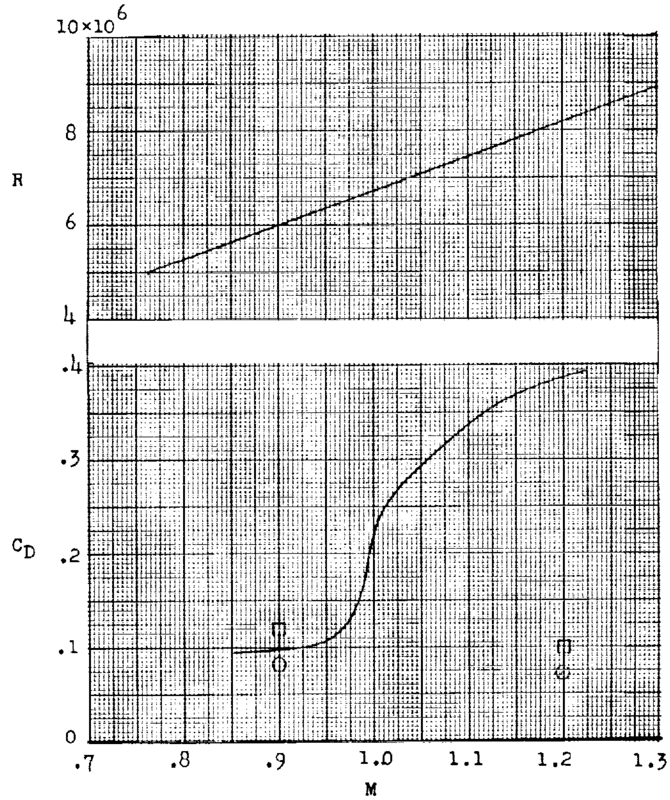

Figure 25.- Concluded.

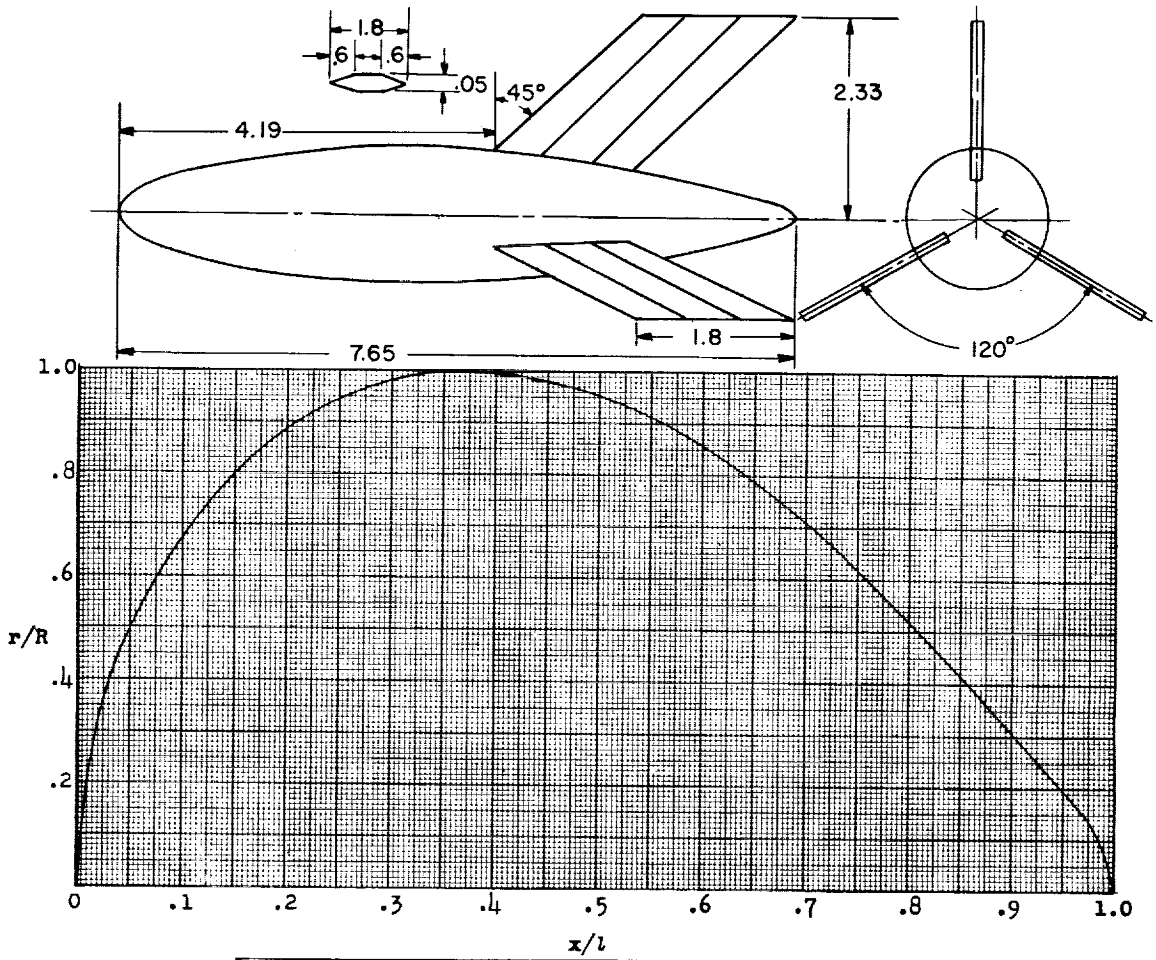

l/d_{Total}	5.10	l/d_{Nose}	1.92	S_b/A	14.60	A_b/A	0.0
l/d_{N+A}	5.10	l/d_{Aft}	3.18	S_f/A	11.0	θ_b	90°

Designation: 18

Test: Helium Gun

Figure 26.

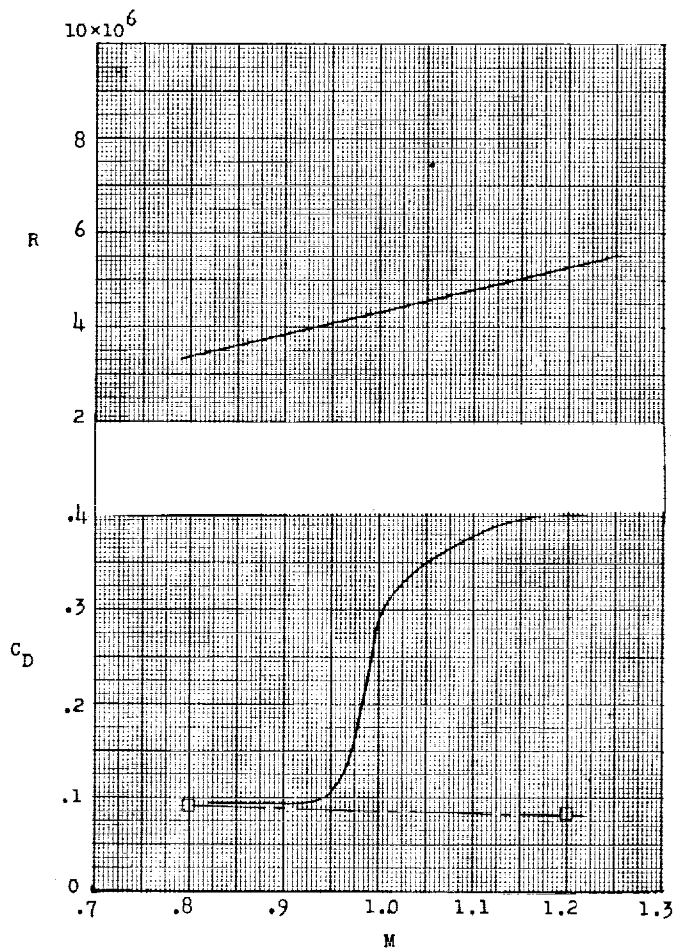

Figure 26.- Concluded.

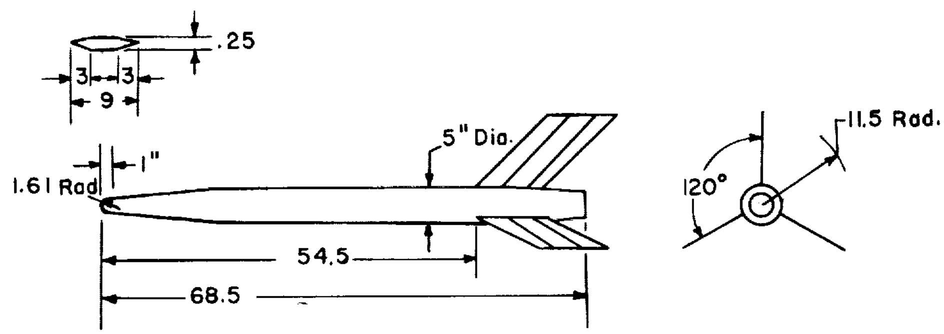

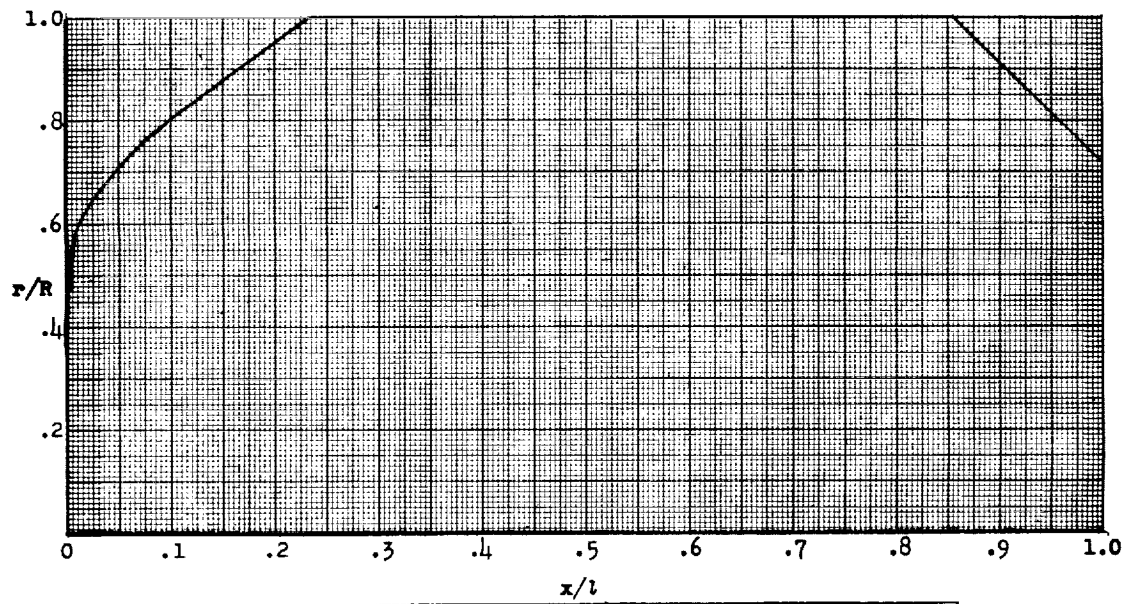

l/d_{Total}	13.7	l/d_{Nose}	3.2	S_b/A	51.0	A_b/A	.52
l/d_{N+A}	5.20	l/d_{Aft}	2.0	S_f/A	24.6	θ_b	4.02°

Designation: 19

Test: Rocket

Remarks: This model 5 times scale of model 20 (fig. 28).

Figure 27.

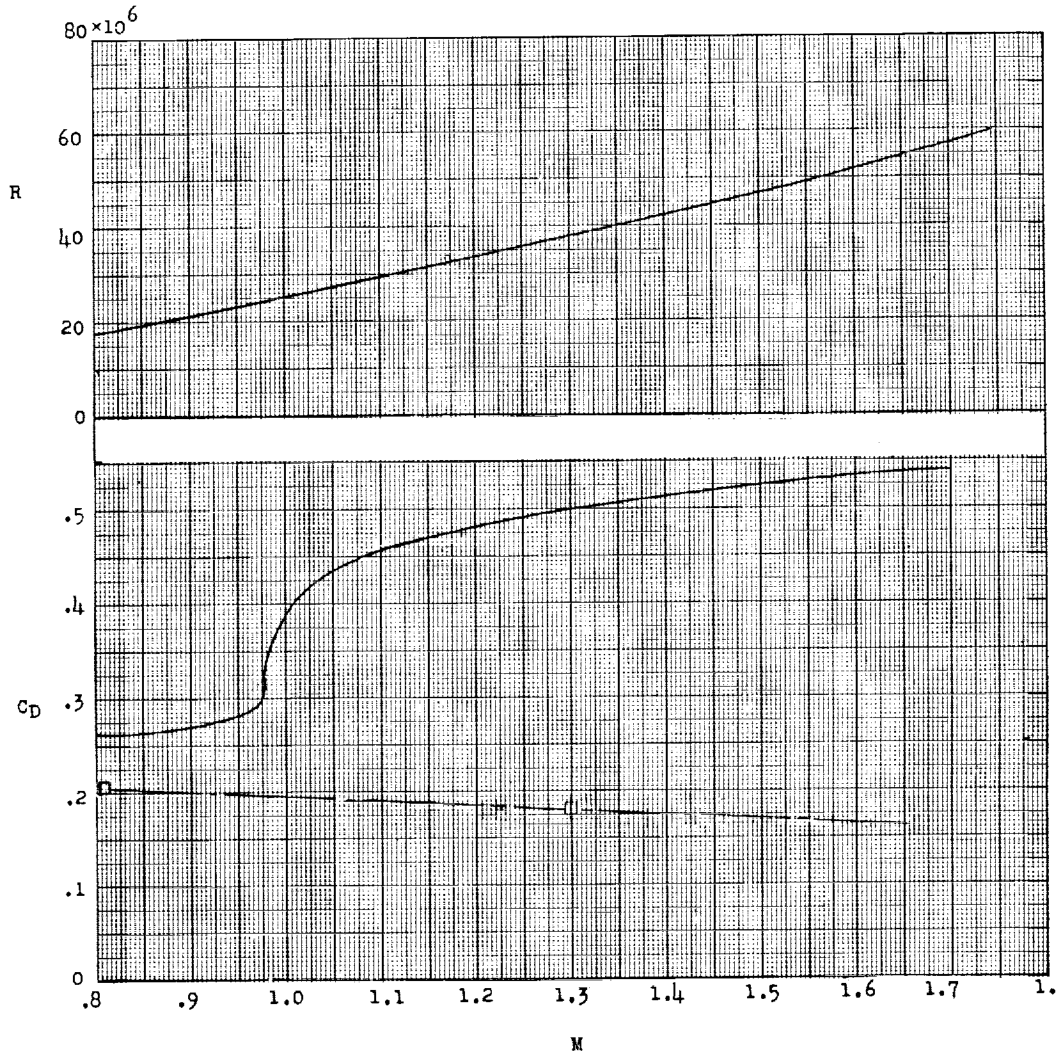

Figure 27.- Concluded.

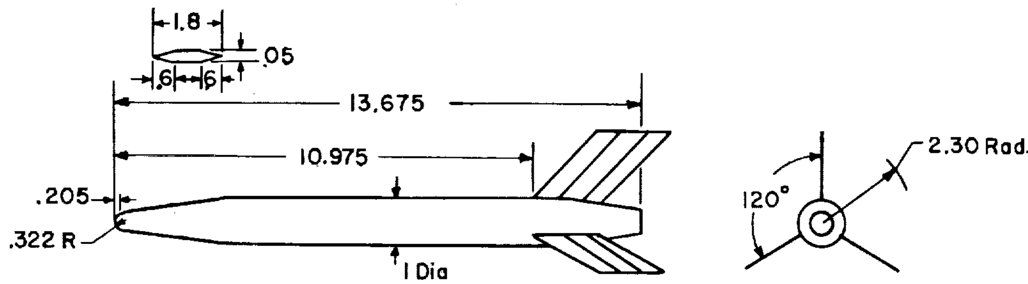

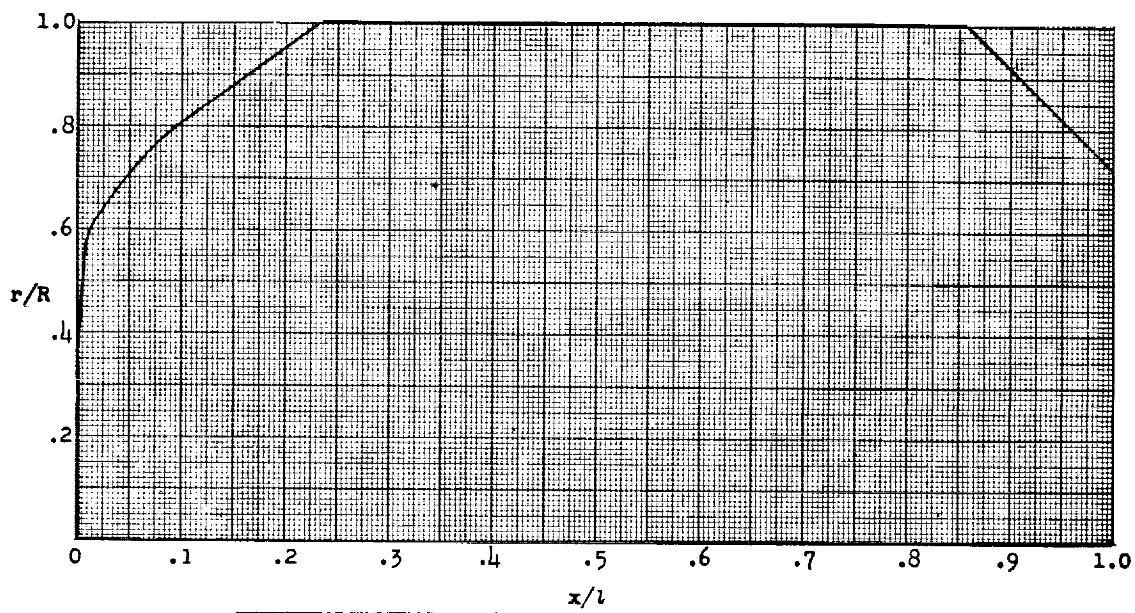

l/d_{Total}	13.7	l/d_{Nose}	3.2	S_b/A	51.0	A_b/A	.52
l/d_{N+A}	5.20	l/d_{Aft}	2.00	S_f/A	24.6	θ_b	4.02°

Designation: 20

Test: **Helium Gun**

Remarks: This model $\frac{1}{5}$ scale of model 19 (fig. 27).

Figure 28.

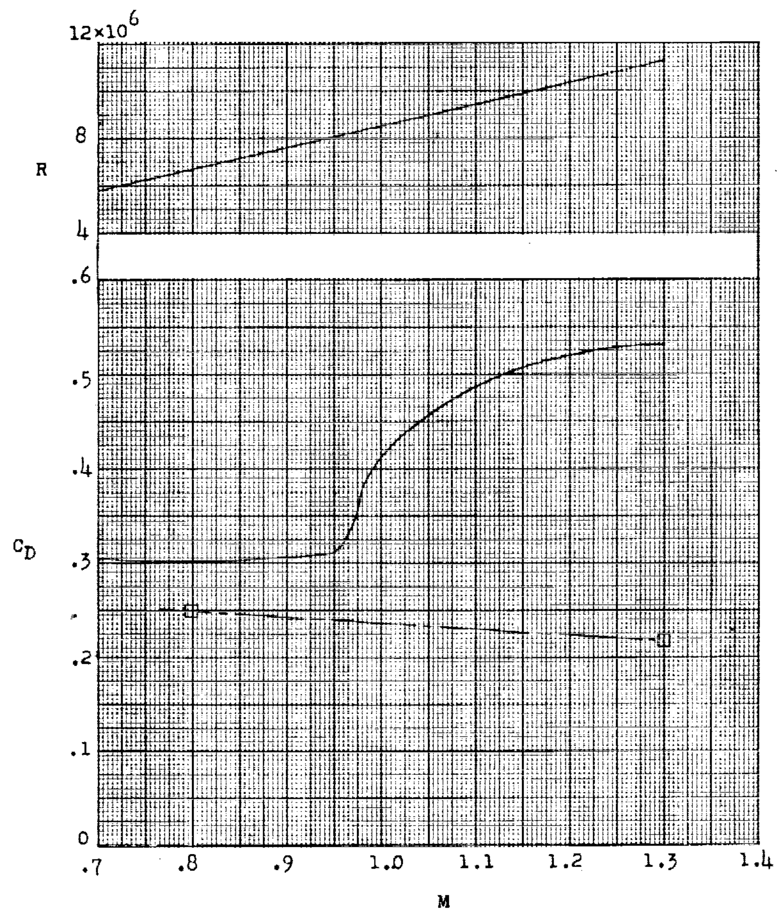

Figure 28.- Concluded.

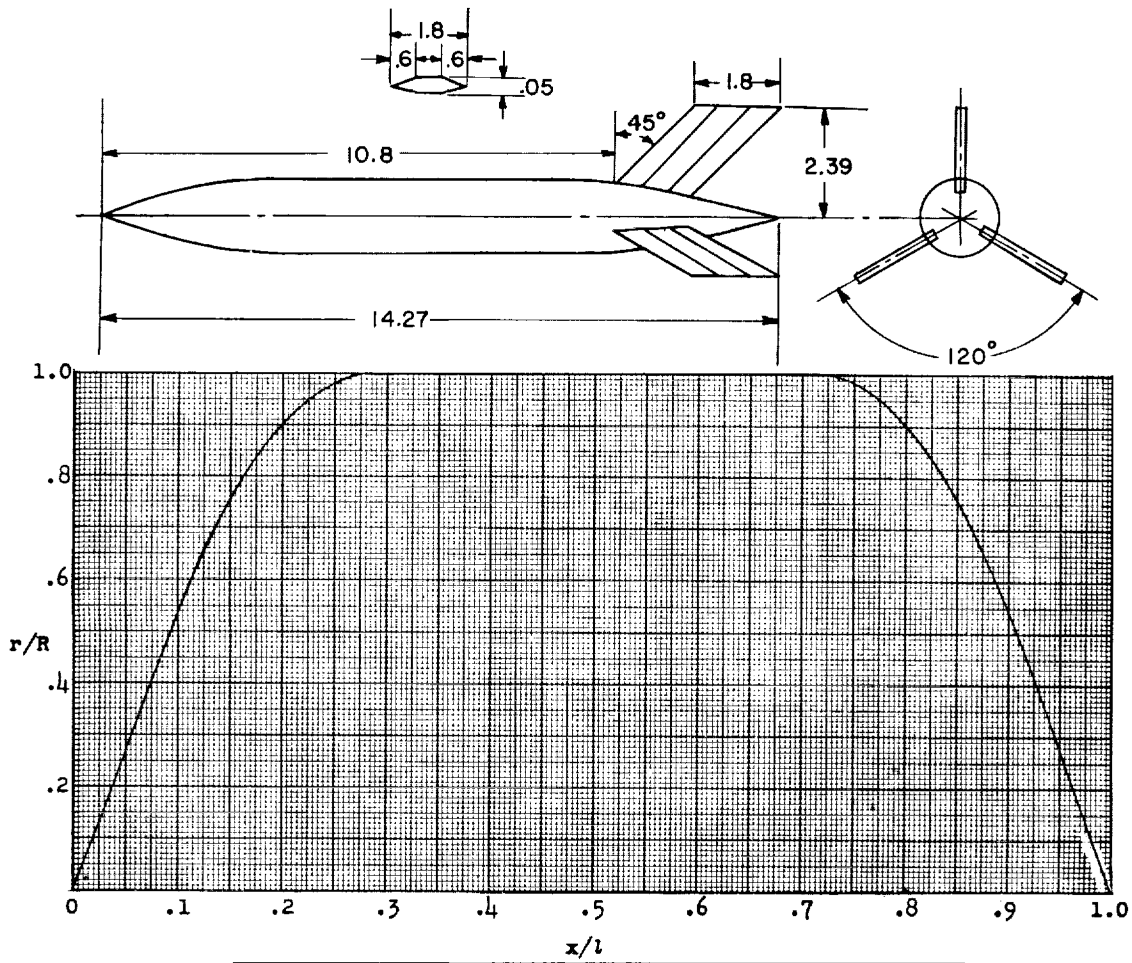

l/d_{Total}	9.51	l/d_{Nose}	2.67	S_b^{*}/A	30.6	A_b/A	0.0
l/d_{N+A}	5.34	l/d_{Aft}	2.67	S_f/A	11.0	θ_b	15.6°

Designation: 21

Test: Helium Gun

Figure 29.

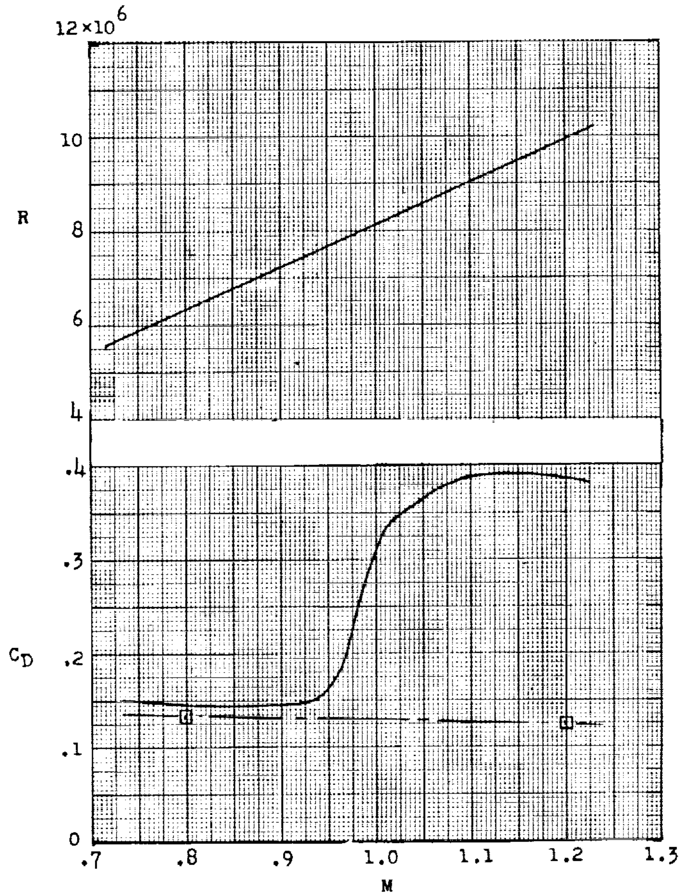

Figure 29.- Concluded.

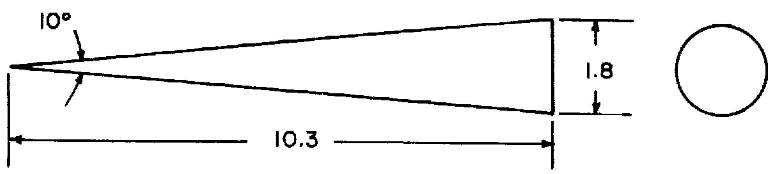

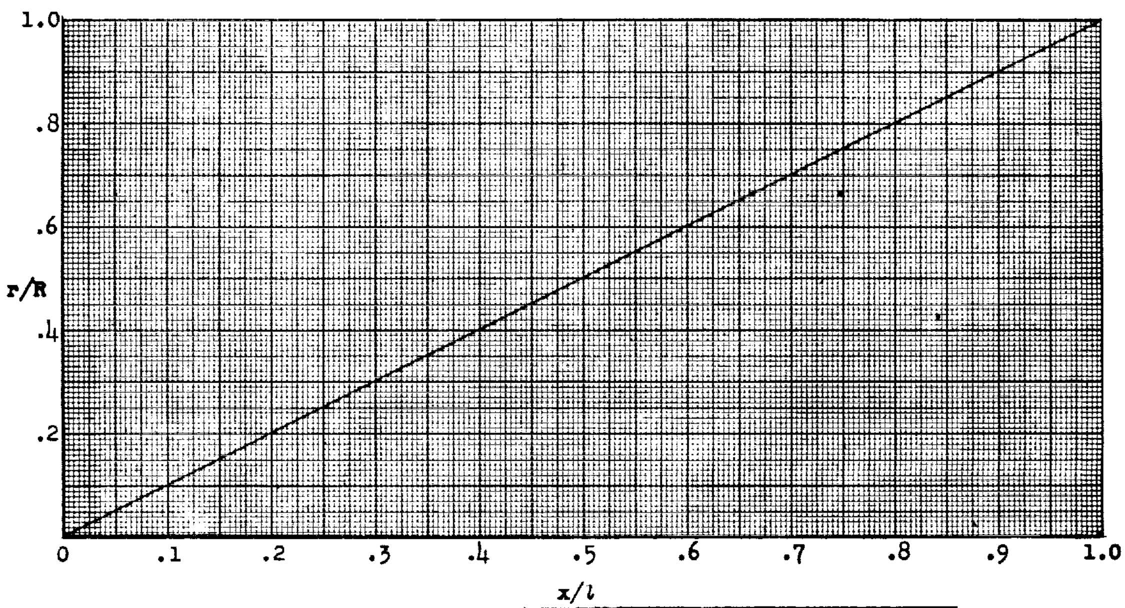

l/d_{Total}	5.7	l/d_{Nose}	5.7	S_b/A	11.40	A_b/A	1.0
l/d_{N+A}	5.7	l/d_{Aft}		S_f/A	0	θ_b	-5.0°

Designation: 22

Test: Helium Gun

Figure 30.

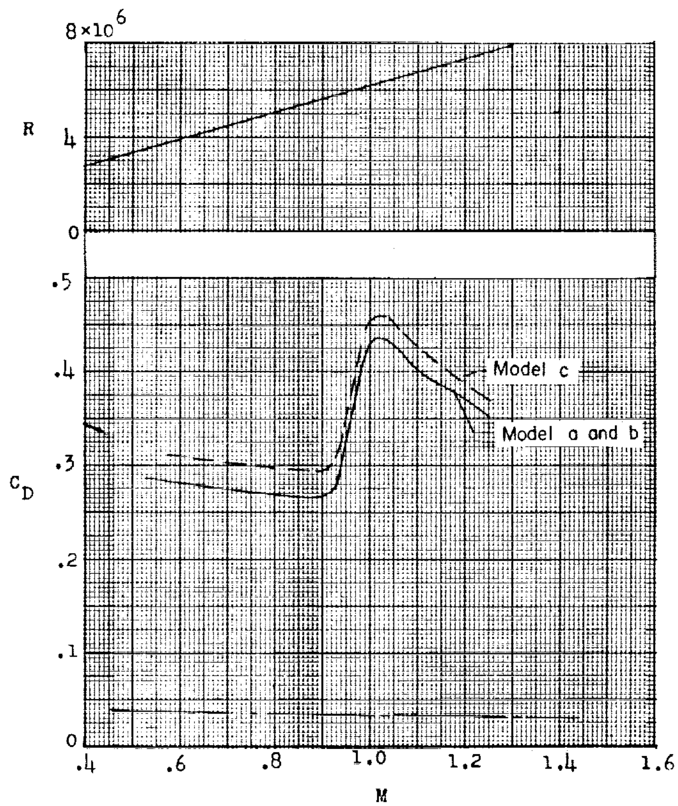

Figure 30.- Concluded.

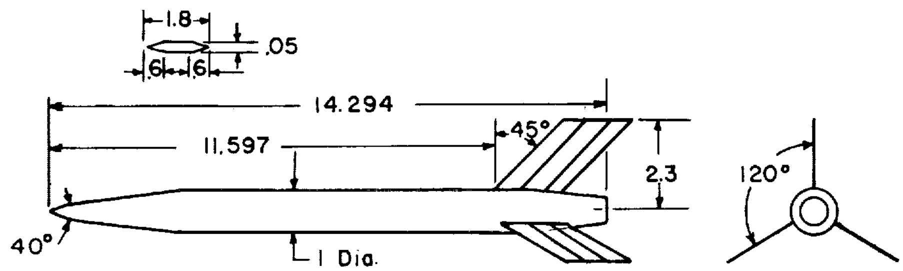

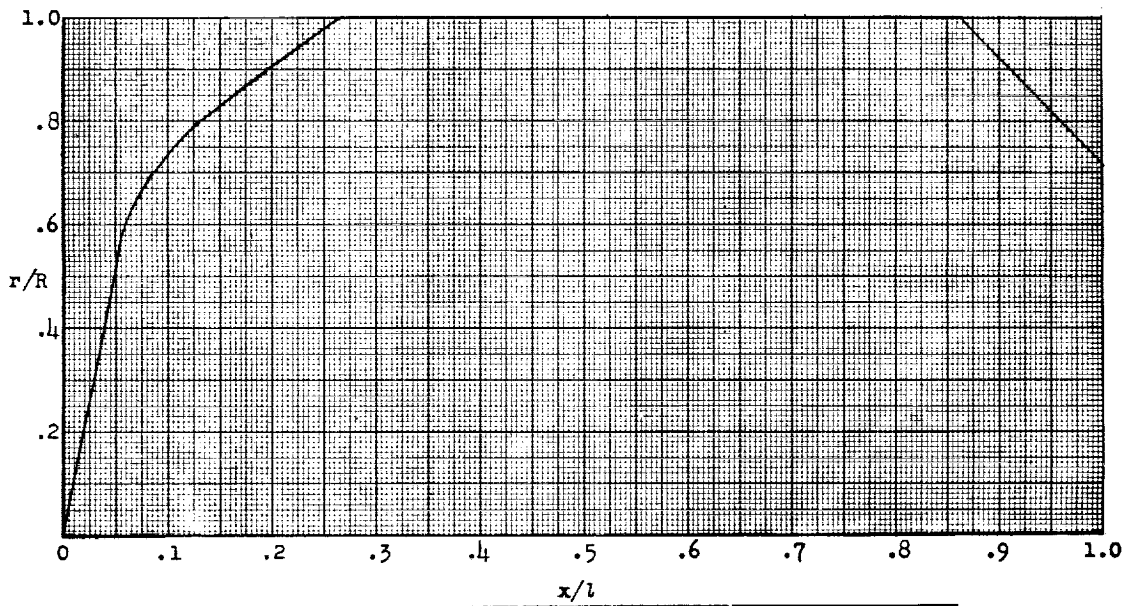

l/d_{Total}	14.29	l/d_{Nose}	3.79	S_b/A	51.9	A_b/A	.52
l/d_{N+A}	5.79	l/d_{Aft}	2.00	S_f/A	24.6	θ_b	4.02°

Designation: 23

Test: Helium Gun

Figure 31.

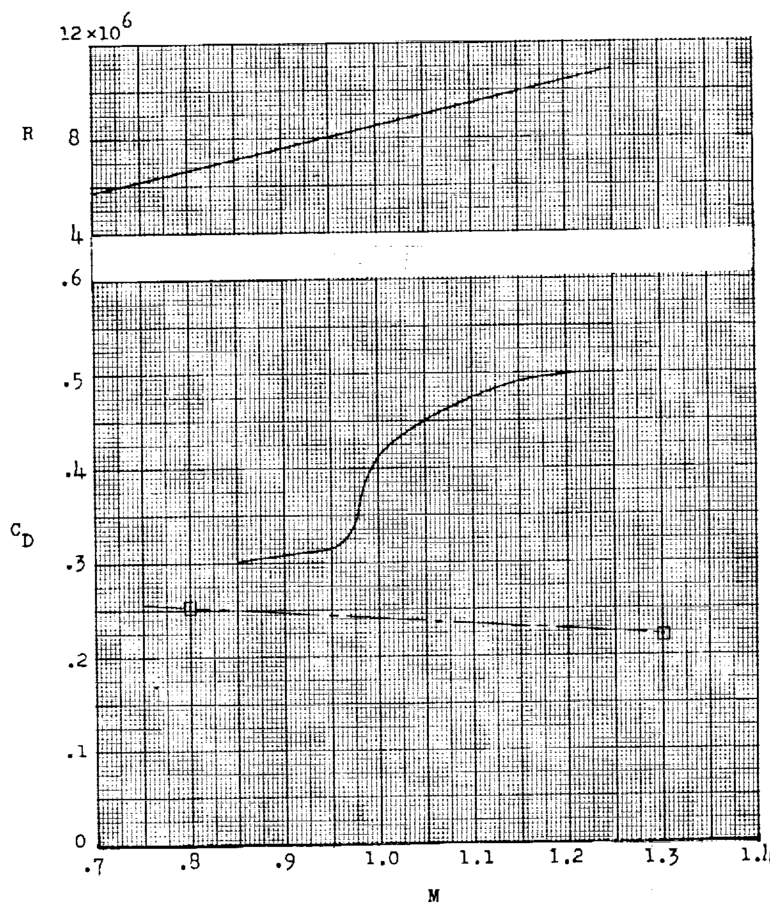

Figure 31.- Concluded.

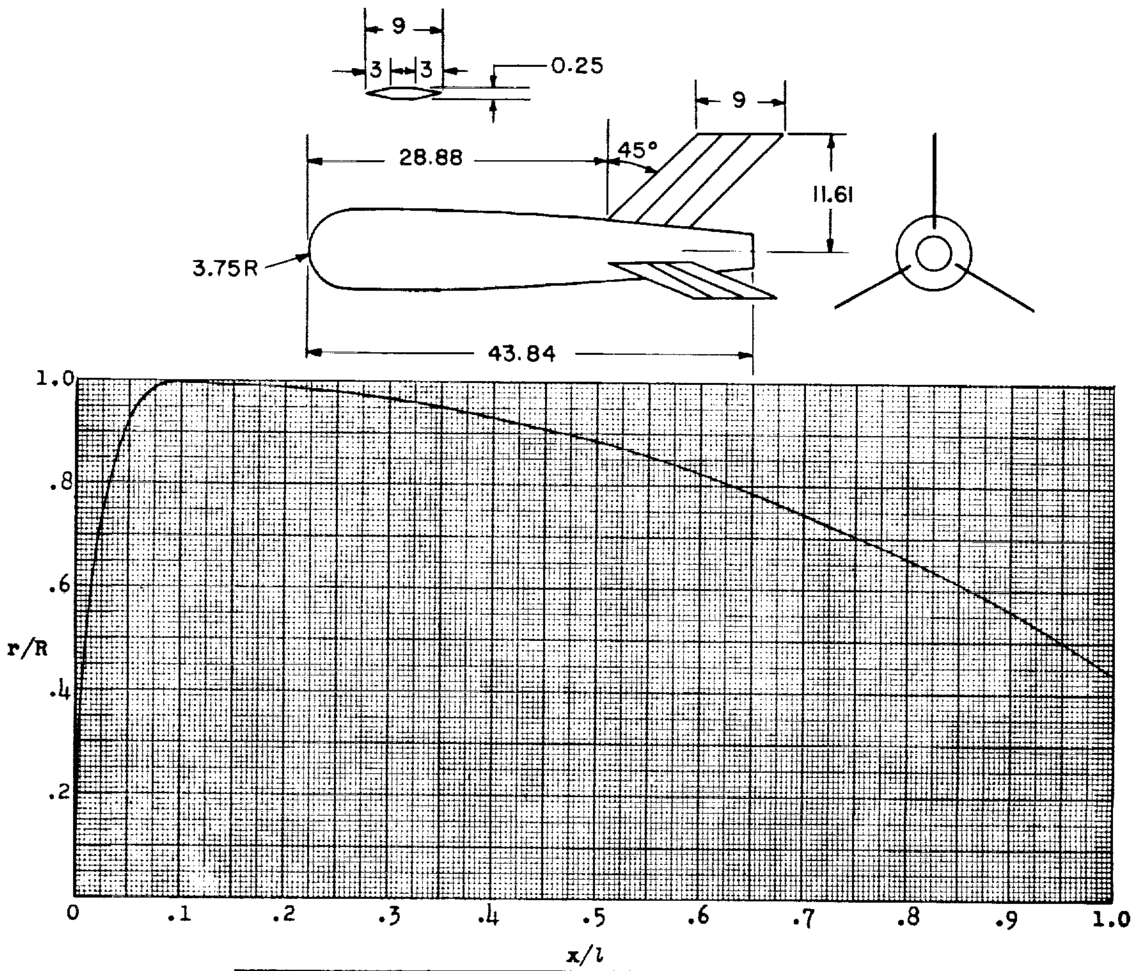

l/d_{Total}	5.84	l/d_{Nose}	0.50	S_b/A	19.00	A_b/A	.19
l/d_{N+A}	5.84	l/d_{Aft}	5.34	S_f/A	11.0	θ_b	7°

Designation: 24

Test: Rocket

Remarks: Hemispherical nose; parabolic afterbody.

Figure 32.

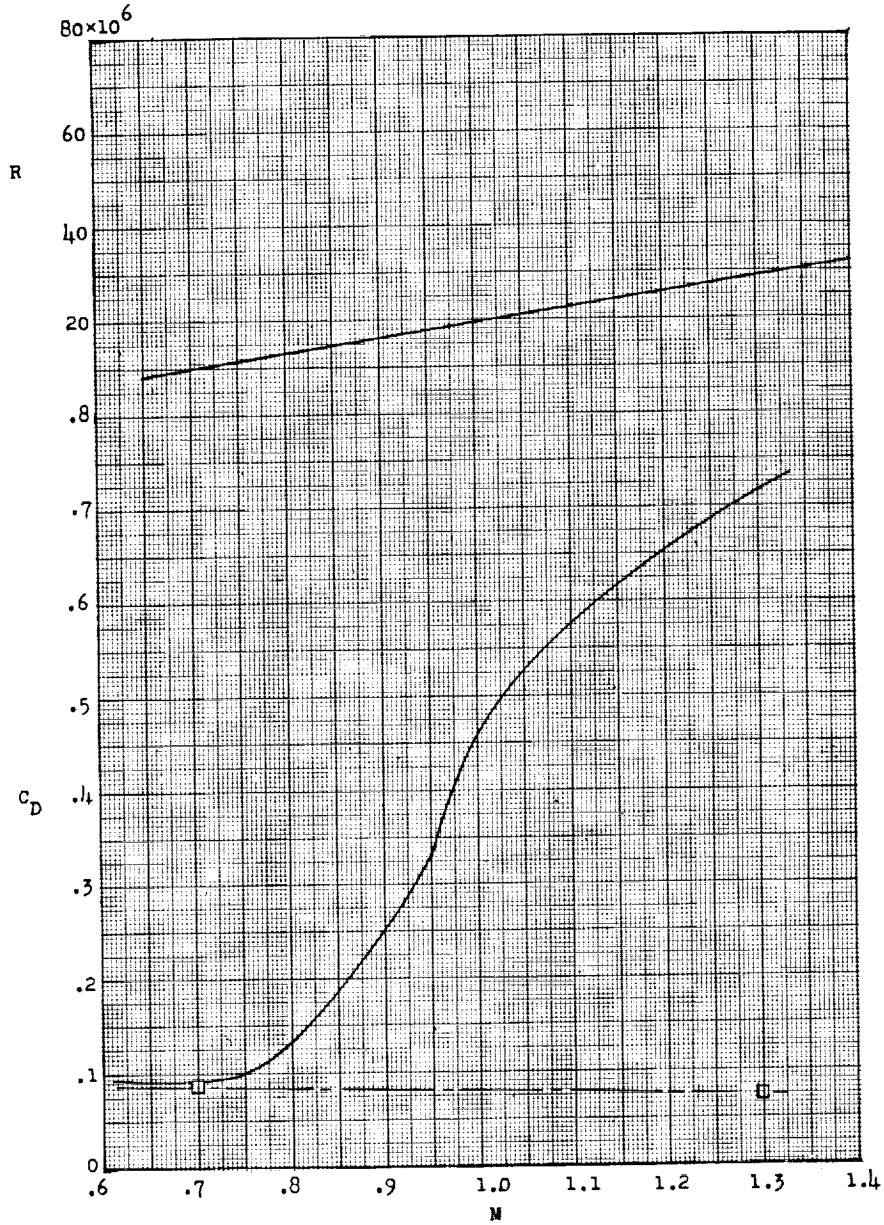

Figure 32.- Concluded.

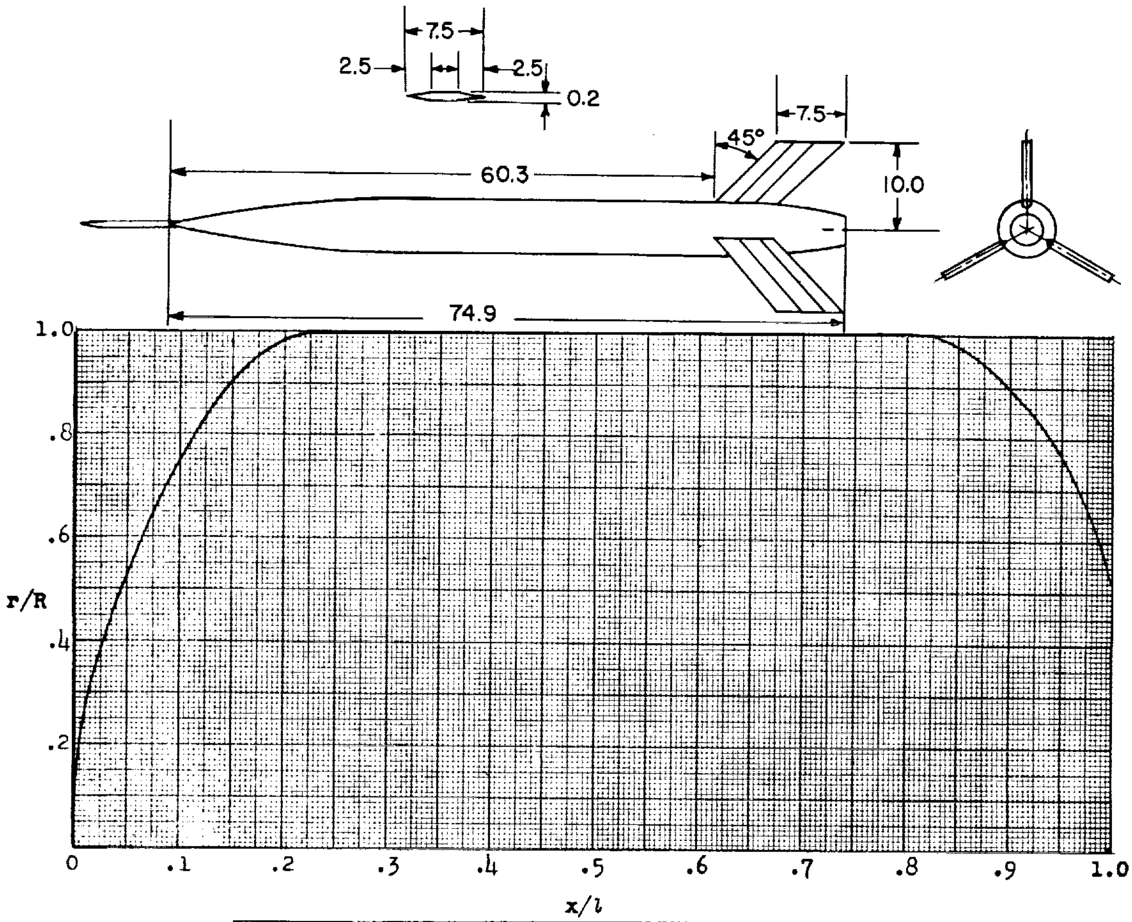

l/d_{Total}	12.9	l/d_{Nose}	3.10	S_b/A	51.8	A_b/A	.25
l/d_{N+A}	5.84	l/d_{Aft}	2.74	S_f/A	12.4	θ_b	18.6°

Designation: 25

Test: Rocket

Remarks: Sting may have some effect on friction drag but hardly any on pressure drag.

Figure 33.

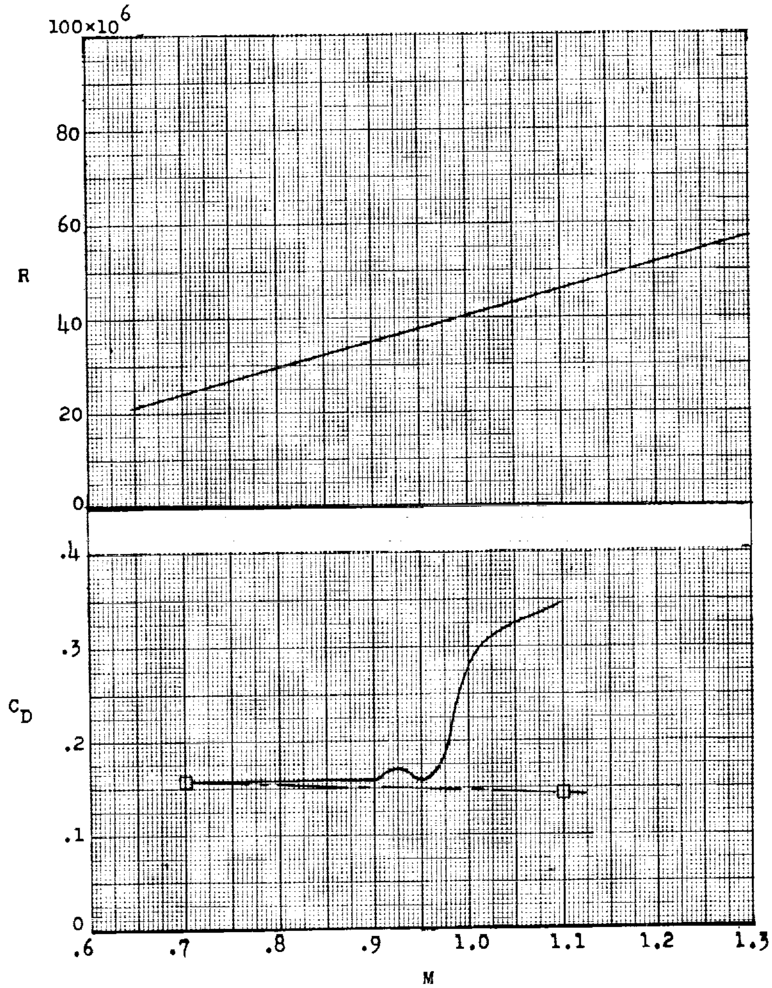

Figure 33.- Concluded.

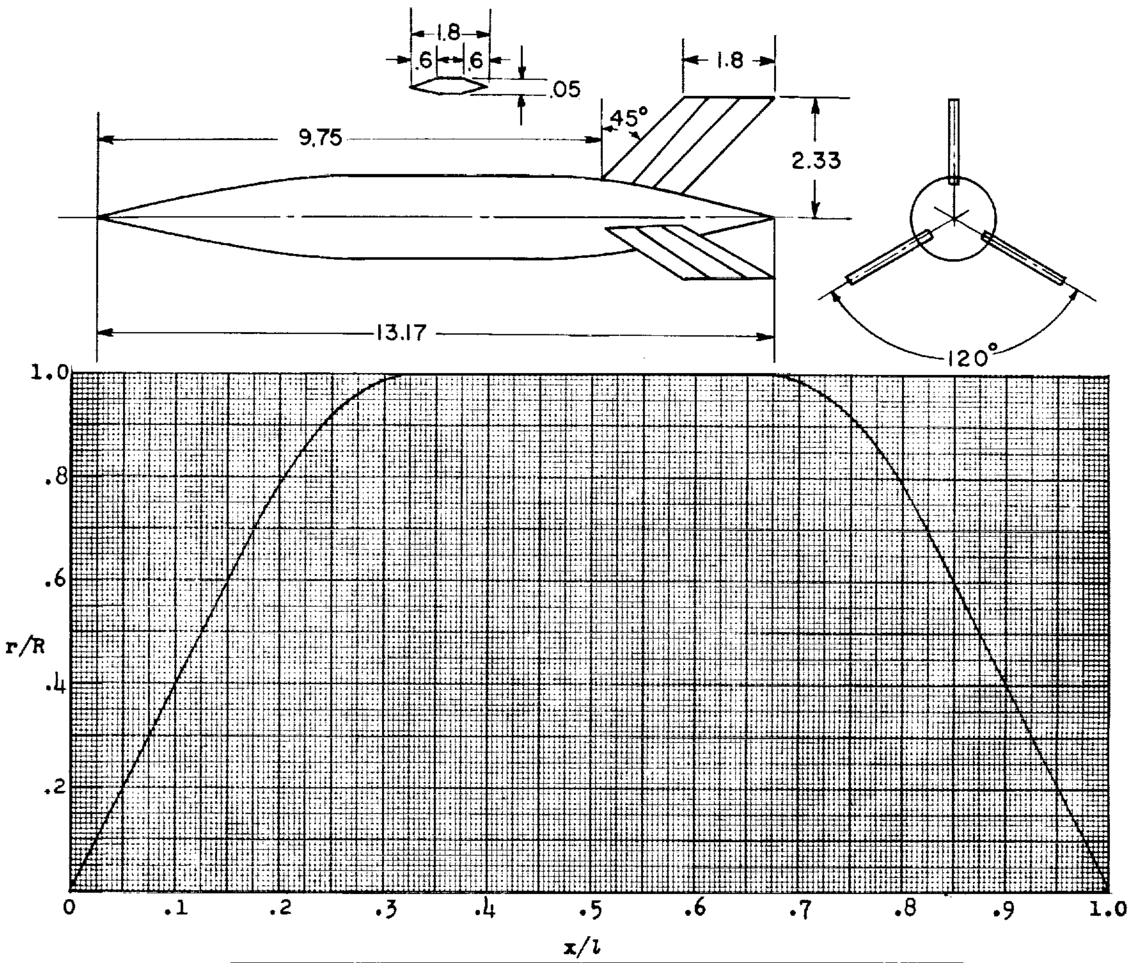

l/d_{Total}	8.78	l/d_{Nose}	3.00	S_b/A	26.20	A_b/A	0.0
l/d_{N+A}	6.00	l/d_{Aft}	3.00	S_f/A	11.0	θ_b	12.9°

Designation: 26

Test: Helium Gun

Figure 34.

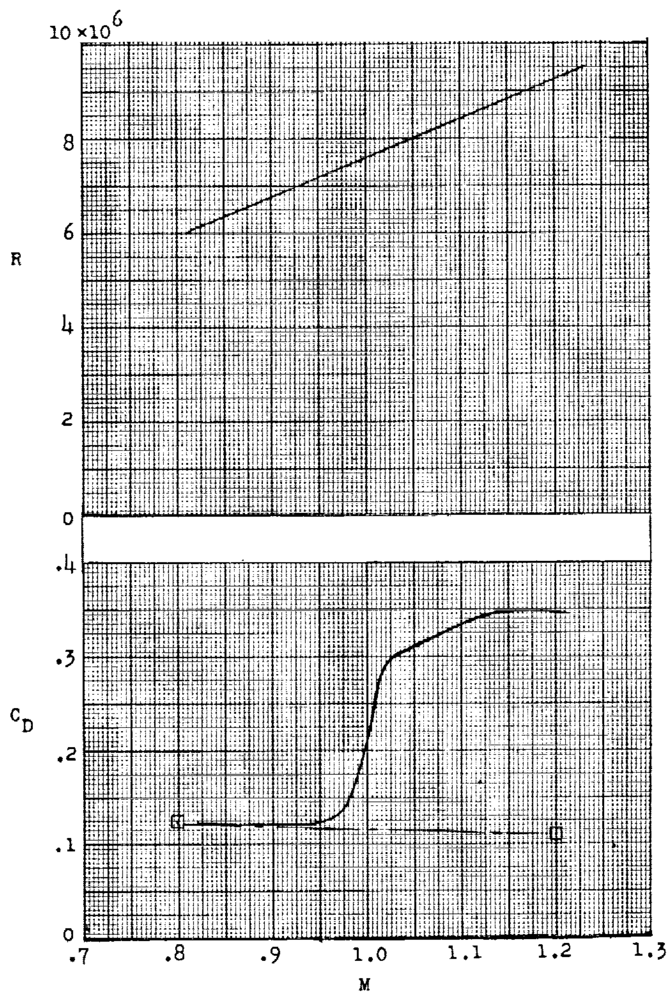

Figure 34.- Concluded.

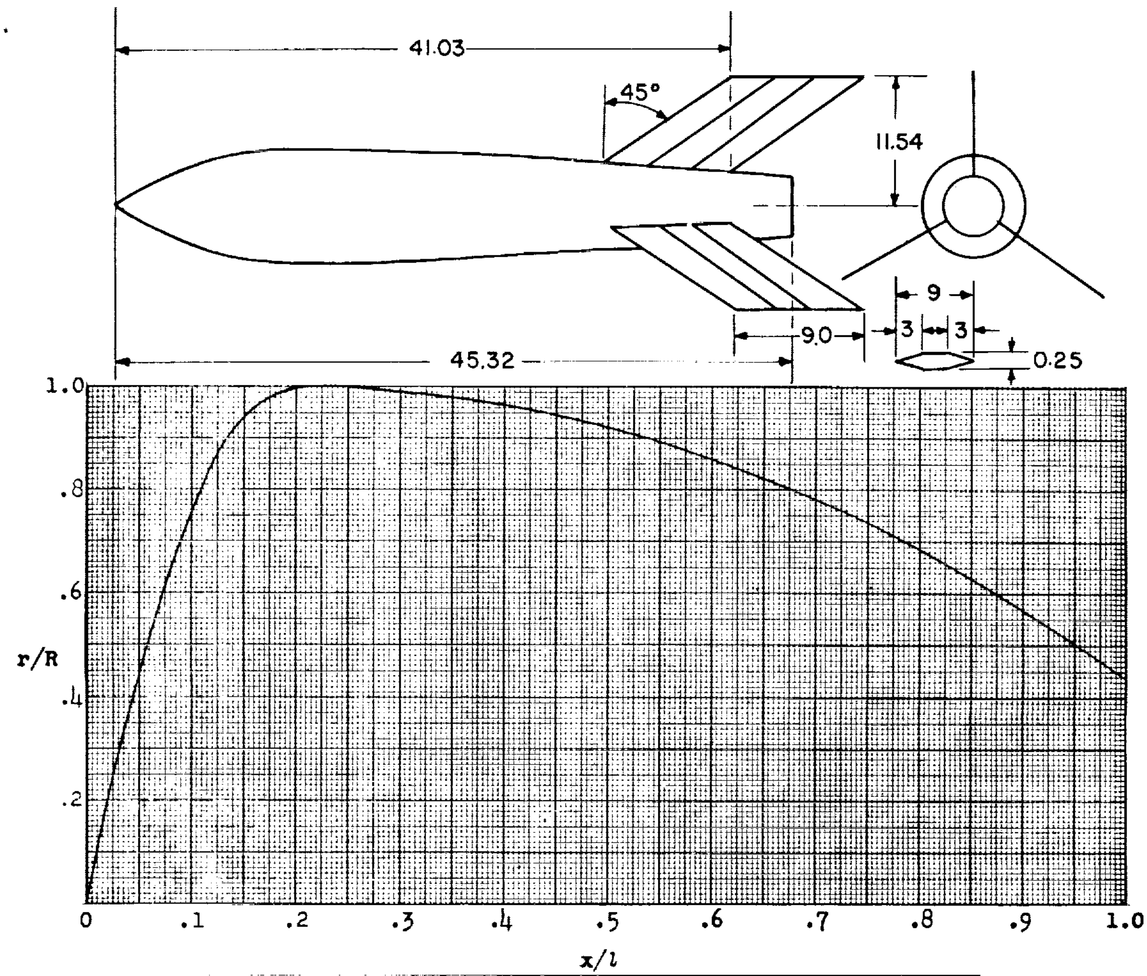

l/d_{Total}	6.04	l/d_{Nose}	1.21	S_b/A	19.16	A_b/A	.19
l/d_{N+A}	6.04	l/d_{Aft}	4.83	S_f/A	11.0	θ_b	9.2°

Designation: 27

Test: Rocket

Remarks: Parabolic nose and afterbody.

Figure 35.

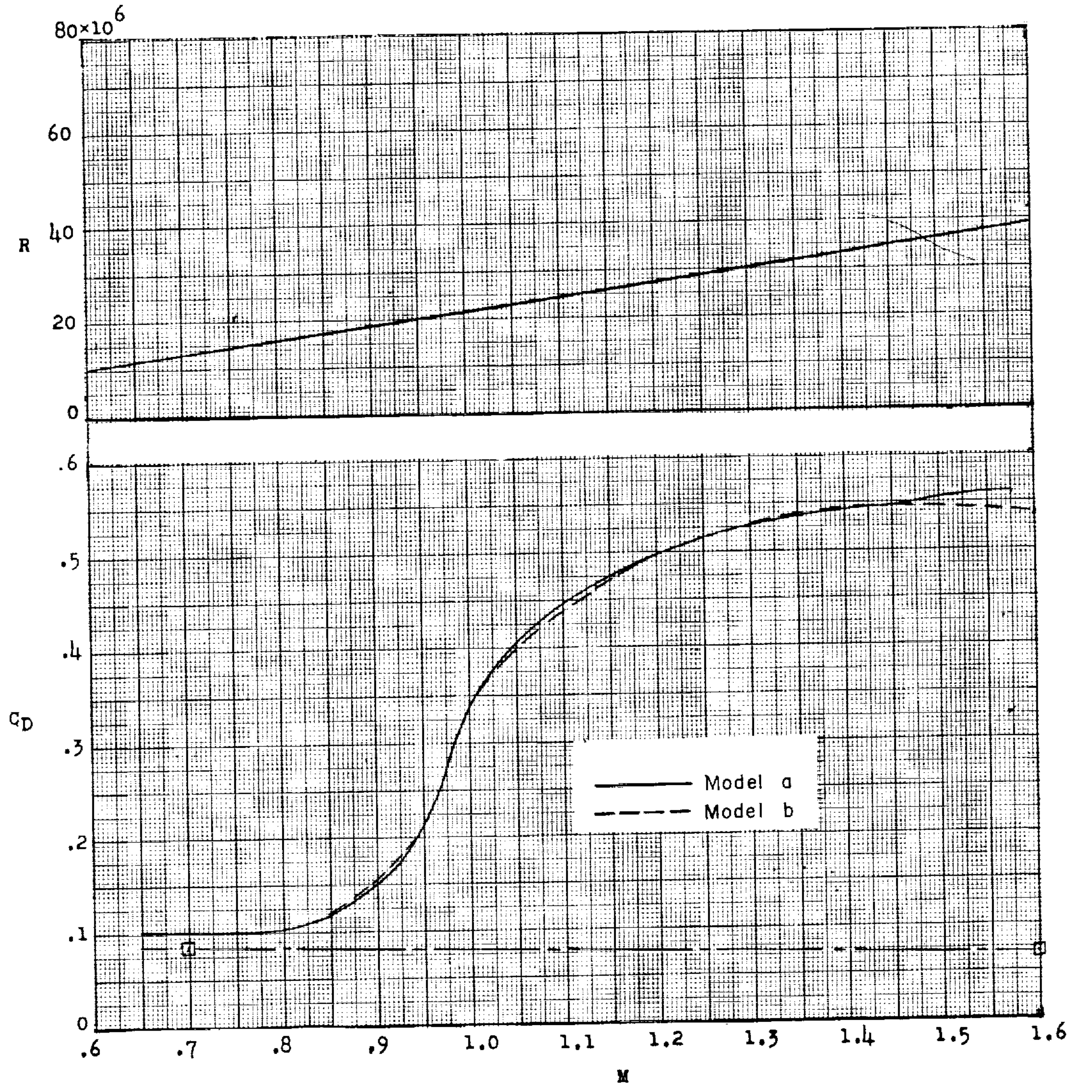

Figure 35.- Concluded.

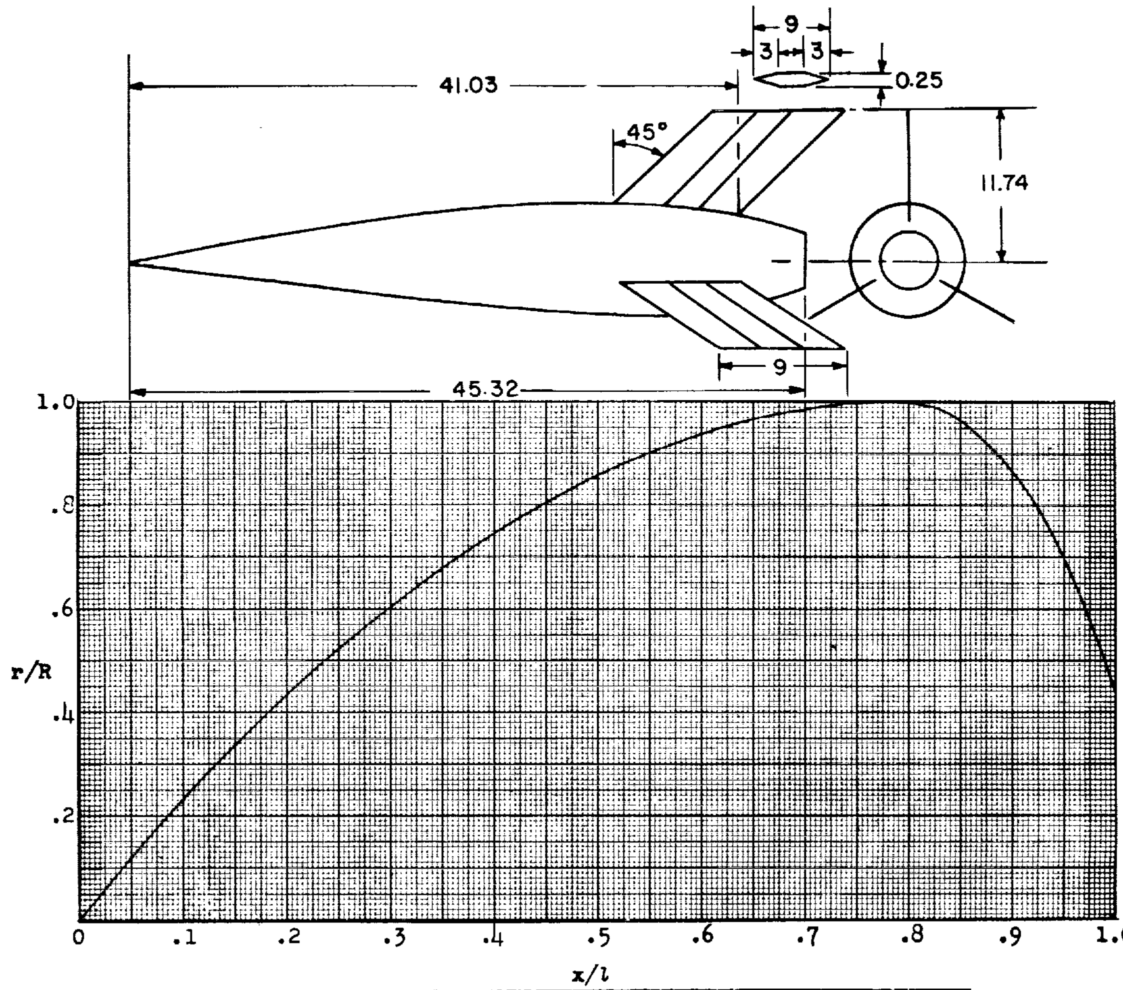

l/d_{Total}	6.04	l/d_{Nose}	4.83	S_b/A	16.84	A_b/A	.19
l/d_{N+A}	6.04	l/d_{Aft}	1.21	S_f/A	11	θ_b	25°

Designation: 28

Test: Rocket

Remarks: Parabolic nose and afterbody.

Figure 36.

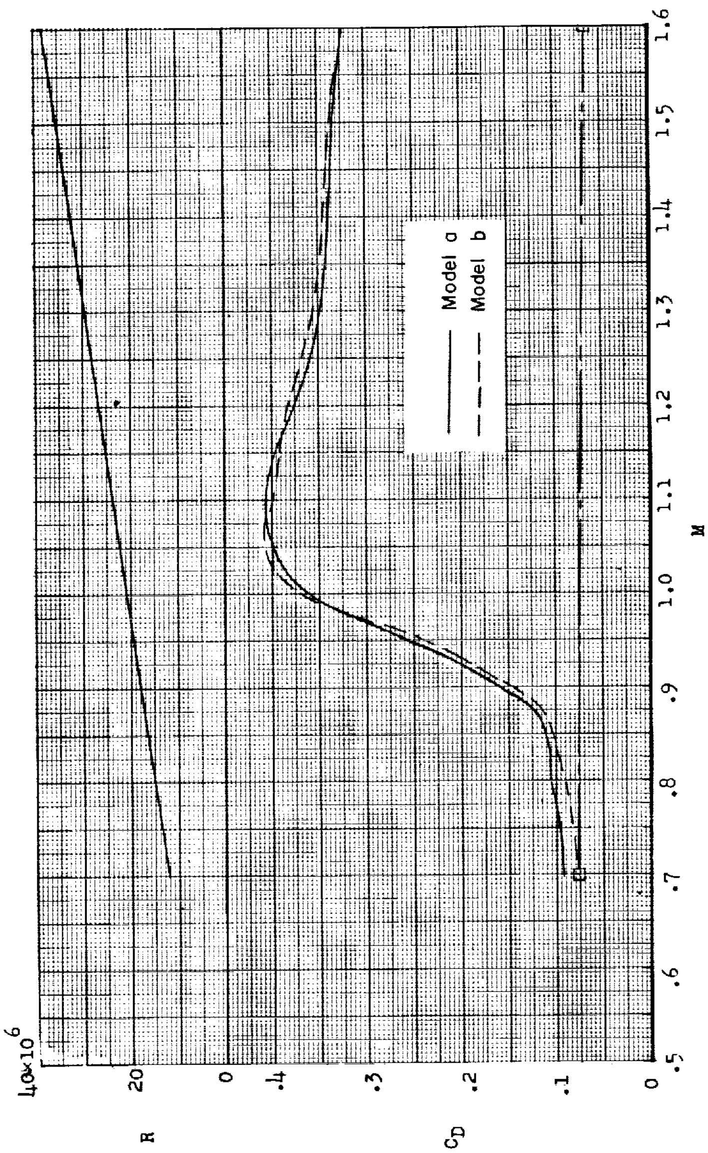

Figure 36.- Concluded.

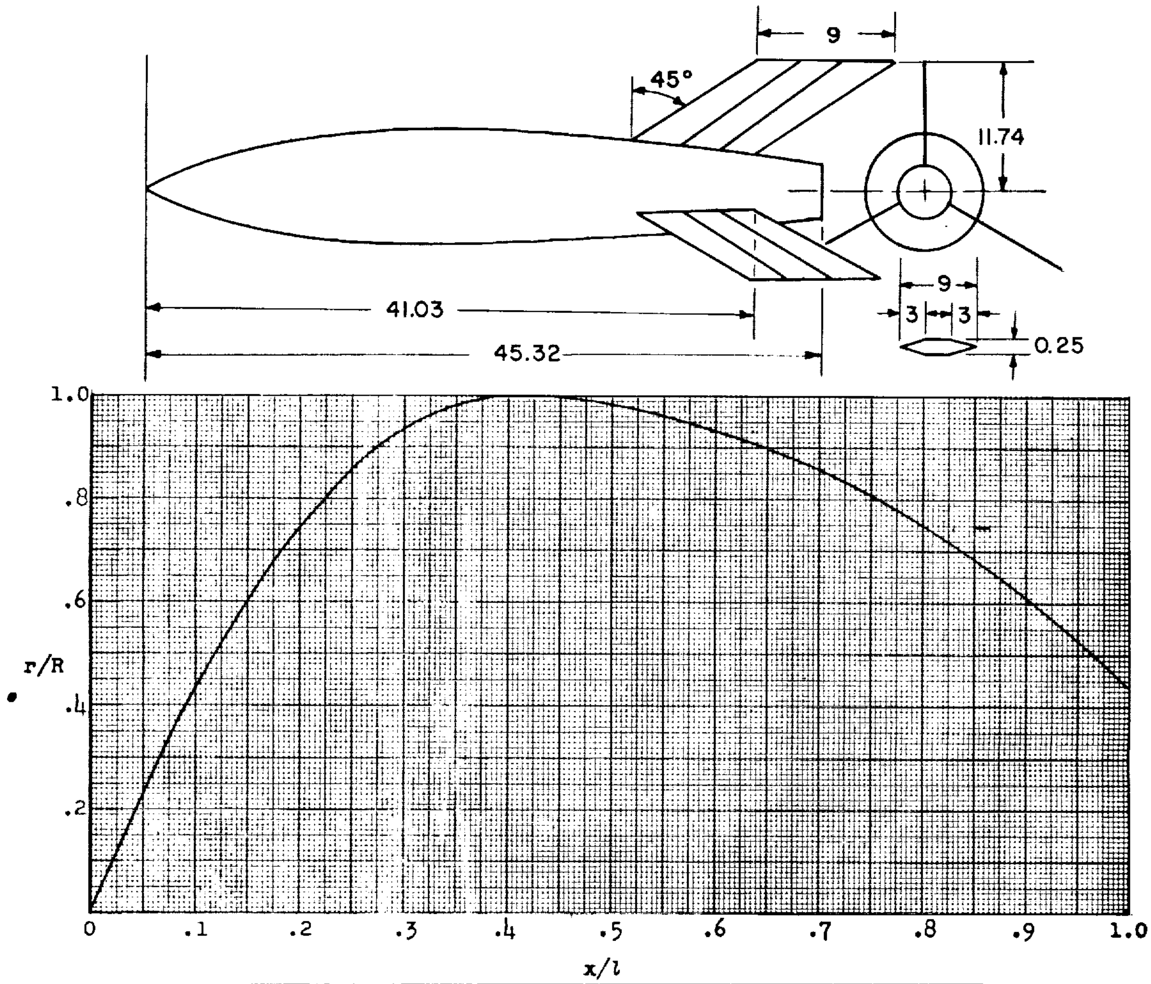

l/d_{Total}	6.04	l/d_{Nose}	2.42	S_b/A	18.39	A_b/A	.19
l/d_{N+A}	6.04	l/d_{Aft}	3.62	S_f/A	11.0	θ_b	8.8°

Designation: 29

Test: Rocket

Remarks: Parabolic nose and afterbody.

Figure 37.

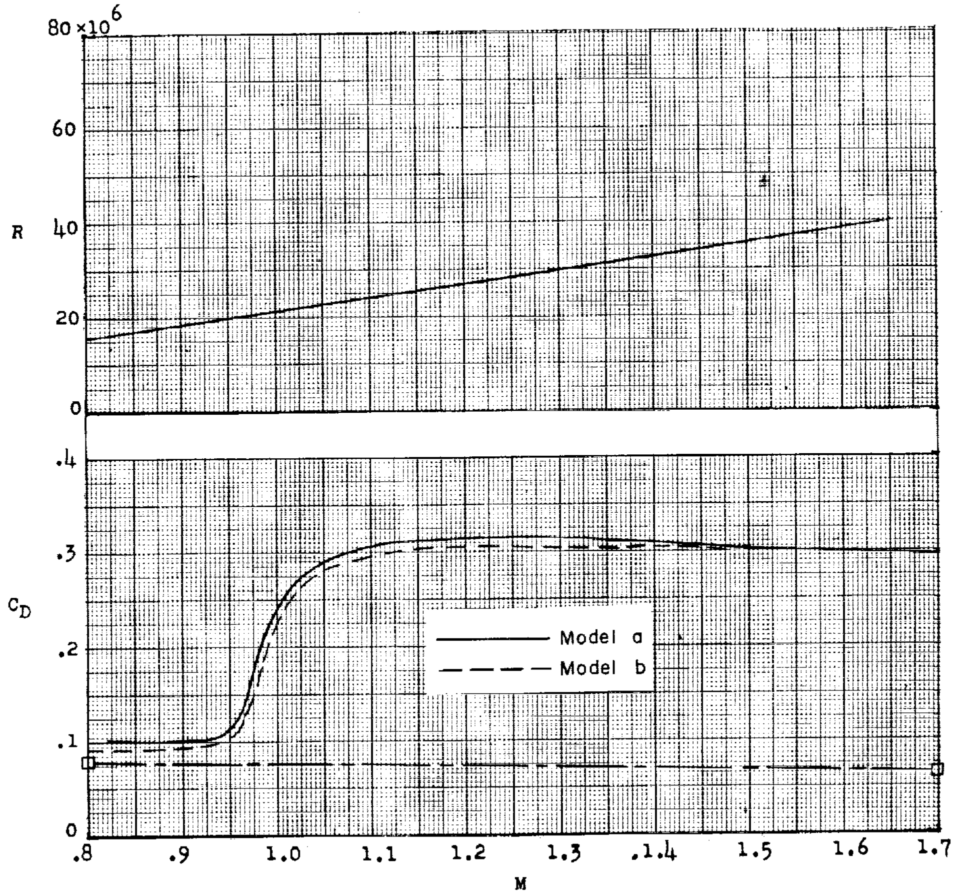

Figure 37.- Concluded.

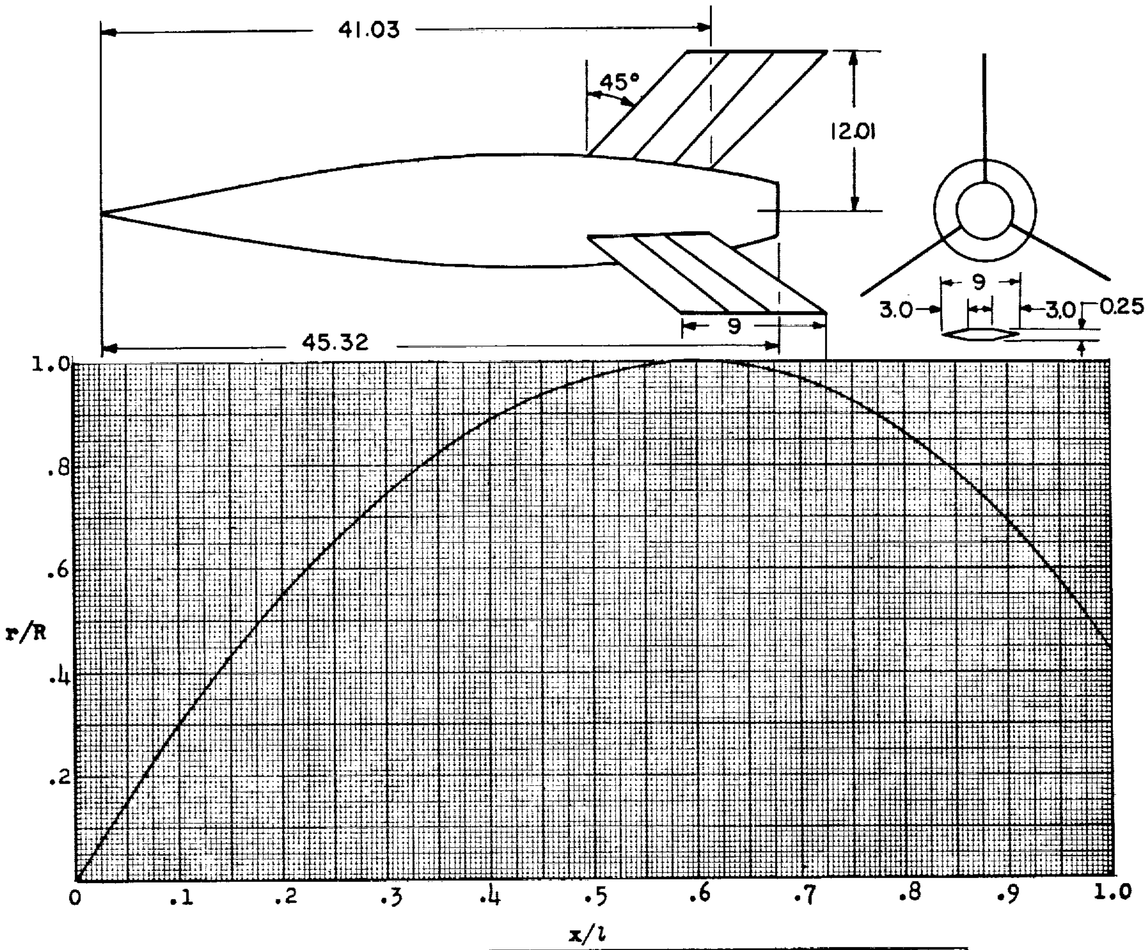

l/d_{Total}	6.04	l/d_{Nose}	3.62	S_b/A	17.64	A_b/A	.19
l/d_{N+A}	6.04	l/d_{Aft}	2.42	S_f/A	11.0	θ_b	13°

Designation: 30

Test: Rocket

Remarks: Parabolic nose and afterbody.

Figure 38.

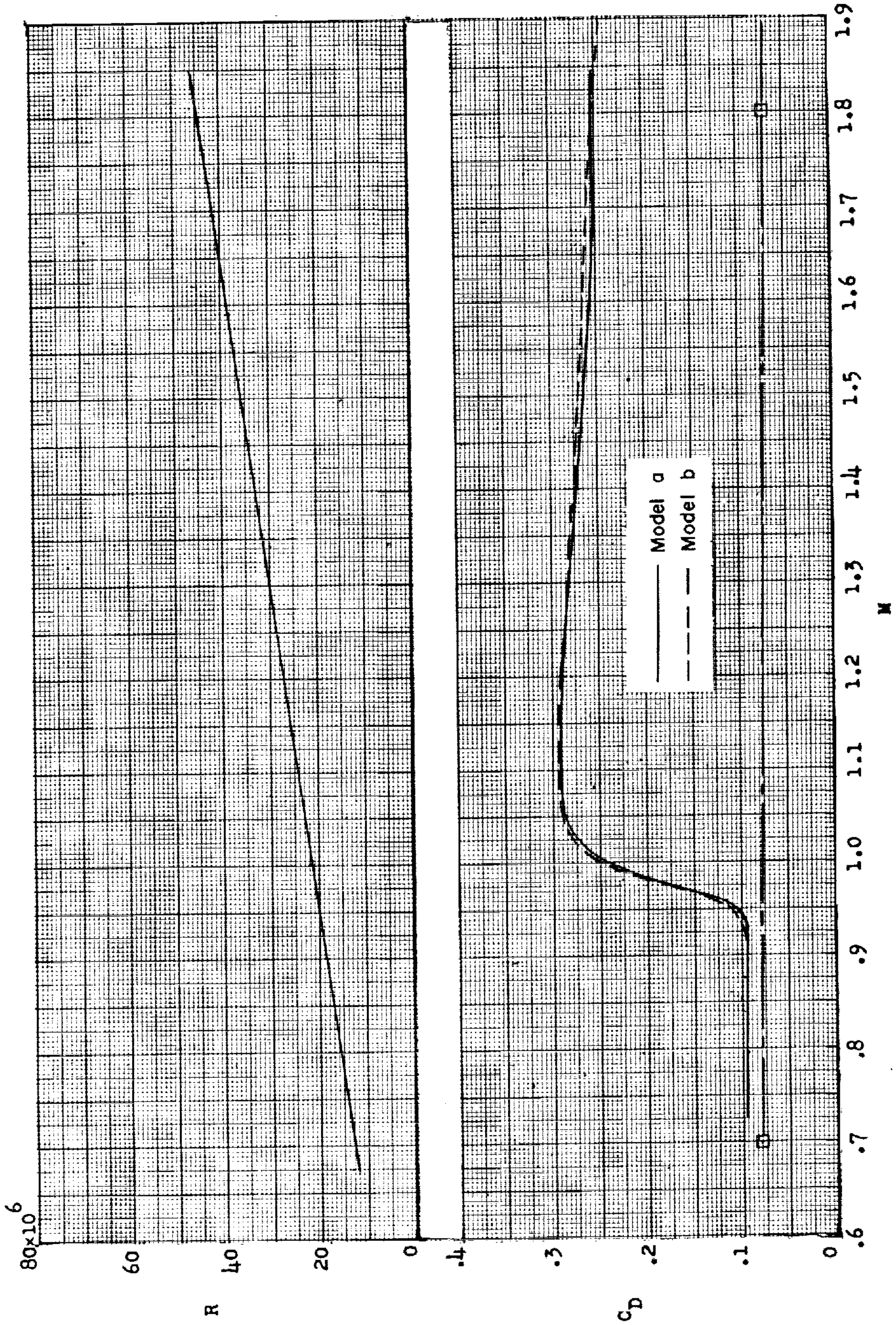

Figure 38.- Concluded.

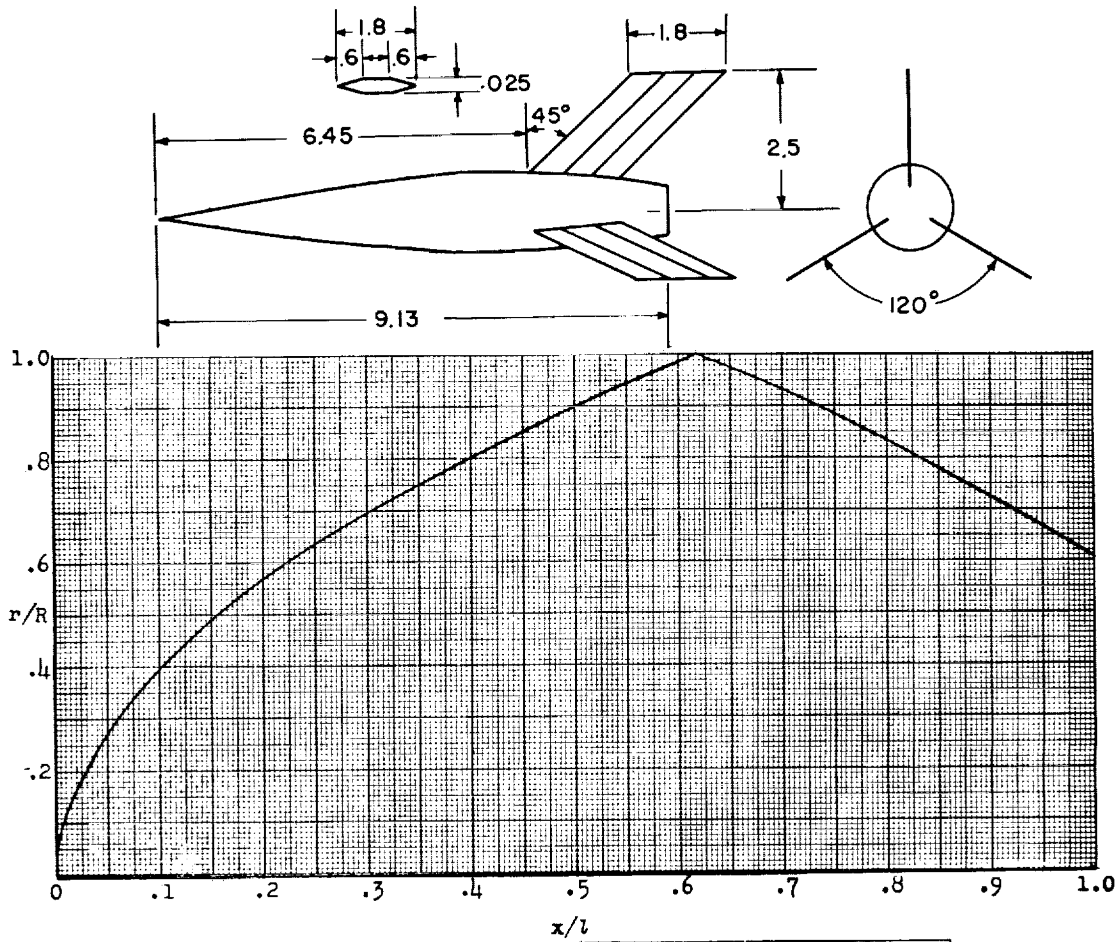

l/d_{Total}	6.04	l/d_{Nose}	3.71	S_b/A	17.60	A_b/A	.37
l/d_{N+A}	6.04	l/d_{Aft}	2.33	S_f/A	11.0	θ_b	6.1°

Designation: 31

Test: **Helium Gun**

Figure 39.

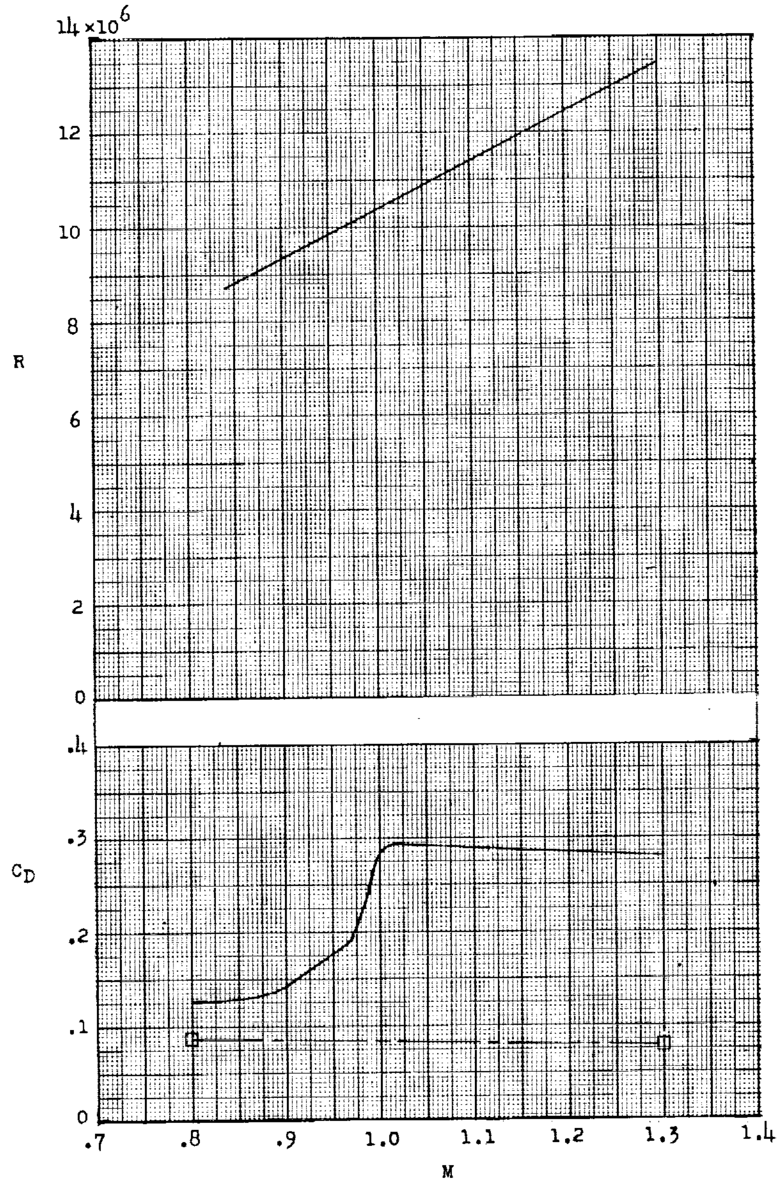

Figure 39.- Concluded.

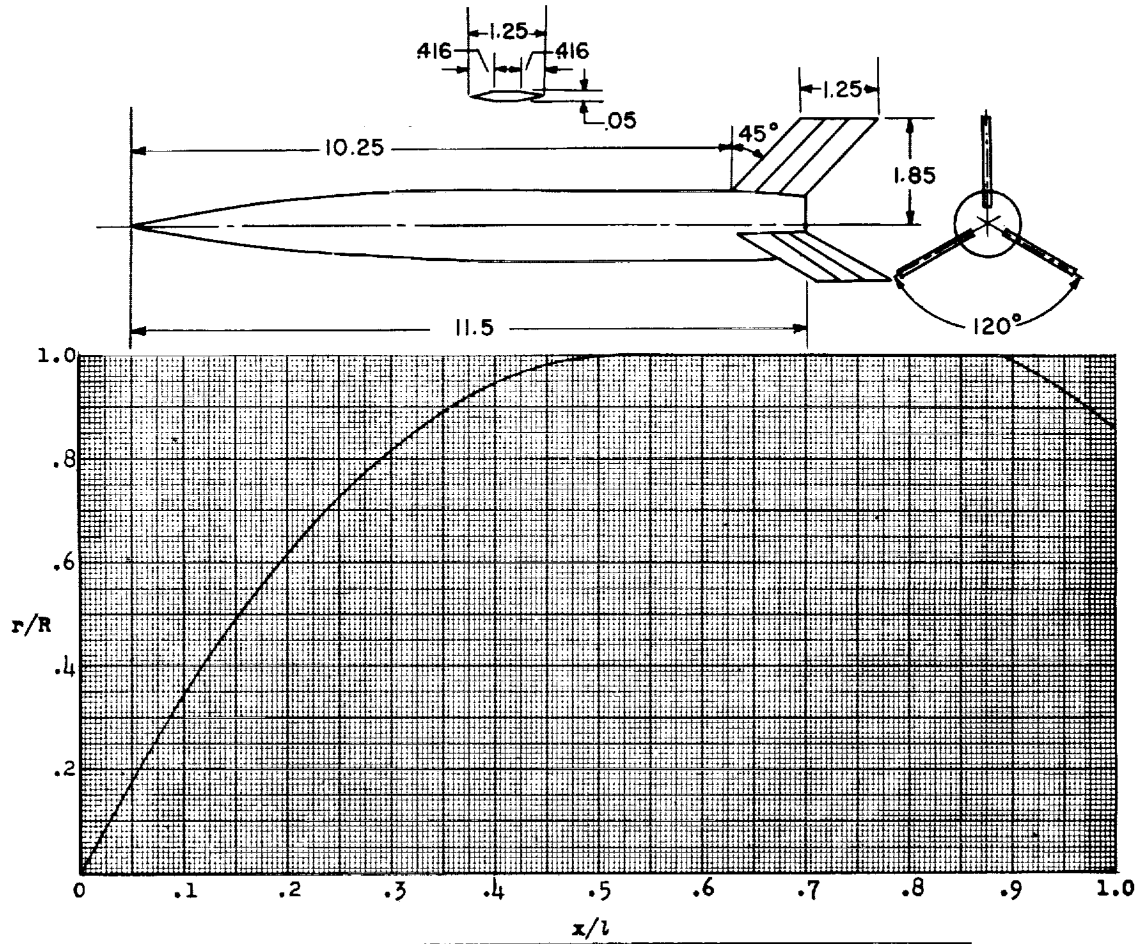

l/d_{Total}	9.6	l/d_{Nose}	5.01	S_b/A	31.6	A_b/A	.69
l/d_{N+A}	6.08	l/d_{Aft}	1.07	S_f/A	12.3	θ_b	5.45°

Designation: 32

Test: Helium Gun

Figure 40.

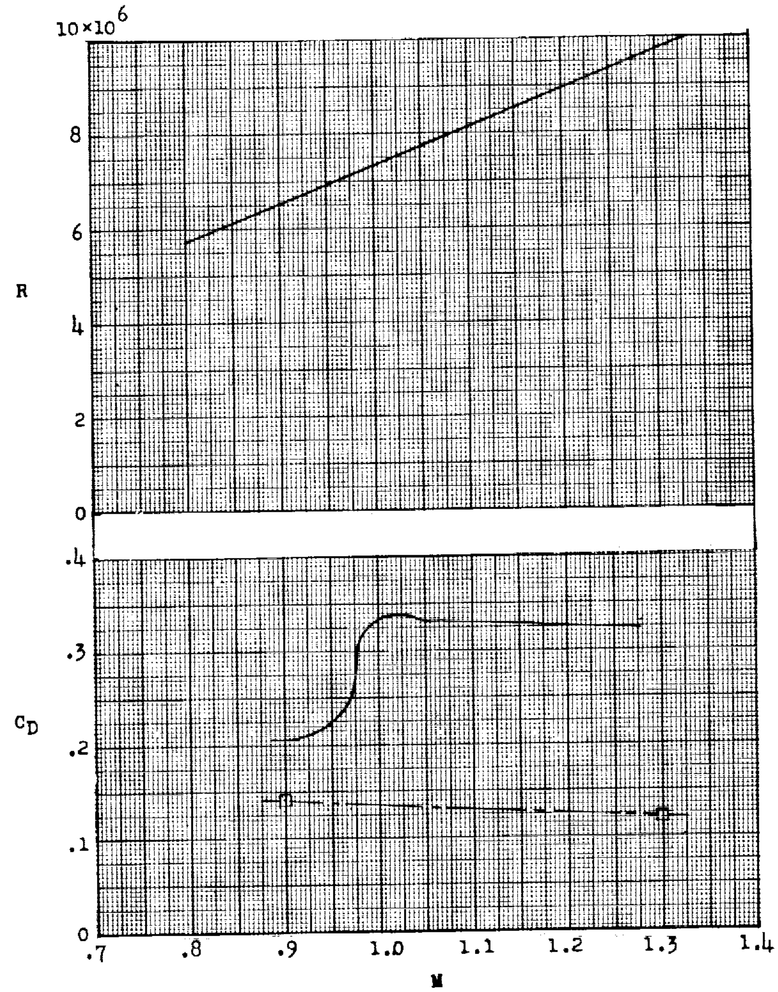

Figure 40.- Concluded.

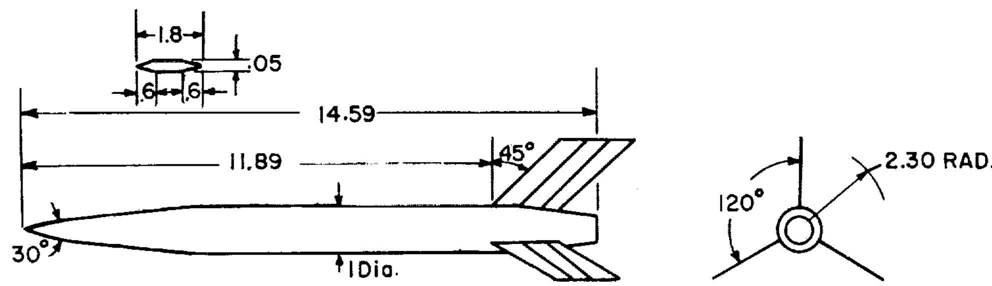

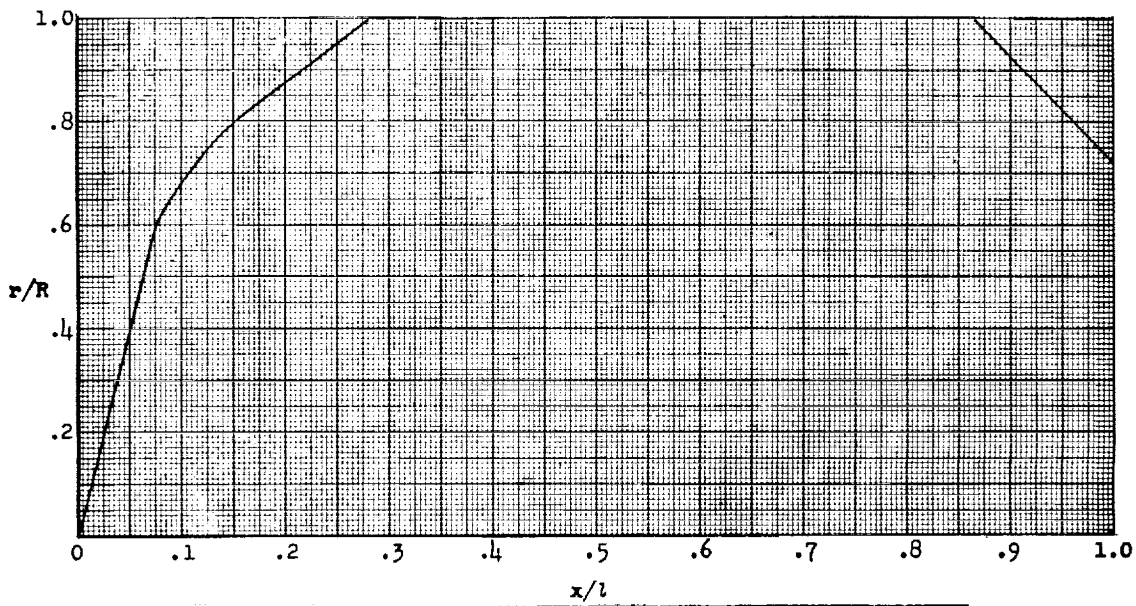

l/d_{Total}	14.6	l/d_{Nose}	4.10	S_b/A	52.3	A_b/A	.52
l/d_{N+A}	6.10	l/d_{Aft}	2.0	S_f/A	24.6	θ_b	4.02°

Designation: 33
Test: Helium Gun
Remarks: This model 1/5 scale of model 34 (fig. 42); thus pressure drags of these two configurations should be the same. That they are not the same is obvious, however, if it is assumed that data of model 34 are in error in M about M = 0.05; then the subsonic levels and the early drag rises are compatible. This seems to be justified since the late drag rise of model 34 would be quite unusual if it really occurred. Model 36 (fig. 44) is similar to 34 and showed the more usual earlier rise. The continued increase in drag coefficient of model 33 above M = 1.1 is also peculiar and is probably in error.

Figure 41.

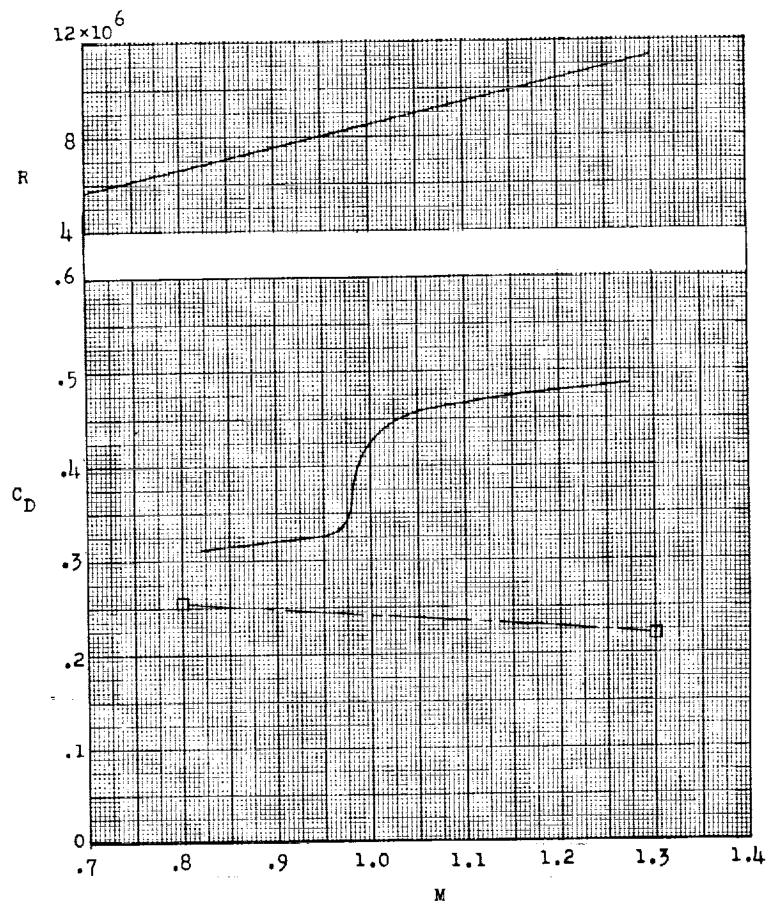

Figure 41.- Concluded.

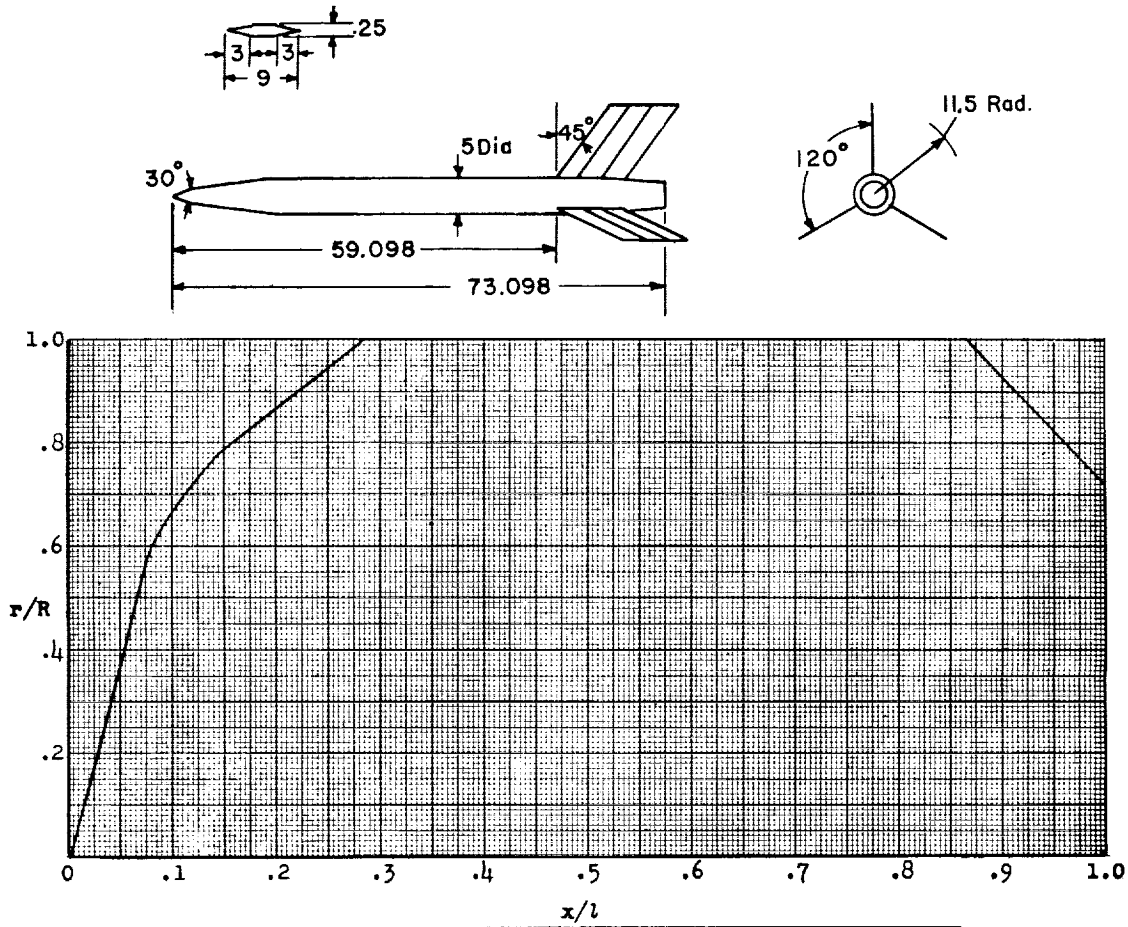

l/d_{Total}	14.6	l/d_{Nose}	4.10	S_b/A	52.3	A_b/A	.52
l/d_{N+A}	6.10	l/d_{Aft}	2.00	S_f/A	24.6	θ_b	4.02°

Designation: 34

Test: Rocket

Remarks: See figure 41.

Figure 42.

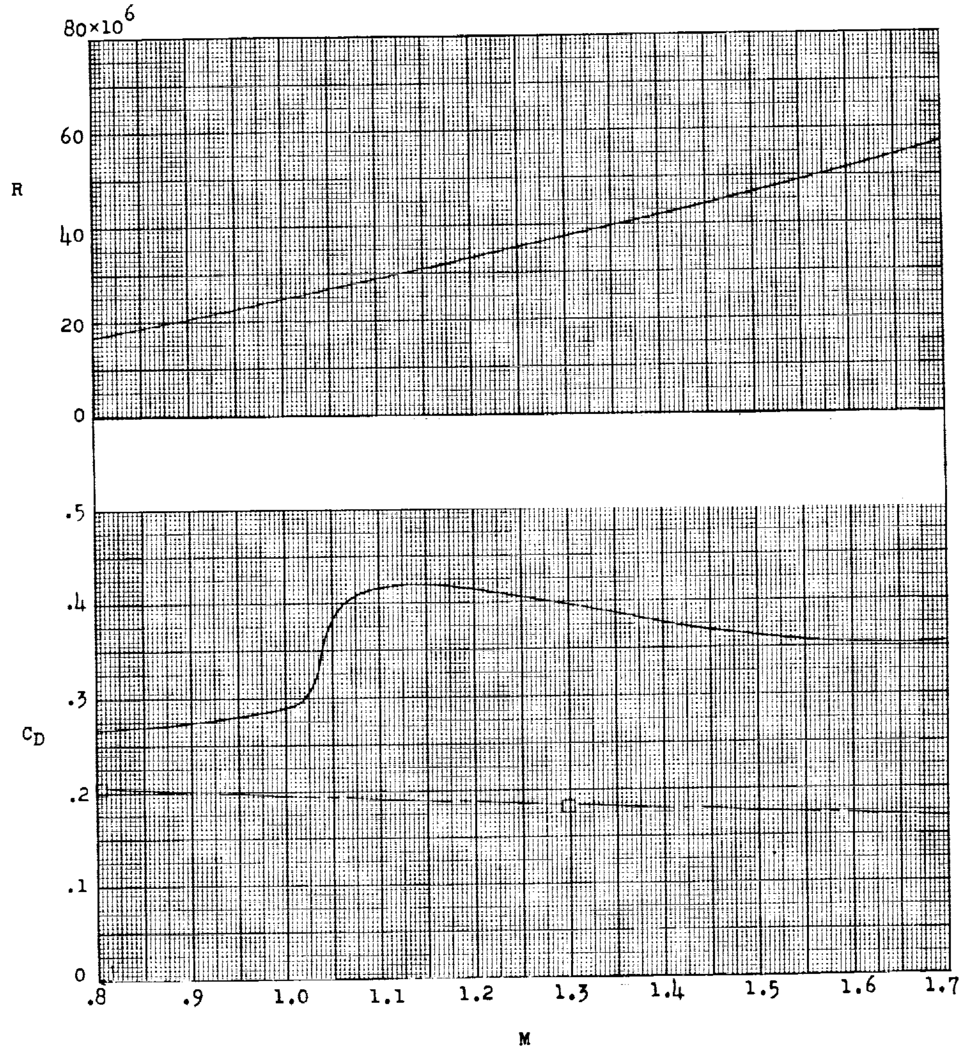

Figure 42.- Concluded.

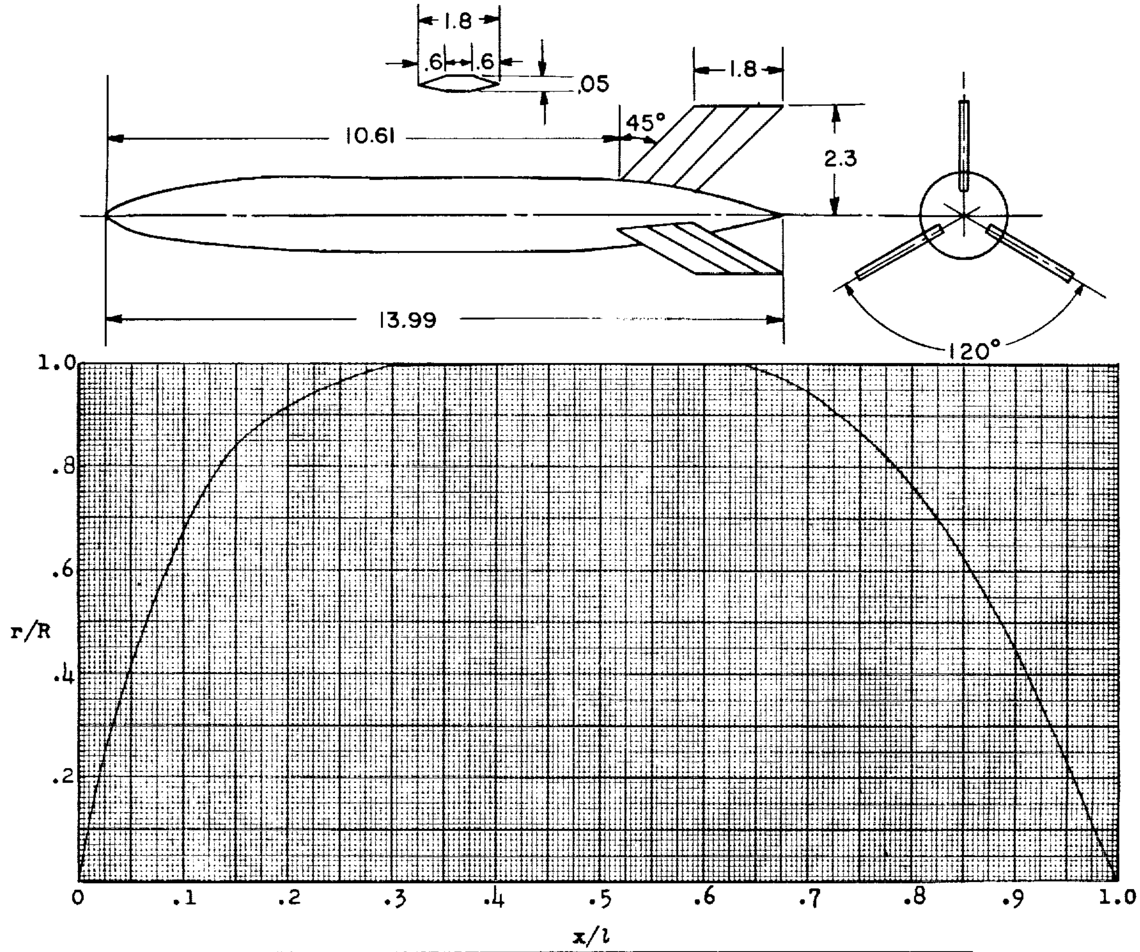

l/d_{Total}	9.32	l/d_{Nose}	2.98	S_b/A	30.20	A_b/A	0.0
l/d_{N+A}	6.42	l/d_{Aft}	3.44	S_f/A	11.0	θ_b	13.3°

Designation: 35

Test: Helium Gun

Figure 43.

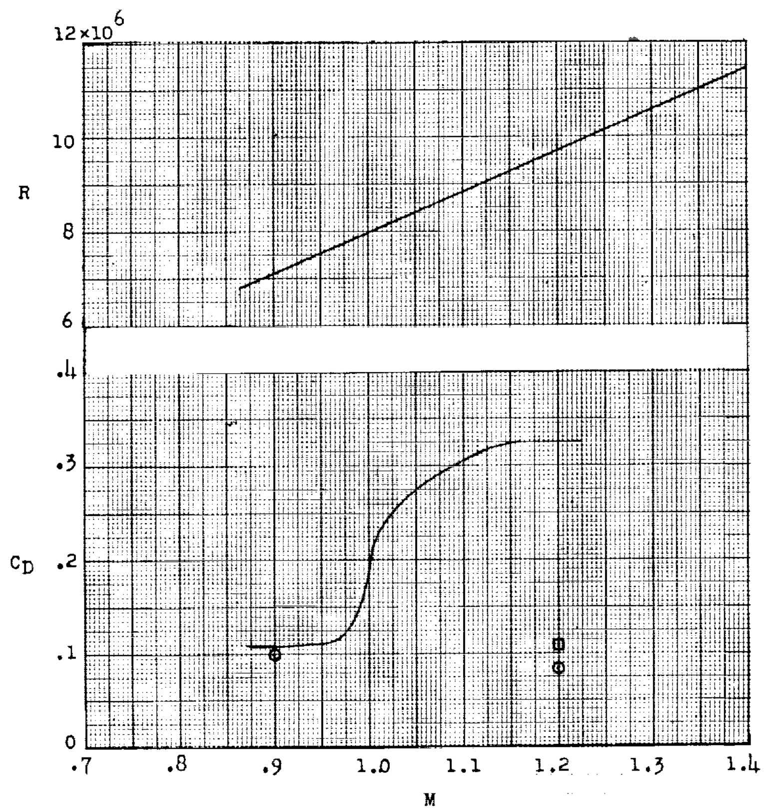

Figure 43.- Concluded.

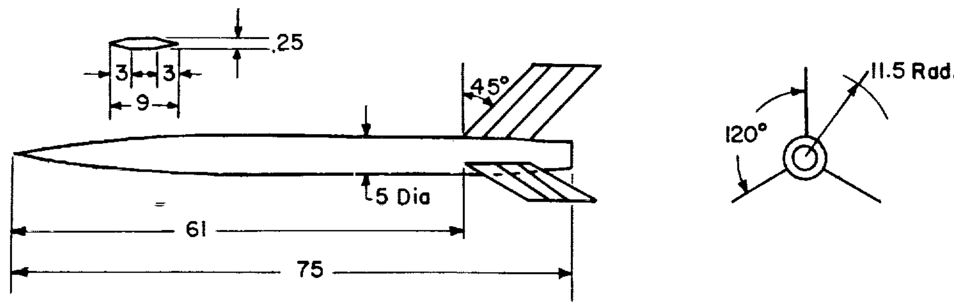

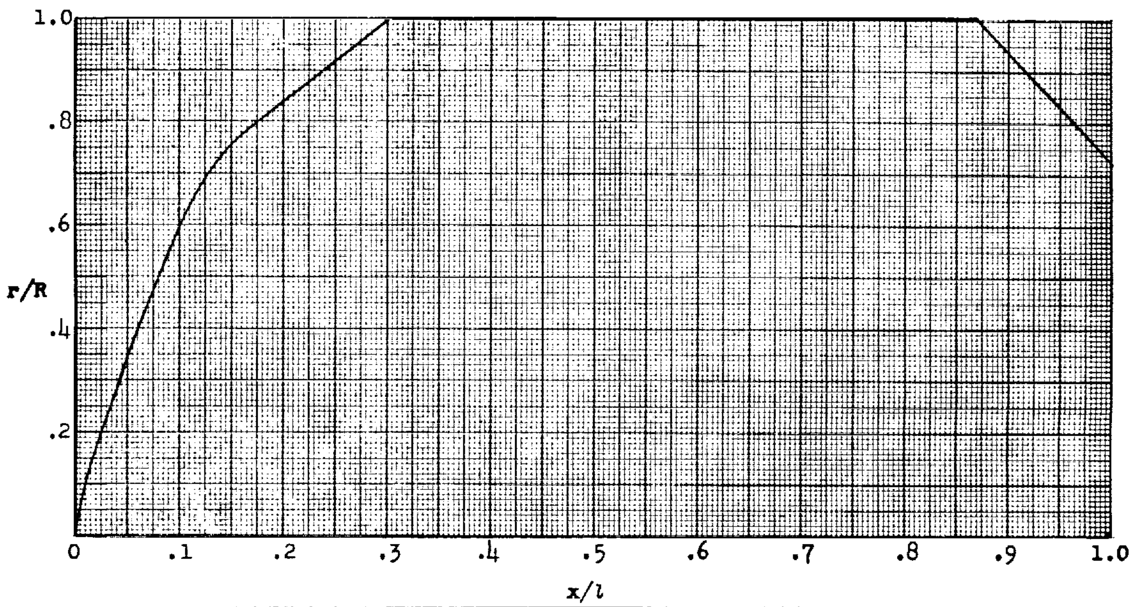

l/d_{Total}	15.00	l/d_{Nose}	4.50	S_b/A	52.6	A_b/A	.52
l/d_{N+A}	6.50	l/d_{Aft}	2.00	S_f/A	24.6	θ_b	4.02°

Designation: 36

Test: Rocket

Remarks: See figure 41.

Figure 44.

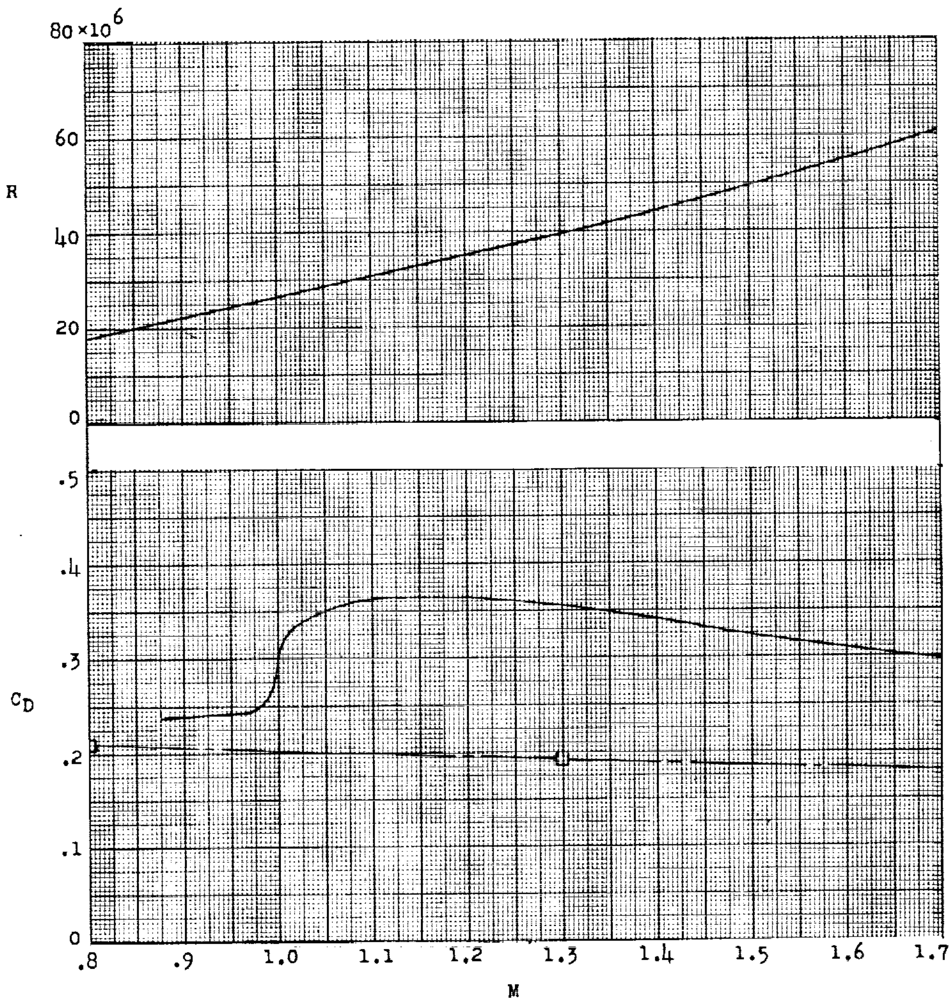

Figure 44.- Concluded.

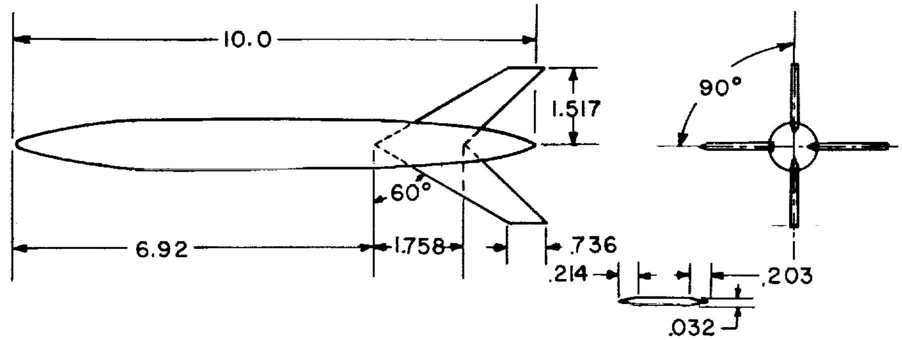

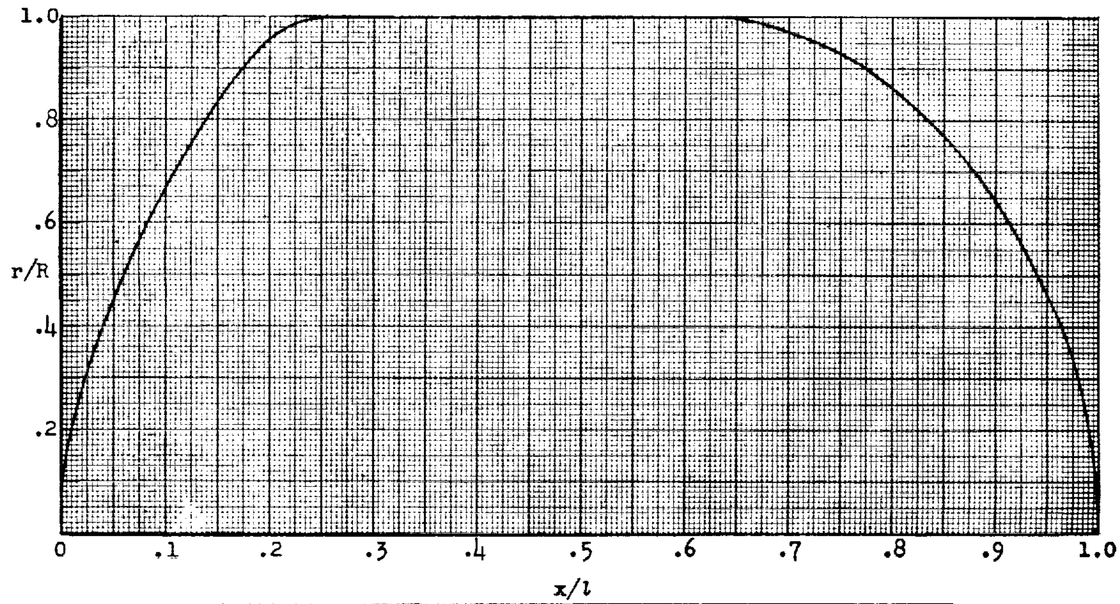

l/d_{Total}	10.87	l/d_{Nose}	2.71	S_b/A	35.6	A_b/A	.0
l/d_{N+A}	6.51	l/d_{Aft}	3.8	S_f/A	12.82	θ_b	60°

Designation: 37

Test: **Helium Gun**

Remarks: Nondimensional ordinates identical to configuration 10 (fig. 18).

Figure 45.

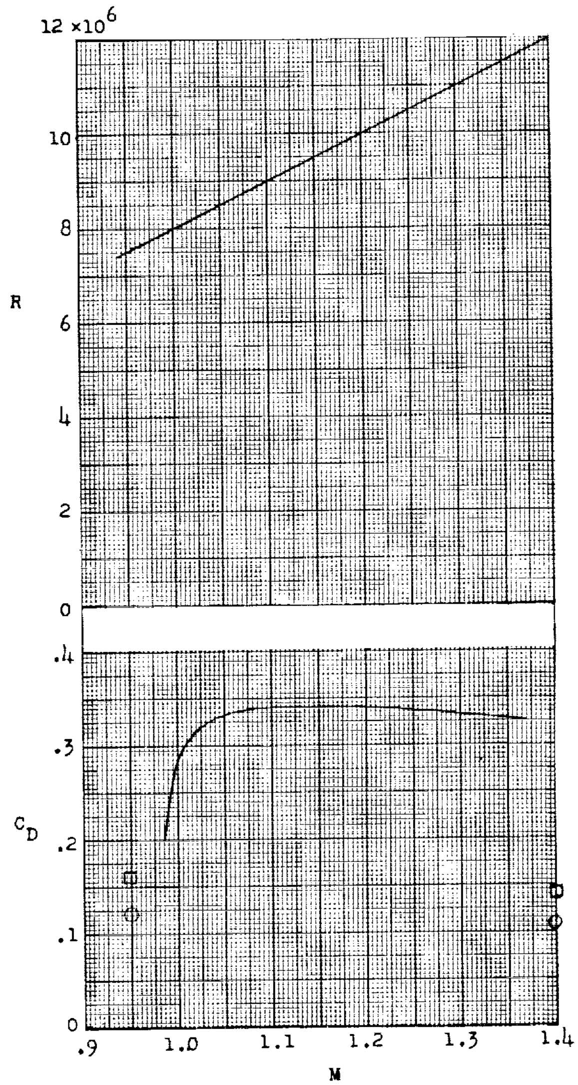

Figure 45.- Concluded.

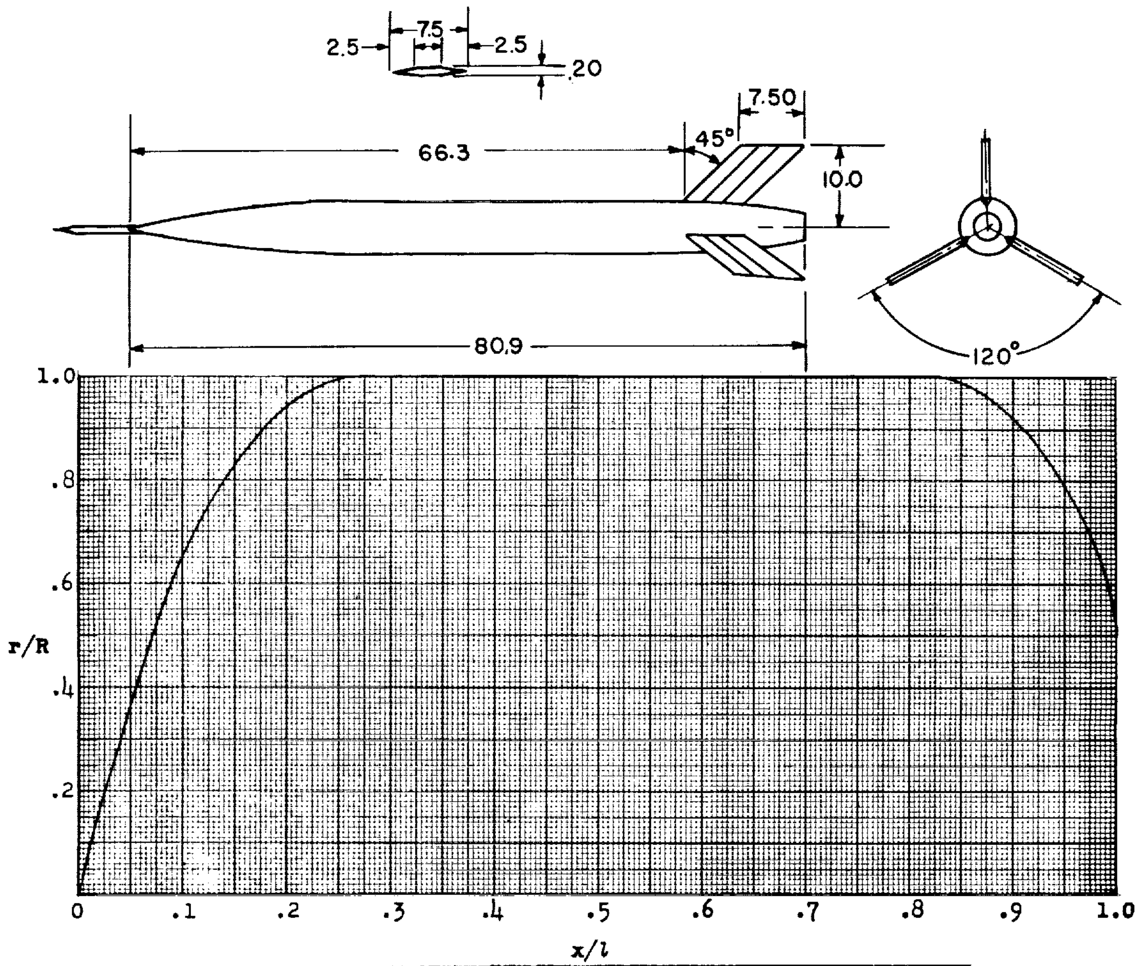

l/d_{Total}	13.9	l/d_{Nose}	3.80	S_b/A	49.6	A_b/A	.25
l/d_{N+A}	6.52	l/d_{Aft}	2.72	S_f/A	12.4	θ_b	17.4°

Designation: 38

Test: Rocket

Remarks: Spike can affect friction drag but is not likely to affect pressure drag.

Figure 46.

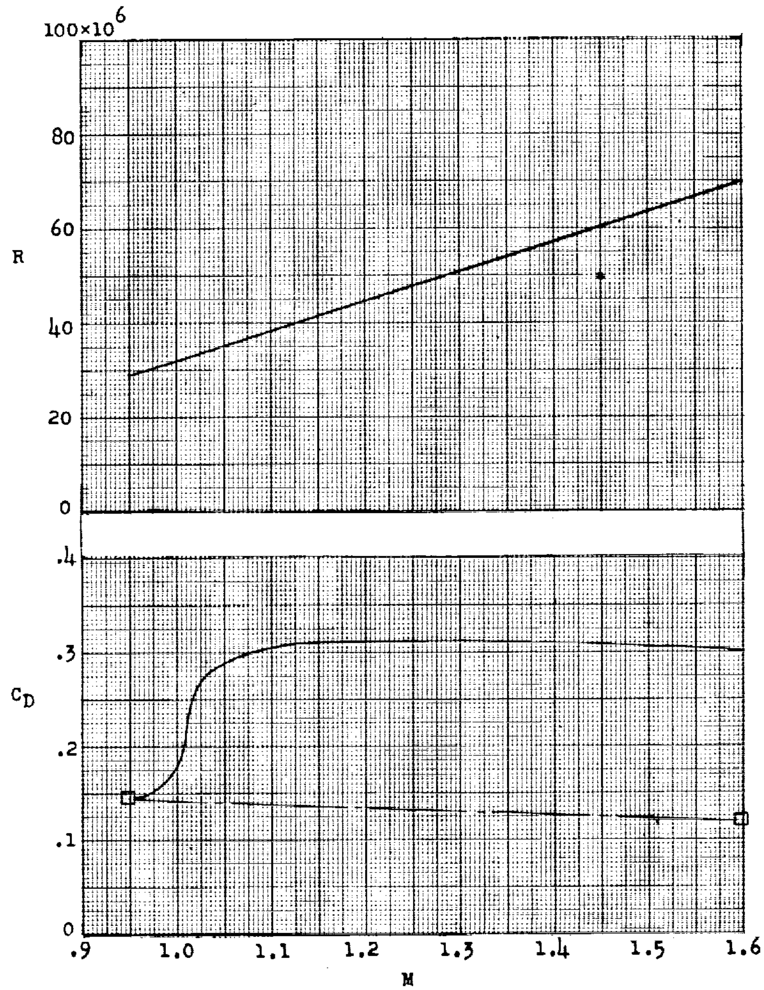

Figure 46.- Concluded.

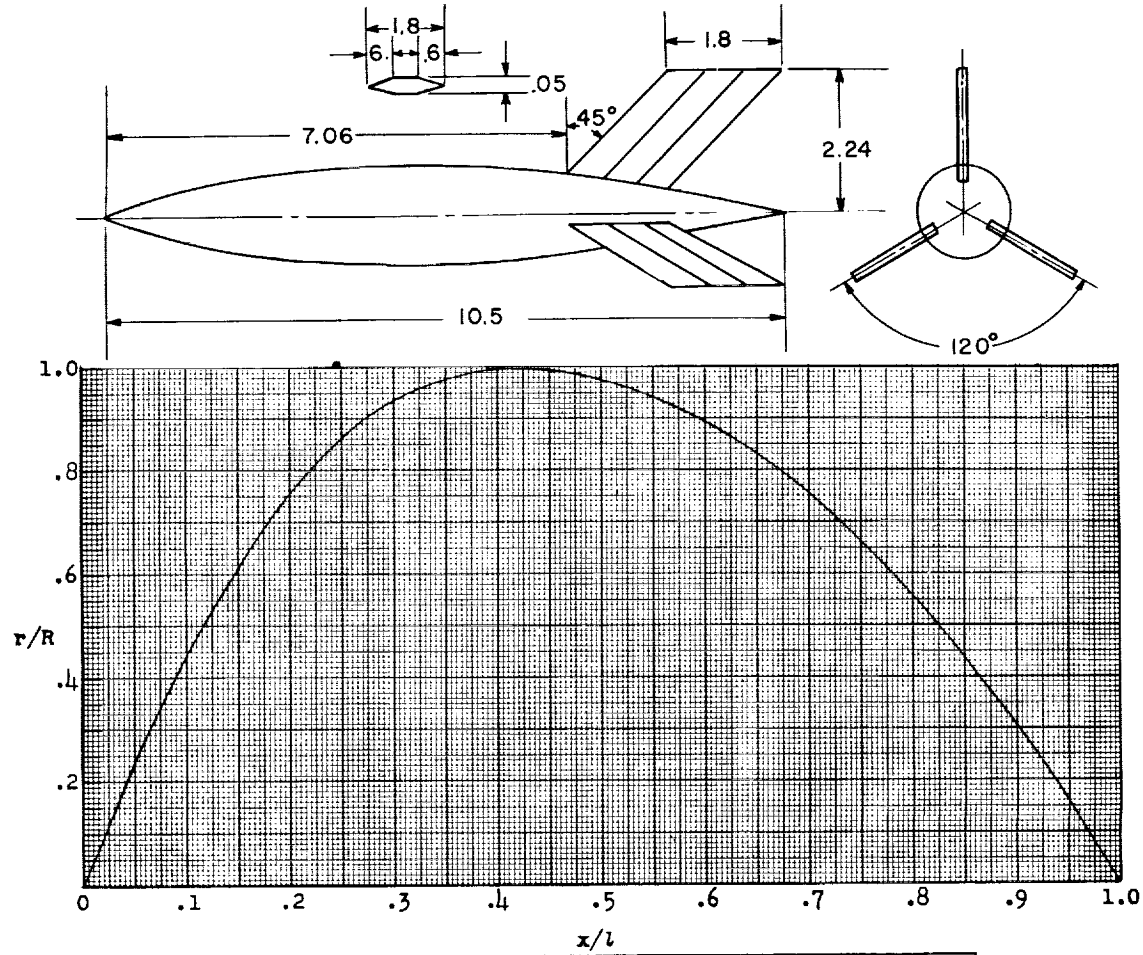

l/d_{Total}	7.00	l/d_{Nose}	2.80	S_b/A	19.00	A_b/A	0.0
l/d_{N+A}	7.00	l/d_{Aft}	4.20	S_f/A	11.0	θ_b	12.9°

Designation: 39

Test: **Helium Gun**

Figure 47.

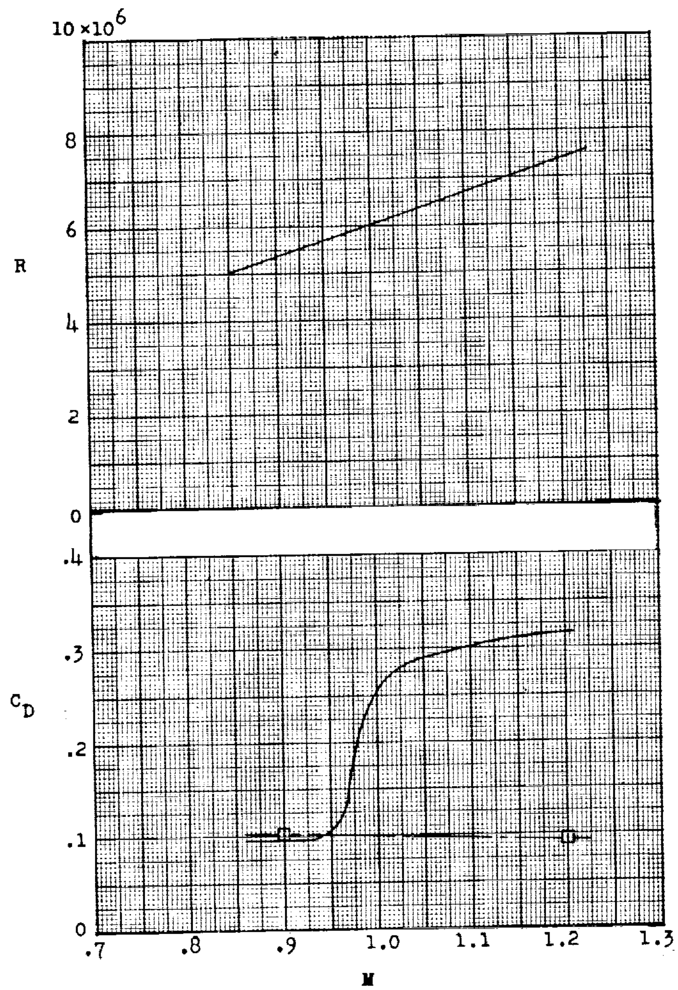

Figure 47.- Concluded.

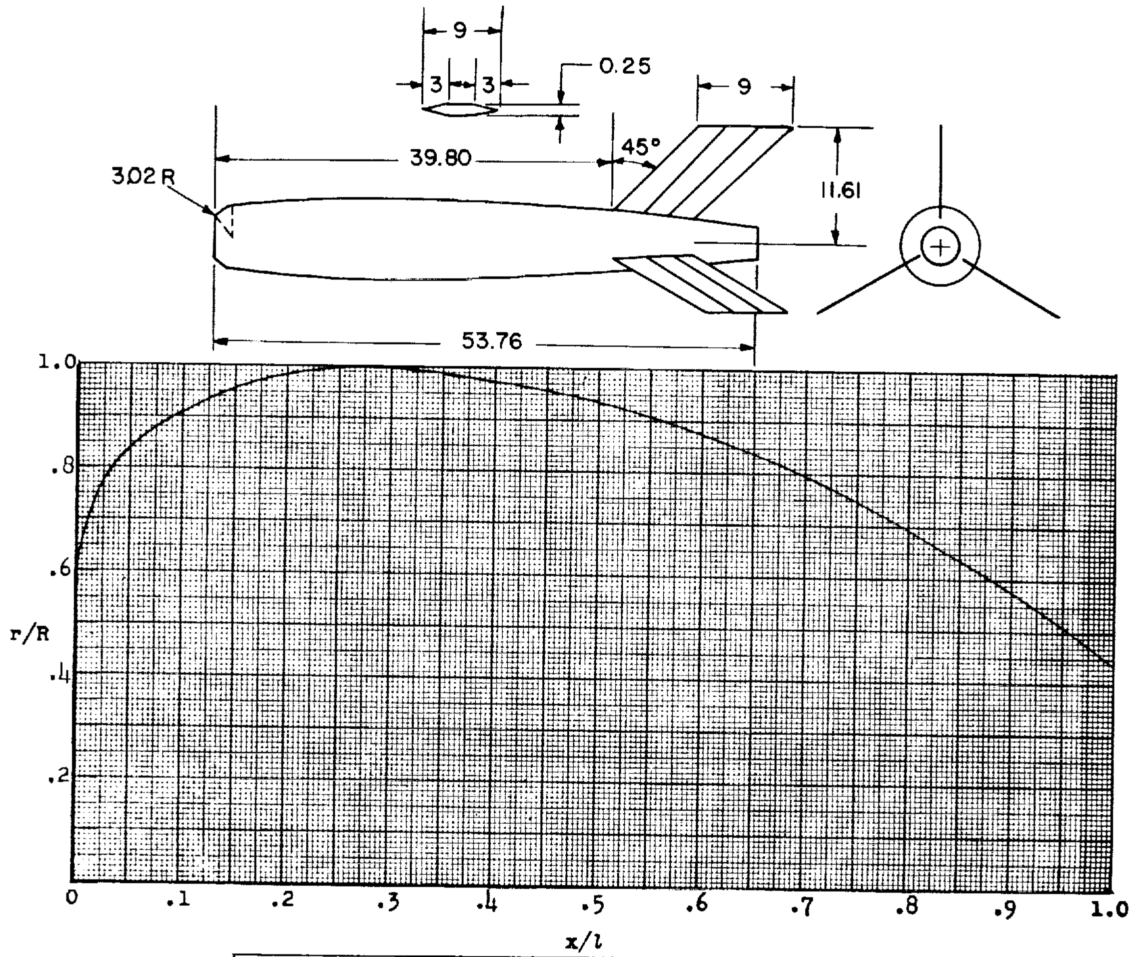

l/d_{Total}	7.16	l/d_{Nose}	1.81	S_b/A	24.00	A_b/A	.19
l/d_{N+A}	7.16	l/d_{Aft}	5.35	S_f/A	11.0	θ_b	7°

Designation: 40

Test: Rocket

Remarks: Flat nose having $r/R = 0.57$ flaired into parabolic segment by 3.02 radius; parabolic afterbody.

Figure 48.

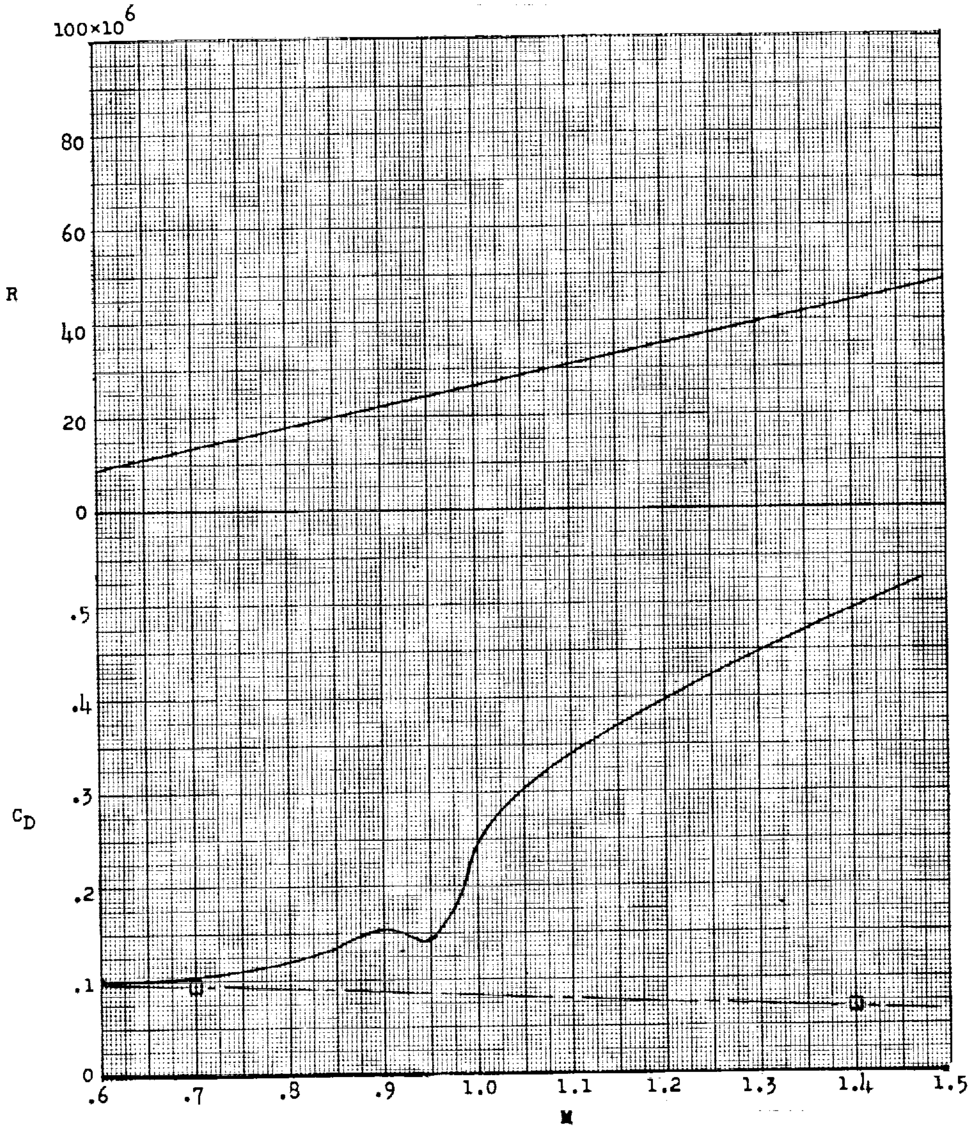

Figure 48.- Concluded.

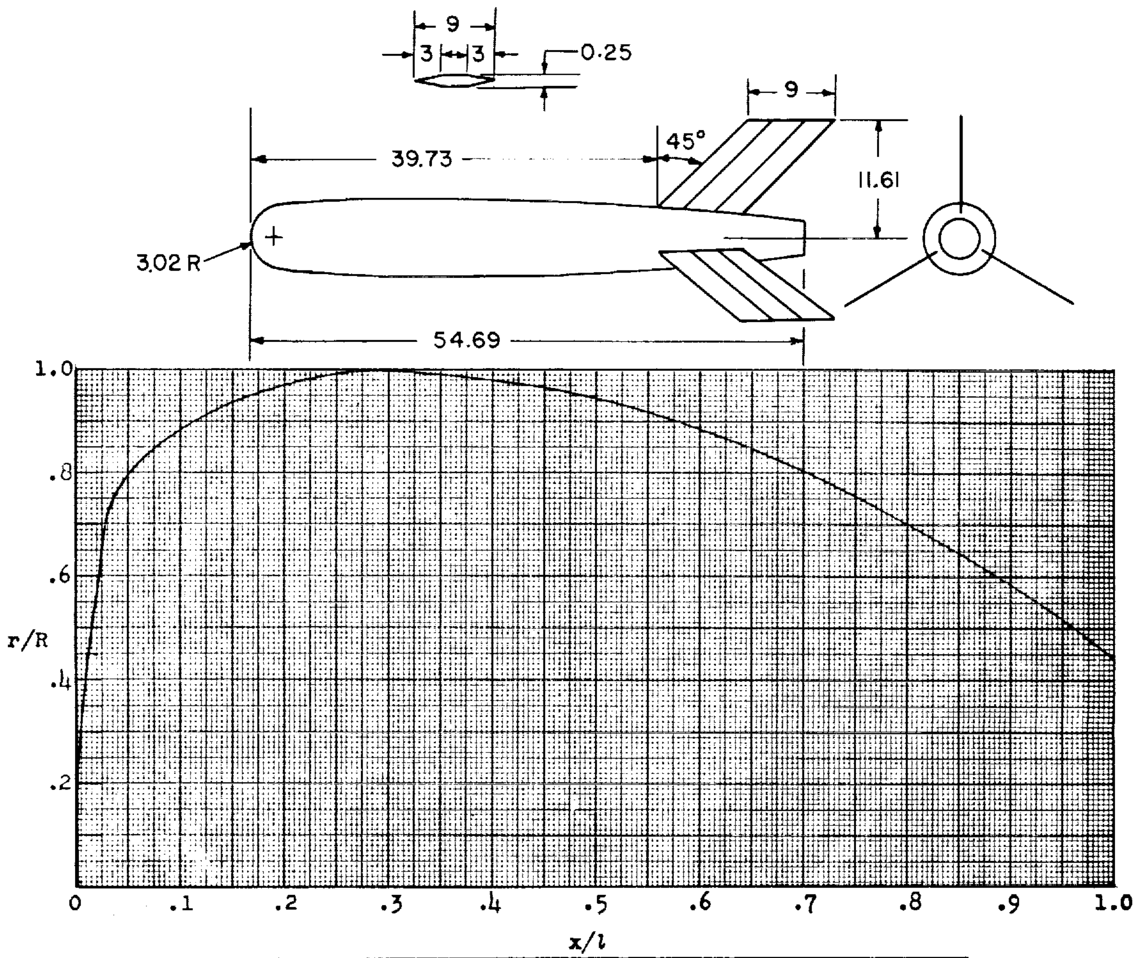

l/d_{Total}	7.30	l/d_{Nose}	1.95	S_b/A	24.2	A_b/A	.19
l/d_{N+A}	7.30	l/d_{Aft}	5.35	S_f/A	11.0	θ_b	7°

Designation: 41

Test: Rocket

Remarks: Nose consists of hemispherical segment plus parabolic segment; parabolic afterbody.

Figure 49.

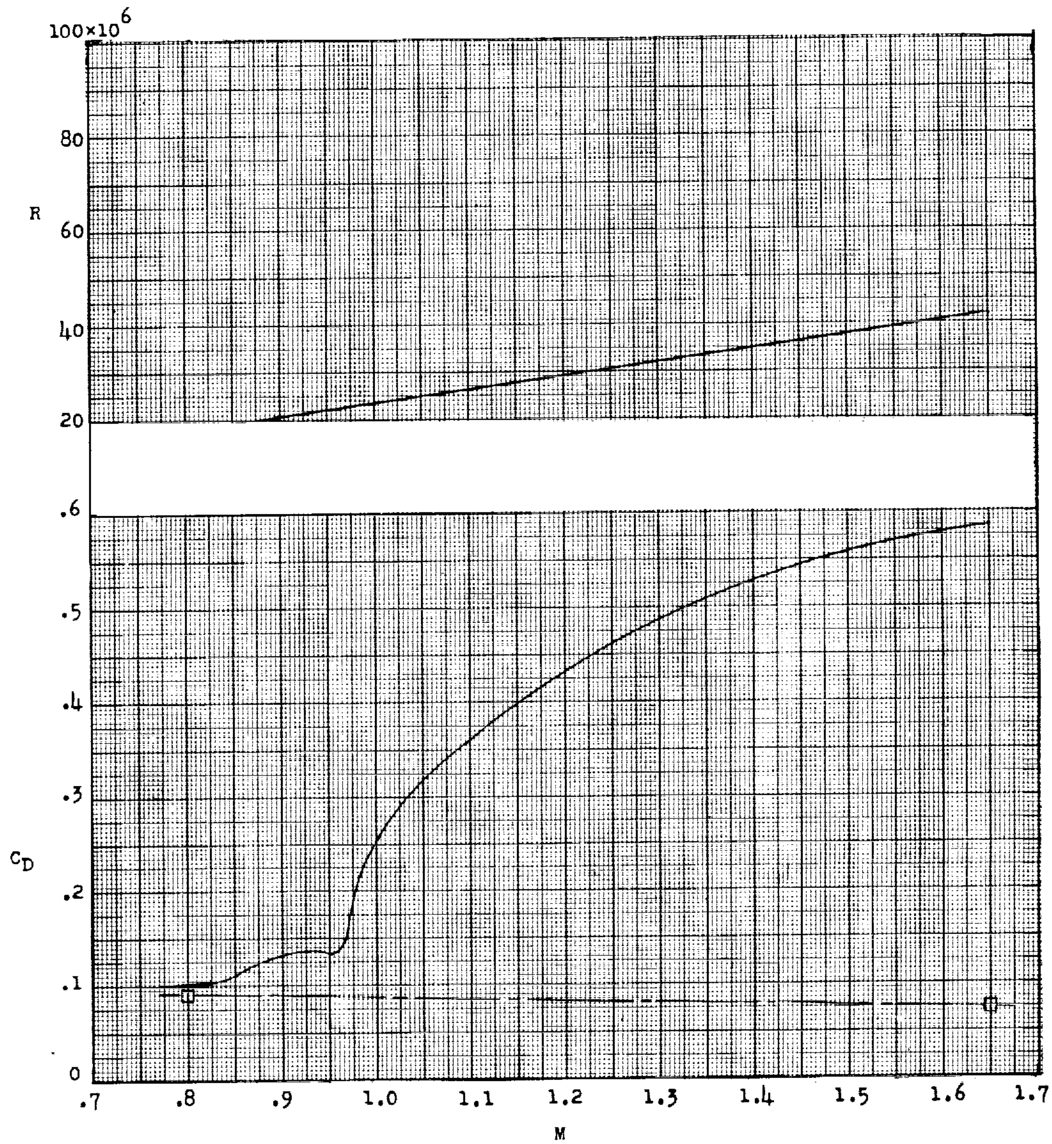

Figure 49.- Concluded.

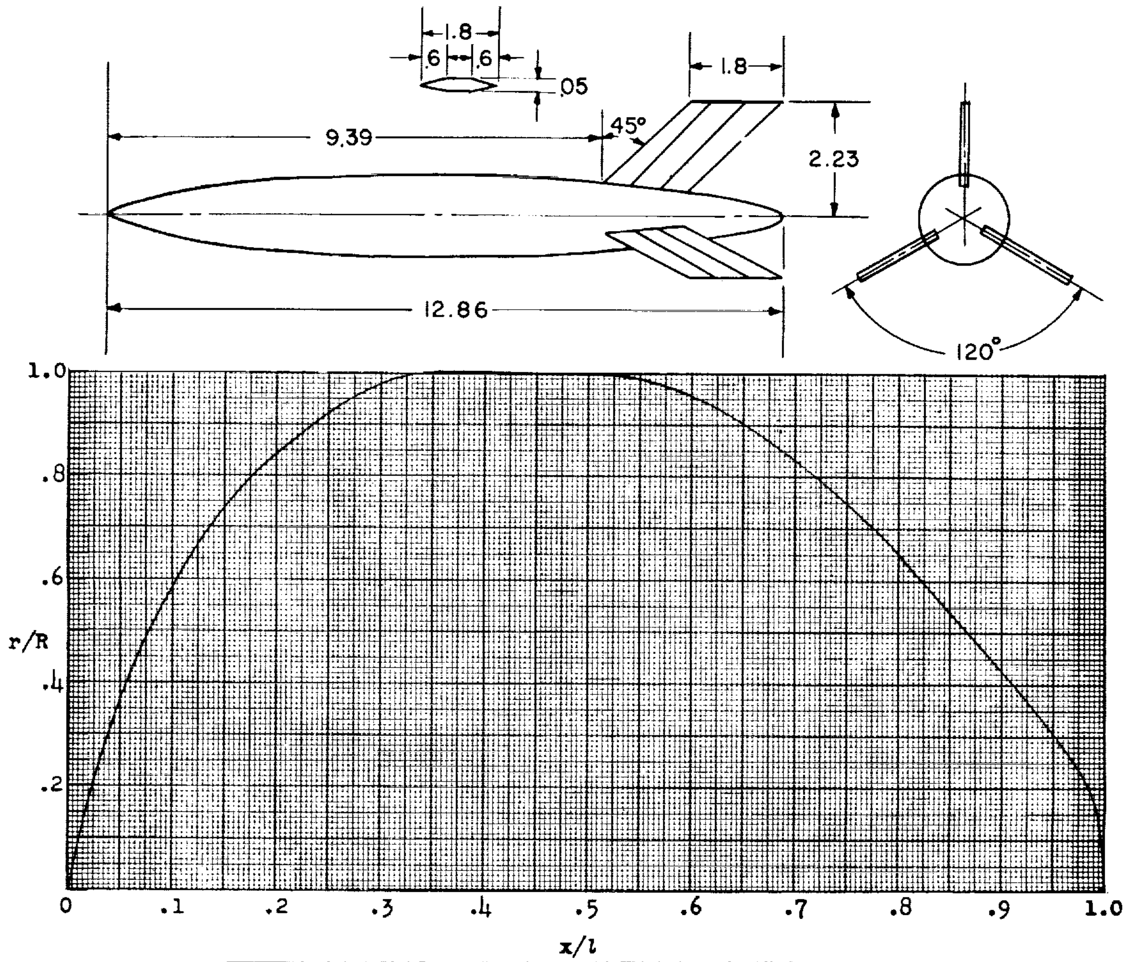

l/d_{Total}	8.57	l/d_{Nose}	3.02	S_b/A	25.60	A_b/A	0.0
l/d_{N+A}	7.33	l/d_{Aft}	4.31	S_f/A	11.0	θ_b	90°

Designation: 42

Test: Helium Gun

Figure 50.

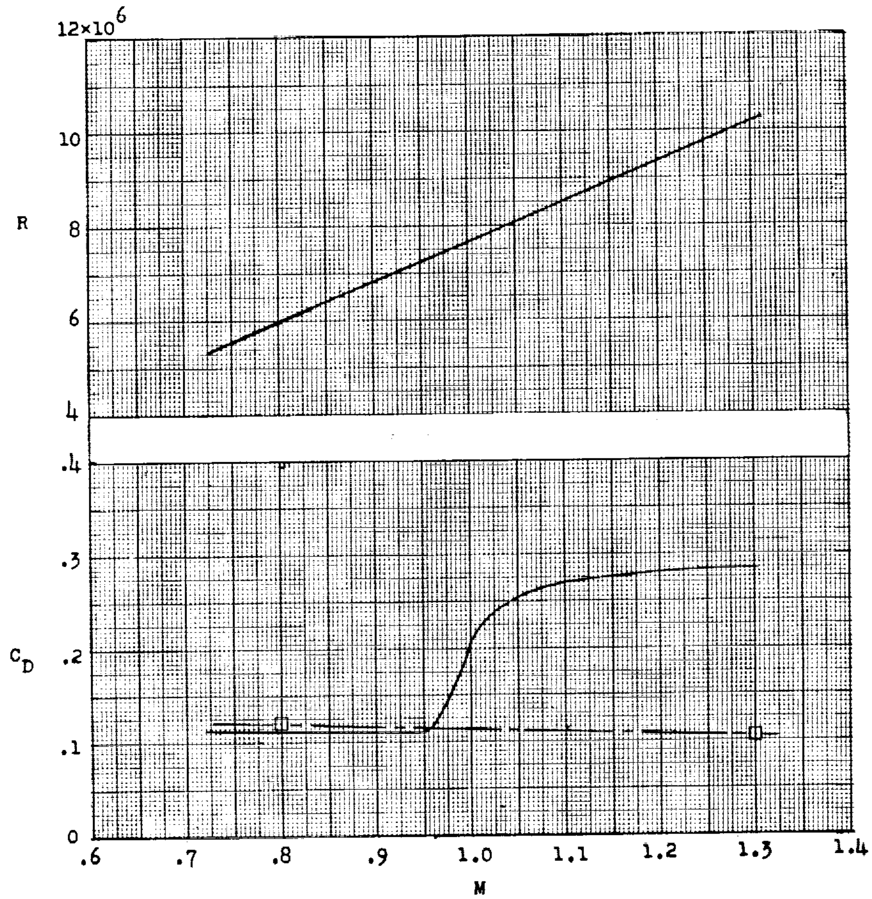

Figure 50.- Concluded.

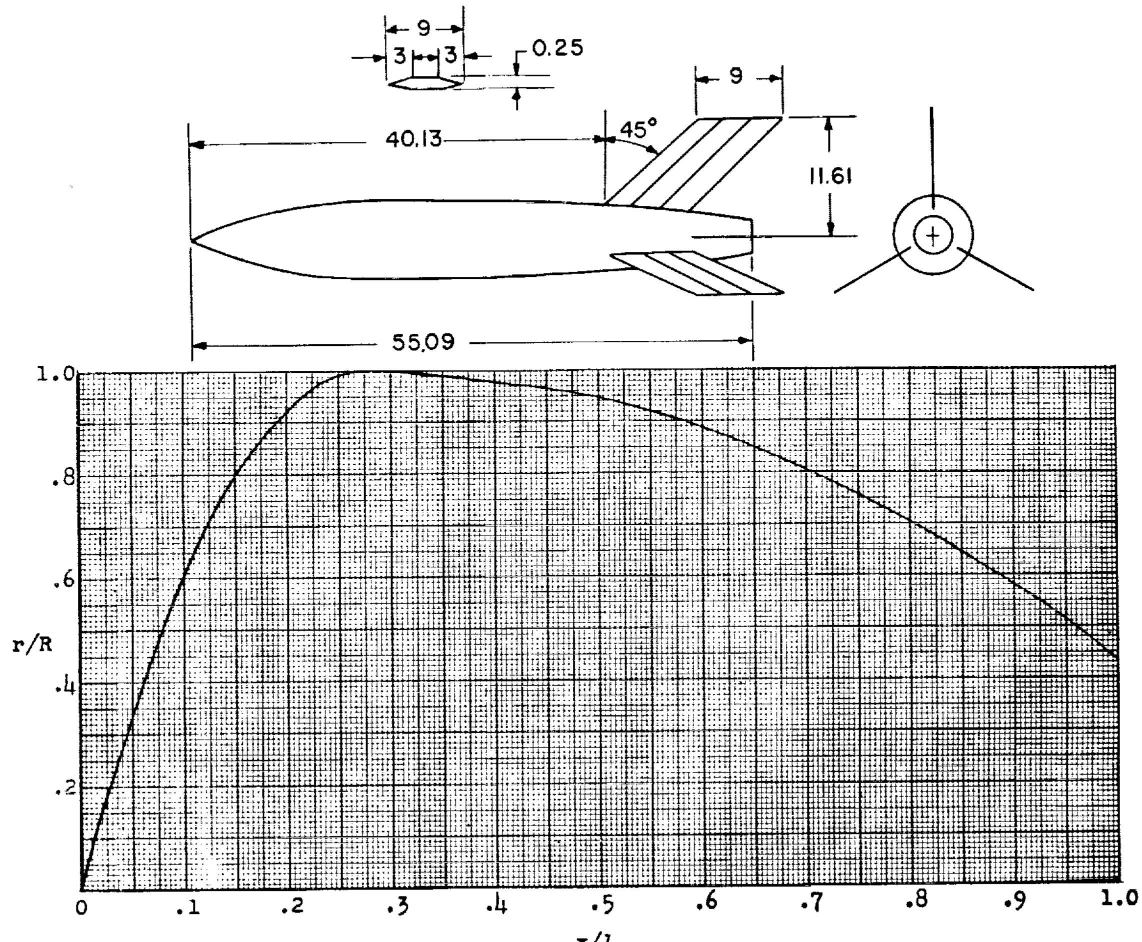

l/d_{Total}	7.35	l/d_{Nose}	2.0	S_b/A	22.70	A_b/A	.19
l/d_{N+A}	7.35	l/d_{Aft}	5.35	S_f/A	11.0	θ_b	6°

Designation: 43

Test: Rocket

Remarks: Parabolic nose and afterbody.

Figure 51.

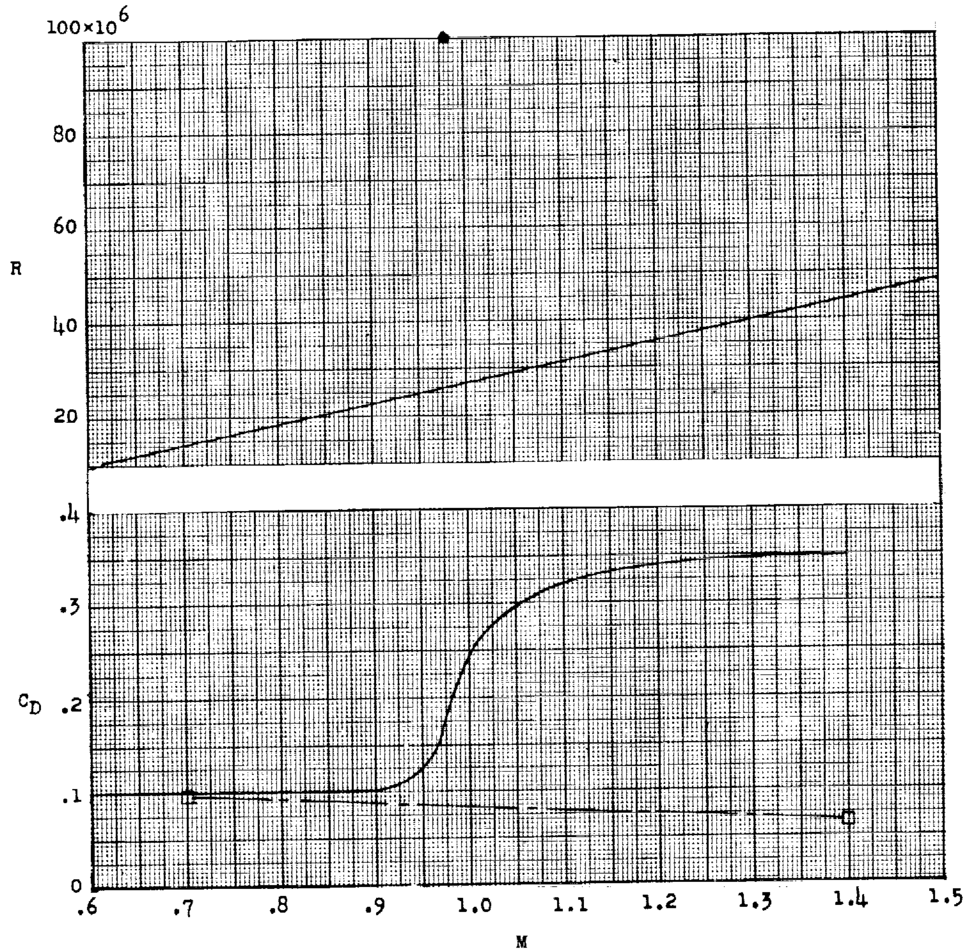

Figure 51.- Concluded.

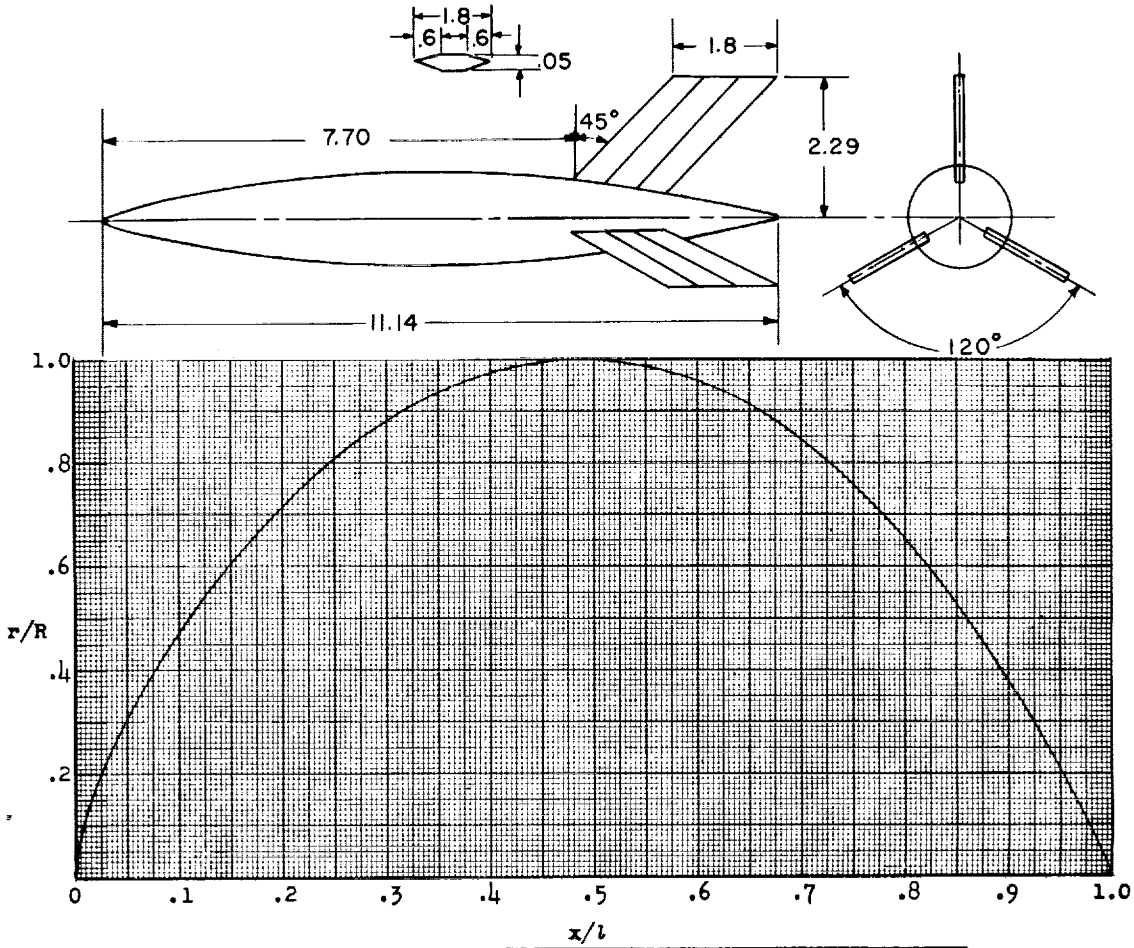

l/d_{Total}	7.43	l/d_{Nose}	3.58	S_b/A	20.90	A_b/A	0.0
l/d_{N+A}	7.43	l/d_{Aft}	3.85	S_f/A	11.0	θ_b	15.0°

Designation: 44

Test: Helium Gun

Figure 52.

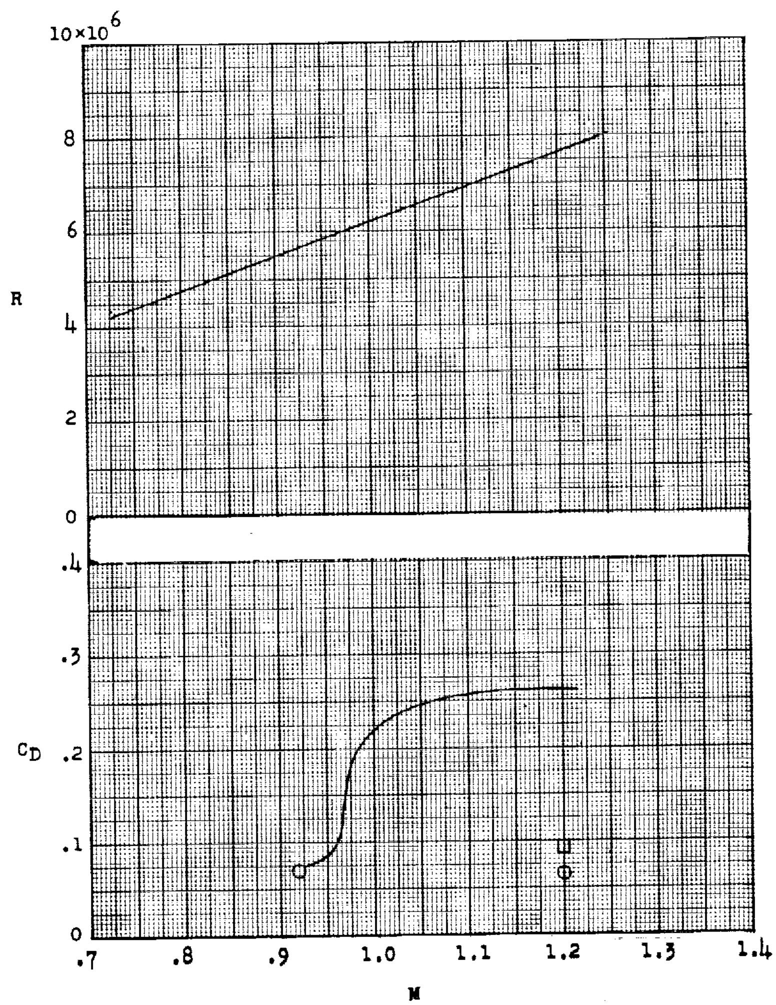

Figure 52.- Concluded.

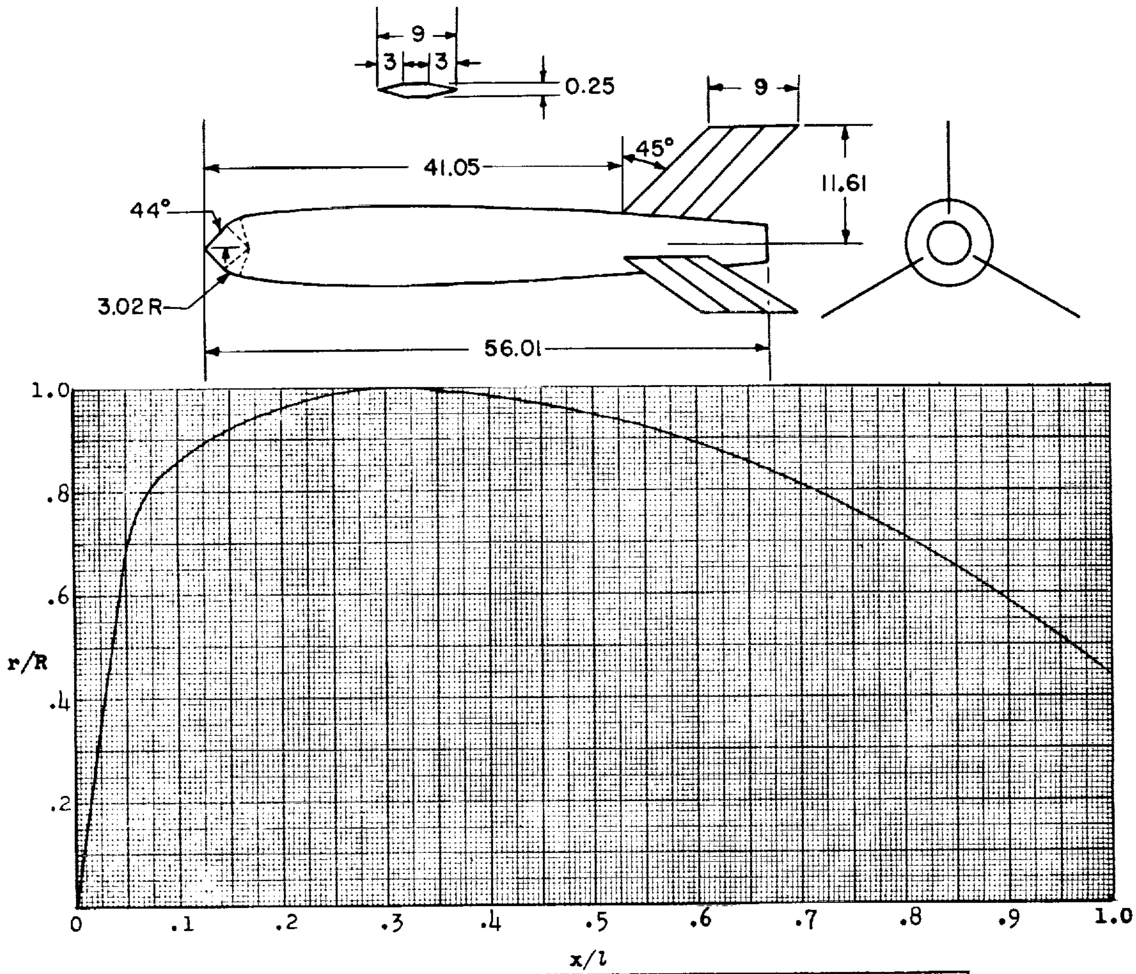

l/d_{Total}	7.47	l/d_{Nose}	2.12	S_b/A	24.30	A_b/A	.19
l/d_{N+A}	7.47	l/d_{Aft}	5.35	S_f/A	11.0	θ_b	6°

Designation: 45

Test: Rocket

Remarks: Conical nose with hemispherical and parabolic segments; parabolic afterbody.

Figure 53.

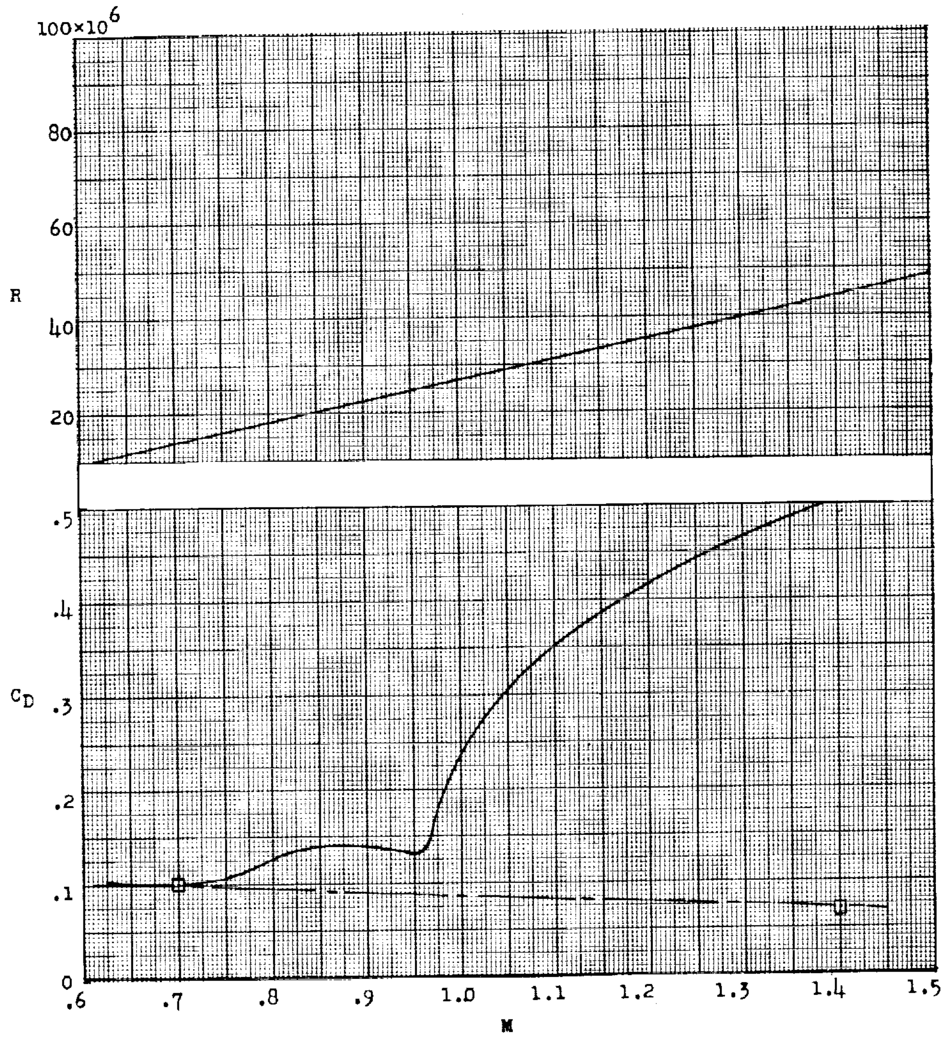

Figure 53.- Concluded.

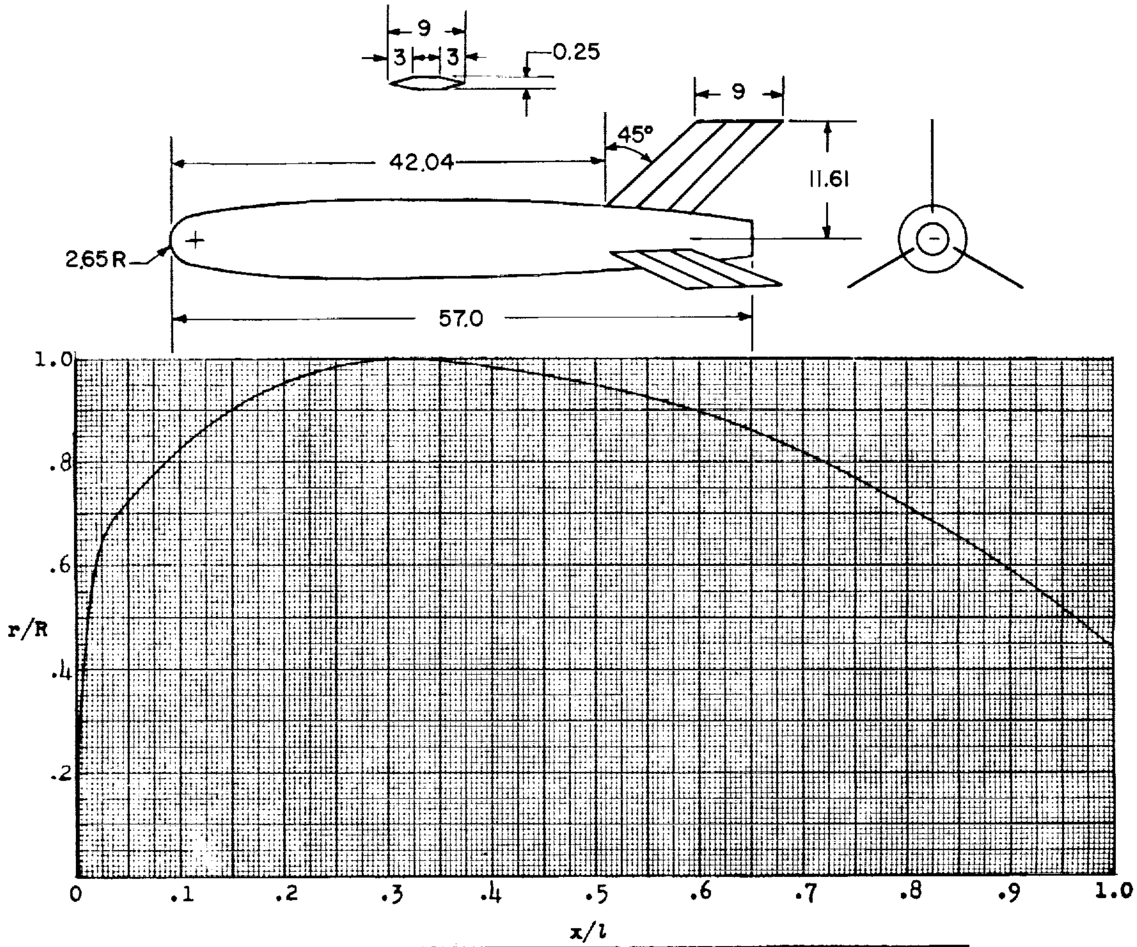

l/d_{Total}	7.60	l/d_{Nose}	2.25	S_b/A	25.10	A_b/A	.19
l/d_{N+A}	7.60	l/d_{Aft}	5.35	S_f/A	11.0	θ_b	7°

Designation: 46

Test: Rocket

Remarks: Nose with hemispherical and parabolic segments; parabolic afterbody.

Figure 54.

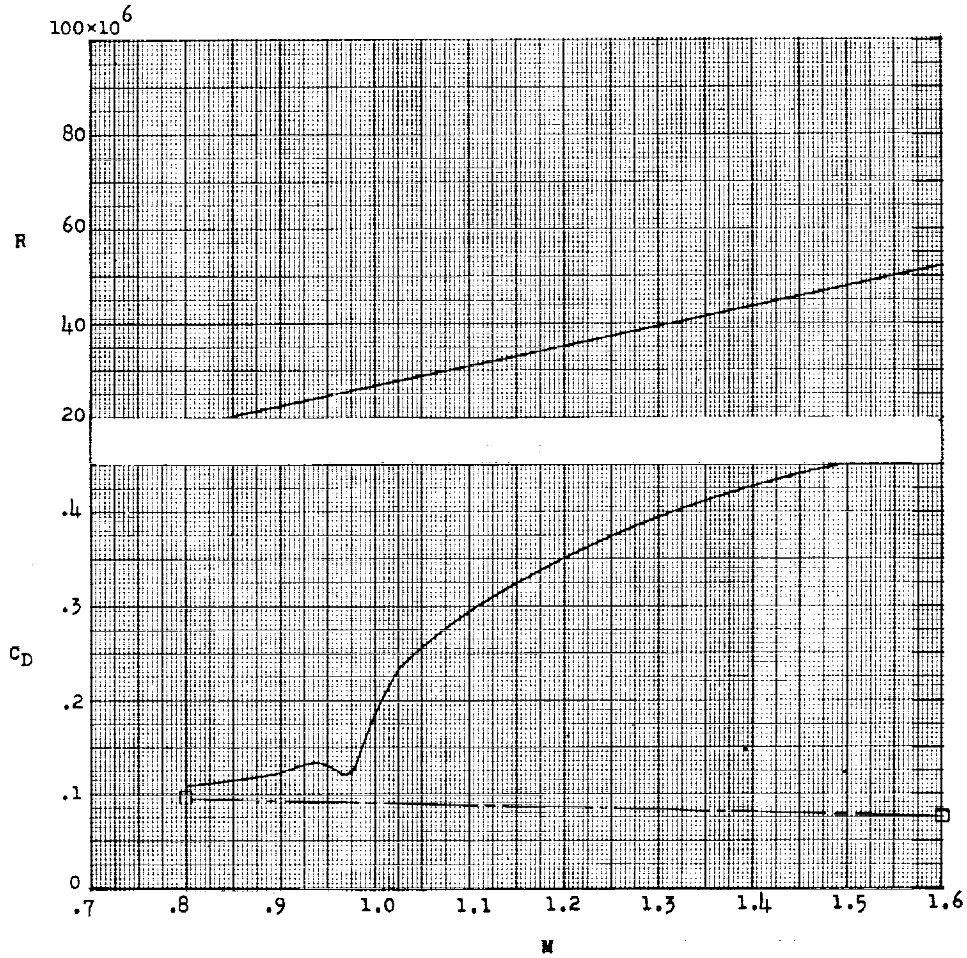

Figure 54.- Concluded.

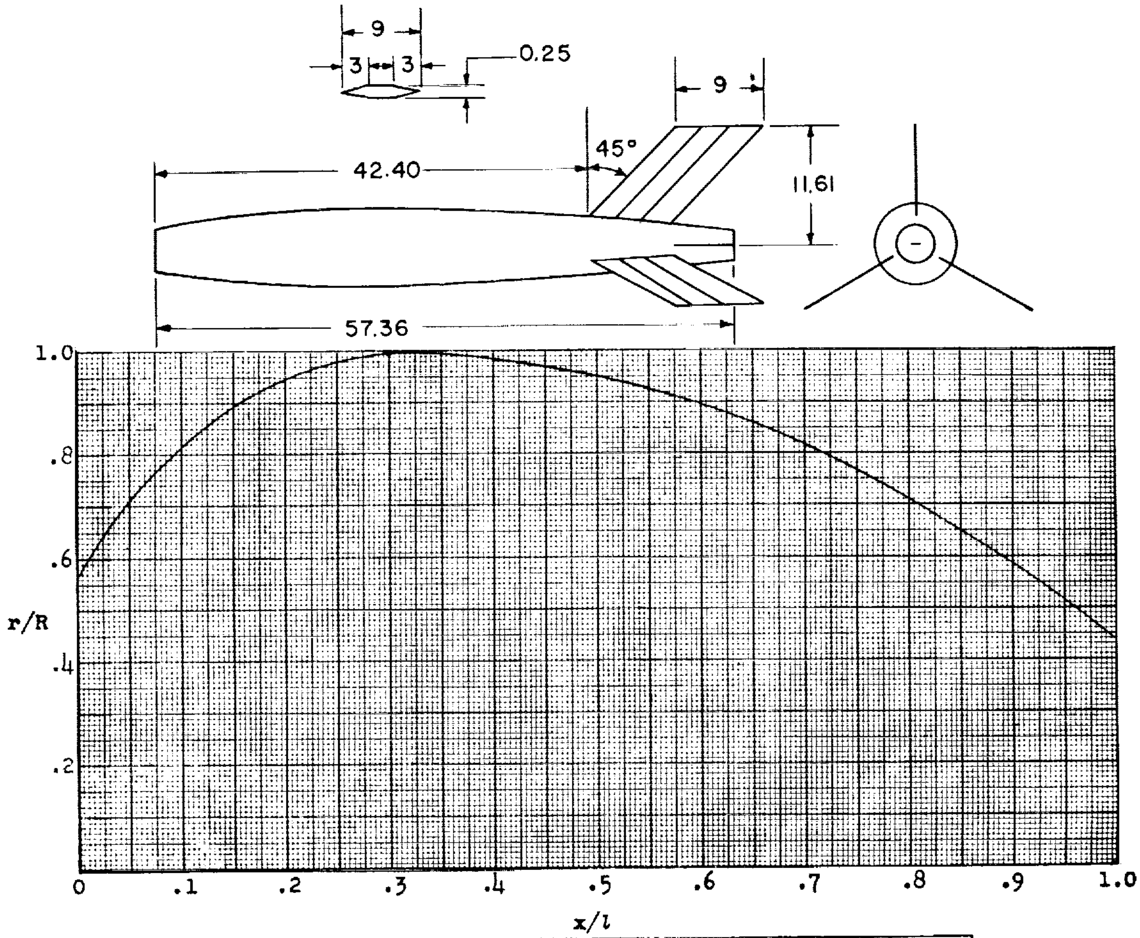

l/d_{Total}	7.66	l/d_{Nose}	2.33	S_b/A	25.3	A_b/A	.19
l/d_{N+A}	7.66	l/d_{Aft}	5.33	S_f/A	11.0	θ_b	7°

Designation: 47

Test: Rocket

Remarks: Nose consists of parabolic segment; parabolic afterbody.

Figure 55.

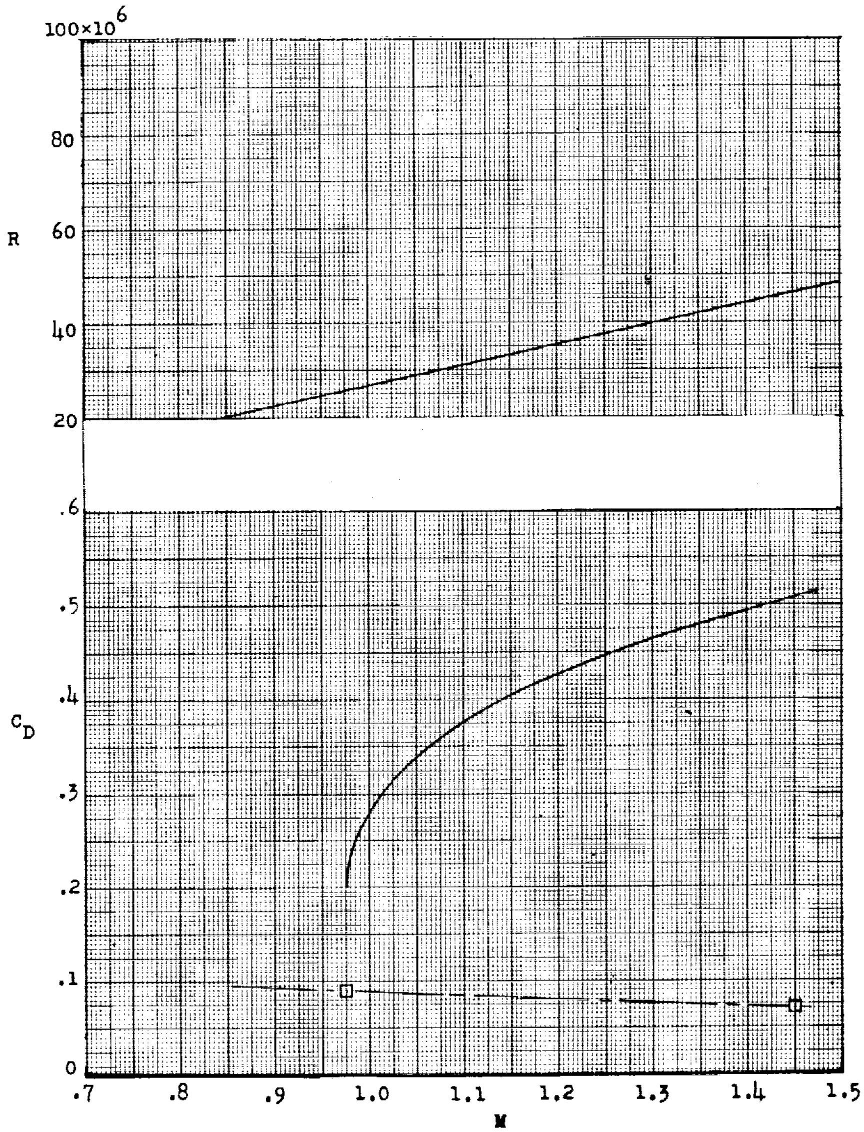

Figure 55.- Concluded.

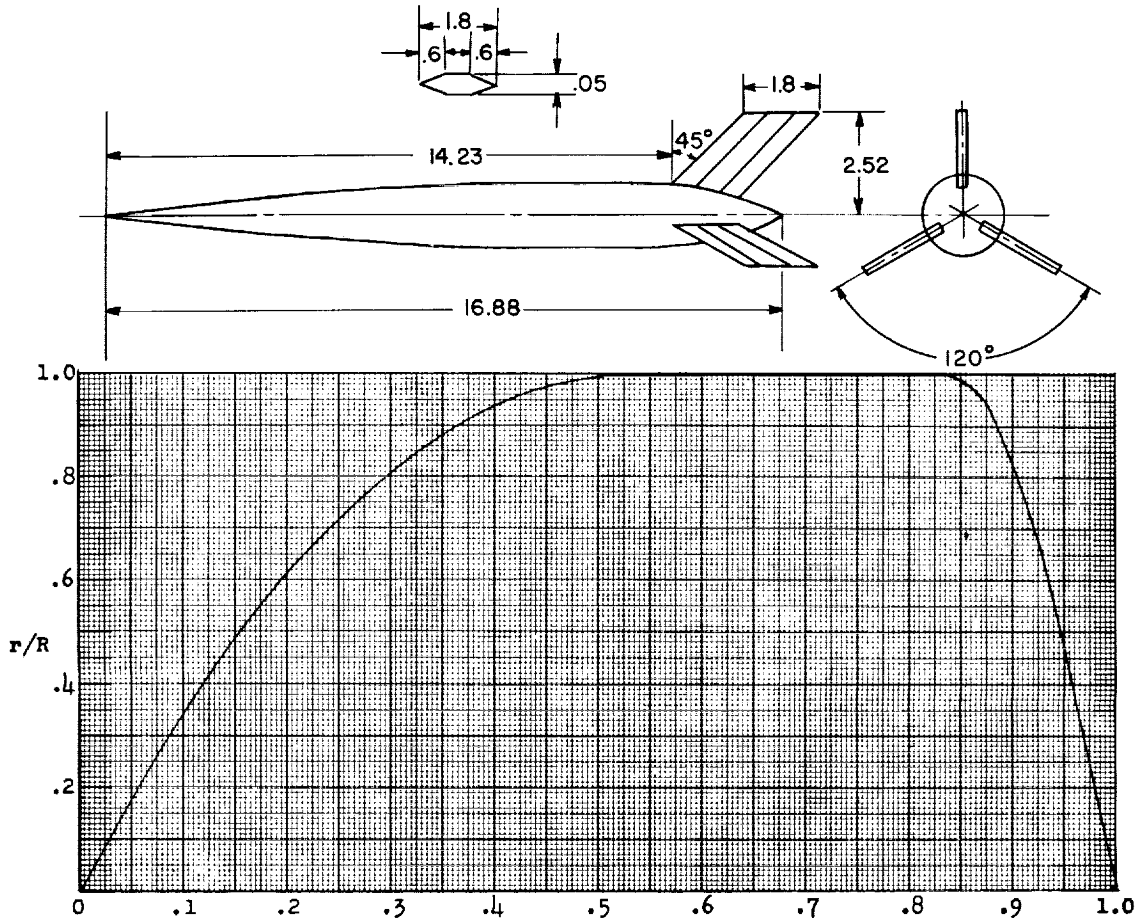

l/d_{Total}	10.9	l/d_{Nose}	6.00	S_b/A	32.6	A_b/A	0.0
l/d_{N+A}	7.72	l/d_{Aft}	1.72	S_f/A	11.0	θ_b	29°

Designation: 48

Test: Helium Gun

Remarks: Body differs from configurations 49 and 50 (figs. 57 and 58) only in removal of Mach 1 area distribution of fins from afterbodies of these models.

Figure 56.

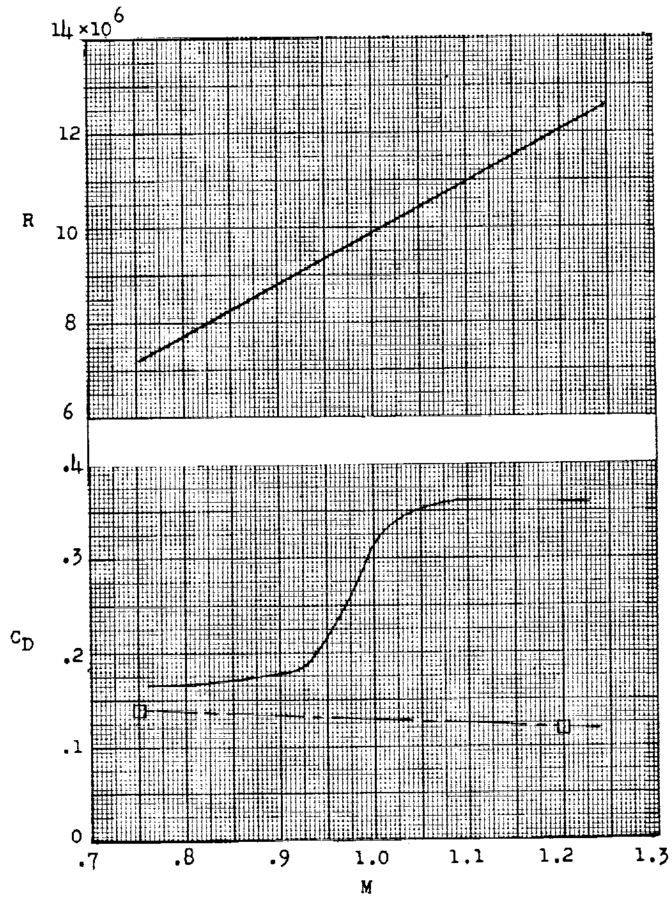

Figure 56.- Concluded.

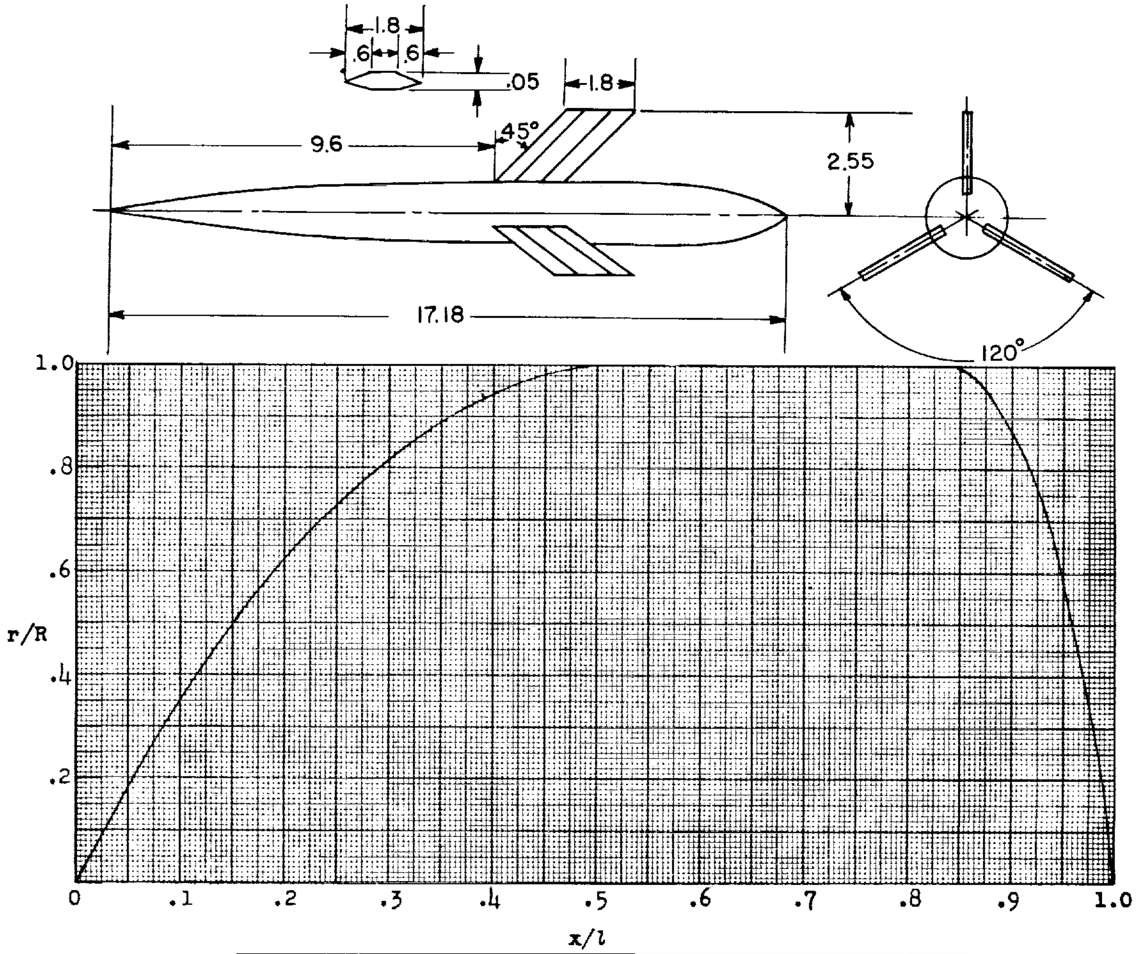

l/d_{Total}	11.50	l/d_{Nose}	6.0	S_b/A	35.50	A_b/A	0.0
l/d_{N+A}	7.78	l/d_{Aft}	1.78	S_f/A	11.0	θ_b	29.5°

Designation: 49

Test: Helium Gun

Remarks: Parabolic nose and afterbody; body identical to configuration 50. (See note for configuration 48 (fig. 56).)

Figure 57.

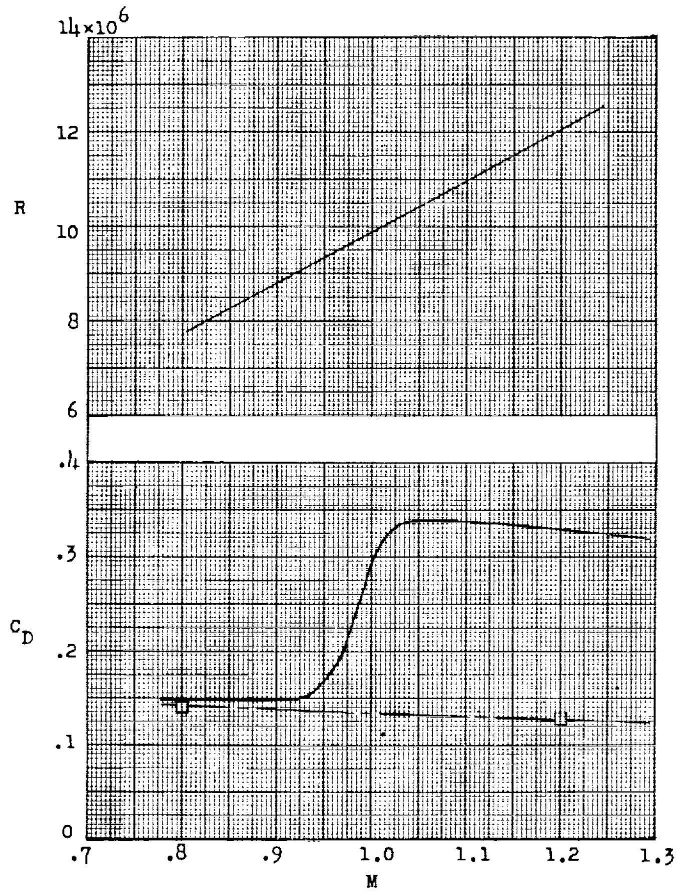

Figure 57.- Concluded.

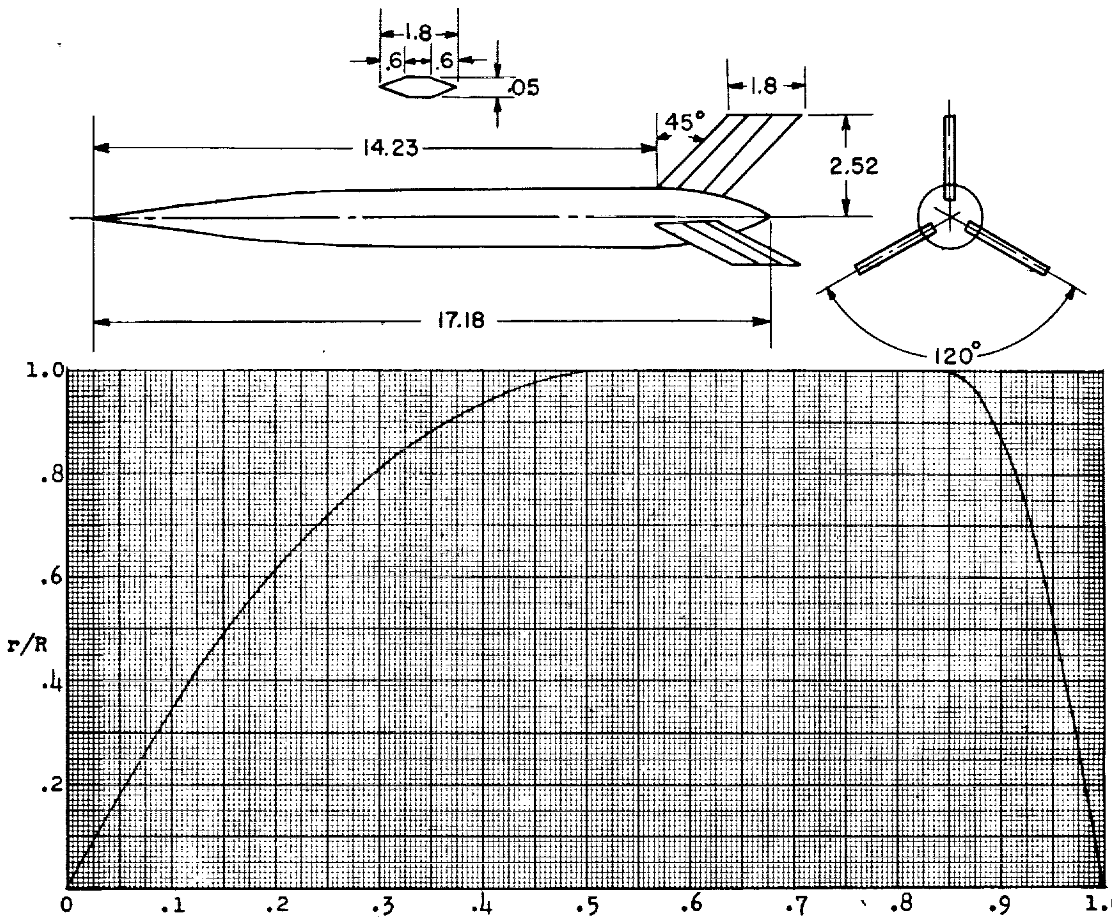

l/d_{Total}	11.5	l/d_{Nose}	6.0	S_b/A	35.5	A_b/A	0.0
l/d_{N+A}	7.78	l/d_{Aft}	1.78	S_f/A	11.0	θ_b	29.3°

Designation: 50

Test: Helium Gun

Remarks: Parabolic nose and afterbody; body identical to configuration 49. (See note for configuration 48 (fig. 56).)

Figure 58.

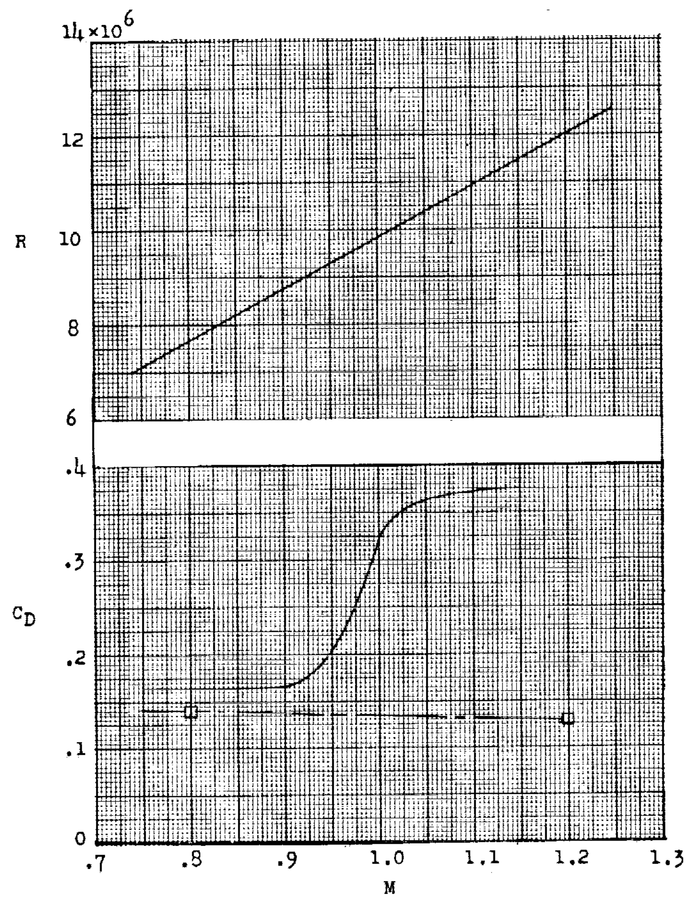

Figure 58.- Concluded.

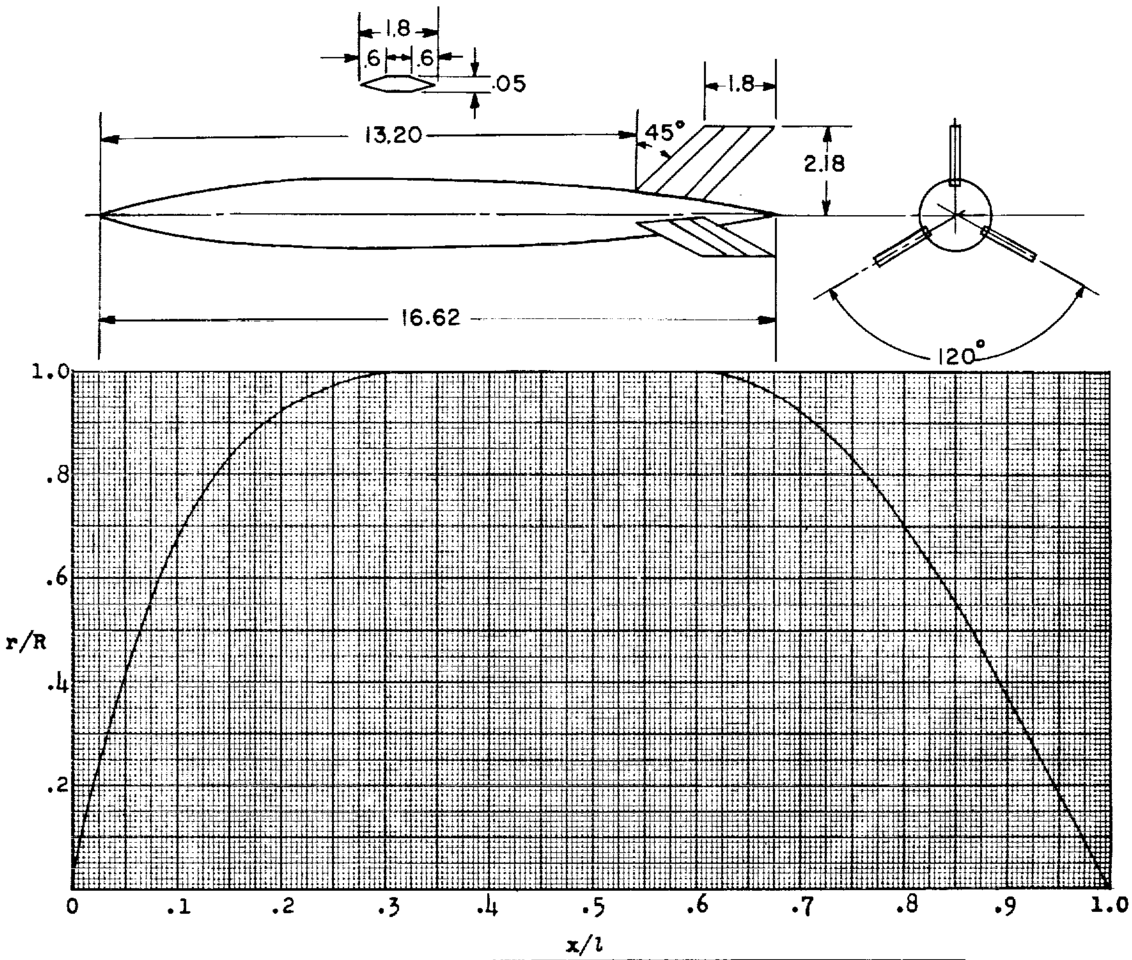

l/d_{Total}	11.08	l/d_{Nose}	3.42	S_b/A	34.40	A_b/A	0.0
l/d_{N+A}	7.80	l/d_{Aft}	4.38	S_f/A	11.0	θ_b	9.8°

Designation: 51

Test: Helium Gun

Figure 59.

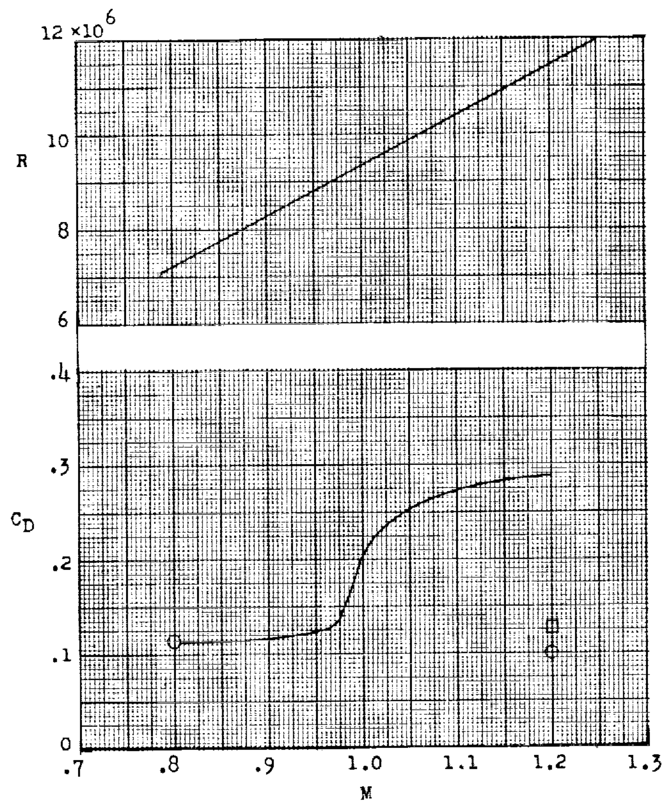

Figure 59.- Concluded.

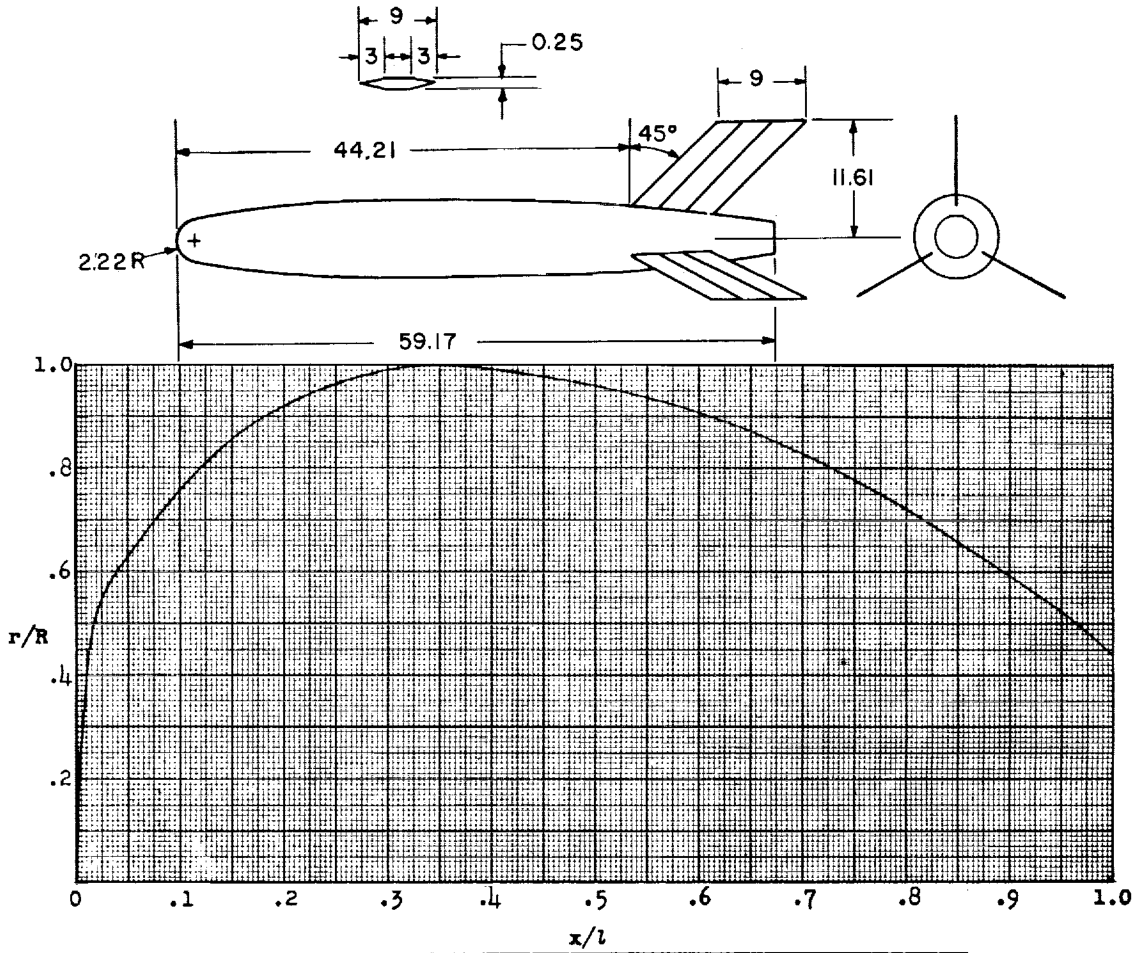

l/d_{Total}	7.9	l/d_{Nose}	2.57	S_b/A	25.70	A_b/A	.19
l/d_{N+A}	7.9	l/d_{Aft}	5.33	S_f/A	11.0	θ_b	7°

Designation: 52

Test: Rocket

Remarks: Nose consists of hemispherical and parabolic segments; parabolic afterbody.

Figure 60.

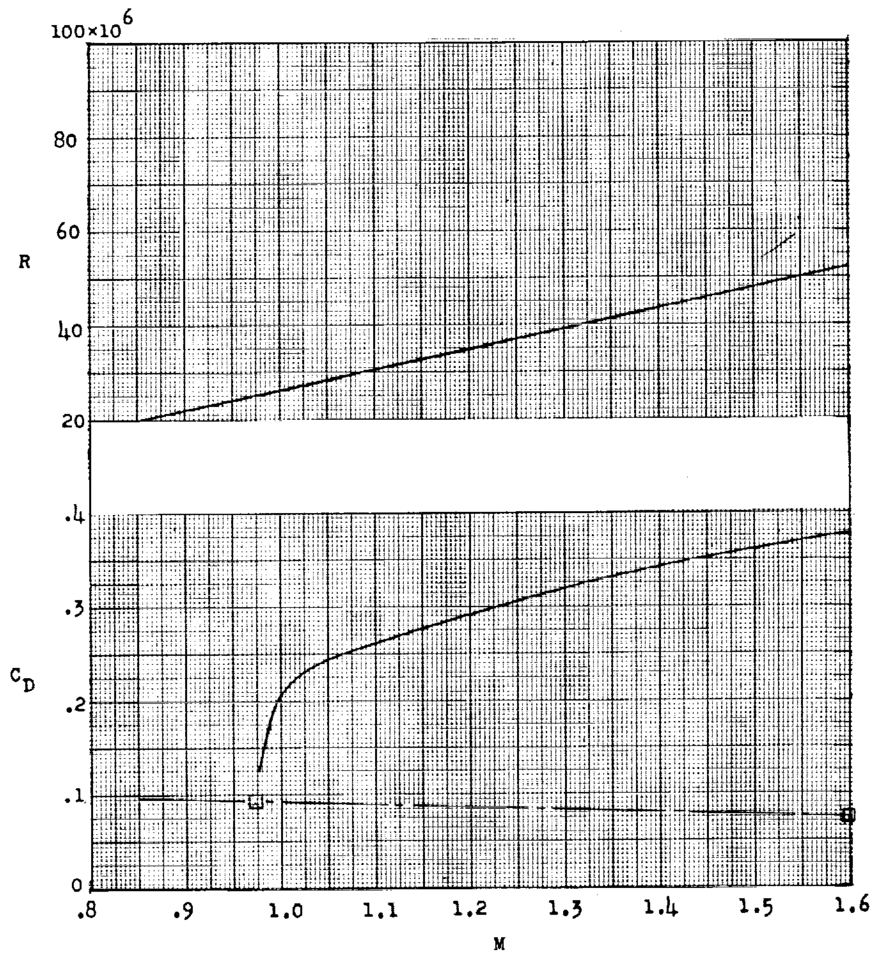

Figure 60.- Concluded.

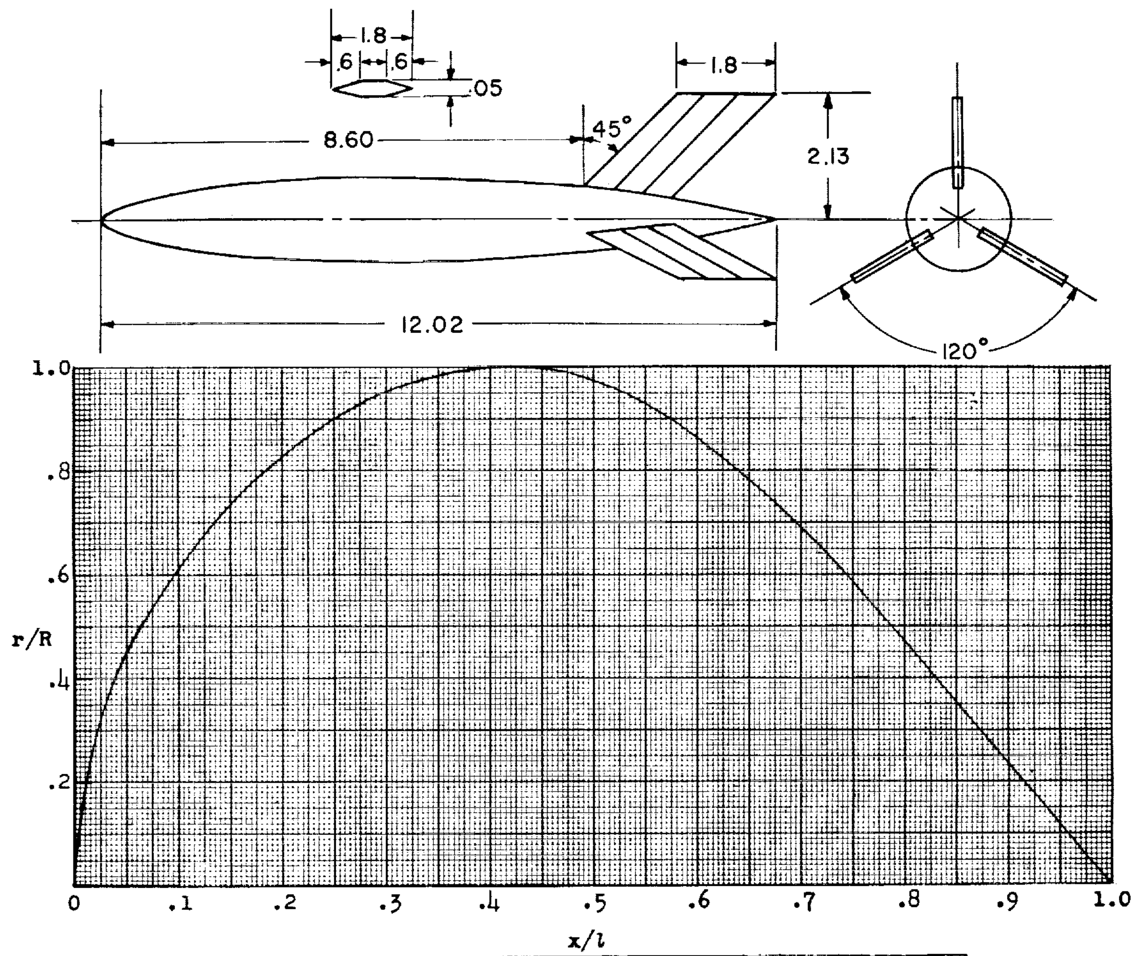

l/d_{Total}	8.00	l/d_{Nose}	3.20	S_b/A	21.9	A_b/A	0.0
l/d_{N+A}	8.00	l/d_{Aft}	4.80	S_f/A	11.0	θ_b	8.5°

Designation: 53

Test: Helium Gun

Figure 61.

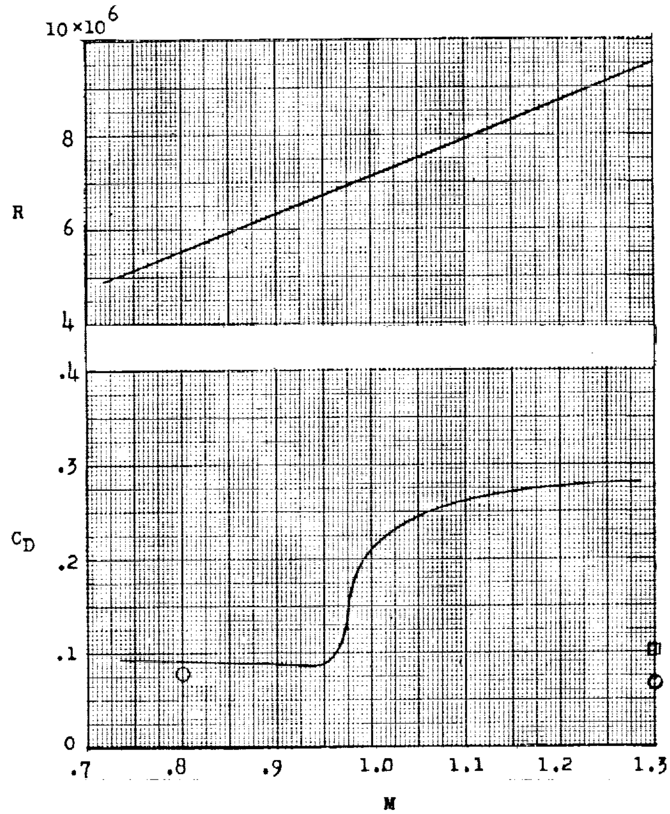

Figure 61.- Concluded.

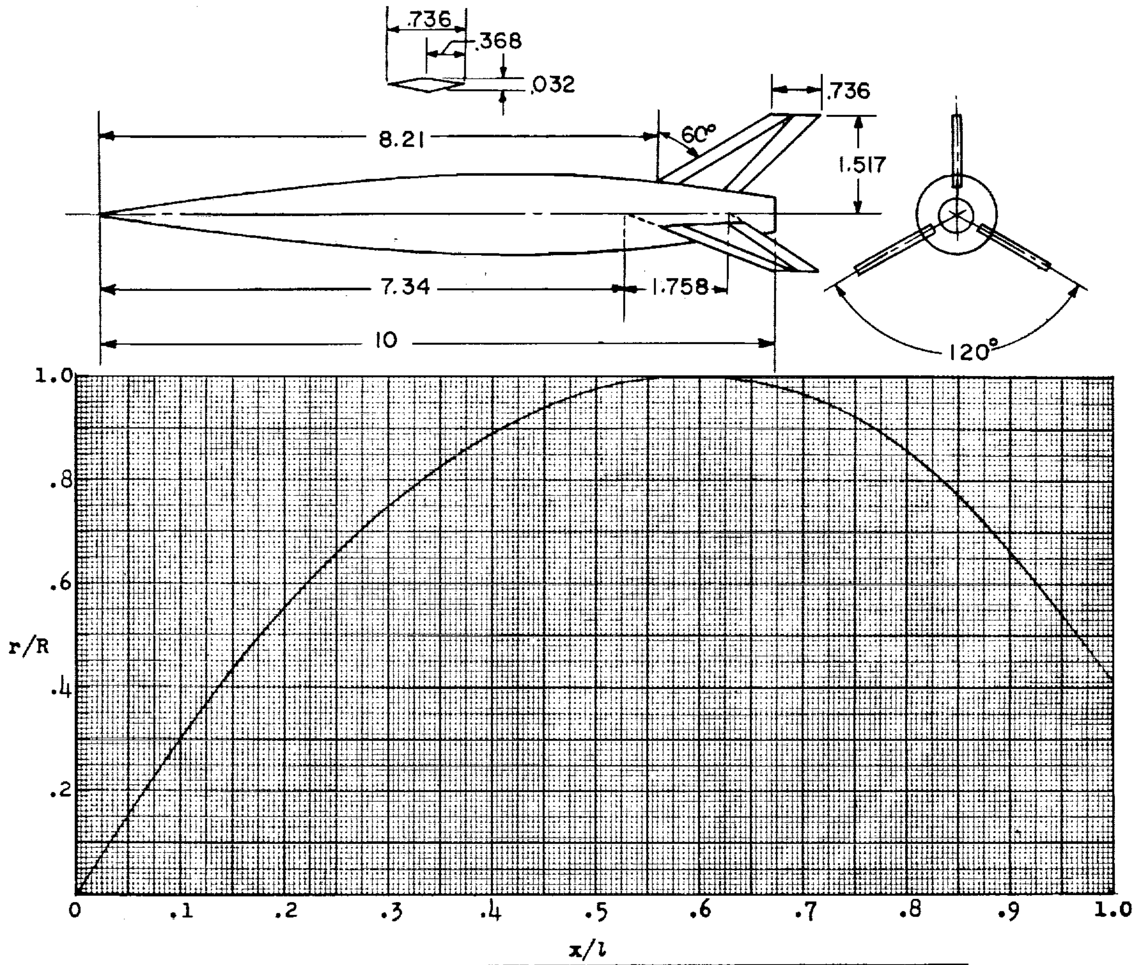

l/d_{Total}	8.0	l/d_{Nose}	4.66	S_b/A	23.16	A_b/A	.17
l/d_{N+A}	8.0	l/d_{Aft}	3.44	S_f/A	5.8	θ_b	9.5°

Designation: 54

Test: Helium Gun

Figure 62.

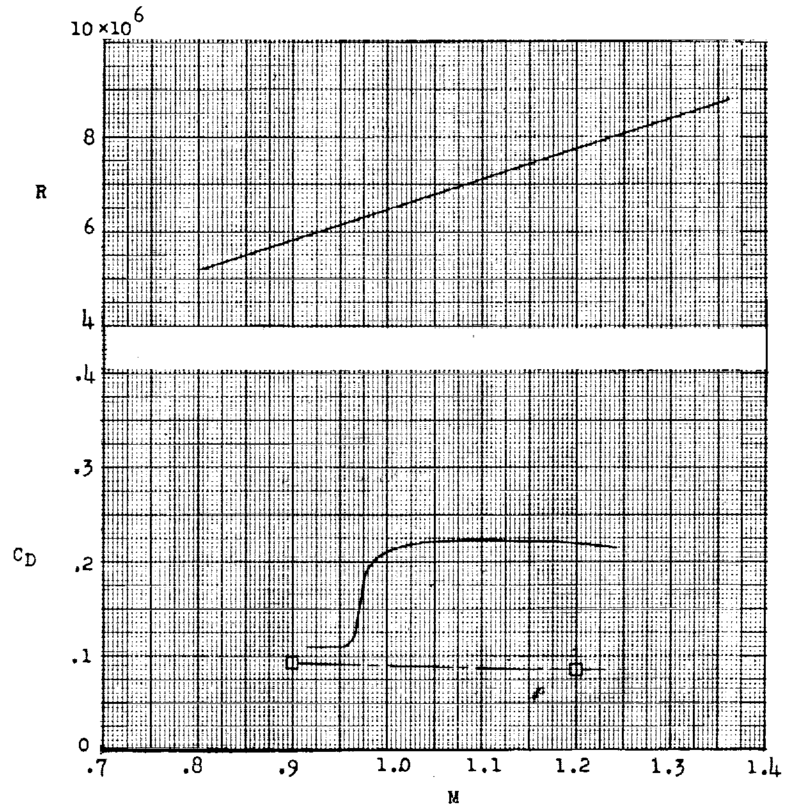

Figure 62.- Concluded.

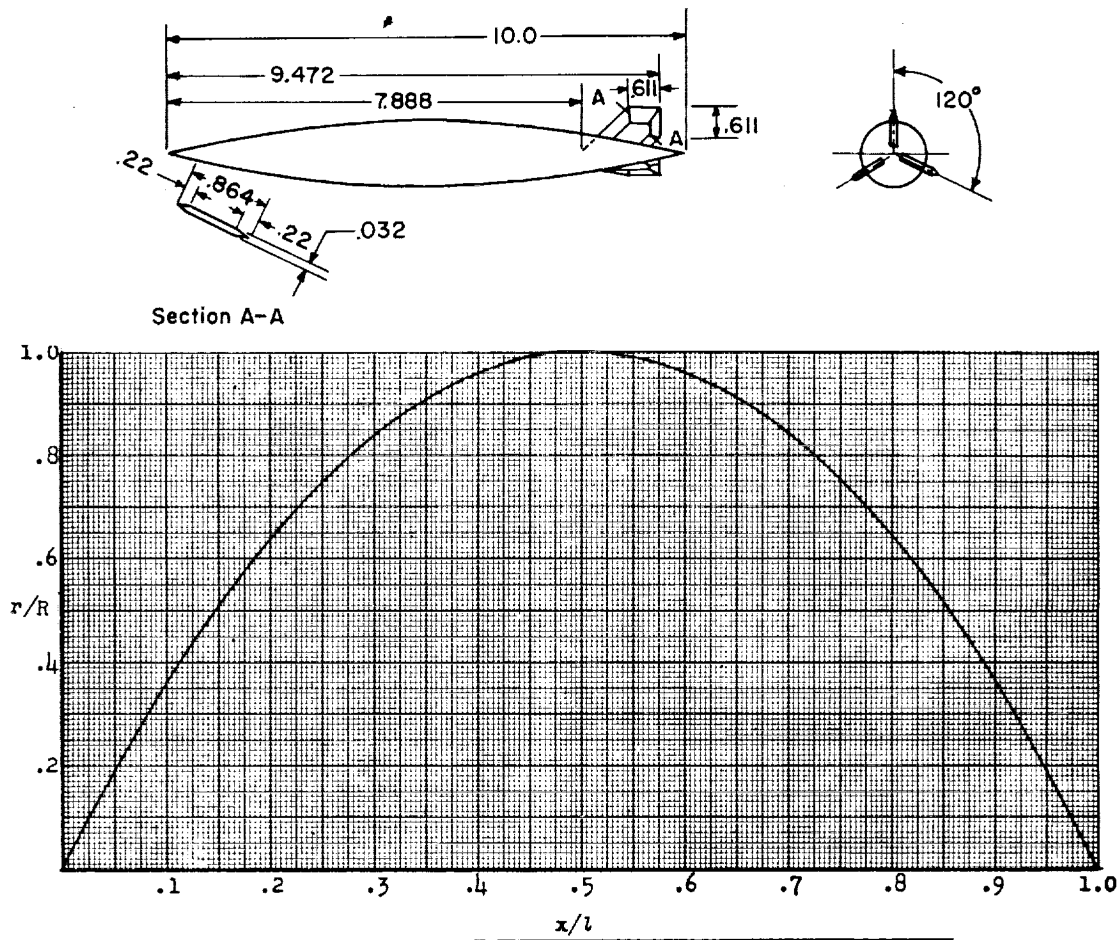

l/d_{Total}	8.0	l/d_{Nose}	4.0	S_b/A	26.3	A_b/A	0
l/d_{N+A}	8.0	l/d_{Aft}	4.0	S_f/A	4.43	θ_b	14.0°

Designation: 55

Test: Helium Gun

Figure 63.

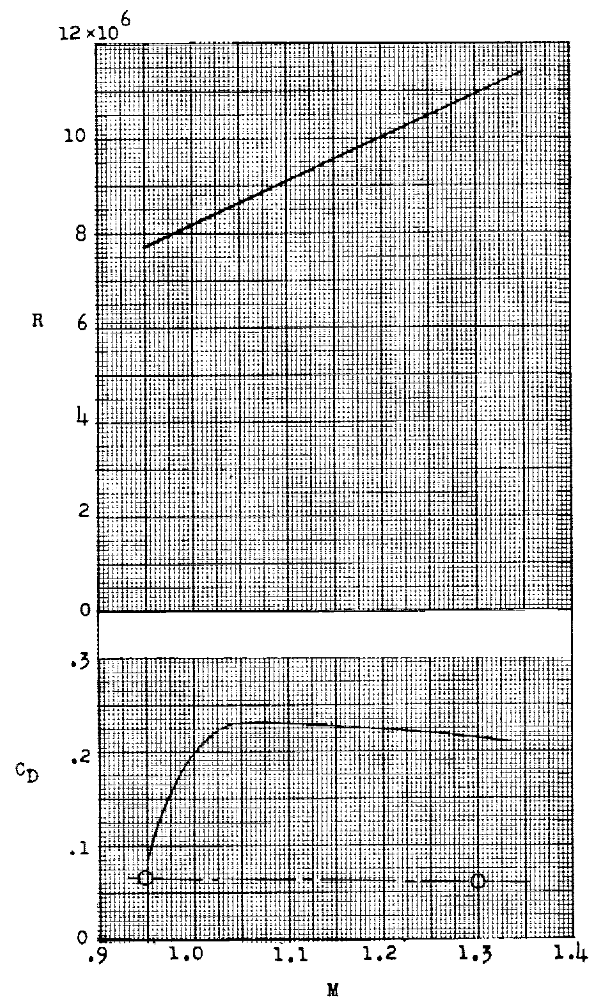

Figure 63.- Concluded.

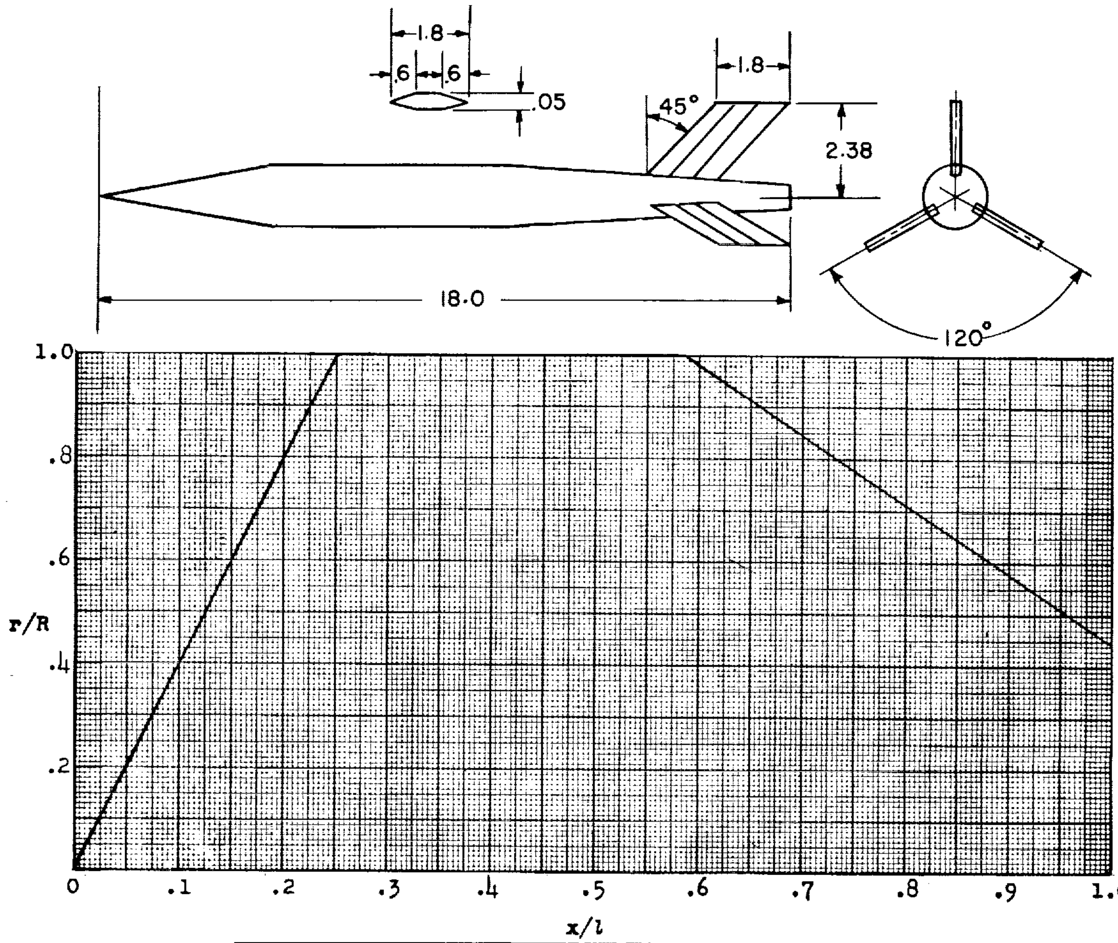

l/d_{Total}	12.00	l/d_{Nose}	3.00	S_b/A	36.38	A_b/A	.19
l/d_{N+A}	8.00	l/d_{Aft}	5.00	S_f/A	11.0	θ_b	3.2°

Designation: 56

Test: **Helium Gun**

Remarks: Conical nose and afterbody.

Figure 64.

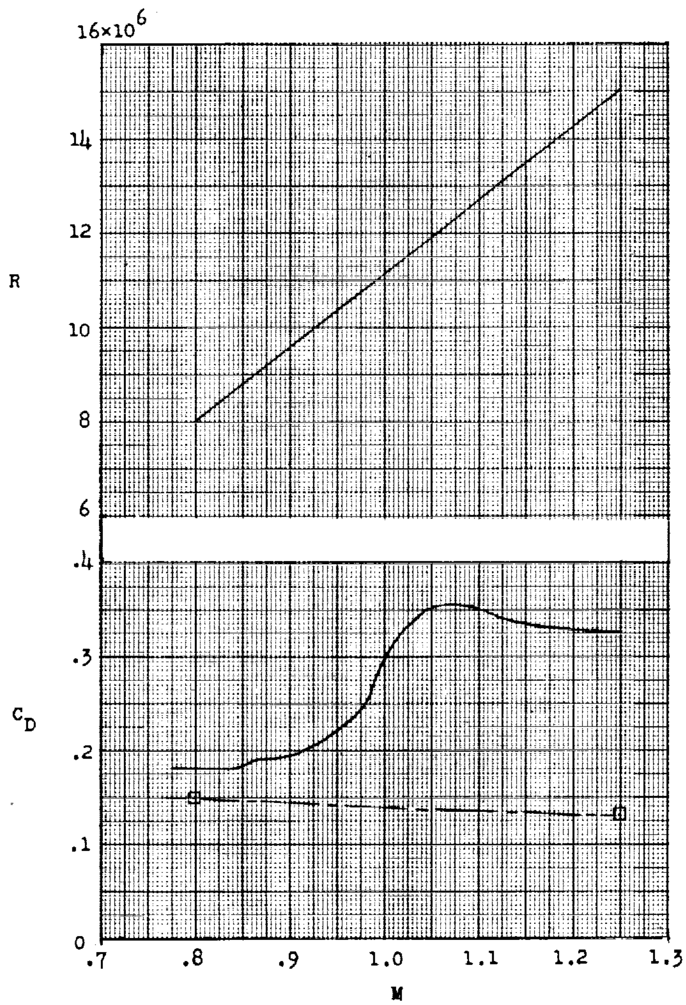

Figure 64.- Concluded.

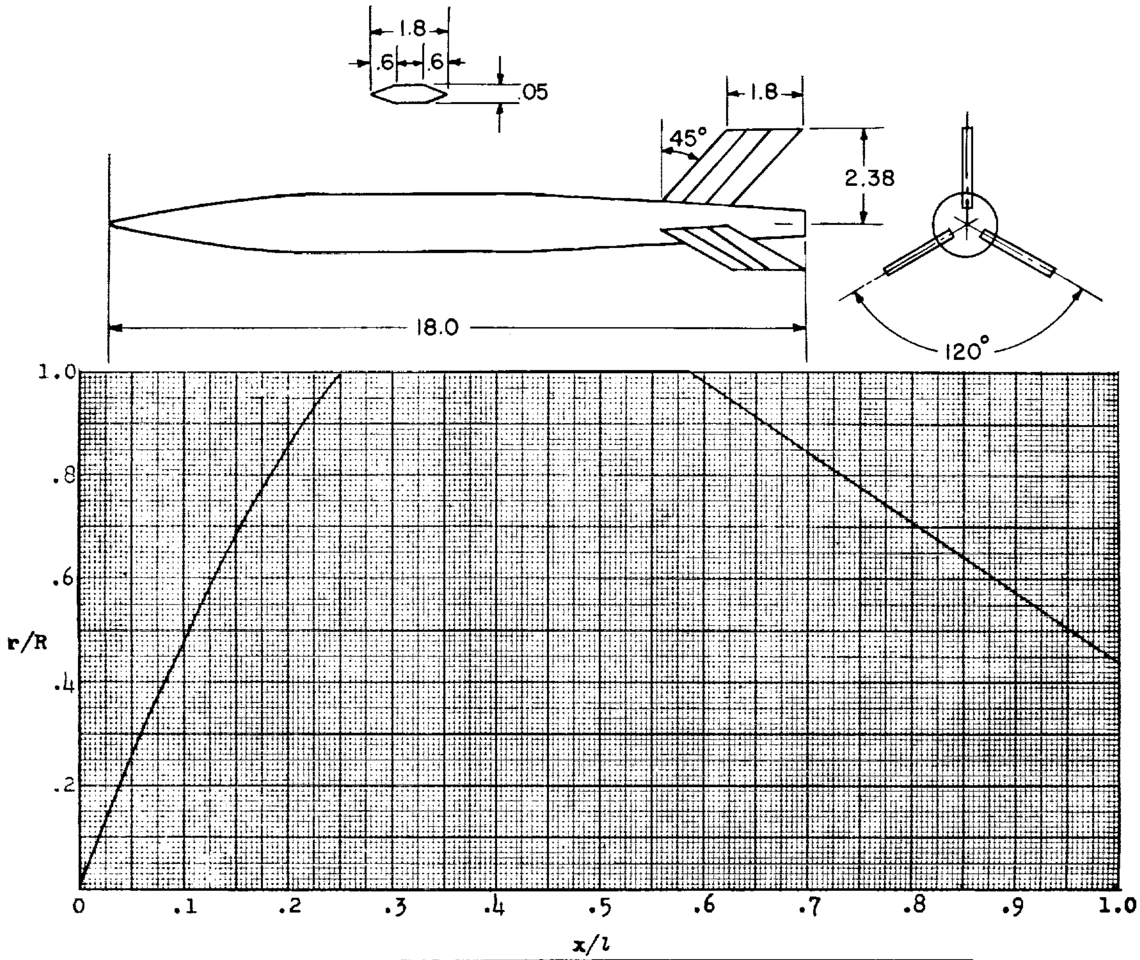

l/d_{Total}	12.0	l/d_{Nose}	3.0	S_b/A	37.05	A_b/A	.19
l/d_{N+A}	8.0	l/d_{Aft}	5.0	S_f/A	11.0	θ_b	3.2°

Designation: 57

Test: **Helium Gun**

Remarks: Nose, $r' = \dfrac{2x' - \frac{1}{2}(x')^2}{1\frac{1}{2}}$; conical afterbody.

Figure 65.

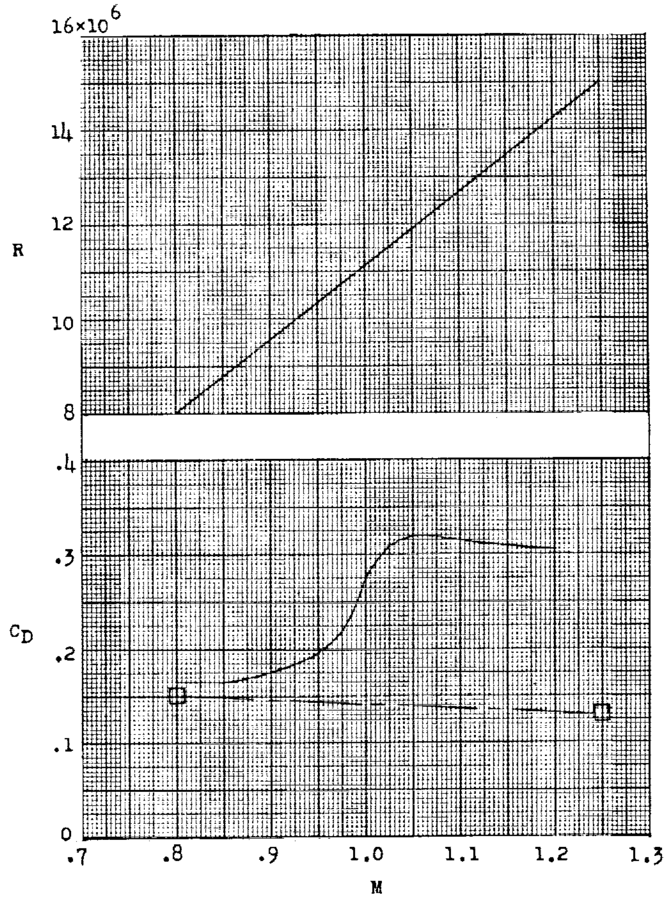

Figure 65.- Concluded.

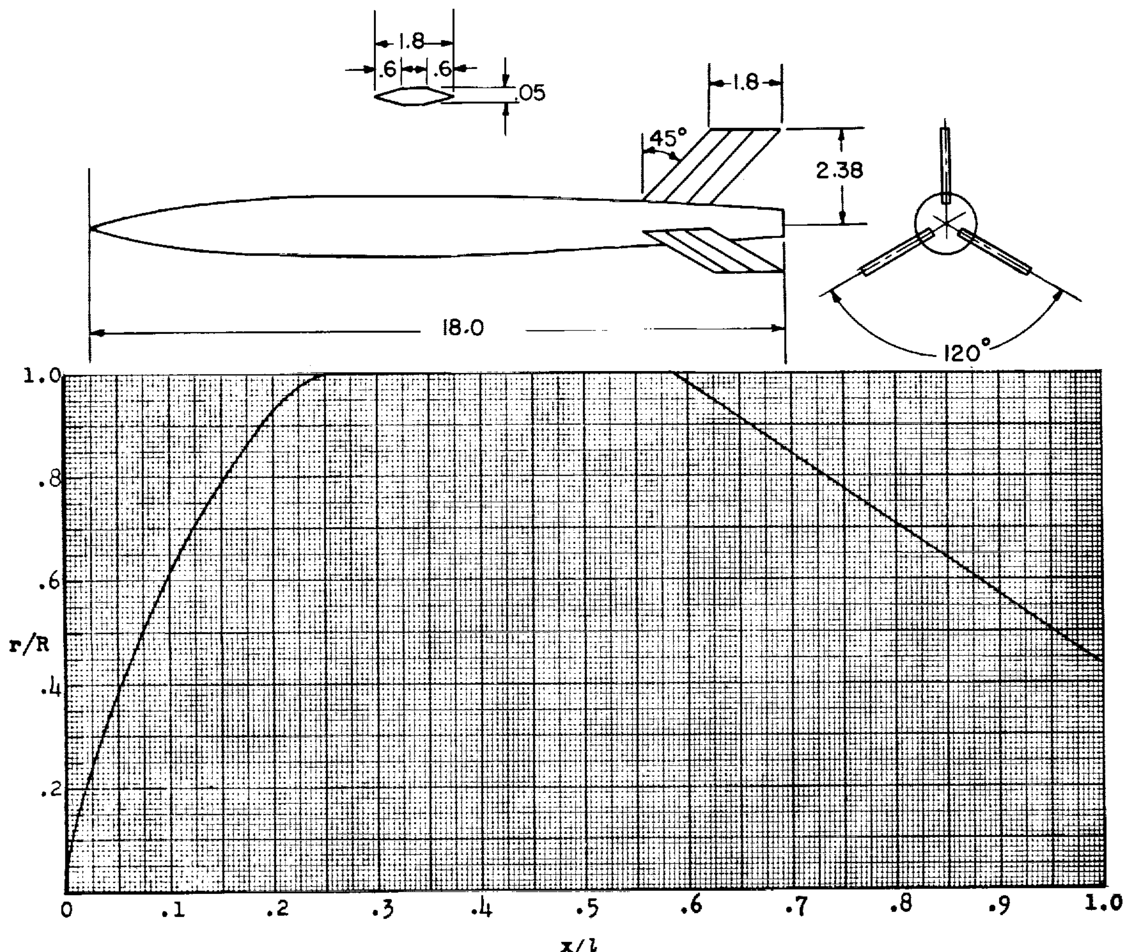

l/d_{Total}	12.00	l/d_{Nose}	3.00	S_b/A	38.35	A_b/A	.19
l/d_{N+A}	8.0	l/d_{Aft}	5.00	S_f/A	11.0	θ_b	3.2°

Designation: 58

Test: Helium Gun

Remarks: Nose, Von Kármán, $r' = \frac{1}{\sqrt{\pi}}\sqrt{\phi - 1/2 \sin^2\phi}$ where $\phi = \cos^{-1}(1 - 2x')$; conical afterbody.

Figure 66.

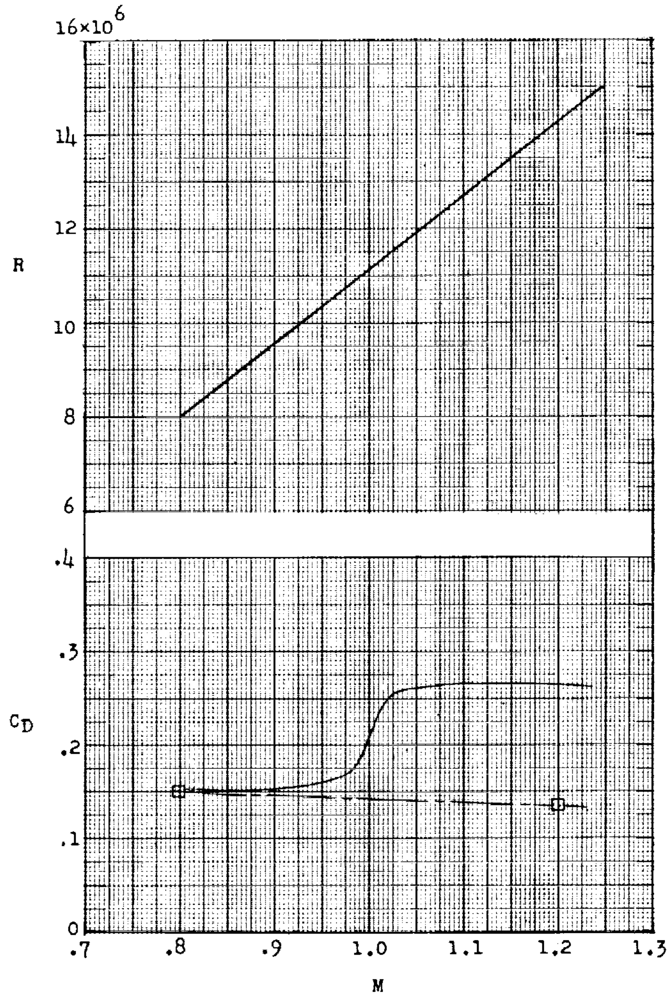

Figure 66.- Concluded.

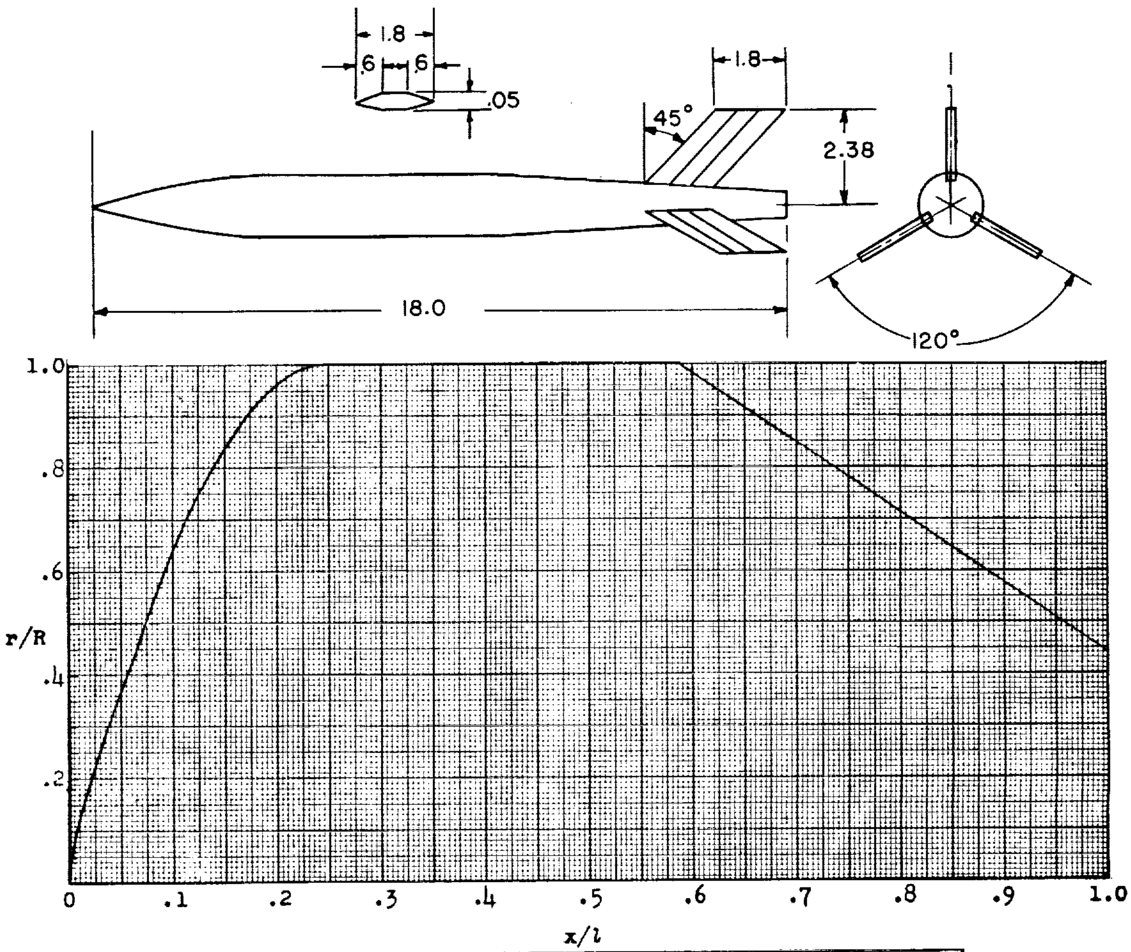

l/d_{Total}	12.00	l/d_{Nose}	3.00	S_b/A	38.40	A_b/A	.19
l/d_{N+A}	8.00	l/d_{Aft}	5.00	S_f/A	11.0	θ_b	3.2°

Designation: 59

Test: Helium Gun

Remarks: Parabolic nose; conical afterbody.

Figure 67.

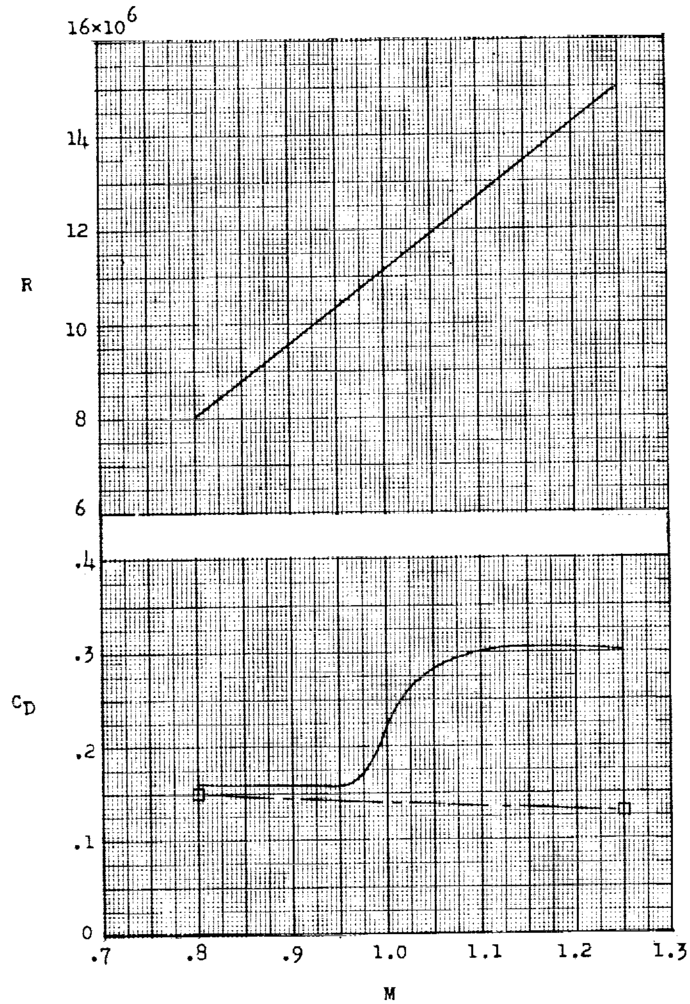

Figure 67.- Concluded.

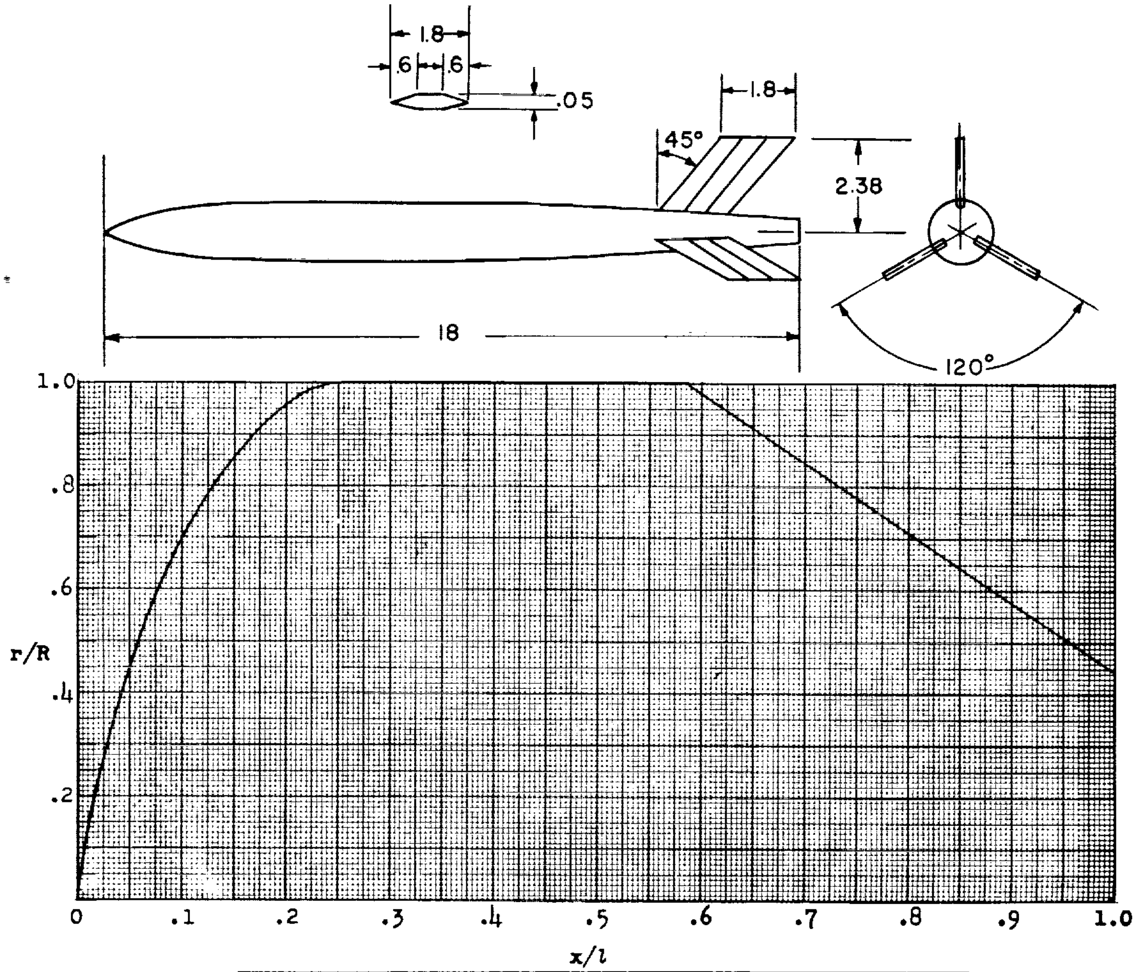

l/d_{Total}	12.0	l/d_{Nose}	3.00	S_b/A	38.78	A_b/A	.19
l/d_{N+A}	8.0	l/d_{Aft}	5.00	S_f/A	11.0	θ_b	3.2°

Designation: 60

Test: **Helium Gun**

Remarks: Nose, L-V Haack, $r' = \frac{1}{\sqrt{\pi}}\sqrt{\phi - 1/2 \sin^2\phi + 1/3 \sin^3\phi}$

where $\phi = \cos^{-1}(1 - 2X')$.

Figure 68.

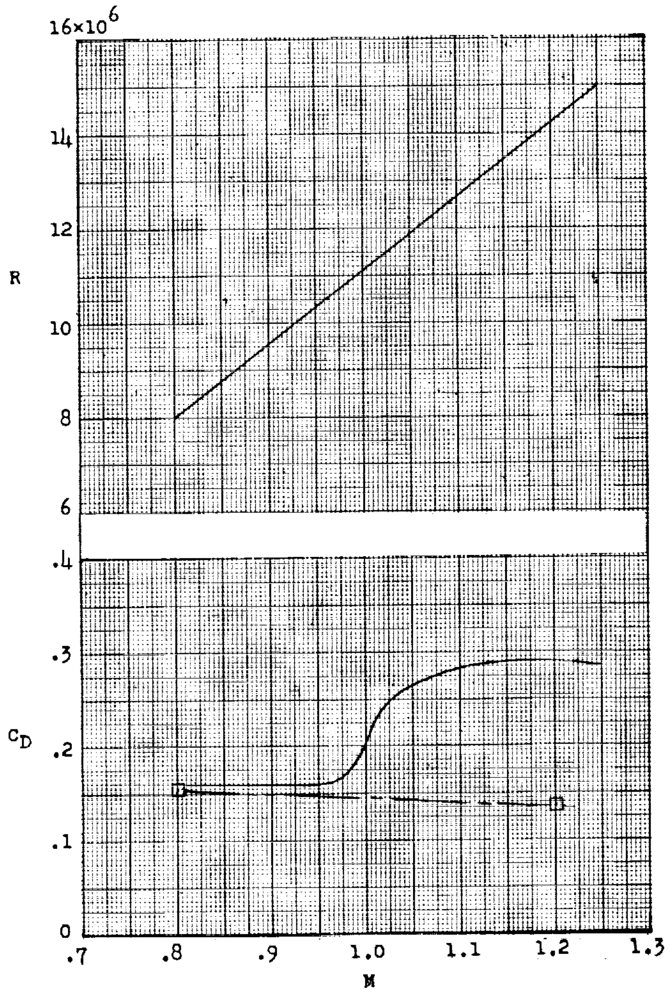

Figure 68.- Concluded.

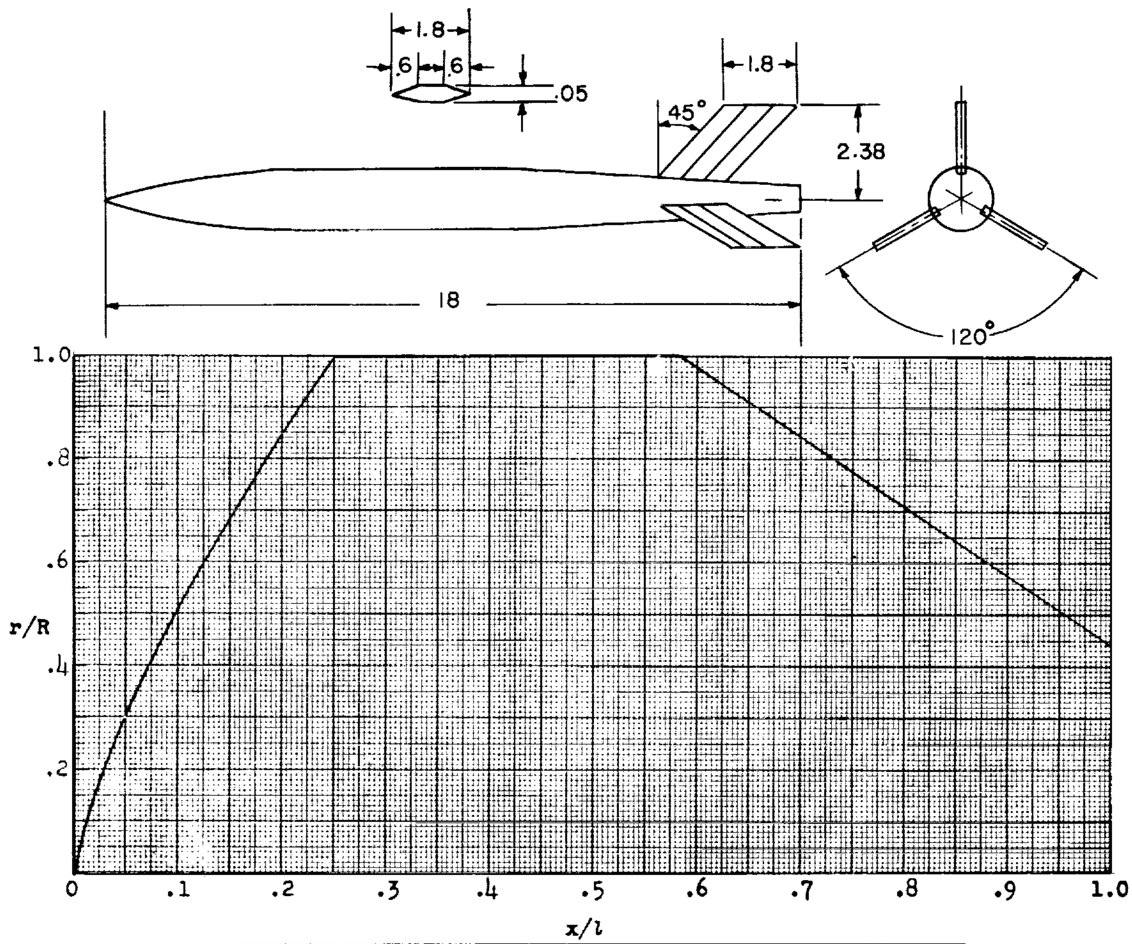

l/d_{Total}	12.00	l/d_{Nose}	3.00	S_b/A	37.24	A_b/A	.19
l/d_{N+A}	8.00	l/d_{Aft}	5.00	S_f/A	11.0	θ_b	3.2°

Designation: 61

Test: Helium Gun

Remarks: Nose, $r' = x'^{3/4}$.

Figure 69.

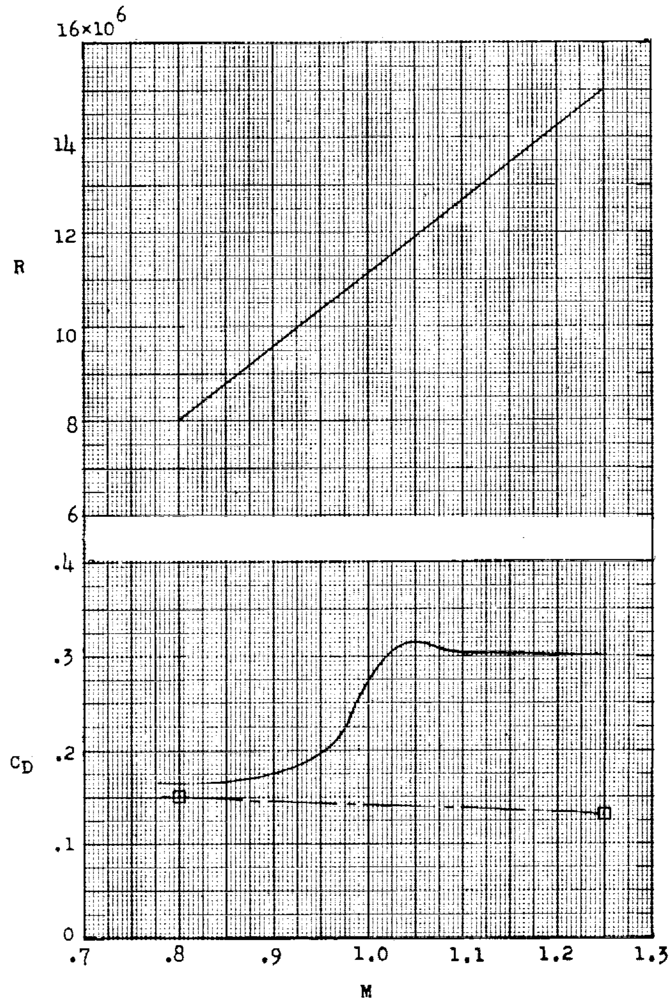

Figure 69.- Concluded.

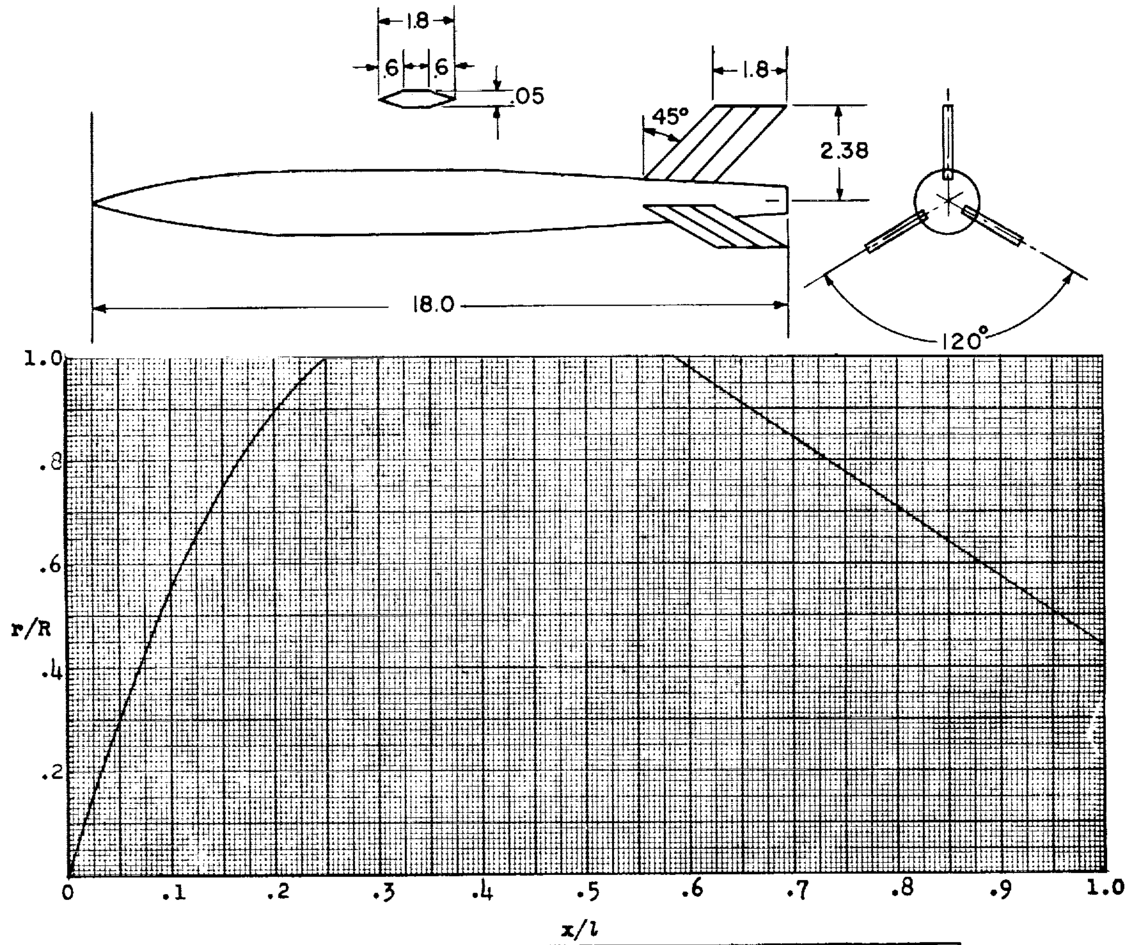

l/d_{Total}	12.0	l/d_{Nose}	3.0	S_b/A	37.58	A_b/A	.19
l/d_{N+A}	8.0	l/d_{Aft}	5.00	S_f/A	11.0	θ_b	3.2°

Designation: 62

Test: **Helium Gun**

Remarks: Nose, $r' = \dfrac{2x' - \frac{3}{4}x'^2}{1.25}$.

Figure 70.

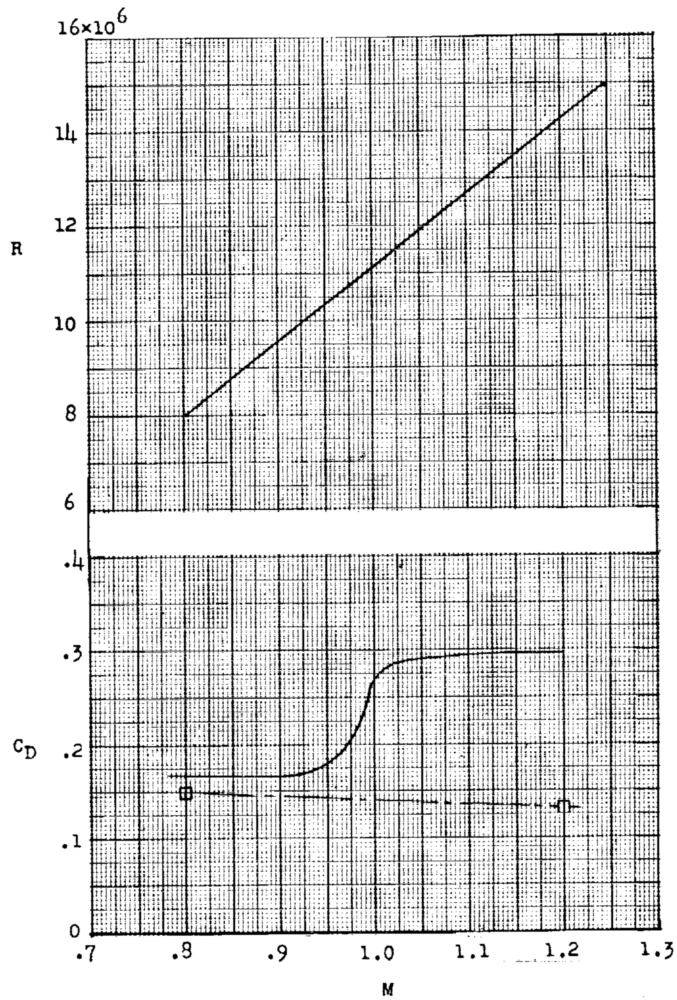

Figure 70.- Concluded.

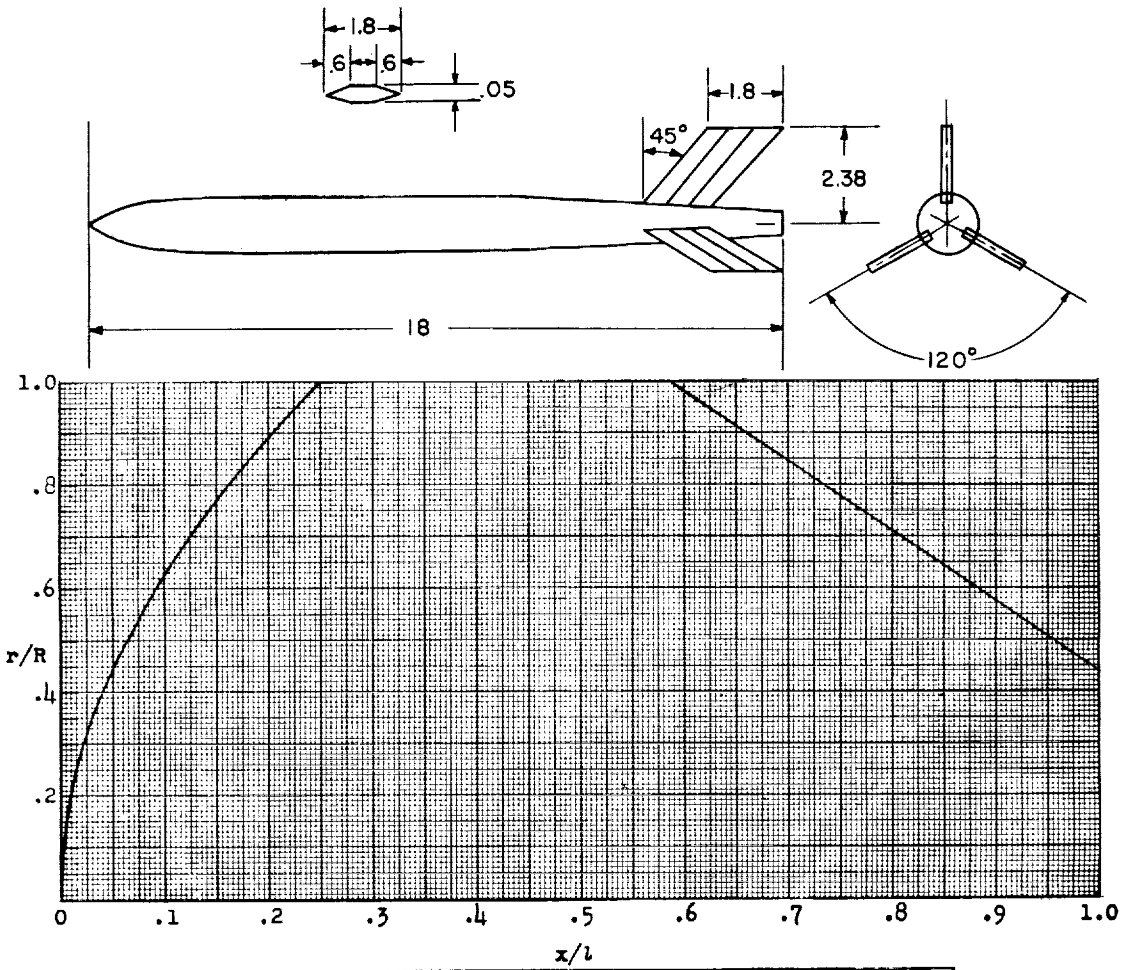

l/d_{Total}	12.00	l/d_{Nose}	3.00	S_b/A	38.40	A_b/A	.19
l/d_{N+A}	8.00	l/d_{Aft}	5.00	S_f/A	11.0	θ_b	3.2°

Designation: 63

Test: Helium Gun

Remarks: Nose, $r' = x'^{\frac{1}{2}}$; conical afterbody.

Figure 71.

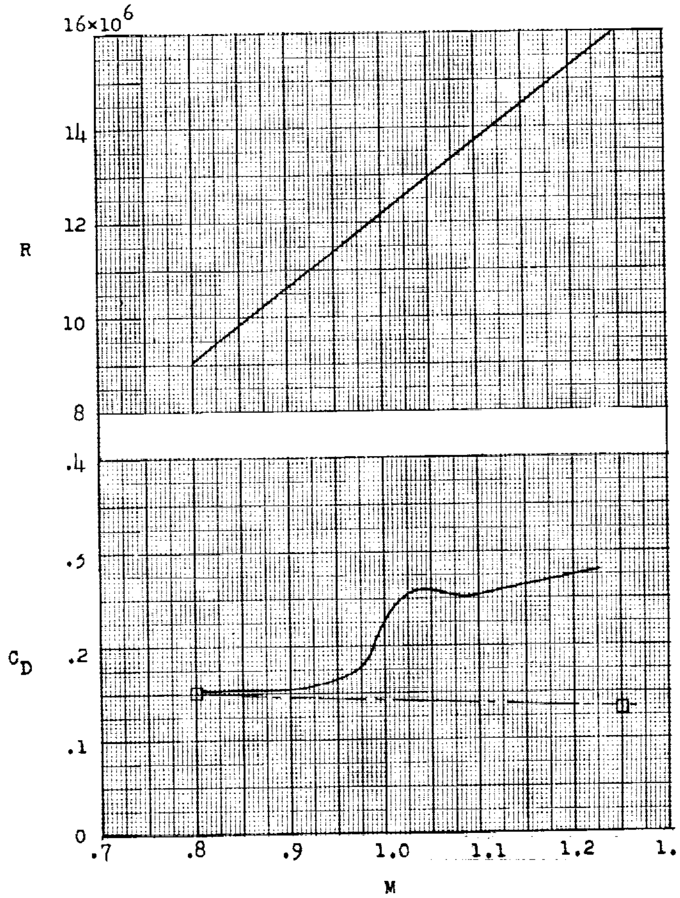

Figure 71.- Concluded.

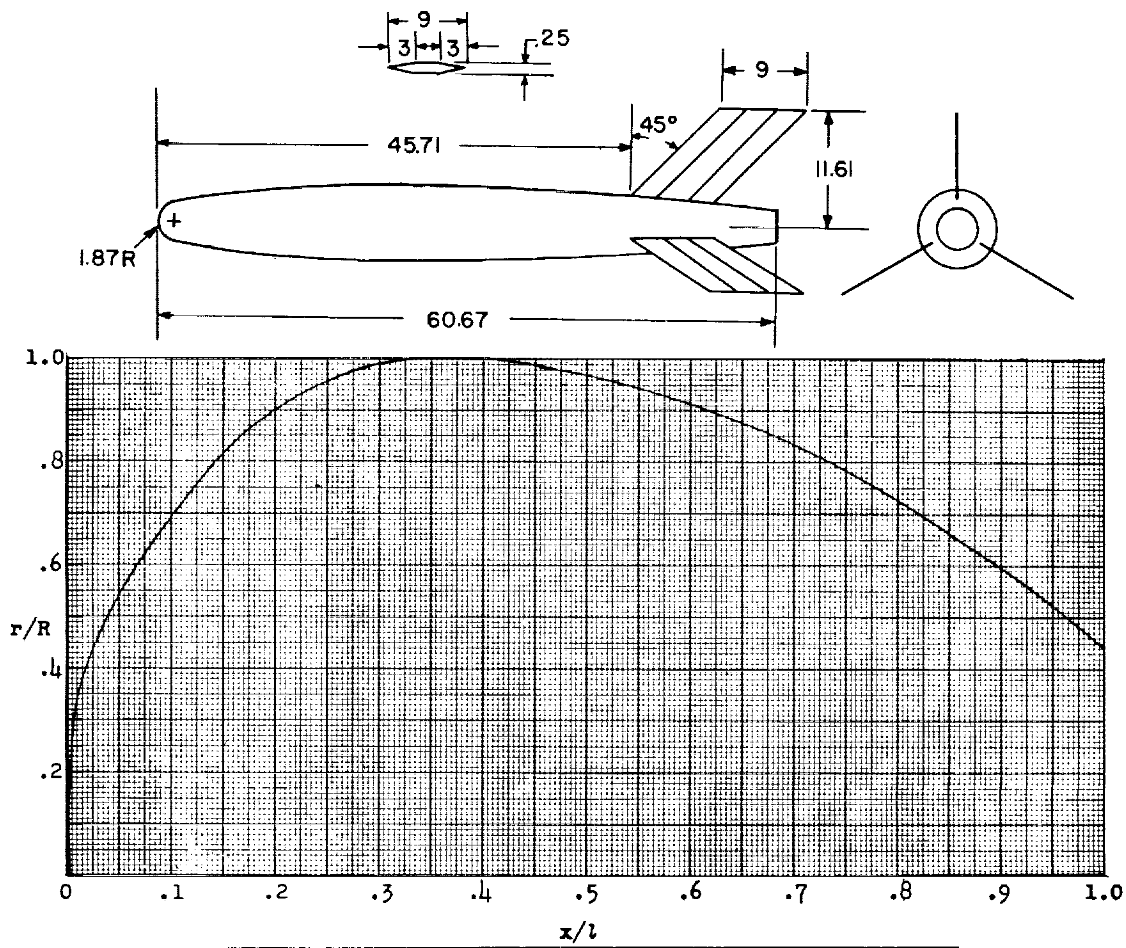

l/d_{Total}	8.10	l/d_{Nose}	2.73	S_b/A	26.08	A_b/A	.19
l/d_{N+A}	8.10	l/d_{Aft}	5.37	S_f/A	11.0	θ_b	7°

Designation: 64

Test: Rocket

Remarks: Nose consists of hemispherical and parabolic segments; parabolic afterbolic.

Figure 72.

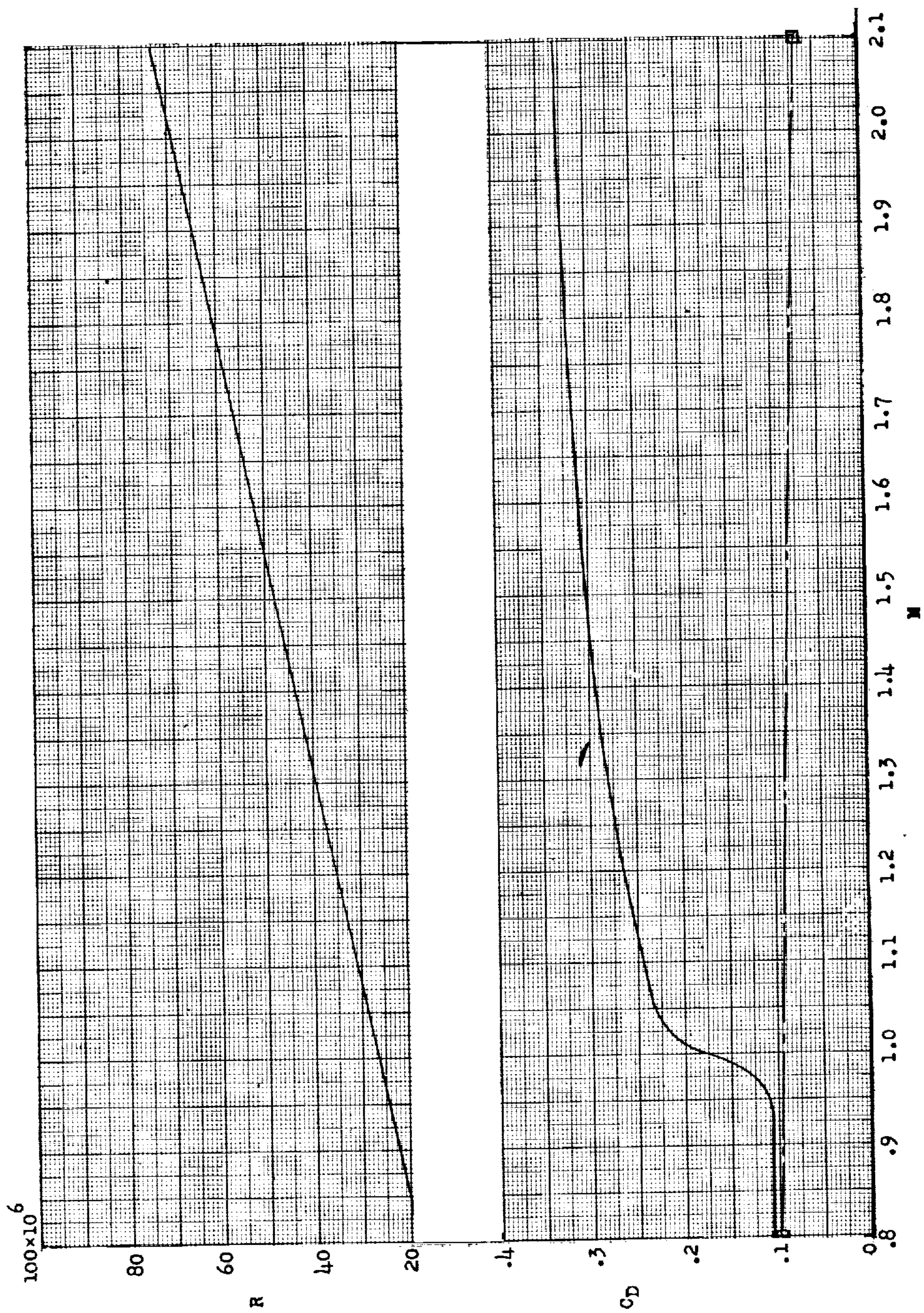

Figure 72.- Concluded.

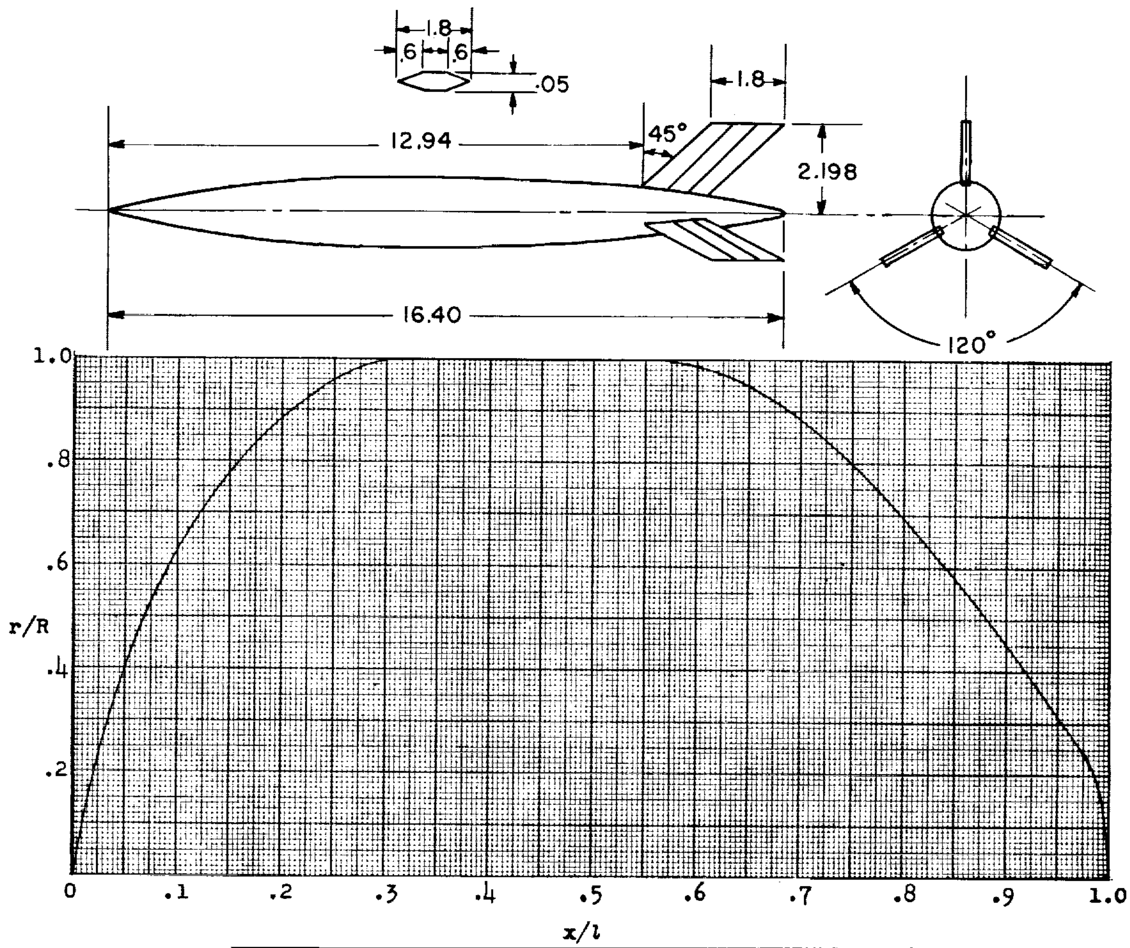

l/d_{Total}	10.93	l/d_{Nose}	3.38	S_b/A	34.10	A_b/A	0.0
l/d_{N+A}	8.20	l/d_{Aft}	4.82	S_f/A	11.0	θ_b	9°

Designation: 65

Test: **Helium Gun**

Figure 73.

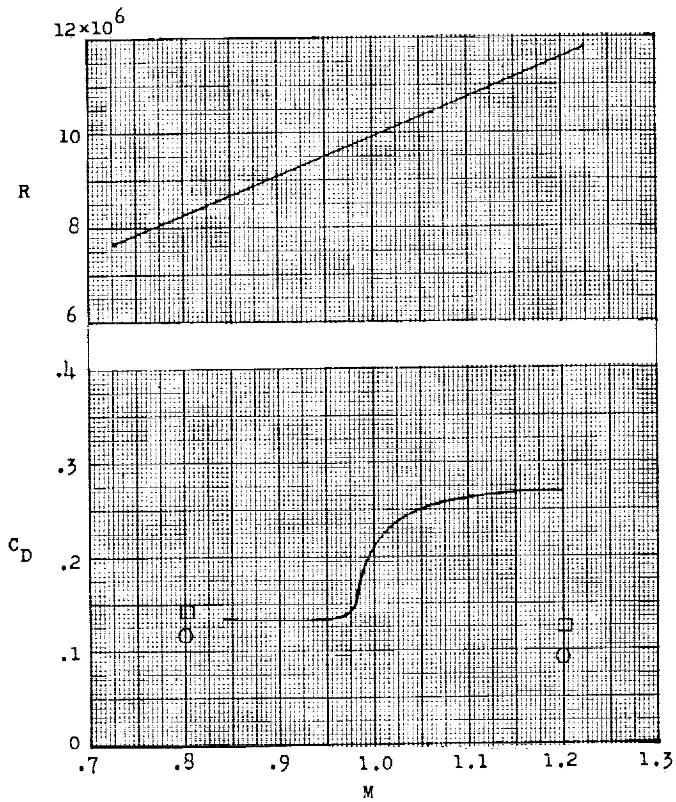

Figure 73.- Concluded.

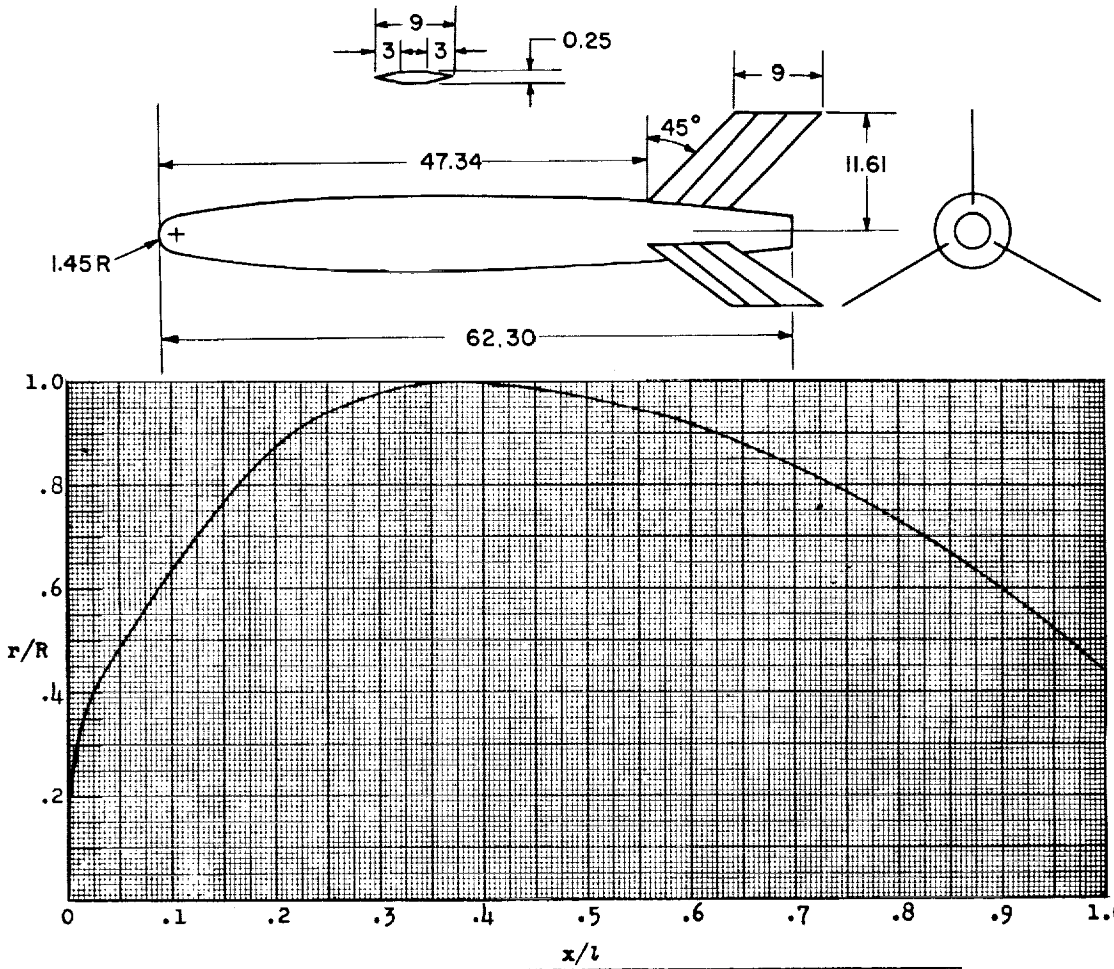

l/d_{Total}	8.3	l/d_{Nose}	2.96	S_b/A	26.5	A_b/A	.19
l/d_{N+A}	8.3	l/d_{Aft}	5.34	S_f/A	11.0	θ_b	7°

Designation: 66

Test: Rocket

Remarks: Nose consists of hemispherical and parabolic segments; parabolic afterbody.

Figure 74.

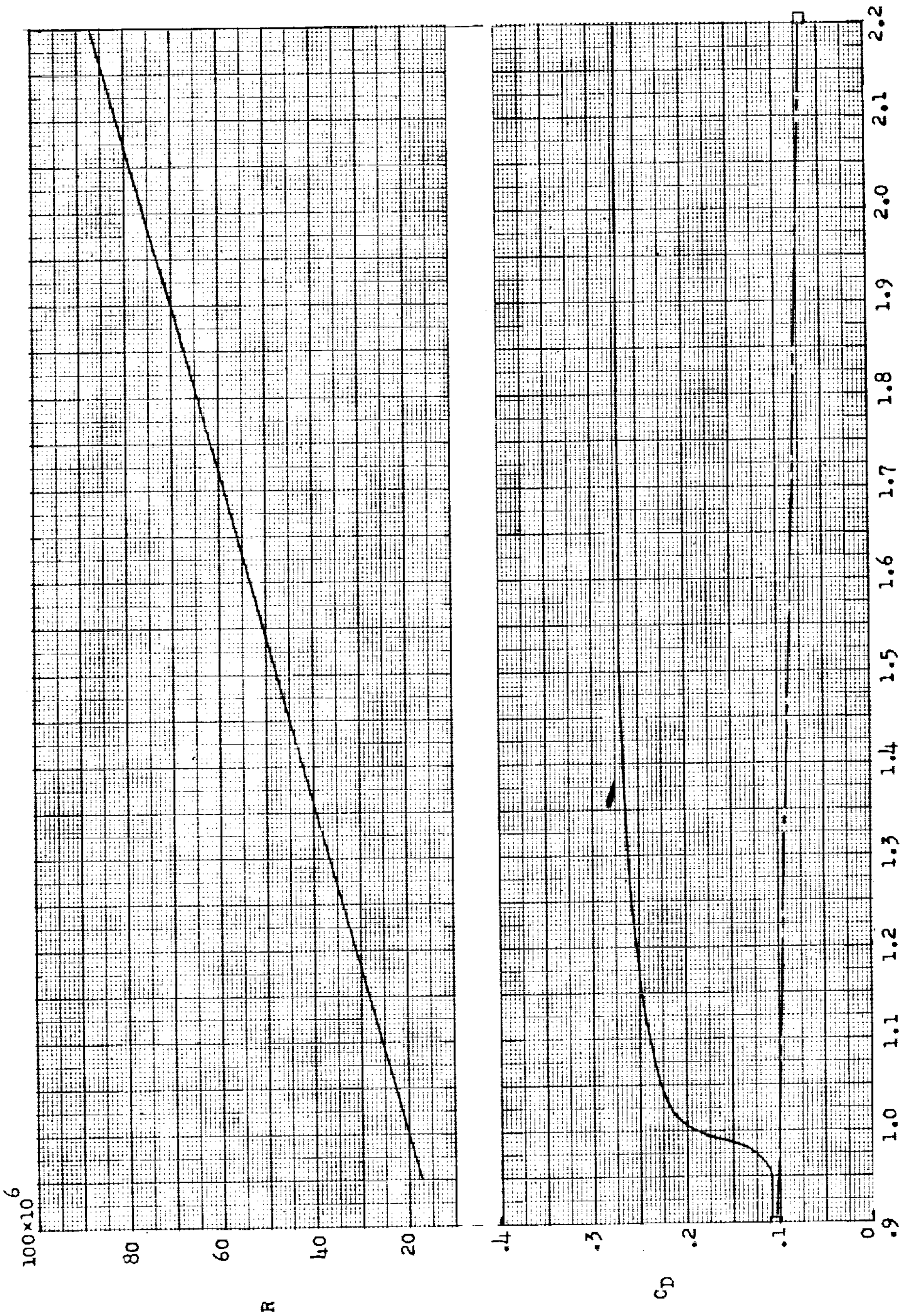

Figure 74.- Concluded.

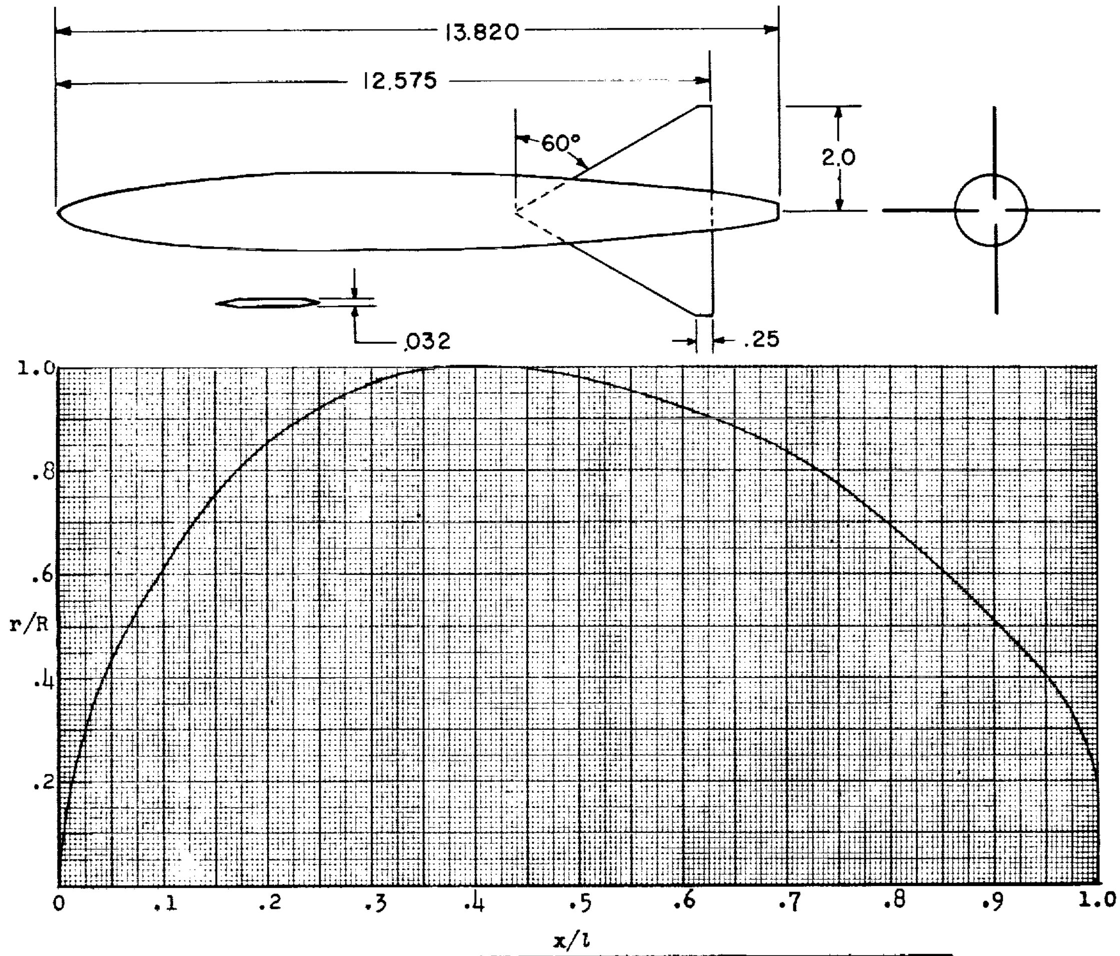

l/d_{Total}	9.02	l/d_{Nose}	3.27	S_b/A	26.6	A_b/A	.038
l/d_{N+A}	8.33	l/d_{Aft}	5.06	S_f/A	9.2	θ_b	23°

Designation 67

Test: Helium Gun

Figure 75.

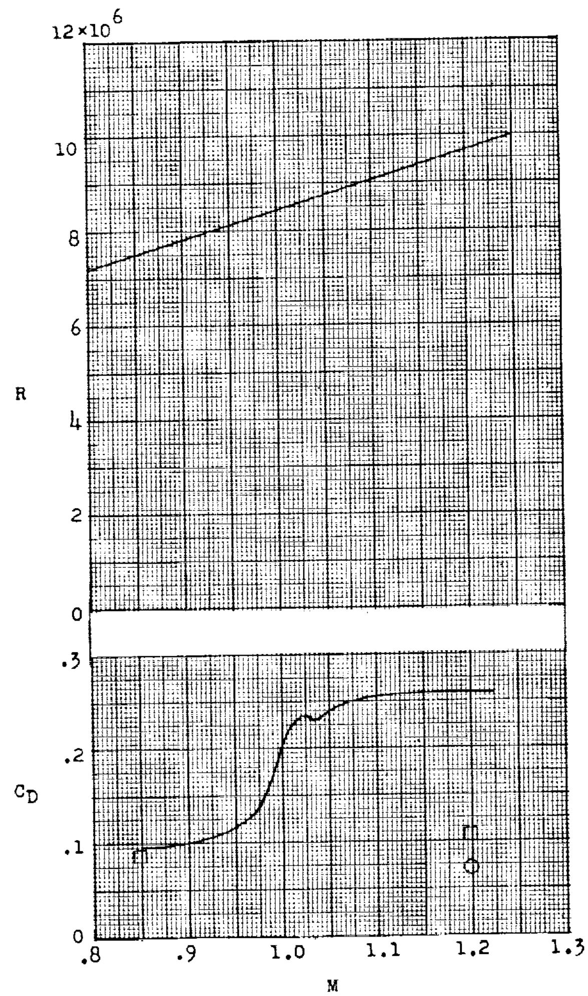

Figure 75.- Concluded.

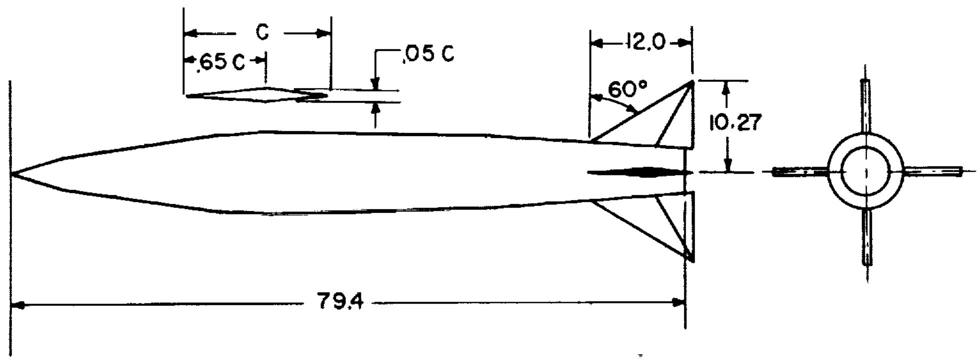

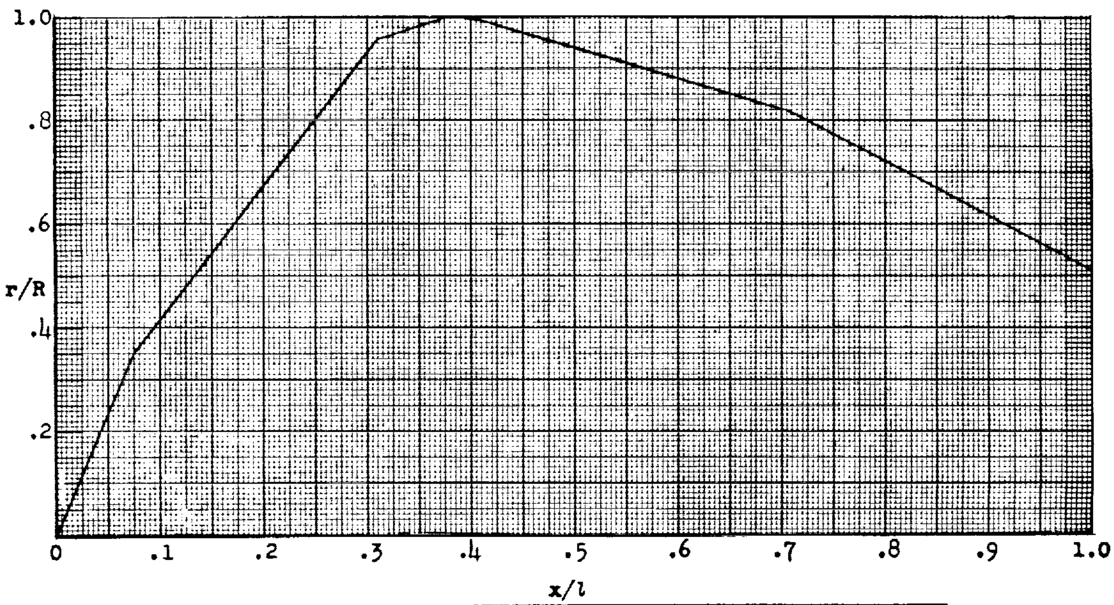

l/d_{Total}	8.44	l/d_{Nose}	3.20	S_b/A	24.90	A_b/A	.26
l/d_{N+A}	8.44	l/d_{Aft}	5.24	S_f/A	5.45	θ_b	3.5°

Designation: 68

Test: Rocket

Remarks: All conical sections.

Figure 76.

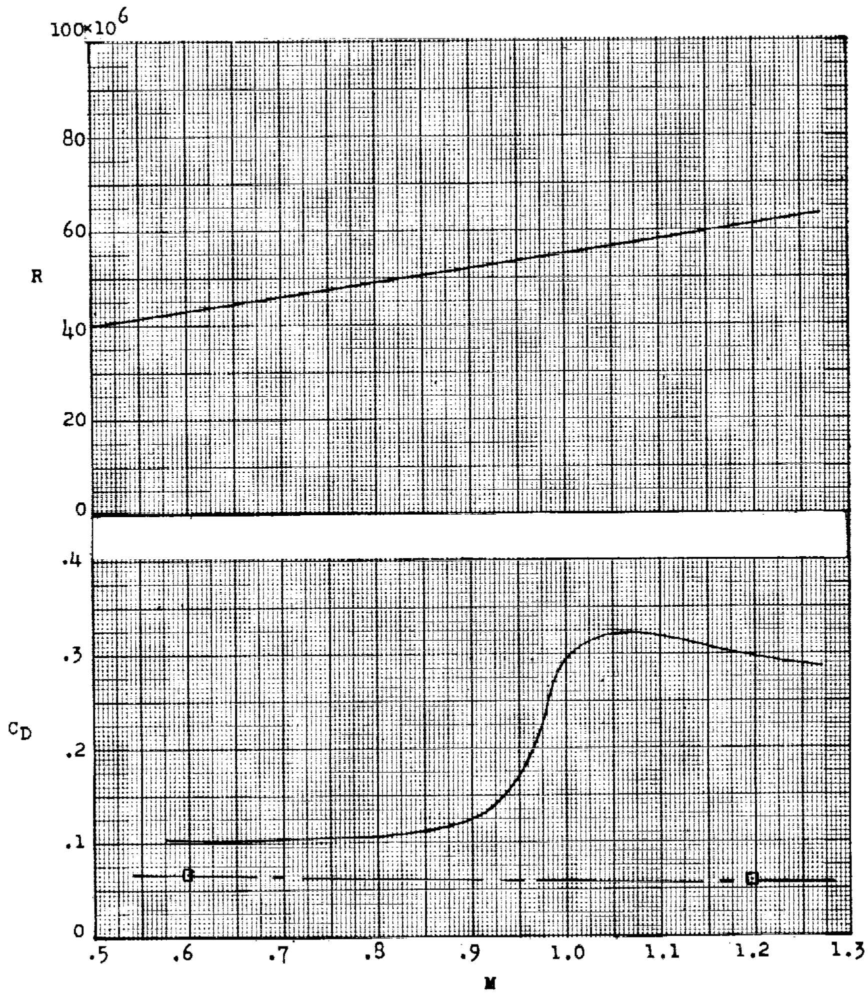

Figure 76.- Concluded.

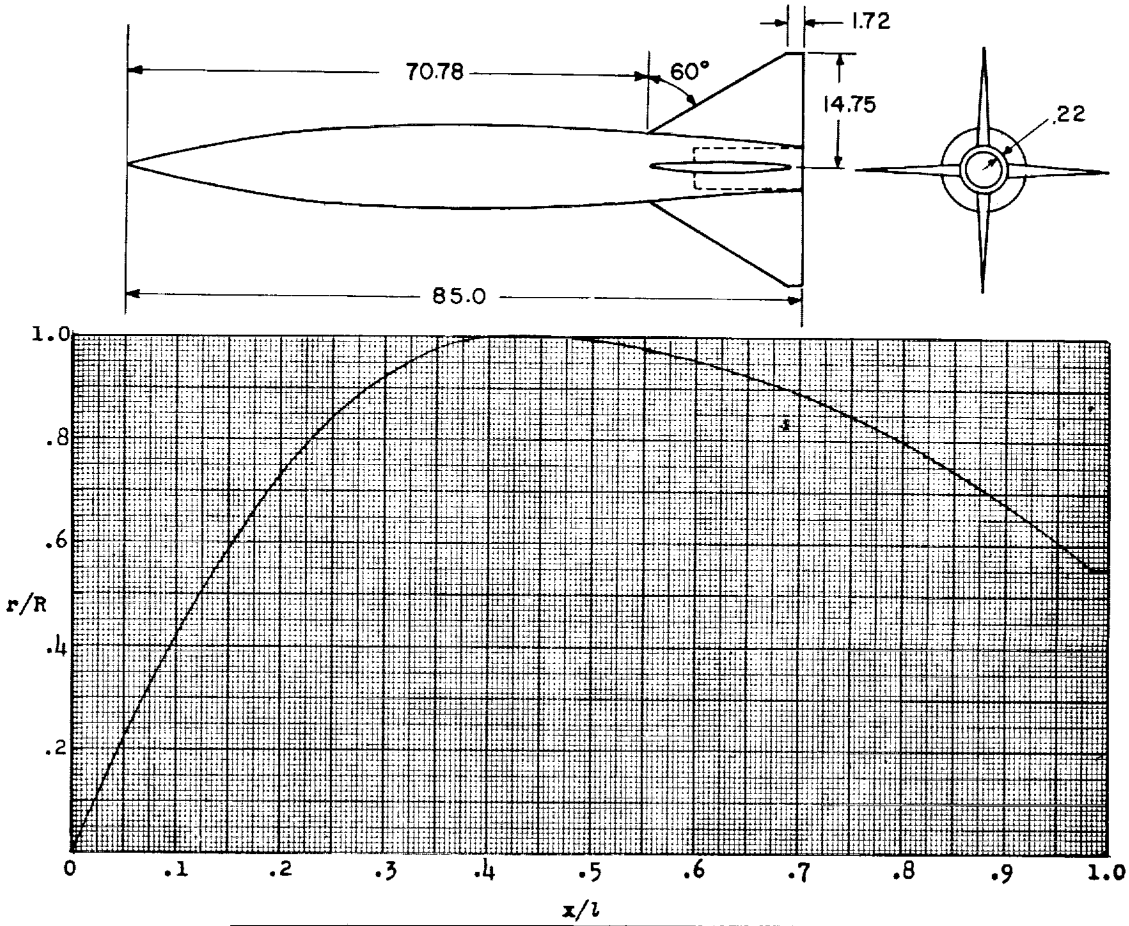

l/d_{Total}	8.5	l/d_{Nose}	3.60	S_b/A	26.30	A_b/A	.30
l/d_{N+A}	8.5	l/d_{Aft}	4.90	S_f/A	9.74	θ_b	5.6°

Designation: 69

Test: Rocket

Figure 77.

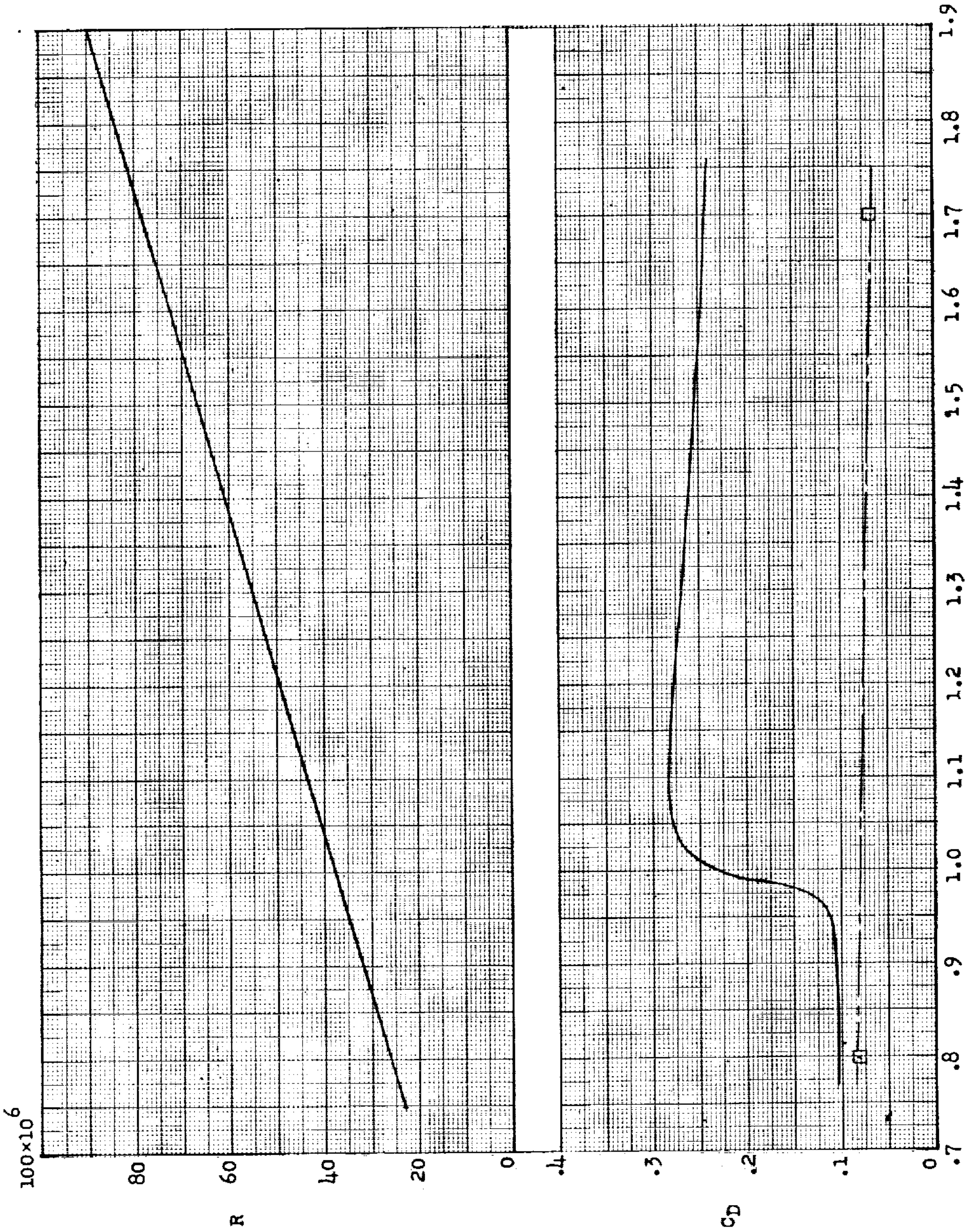

Figure 77.- Concluded.

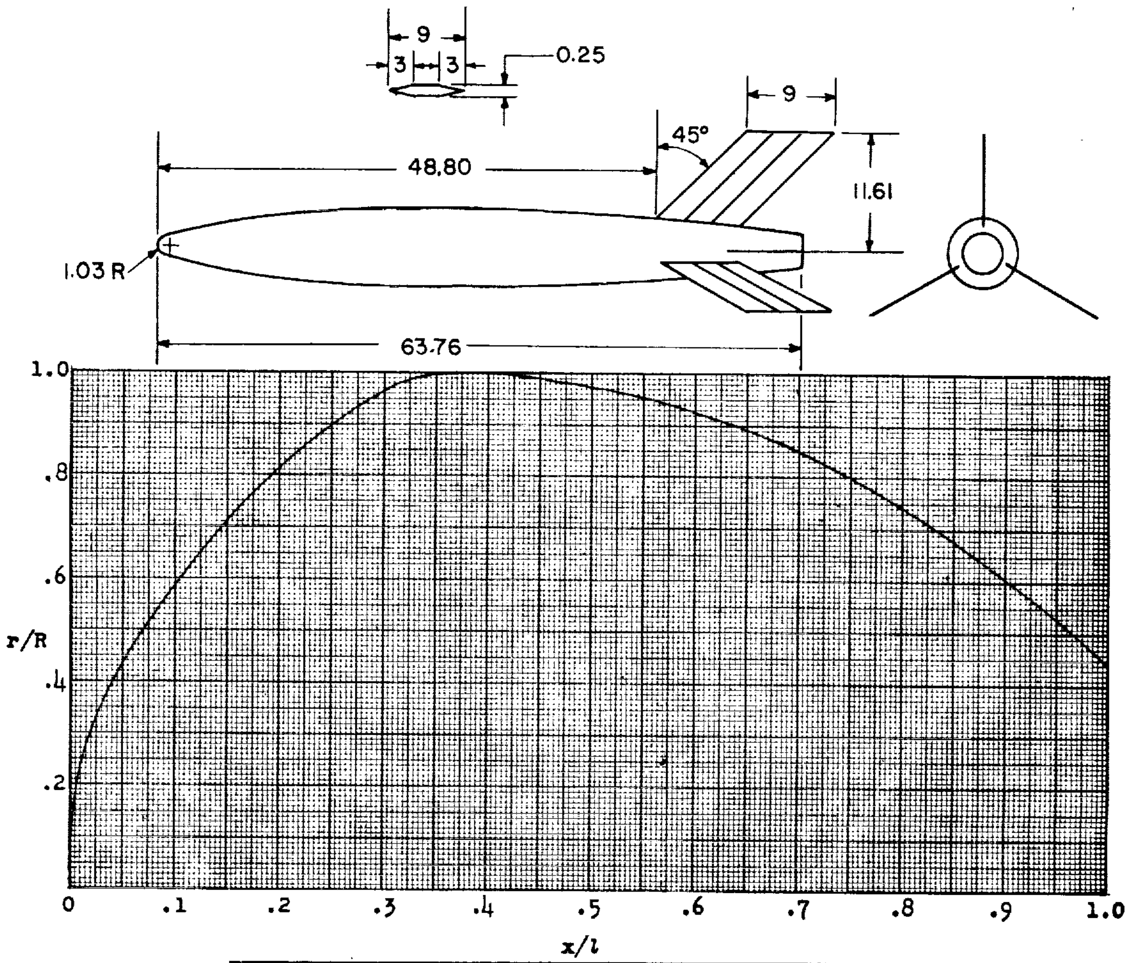

l/d_{Total}	8.5	l/d_{Nose}	3.16	S_b/A	26.80	A_b/A	.19
l/d_{N+A}	8.5	l/d_{Aft}	5.34	S_f/A	11.0	θ_b	7°

Designation: 70

Test: **Rocket**

Remarks: Nose consists of hemispherical and parabolic segments; parabolic afterbody.

Figure 78.

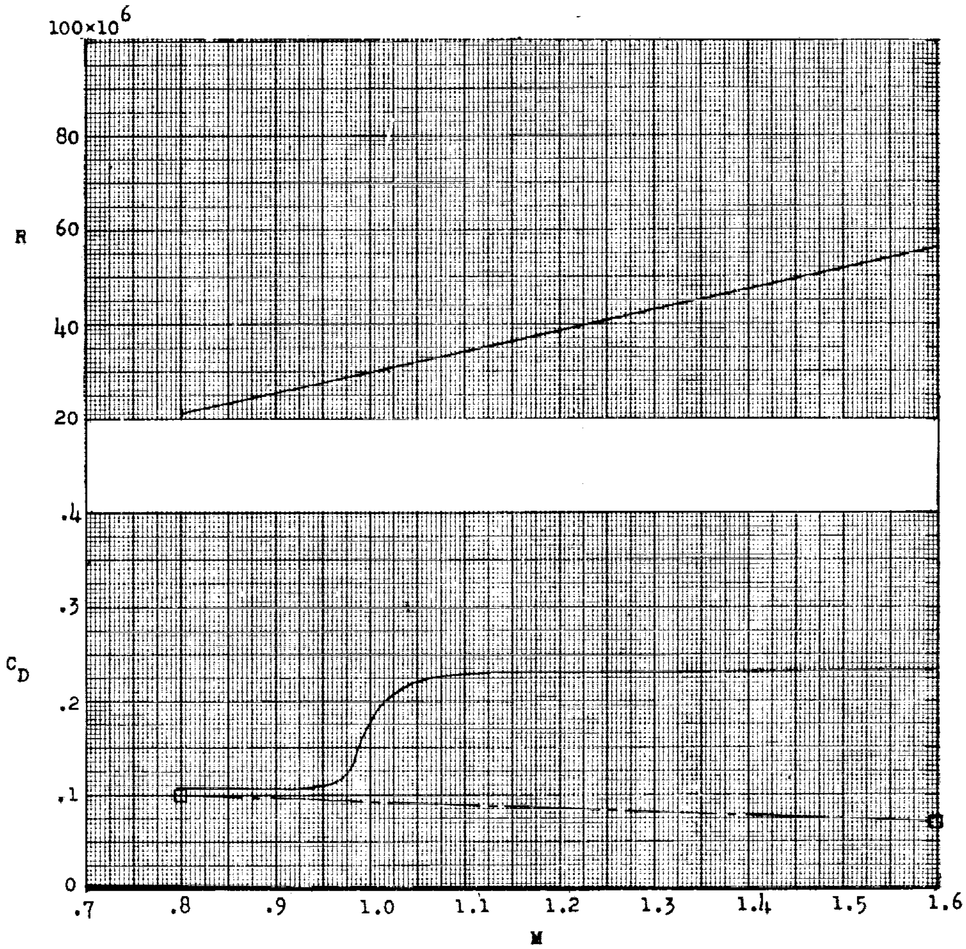

Figure 78.- Concluded.

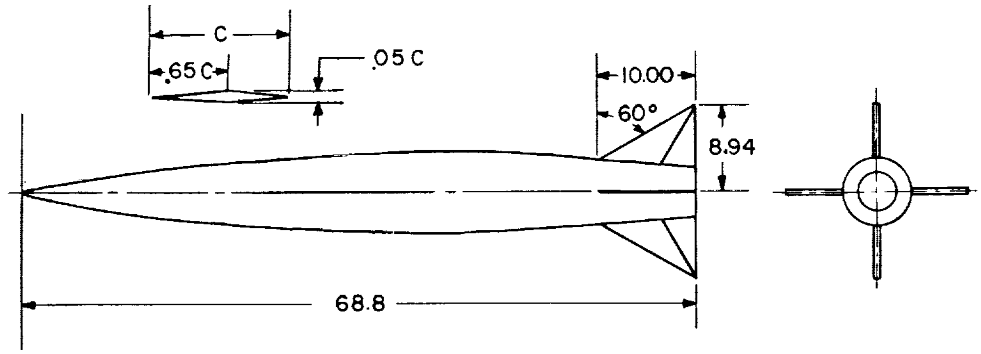

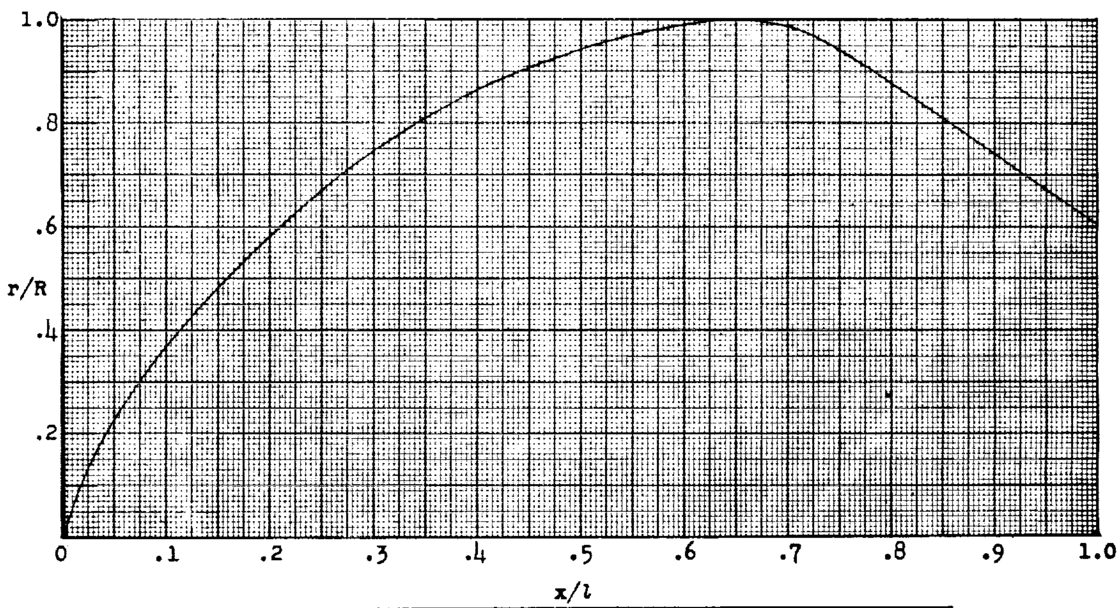

l/d_{Total}	8.60	l/d_{Nose}	5.59	S_b/A	25.70	A_b/A	.36
l/d_{N+A}	8.60	l/d_{Aft}	3.01	S_f/A	5.2	θ_b	4.55°

Designation: 71

Test: Rocket

Figure 79.

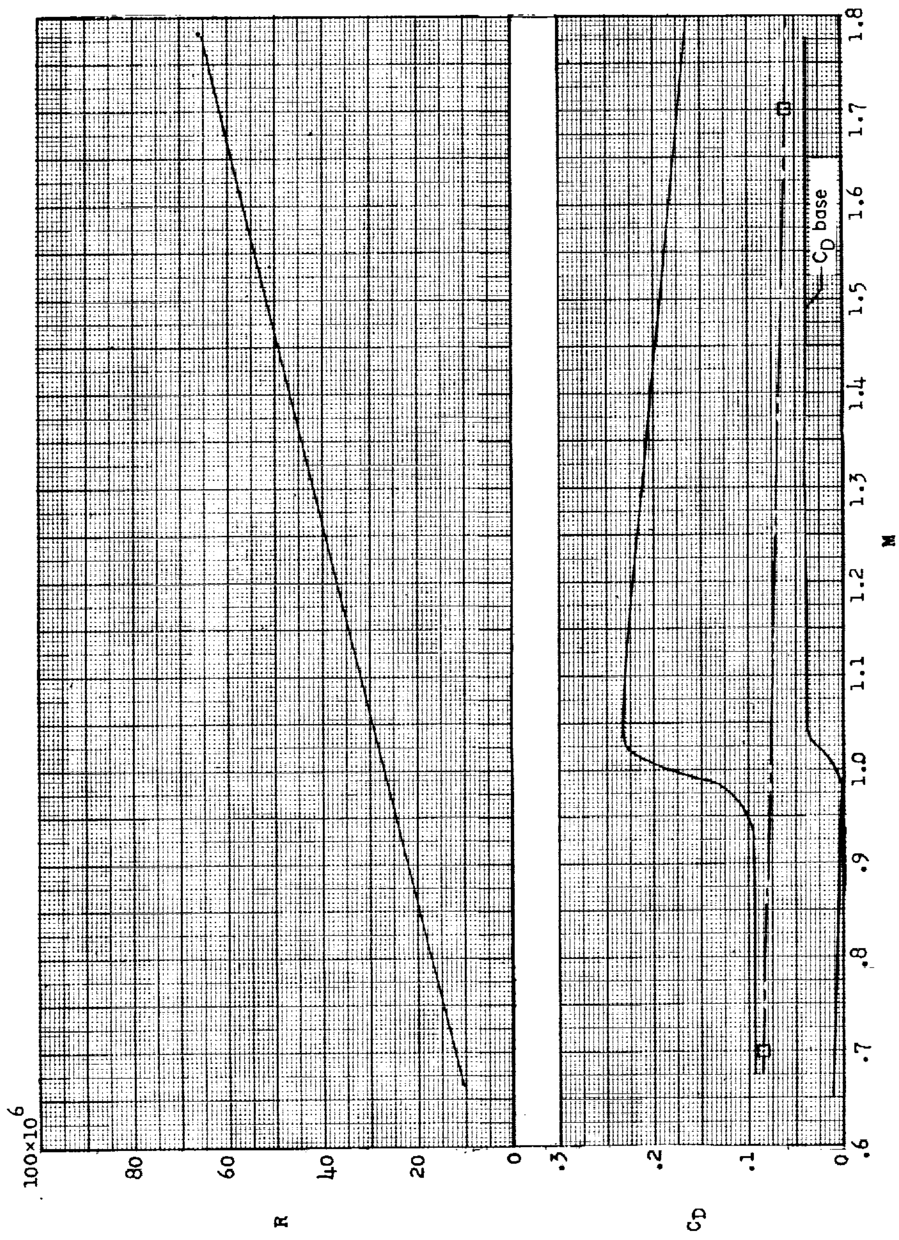

Figure 79.- Concluded.

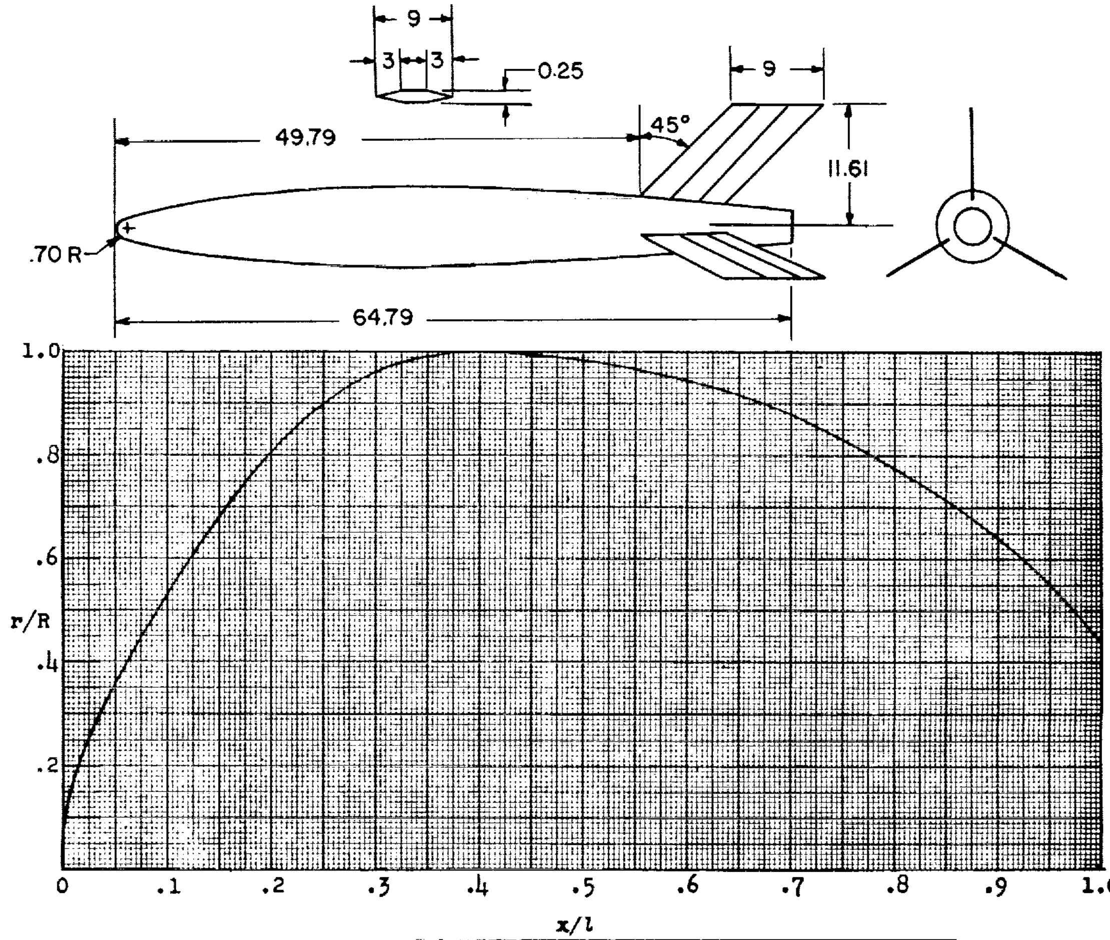

l/d_{Total}	8.65	l/d_{Nose}	3.28	S_b/A	27.3	A_b/A	.19
l/d_{N+A}	8.65	l/d_{Aft}	5.37	S_f/A	11.0	θ_b	7°

Designation: 72

Test: Rocket

Remarks: Nose consists of hemispherical and parabolic segments; parabolic afterbody.

Figure 80.

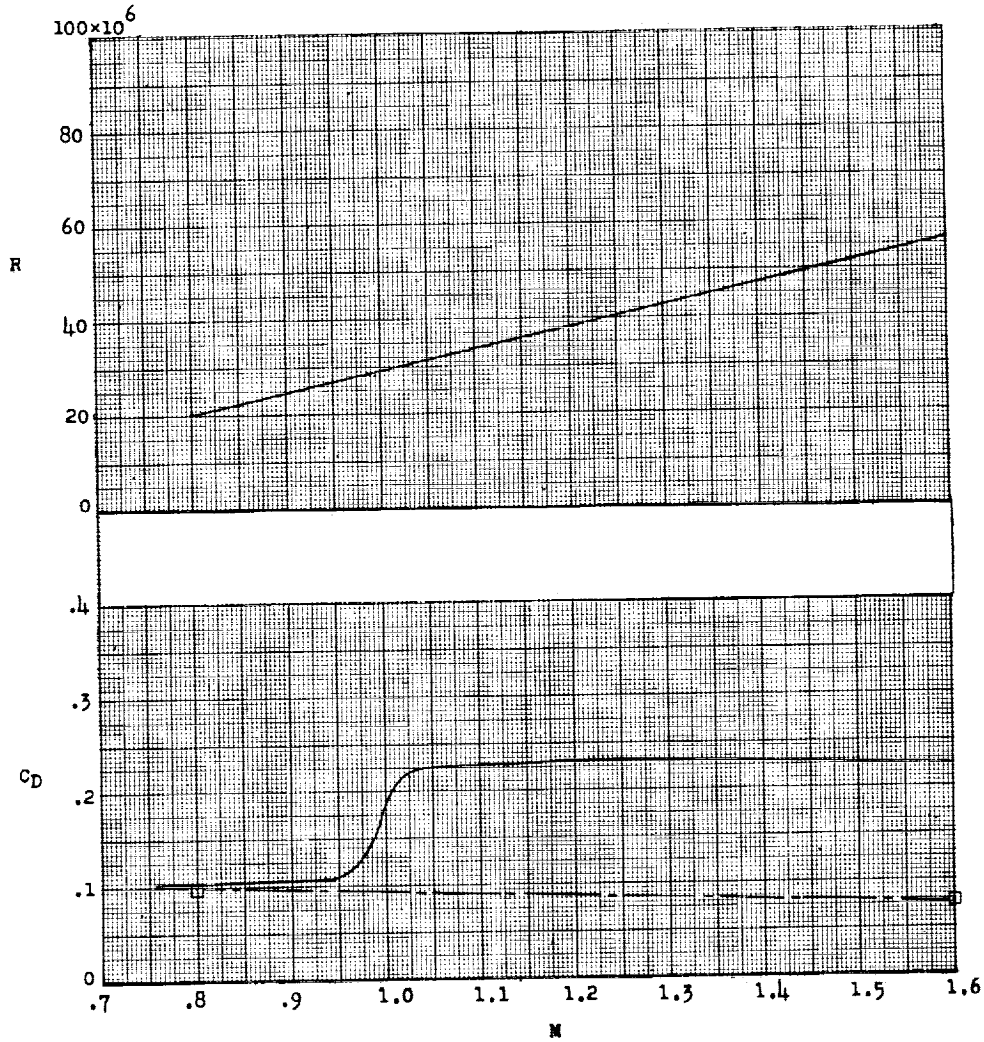

Figure 80.- Concluded.

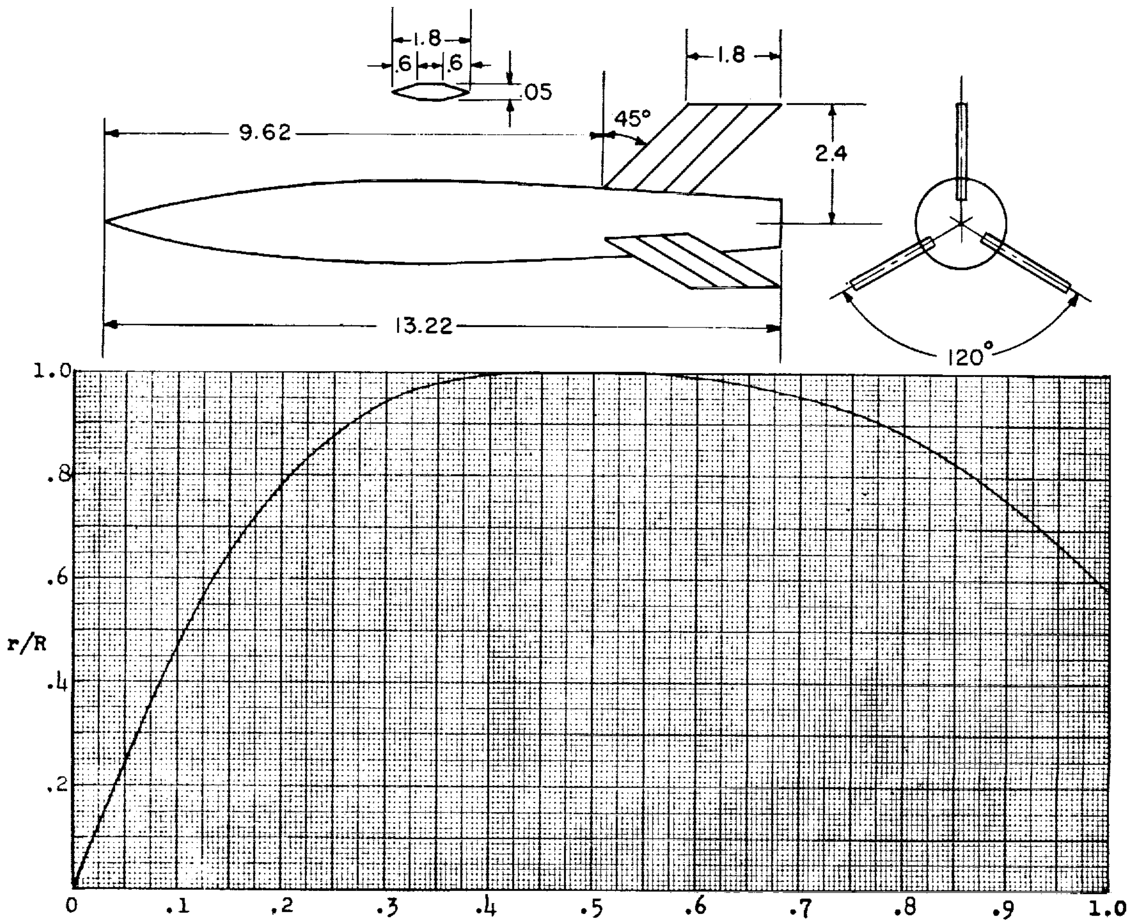

l/d_{Total}	8.81	l/d_{Nose}	4.04	S_b/A	28.8	A_b/A	.33
l/d_{N+A}	8.81	l/d_{Aft}	4.77	S_f/A	11	θ_b	6.9°

Designation: 73

Test: Helium Gun

Figure 81.

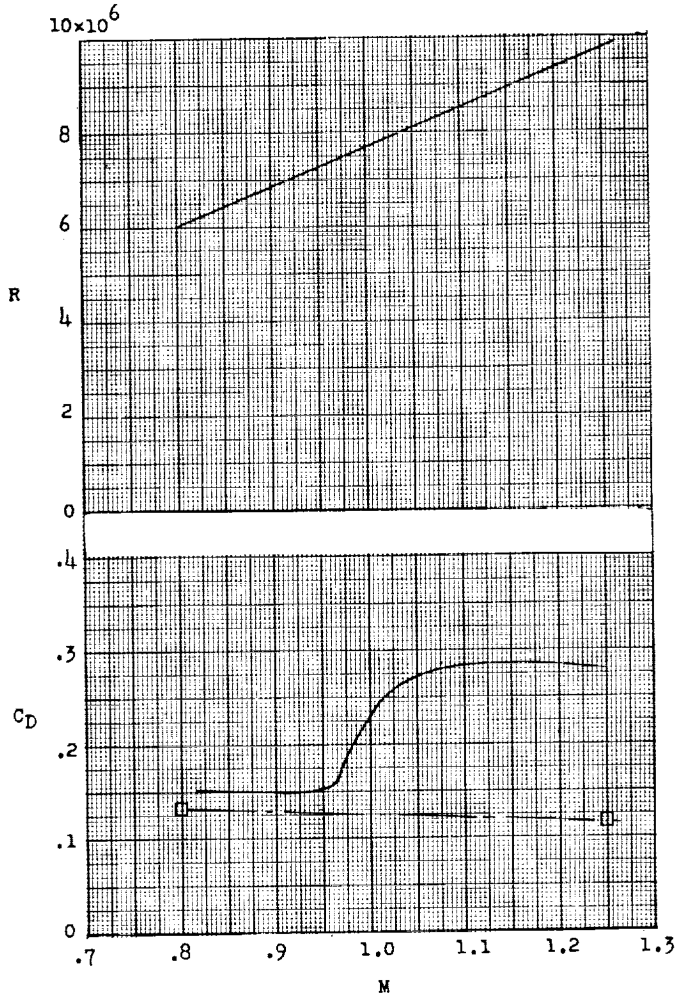

Figure 81.- Concluded.

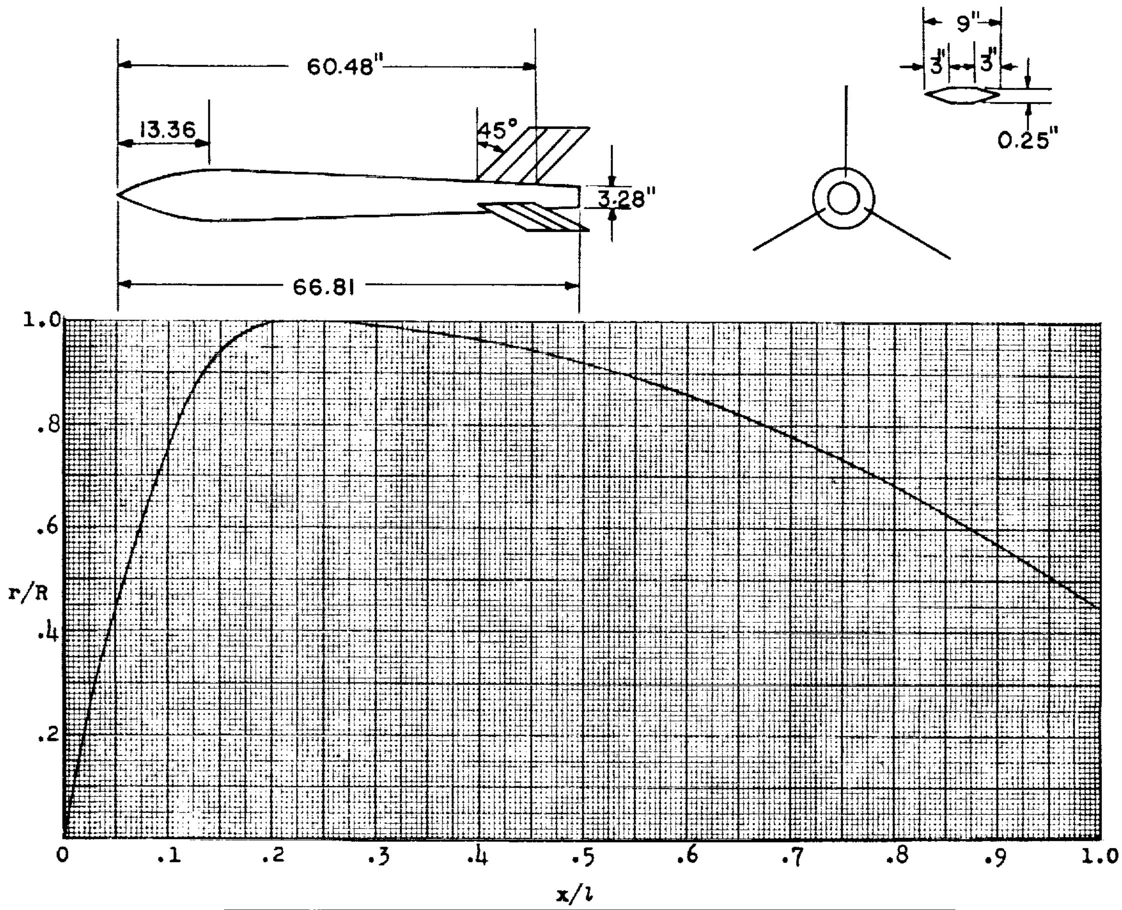

l/d_{Total}	8.91	l/d_{Nose}	1.78	S_b/A	28.26	A_b/A	.19
l/d_{N+A}	8.91	l/d_{Aft}	7.13	S_f/A	11.0	θ_b	6.5°

Designation: 74

Test: Rocket

Remarks: Parabolic nose and afterbody.

Figure 82.

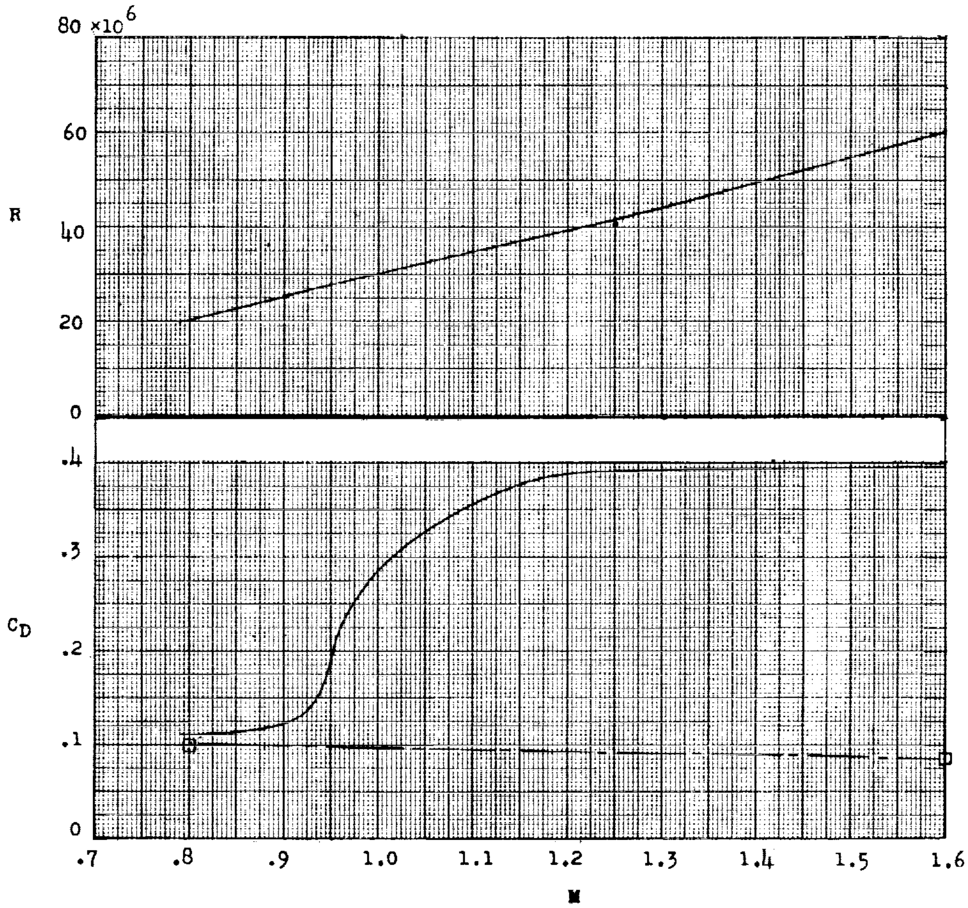

Figure 82.- Concluded.

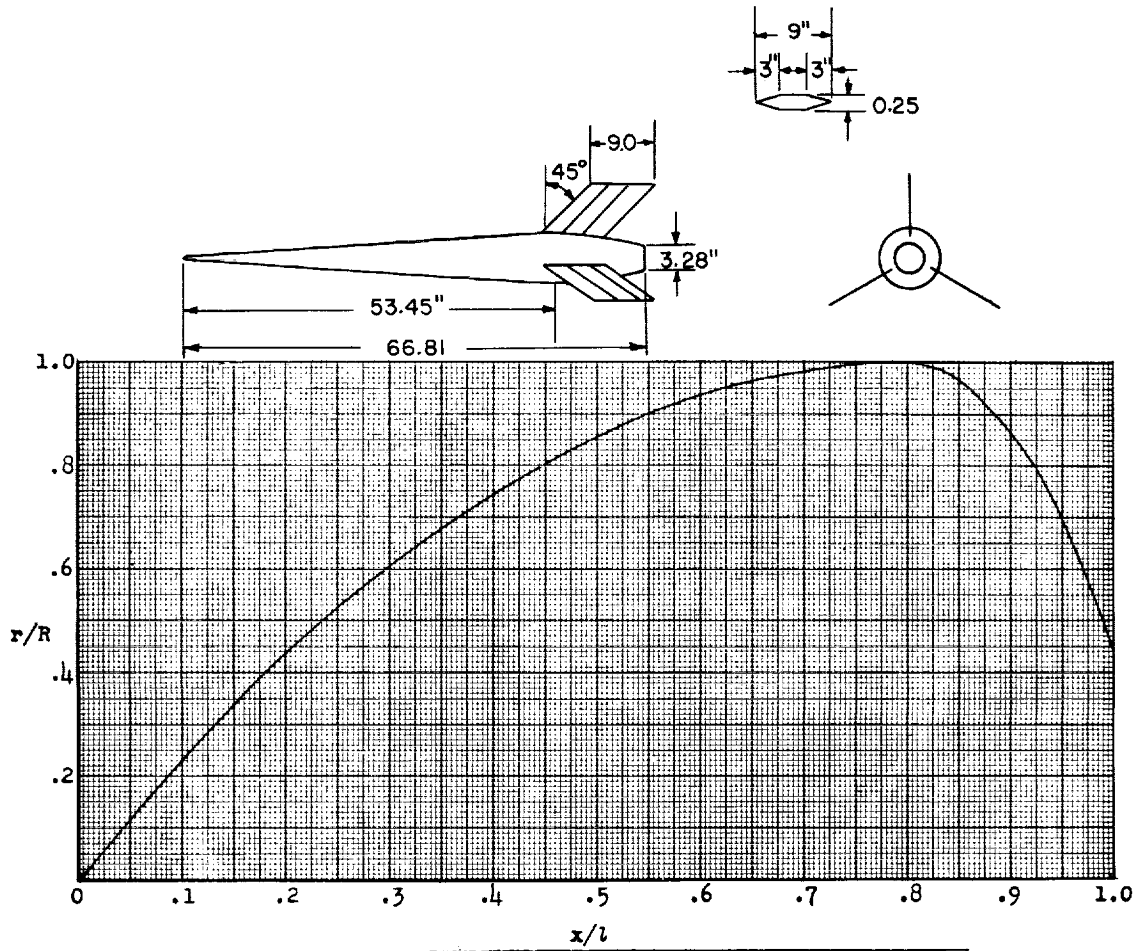

l/d_{Total}	8.91	l/d_{Nose}	7.13	S_b/A	24.84	A_b/A	.19
l/d_{N+A}	8.91	l/d_{Aft}	1.78	S_f/A	11.0	θ_b	18.3°

Designation: 75

Test: Rocket

Remarks: Parabolic nose and afterbody.

Figure 83.

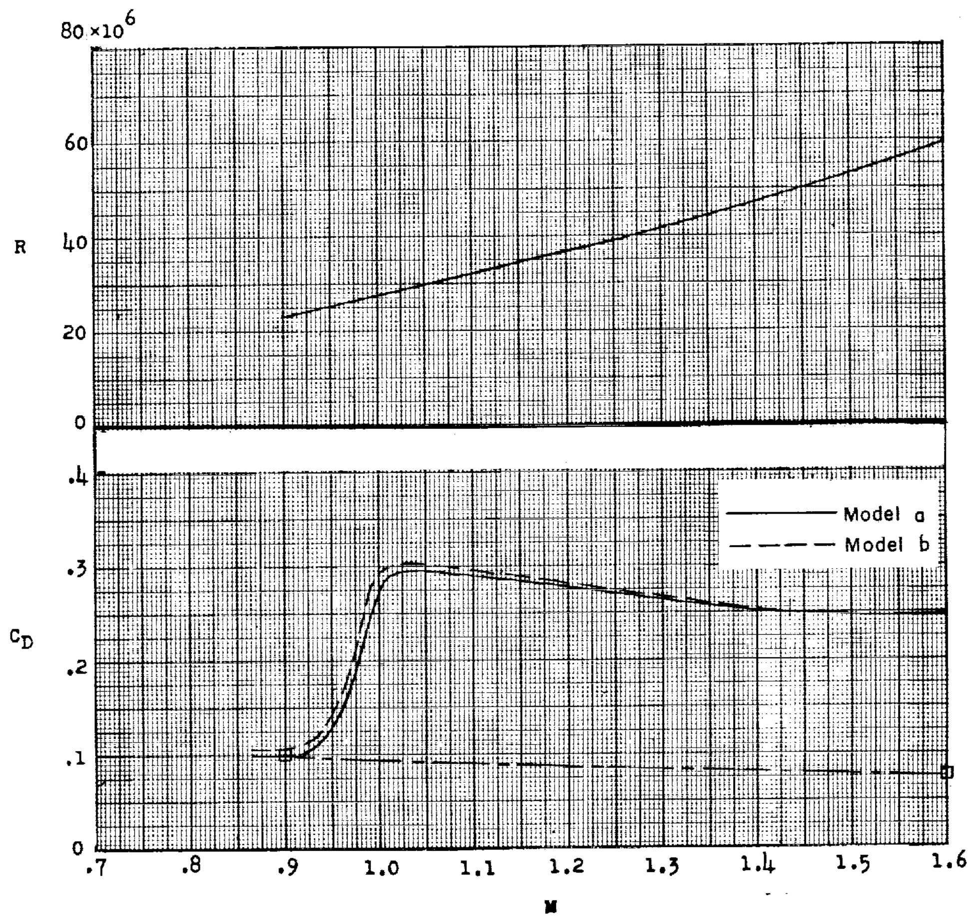

Figure 83.- Concluded.

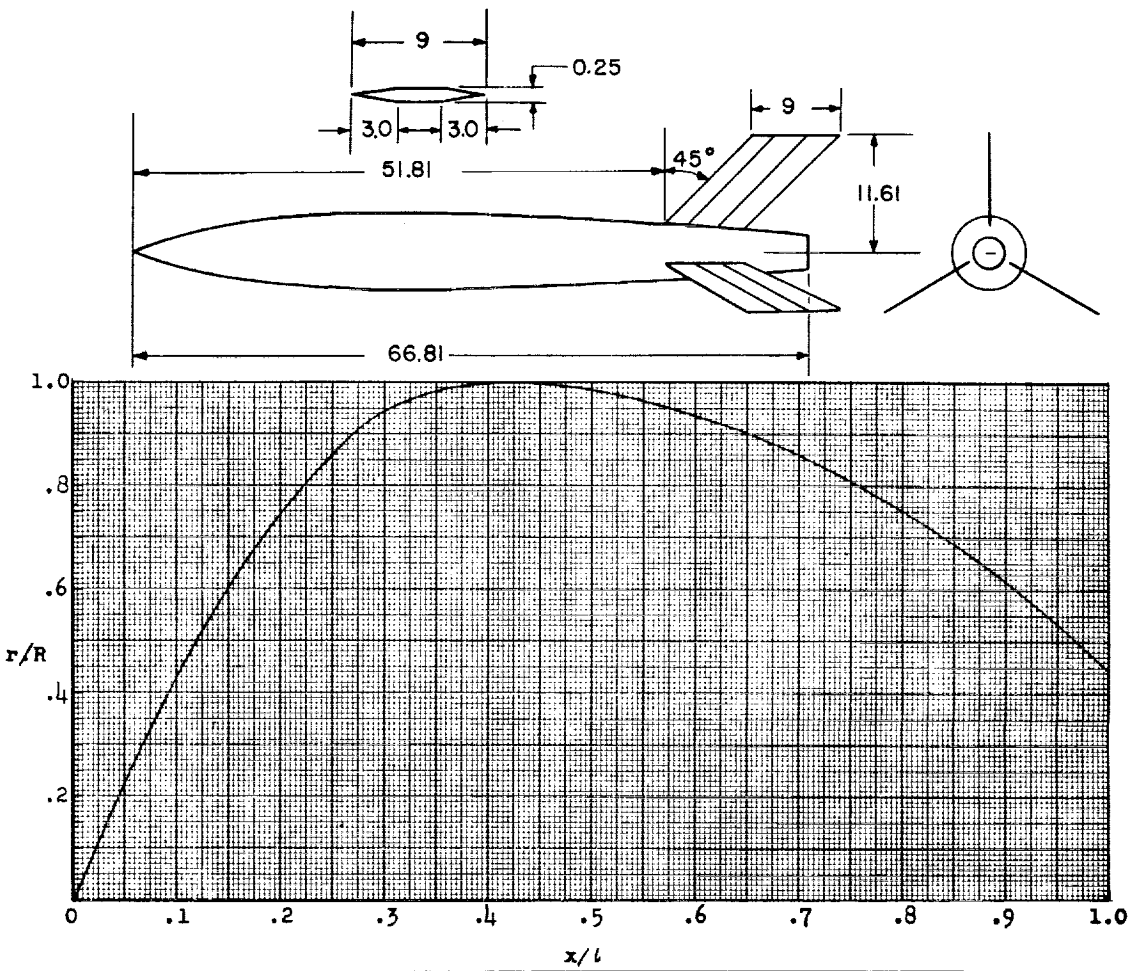

l/d_{Total}	8.91	l/d_{Nose}	3.56	S_b/A	27.00	A_b/A	.19
l/d_{N+A}	8.91	l/d_{Aft}	5.35	S_f/A	11.0	θ_b	6.0°

Designation: 76

Test: Rocket

Remarks: Parabolic nose and afterbody; waviness of coefficient of low Mach number models is probably due to afterburning of their sustainer rockets.

Figure 84.

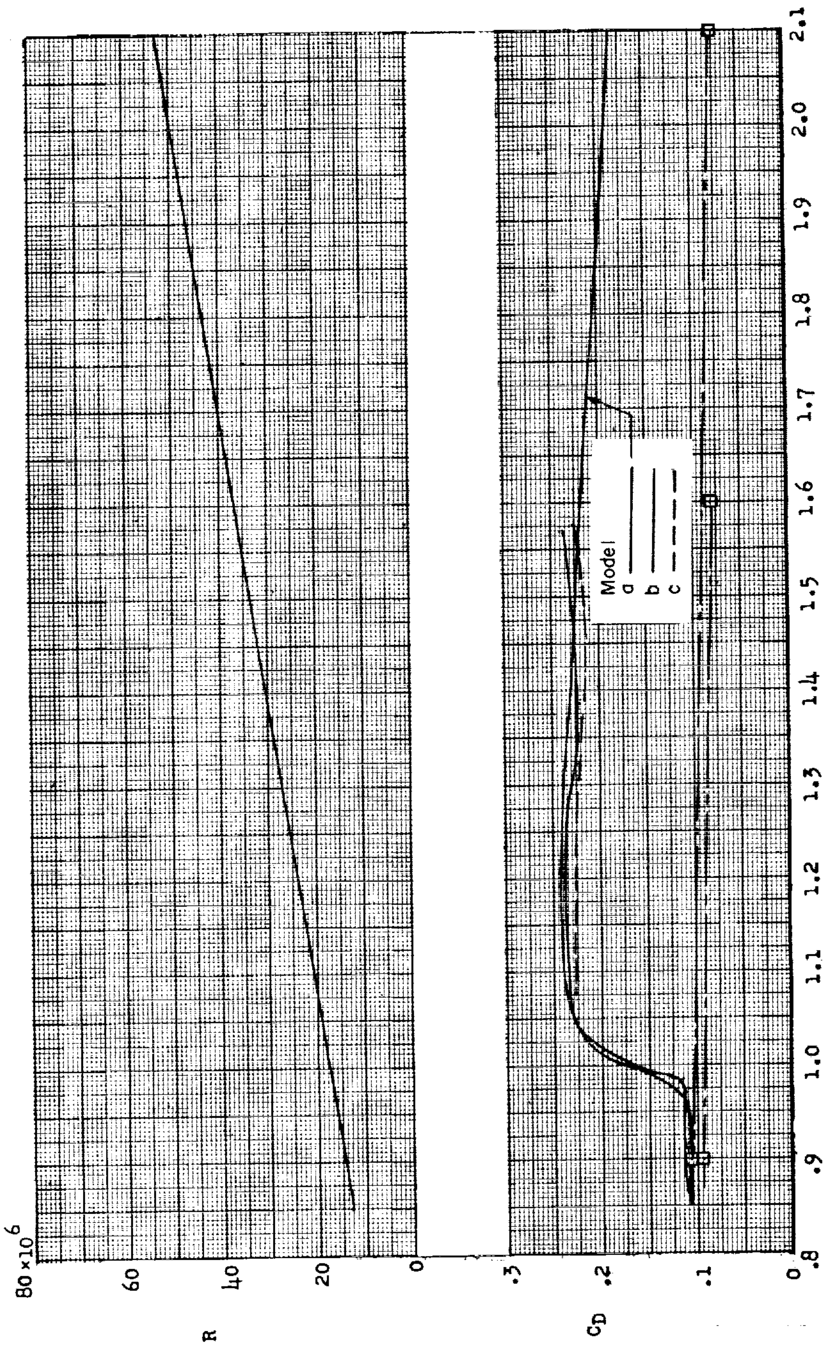

Figure 84.- Concluded.

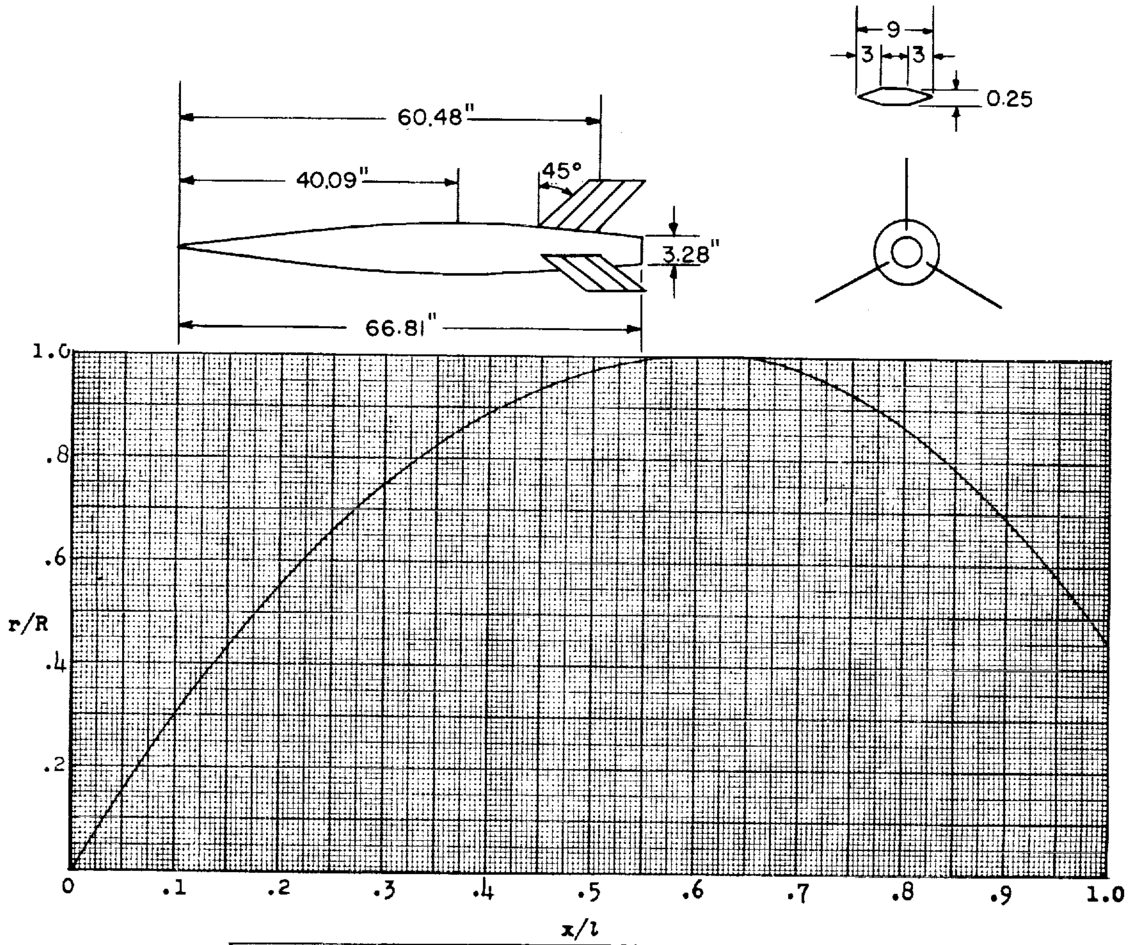

l/d_{Total}	8.91	l/d_{Nose}	5.35	S_b/A	26.02	A_b/A	.19
l/d_{N+A}	8.91	l/d_{Aft}	3.56	S_f/A	11.0	θ_b	10.2°

Designation: 77

Test: Rocket

Remarks: Parabolic nose and afterbody.

Figure 85.

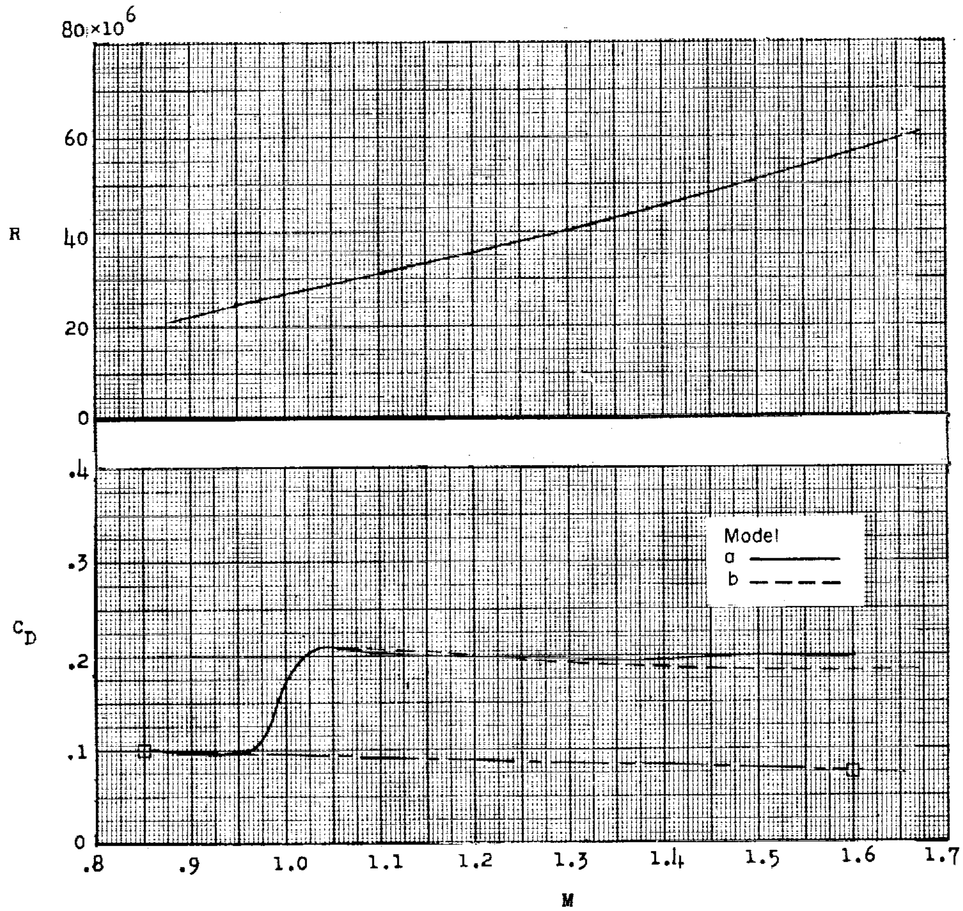

Figure 85.- Concluded.

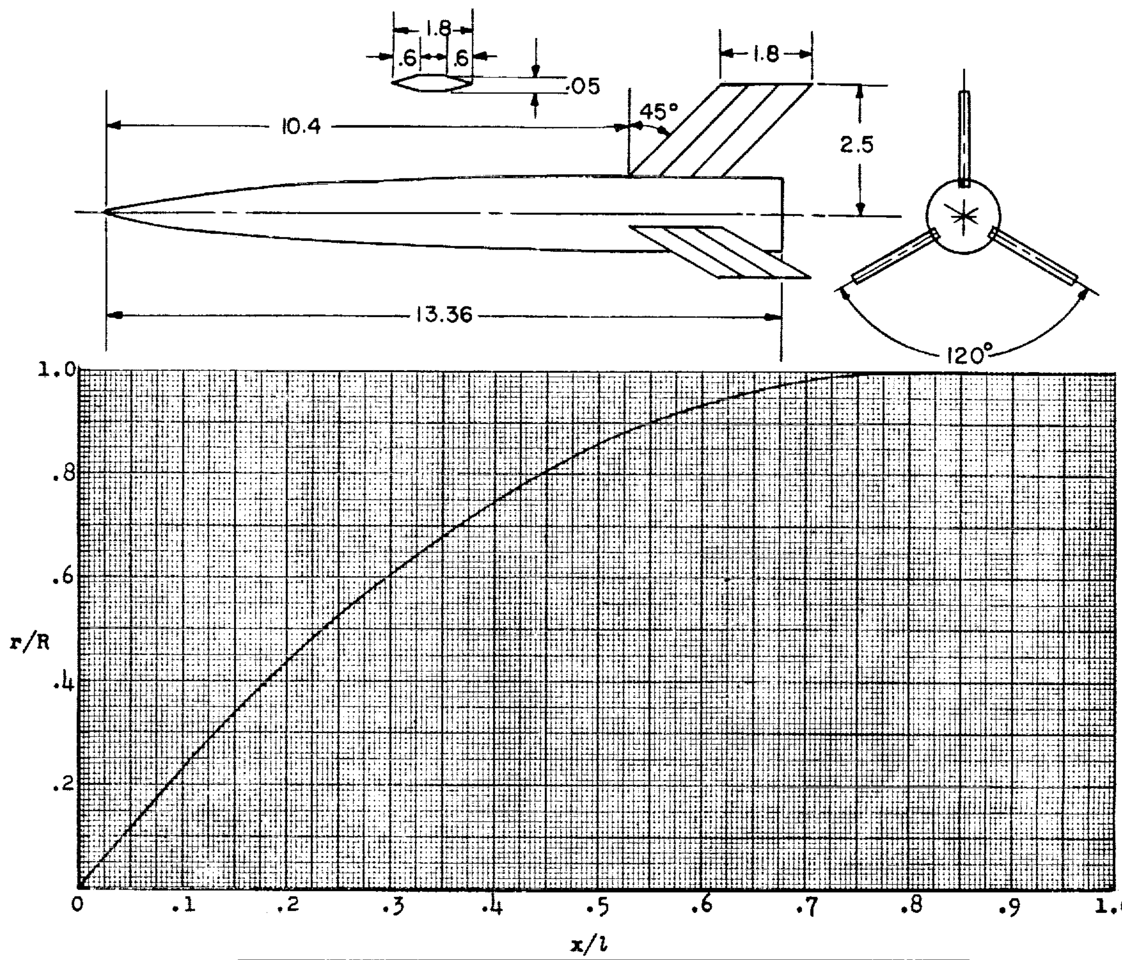

l/d_{Total}	8.91	l/d_{Nose}	7.13	S_b/A	26.10	A_b/A	1.00
l/d_{N+A}	8.91	l/d_{Aft}	1.78	S_f/A	11.0	θ_b	0°

Designation: 78

Test: Helium Gun

Remarks: Parabolic nose.

Figure 86.

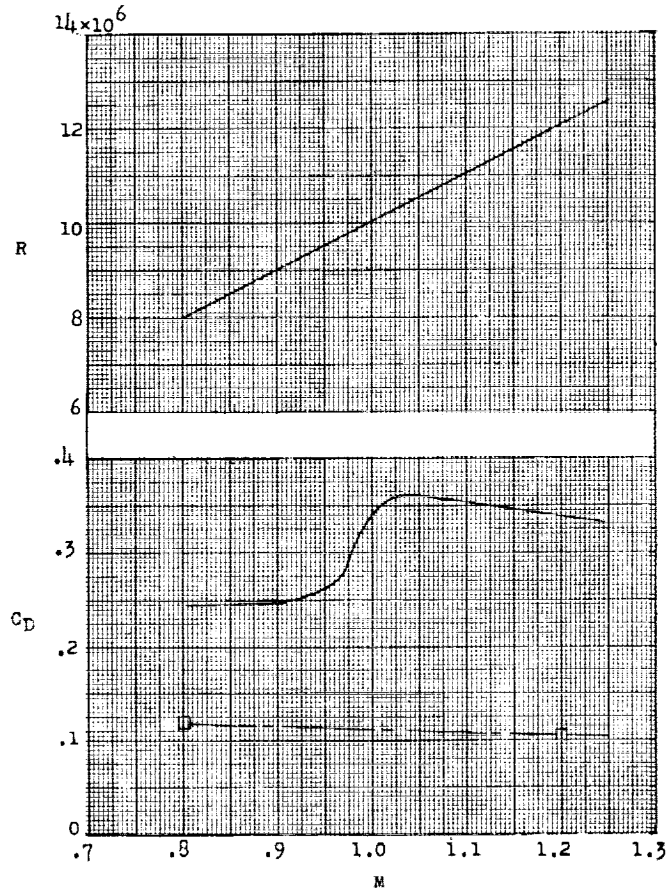

Figure 86.- Concluded.

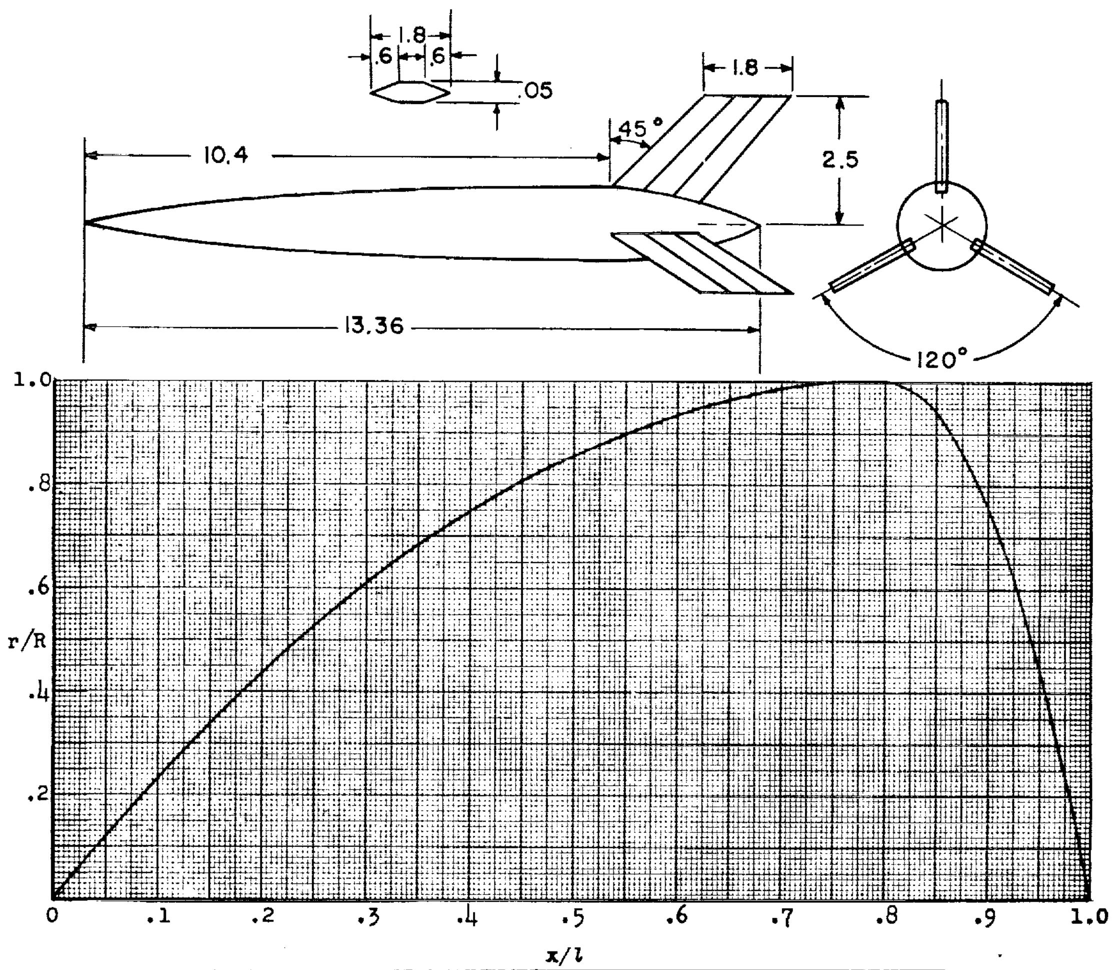

l/d_{Total}	8.91	l/d_{Nose}	7.13	S_b/A	23.70	A_b/A	0
l/d_{N+A}	8.91	l/d_{Aft}	1.78	S_f/A	11.0	θ_b	29.3°

Designation: 79

Test: Helium Gun

Figure 87.

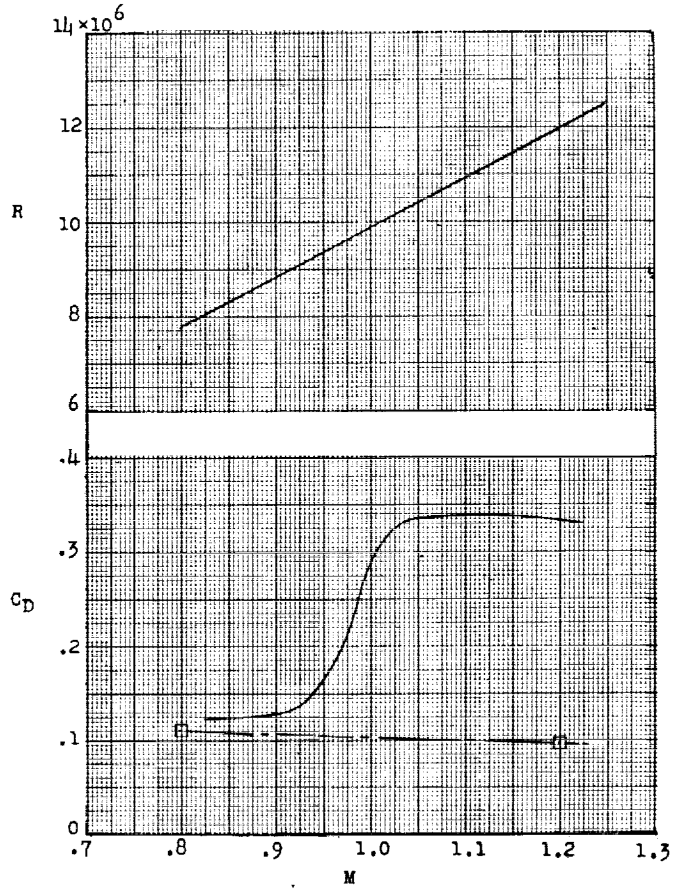

Figure 87.- Concluded.

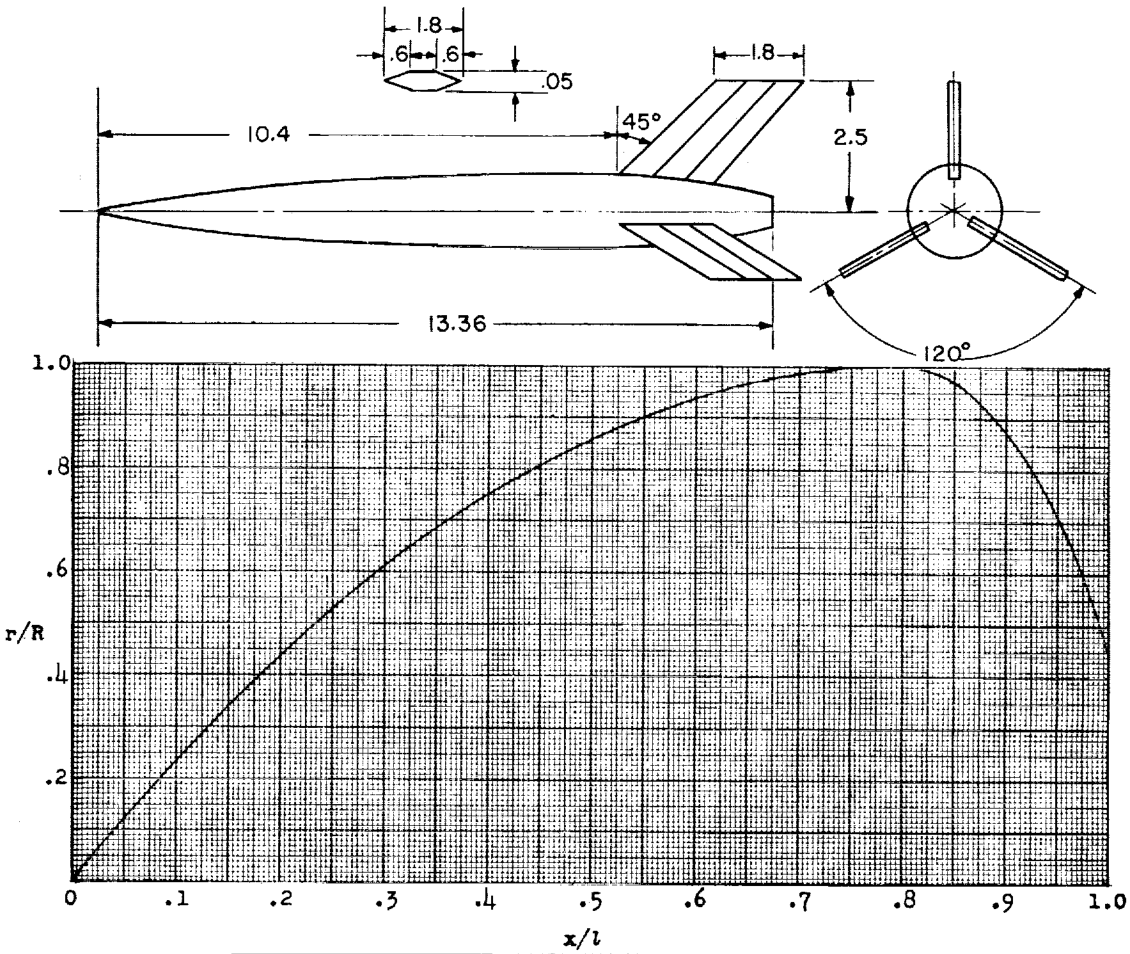

l/d_{Total}	8.91	l/d_{Nose}	7.13	S_b/A	24.8	A_b/A	.19
l/d_{N+A}	8.91	l/d_{Aft}	1.78	S_f/A	11.0	θ_b	17.5°

Designation: 80

Test: Helium Gun

Remarks: Parabolic nose and afterbody.

Figure 88.

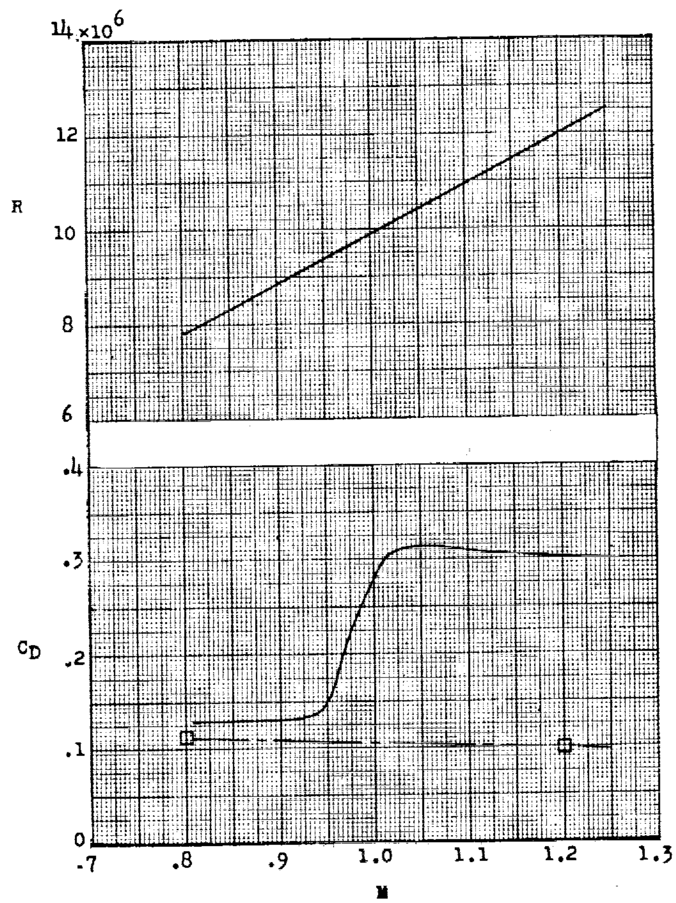

Figure 88.- Concluded.

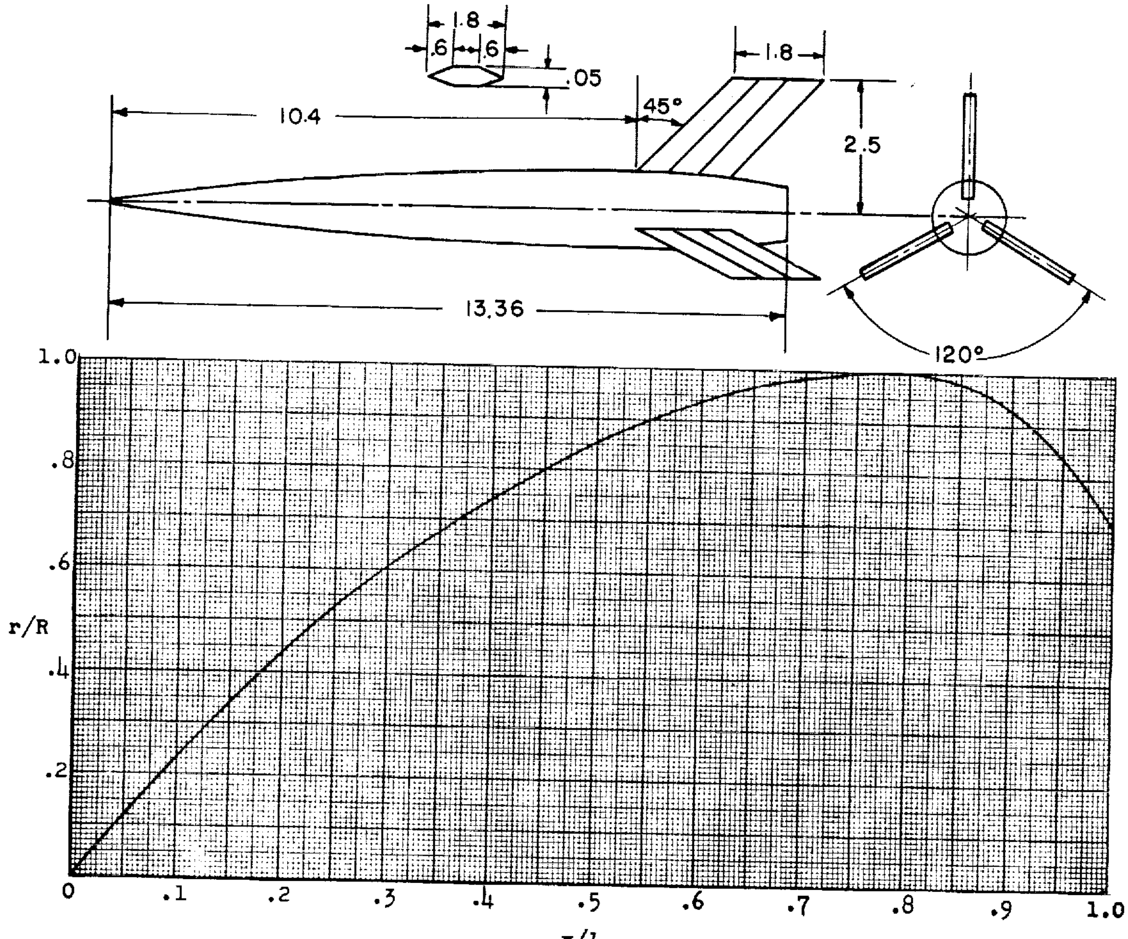

l/d_{Total}	8.91	l/d_{Nose}	7.13	S_b/A	25.4	A_b/A	.49
l/d_{N+A}	8.91	l/d_{Aft}	1.78	S_f/A	11.0	θ_b	9.6°

Designation: 81

Test: Helium Gun

Remarks: Parabolic nose and afterbody.

Figure 89.

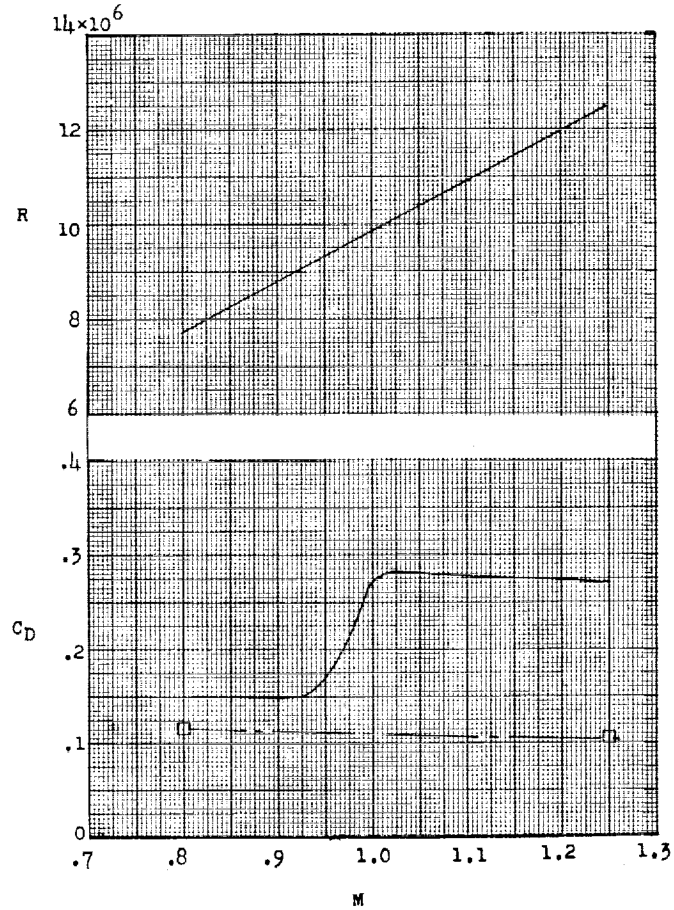

Figure 89.- Concluded.

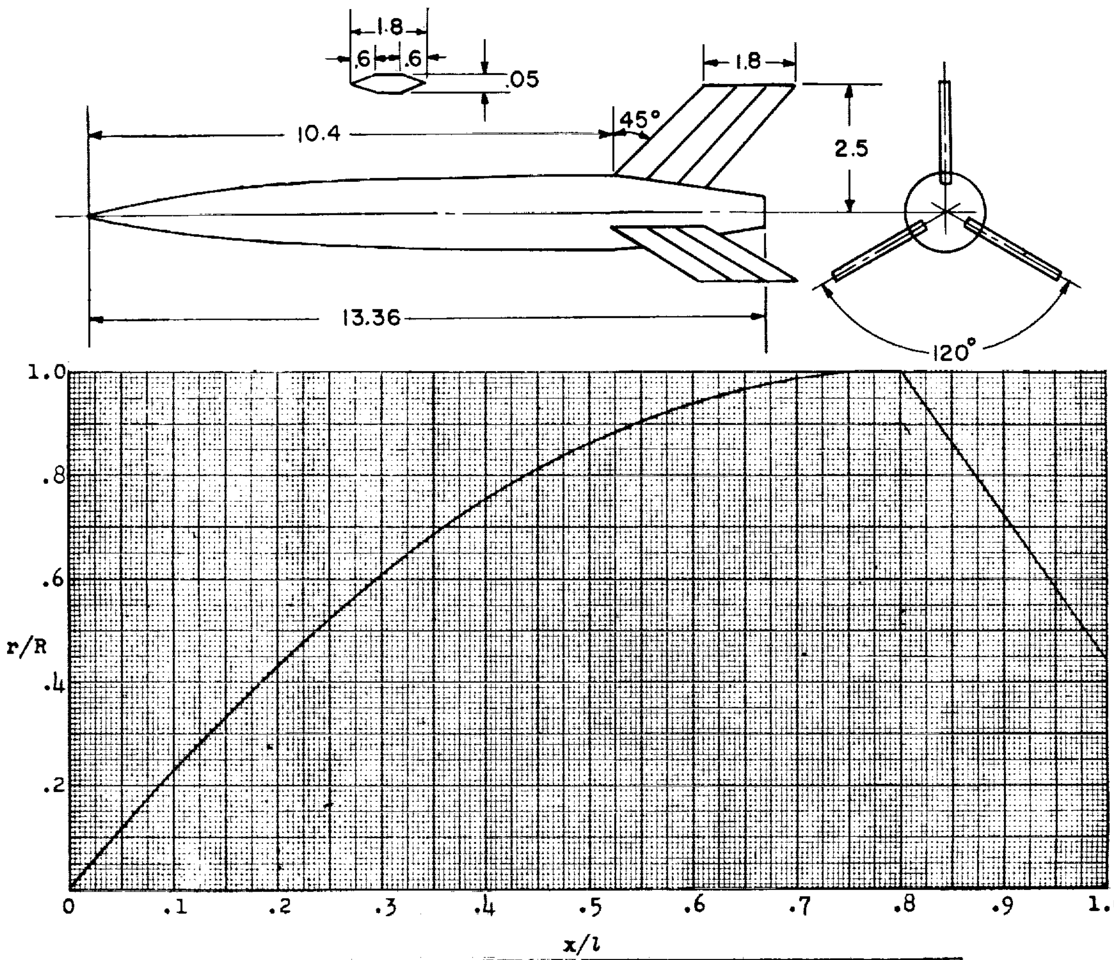

l/d_{Total}	8.91	l/d_{Nose}	7.13	S_b/A	24.2	A_b/A	.19
l/d_{N+A}	8.91	l/d_{Aft}	1.78	S_f/A	11.0	θ_b	9°

Designation: 82

Test: **Helium Gun**

Remarks: Parabolic nose; conical afterbody.

Figure 90.

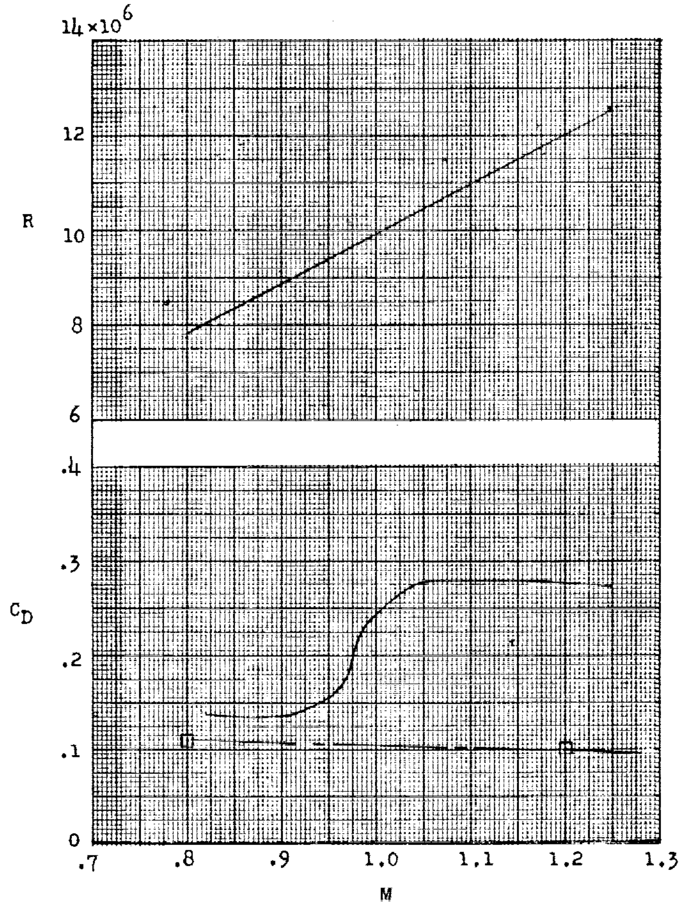

Figure 90.- Concluded.

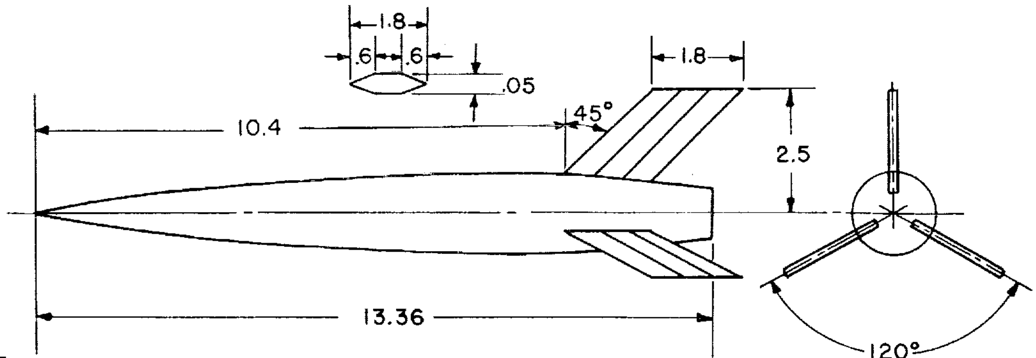

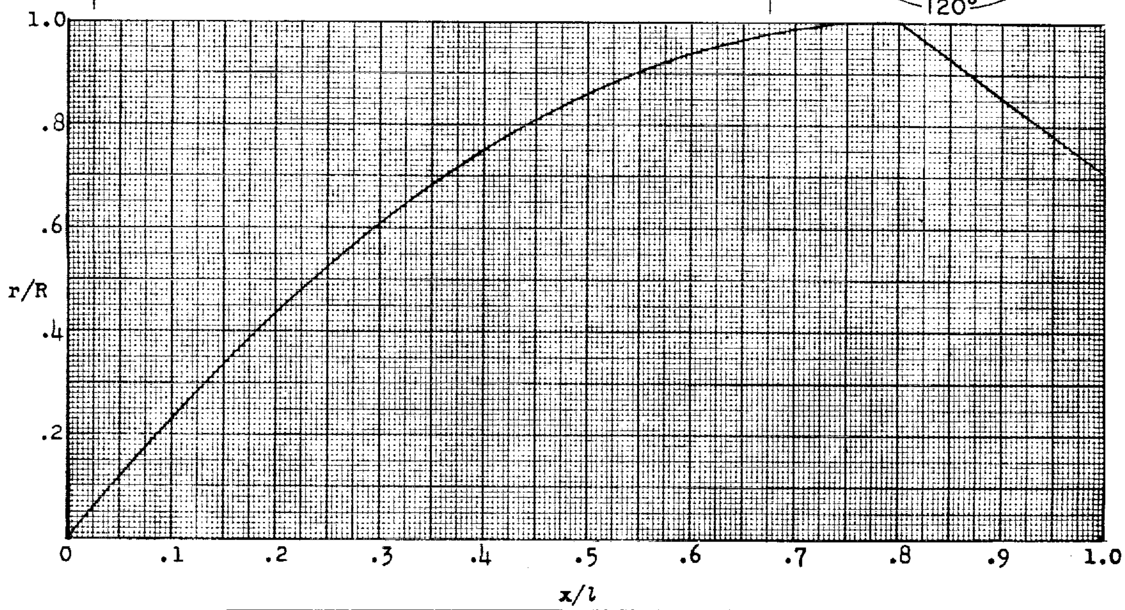

l/d_{Total}	8.91	l/d_{Nose}	7.13	S_b/A	25.10	A_b/A	.49
l/d_{N+A}	8.91	l/d_{Aft}	1.78	S_f/A	11	θ_b	4.87°

Designation: 83

Test: **Helium Gun**

Remarks: Parabolic nose and afterbody.

Figure 91.

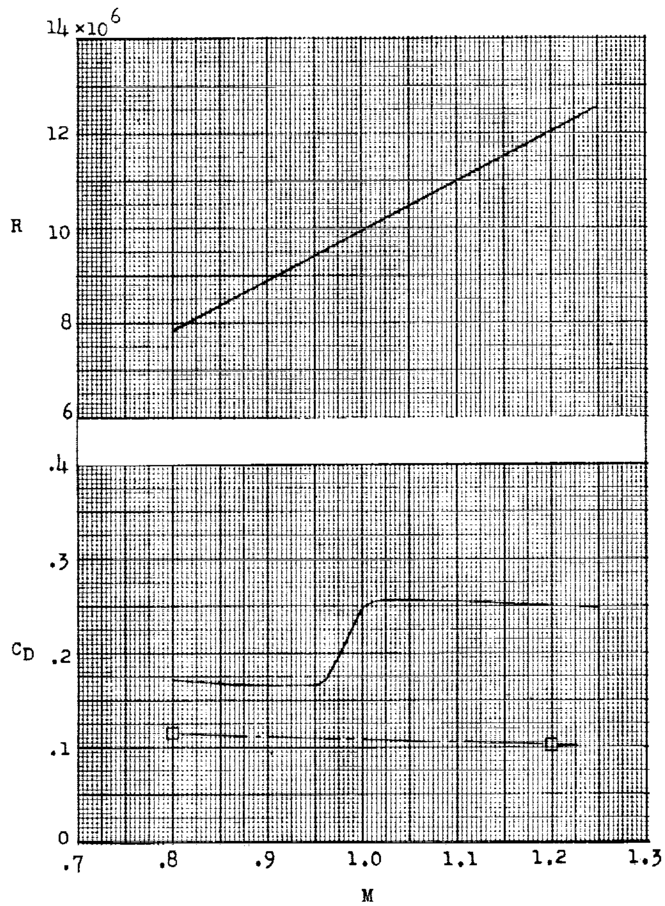

Figure 91.- Concluded.

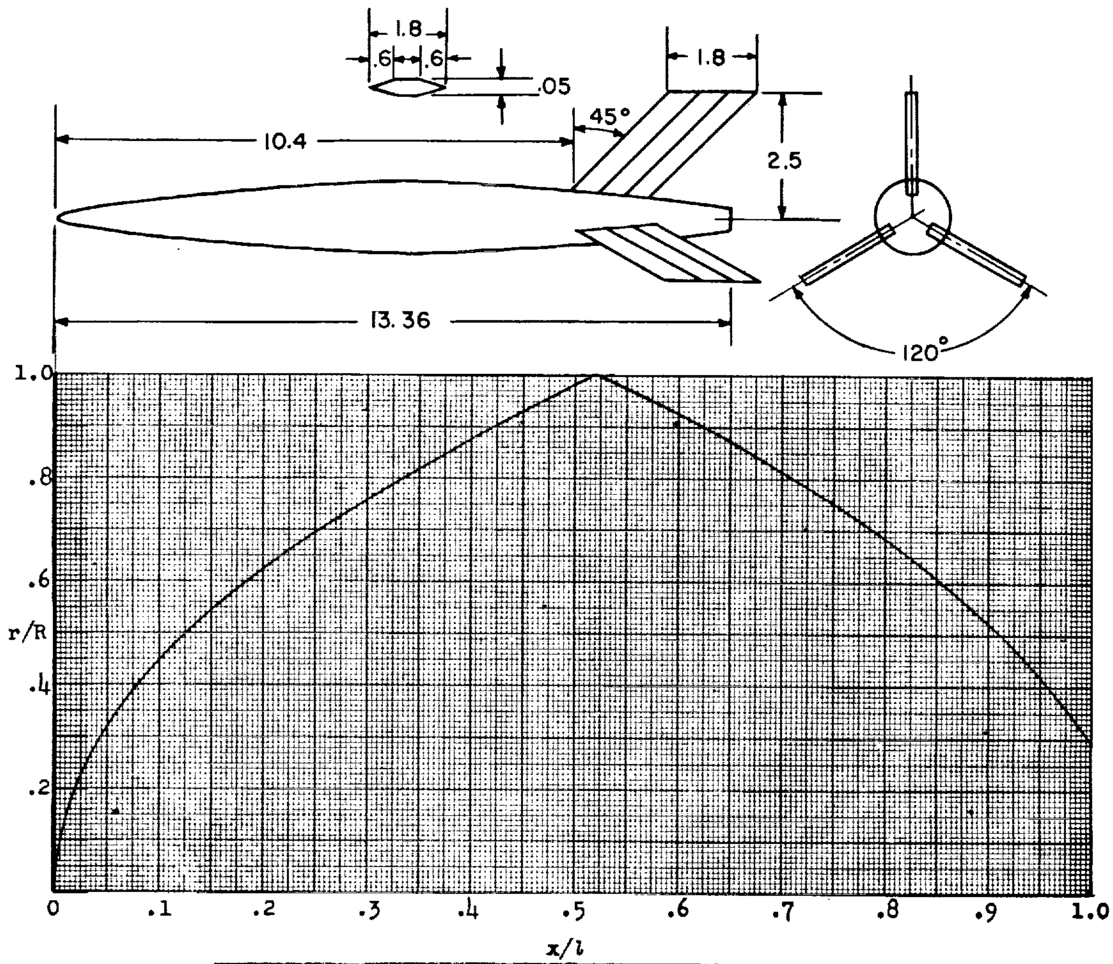

l/d_{Total}	8.91	l/d_{Nose}	4.66	S_b/A	24.5	A_b/A	.09
l/d_{N+A}	8.91	l/d_{Aft}	4.25	S_f/A	11.0	θ_b	9.7°

Designation: 84

Test: **Helium Gun**

Remarks: Contour of nose and afterbody exactly the same as those of configuration 85 (fig. 93).

Figure 92.

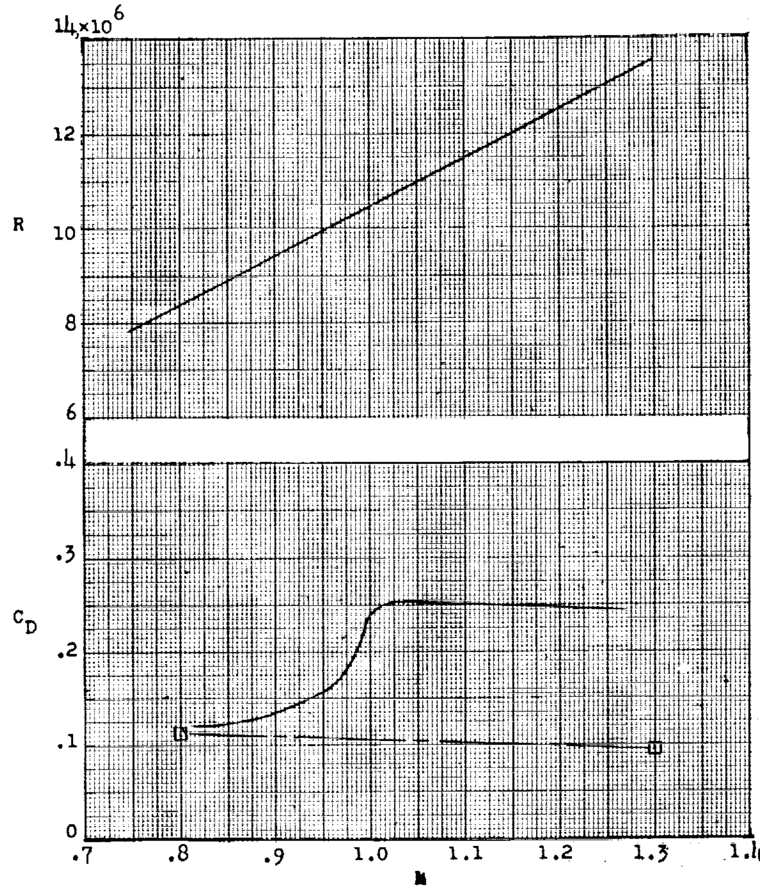

Figure 92.- Concluded.

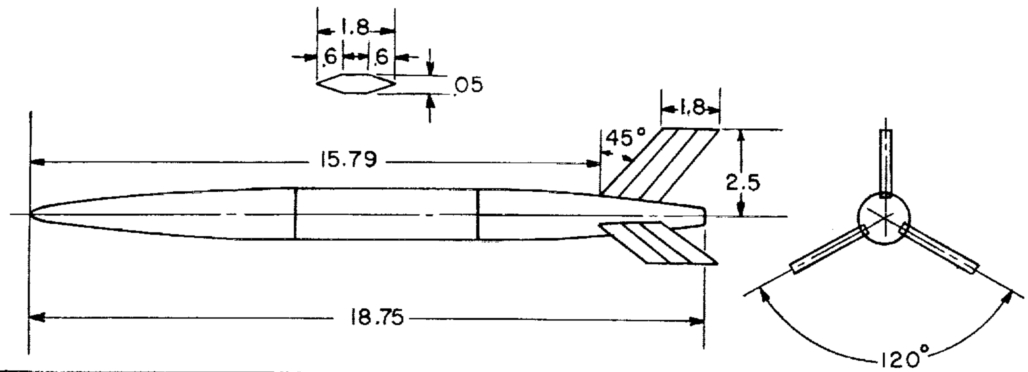

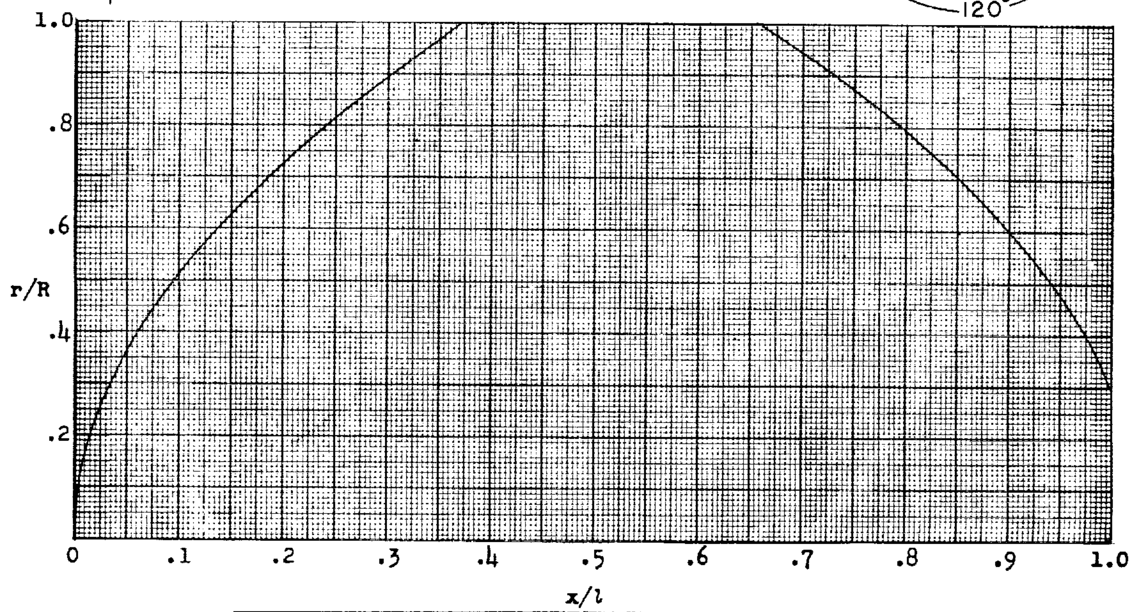

l/d_{Total}	12.5	l/d_{Nose}	4.66	S_b/A	38.8	A_b/A	.09
l/d_{N+A}	8.91	l/d_{Aft}	4.25	S_f/A	11.0	θ_b	10.7°

Designation: 85

Test: **Helium Gun**

Remarks: Contour of nose and afterbody exactly the same as configuration 84 (fig. 92).

Figure 93.

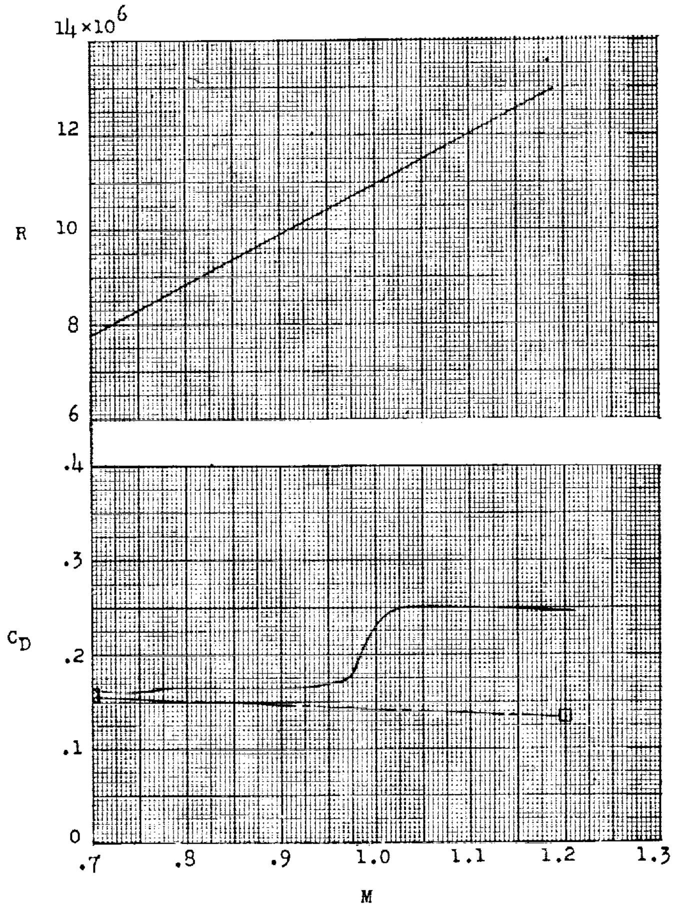

Figure 93.- Concluded.

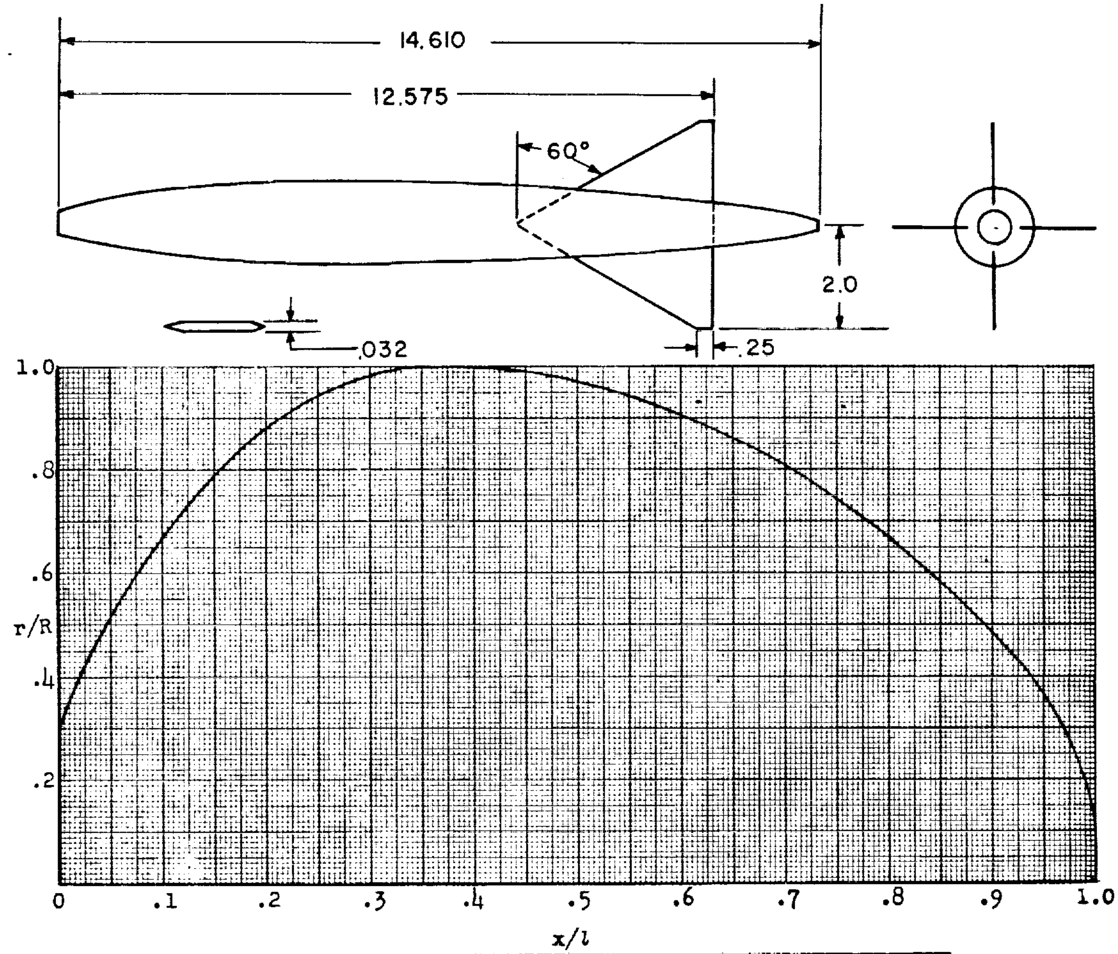

l/d_{Total}	9.13	l/d_{Nose}	3.28	S_b/A	28.0	A_b/A	.008
l/d_{N+A}	9.13	l/d_{Aft}	5.85	S_f/A	8.30	θ_b	30°

Designation: 86

Test: **Helium Gun**

Remarks: Flat face of model caused high subsonic drag. (See also configuration 47 (fig. 55).)

Figure 94.

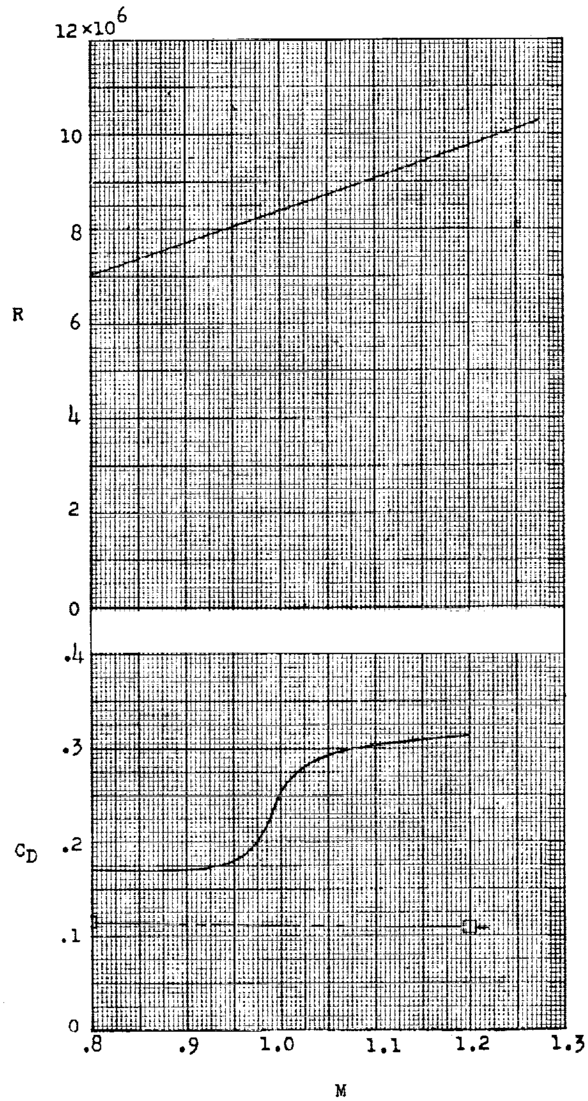

Figure 94.- Concluded.

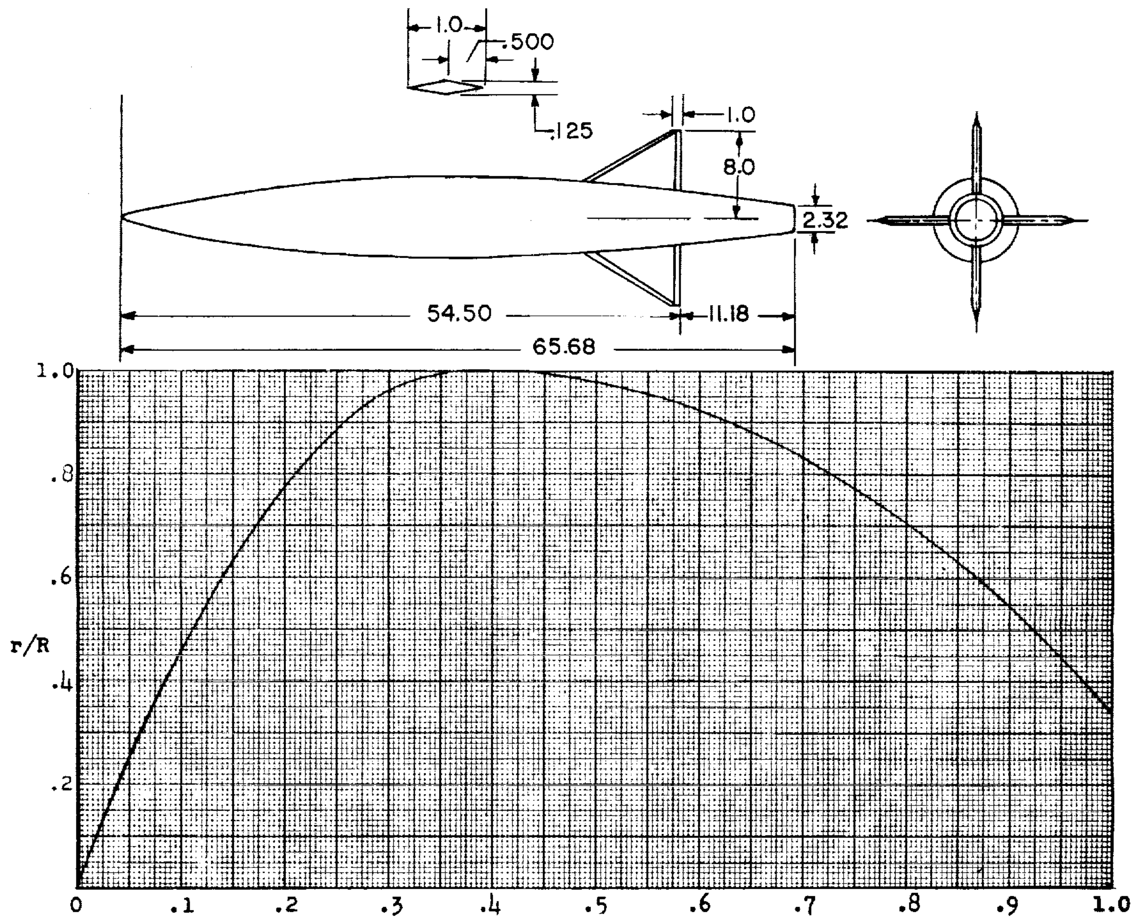

l/d_{Total}	9.38	l/d_{Nose}	3.63	S_b/A	28.00	A_b/A	.11
l/d_{N+A}	9.38	l/d_{Aft}	5.75	S_f/A	6.40	θ_b	7.0°

Designation: 87

Test: **Rocket**

Remarks: Parabolic nose and afterbolic.

Figure 95.

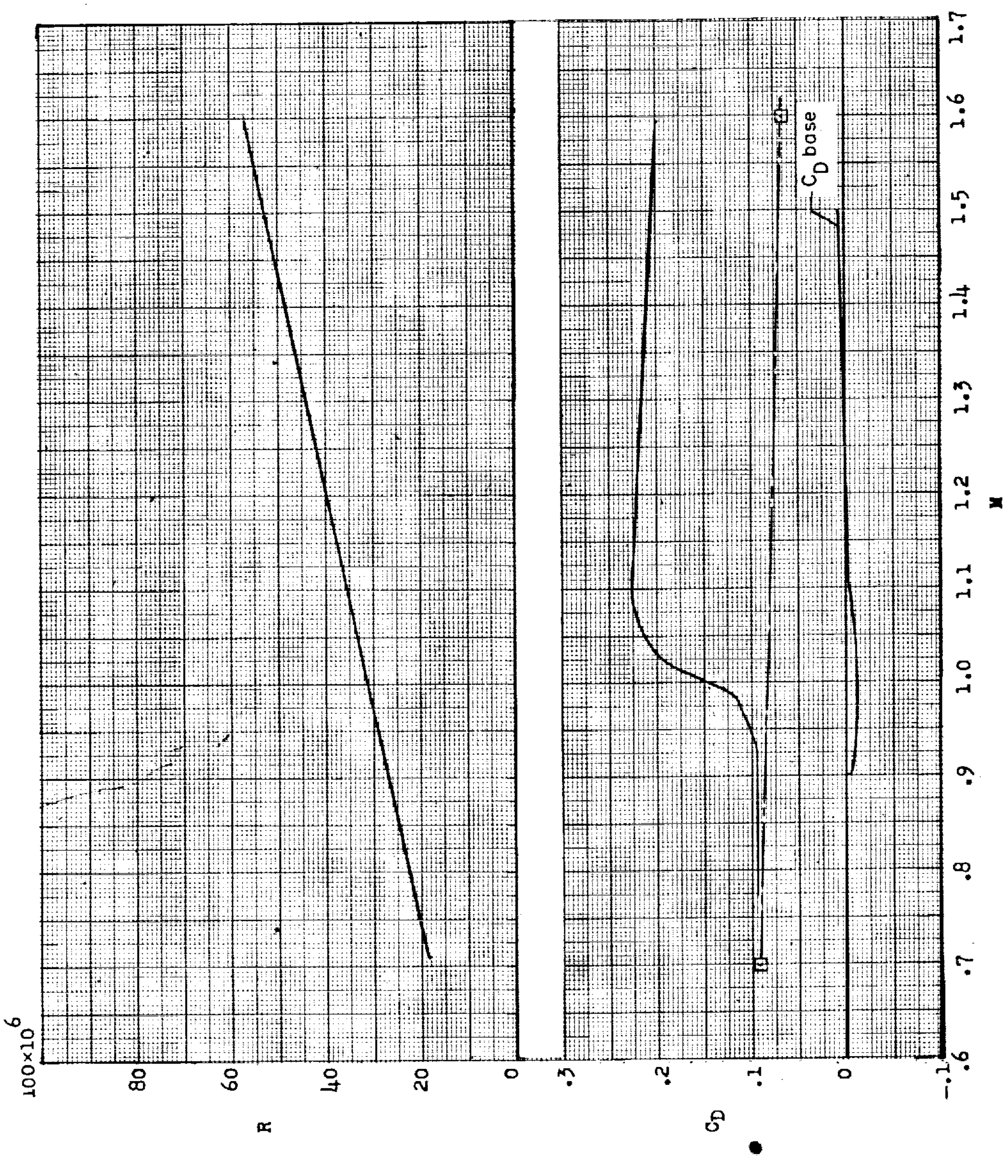

Remarks: Parabolic nose and afterbody.

Figure 95.

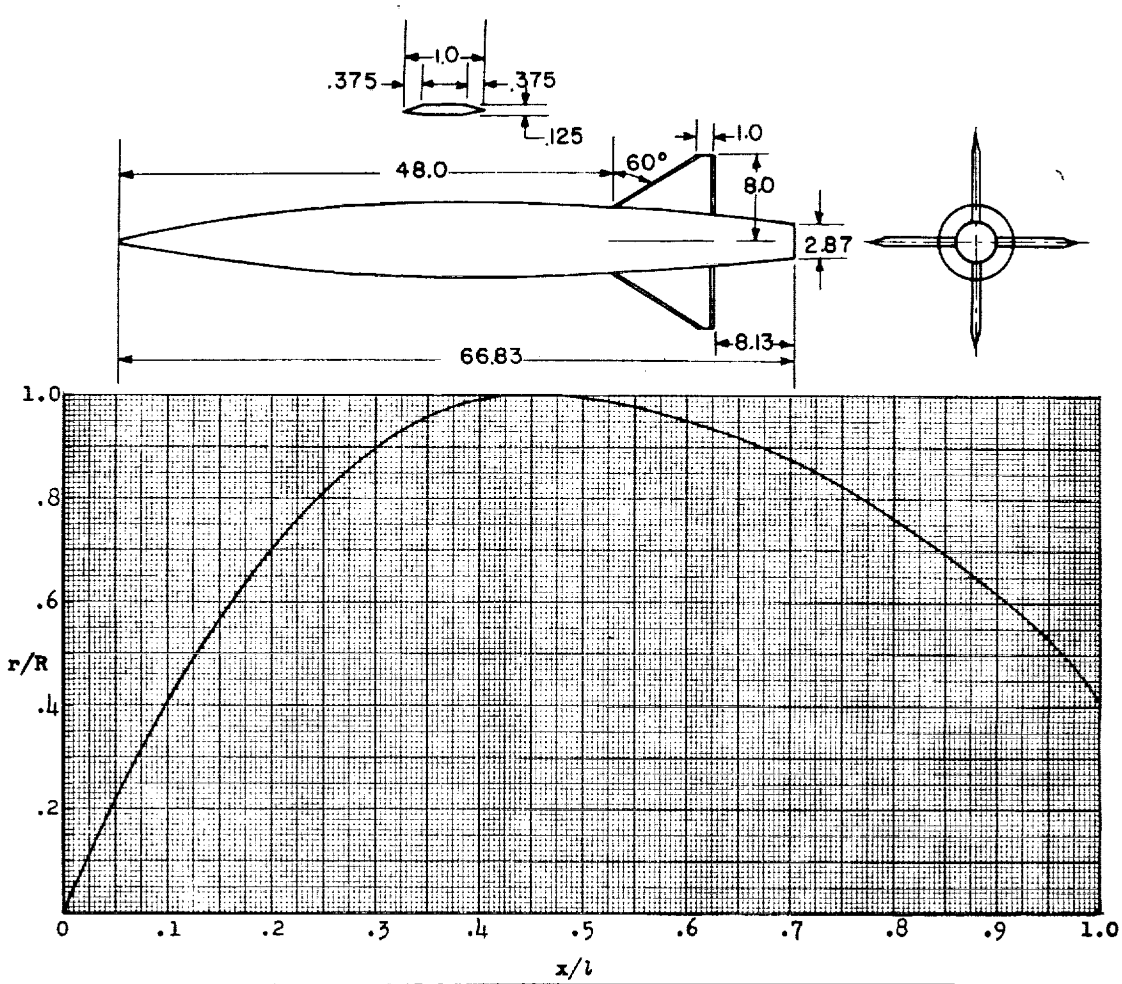

l/d_{Total}	9.54	l/d_{Nose}	4.20	S_b/A	28.60	A_b/A	.17
l/d_{N+A}	9.54	l/d_{Aft}	5.34	S_f/A	6.4	θ_b	8.75°

Designation: 88

Test: **Rocket**

Remarks: Parabolic nose and afterbody.

Figure 96.

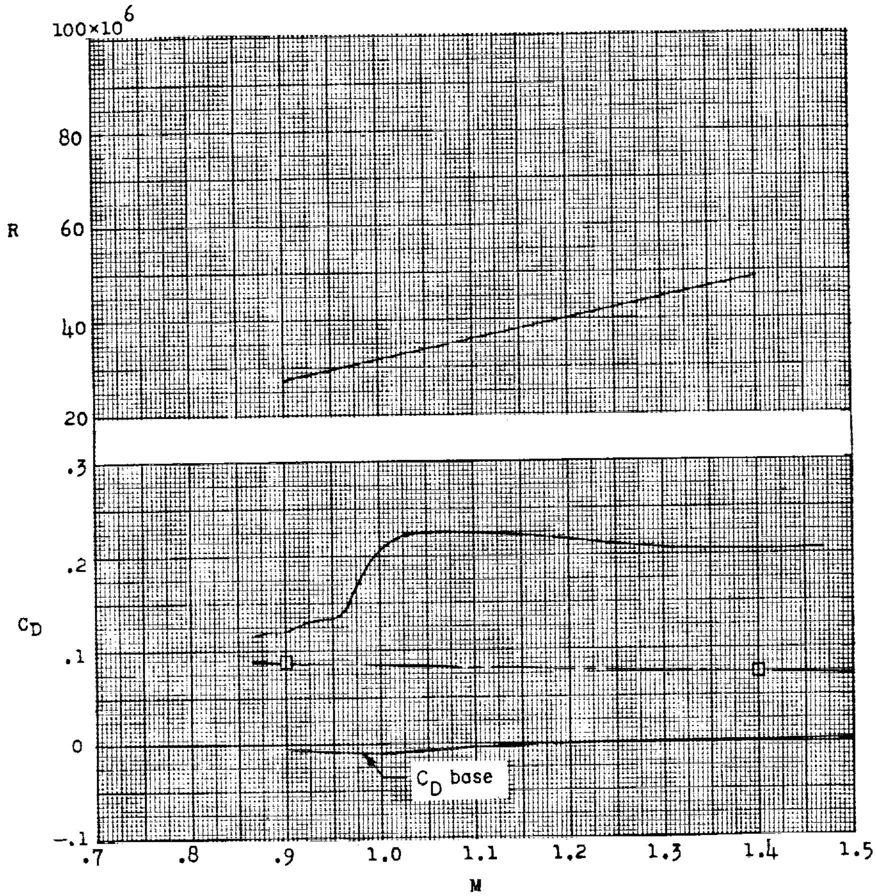

Figure 96.- Concluded.

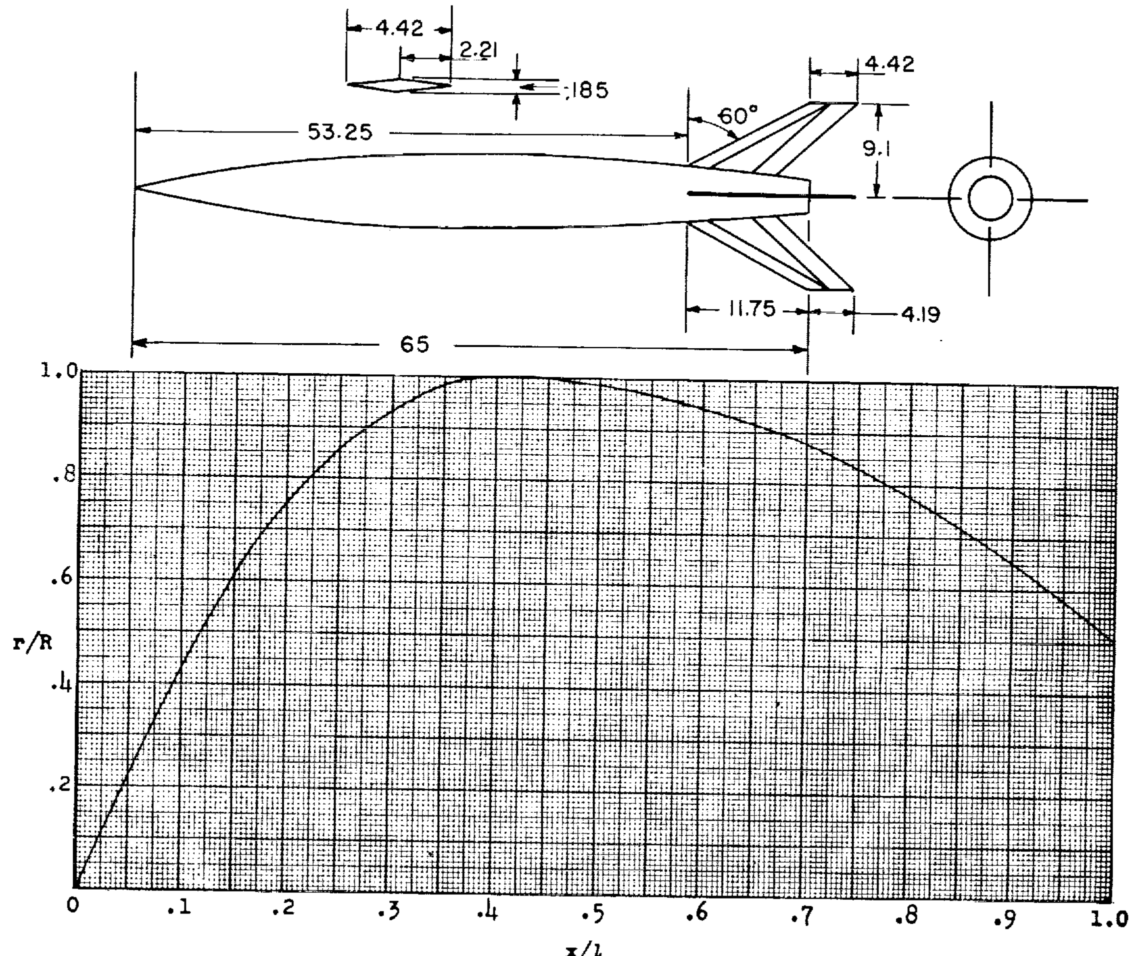

l/d_{Total}	10.0	l/d_{Nose}	4.00	S_b/A	30.88	A_b/A	.25
l/d_{N+A}	10.0	l/d_{Aft}	6.00	S_f/A	11.4	θ_b	4.47°

Designation: 89

Test: Rocket

Remarks: Parabolic nose and afterbody.

Figure 97.

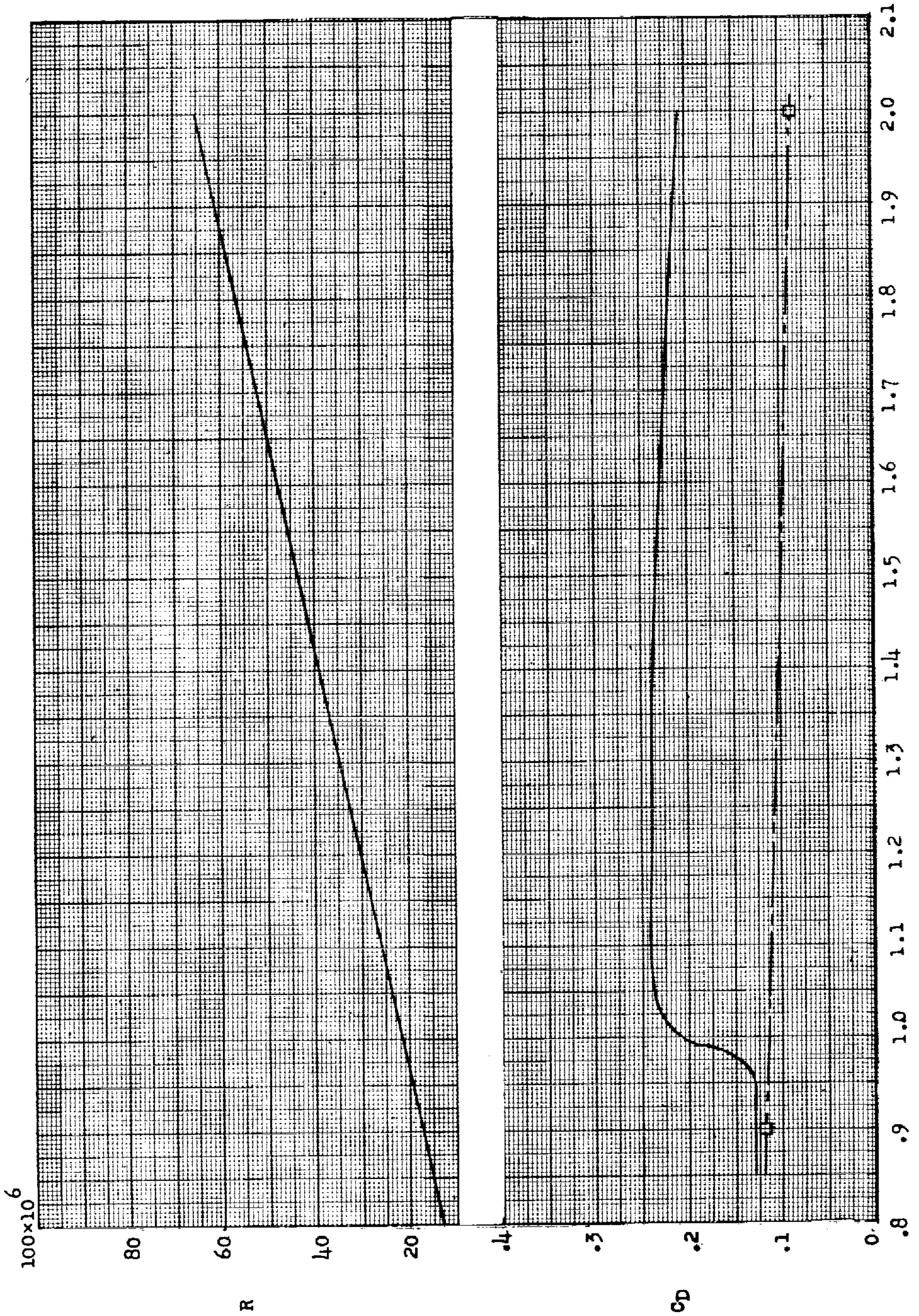

Figure 97.- Concluded.

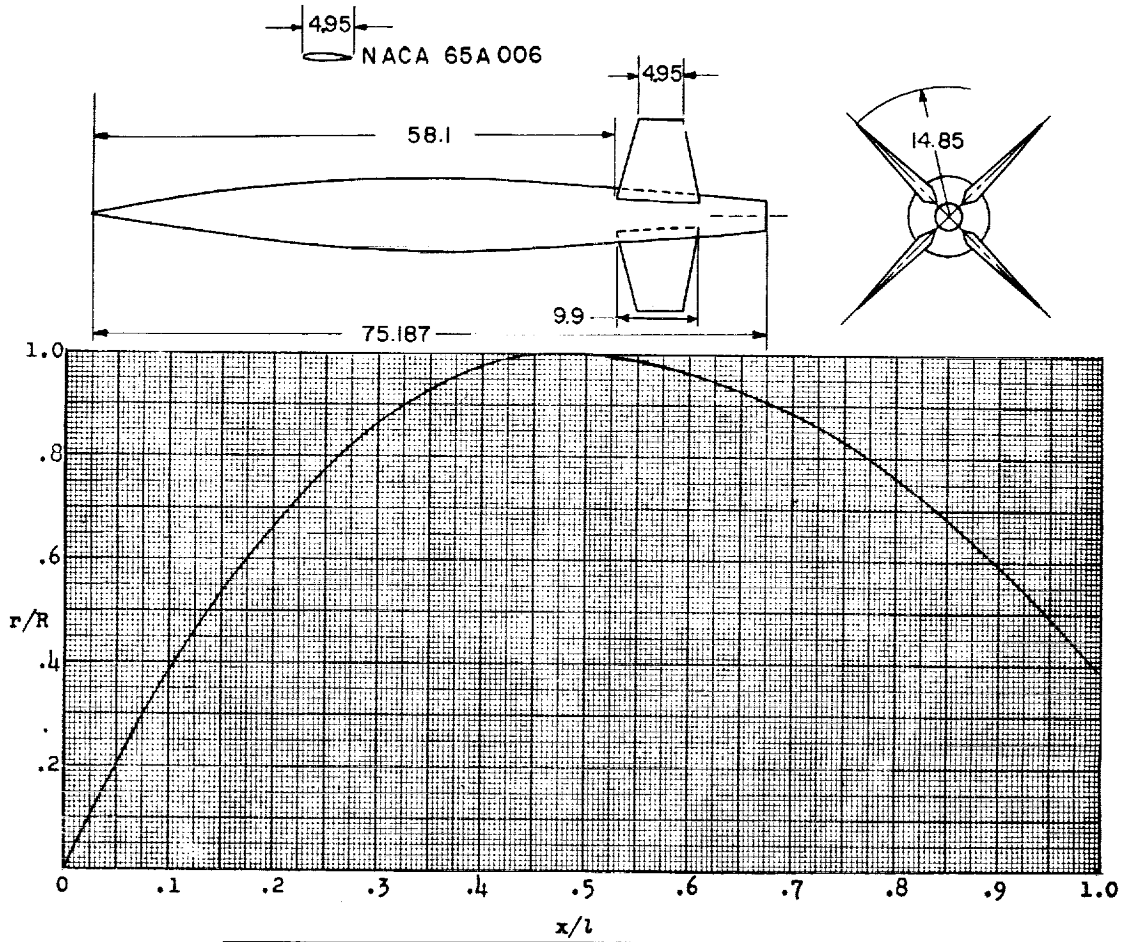

l/d_{Total}	10.0	l/d_{Nose}	4.73	S_b/A	29.6	A_b/A	.15
l/d_{N+A}	10.0	l/d_{Aft}	5.27	S_f/A	17.76	θ_b	6.45°

Designation: 90

Test: Rocket

Figure 98.

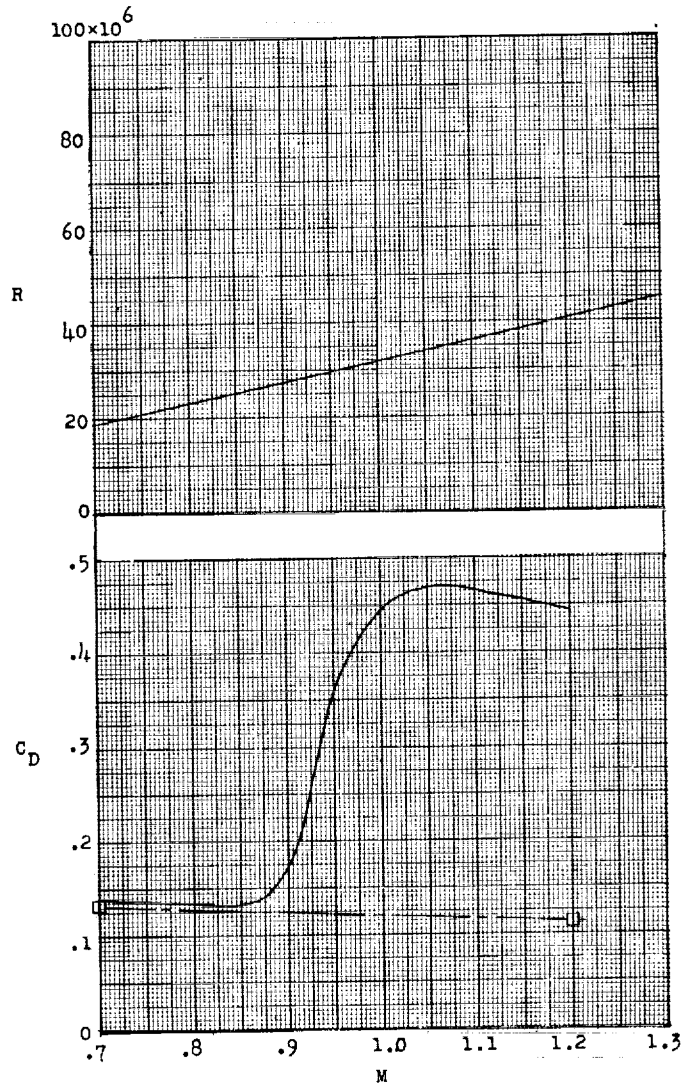

Figure 98.- Concluded.

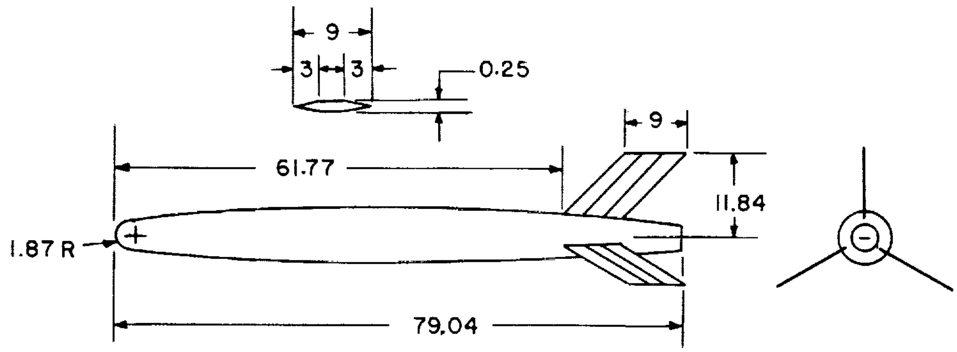

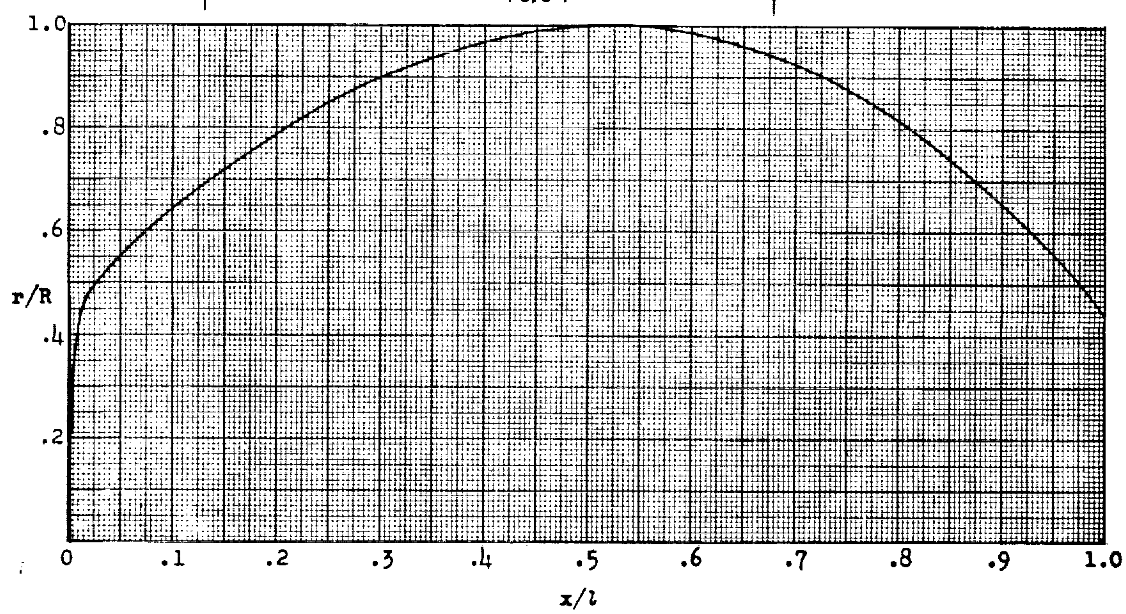

l/d_{Total}	10.54	l/d_{Nose}	5.38	S_b/A	34.40	A_b/A	.19
l/d_{N+A}	10.54	l/d_{Aft}	5.16	S_f/A	11.0	θ_b	7.0°

Designation: 91

Test: **Rocket**

Remarks: Nose consists of hemispherical and parabolic segments; parabolic afterbody.

Figure 99.

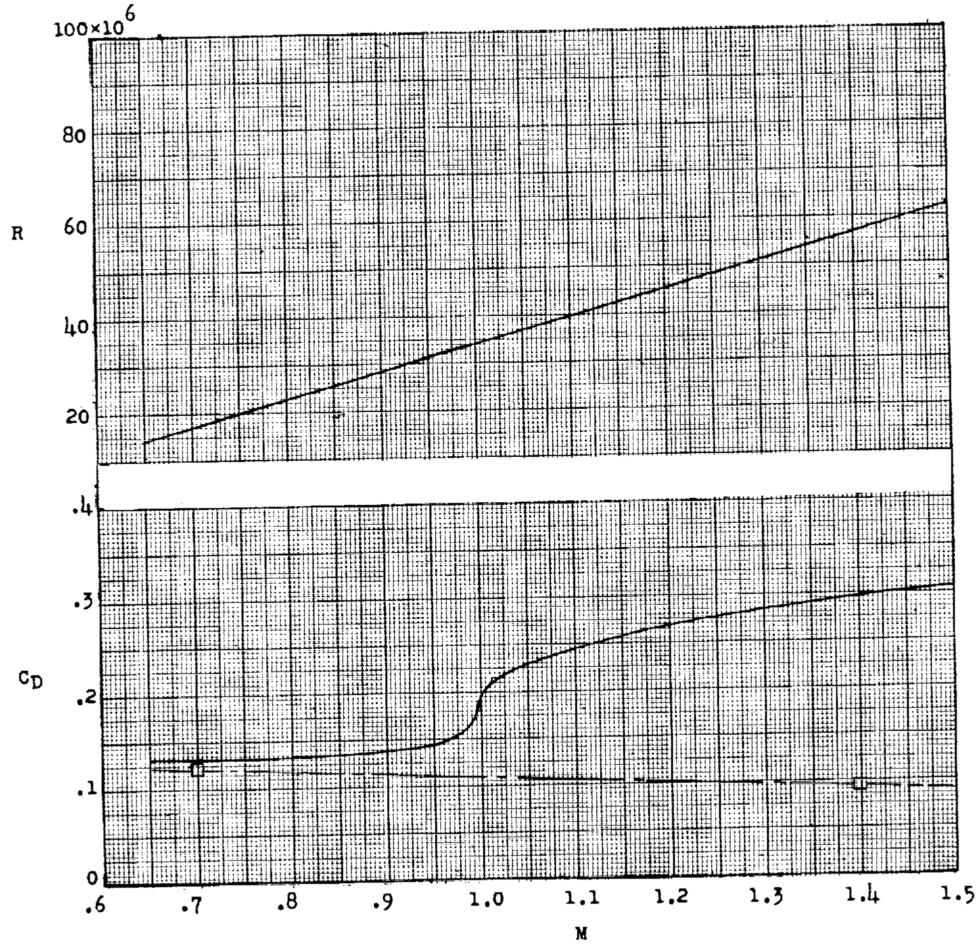

Figure 99.- Concluded.

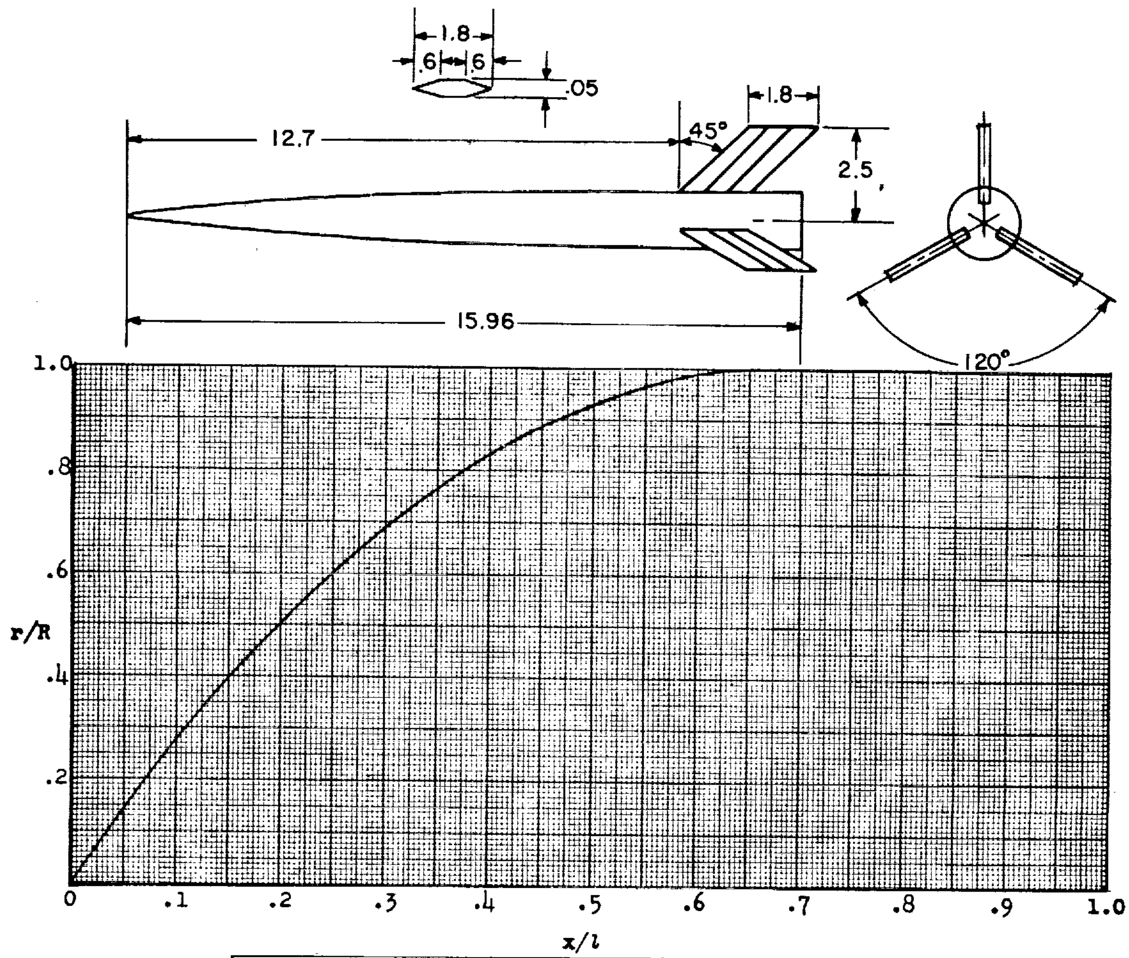

l/d_{Total}	10.63	l/d_{Nose}	7.13	S_b/A	33.0	A_b/A	1.0
l/d_{N+A}	10.63	l/d_{Aft}	3.50	S_f/A	11.0	θ_b	0°

Designation: 92

Test: Helium Gun

Remarks: Parabolic nose; cylindrical afterbody.

Figure 100.

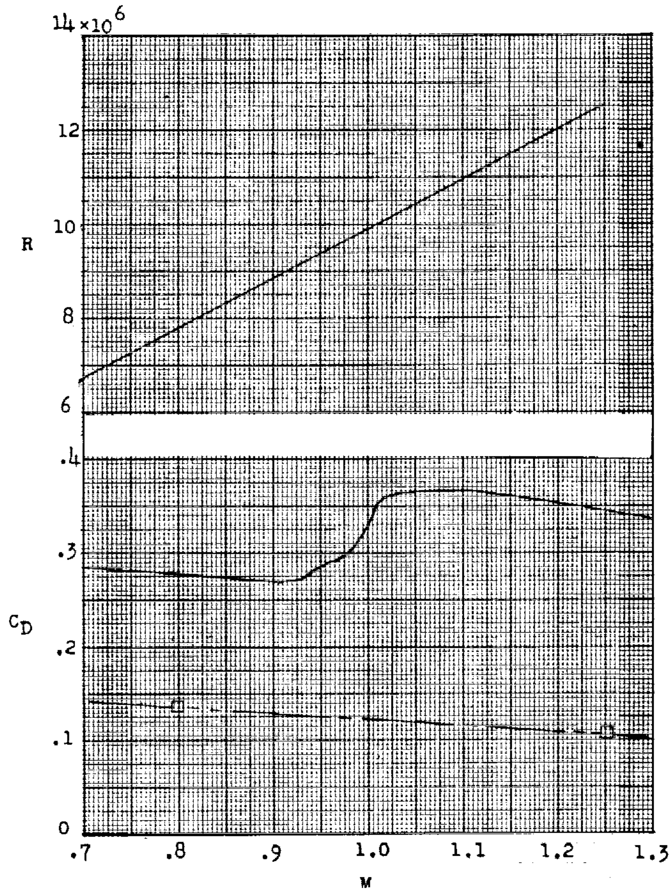

Figure 100.- Concluded.

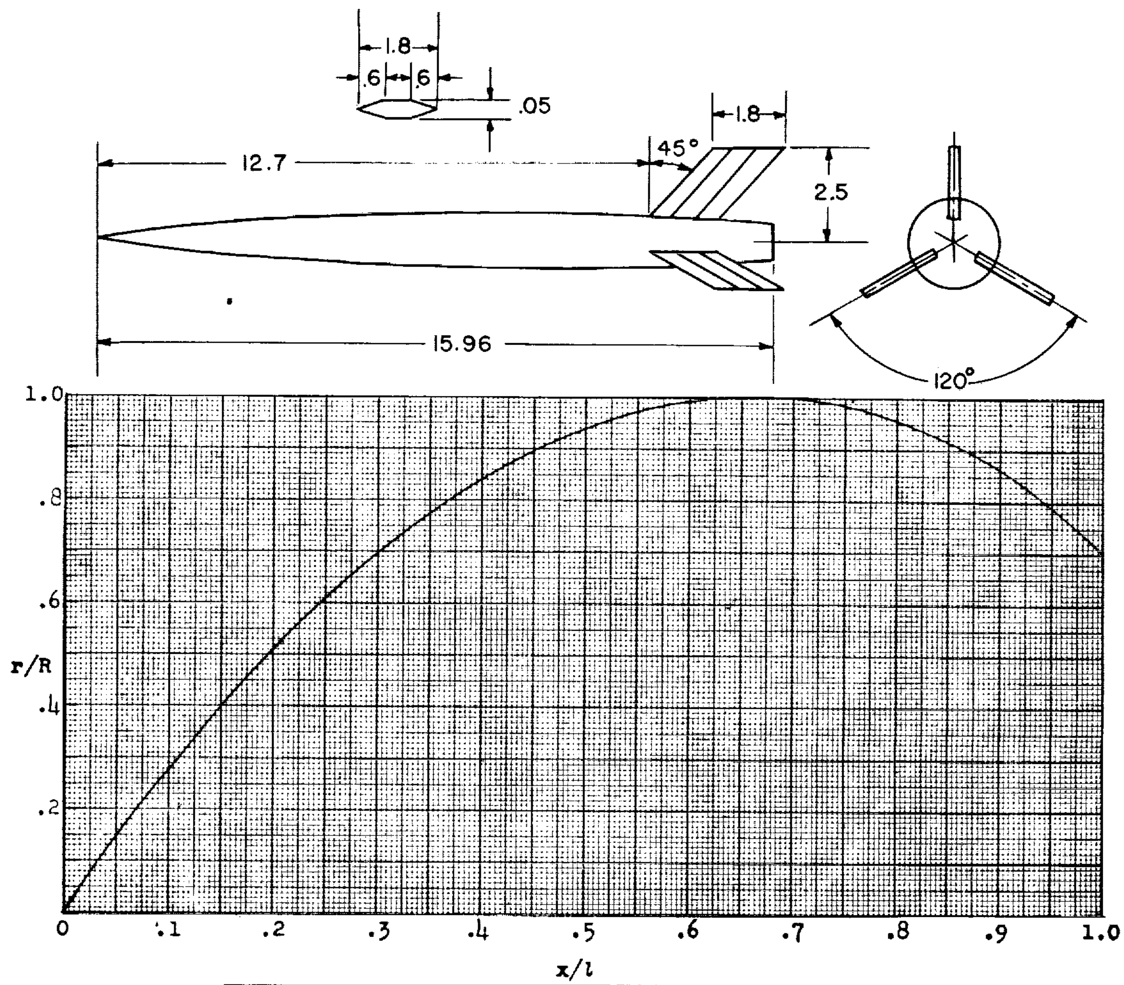

l/d_{Total}	10.63	l/d_{Nose}	7.13	S_b/A	31.60	A_b/A	.49
l/d_{N+A}	10.63	l/d_{Aft}	3.50	S_f/A	11	θ_b	5.4°

Designation: 93

Test: Helium Gun

Remarks: Parabolic nose and afterbody.

Figure 101.

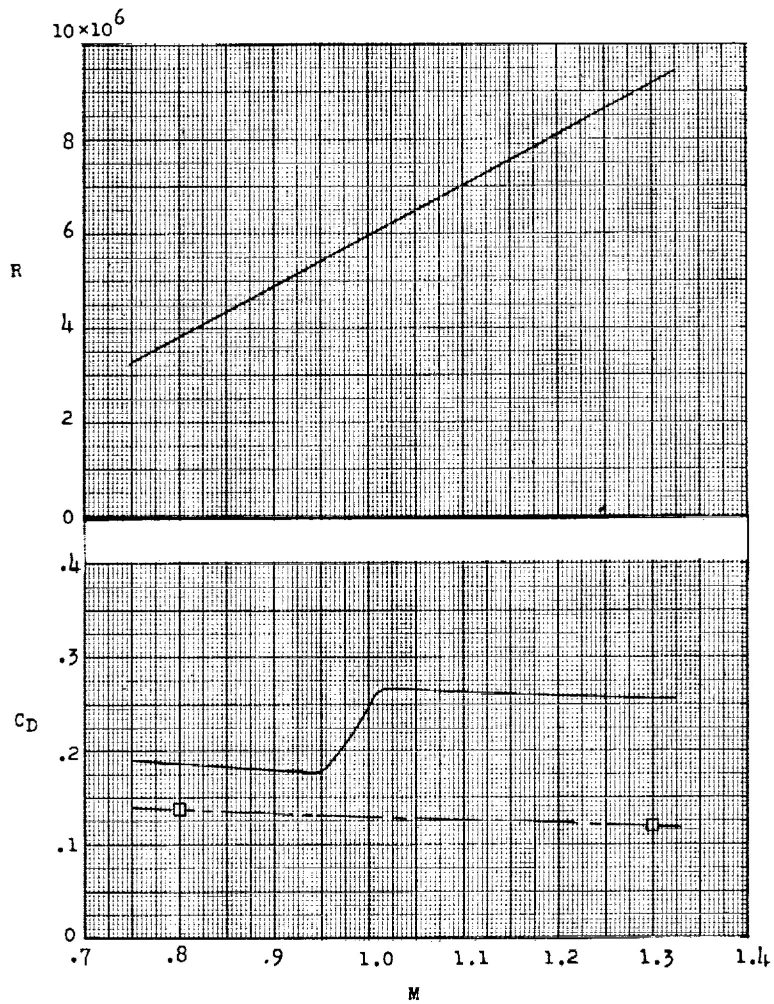

Figure 101.- Concluded.

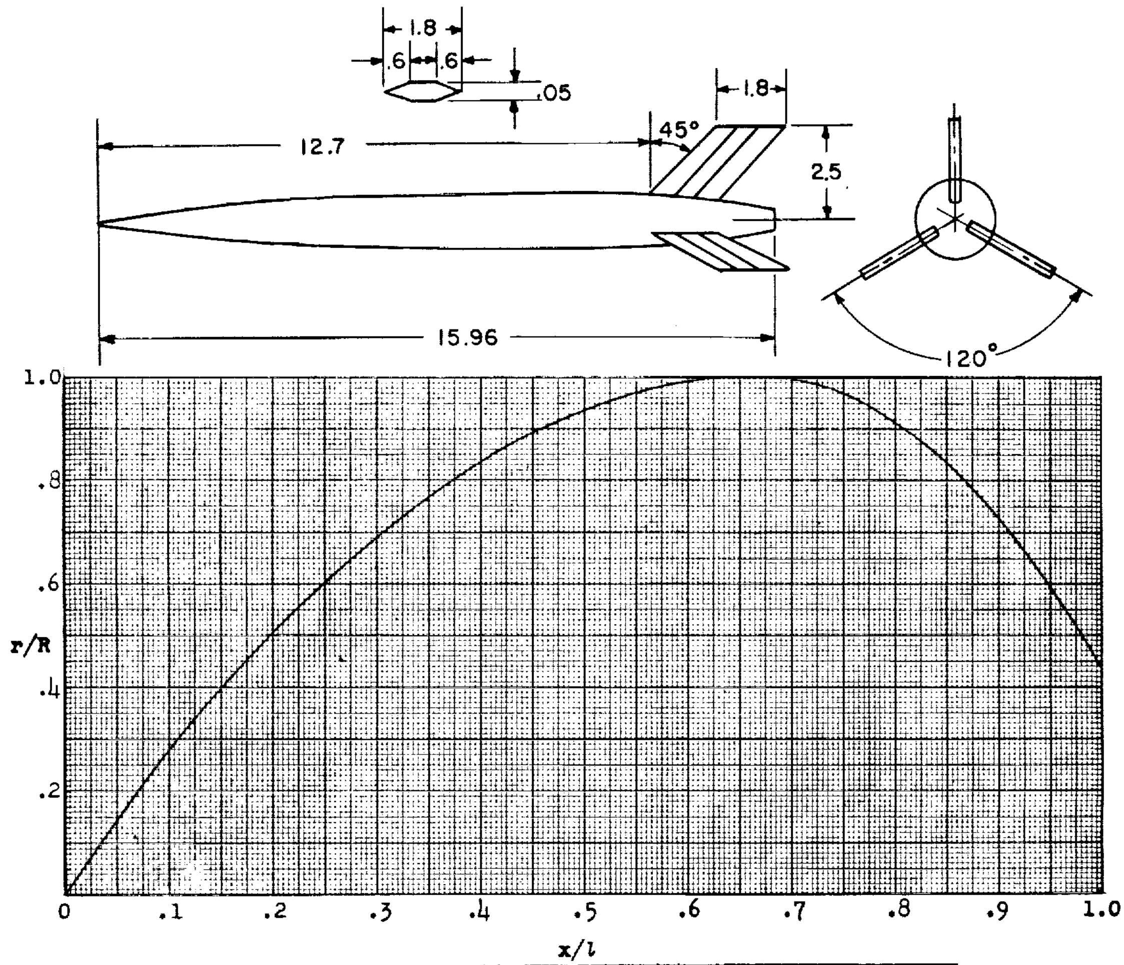

l/d_{Total}	10.63	l/d_{Nose}	7.13	S_b/A	30.06	A_b/A	.19
l/d_{N+A}	10.63	l/d_{Aft}	3.50	S_f/A	11.0	θ_b	14.8°

Designation: 94

Test: Helium Gun

Remarks: Parabolic nose and afterbody.

Figure 102.

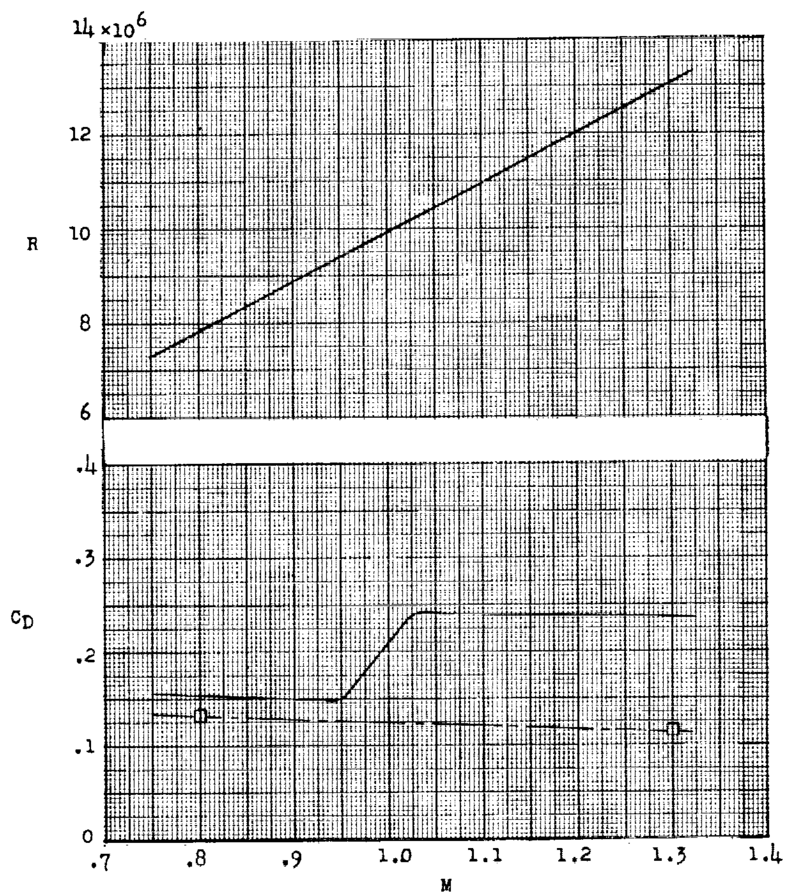

Figure 102.- Concluded.

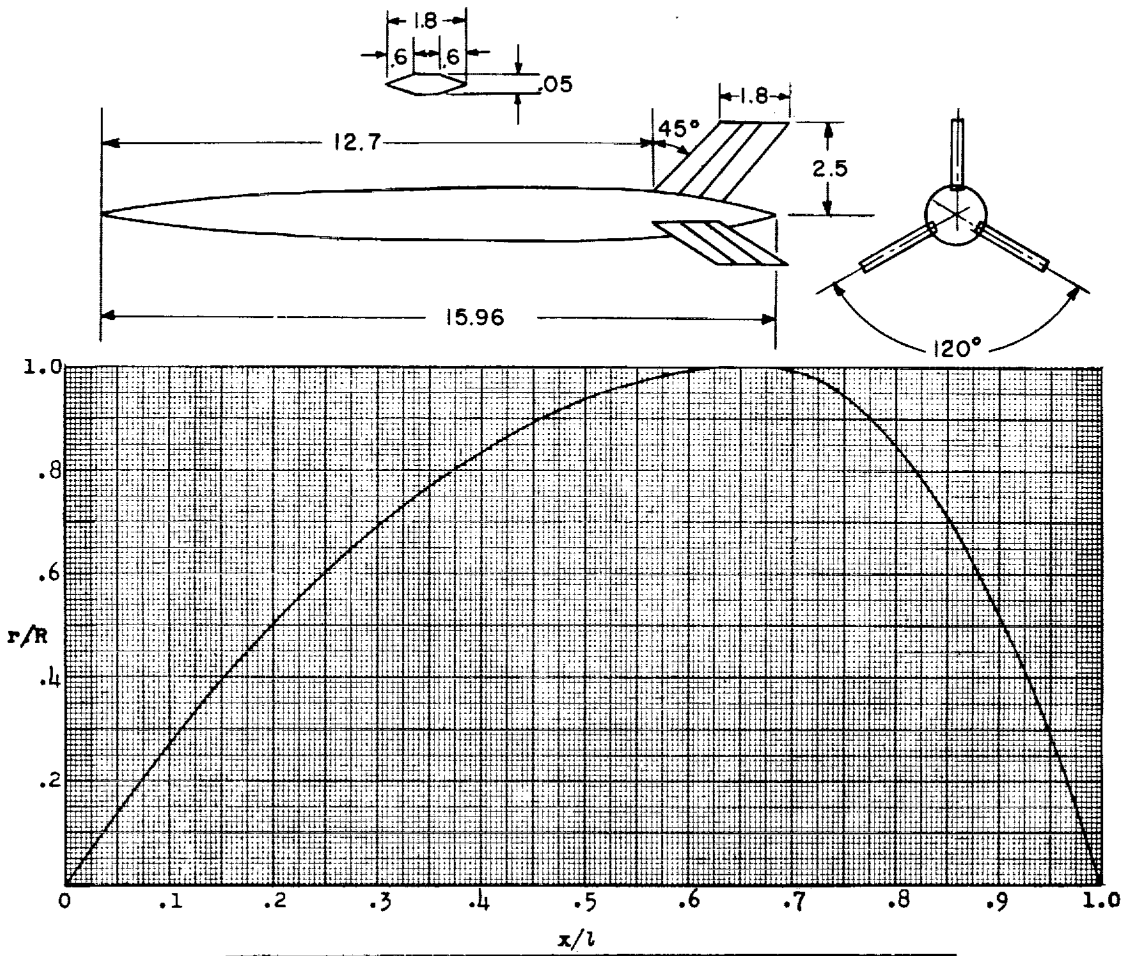

l/d_{Total}	10.63	l/d_{Nose}	7.13	S_b/A	28.30	A_b/A	0.0
l/d_{N+A}	10.63	l/d_{Aft}	3.50	S_f/A	11.0	θ_b	15.8°

Designation: 95

Test: Helium Gun

Remarks: Parabolic nose and afterbody.

Figure 103.

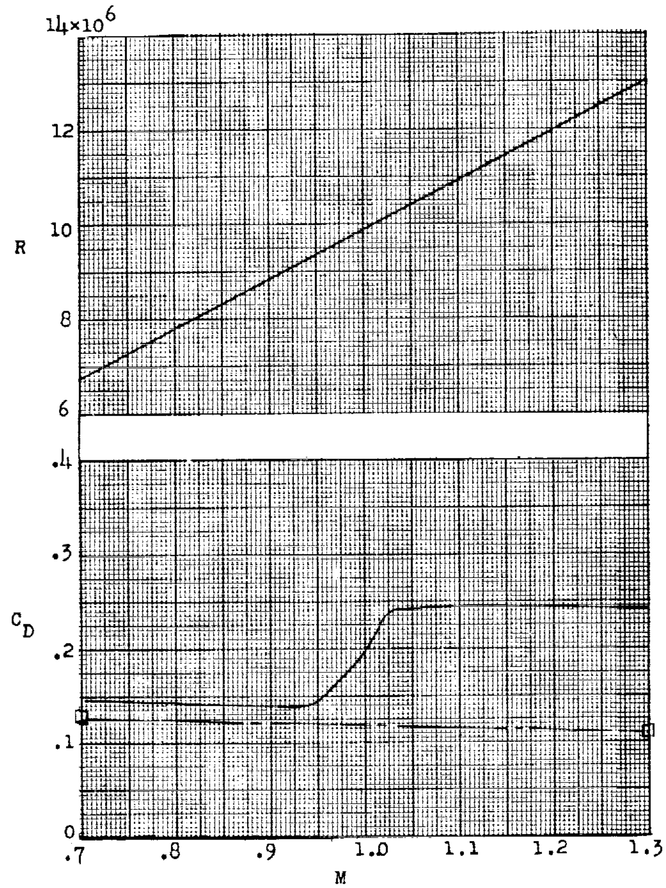

Figure 103.- Concluded.

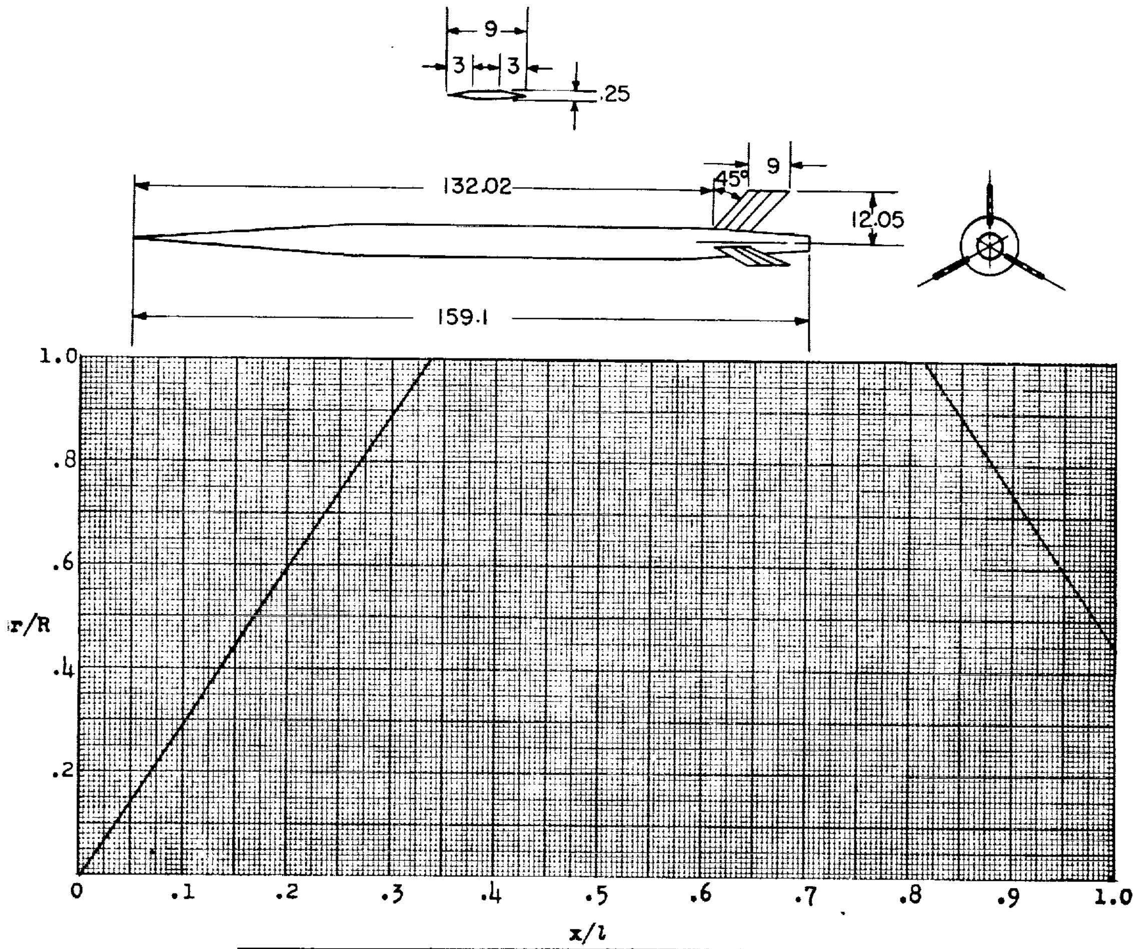

l/d_{Total}	21.2	l/d_{Nose}	7.16	S_b/A	62.5	A_b/A	.19
l/d_{N+A}	11.19	l/d_{Aft}	4.03	S_f/A	11.0	θ_b	4°

Designation: 96

Test: Rocket

Remarks: Conical nose and afterbody.

Figure 104.

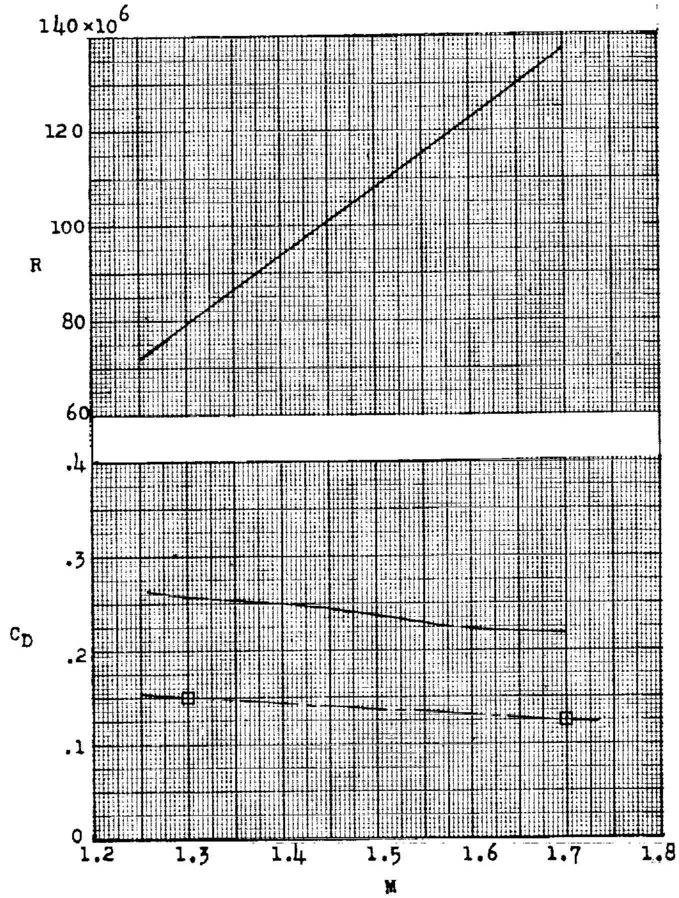

Figure 104.- Concluded.

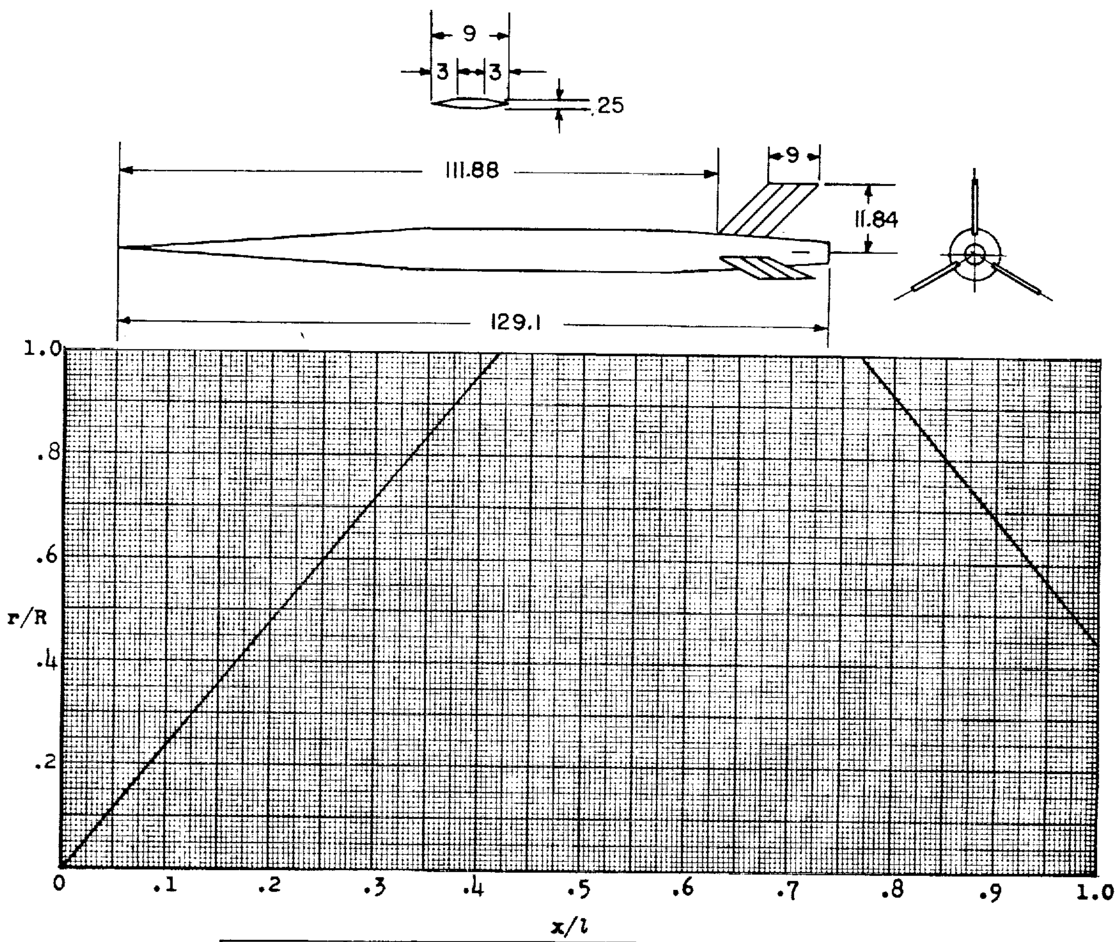

l/d_{Total}	17.2	l/d_{Nose}	7.16	S_b/A	48.8	A_b/A	.19
l/d_{N+A}	11.19	l/d_{Aft}	4.03	S_f/A	11.0	θ_b	4°

Designation: 97

Test: Rocket

Remarks: Conical nose and afterbody.

Figure 105.

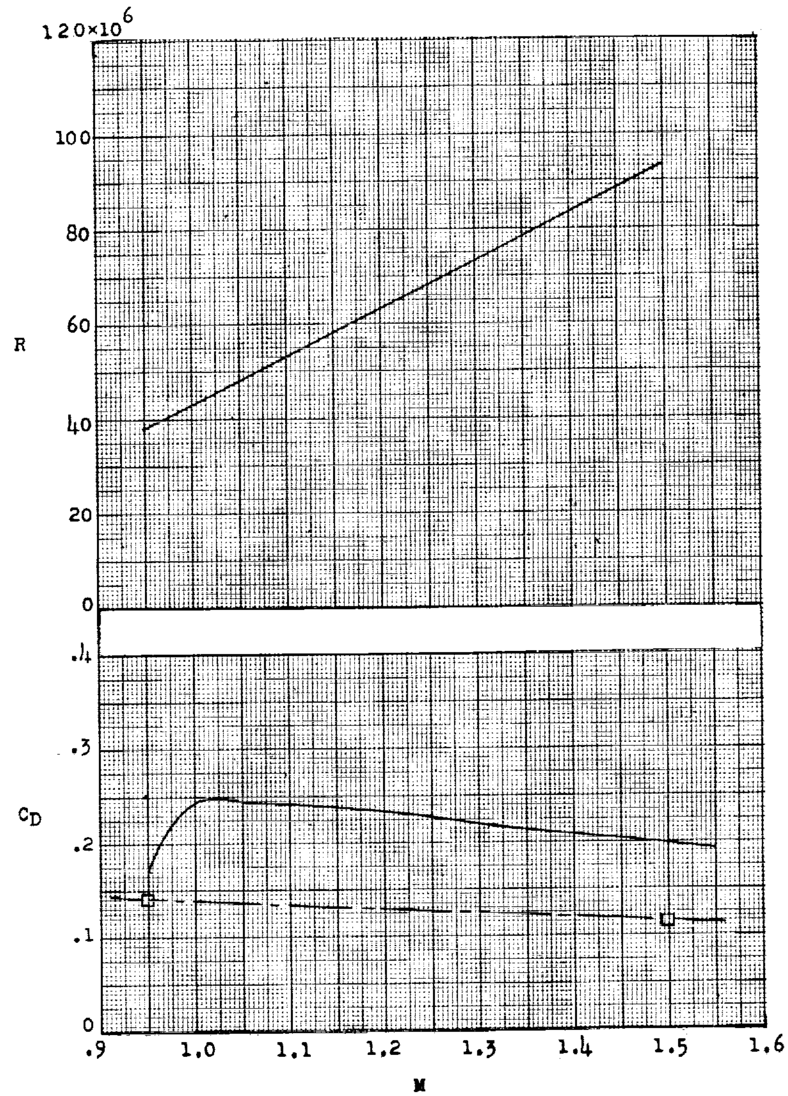

Figure 105.- Concluded.

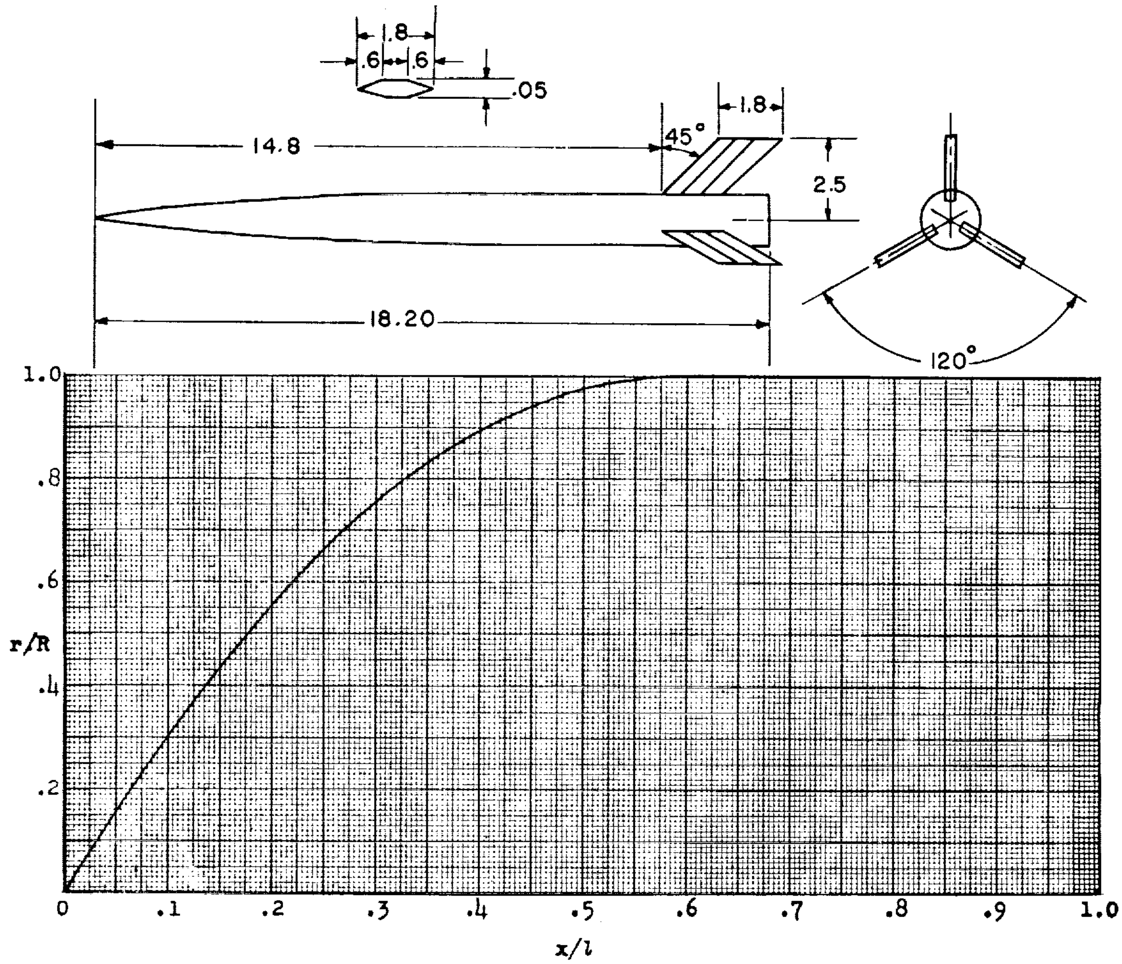

l/d_{Total}	12.13	l/d_{Nose}	7.13	S_b/A	38.9	A_b/A	1.00
l/d_{N+A}	12.13	l/d_{Aft}	5.00	S_f/A	11.0	θ_b	0°

Designation: 98

Test: Helium Gun

Remarks: Parabolic nose; cylindrical afterbody.

Figure 106.

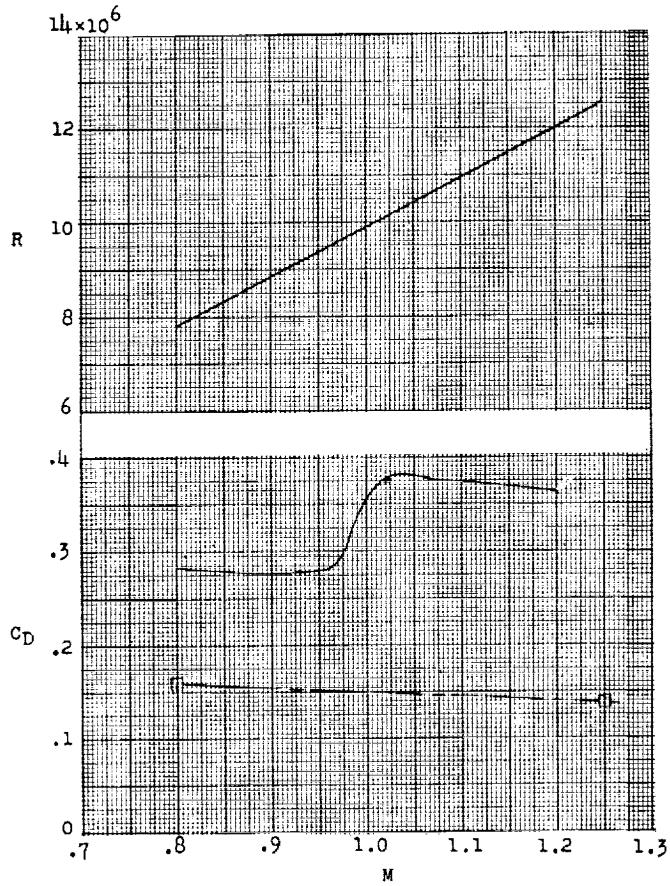

Figure 106.- Concluded.

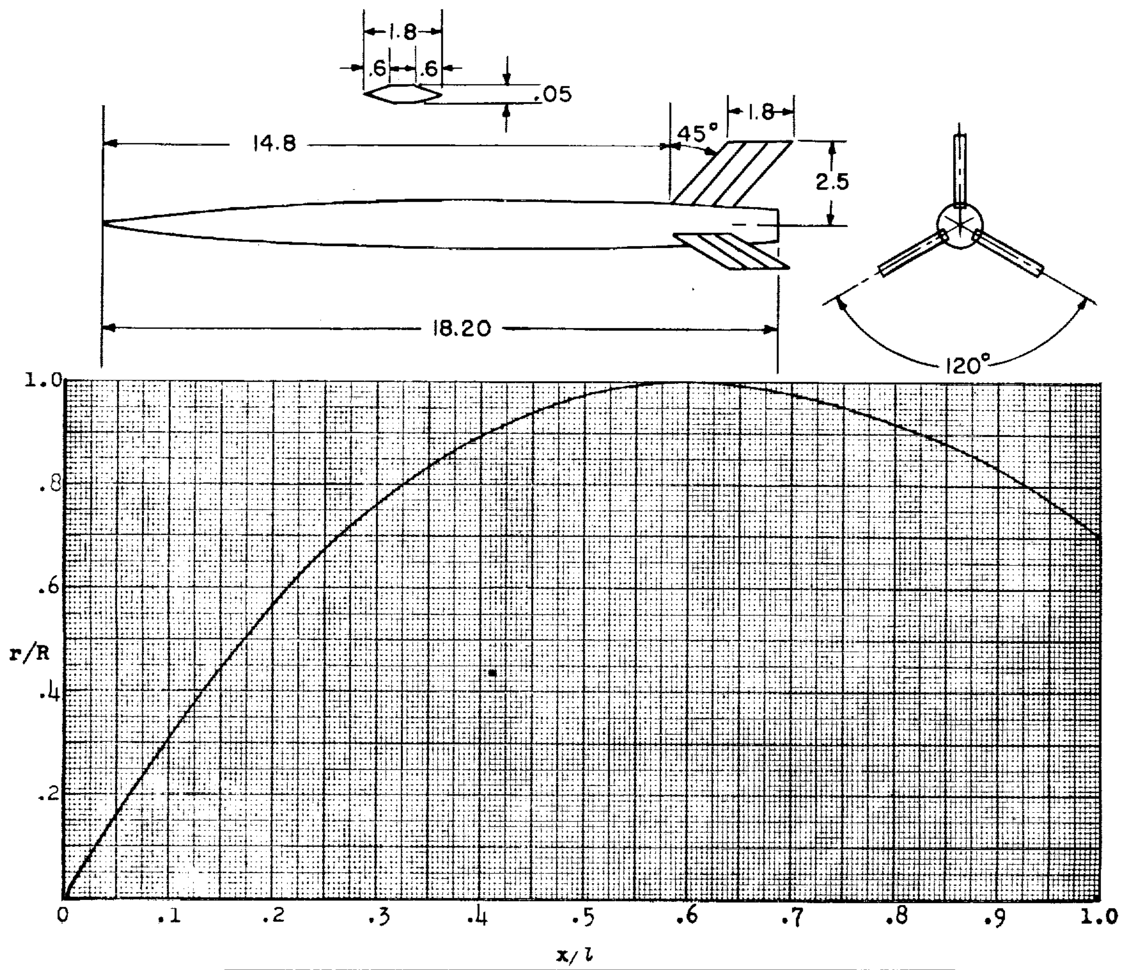

l/d_{Total}	12.13	l/d_{Nose}	7.13	S_b/A	36.9	A_b/A	.49
l/d_{N+A}	12.13	l/d_{Aft}	5.00	S_f/A	11.0	θ_b	3.42

Designation: 99

Test: Helium Gun

Remarks: Parabolic nose and afterbody.

Figure 107.

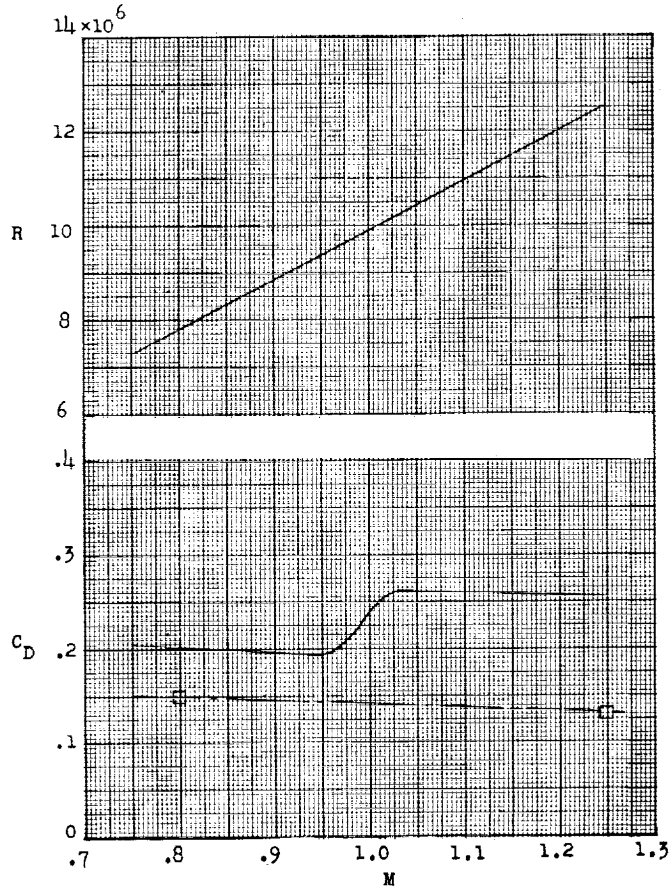

Figure 107.- Concluded.

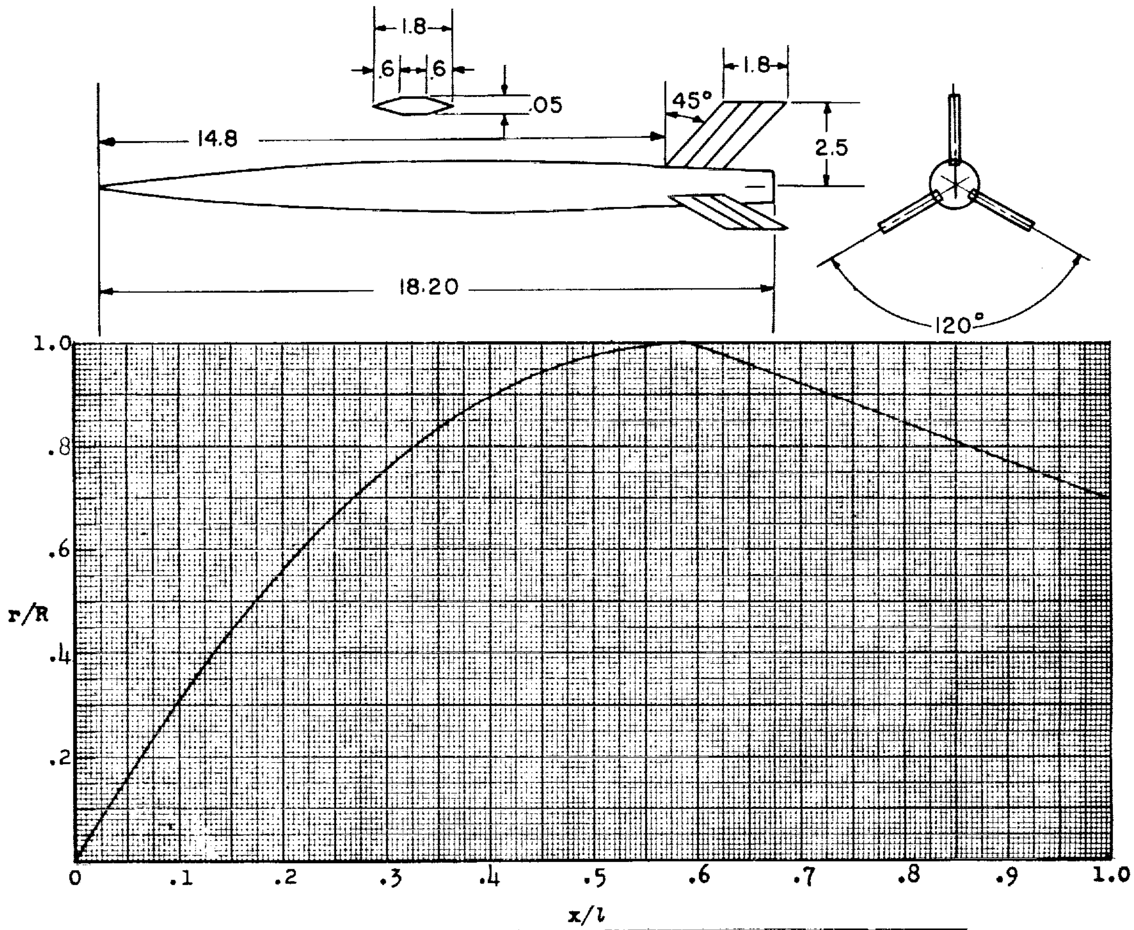

l/d_{Total}	12.13	l/d_{Nose}	7.13	S_b/A	35.8	A_b/A	.49
l/d_{N+A}	12.13	l/d_{Aft}	5.00	S_f/A	11.0	θ_b	1.7°

Designation: 100

Test: **Helium Gun**

Remarks: Parabolic nose; conical afterbody.

Figure 108.

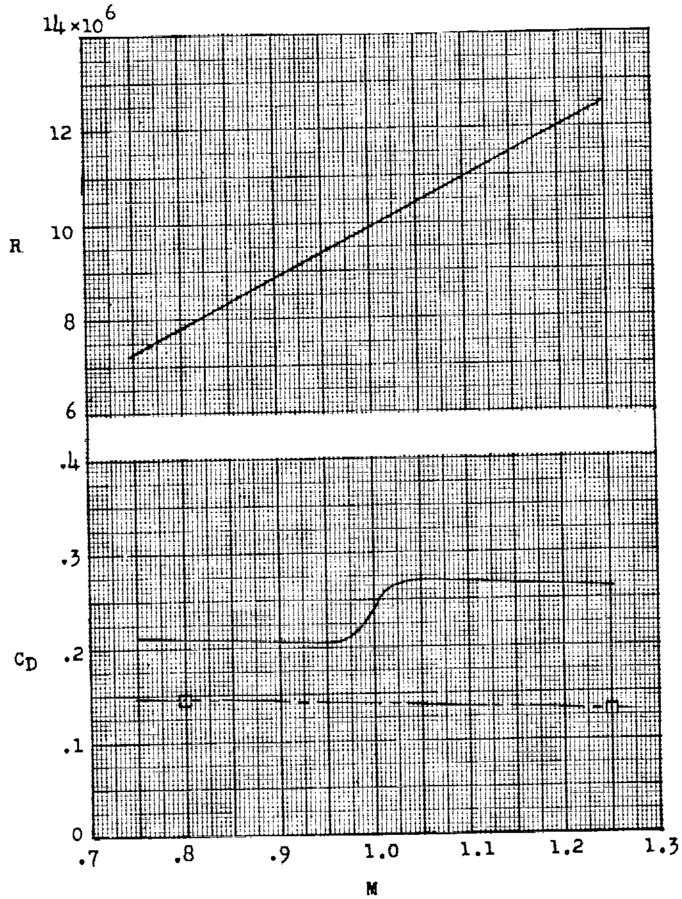

Figure 108.- Concluded.

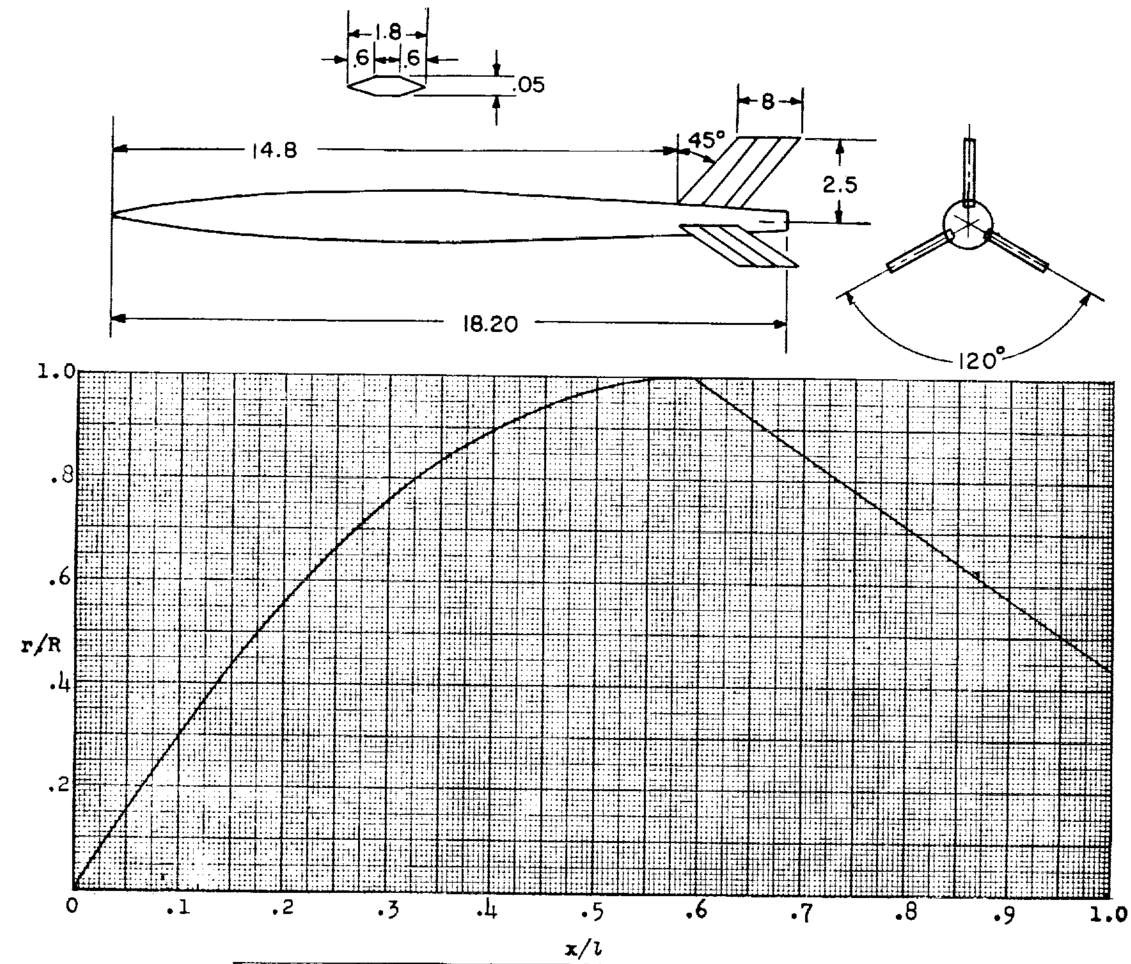

l/d_{Total}	12.13	l/d_{Nose}	7.13	S_b/A	33.3	A_b/A	.19
l/d_{N+A}	12.13	l/d_{Aft}	5.00	S_f/A	11.0	θ_b	3.2°

Designation: 101

Test: Helium Gun

Remarks: Parabolic nose; conical afterbody.

Figure 109.

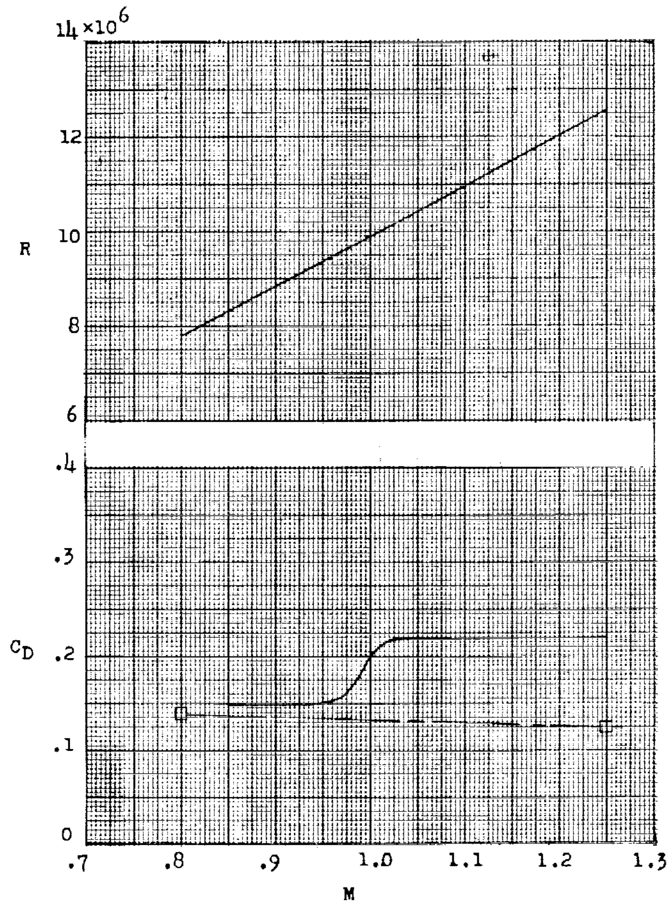

Figure 109.- Concluded.

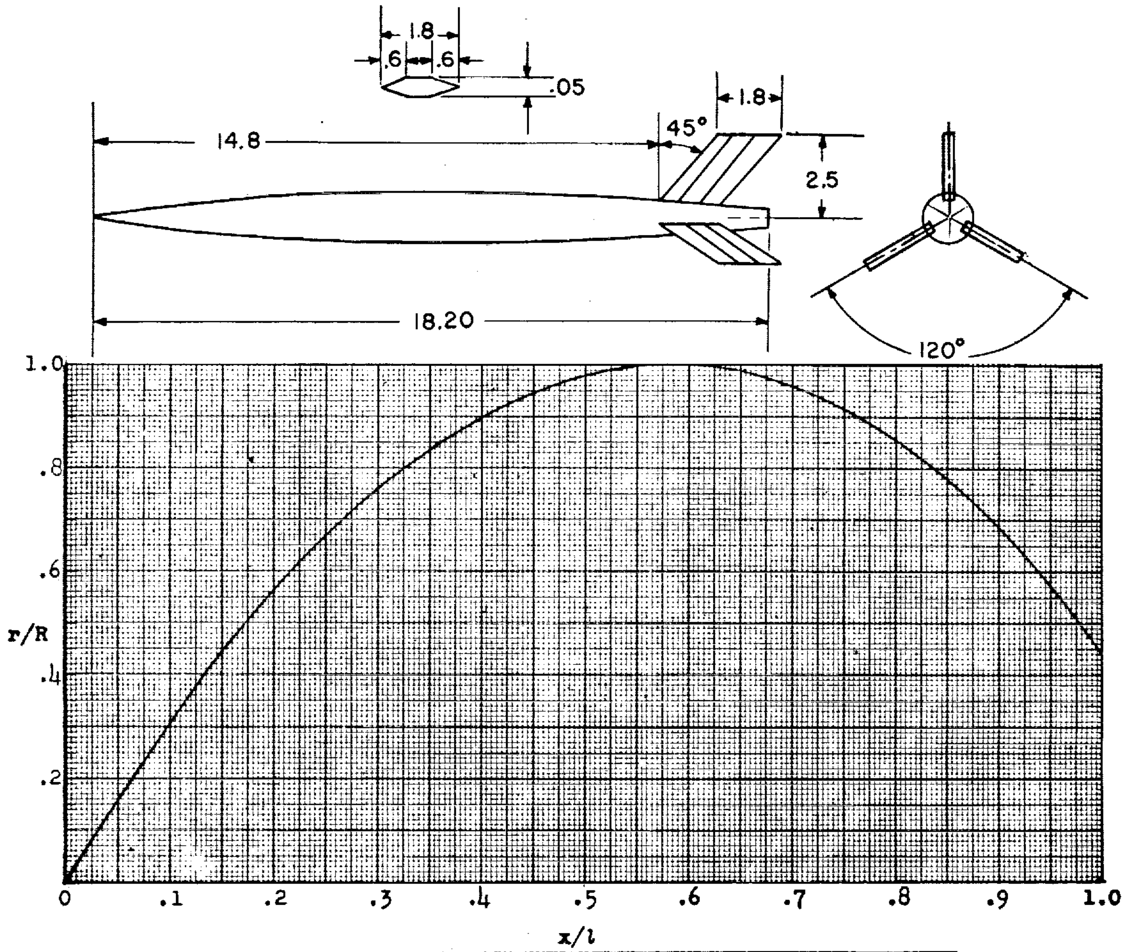

l/d_{Total}	12.13	l/d_{Nose}	7.13	S_b/A	35.20	A_b/A	.19
l/d_{N+A}	12.13	l/d_{Aft}	5.00	S_f/A	11.0	θ_b	6.4°

Designation: 102

Test: Helium Gun

Remarks: Parabolic nose and afterbody.

Figure 110.

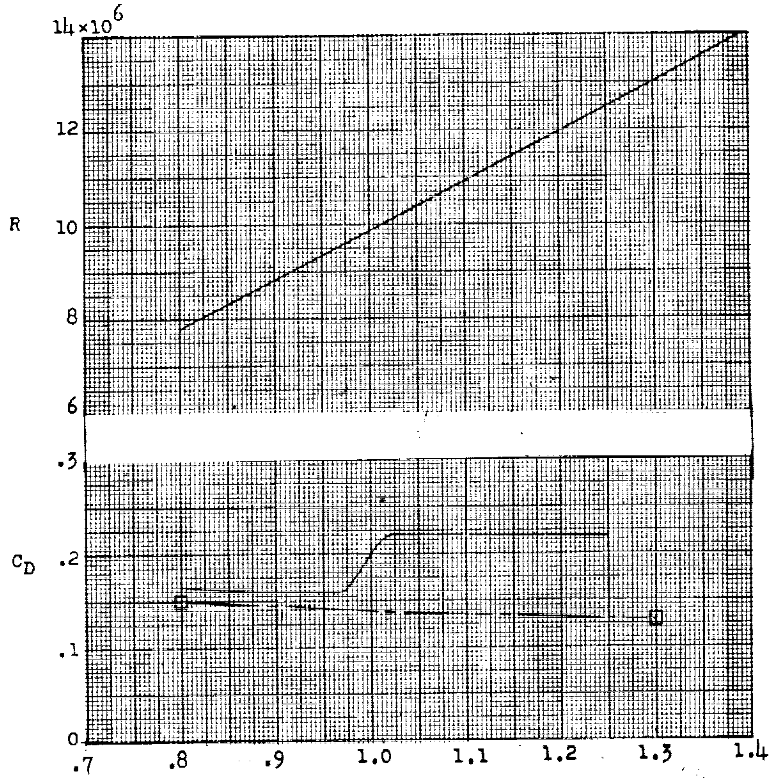

Figure 110.- Concluded.

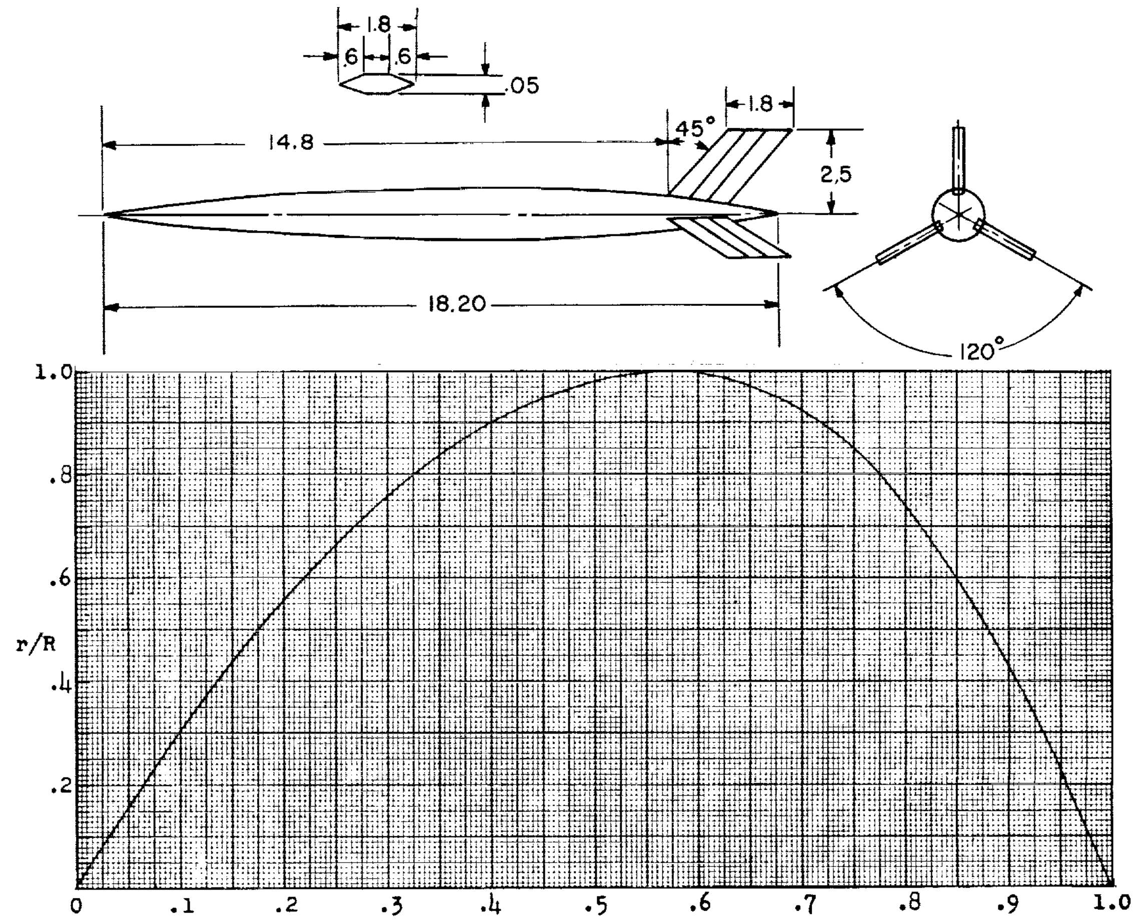

l/d_{Total}	12.13	l/d_{Nose}	7.13	S_b/A	32.2	A_b/A	0.0
l/d_{N+A}	12.13	l/d_{Aft}	5.00	S_f/A	11.0	θ_b	11.7°

Designation: 103

Test: **Helium Gun**

Remarks: Parabolic nose and afterbody.

Figure 111.

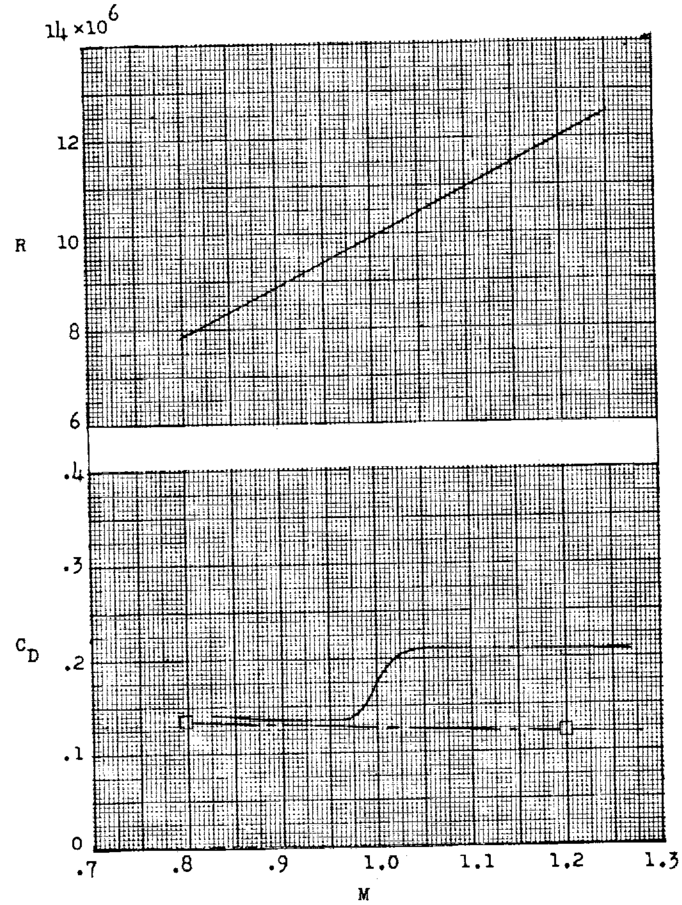

Figure 111.- Concluded.

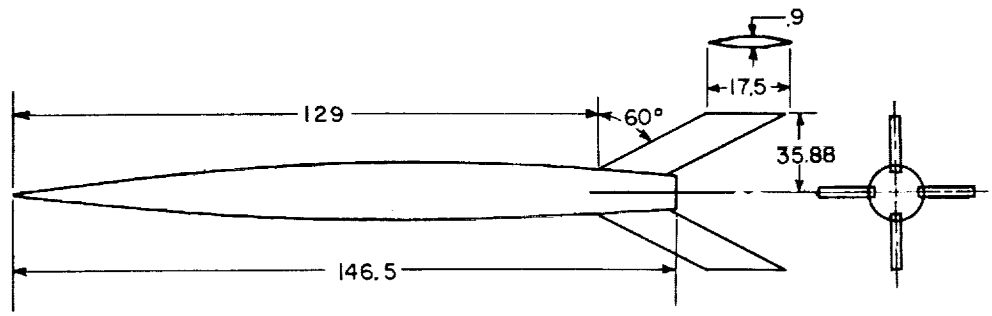

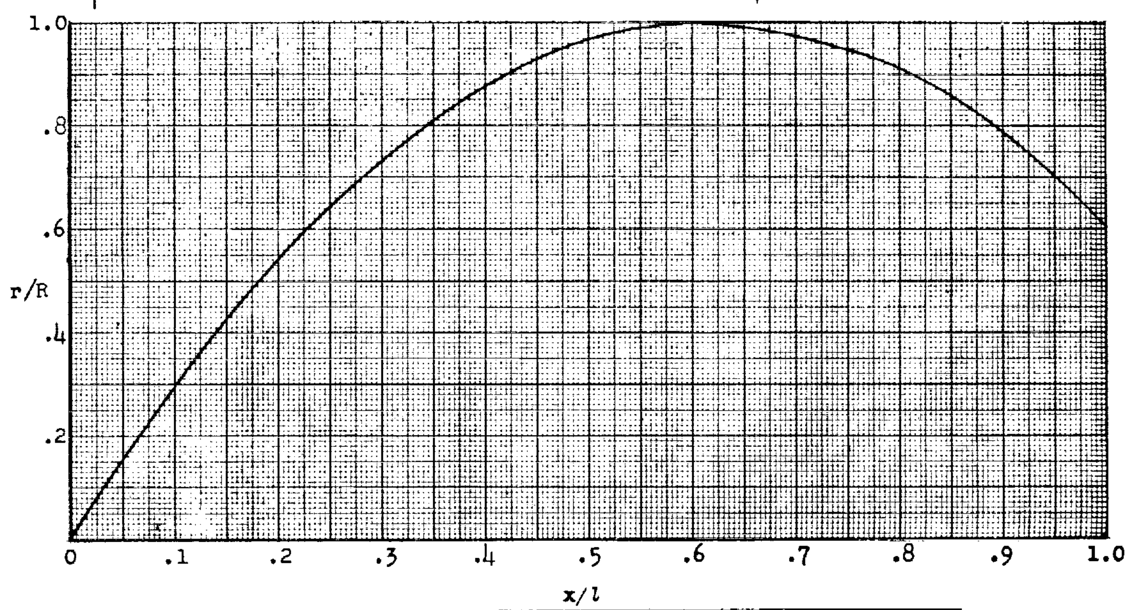

l/d_{Total}	12.2	l/d_{Nose}	7.5	S_b/A	36.3	A_b/A	.364
l/d_{N+A}	12.2	l/d_{Aft}	4.7	S_f/A	30.8	θ_b	7.6°

Designation: 104

Test: Rocket

Remarks: Parabolic nose and afterbody twice scale of model 105. Calculated friction drag coefficients are obviously too high. (See note for model 105 (fig. 113) about oscillations in drag curves.)

Figure 112.

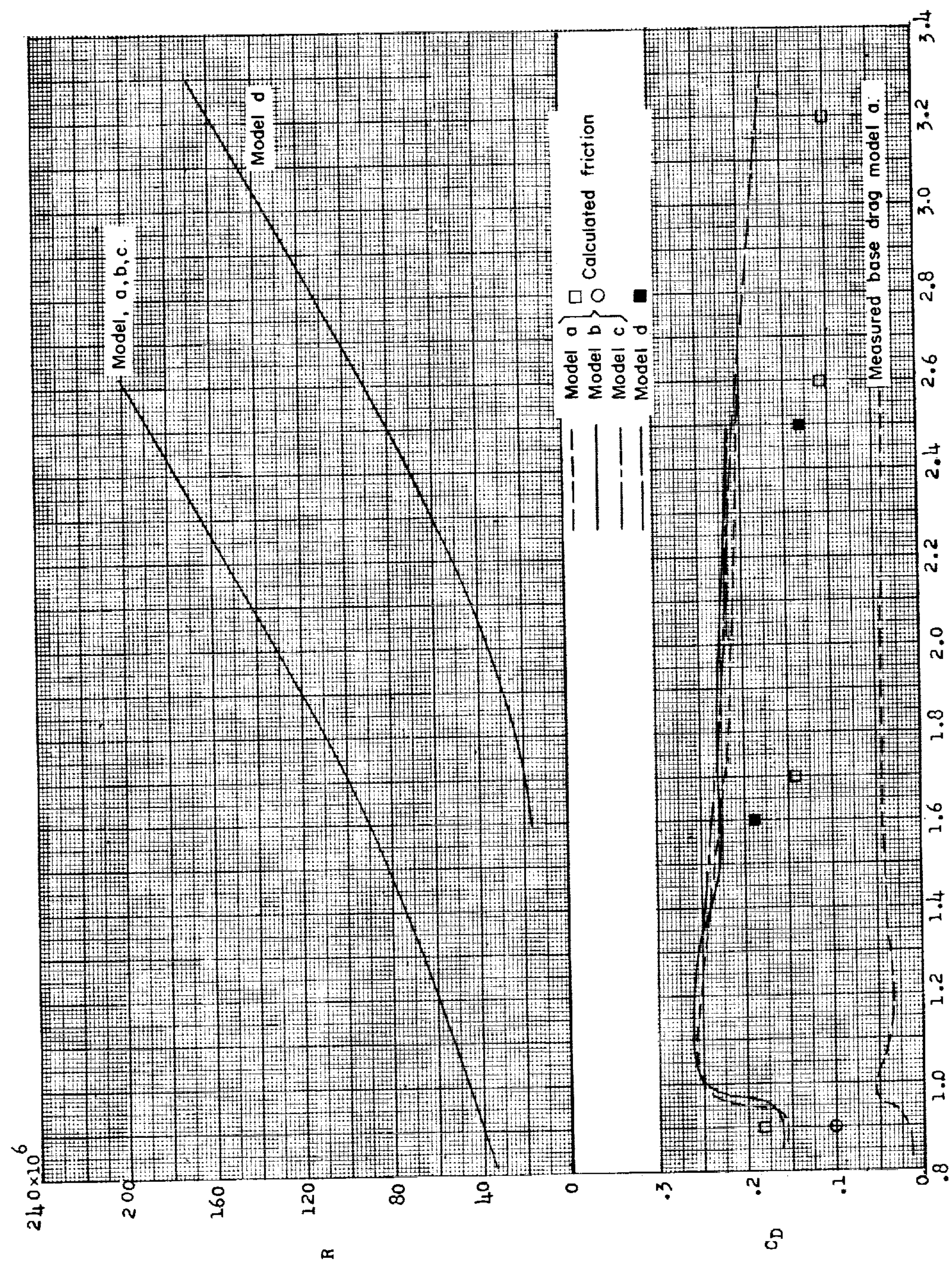

Figure 112.- Concluded.

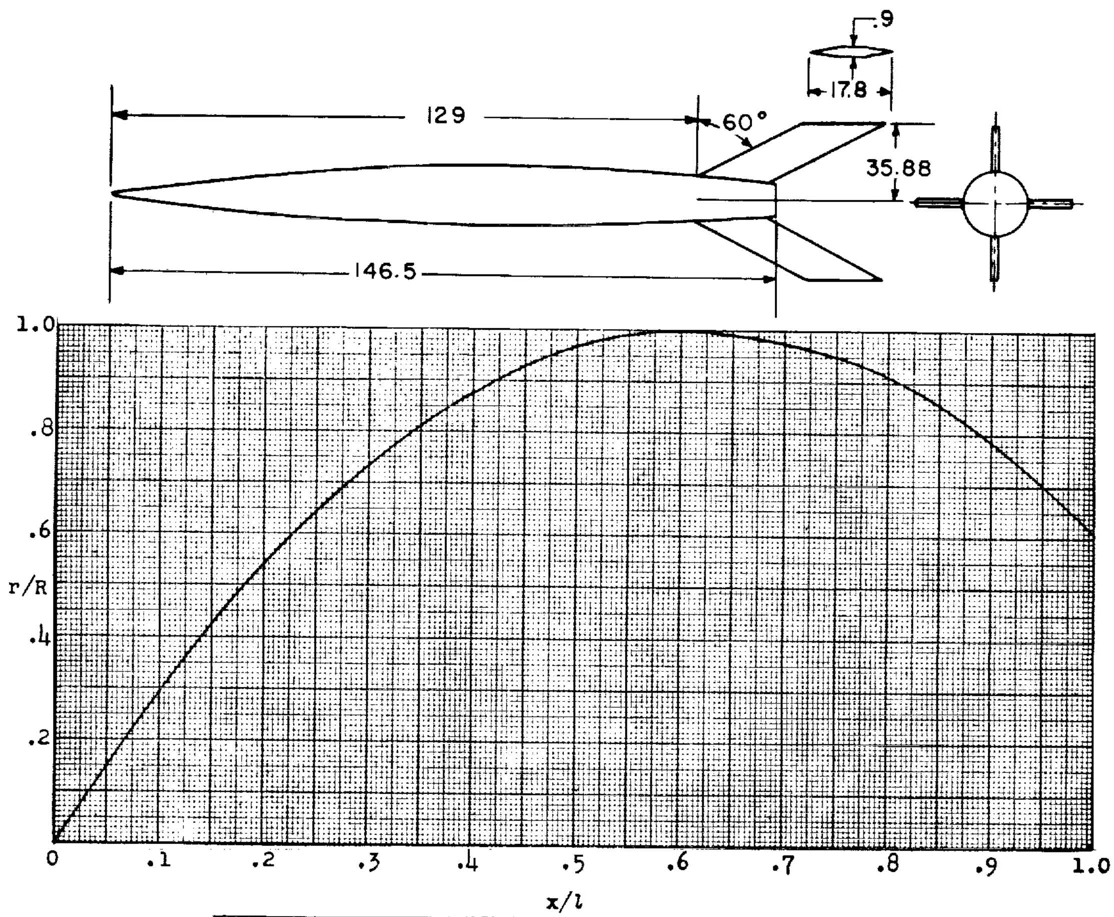

l/d_{Total}	12.2	l/d_{Nose}	7.5	S_b/A	36.3	A_b/A	.364
l/d_{N+A}	12.2	l/d_{Aft}	4.7	S_f/A	30.8	θ_b	7.6°

Designation: 105

Test: Rocket

Figure 113.

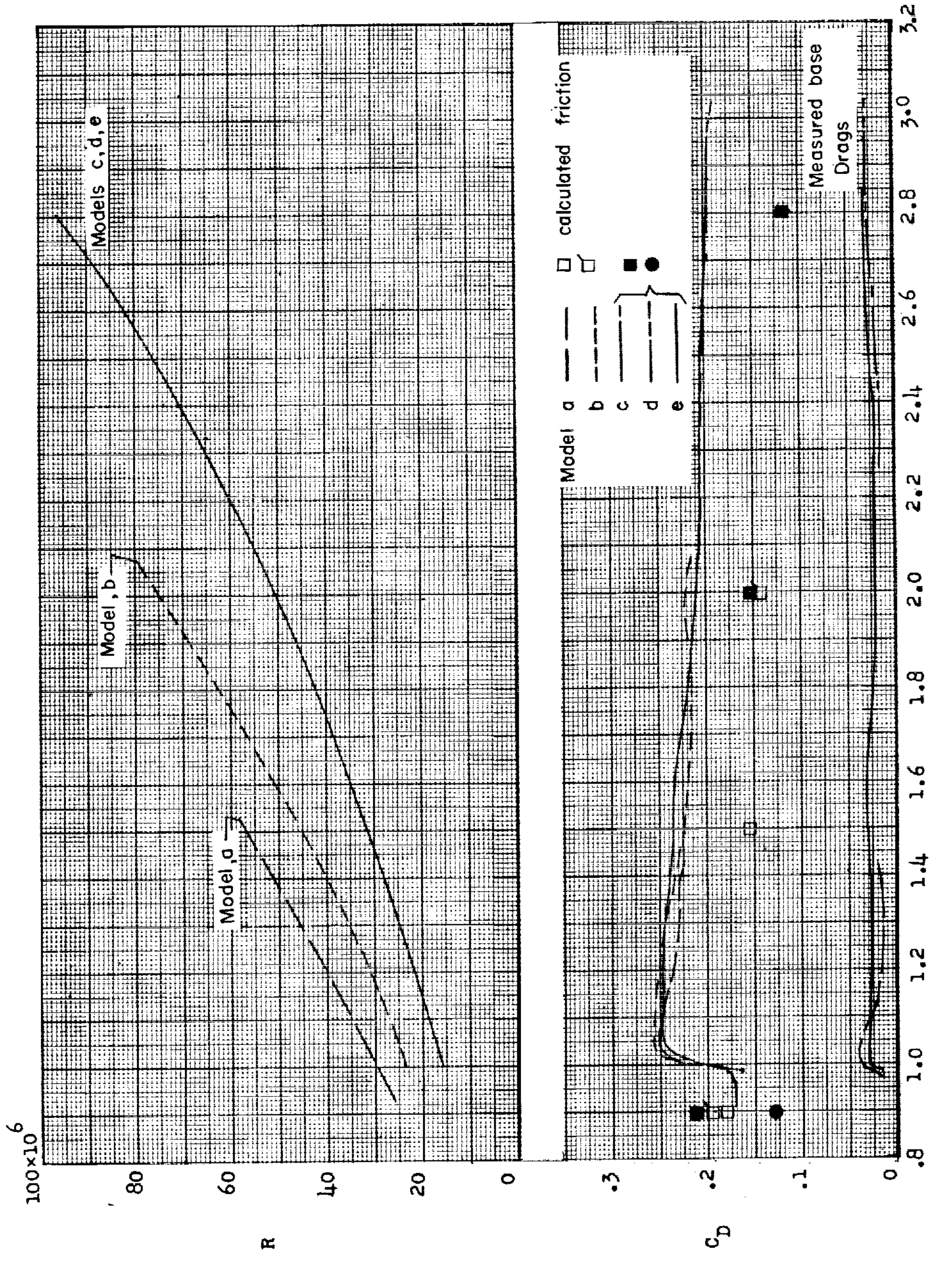

Figure 113.- Concluded.

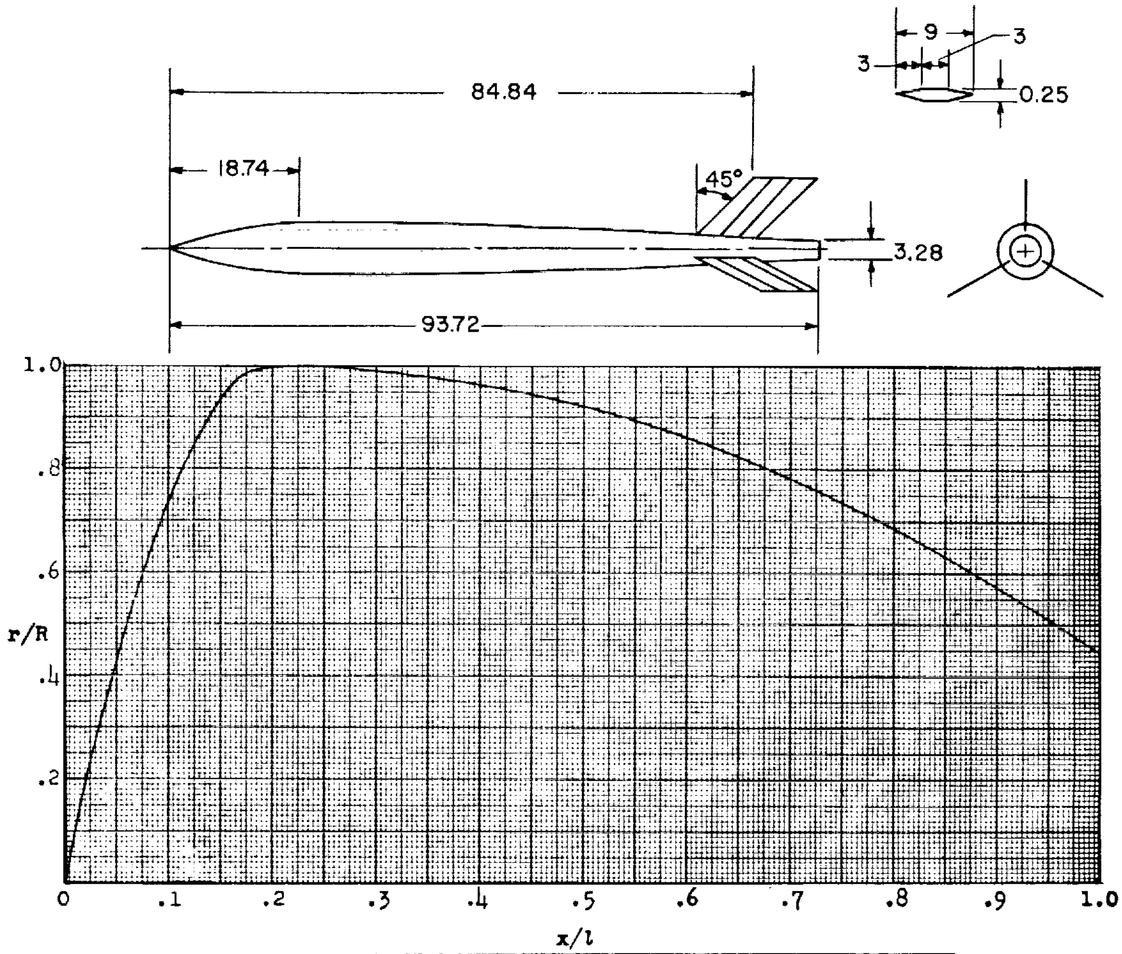

l/d_{Total}	12.5	l/d_{Nose}	2.5	S_b/A	39.65	A_b/A	.19
l/d_{N+A}	12.5	l/d_{Aft}	10.00	S_f/A	11.0	θ_b	3.2°

Designation: 106

Test: Rocket

Remarks: Parabolic nose and afterbody.

Figure 114.

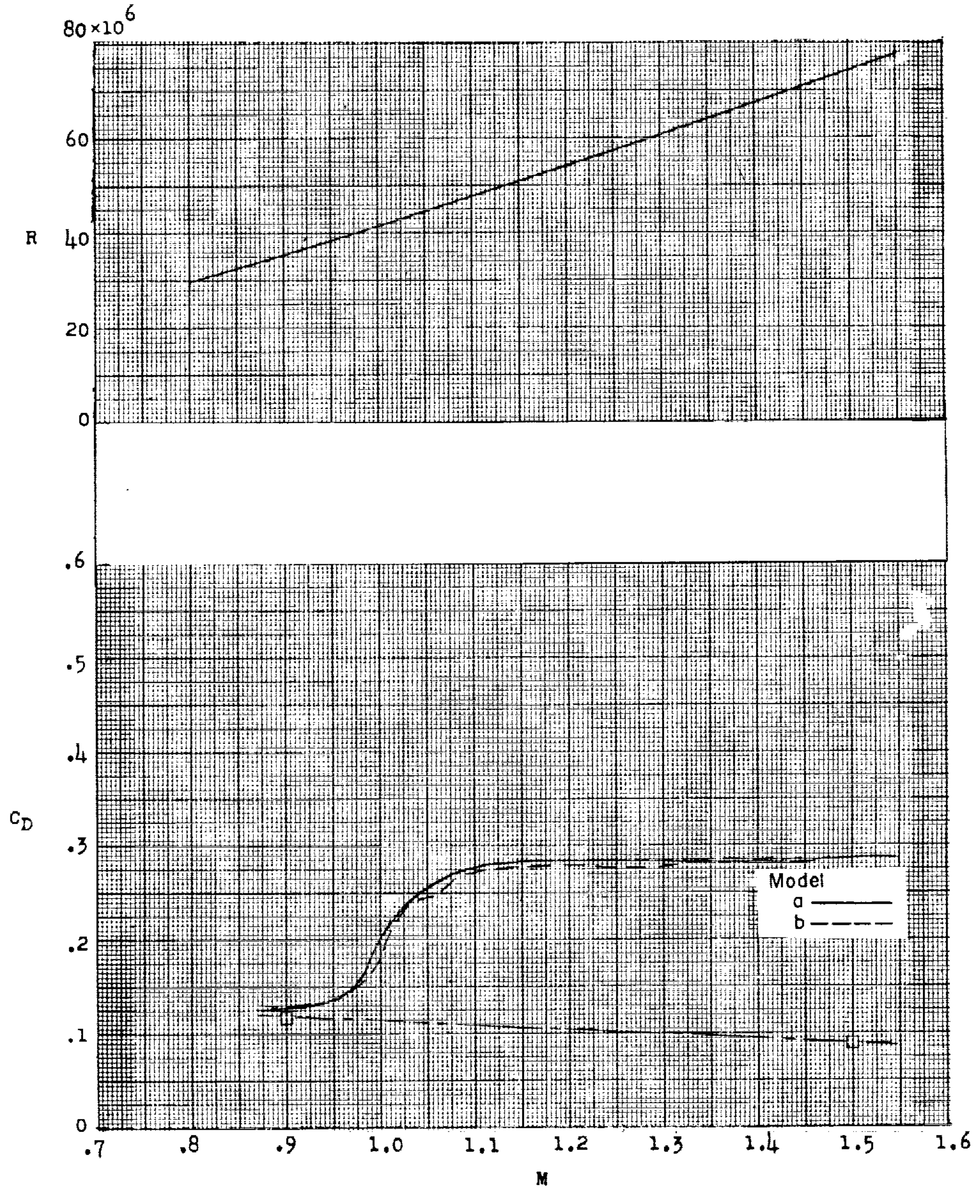

Figure 114.- Concluded.

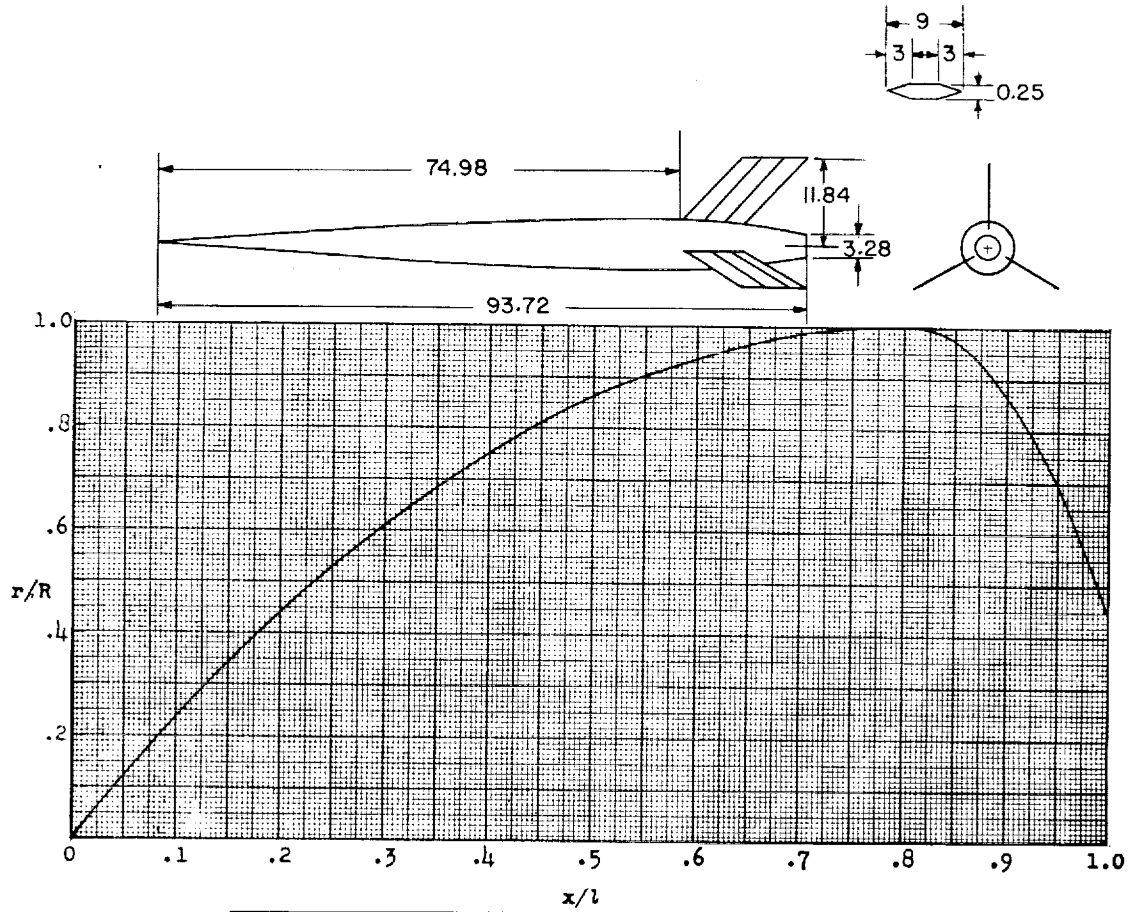

l/d_{Total}	12.5	l/d_{Nose}	10.00	S_b/A	34.85	A_b/A	.19
l/d_{N+A}	12.5	l/d_{Aft}	2.5	S_f/A	11.0	θ_b	12.6°

Designation: 107

Test: Rocket

Remarks: Parabolic nose and afterbody.

Figure 115.

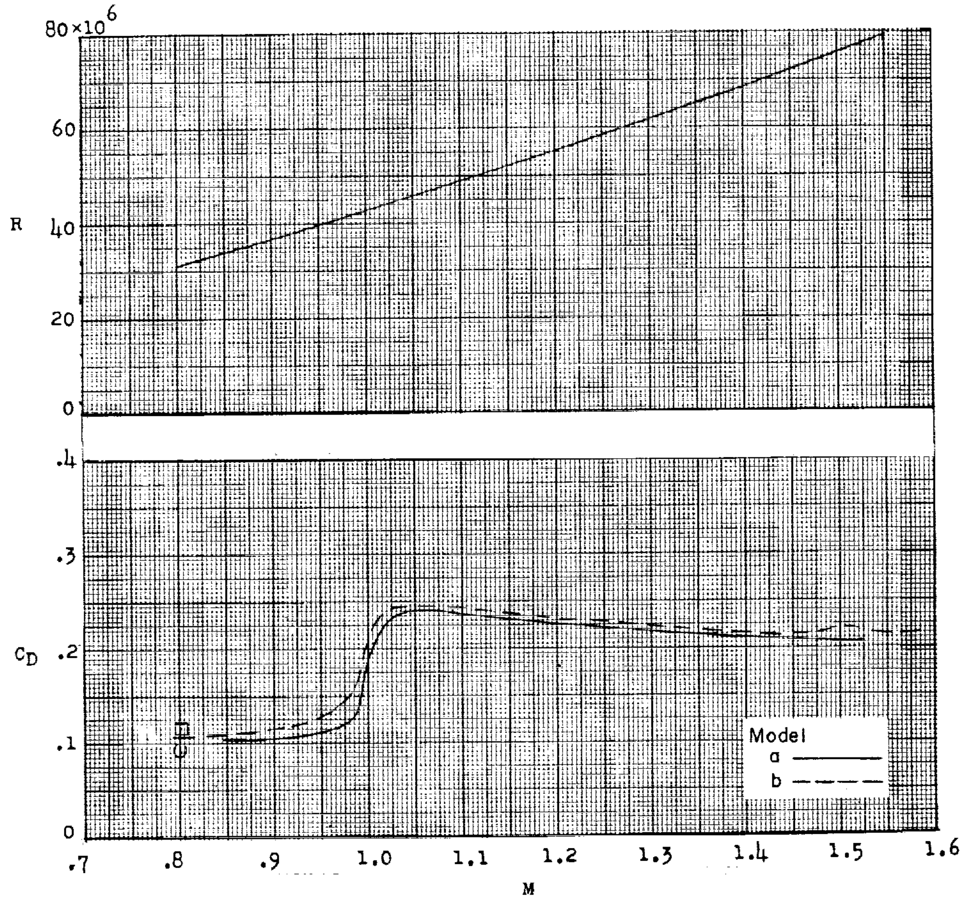

Figure 115.- Concluded.

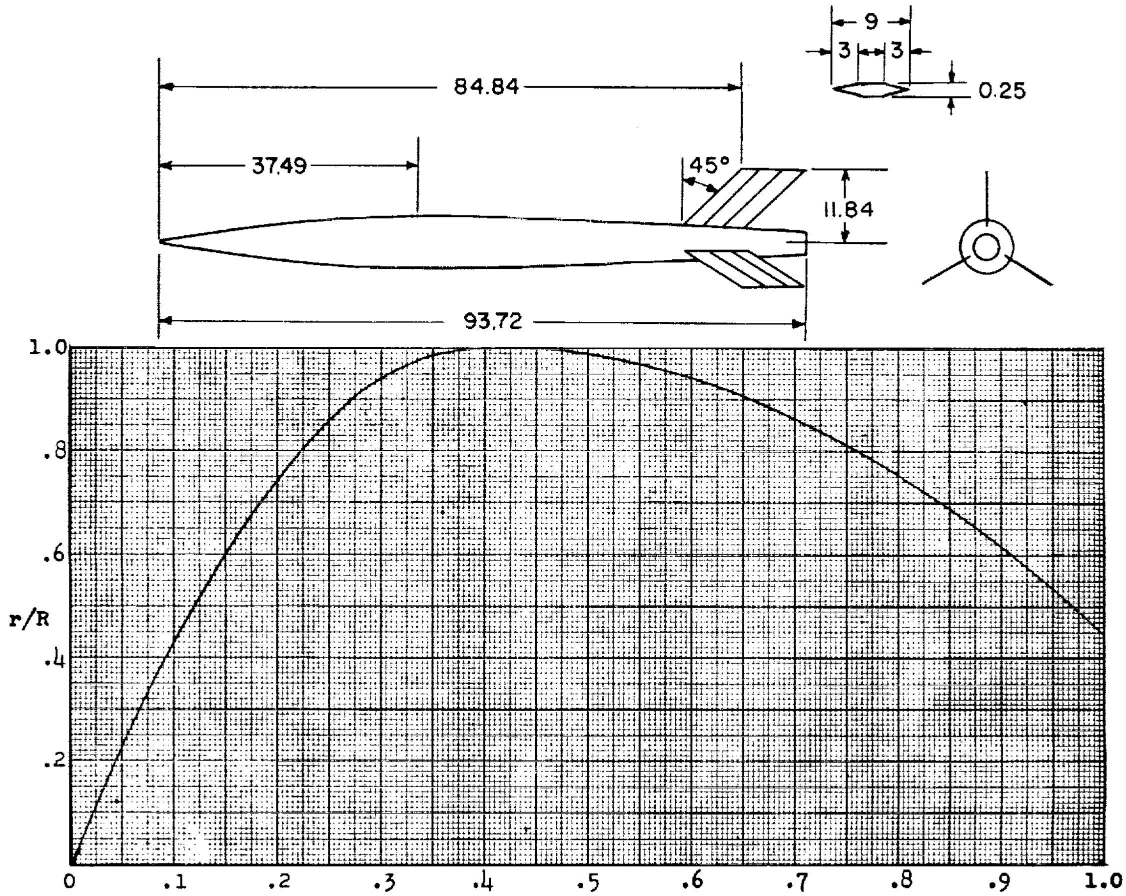

l/d_{Total}	12.5	l/d_{Nose}	5.00	S_b/A	38.10	A_b/A	.19
l/d_{N+A}	12.5	l/d_{Aft}	7.50	S_f/A	11.0	θ_b	4.3°

Designation: 108

Test: **Rocket**

Remarks: Parabolic nose and afterbody; both models appear to have been affected by rocket afterburning which caused the wavy curve of C_D at supersonic Mach numbers.

Figure 116.

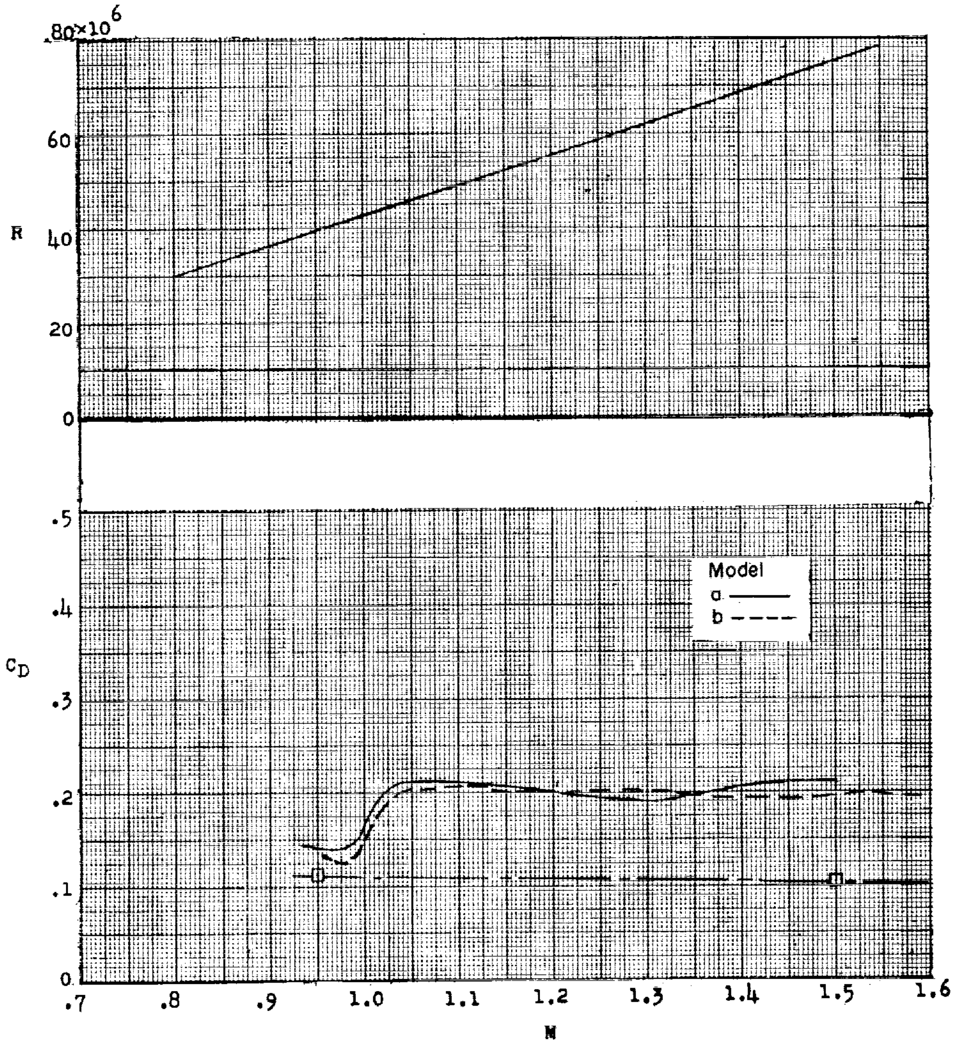

Figure 116.- Concluded.

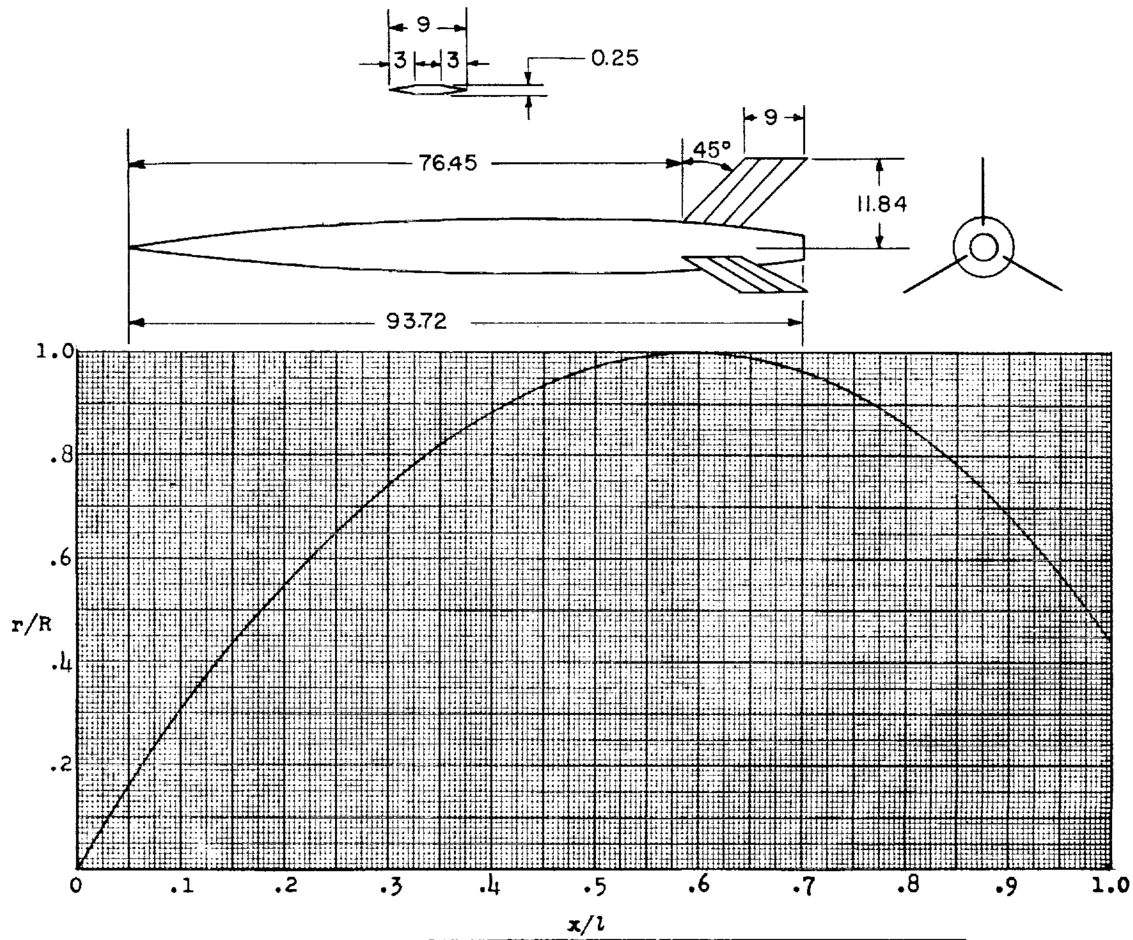

l/d_{Total}	12.5	l/d_{Nose}	7.50	S_b/A	36.50	A_b/A	.19
l/d_{N+A}	12.5	l/d_{Aft}	5.00	S_f/A	11.0	θ_b	6.4°

Designation: 109

Test: Rocket

Remarks: Parabolic nose and afterbody.

Figure 117.

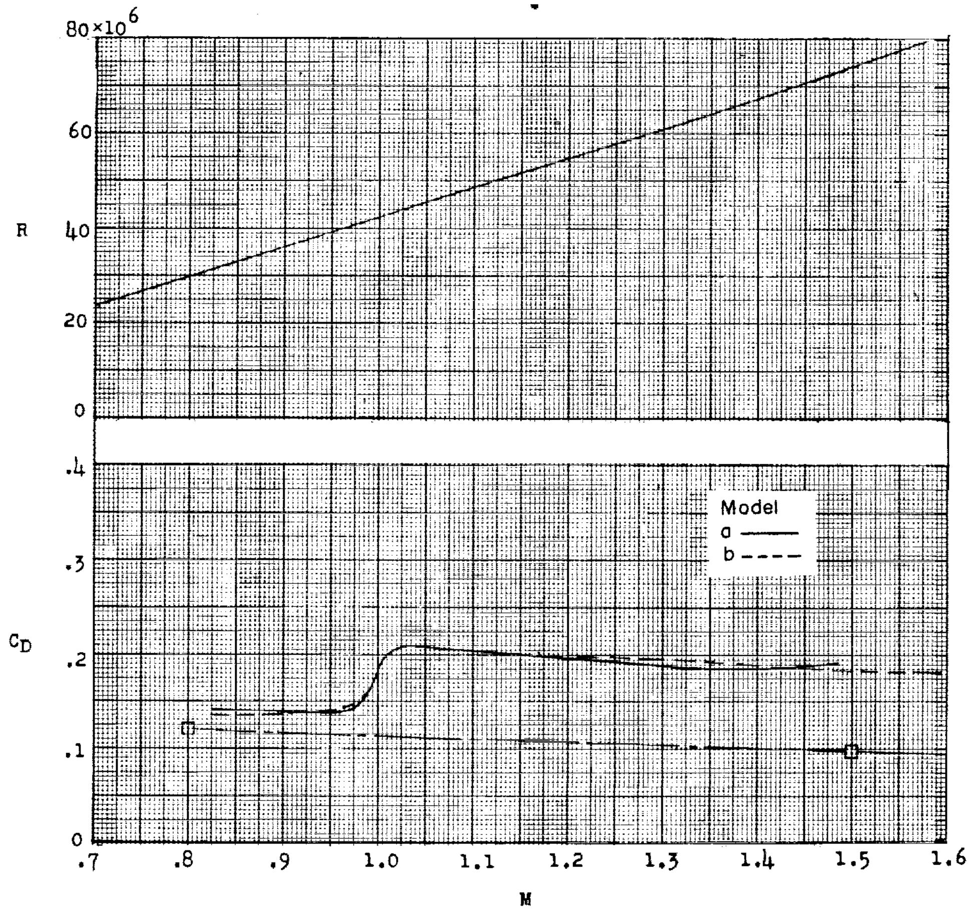

Figure 117.- Concluded.

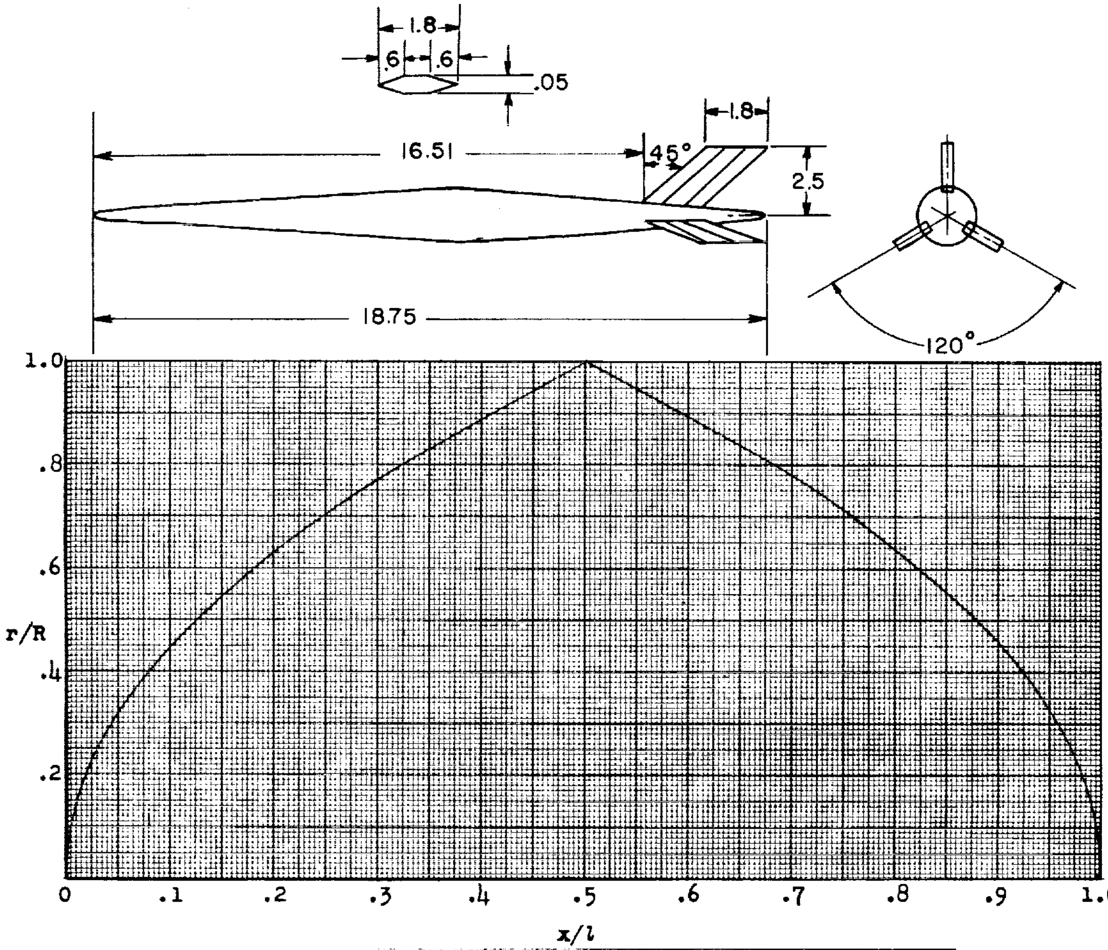

l/d_{Total}	12.5	l/d_{Nose}	6.25	S_b/A	33.40	A_b/A	0.0
l/d_{N+A}	12.5	l/d_{Aft}	6.25	S_f/A	11.0	θ_b	90°

Designation: 110

Test: Helium Gun

Remarks: Nose and afterbody, $r' = x'^{3/4}$.

Figure 118.

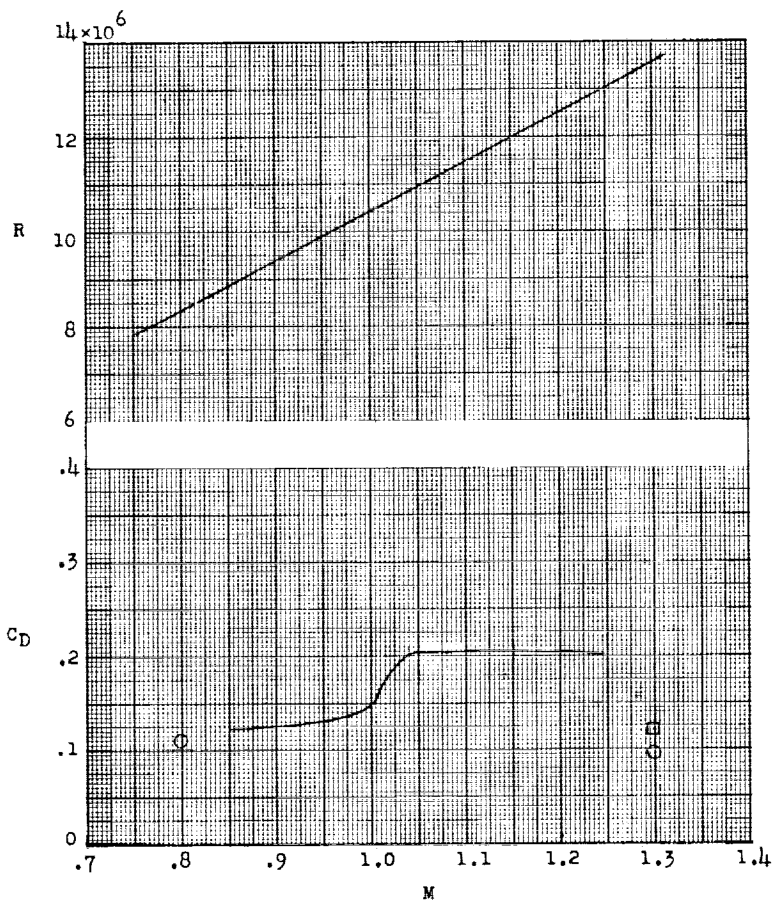

Figure 118.- Concluded.

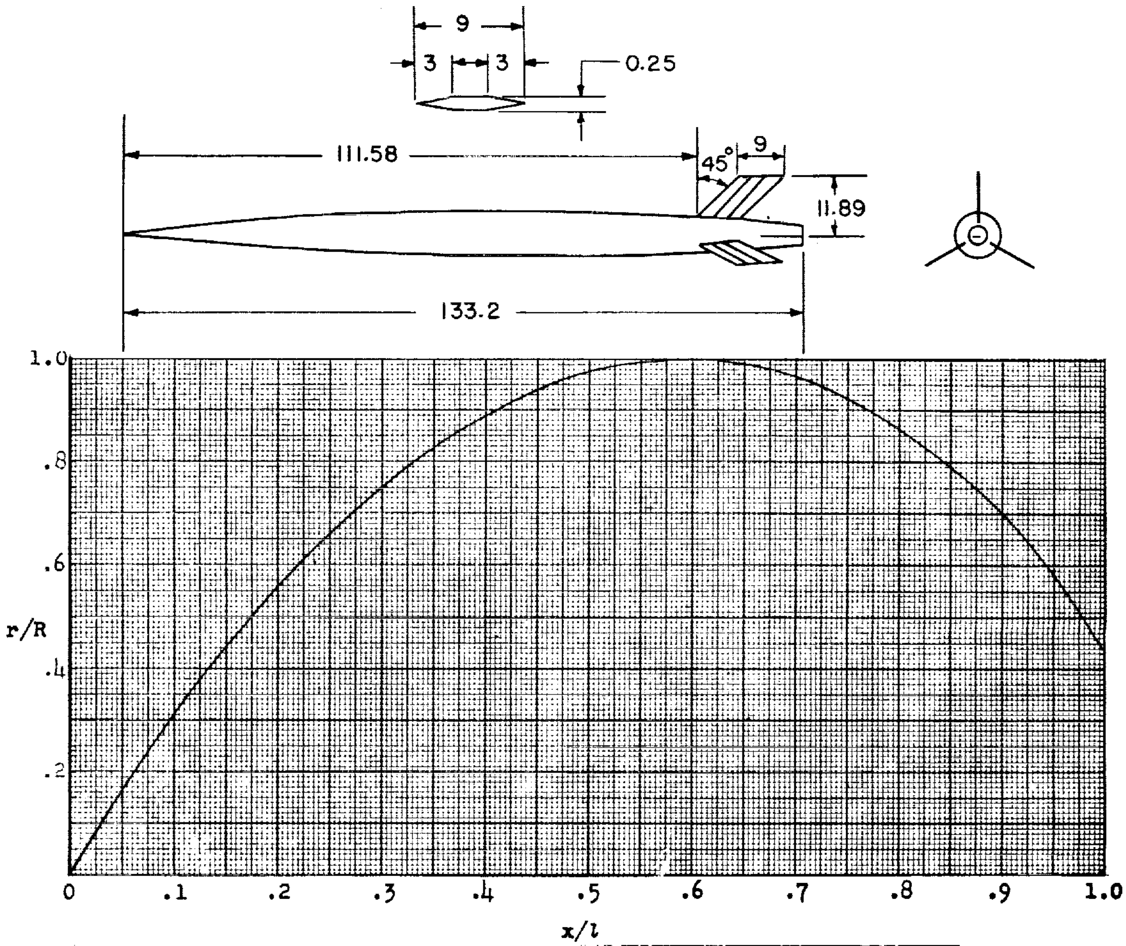

l/d_{Total}	17.78	l/d_{Nose}	10.65	S_b/A	52 0	A_b/A	.19
l/d_{N+A}	17.78	l/d_{Aft}	7.1	S_f/A	11.0	θ_b	4.6°

Designation: 111

Test: Rocket

Remarks: Parabolic nose and afterbody.

Figure 119.

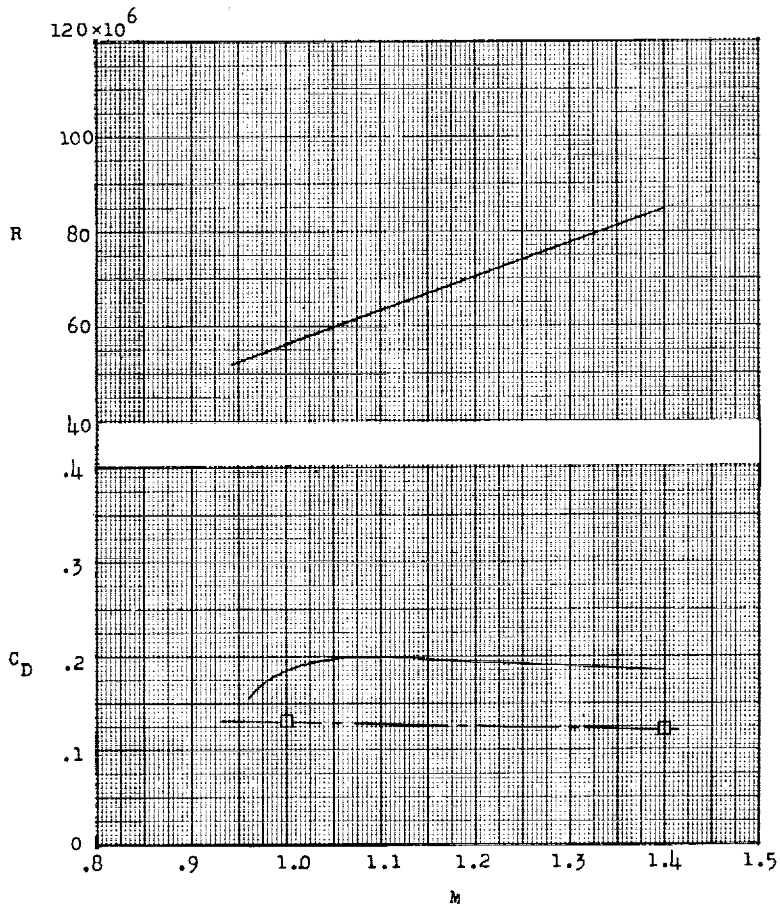

Figure 119.- Concluded.

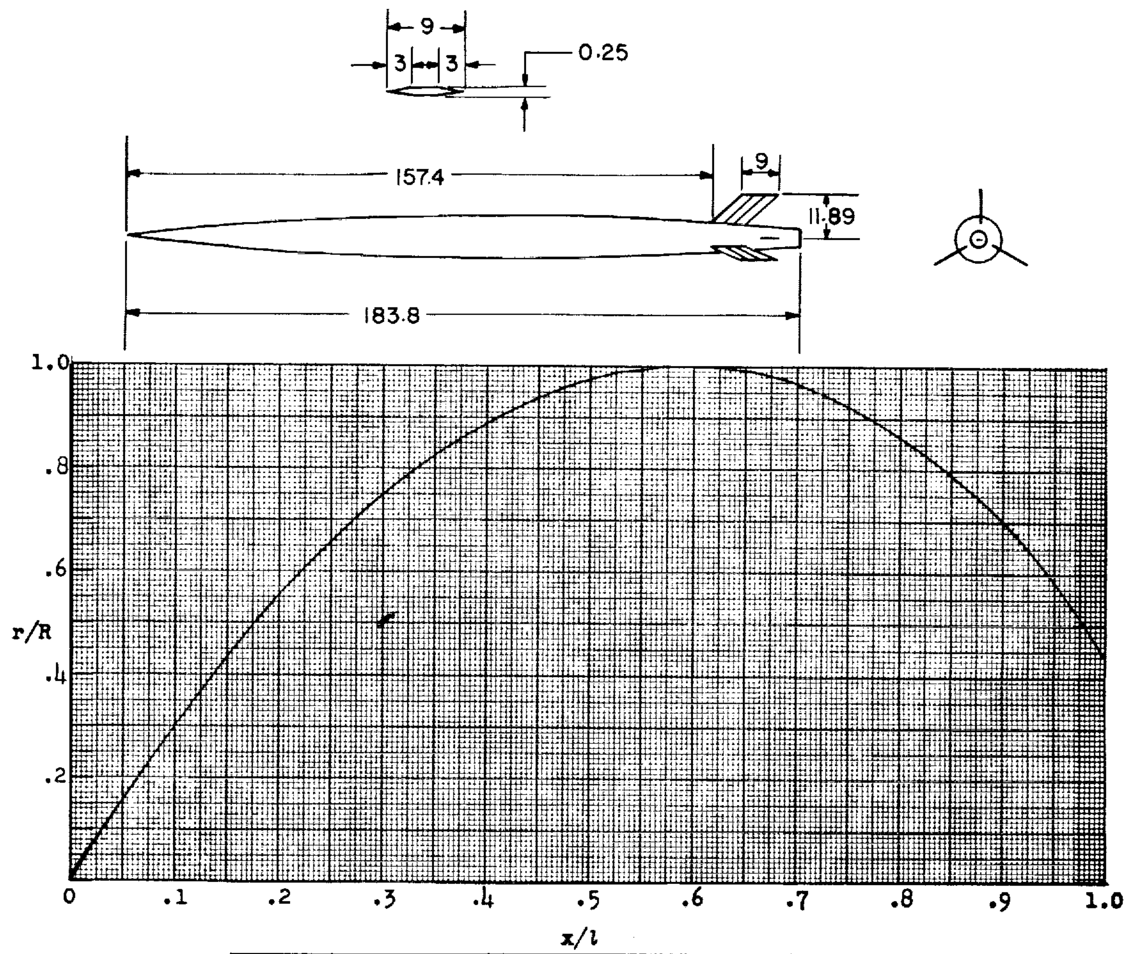

l/d_{Total}	24.5	l/d_{Nose}	14.7	S_b/A	71.6	A_b/A	.19
l/d_{N+A}	24.5	l/d_{Aft}	9.8	S_f/A	11.0	θ_b	3.3°

Designation: 112

Test: Rocket

Figure 120.

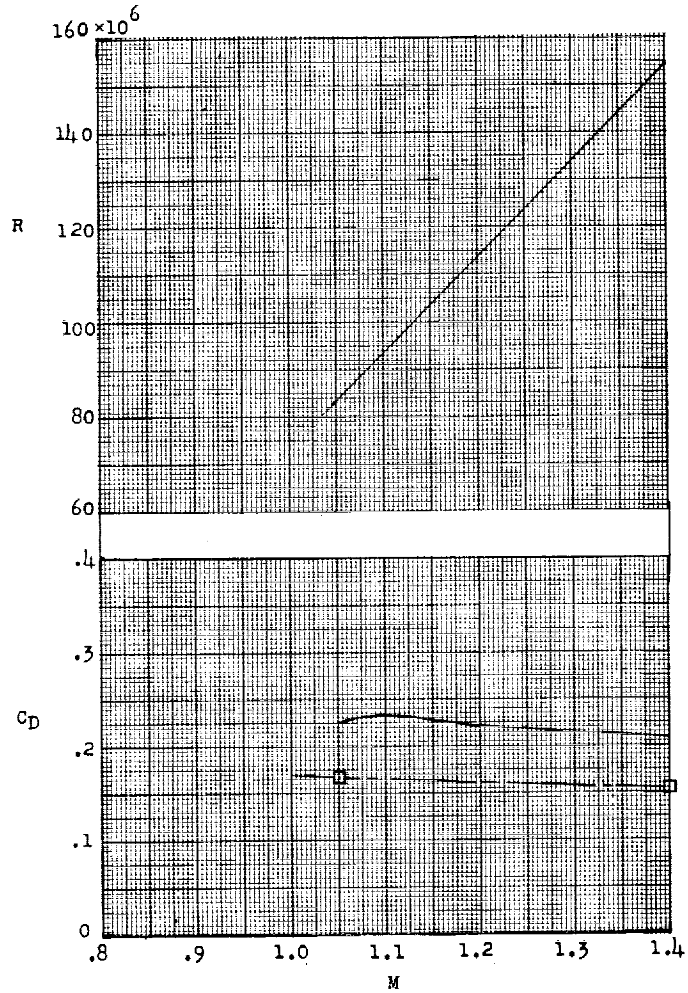

Figure 120.- Concluded.

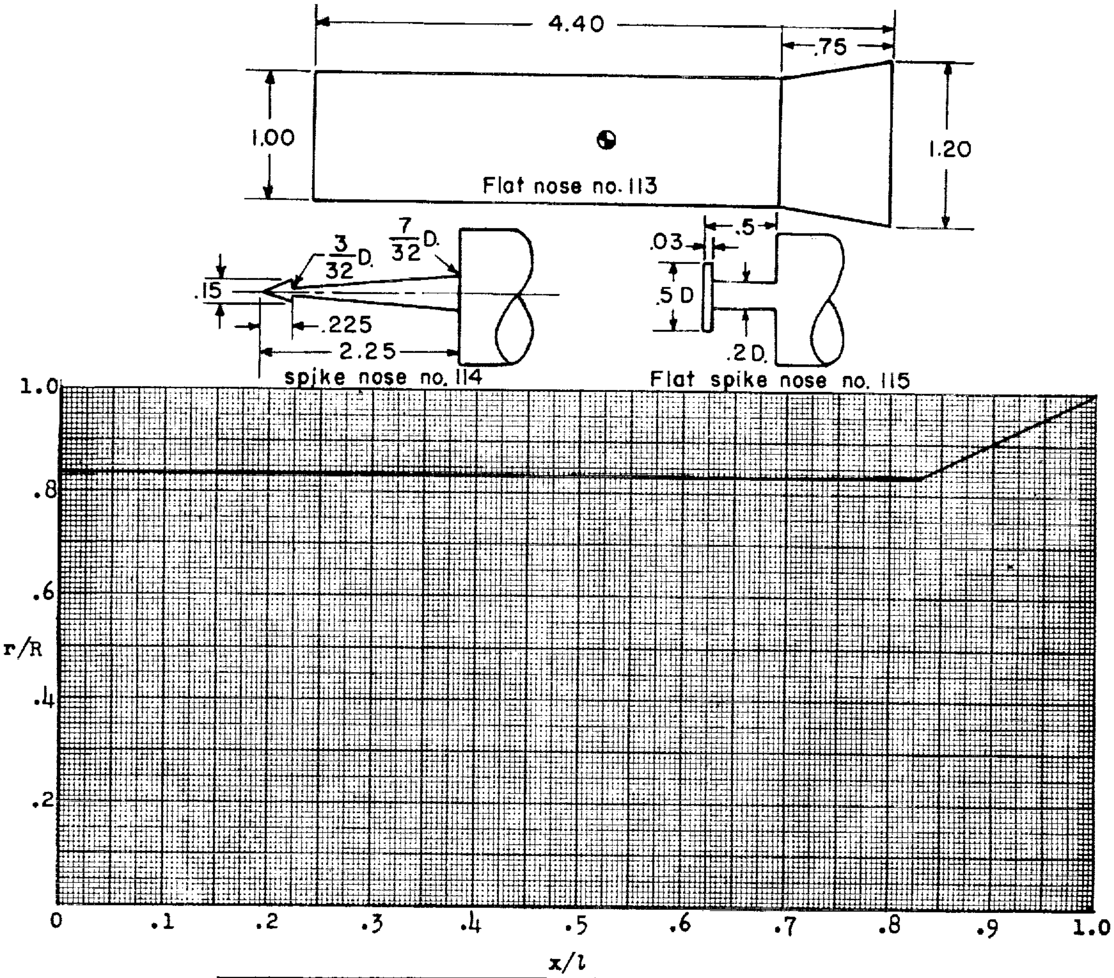

l/d_{Total}	3.67	l/d_{Nose}		S_b/A	12.4	A_b/A	1.0
l/d_{N+A}		l/d_{Aft}		S_f/A	0	θ_b	-7.6°

Designation: 113-114-115

Test: **Helium Gun**

Remarks: Curves presented are faired values obtained from the drag of two models for each of the configurations. In each case the drags of the identical models were quite close, indicating that the models were at essentially 0° angle of attack since it does not appear reasonable that the drag due to oscillations would be a repeatable phenomena.

Figure 121.

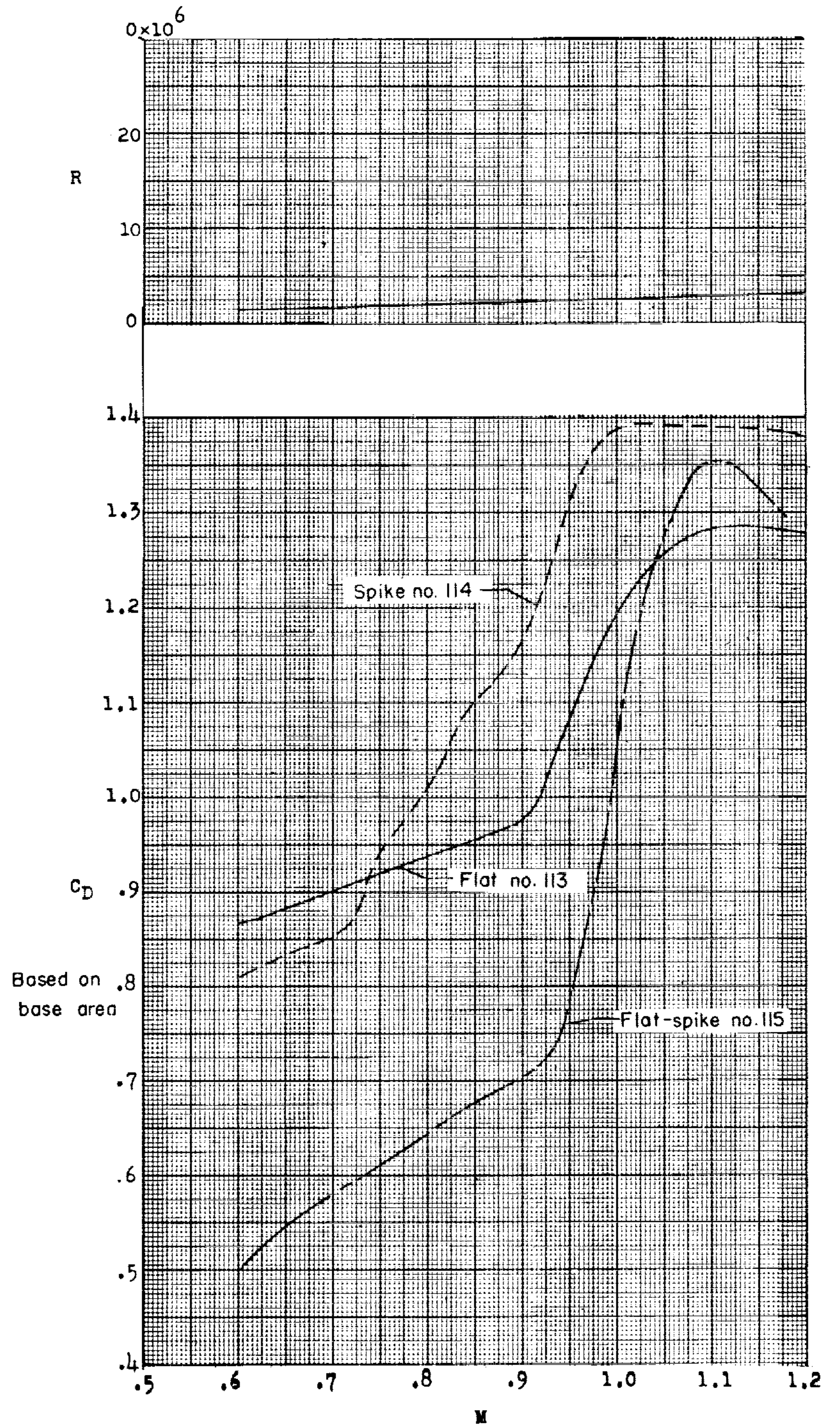

Figure 121.- Concluded.

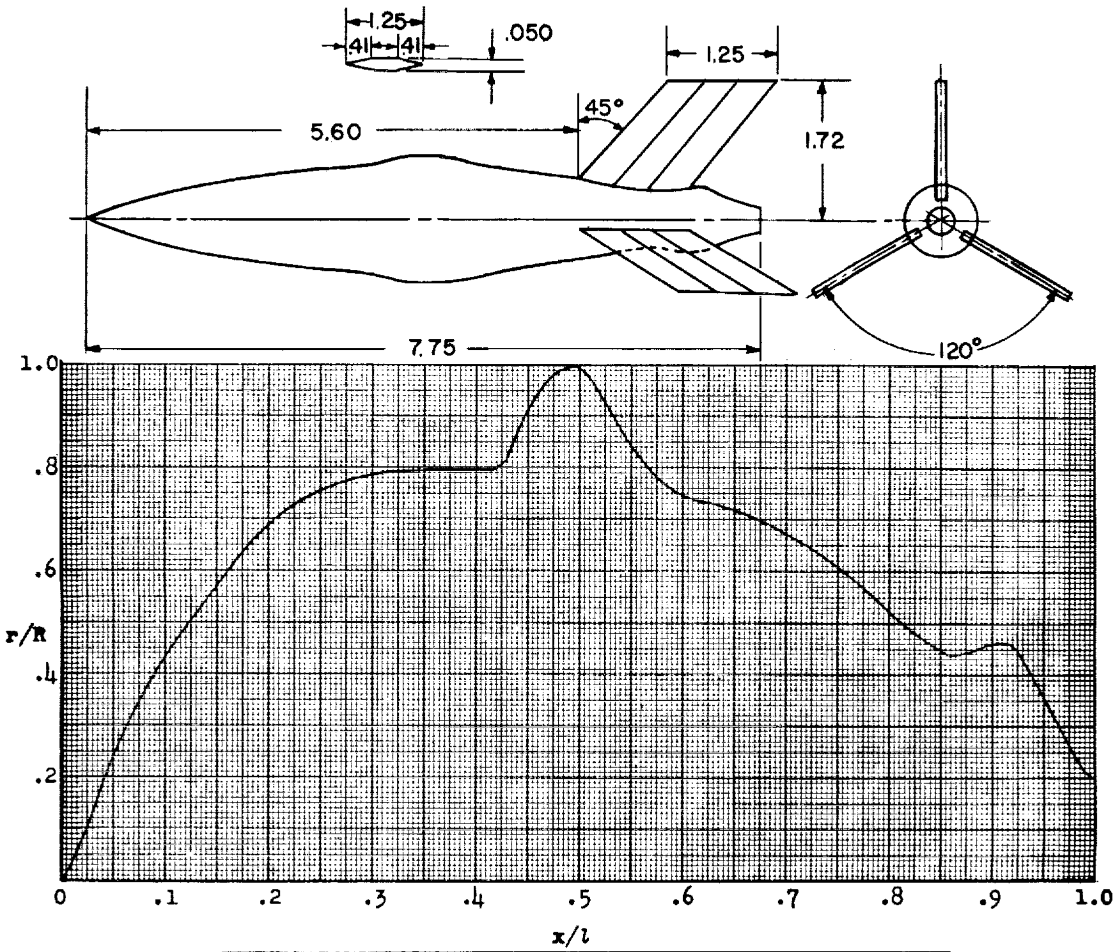

l/d_{Total}	5.23	l/d_{Nose}		S_b/A	13.1	A_b/A	.04
l/d_{N+A}	5.23	l/d_{Aft}		S_f/A	5.8	θ_b	5.5°

Designation: 116

Test: Helium Gun

Figure 122.

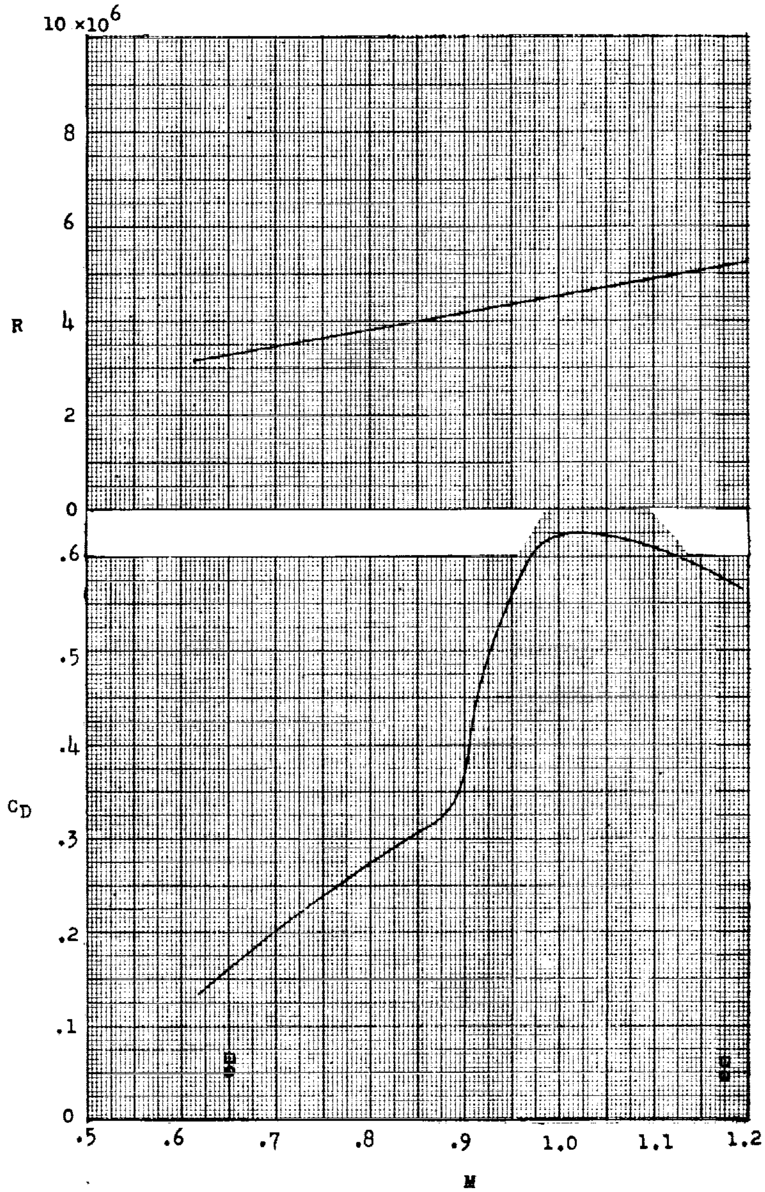

Figure 122.- Concluded.

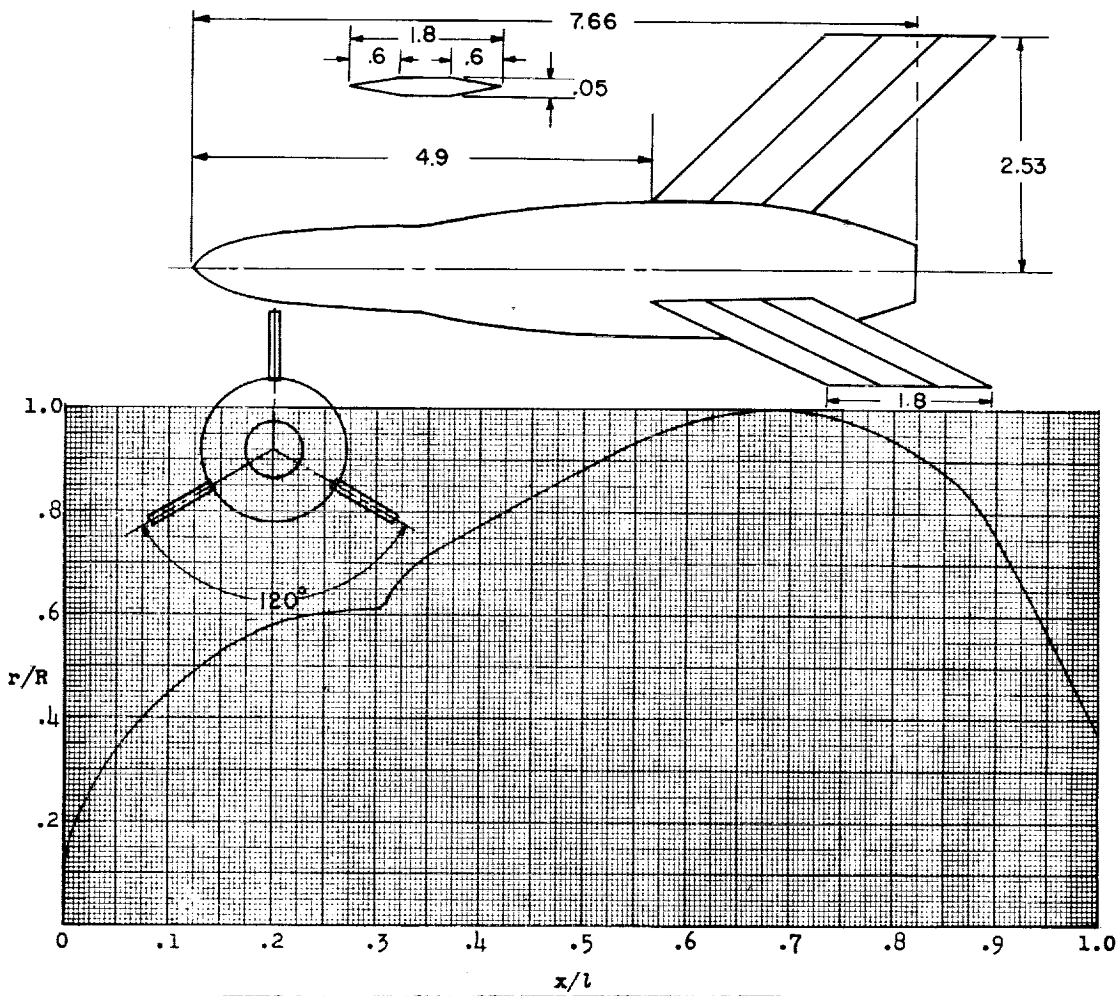

l/d_{Total}	5.26	l/d_{Nose}		S_b/A	24.79	A_b/A	.14
l/d_{N+A}	5.26	l/d_{Aft}		S_f/A	11.64	θ_b	23.9°

Designation: 117

Test: Helium Gun

Figure 123.

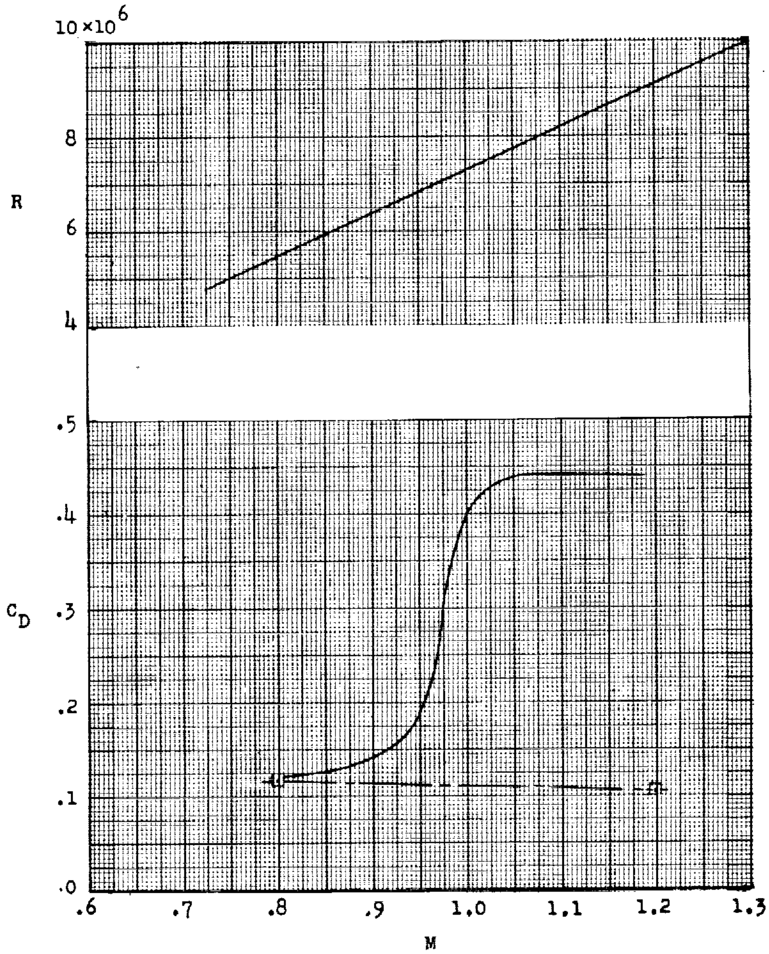

Figure 123.- Concluded.

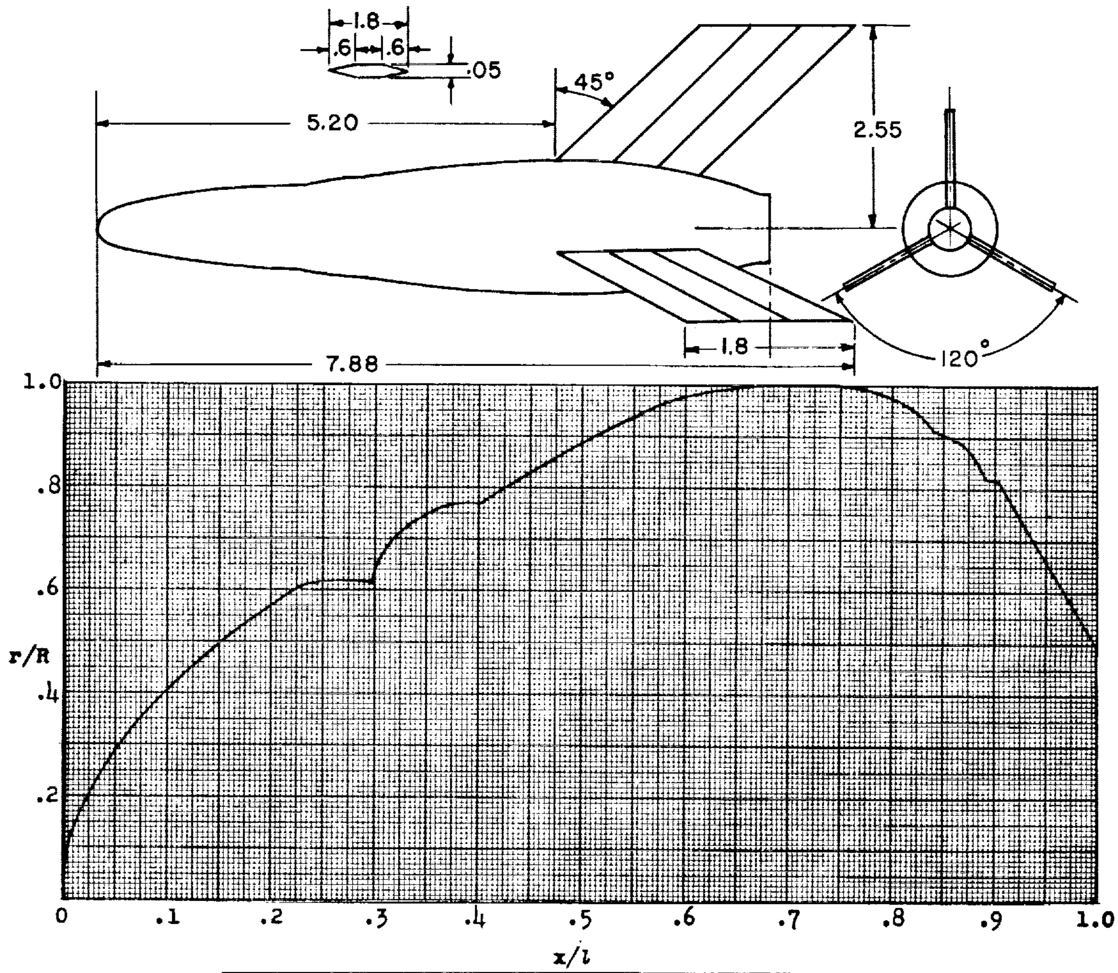

l/d_{Total}	5.29	l/d_{Nose}		S_b/A	16.0	A_b/A	.23
l/d_{N+A}	5.29	l/d_{Aft}		S_f/A	11.64	θ_b	17.3°

Designation: 118

Test: Helium Gun

Figure 124.

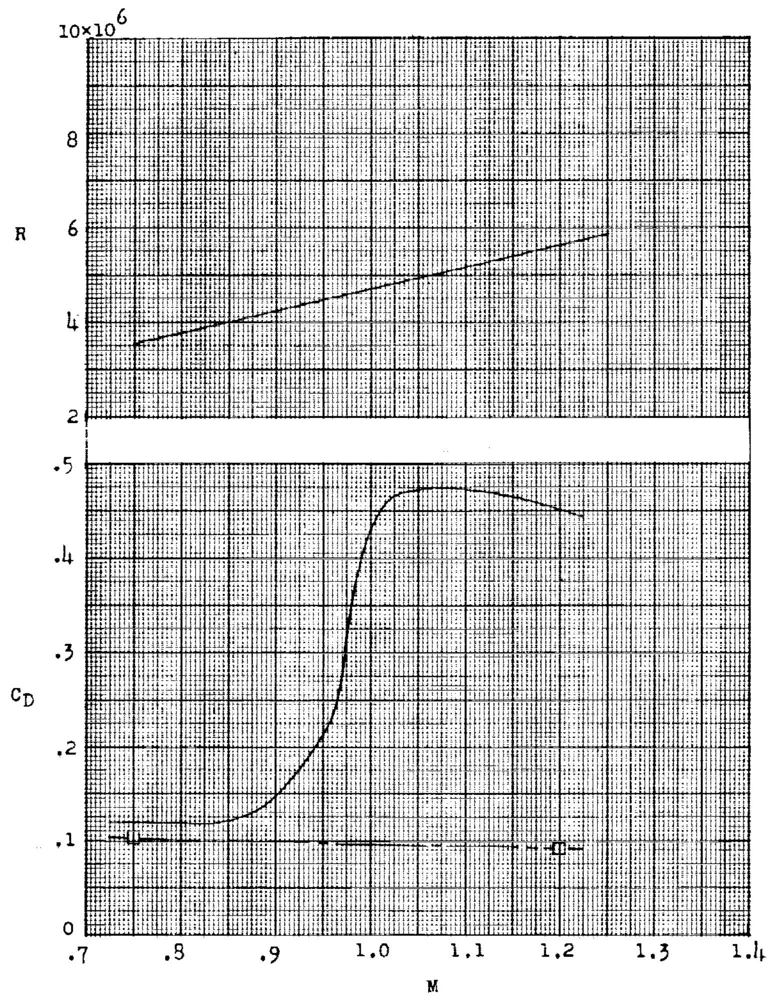

Figure 124.- Concluded.

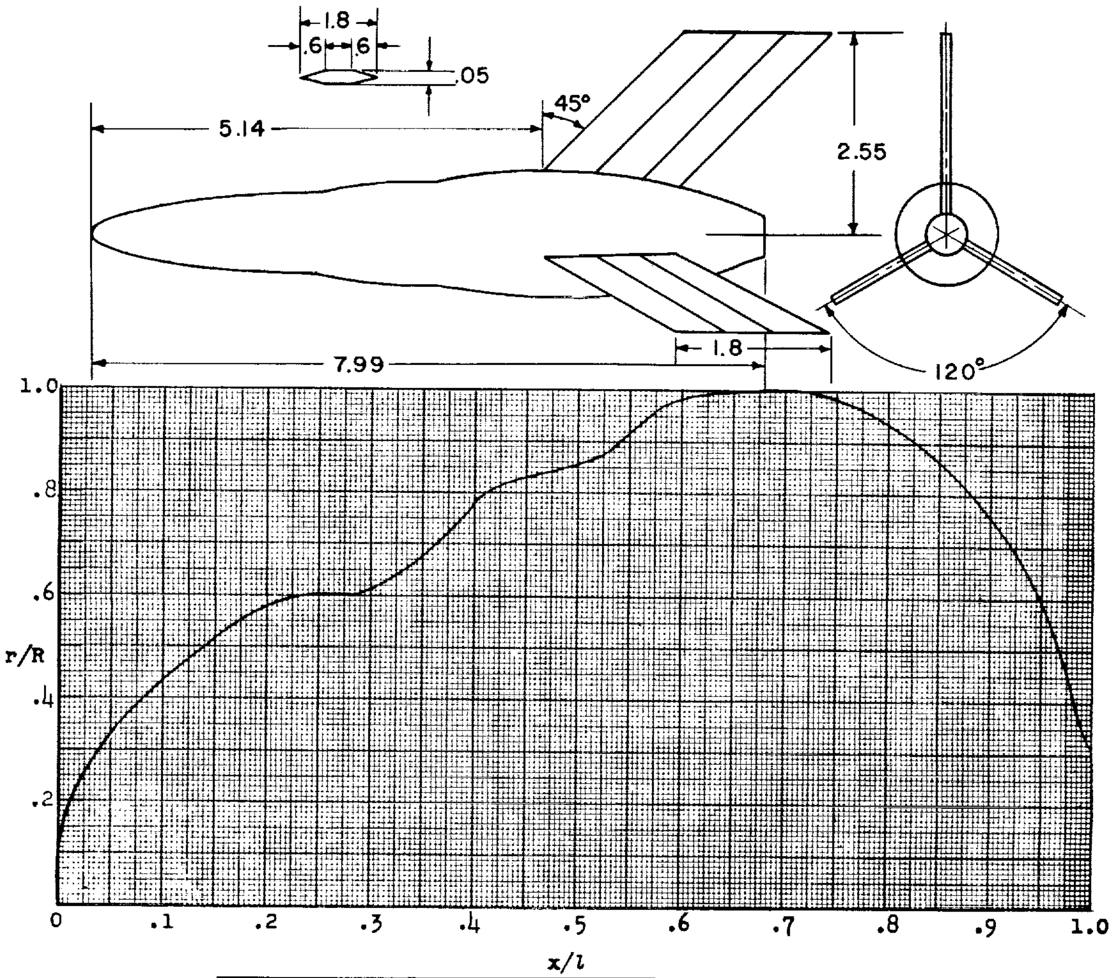

l/d_{Total}	5.36	l/d_{Nose}		S_b/A	15.6	A_b/A	.09
l/d_{N+A}	5.36	l/d_{Aft}		S_f/A	11.28	θ_b	24.2°

Designation: 119

Test: Helium Gun

Figure 125.

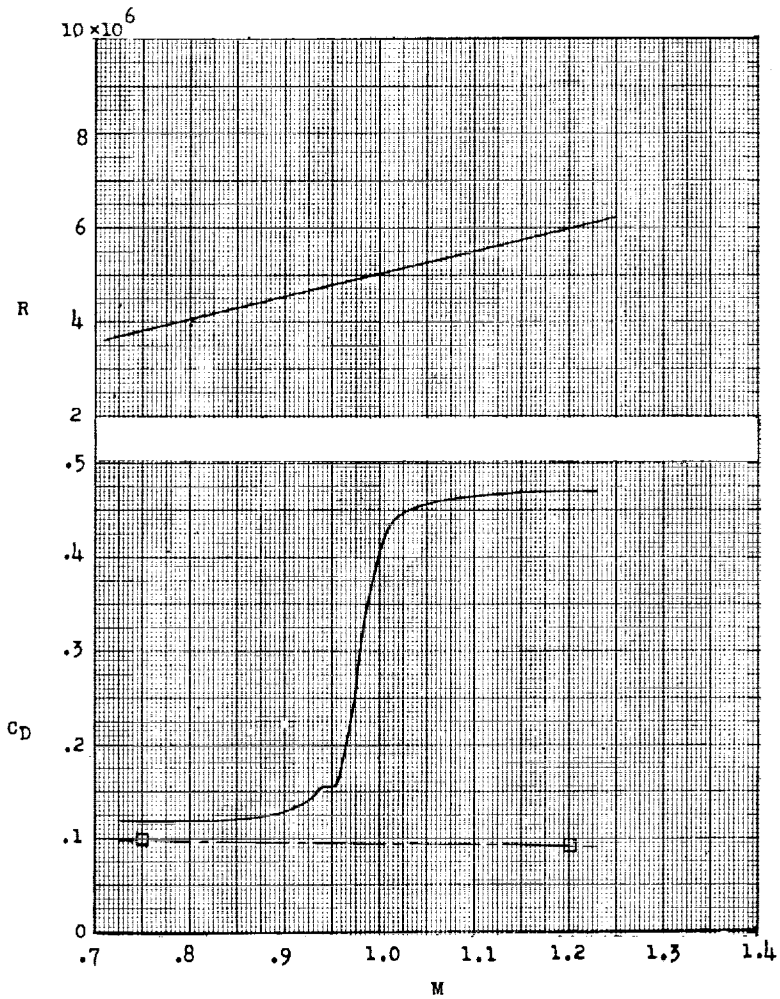

Figure 125.- Concluded.

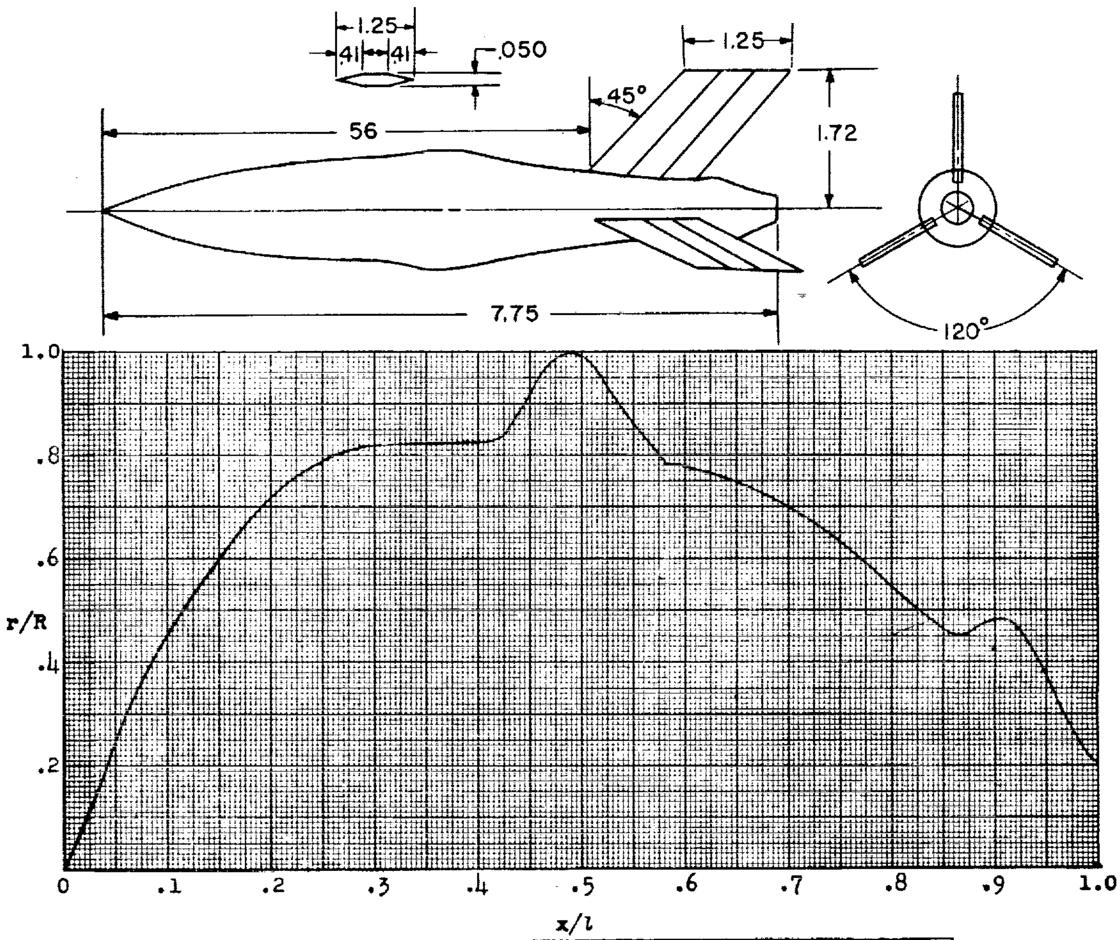

l/d_{Total}	5.45	l/d_{Nose}		S_b/A	14.1	A_b/A	.04
l/d_{N+A}	5.45	l/d_{Aft}		S_f/A	6.28	θ_b	5.5°

Designation: 120

Test: Helium Gun

Figure 126.

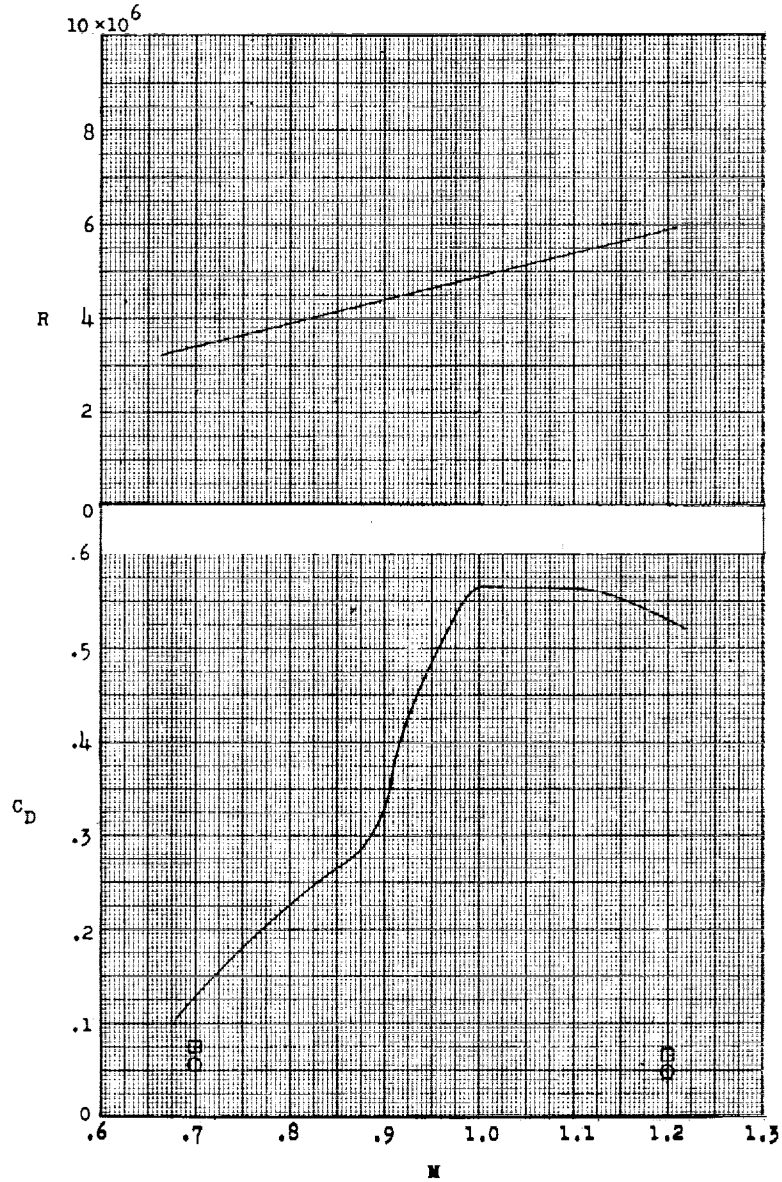

Figure 126.- Concluded.

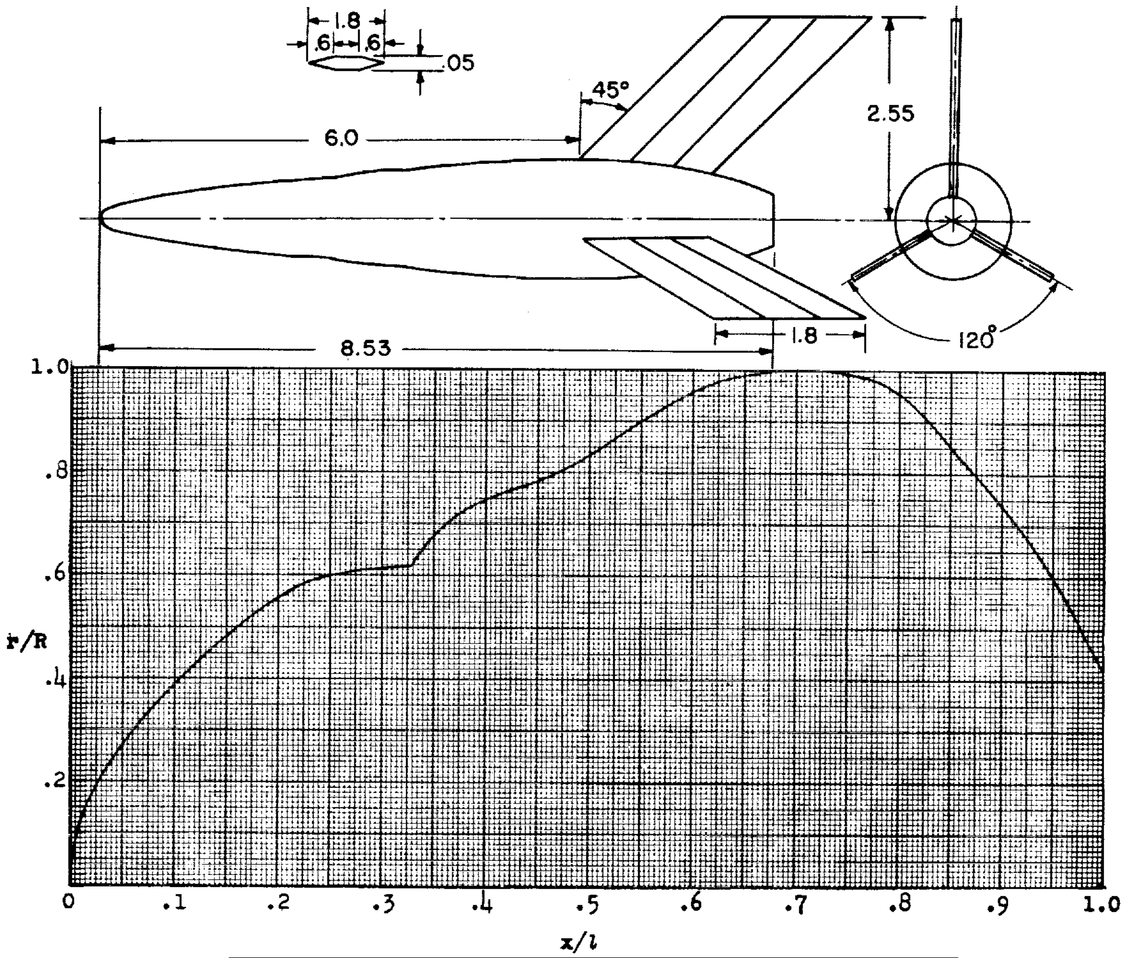

l/d_{Total}	5.68	l/d_{Nose}		S_b/A	16.6	A_b/A	.17
l/d_{N+A}	5.68	l/d_{Aft}		S_f/A	11.6	θ_b	20.2°

Designation: 121

Test: Helium Gun

Figure 127.

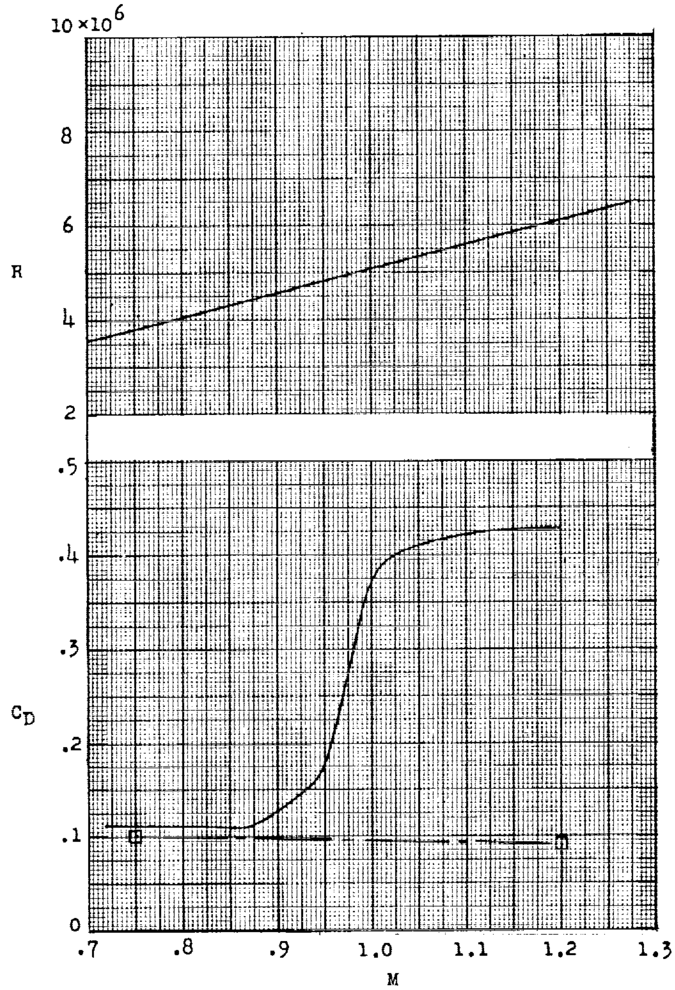

Figure 127.- Concluded.

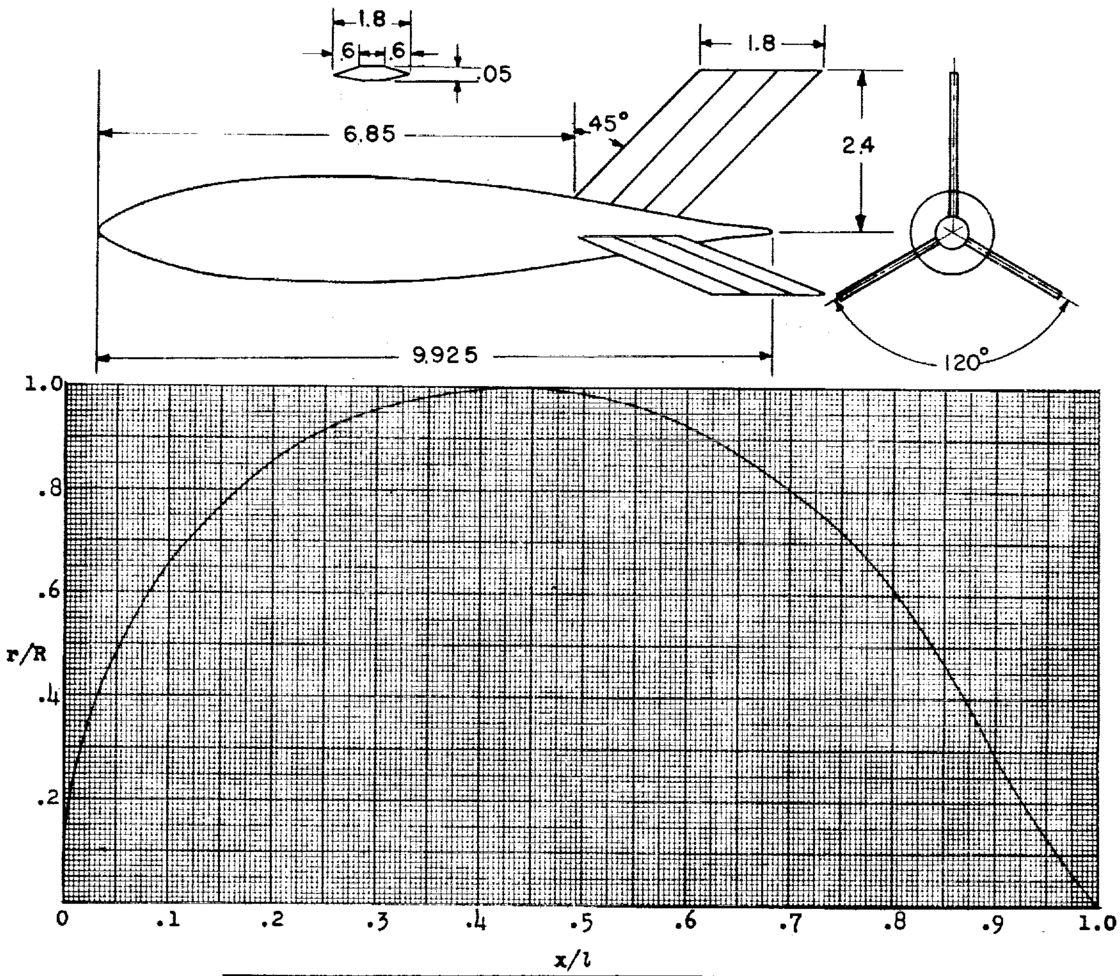

l/d_{Total}	6.00	l/d_{Nose}	2.54	S_b/A	17.50	A_b/A	0.0
l/d_{N+A}	6.00	l/d_{Aft}	3.46	S_f/A	12.0	θ_b	13.6°

Designation: 122

Test: **Helium Gun**

Figure 128.

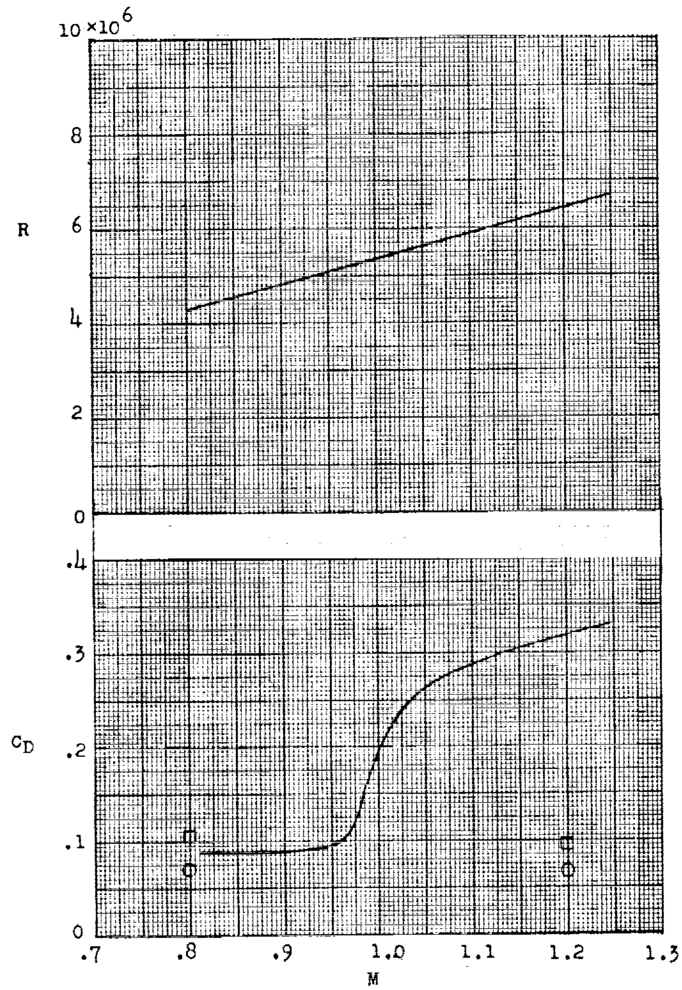

Figure 128.- Concluded.

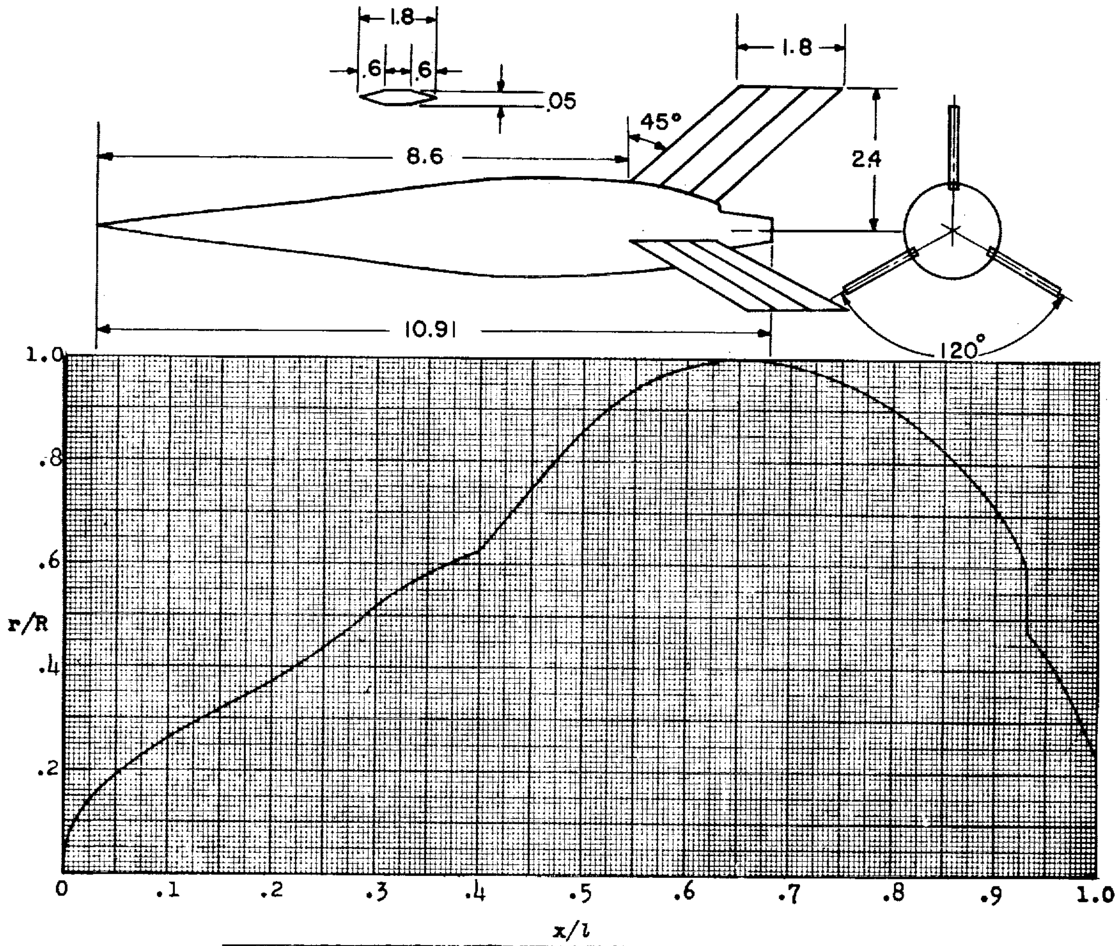

l/d_{Total}	6.66	l/d_{Nose}		S_b/A	17.19	A_b/A	.06
l/d_{N+A}	6.66	l/d_{Aft}		S_f/A	9.22	θ_b	16.7°

Designation: 123

Test: Helium Gun

Remarks: Subsonic flow probably separated at rear step.

Figure 129.

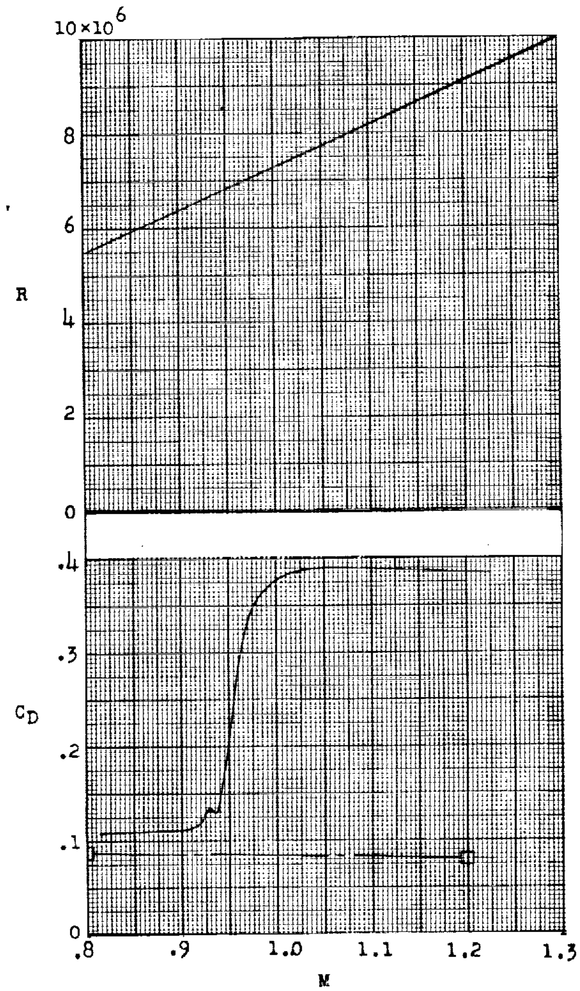

Figure 129.- Concluded.

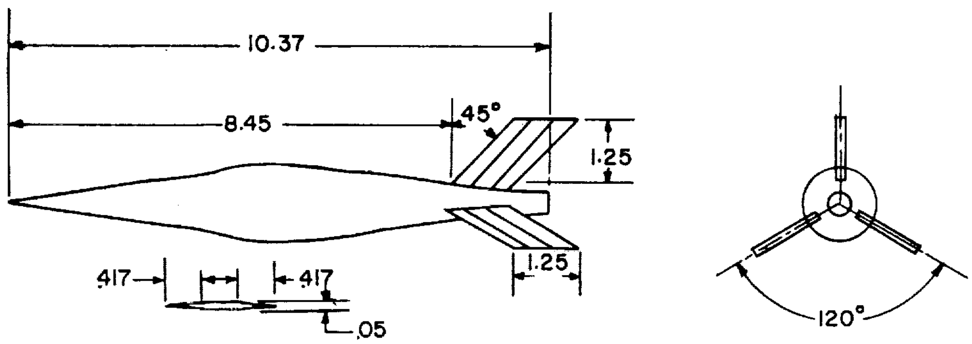

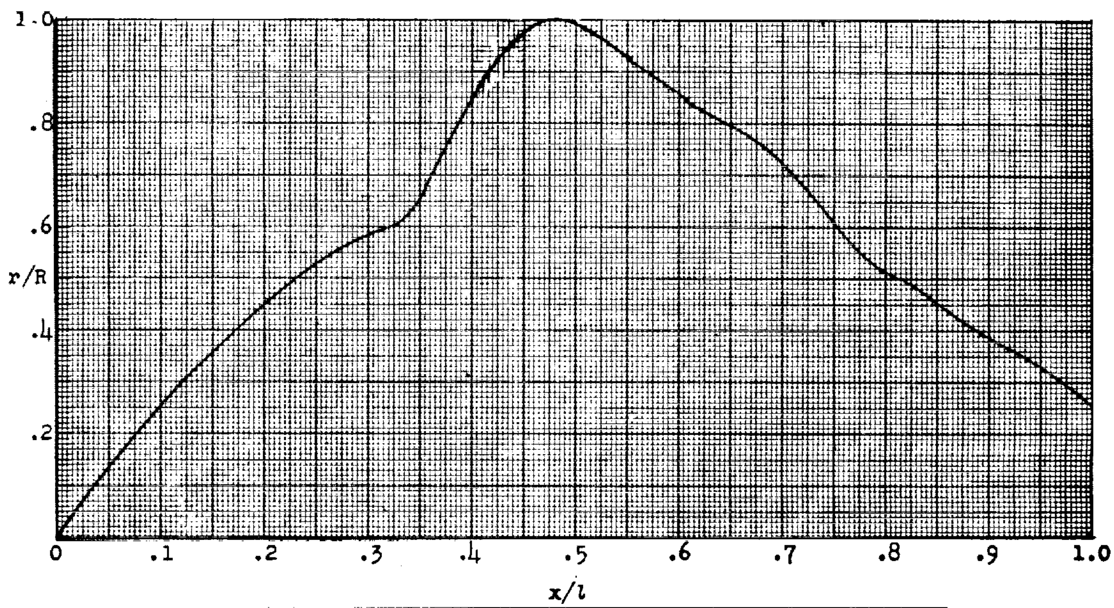

l/d_{Total}	6.82	l/d_{Nose}		S_b/A	15.7	A_b/A	.065
l/d_{N+A}	6.82	l/d_{Aft}		S_f/A	5.43	θ_b	5.0°

Designation: 124

Test: Helium Gun

Figure 130.

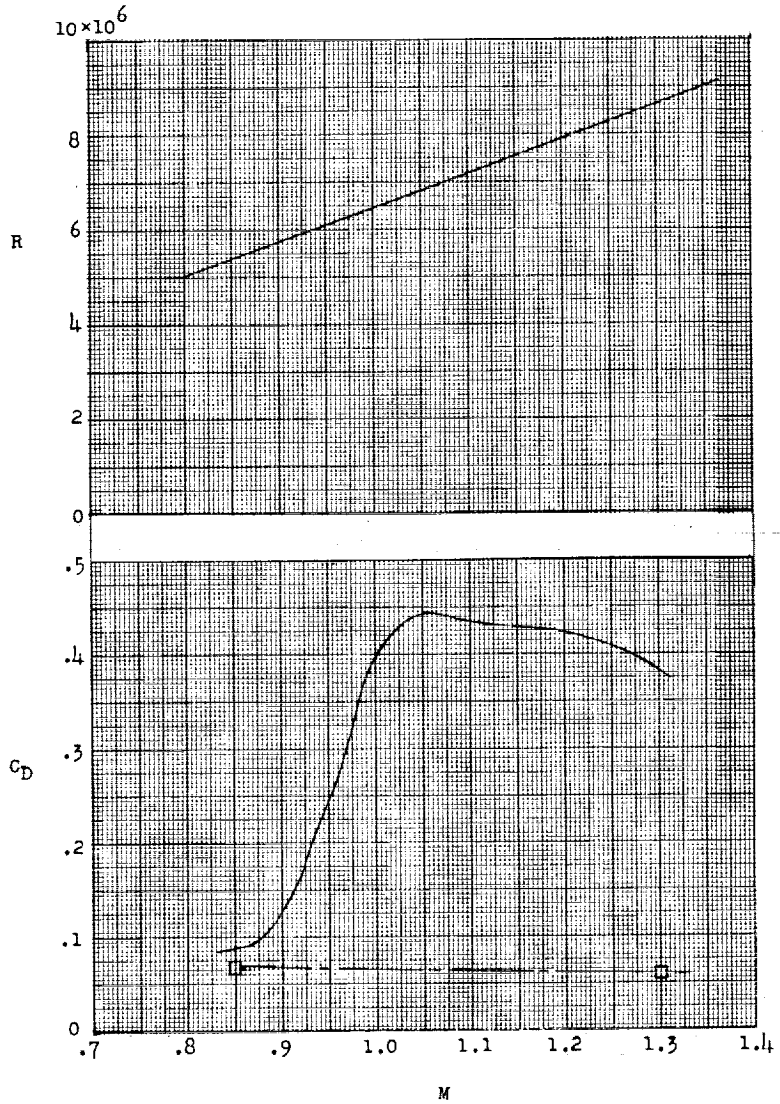

Figure 130.- Concluded.

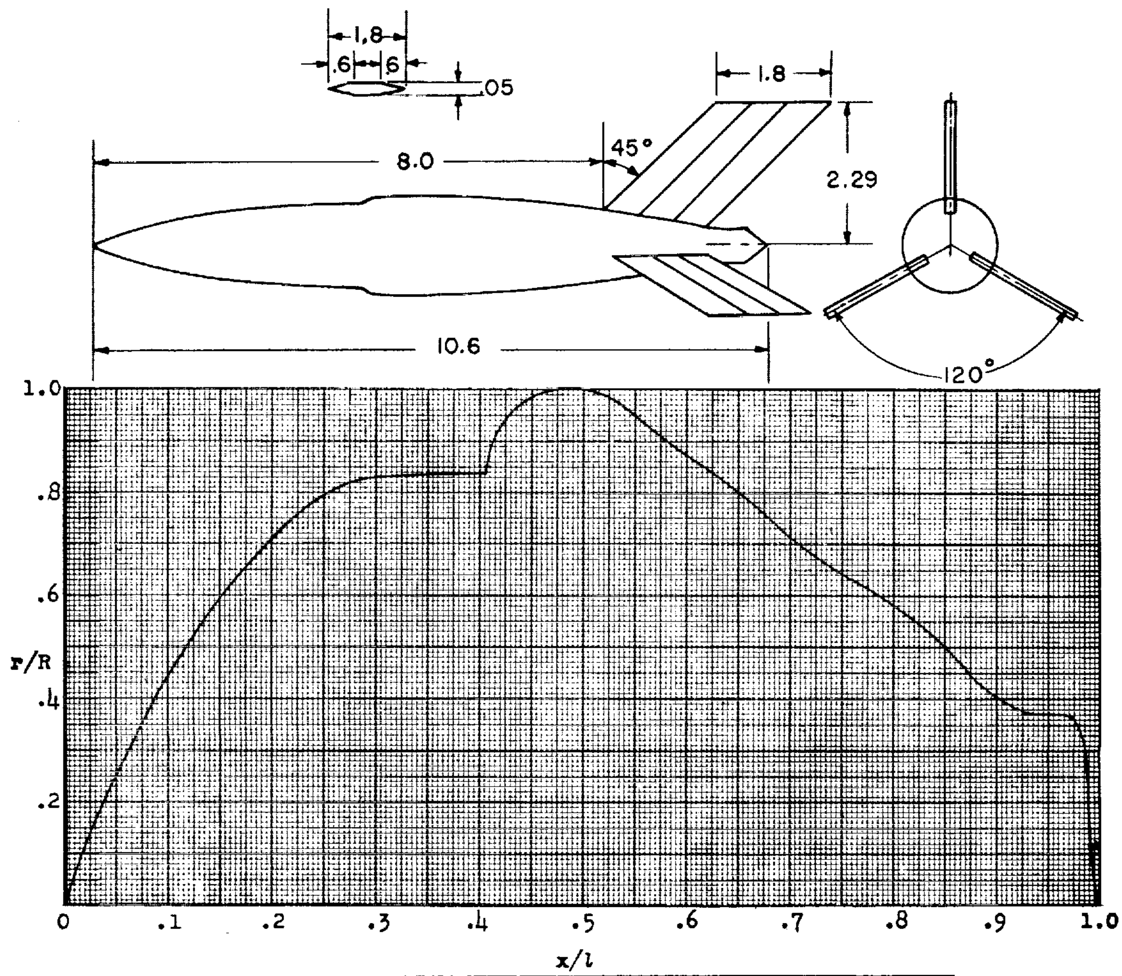

l/d_{Total}	6.84	l/d_{Nose}		S_b/A	18.2	A_b/A	0.0
l/d_{N+A}	6.84	l/d_{Aft}		S_f/A	10.76	θ_b	90°

Designation: 125

Test: Helium Gun

Remarks: Although the calculated friction drag indicates that the fins may be in turbulent flow at subsonic values of M, it is possible that they may be in laminar as their low Reynolds number would predict. The drag difference between the laminar friction calculations and the experimental subsonic values may be due to separation over the base $\left(\frac{x}{l} \approx 0.970\right)$ and over the forward step at $\frac{x}{l} = 0.4$.

Figure 131.

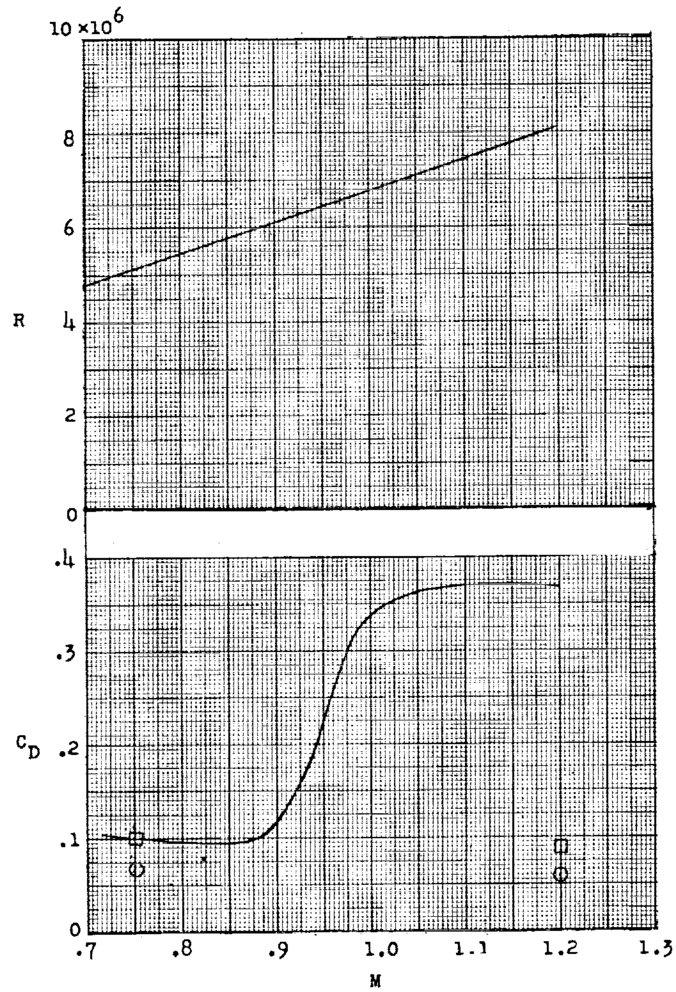

Figure 131.- Concluded.

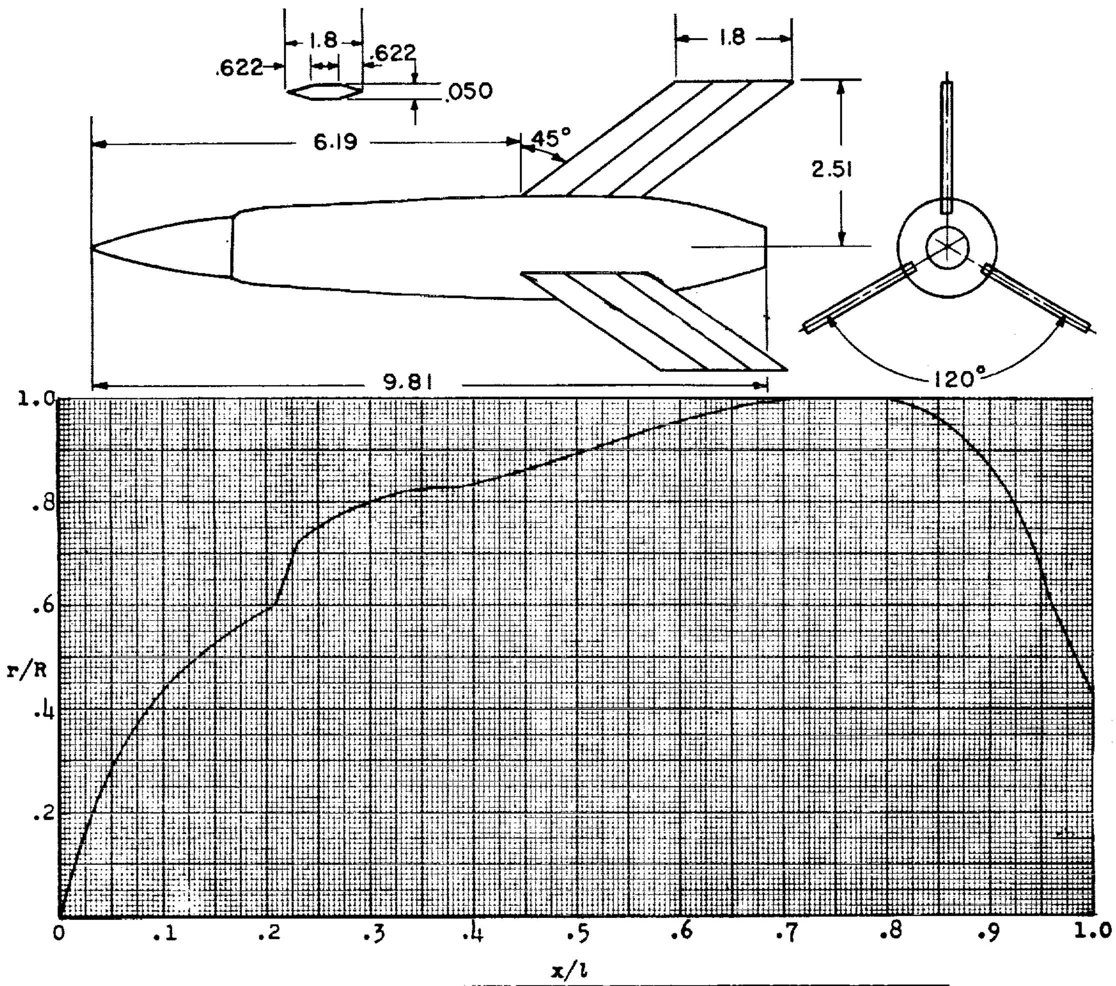

l/d_{Total}	6.86	l/d_{Nose}		S_b/A	21.15	A_b/A	.18
l/d_{N+A}	6.86	l/d_{Aft}		S_f/A	12.2	θ_b	18°

Designation: 126

Test: **Helium Gun**

Figure 132.

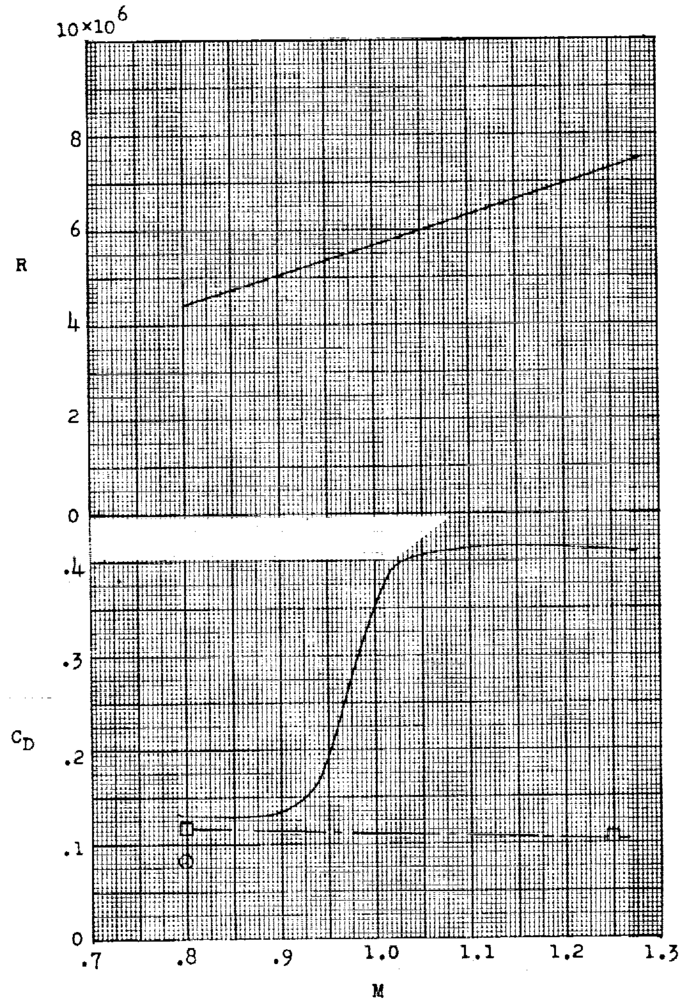

Figure 132.- Concluded.

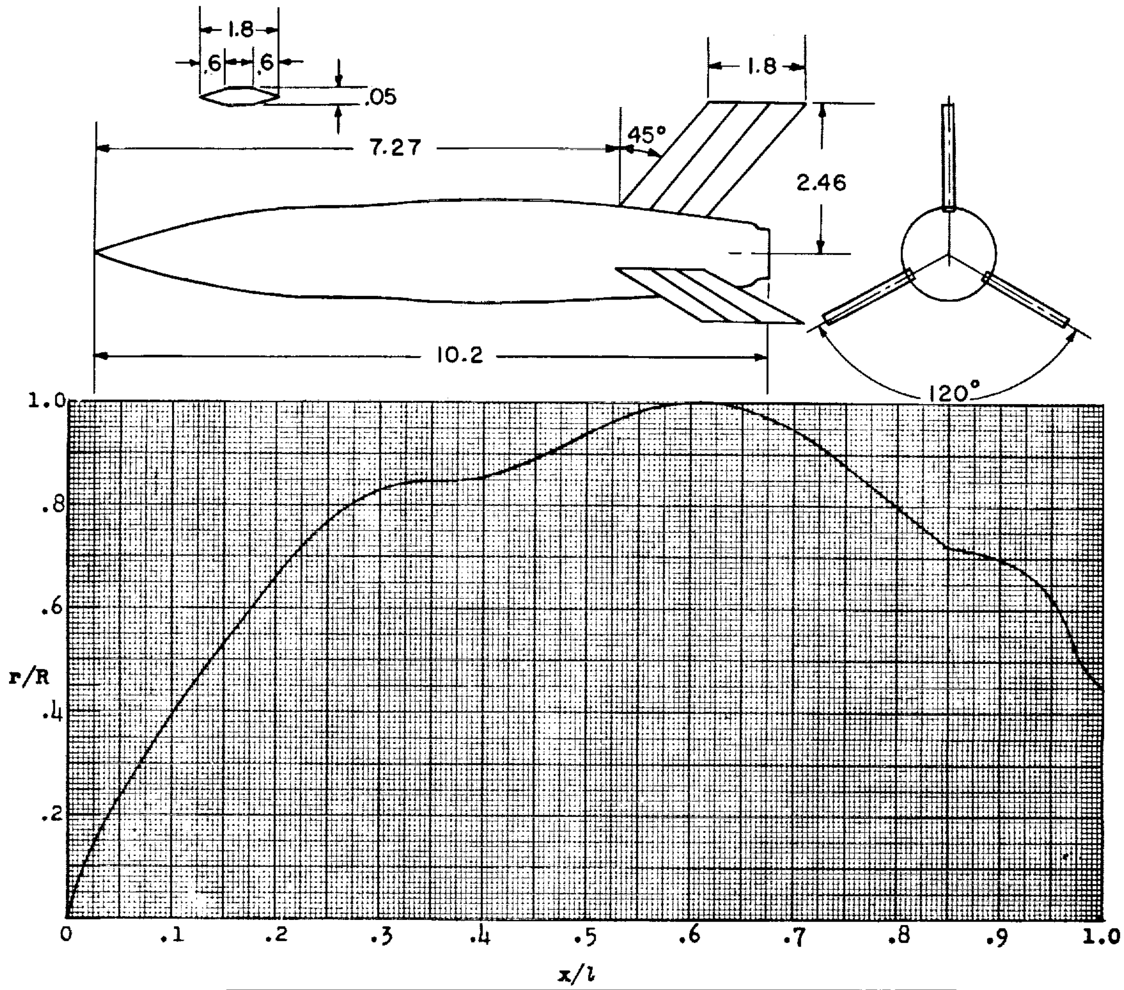

l/d_{Total}	6.95	l/d_{Nose}		S_b/A	19.90	A_b/A	.20
l/d_{N+A}	6.95	l/d_{Aft}		S_f/A	11.64	θ_b	8.8°

Designation: 127

Test: Helium Gun

Remarks: Assuming separation at step $\left(\frac{x}{l} \approx 0.9\right)$ and subsonic $C_p = -0.1$, the subsonic base drag would be $C_{D_{base}} = 0.1 \times 0.5 = 0.05$. This would indicate that subsonic fin flow was laminar.

Figure 133.

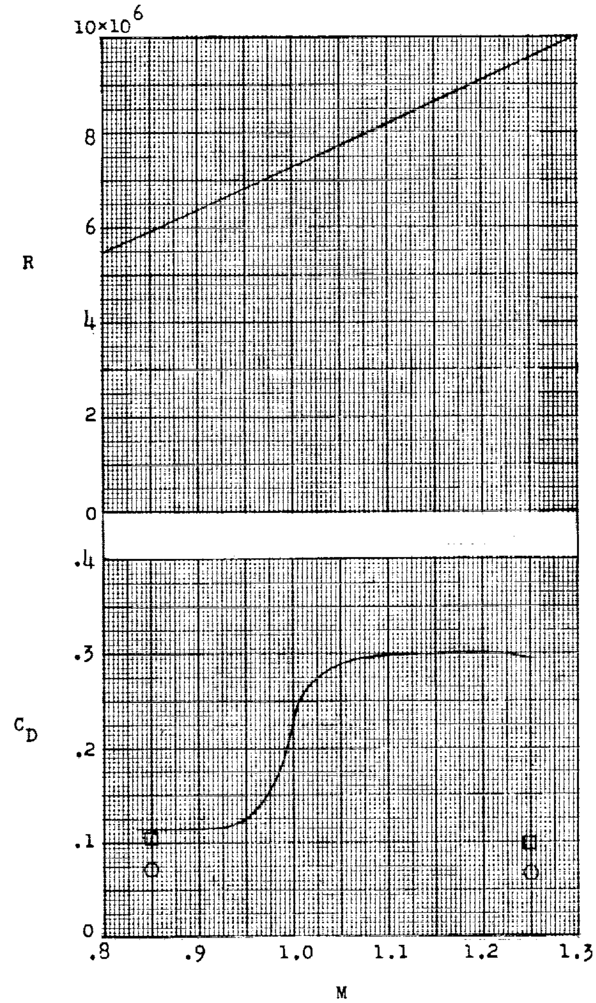

Figure 133.- Concluded.

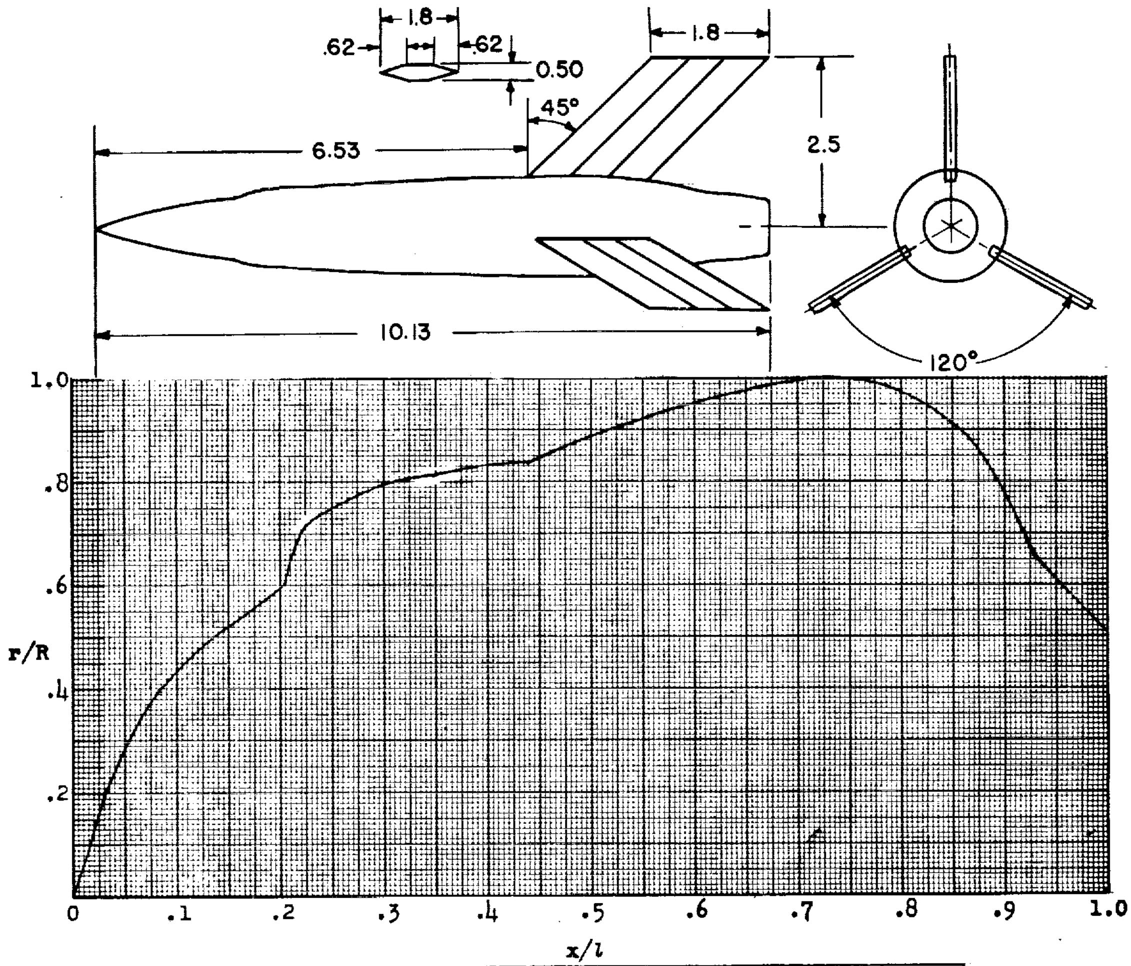

l/d_{Total}	6.98	l/d_{Nose}		S_b/A	21.16	A_b/A	.26
l/d_{N+A}	6.98	l/d_{Aft}		S_f/A	11.8	θ_b	10.3°

Designation: 128

Test: Helium Gun

Figure 134.

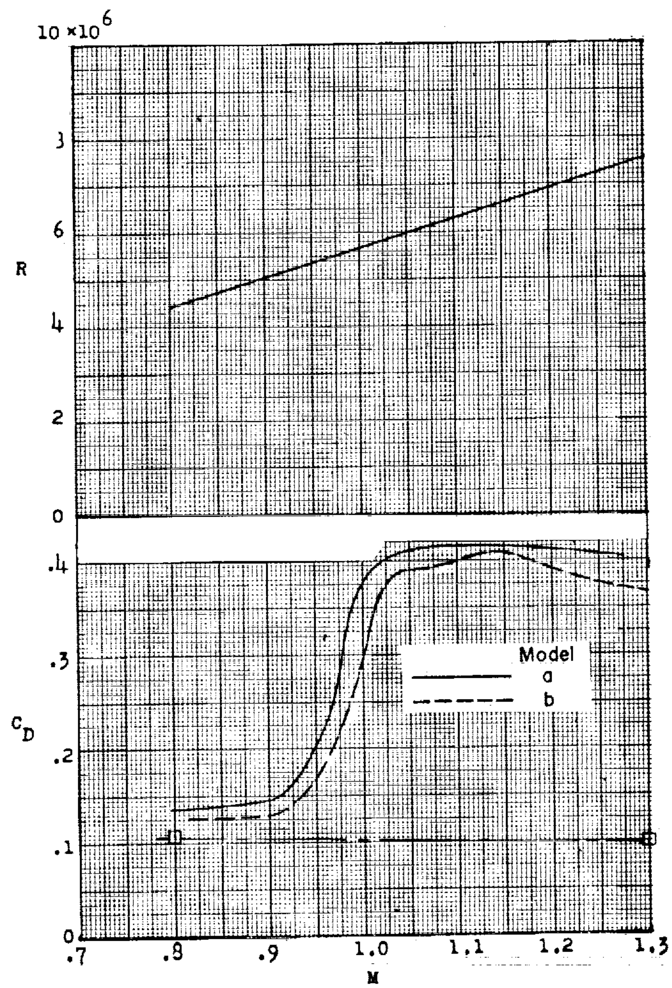

Figure 134.- Concluded.

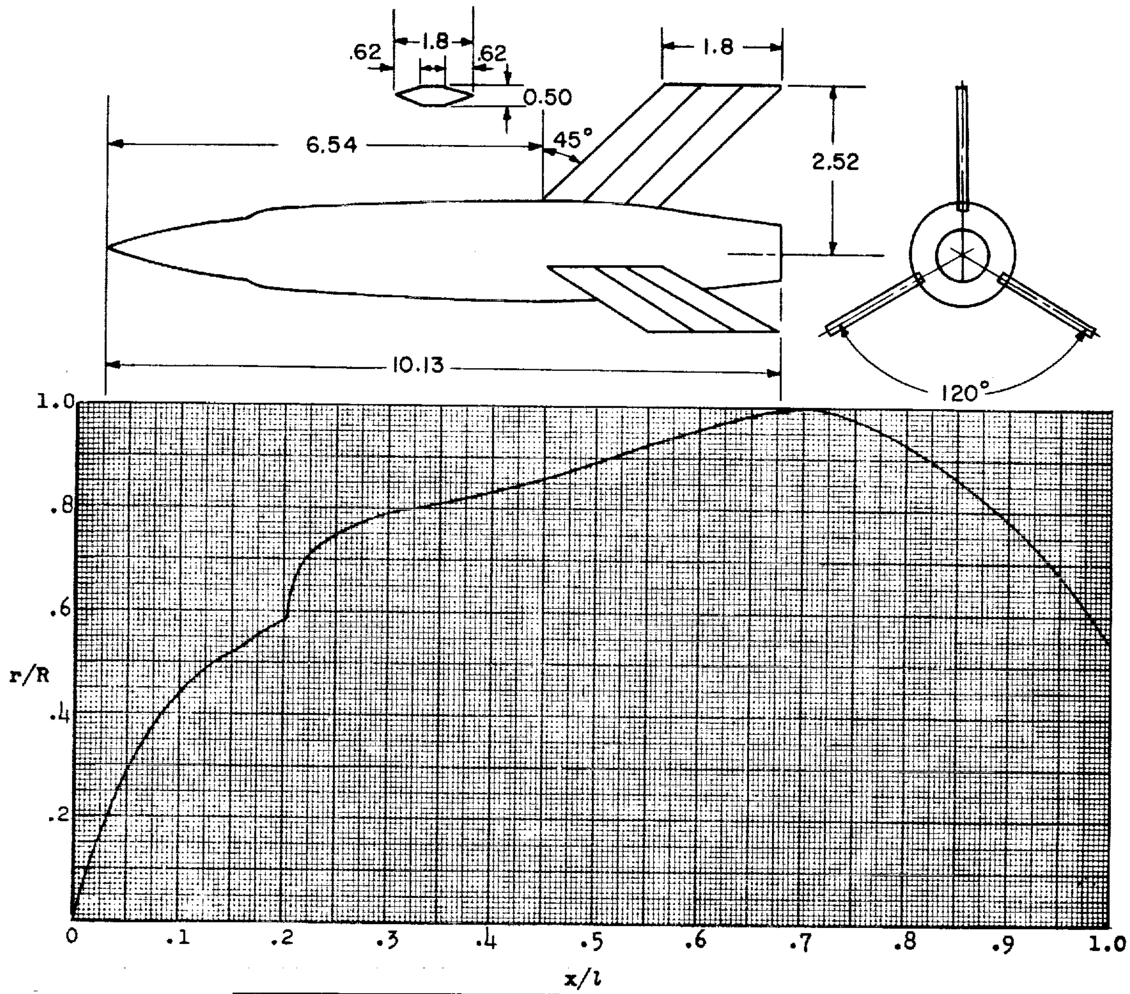

l/d_{Total}	6.98	l/d_{Nose}		S_b/A	21.27	A_b/A	.29
l/d_{N+A}	6.98	l/d_{Aft}		S_f/A	11.8	θ_b	9.7°

Designation: 129

Test: Helium Gun

Figure 135.

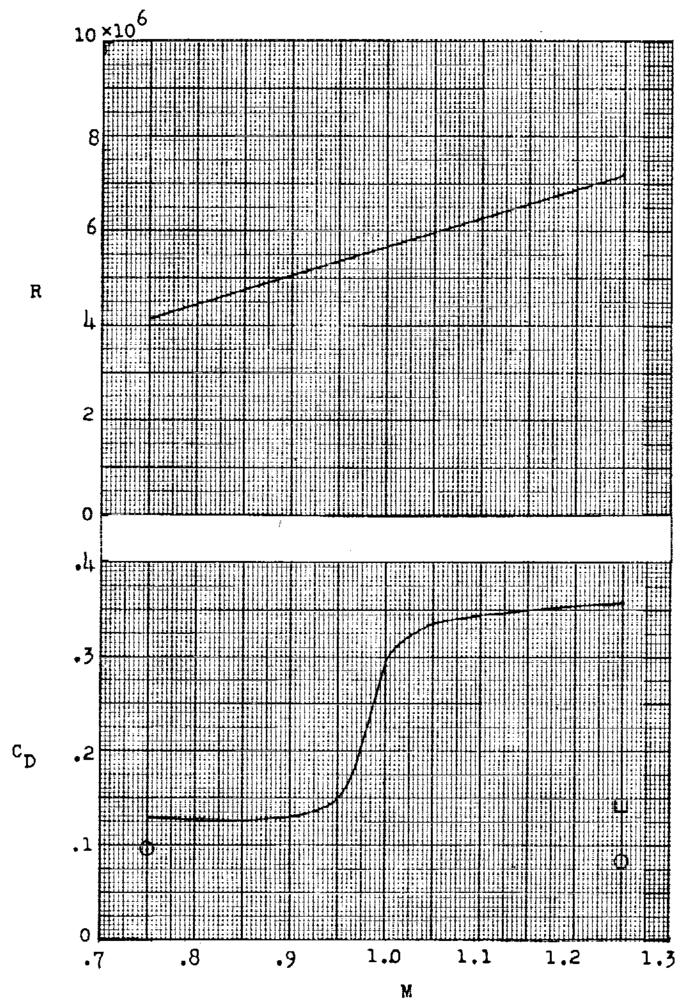

Figure 135.- Concluded.

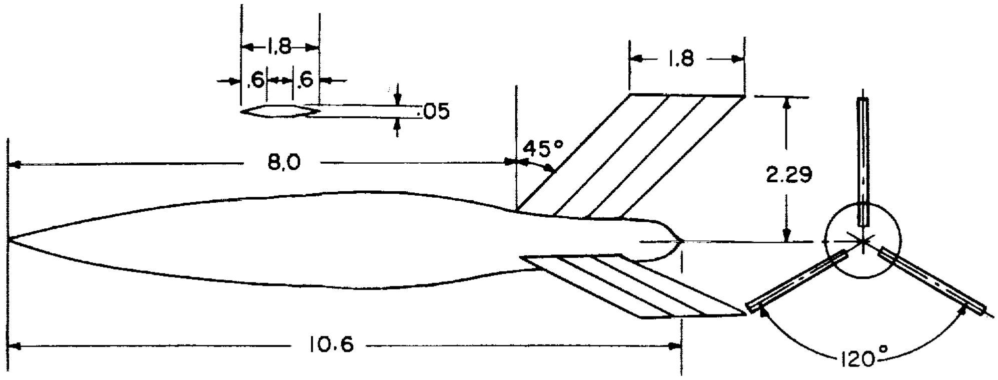

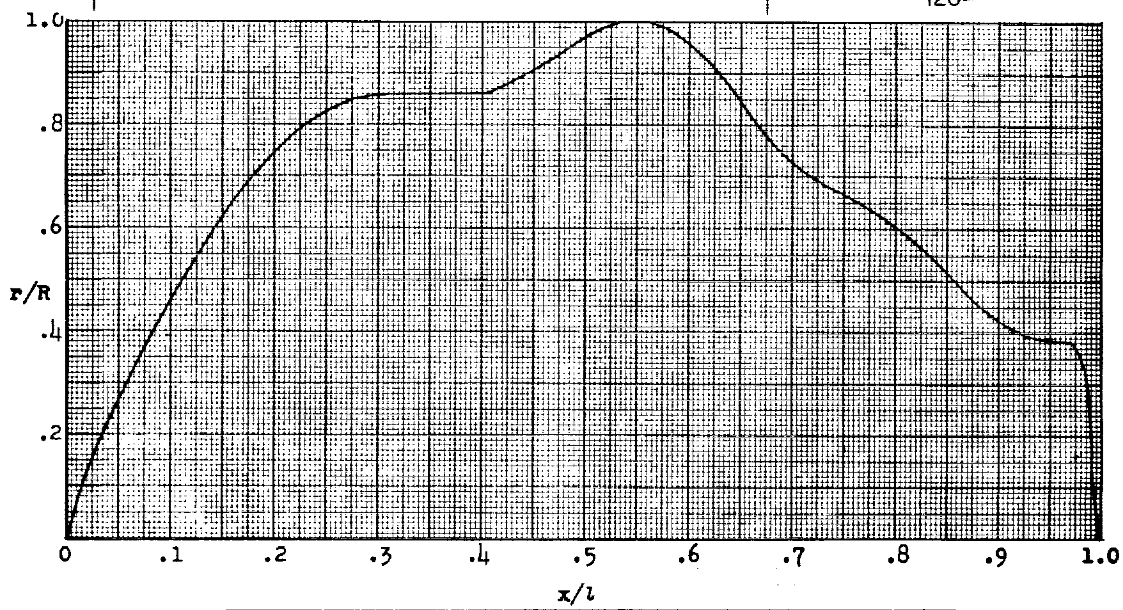

l/d_{Total}	7.08	l/d_{Nose}	—	S_b/A	19.4	A_b/A	0.0
l/d_{N+A}	7.08	l/d_{Aft}		S_f/A	13.00	θ_b	90°

Designation: 130

Test: Helium Gun

Remarks: Subsonic flow probably separated about $\frac{x}{l} = 0.97$.

Figure 136.

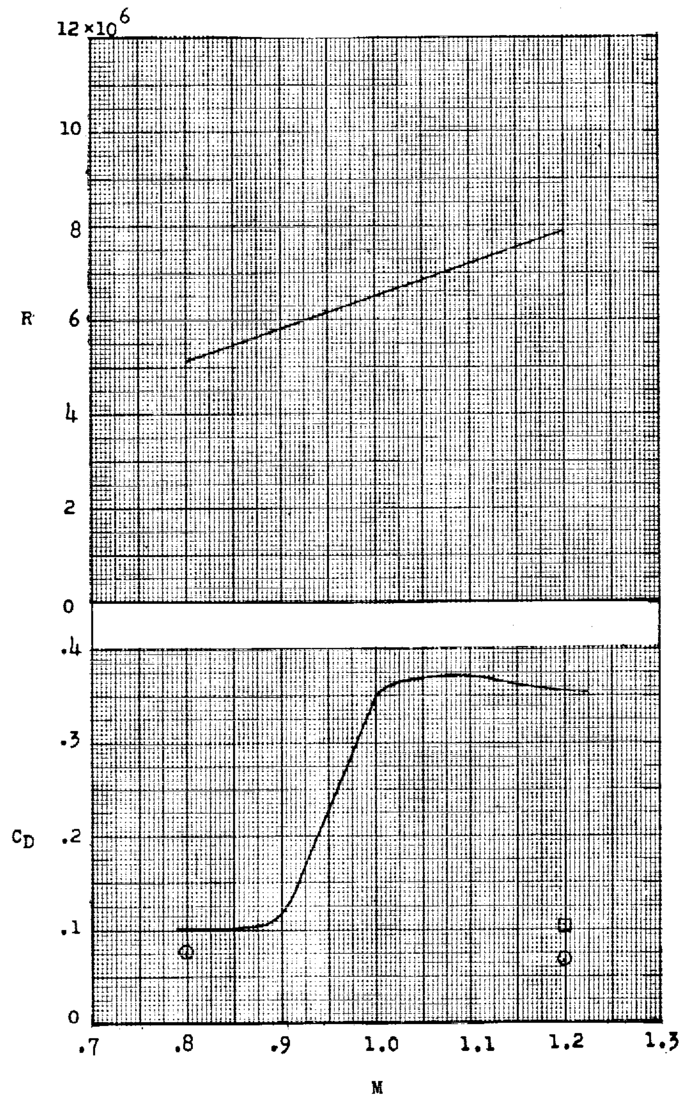

Figure 136.- Concluded.

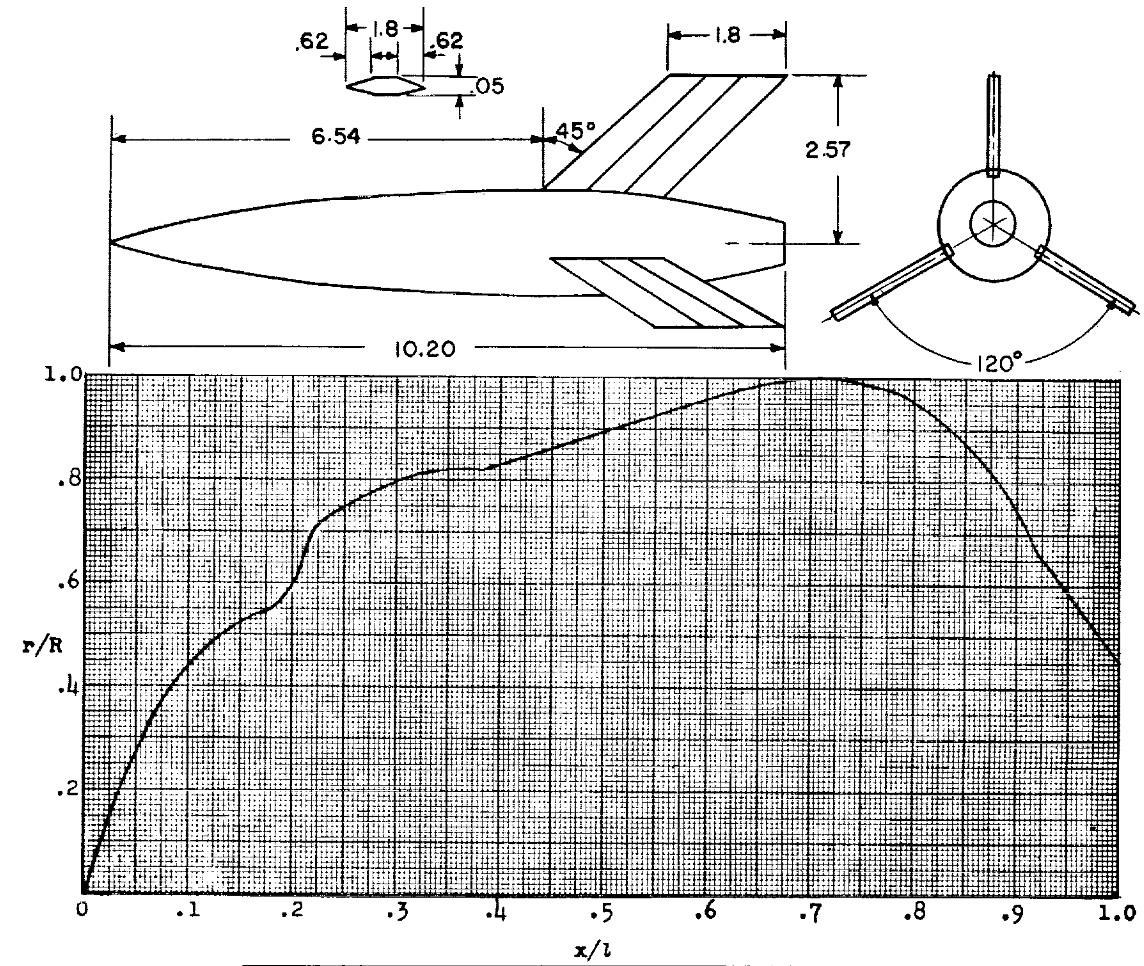

l/d_{Total}	7.08	l/d_{Nose}		S_b/A	21.35	A_b/A	.20
l/d_{N+A}	7.08	l/d_{Aft}		S_f/A	11.86	θ_b	11.3°

Designation: 131

Test: Helium Gun

Figure 137.

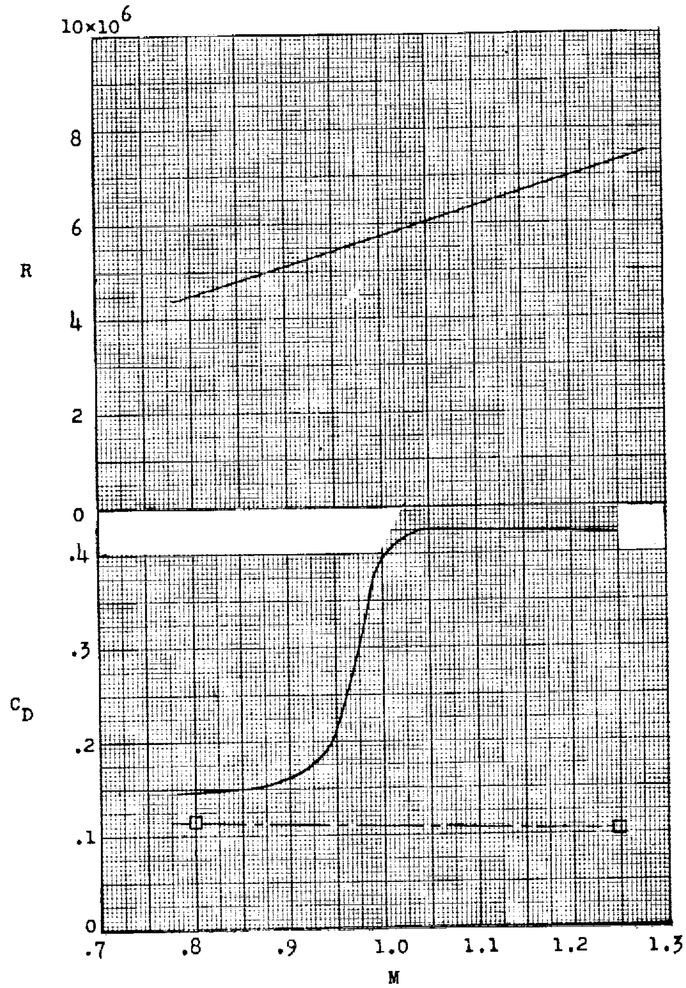

Figure 137.- Concluded.

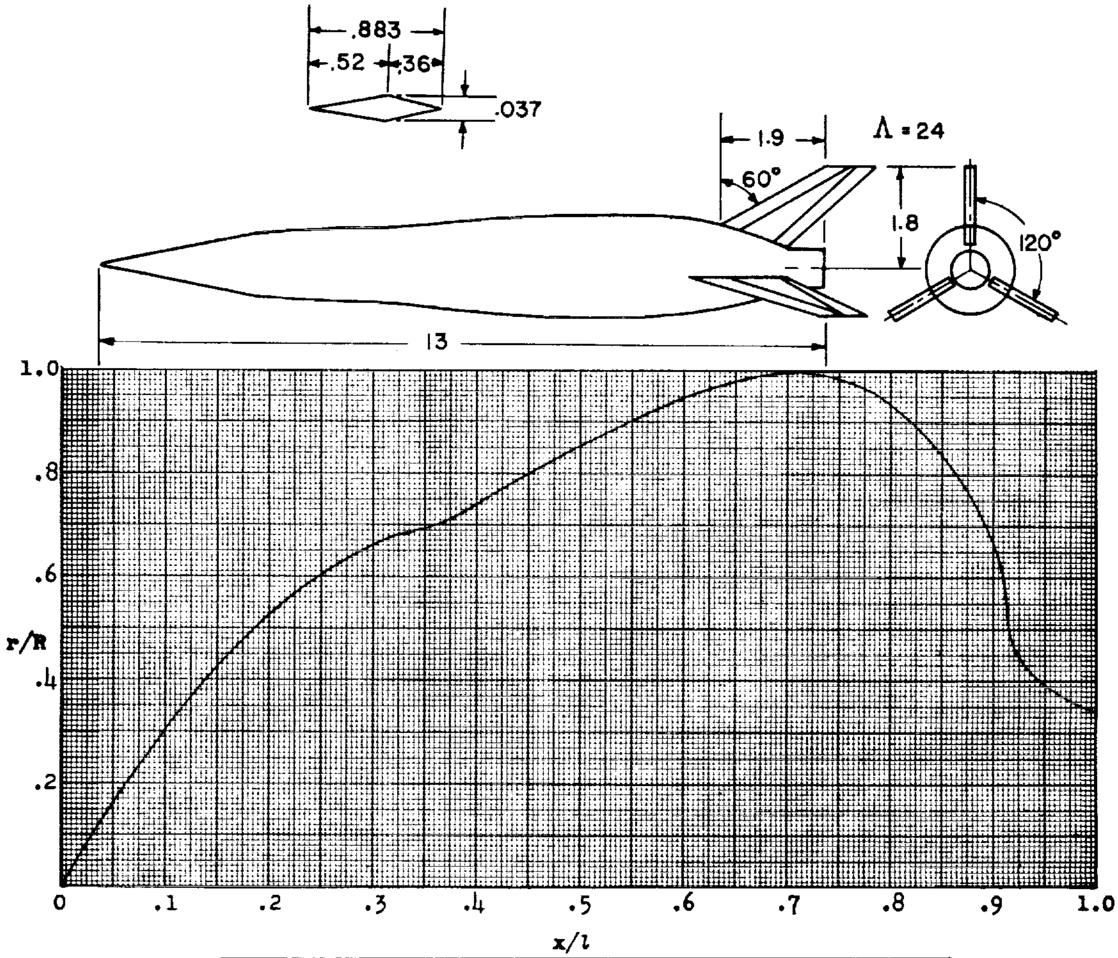

l/d_{Total}	7.08	l/d_{Nose}		S_b/A	19.6	A_b/A	.12
l/d_{N+A}	7.08	l/d_{Aft}		S_f/A	3.56	θ_b	6.5°

Designation: 132

Test: Helium Gun

Figure 138.

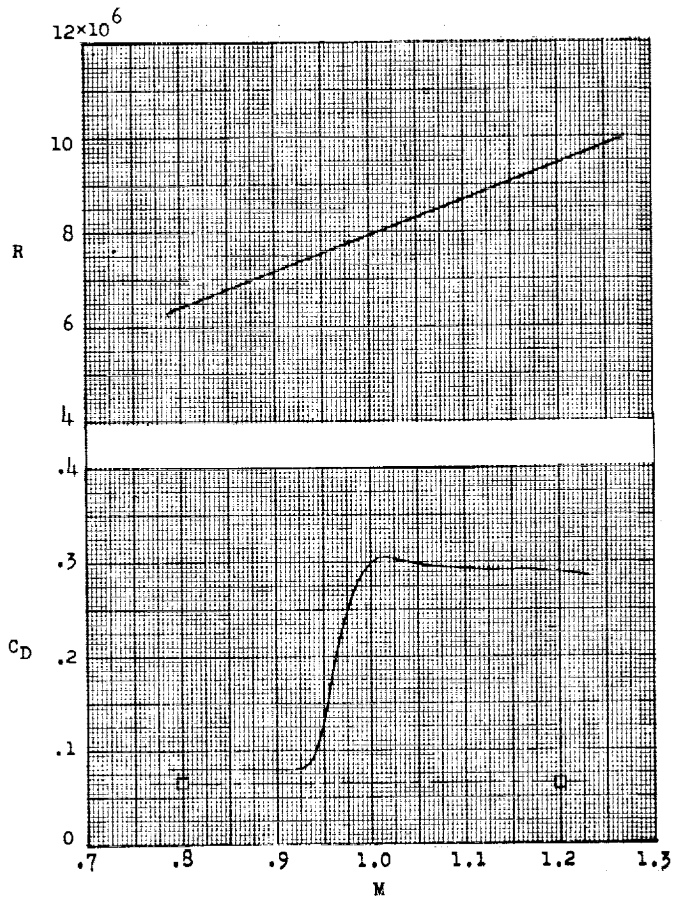

Figure 138.- Concluded.

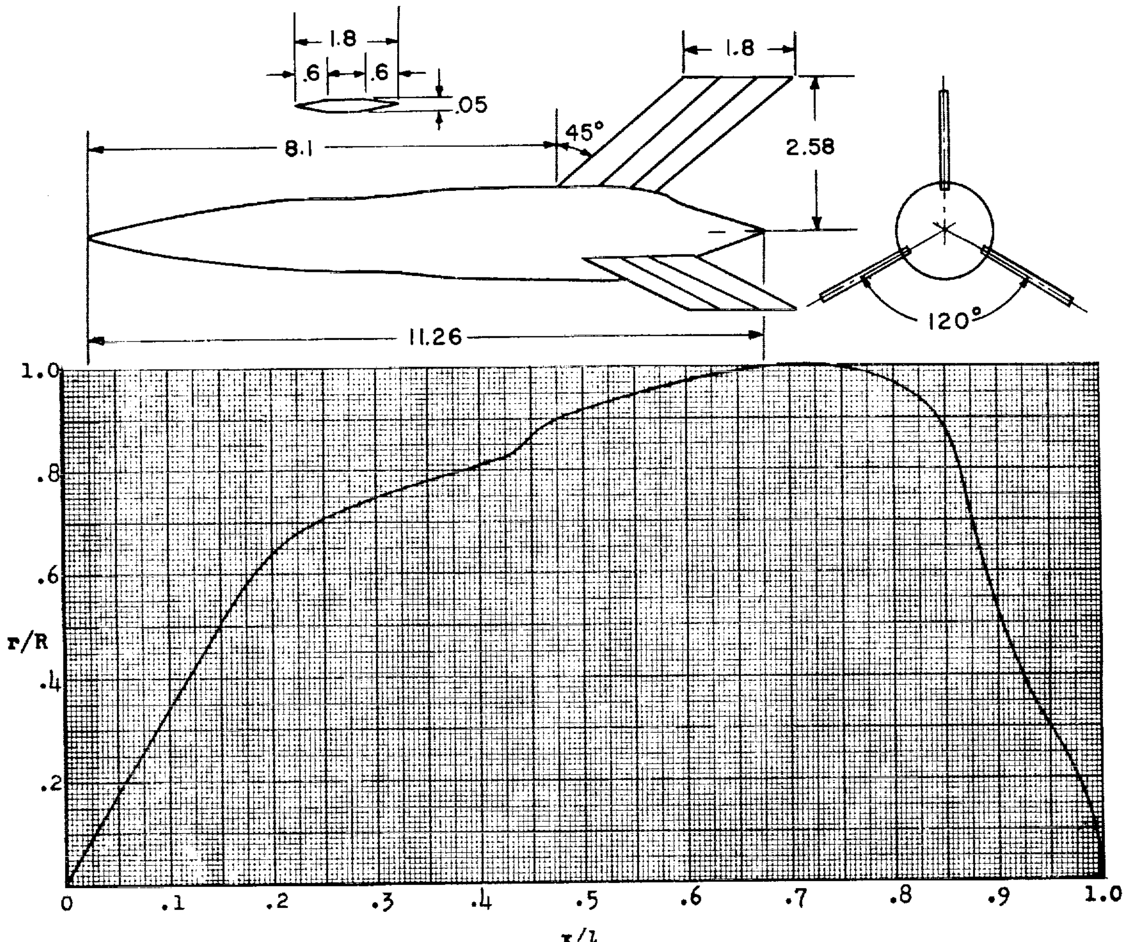

l/d_{Total}	7.14	l/d_{Nose}		S_b/A	20.26	A_b/A	0.0
l/d_{N+A}	7.14	l/d_{Aft}		S_f/A	9.90	θ_b	90°

Designation: 133

Test: Helium Gun

Remarks: Flow is probably separated at subsonic speeds.

Figure 139.

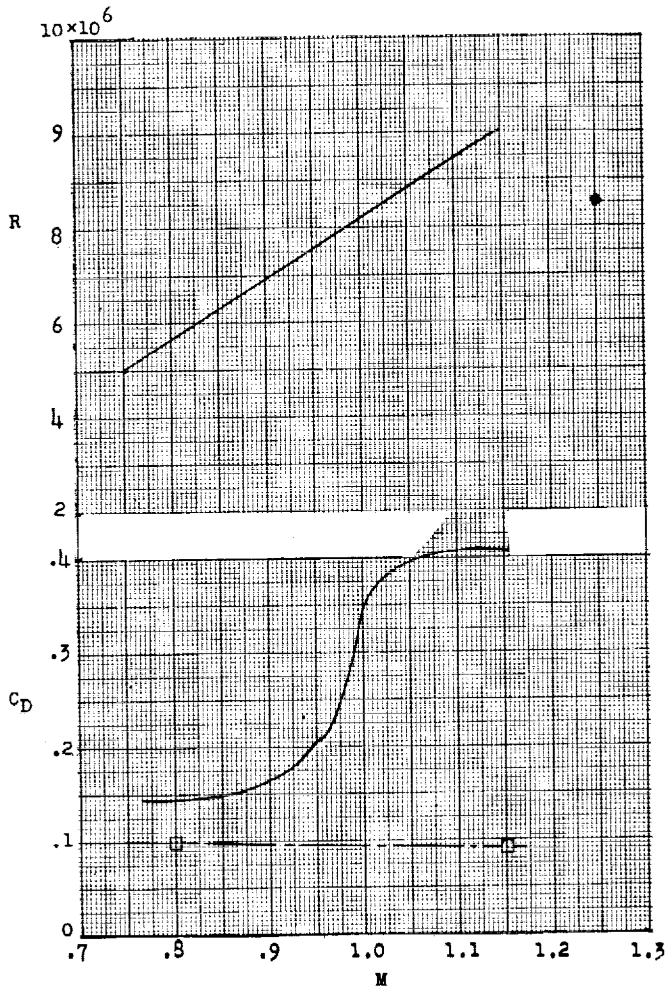

Figure 139.- Concluded.

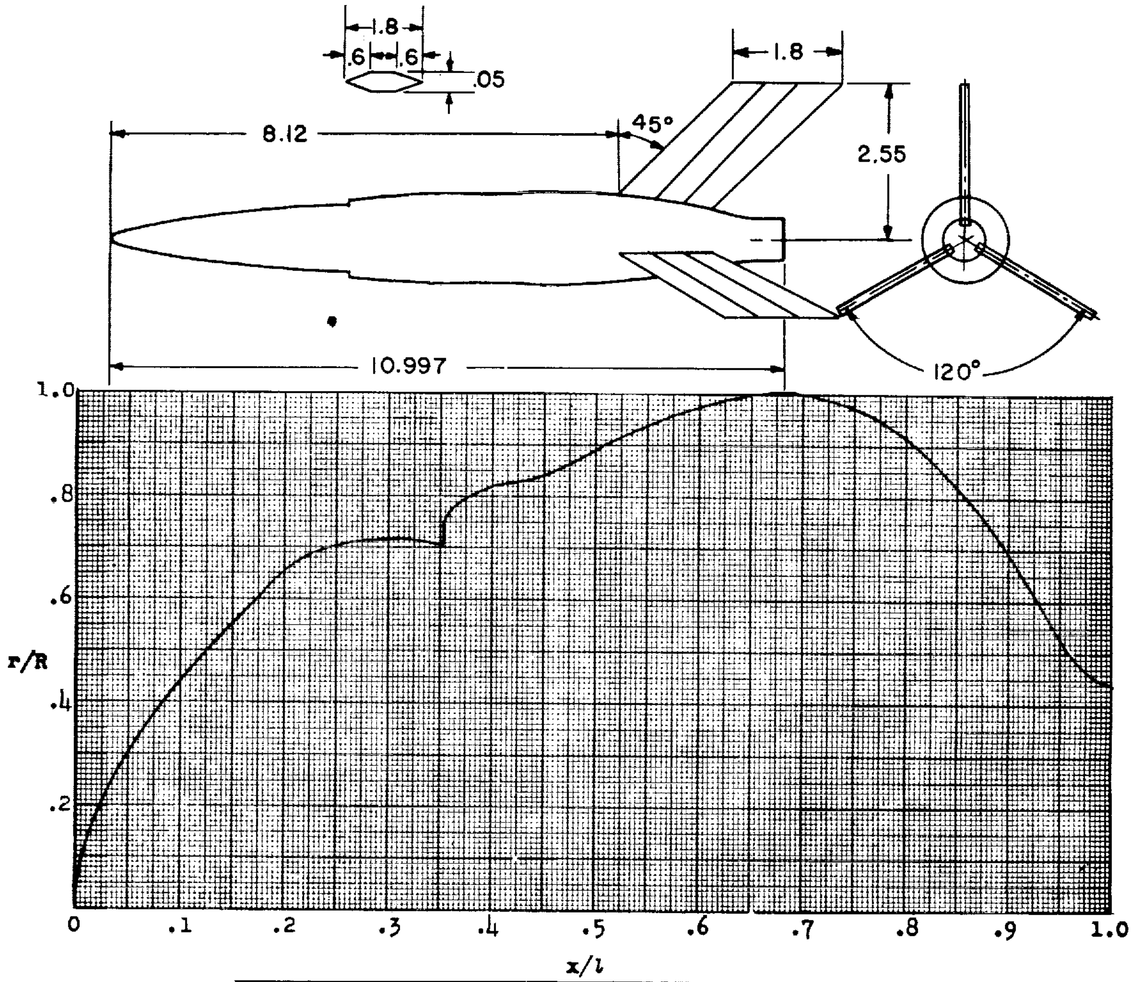

l/d_{Total}	7.33	l/d_{Nose}		S_b/A	21.70	A_b/A	.19
l/d_{N+A}	7.33	l/d_{Aft}		S_f/A	11.70	θ_b	0°

Designation: 134

Test: **Helium Gun**

Remarks: Probable that subsonic flow was laminar. (See note for model 125 (fig. 131).)

Figure 140.

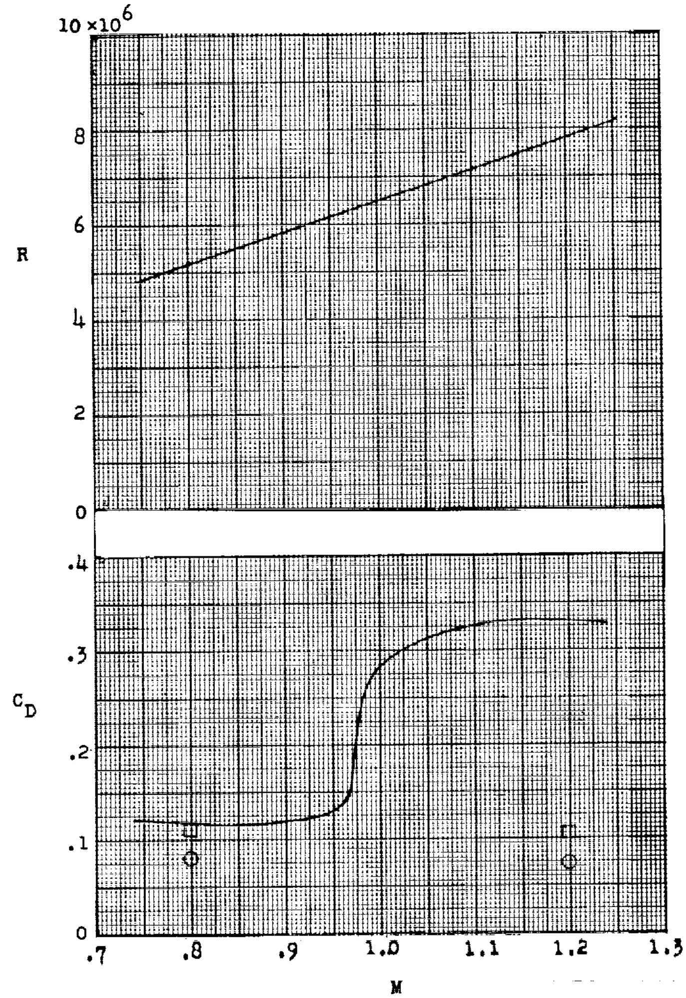

Figure 140.- Concluded.

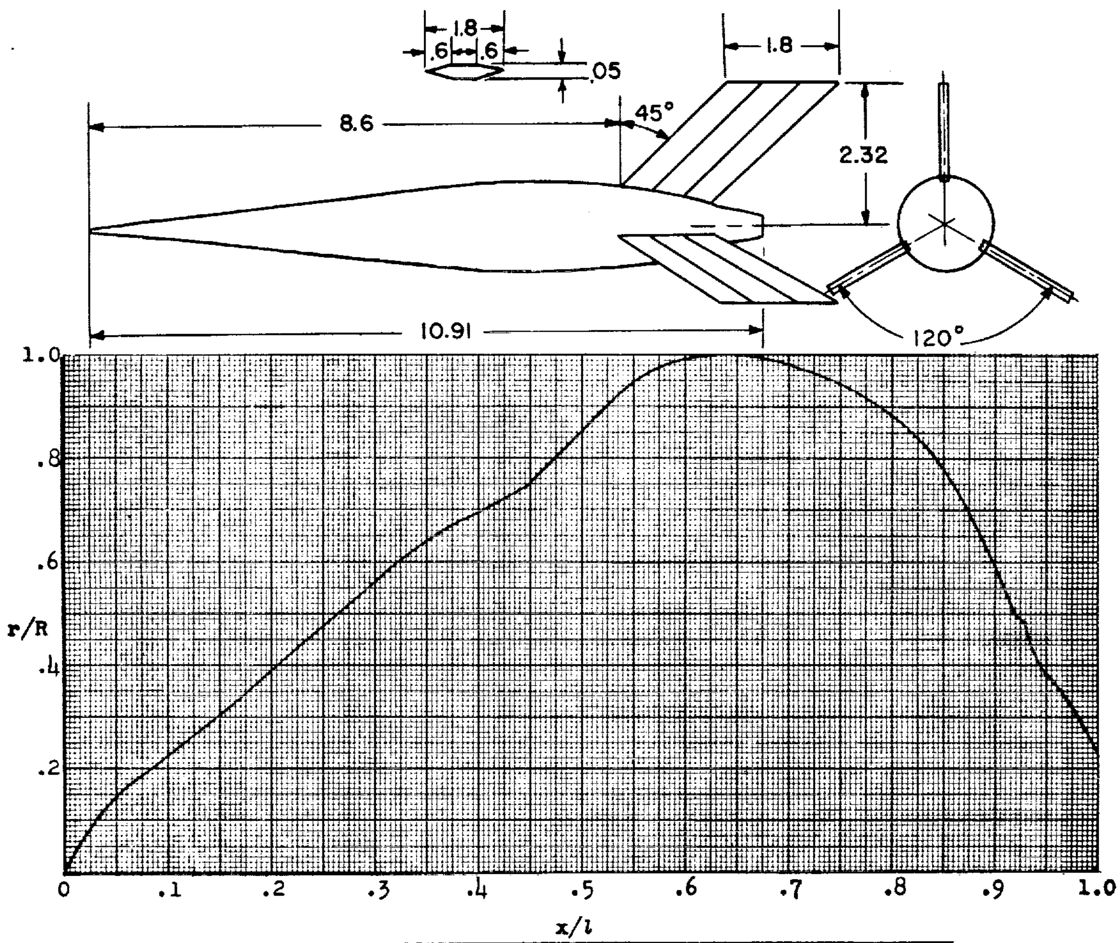

l/d_{Total}	7.42	l/d_{Nose}		S_b/A	19.00	A_b/A	.05
l/d_{N+A}	7.42	l/d_{Aft}		S_f/A	11.50	θ_b	15.4°

Designation: 135

Test: Helium Gun

Remarks: Subsonic drag looks too high.

Figure 141.

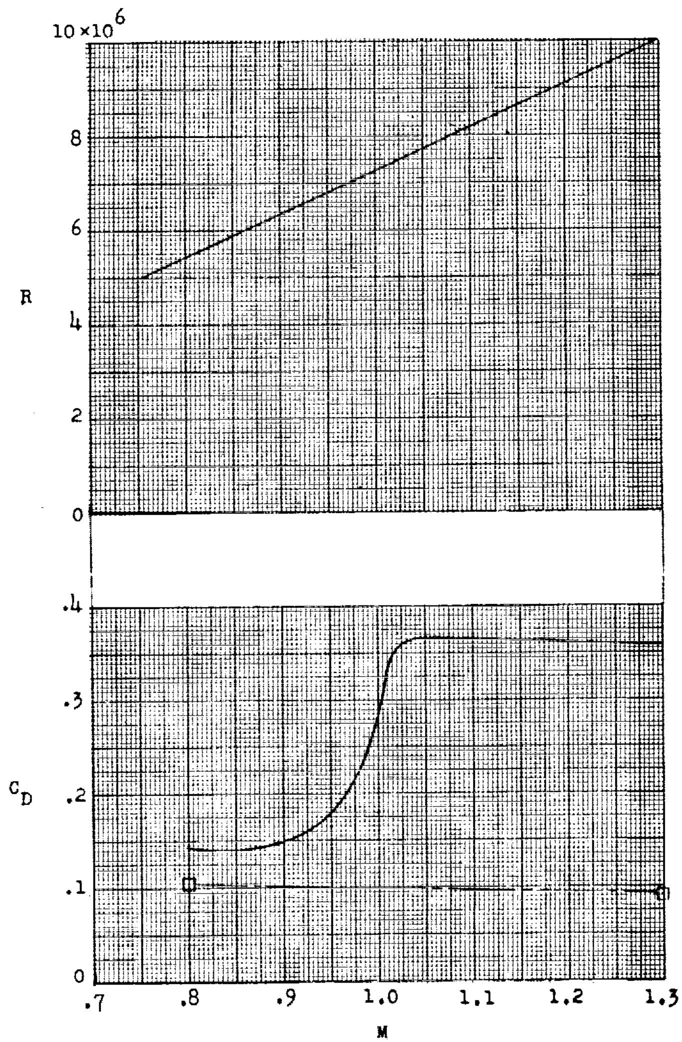

Figure 141.- Concluded.

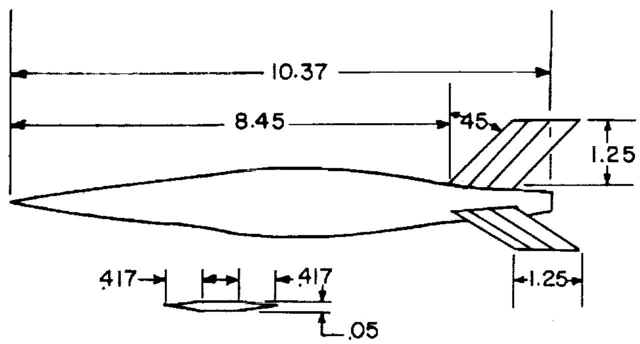

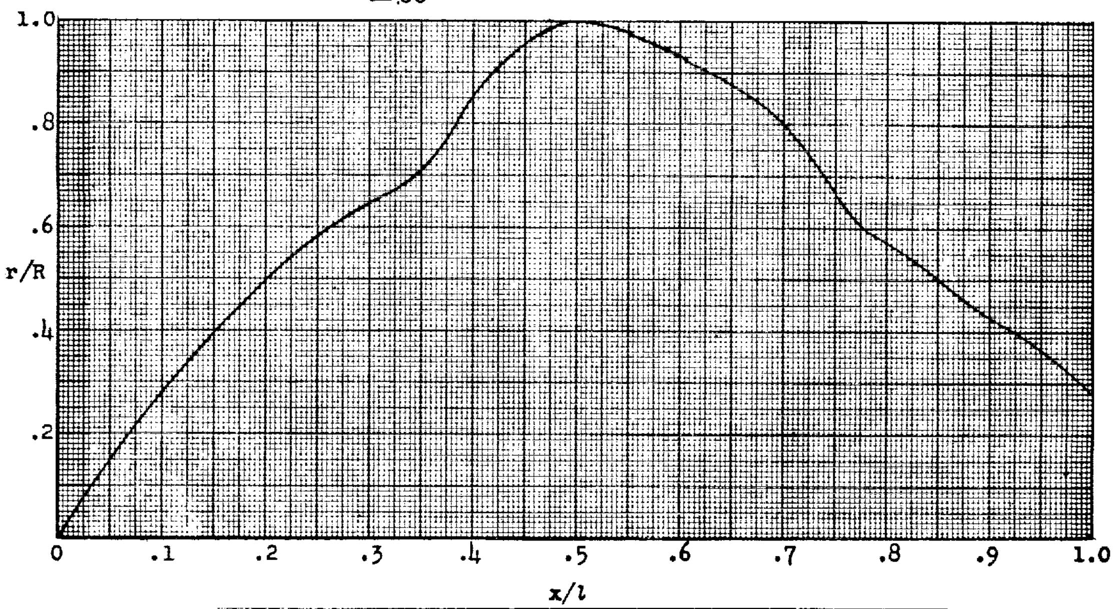

l/d_{Total}	7.55	l/d_{Nose}		S_b/A	18.7	A_b/A	.08
l/d_{N+A}	7.55	l/d_{Aft}		S_f/A	6.63	θ_b	5.0°

Designation: 136

Test: **Helium Gun**

Figure 142.

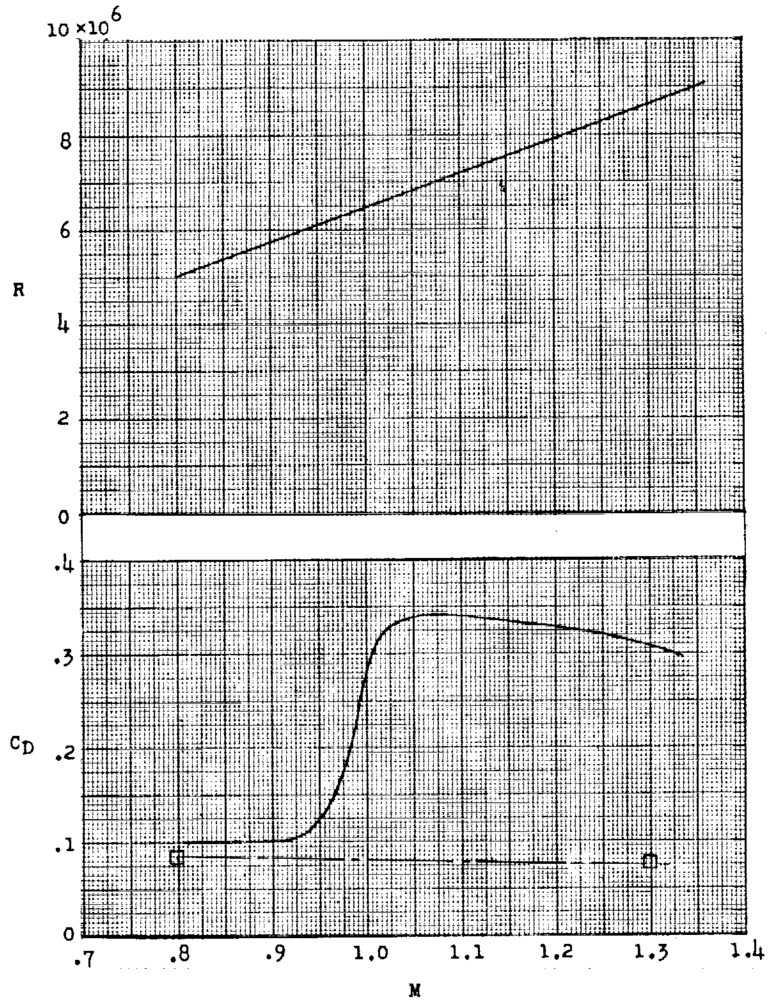

Figure 142.- Concluded.

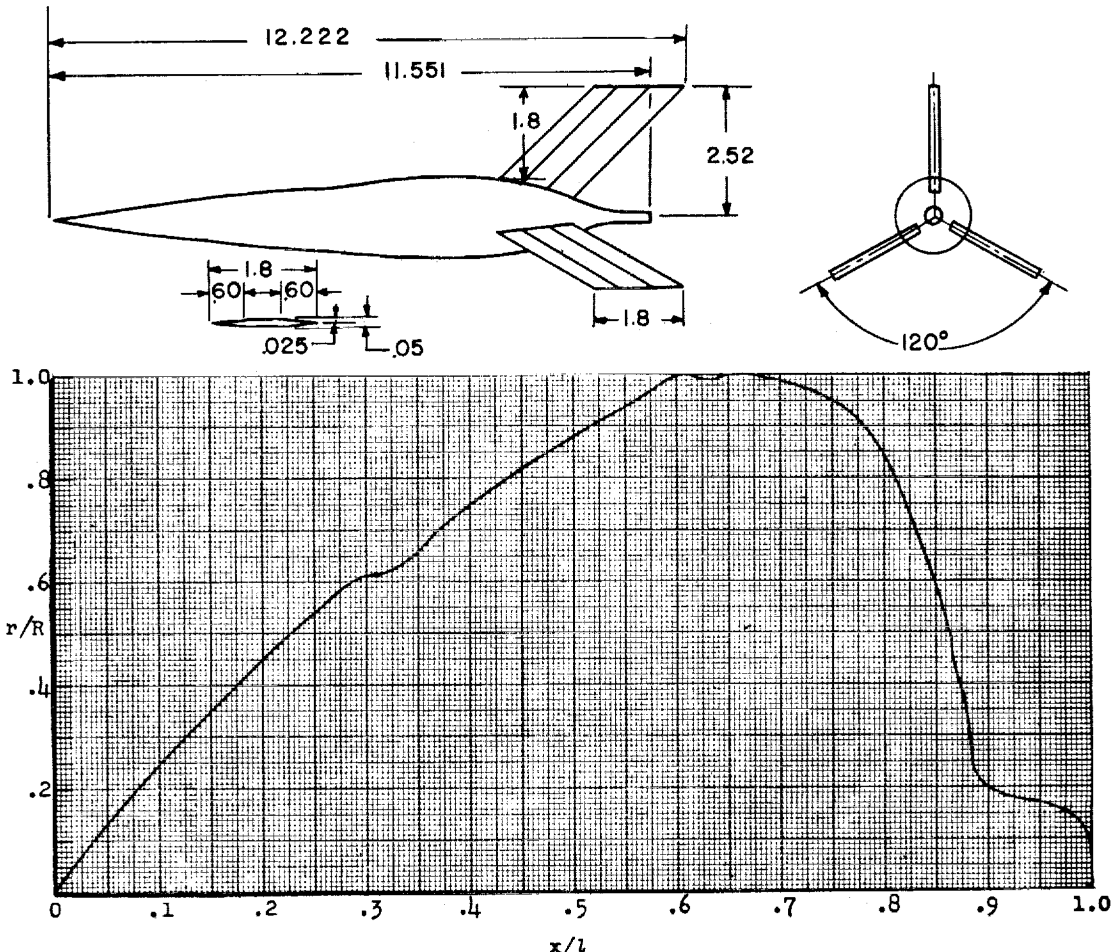

l/d_{Total}	7.7	l/d_{Nose}		S_b/A	18.8	A_b/A	.00568
l/d_{N+A}	7.7	l/d_{Aft}		S_f/A	11.95	θ_b	90°

Designation: 137

Test: **Helium Gun**

Figure 143.

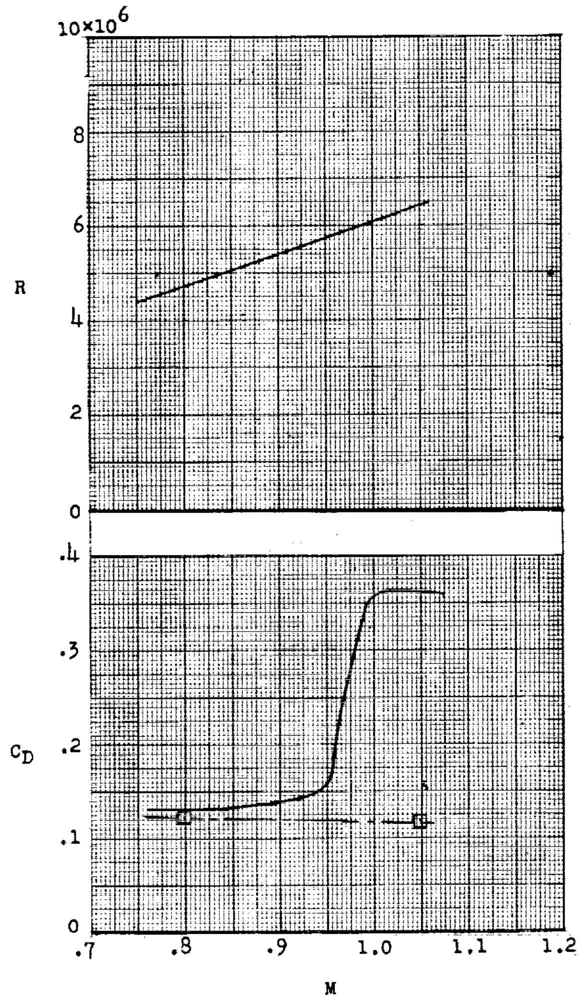

Figure 143.- Concluded.

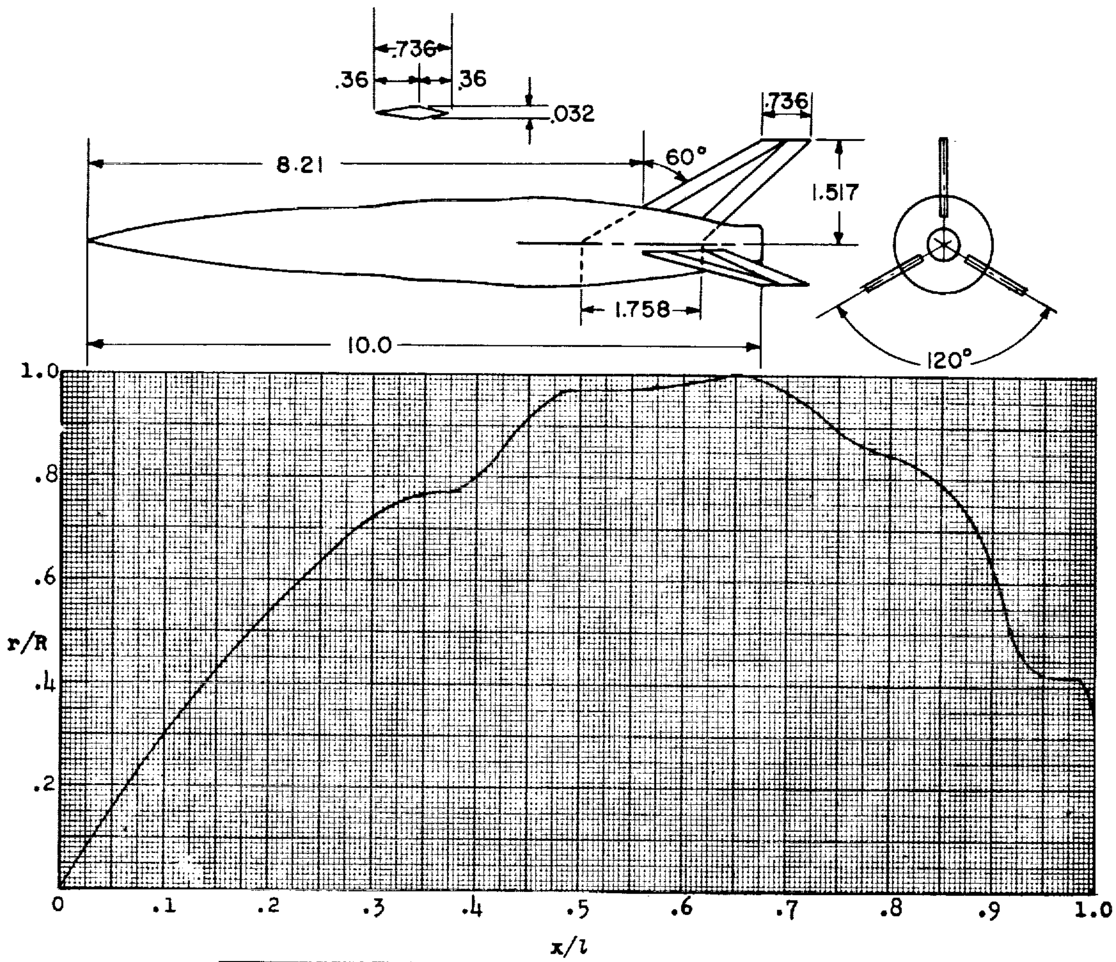

l/d_{Total}	7.75	l/d_{Nose}		S_b/A	20.90	A_b/A	.20
l/d_{N+A}	7.75	l/d_{Aft}		S_f/A	5.78	θ_b	26.5°

Designation: 138

Test: Helium Gun

Remarks: Remarks for configuration 125 (fig. 131) may apply to these models also.

Figure 144.

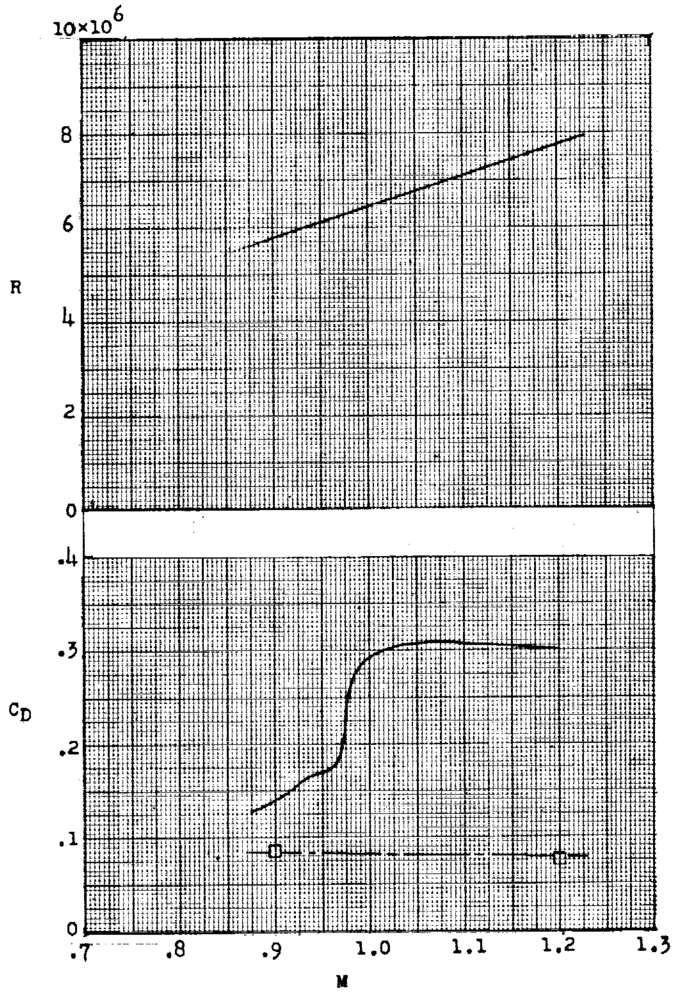

Figure 144.- Concluded.

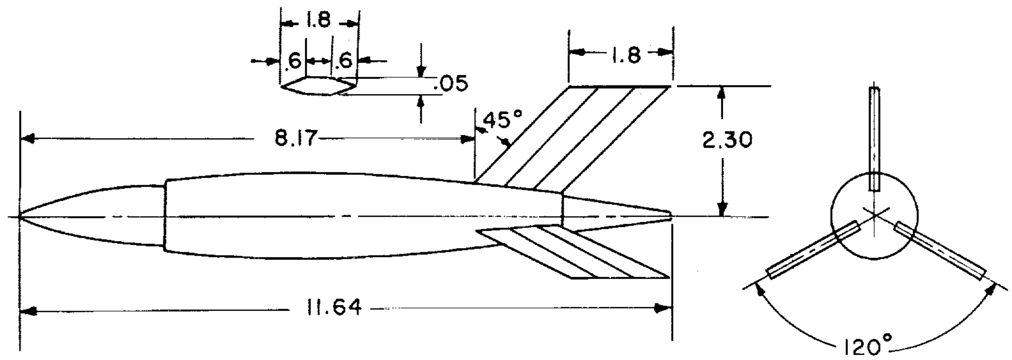

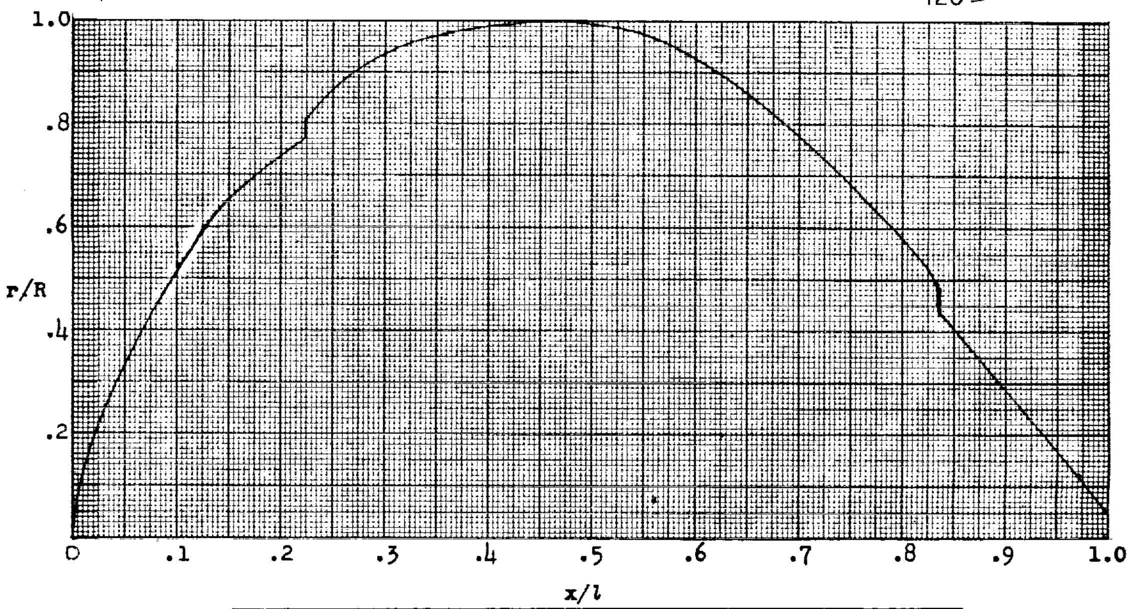

l/d_{Total}	7.76	l/d_{Nose}		S_b/A	21.54	A_b/A	0.0
l/d_{N+A}	7.76	l/d_{Aft}		S_f/A	11.0	θ_b	9.4°

Designation: 139

Test: Helium Gun

Remarks: Remarks for configuration 125 (fig. 131) may apply to these models also.

Figure 145.

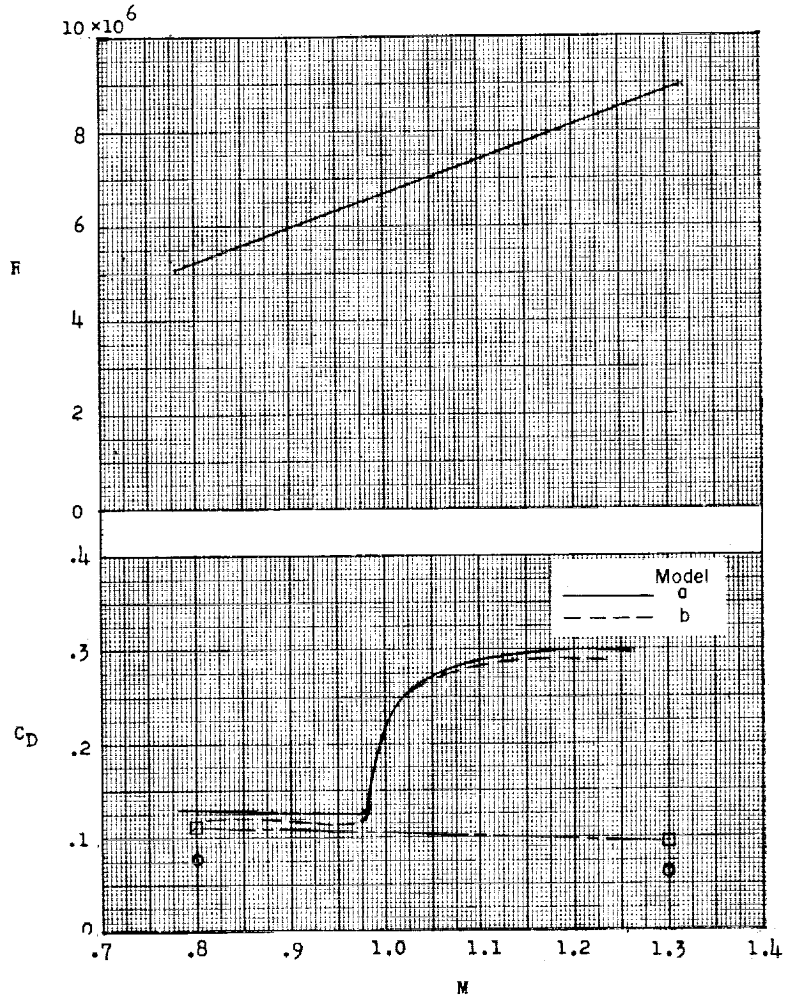

Figure 145.- Concluded.

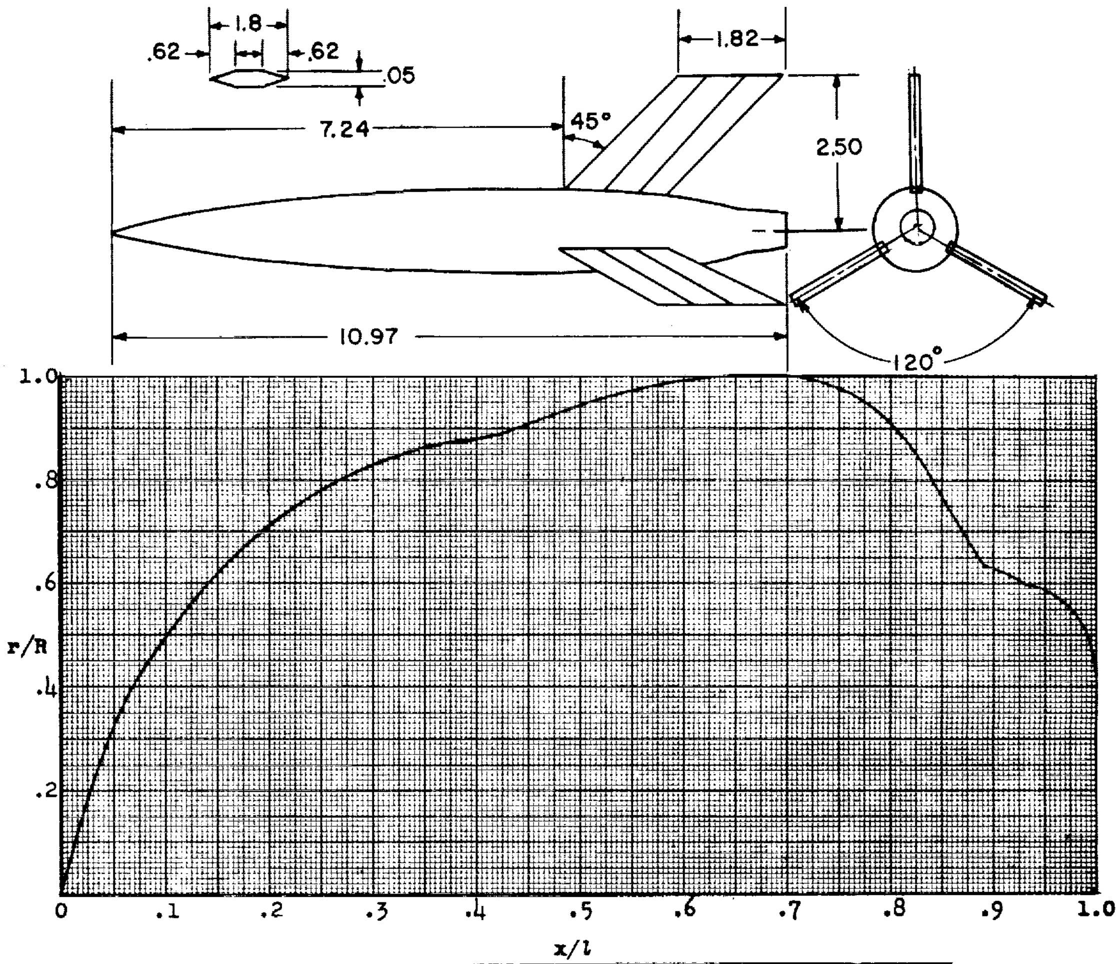

l/d_{Total}	8.00	l/d_{Nose}		S_b/A	24.80	A_b/A	.18
l/d_{N+A}	8.00	l/d_{Aft}		S_f/A	13.2	θ_b	33.2°

Designation: 140

Test: Helium Gun

Figure 146.

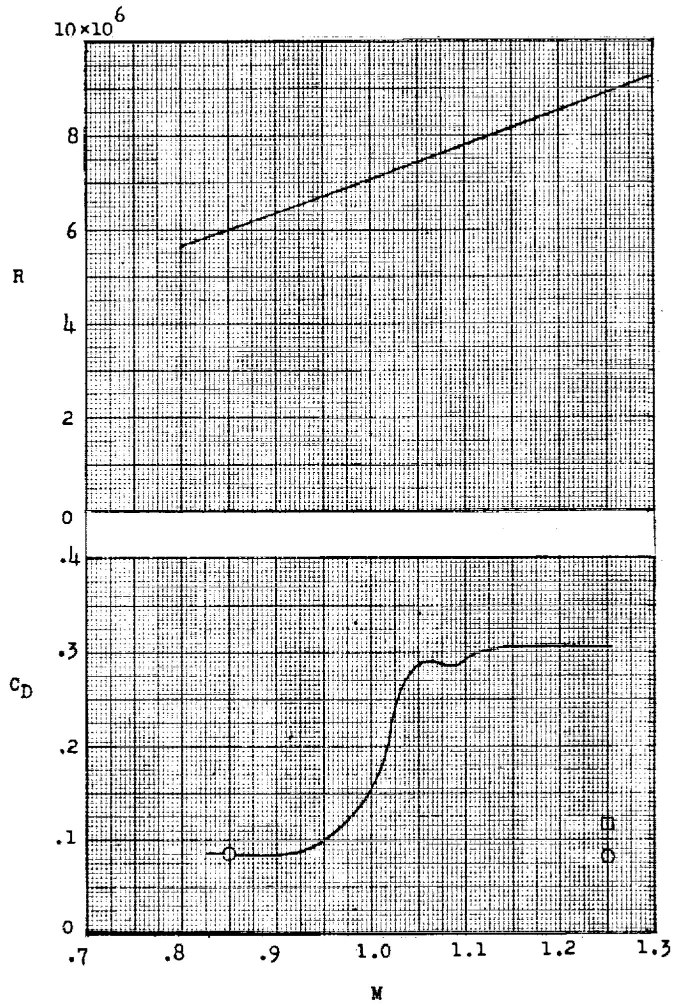

Figure 146.- Concluded.

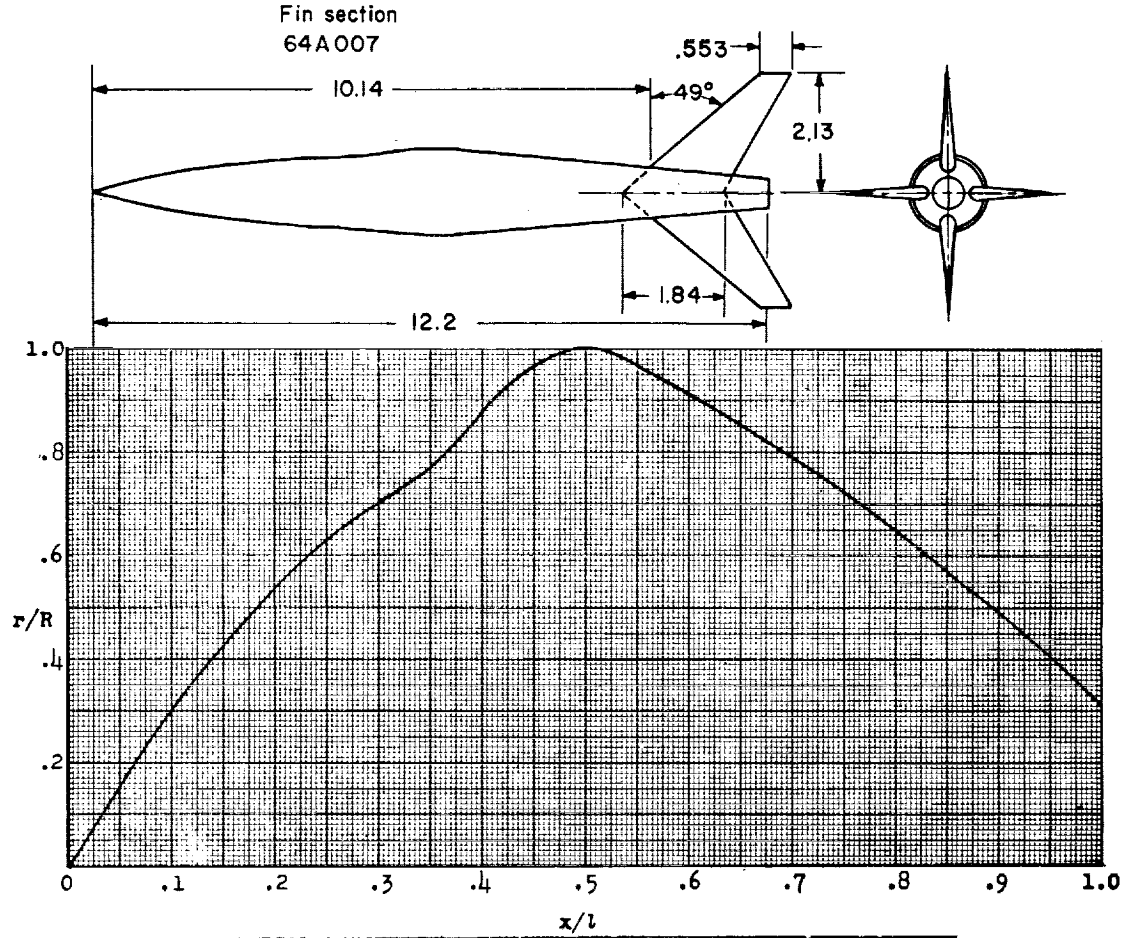

l/d_{Total}	8.03	l/d_{Nose}		S_b/A	20.70	A_b/A	.09
l/d_{N+A}	8.03	l/d_{Aft}		S_f/A	9.0	θ_b	7.9°

Designation: 141

Test: Helium Gun

Figure 147.

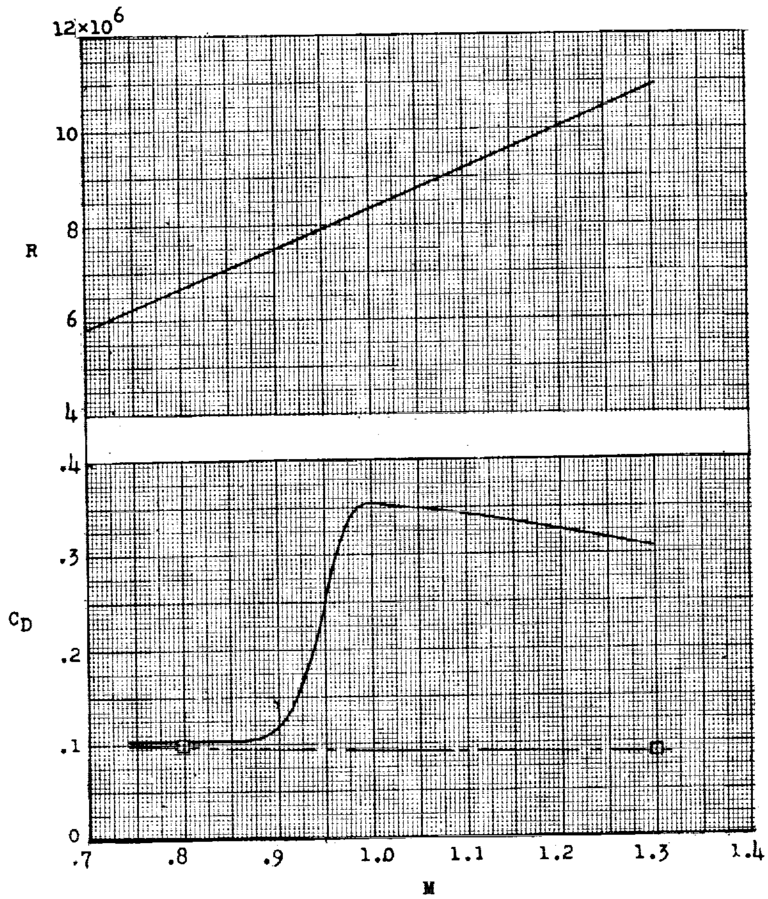

Figure 147.- Concluded.

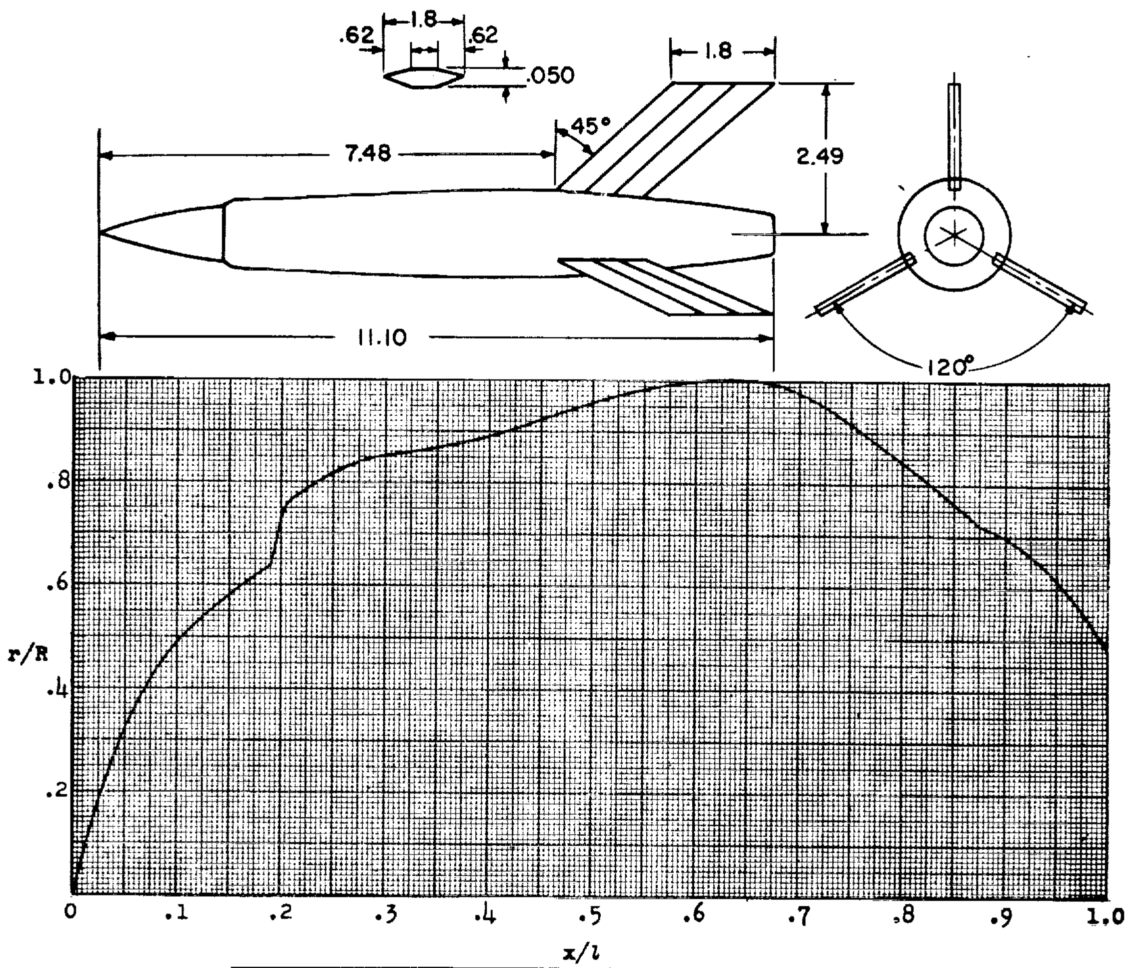

l/d_{Total}	8.04	l/d_{Nose}		S_b/A	24.04	A_b/A	.23
l/d_{N+A}	8.04	l/d_{Aft}		S_f/A	13.00	θ_b	12.6°

Designation: 142

Test: Helium Gun

Figure 148.

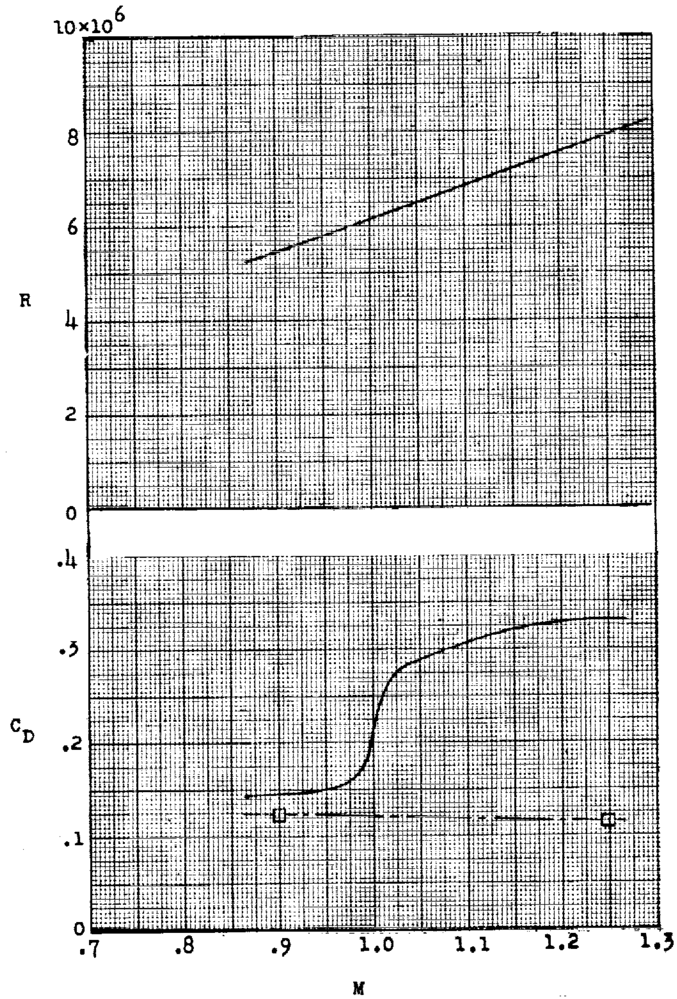

Figure 148.- Concluded.

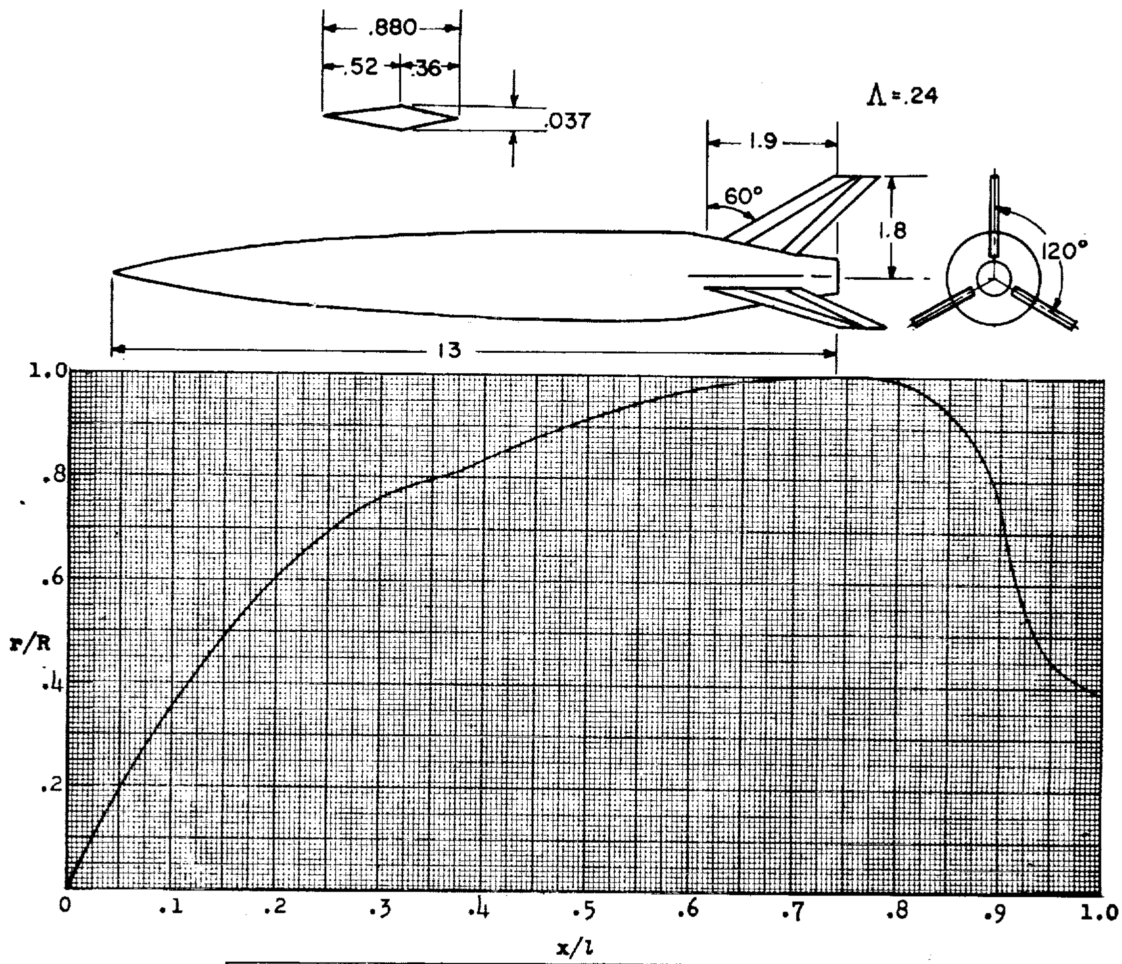

l/d_{Total}	8.07	l/d_{Nose}		S_b/A	23.75	A_b/A	.15
l/d_{N+A}	8.07	l/d_{Aft}		S_f/A	4.12	θ_b	4.3°

Designation: 143

Test: Helium Gun

Figure 149.

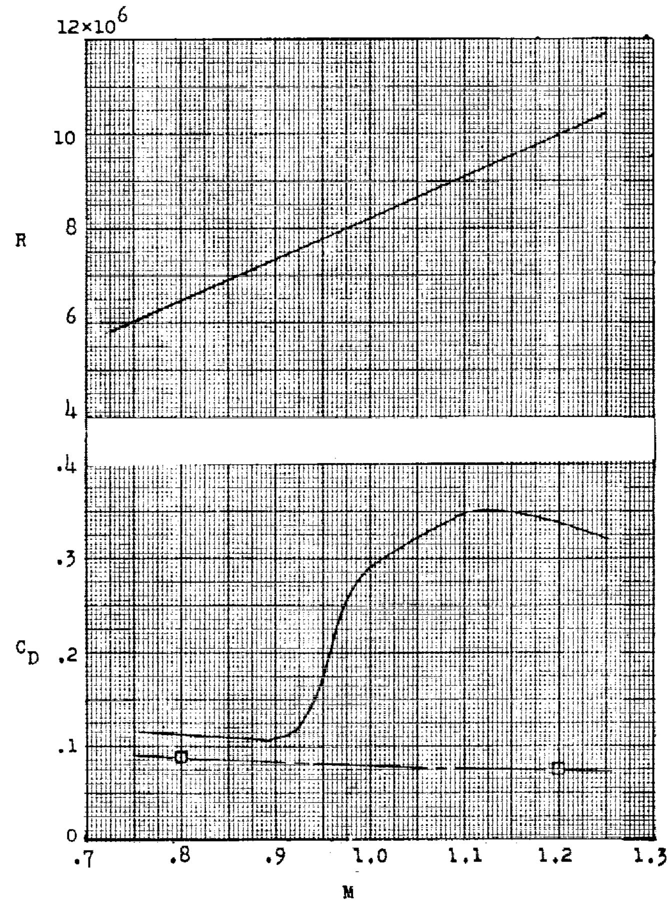

Figure 149.- Concluded.

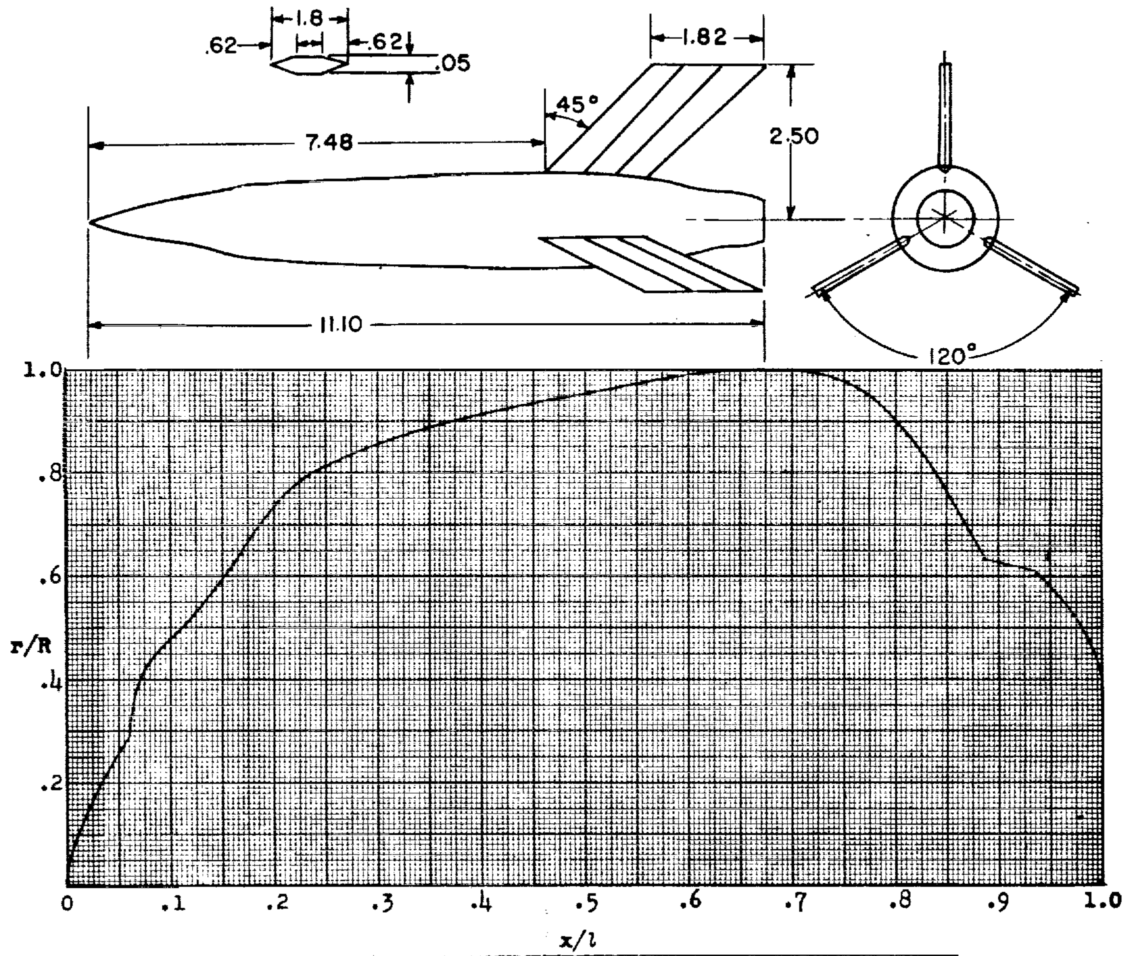

l/d_{Total}	8.10	l/d_{Nose}		S_b/A	25.11	A_b/A	.18
l/d_{N+A}	8.10	l/d_{Aft}		S_f/A	13.2	θ_b	21.5°

Designation: 144

Test: Helium Gun

Figure 150.

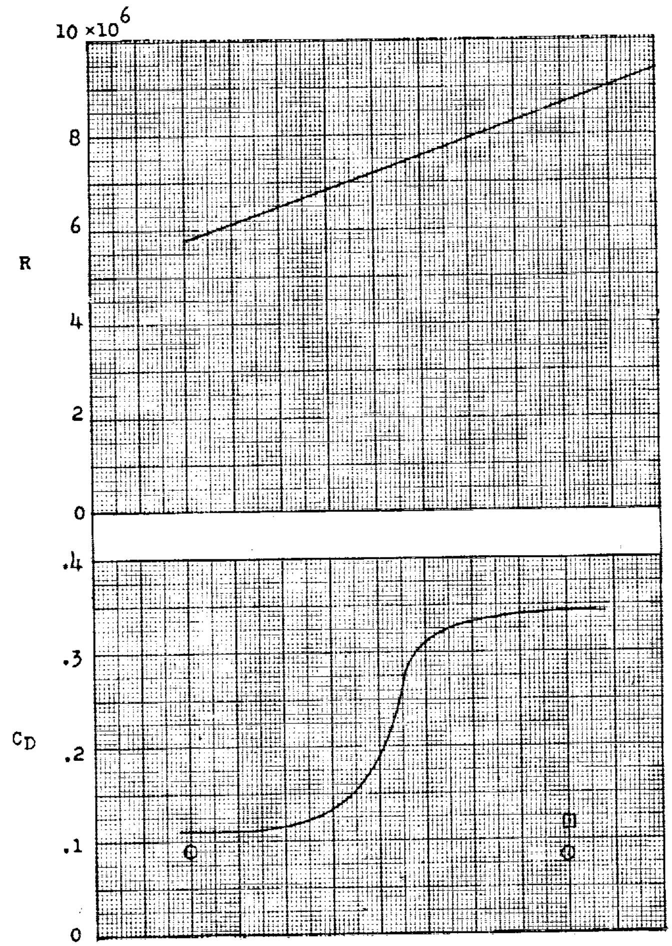

Figure 150.- Concluded.

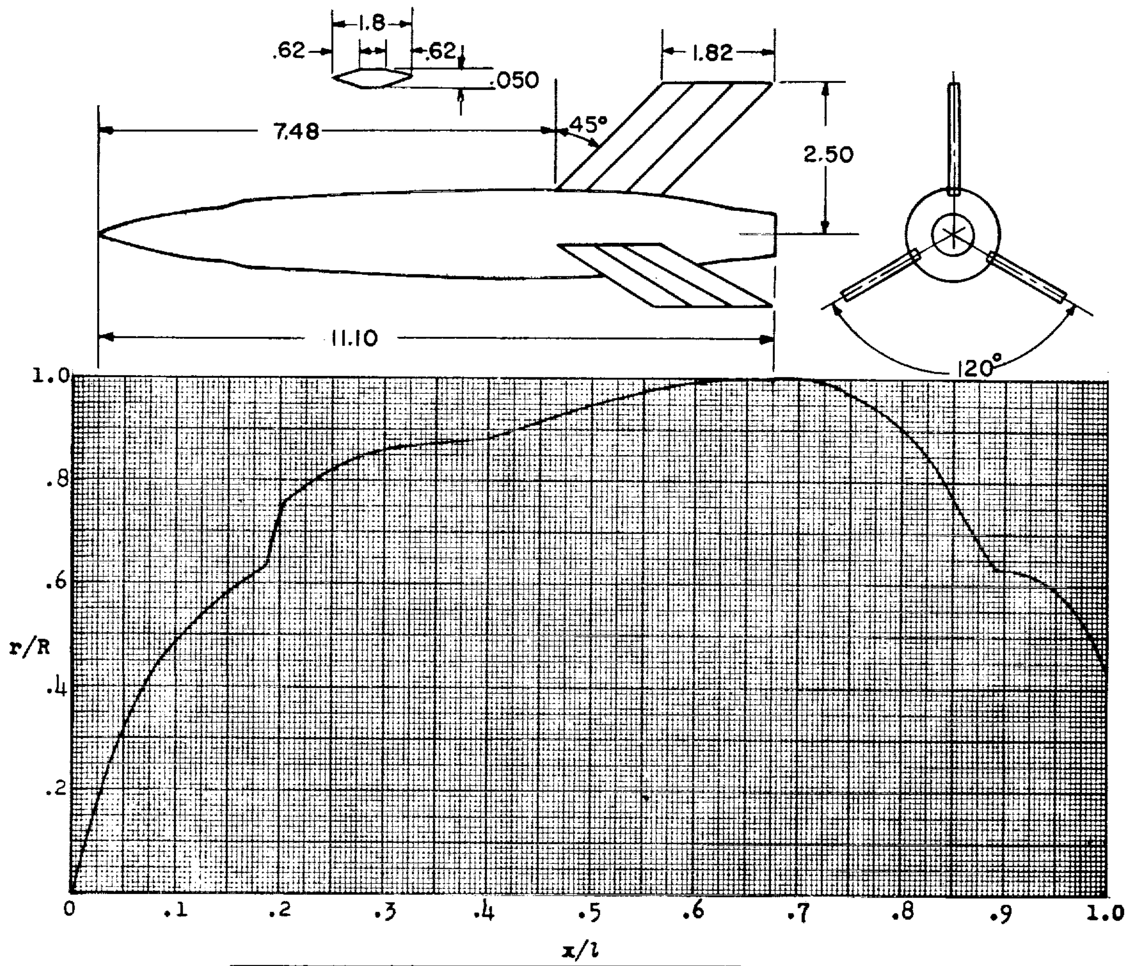

l/d_{Total}	8.10	l/d_{Nose}		S_b/A	25.08	A_b/A	.18
l/d_{N+A}	8.10	l/d_{Aft}		S_f/A	13.2	θ_b	17.1°

Designation: 145

Test: Helium Gun

Figure 151.

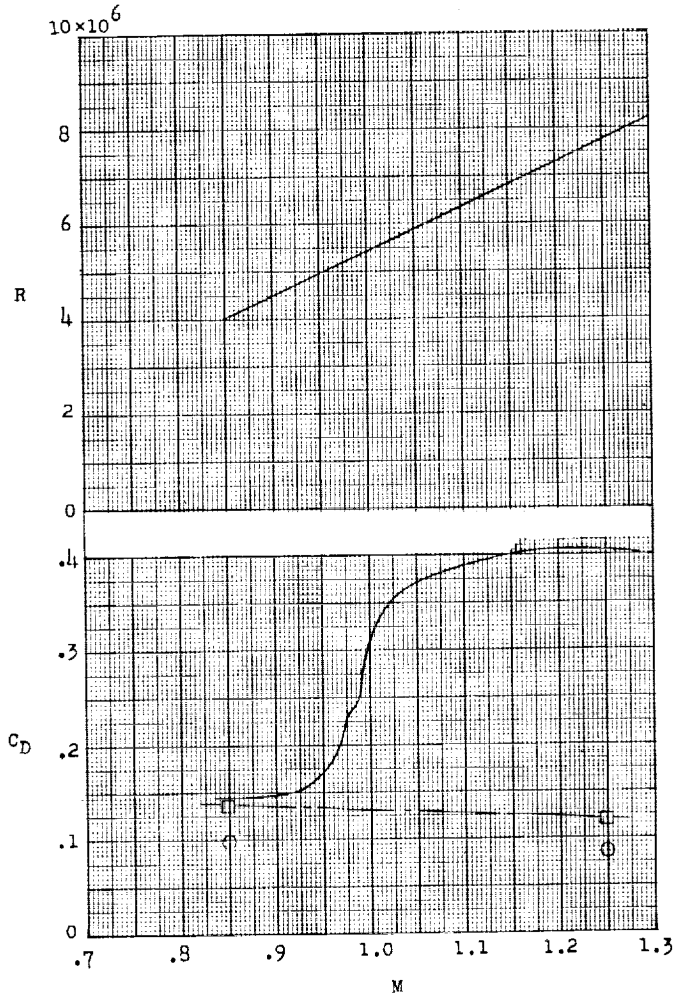

Figure 151.- Concluded.

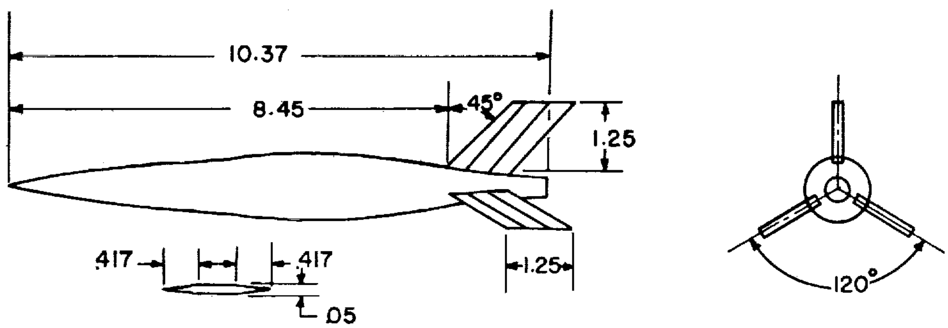

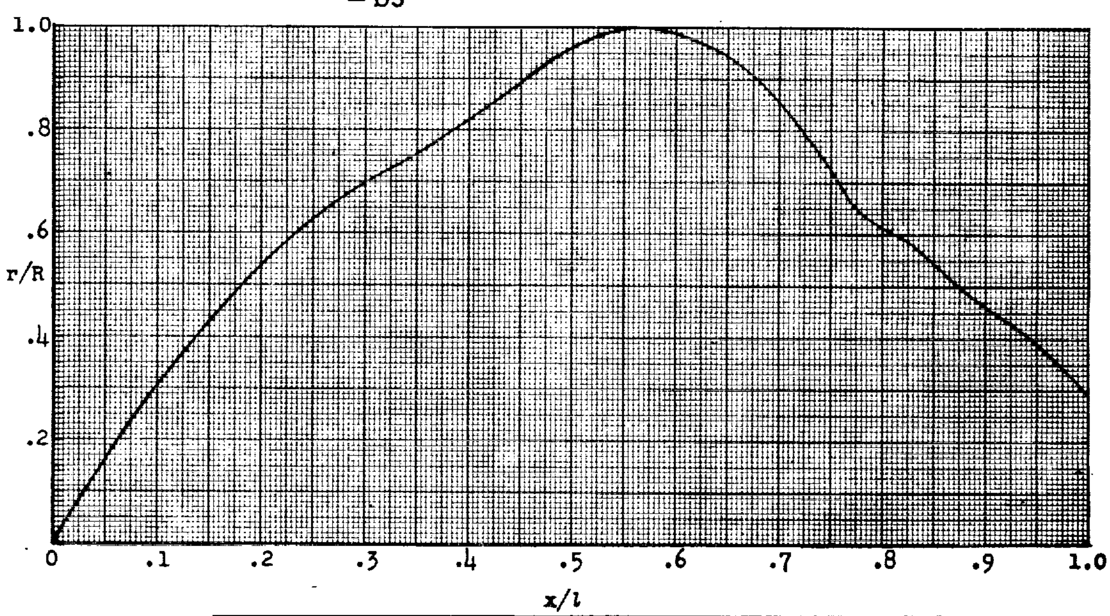

l/d_{Total}	8.11	l/d_{Nose}		S_b/A	21.0	A_b/A	.09
l/d_{N+A}	8.11	l/d_{Aft}		S_f/A	7.67	θ_b	5.0°

Designation: 146

Test: **Helium Gun**

Figure 152.

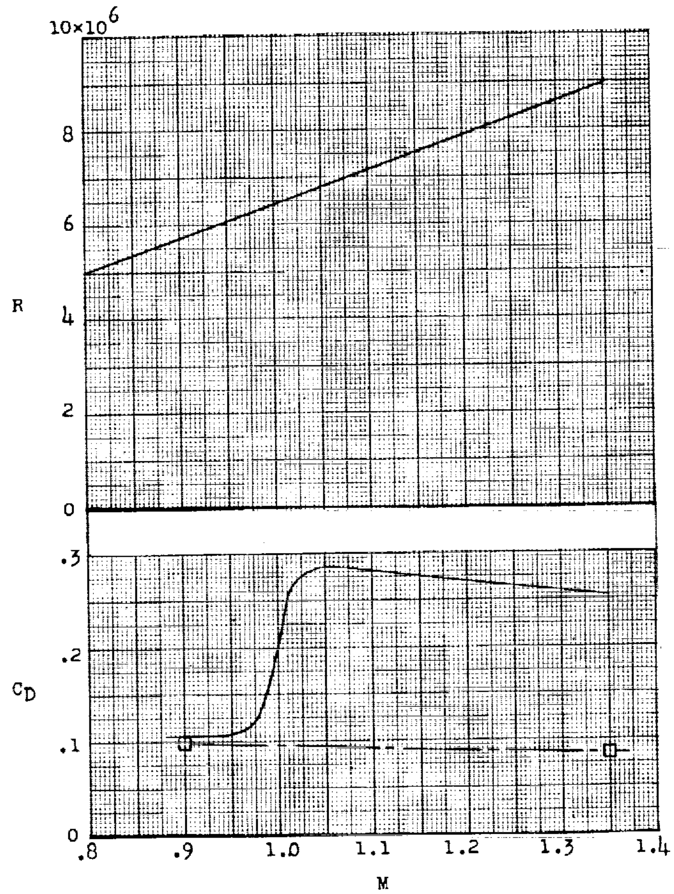

Figure 152.- Concluded.

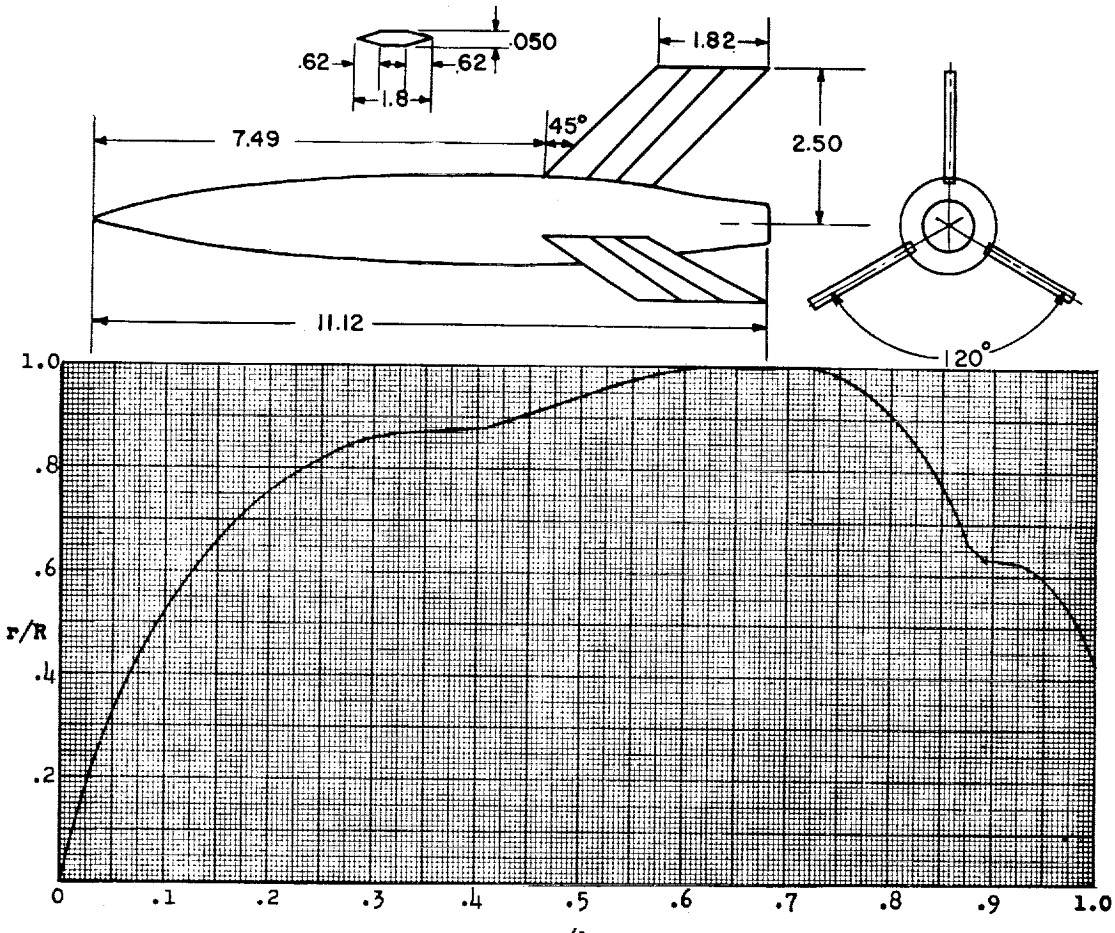

l/d_{Total}	8.12	l/d_{Nose}		S_b/A	25.40	A_b/A	.18
l/d_{N+A}	8.12	l/d_{Aft}		S_f/A	13.20	θ_b	17.9°

Designation: 147

Test: Helium Gun

Figure 153.

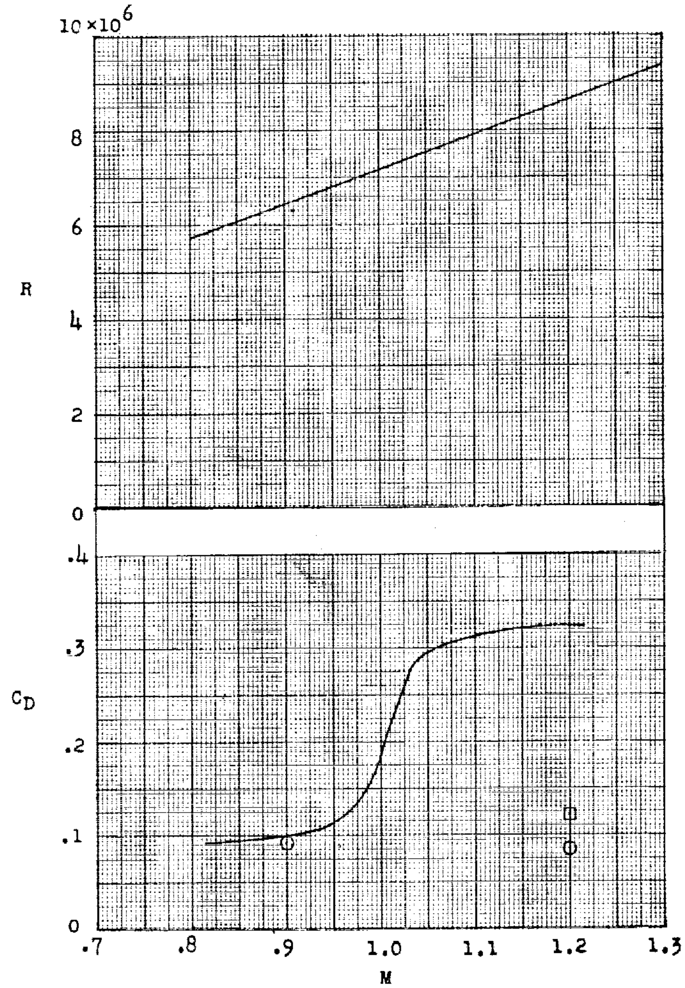

Figure 153.- Concluded.

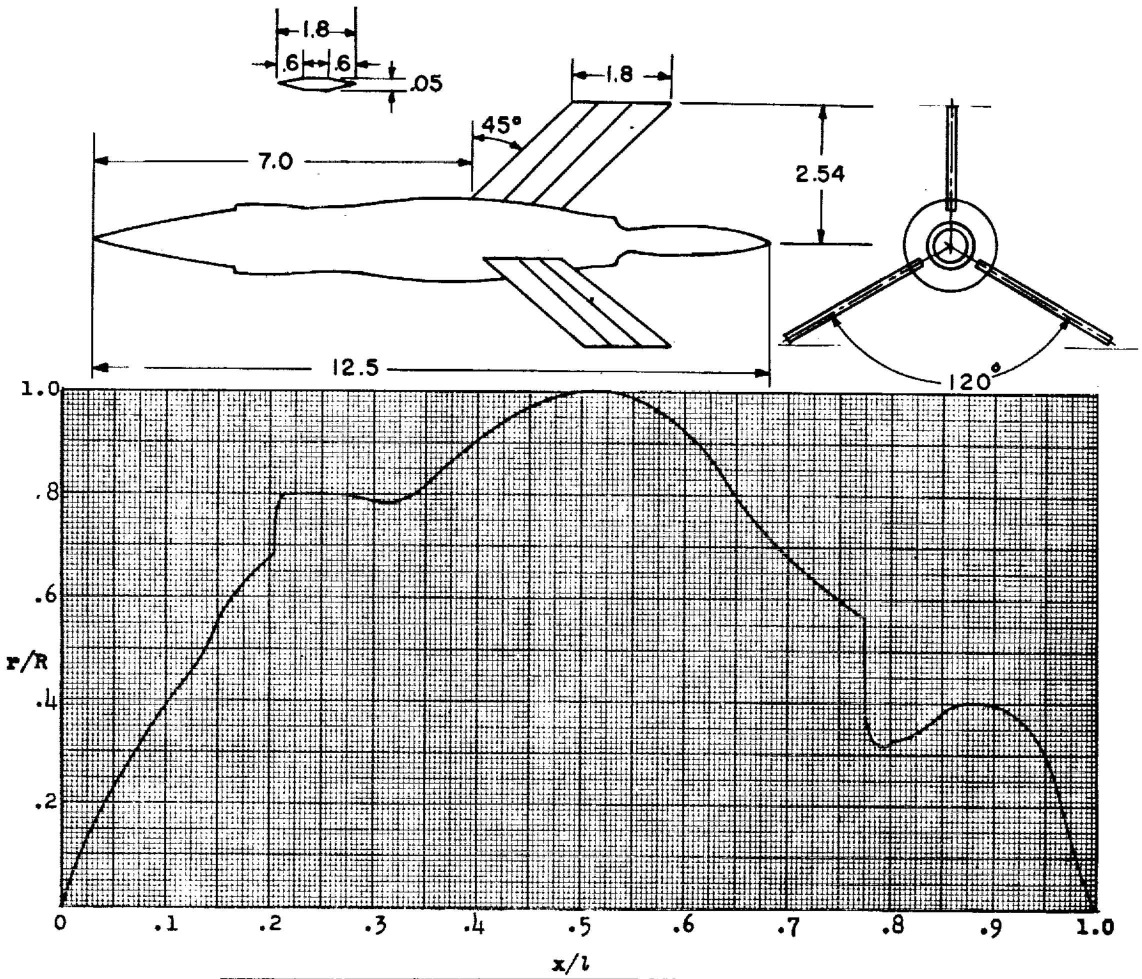

l/d_{Total}	8.23	l/d_{Nose}		S_b/A	20.80	A_b/A	0.0
l/d_{N+A}	8.23	l/d_{Aft}		S_f/A	11.72	θ_b	16.8°

Designation: 148

Test: Helium Gun

Figure 154.

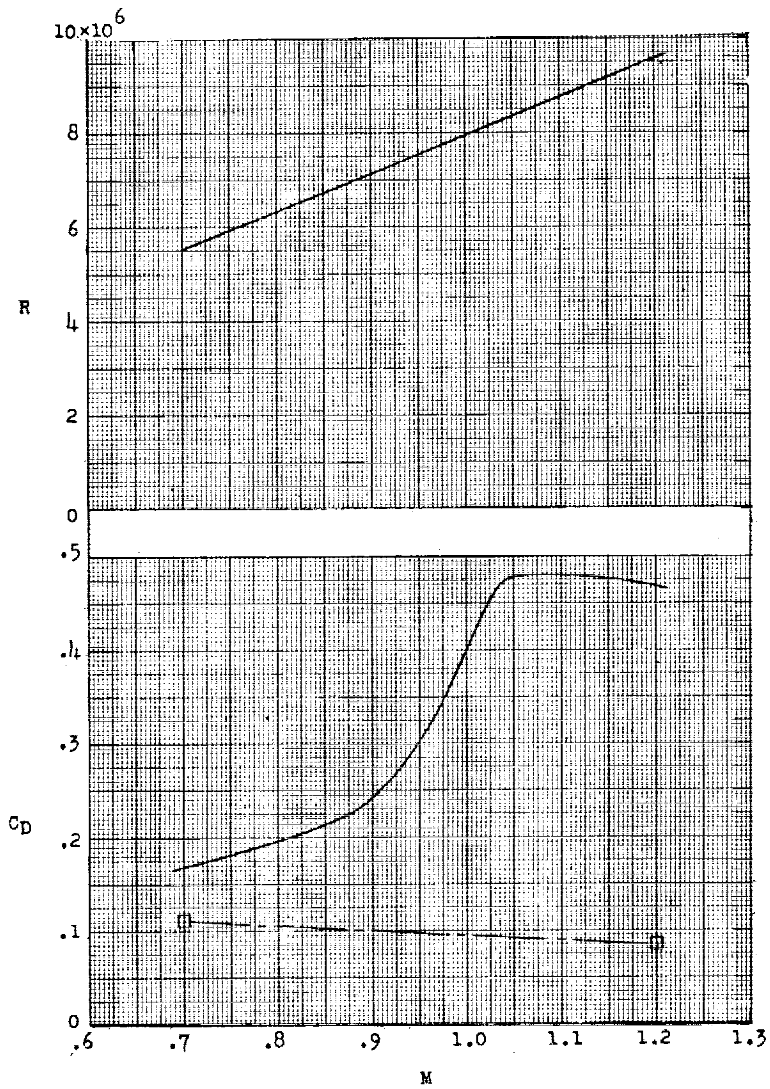

Figure 154.- Concluded.

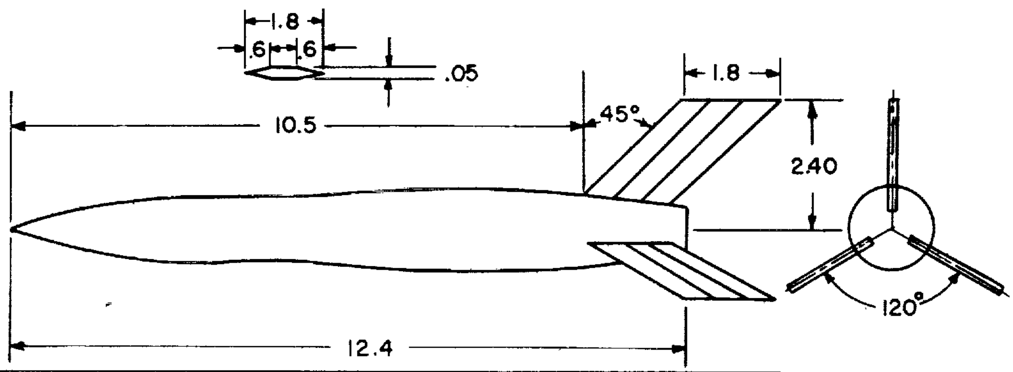

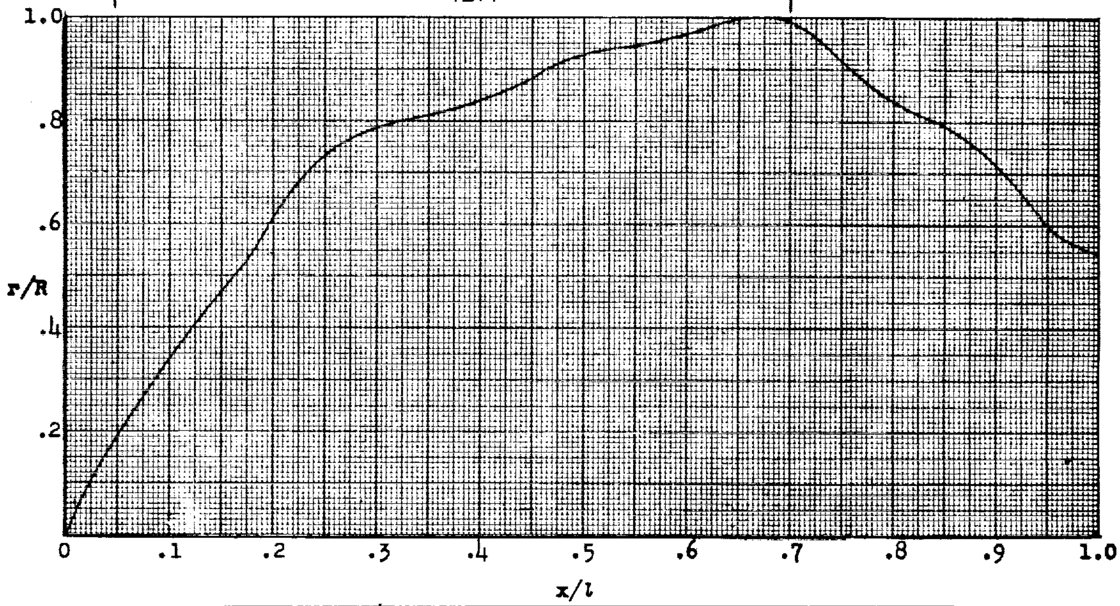

l/d_{Total}	8.27	l/d_{Nose}		S_b/A	24.0	A_b/A	.29
l/d_{N+A}	8.27	l/d_{Aft}		S_f/A	10.9	θ_b	2.8°

Designation: 149

Test: Helium Gun

Figure 155.

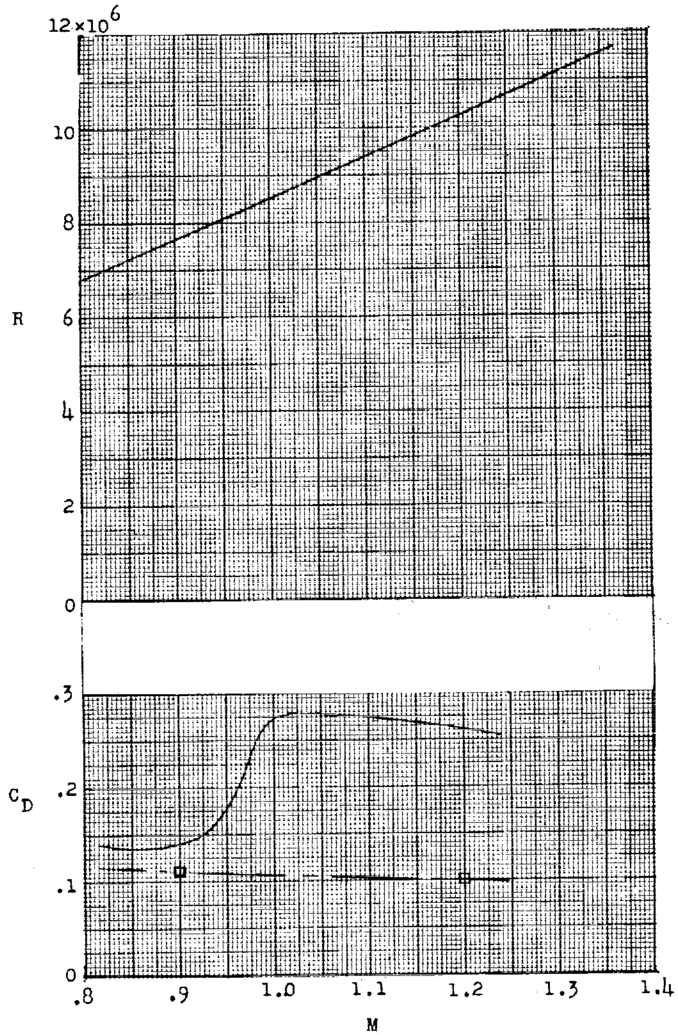

Figure 155.- Concluded.

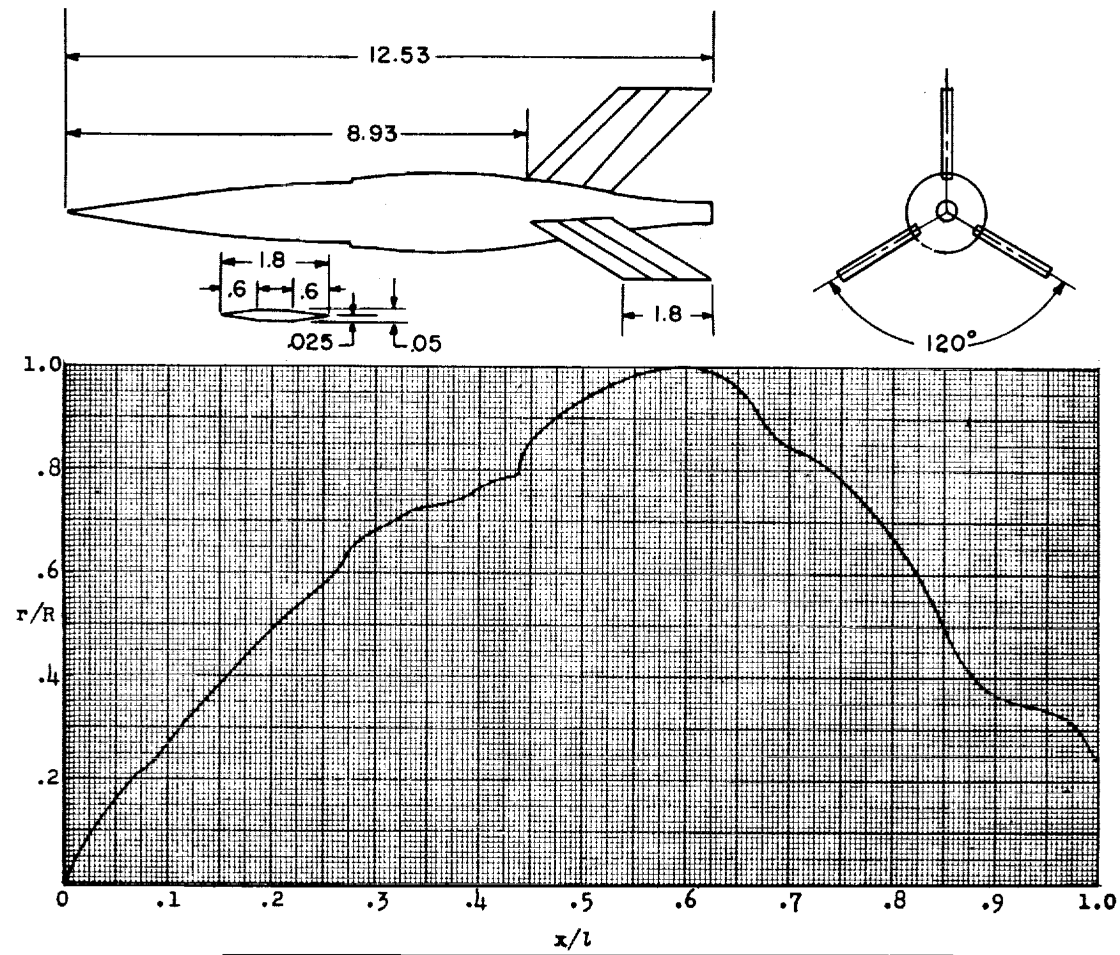

l/d_{Total}	8.28	l/d_{Nose}		S_b/A	20.7	A_b/A	.06
l/d_{N+A}	8.28	l/d_{Aft}		S_f/A	11.8	θ_b	15.0°

Designation: 150

Test: Helium Gun

Figure 156.

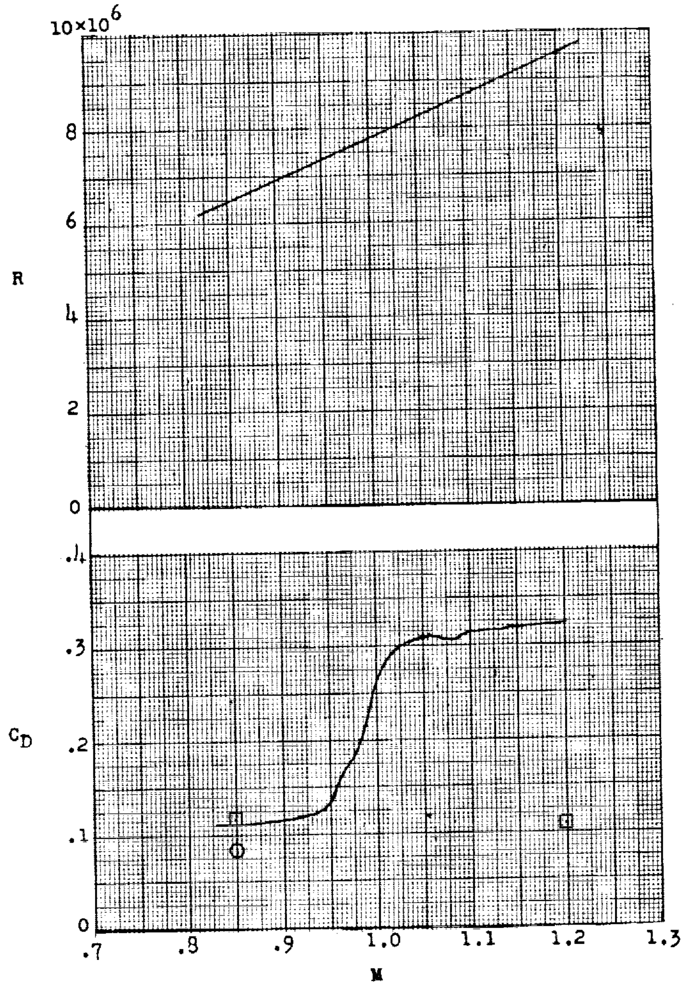

Figure 156.- Concluded.

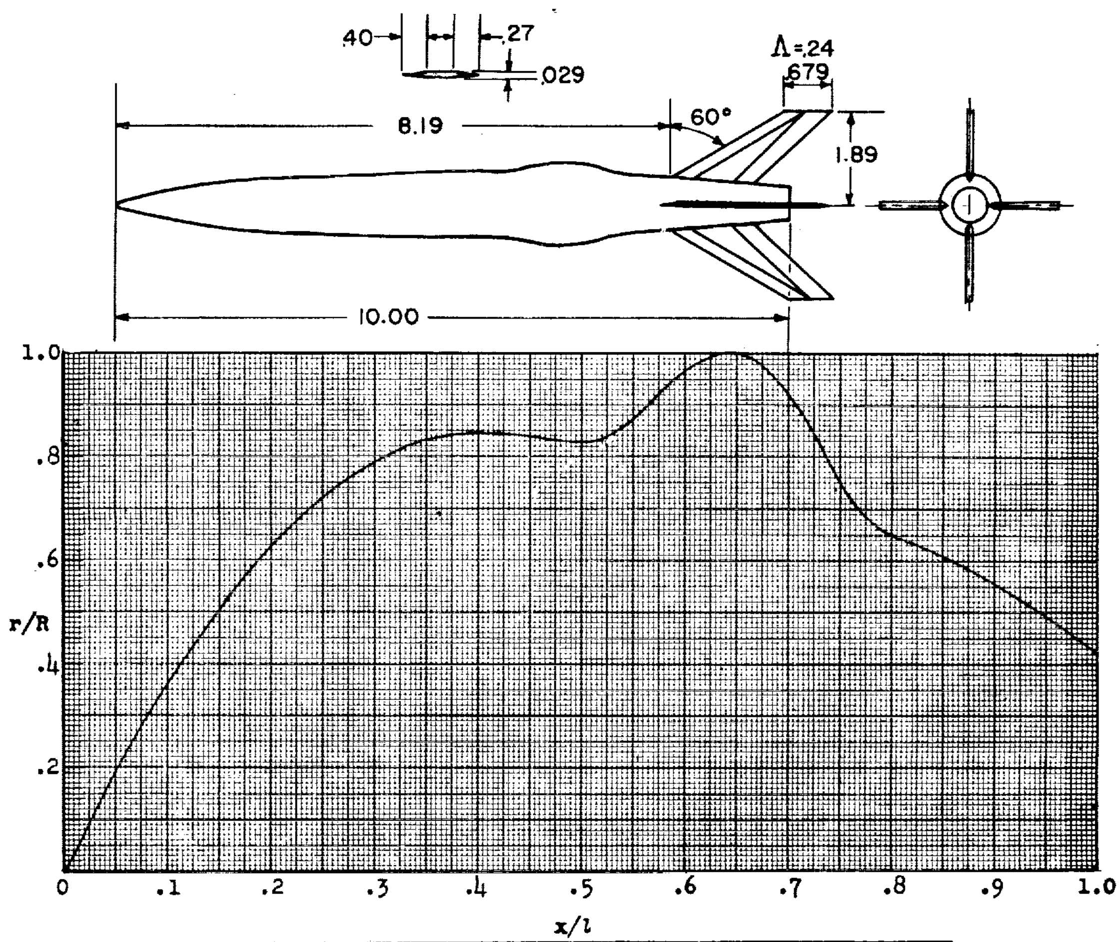

l/d_{Total}	8.40	l/d_{Nose}		S_b/A	23.00	A_b/A	.17
l/d_{N+A}	8.40	l/d_{Aft}		S_f/A	7.88	θ_b	6.1°

Designation: 151

Test: Helium Gun

Figure 157.

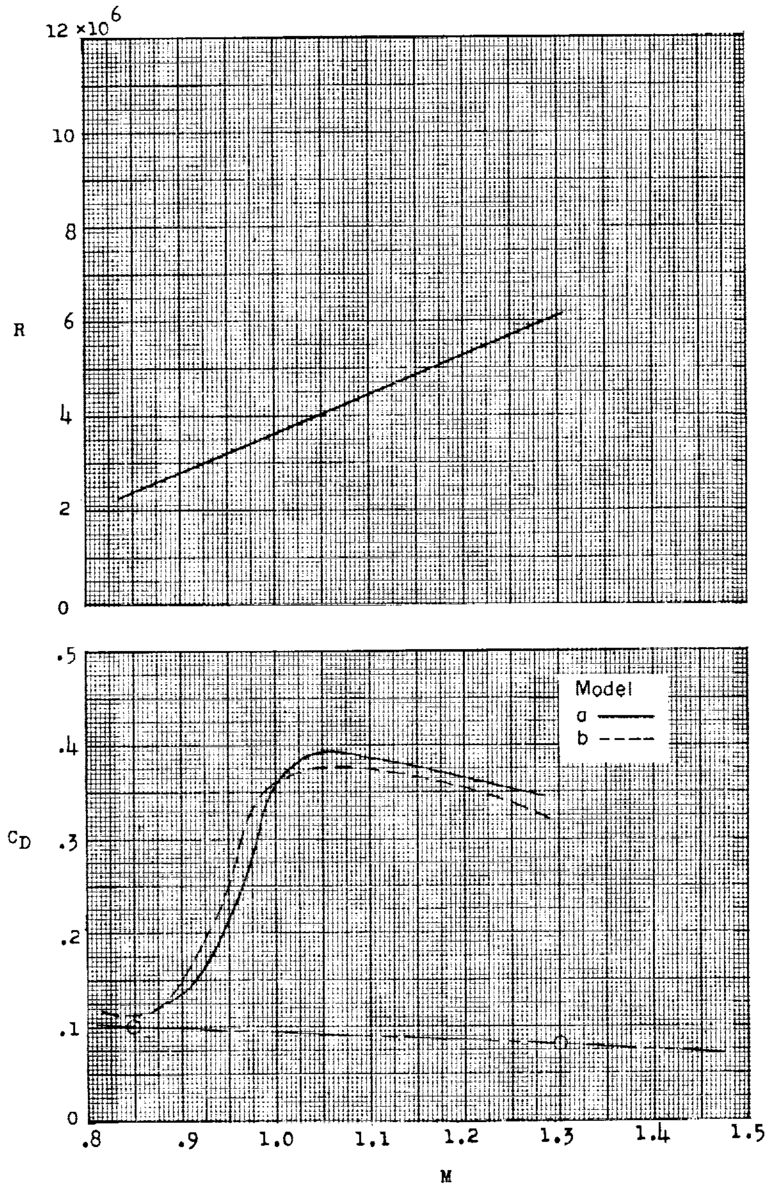

Figure 157.- Concluded.

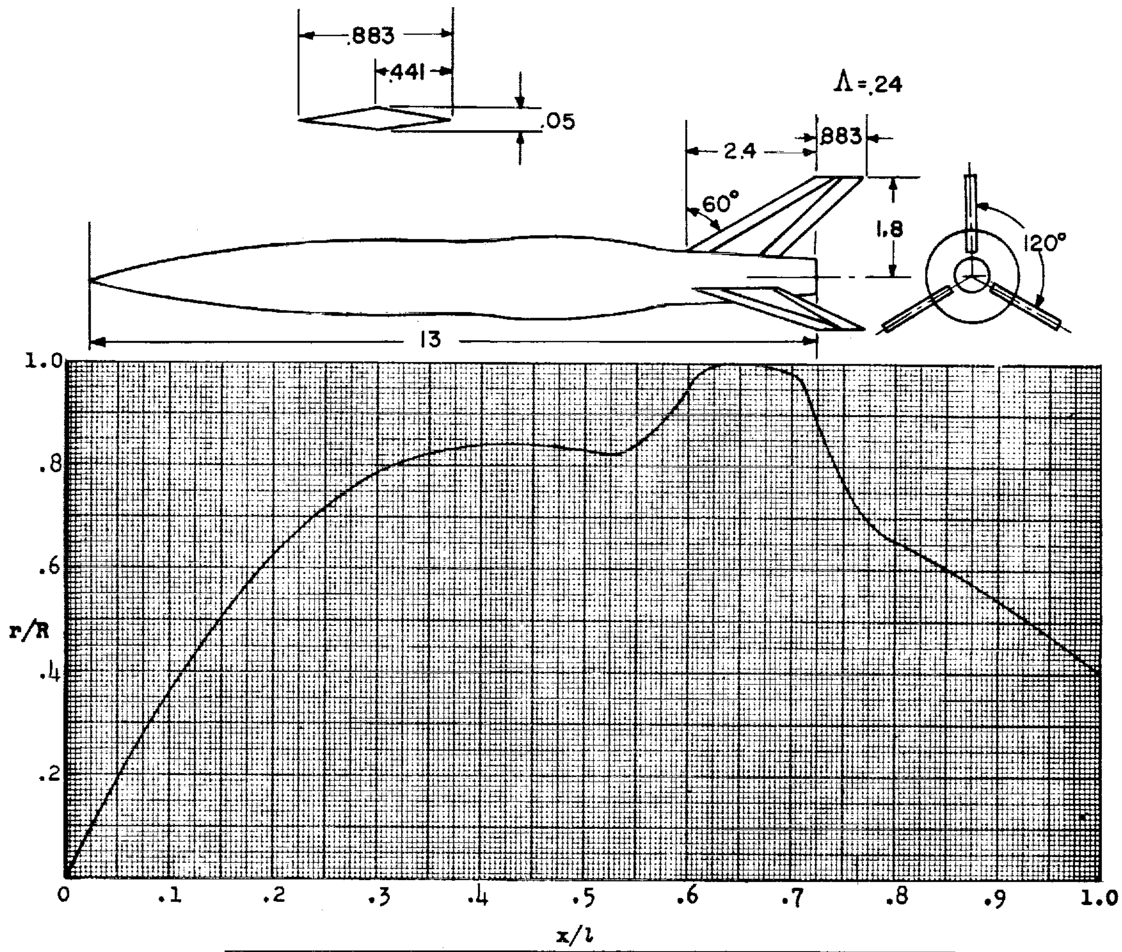

l/d_{Total}	8.43	l/d_{Nose}		S_b/A	23.1	A_b/A	.17
l/d_{N+A}	8.43	l/d_{Aft}		S_f/A	6.00	θ_b	6.8°

Designation: 152

Test: Helium Gun

Figure 158.

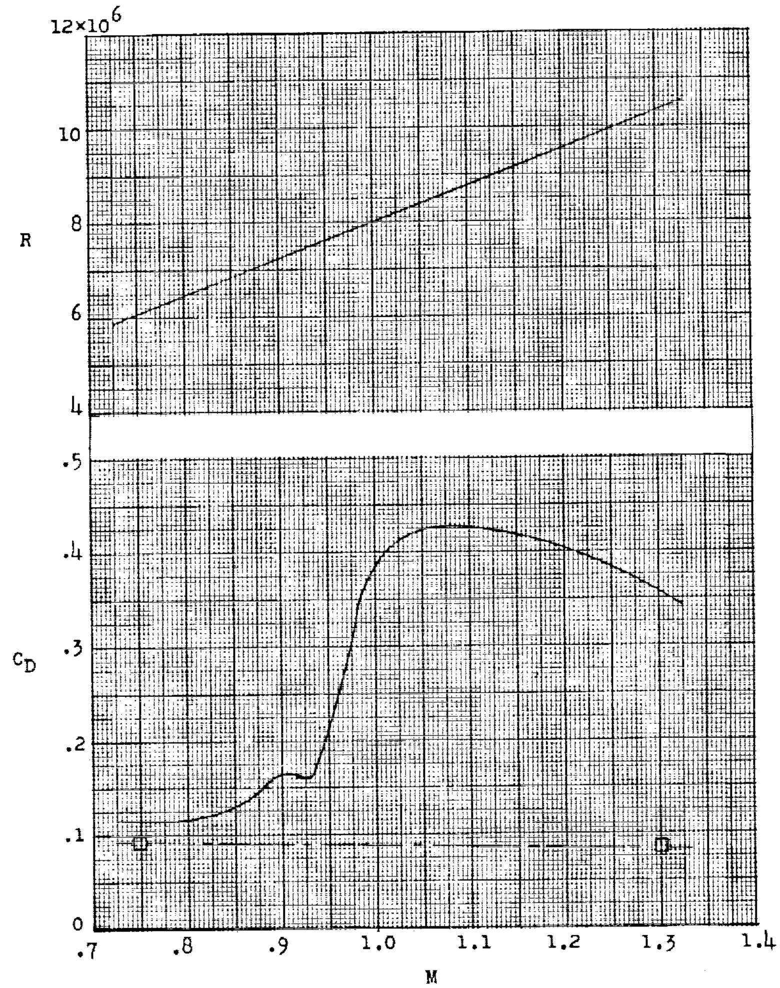

Figure 158.- Concluded.

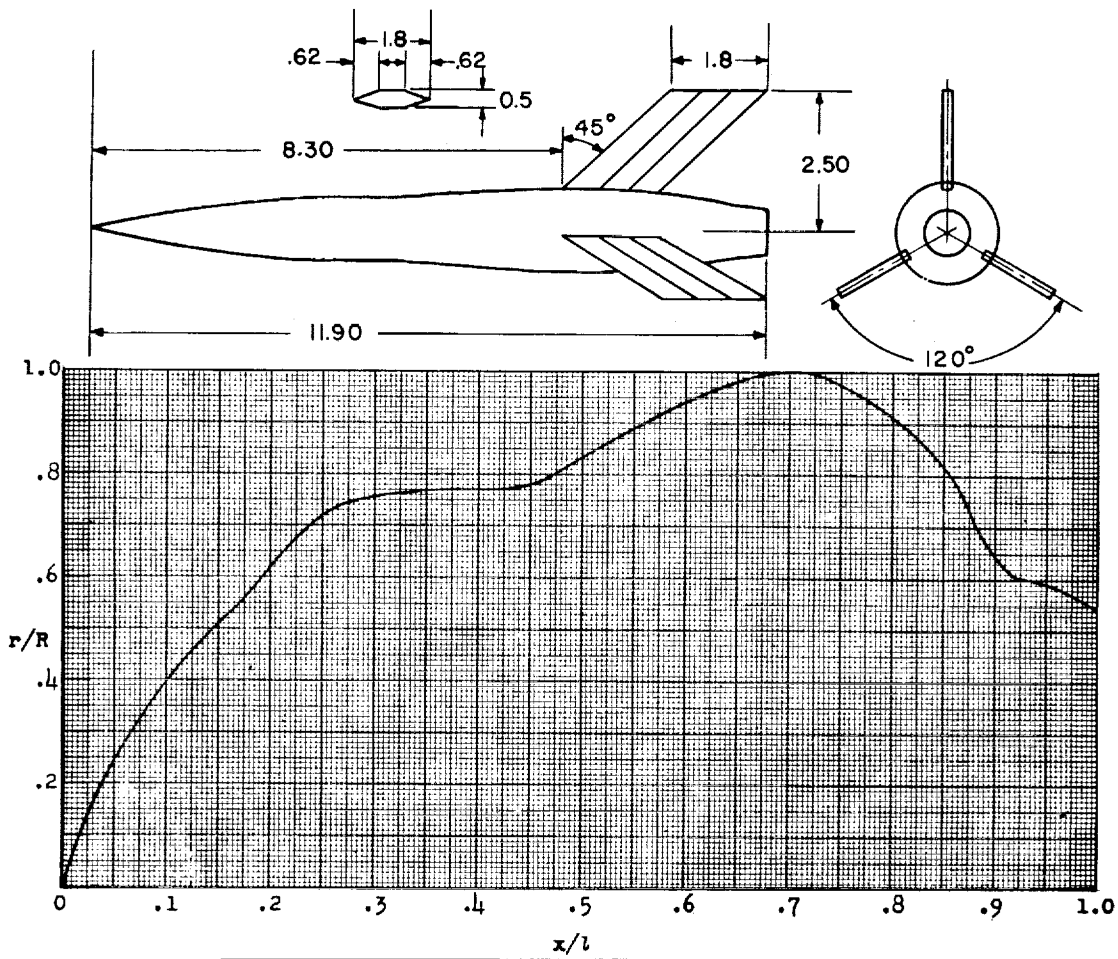

l/d_{Total}	8.48	l/d_{Nose}		S_b/A	23.76	A_b/A	.30
l/d_{N+A}	8.48	l/d_{Aft}		S_f/A	12.62	θ_b	2.4°

Designation: 153

Test: Helium Gun

Figure 159.

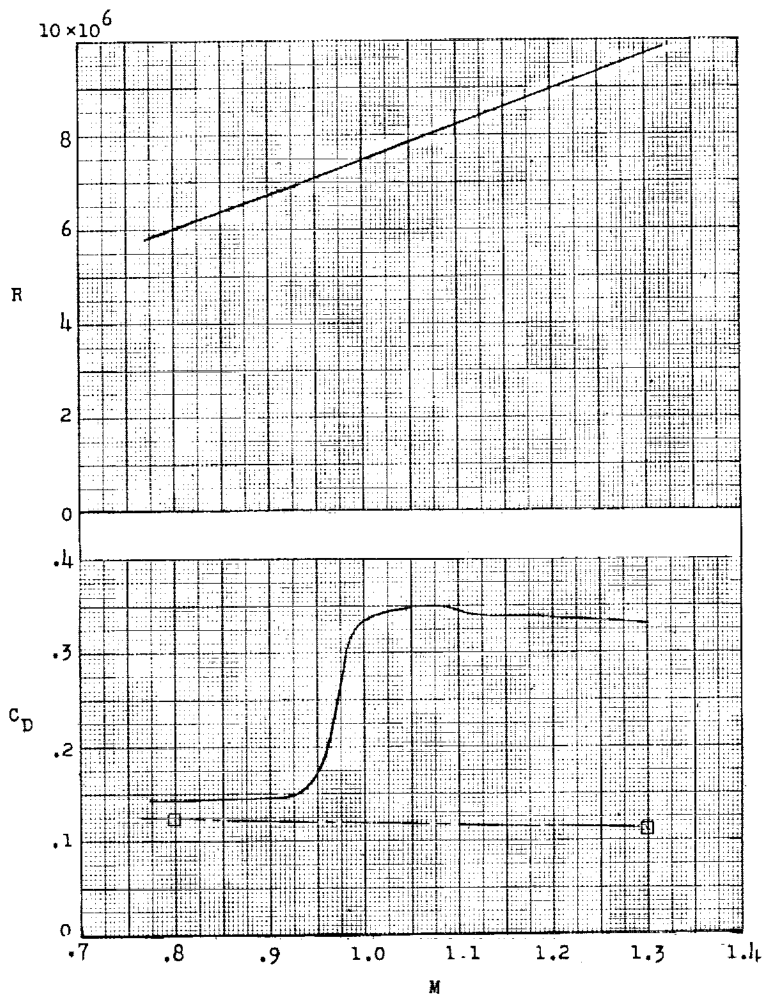

Figure 159.- Concluded.

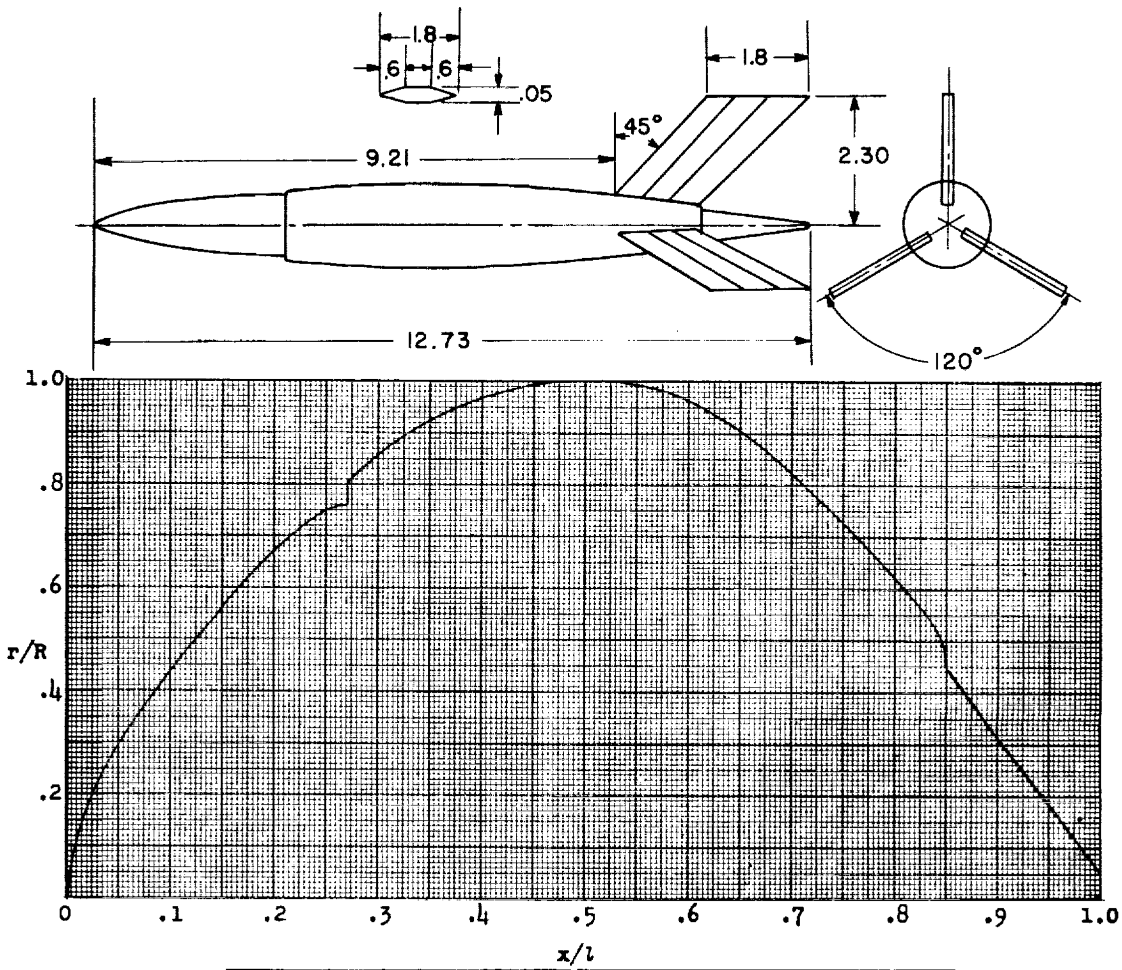

l/d_{Total}	8.49	l/d_{Nose}		S_b/A	23.12	A_b/A	0.0
l/d_{N+A}	8.49	l/d_{Aft}		S_f/A	11.0	θ_b	7.4°

Designation: 154

Test: Helium Gun

Figure 160.

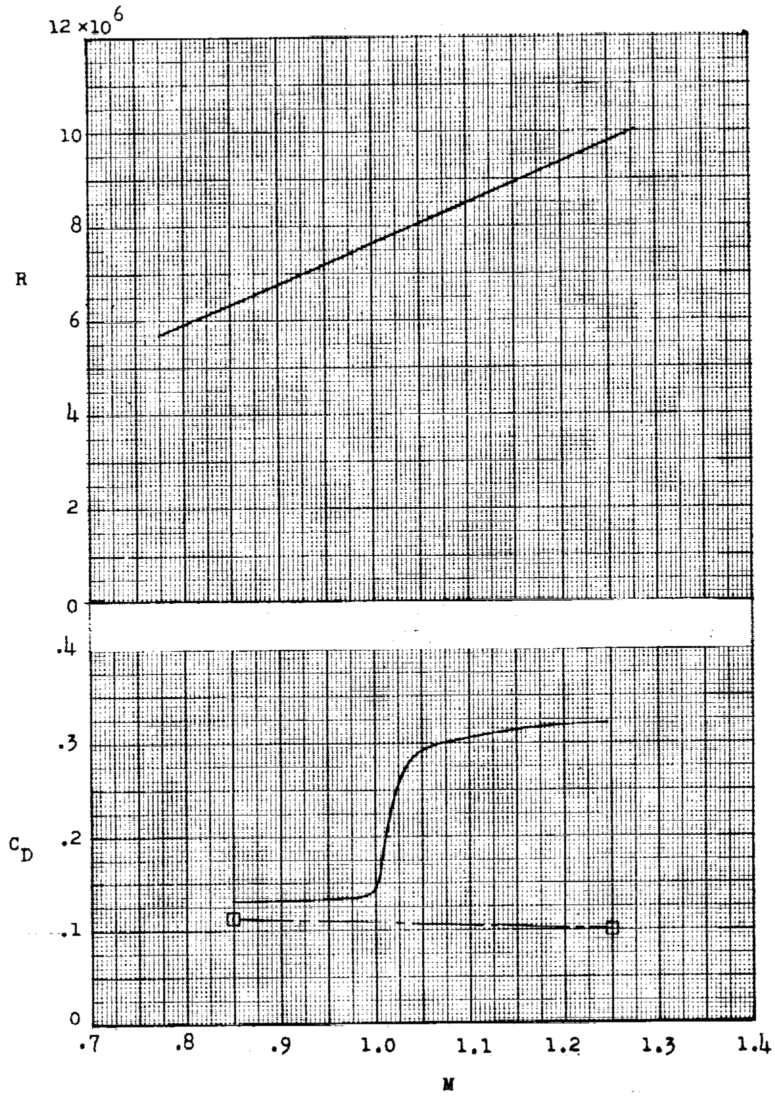

Figure 160.- Concluded.

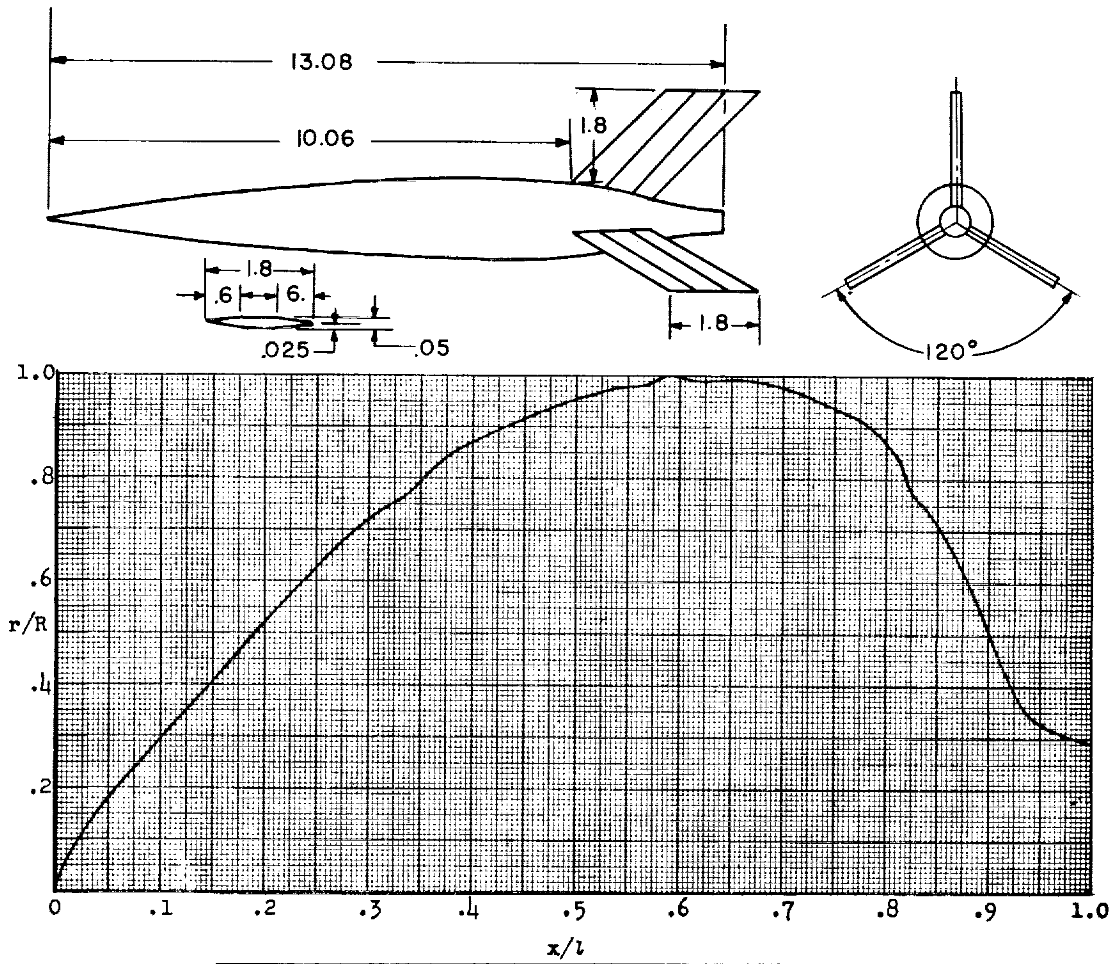

l/d_{Total}	8.52	l/d_{Nose}		S_b/A	23.4	A_b/A	.08
l/d_{N+A}	8.52	l/d_{Aft}		S_f/A	11.5	θ_b	2.5°

Designation: 155

Test: Helium Gun

Figure 161..

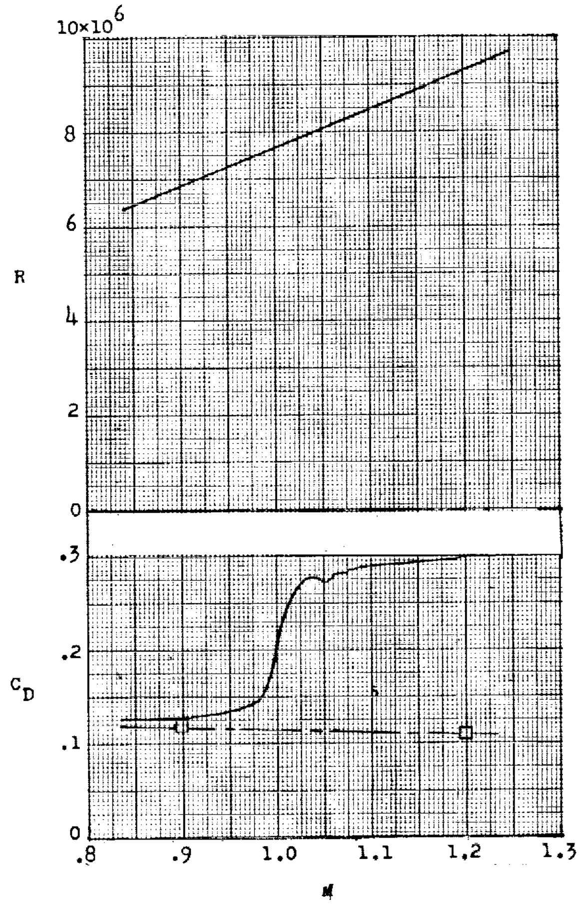

Figure 161.- Concluded.

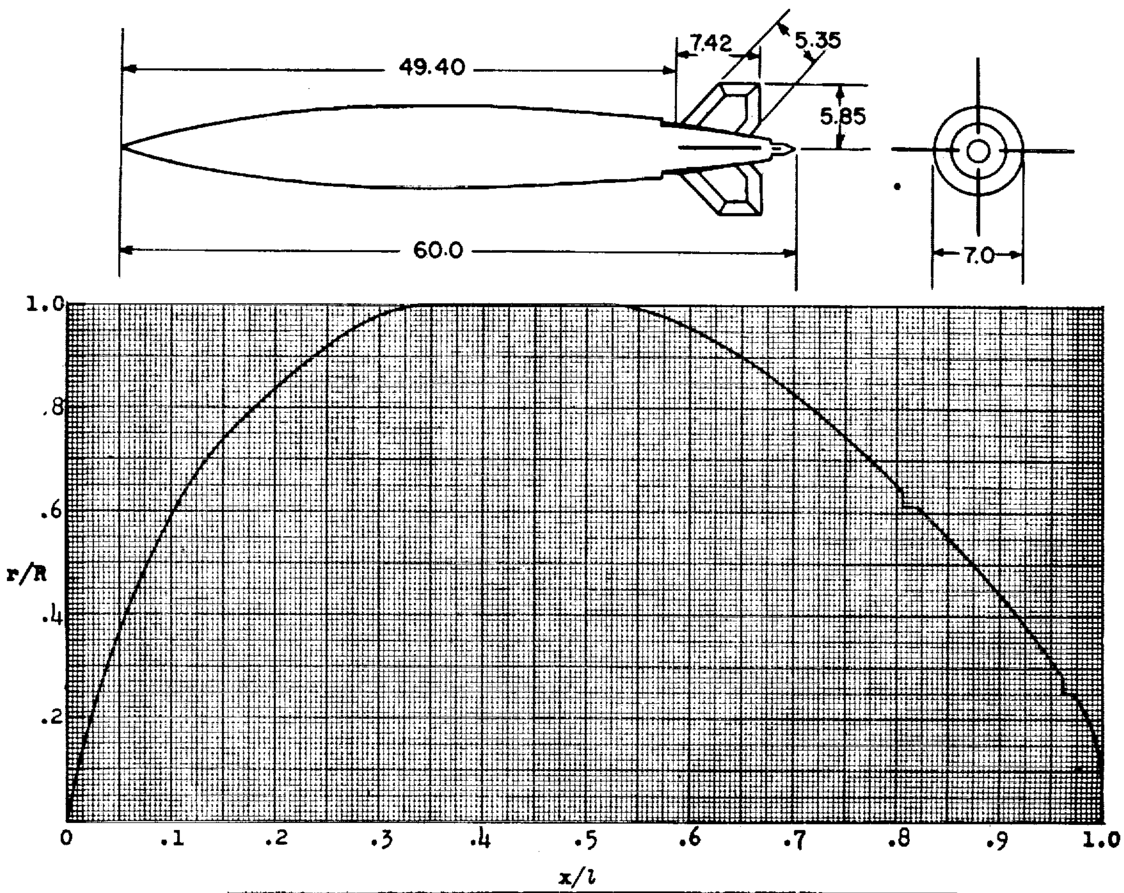

l/d_{Total}	8.57	l/d_{Nose}		S_b/A	25.70	A_b/A	0.0
l/d_{N+A}	7.32	l/d_{Aft}		S_f/A	6.7	θ_b	90°

Designation: 156

Test: Rocket

Figure 162.

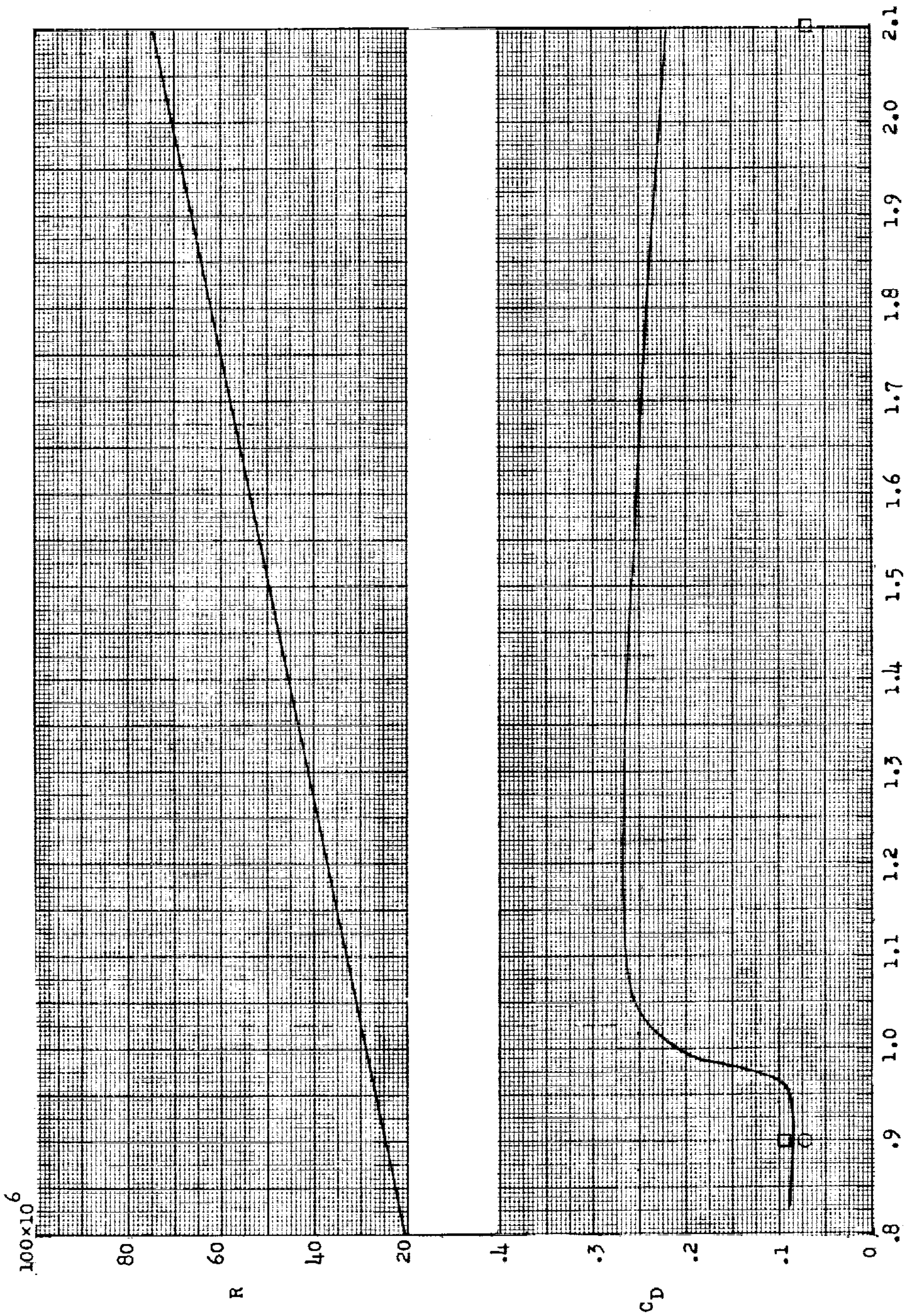

Figure 162.- Concluded.

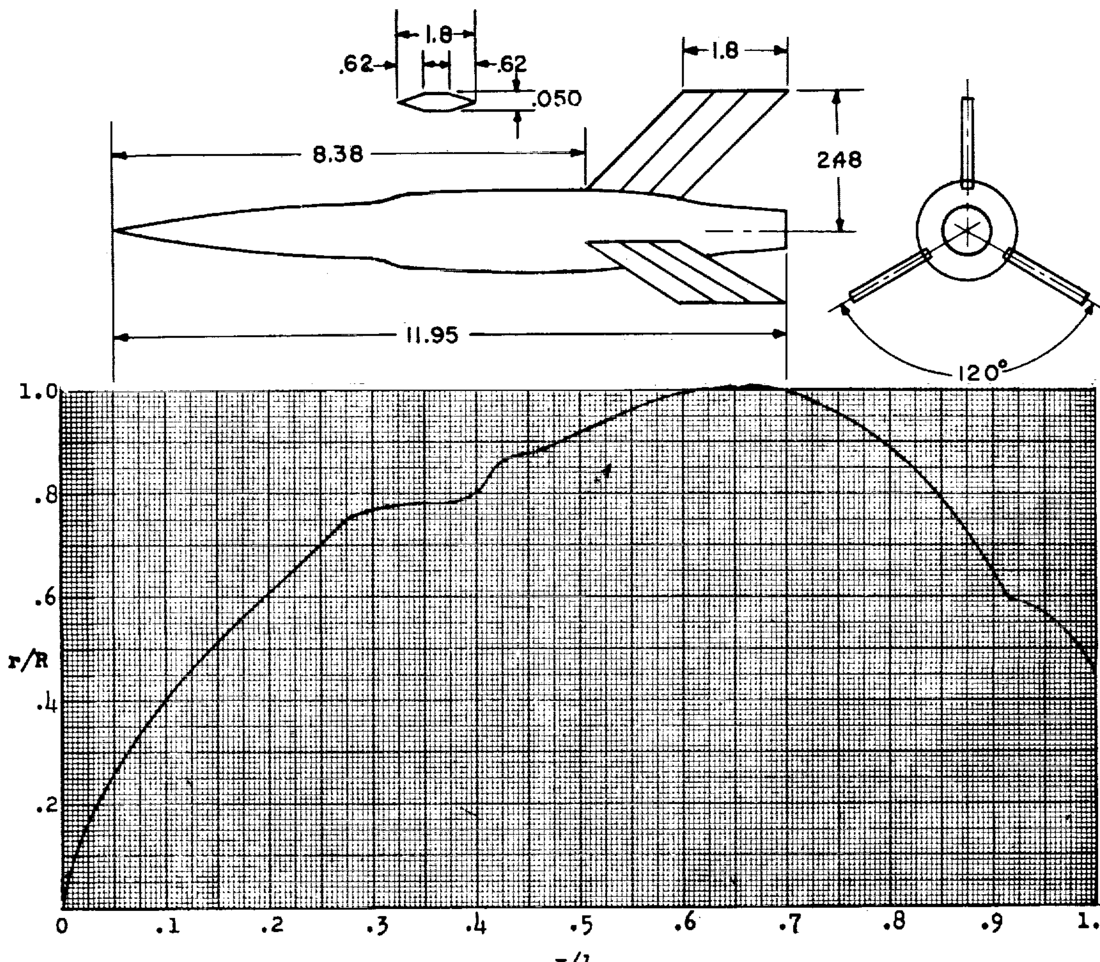

l/d_{Total}	8.7	l/d_{Nose}		S_b/A	24.54	A_b/A	.20
l/d_{N+A}	8.7	l/d_{Aft}		S_f/A	13.12	θ_b	12.1°

Designation: 157

Test: Helium Gun

Figure 163.

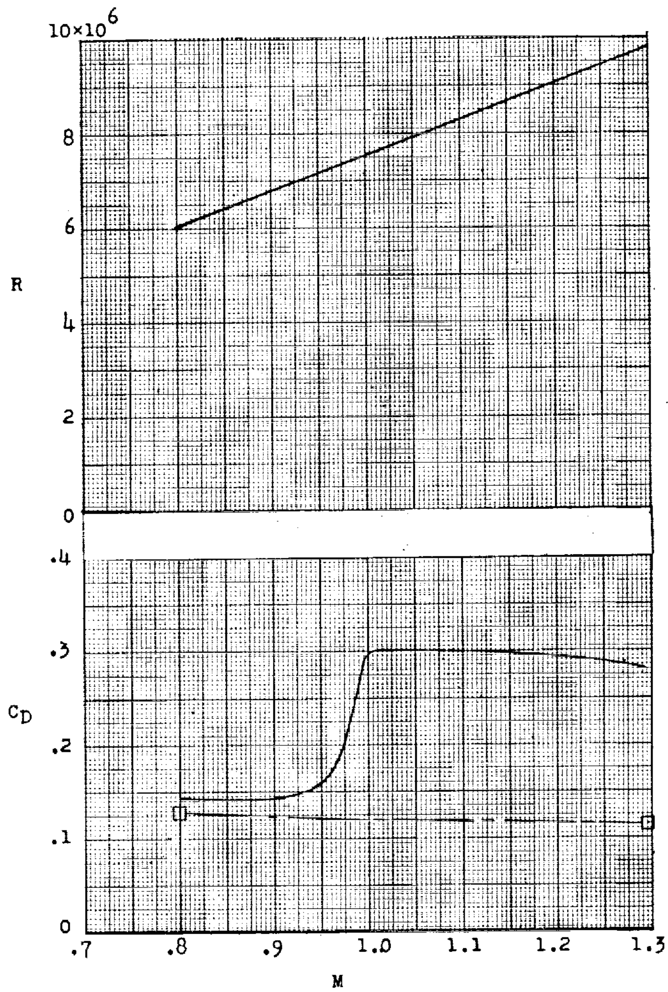

Figure 163.- Concluded.

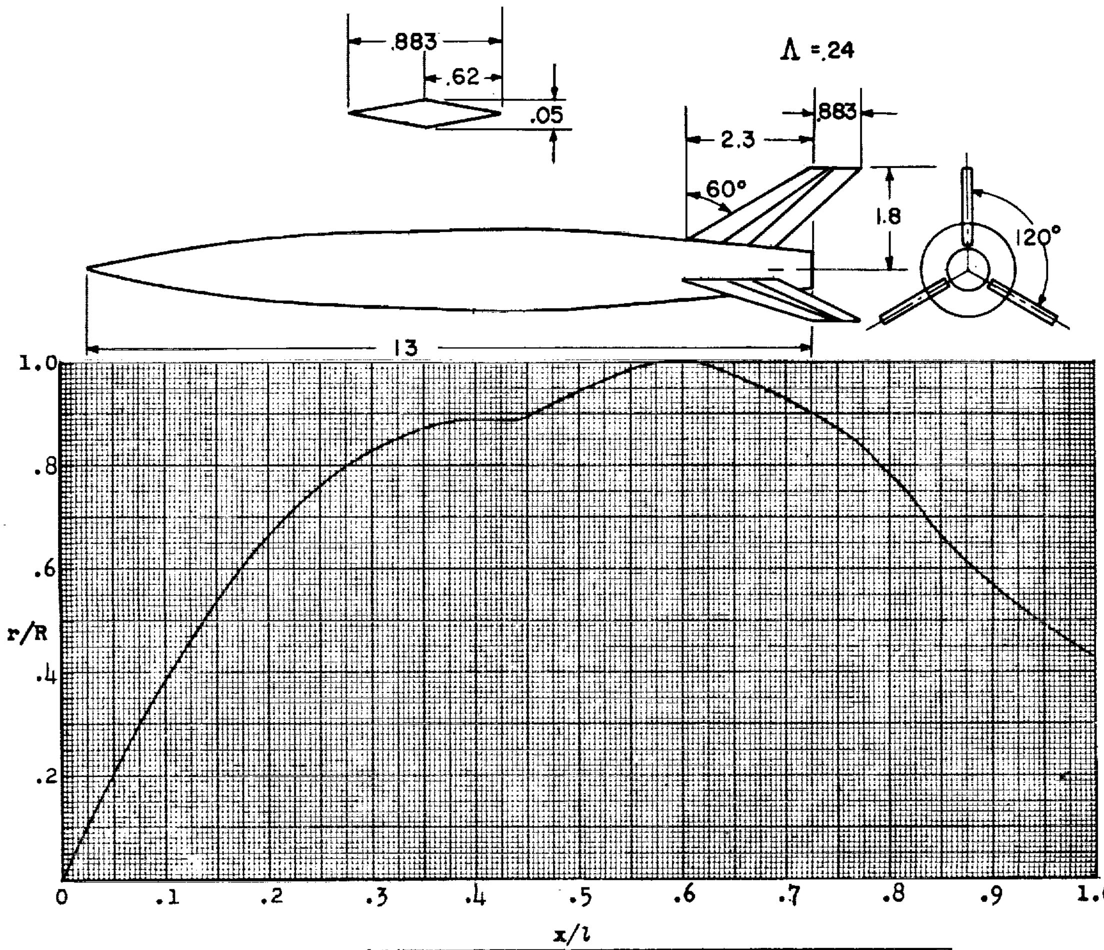

l/d_{Total}	8.84	l/d_{Nose}		S_b/A	25.64	A_b/A	.18
l/d_{N+A}	8.84	l/d_{Aft}		S_f/A	6.64	θ_b	4.6°

Designation: 158

Test: Helium Gun

Figure 164.

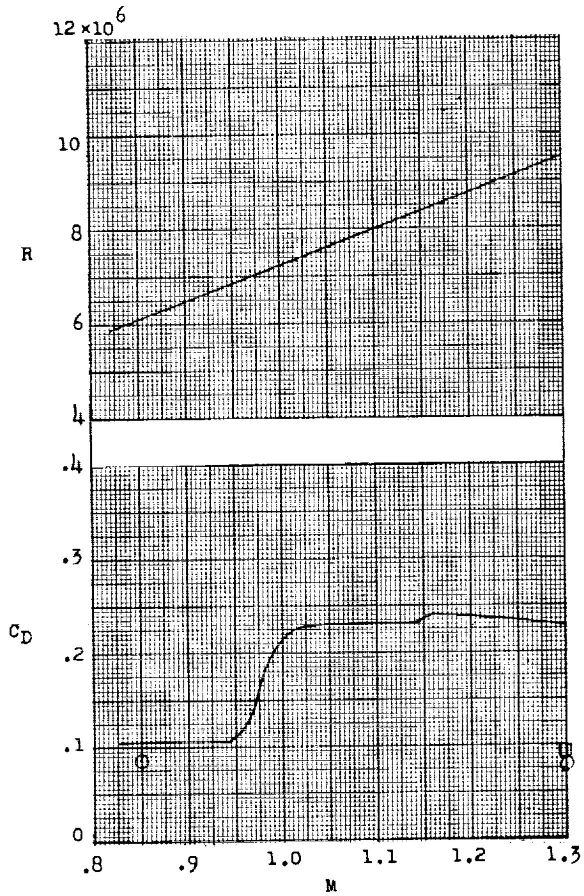

Figure 164.- Concluded.

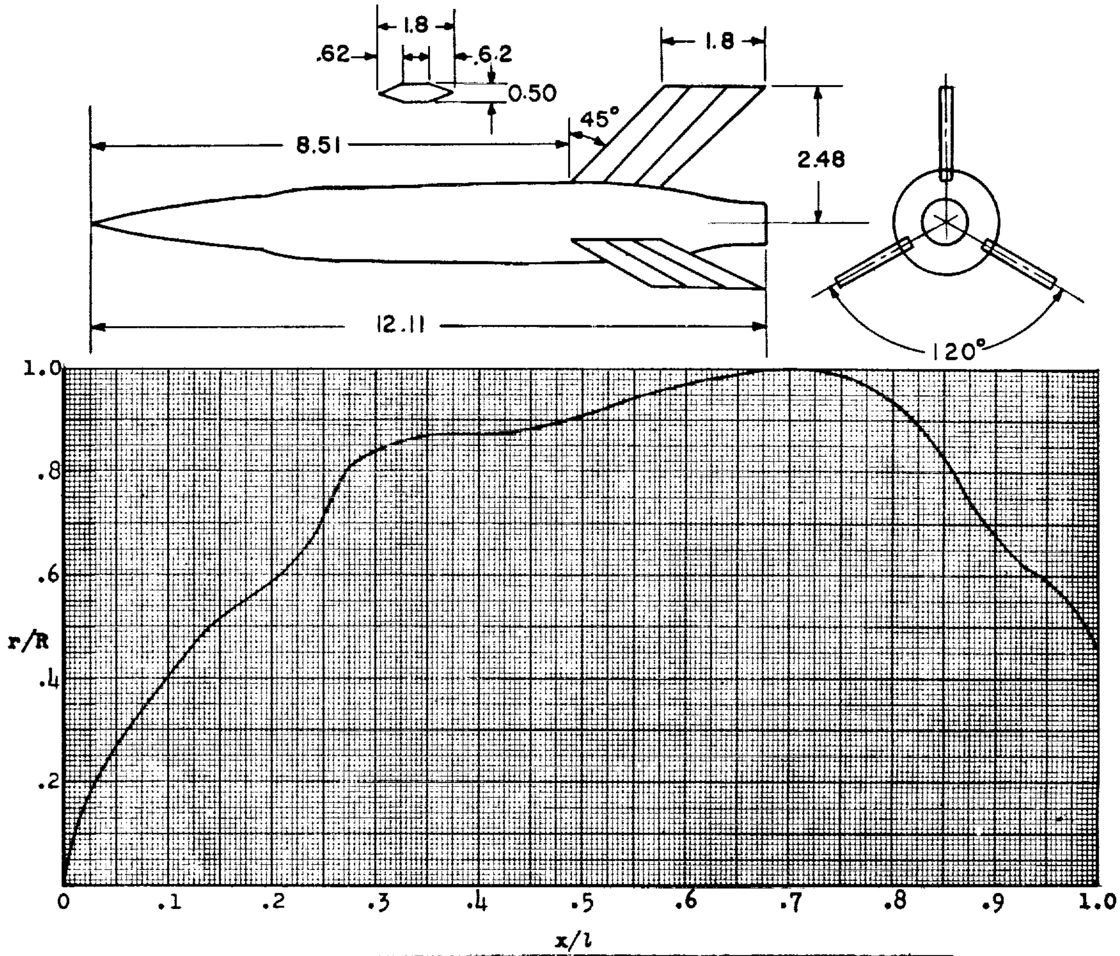

l/d_{Total}	8.85	l/d_{Nose}		S_b/A	25.75	A_b/A	.21
l/d_{N+A}	8.85	l/d_{Aft}		S_f/A	13.14	θ_b	12.3°

Designation: 159

Test: Helium Gun

Figure 165.

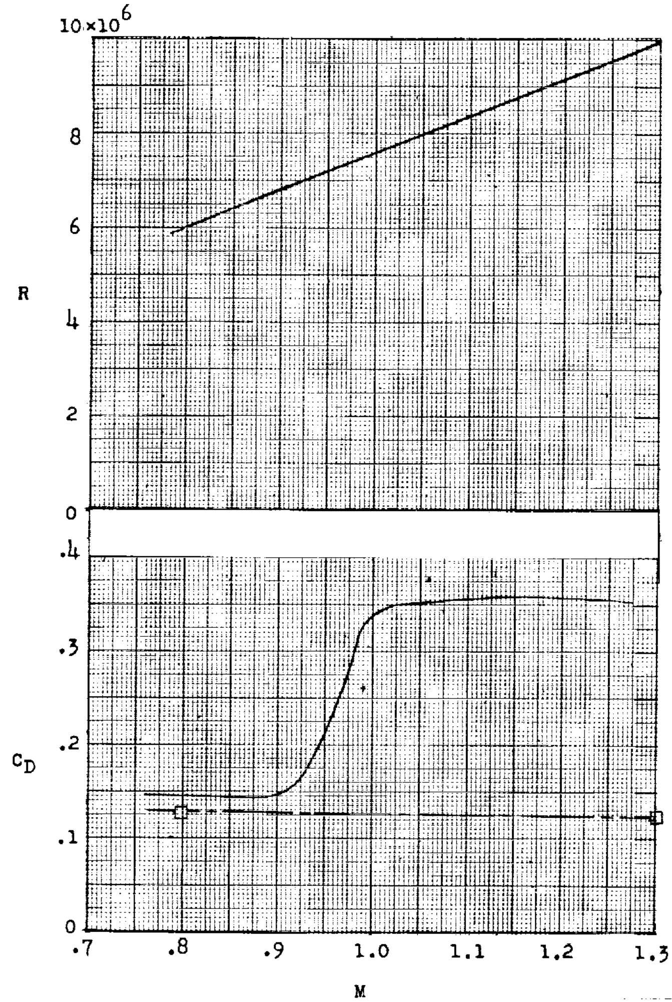

Figure 165.- Concluded.

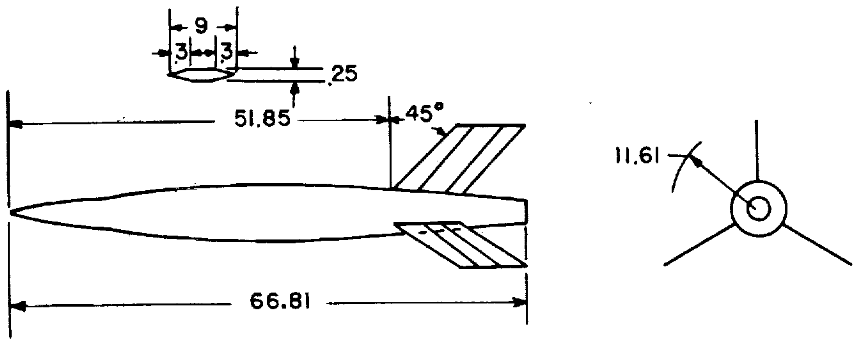

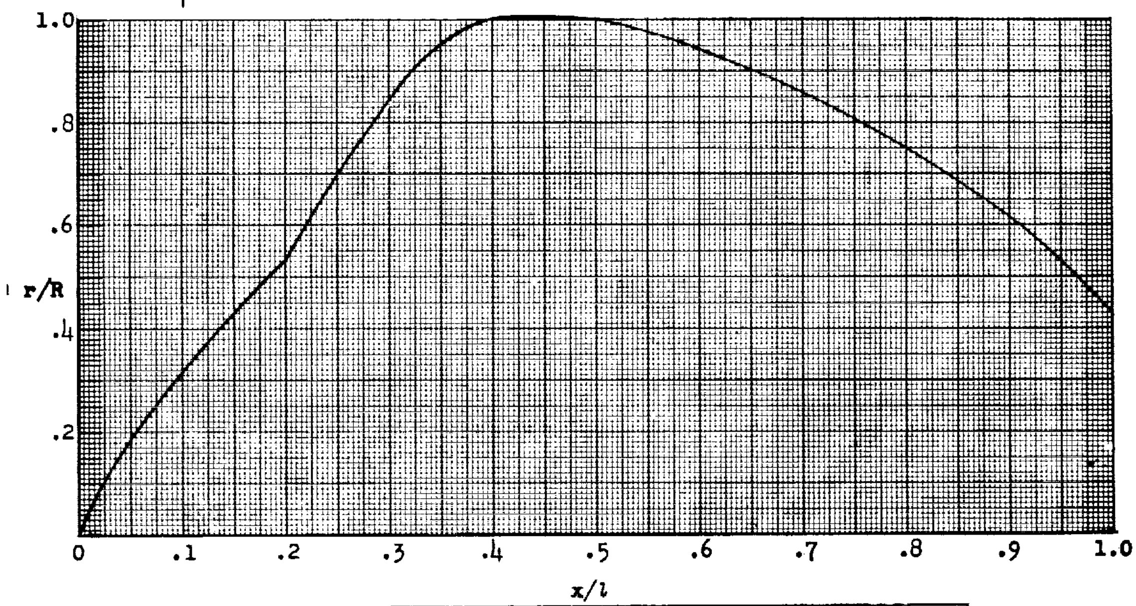

l/d_{Total}	8.91	l/d_{Nose}		S_b/A	25.00	A_b/A	.19
l/d_{N+A}	8.91	l/d_{Aft}		S_f/A	11	θ_b	7.0°

Designation: 160

Test: Rocket

Remarks: Parabolic afterbody.

Figure 166.

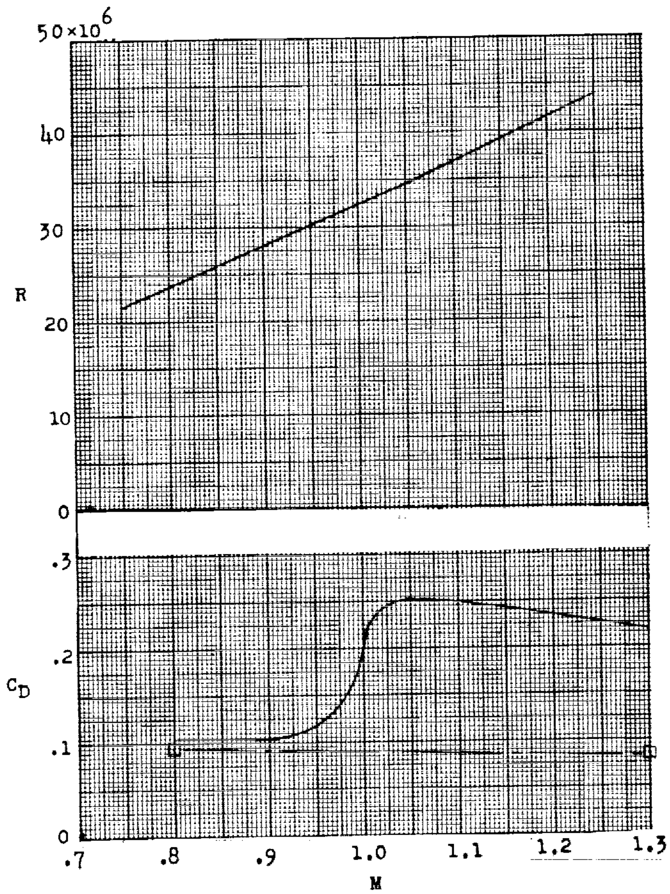

Figure 166.- Concluded.

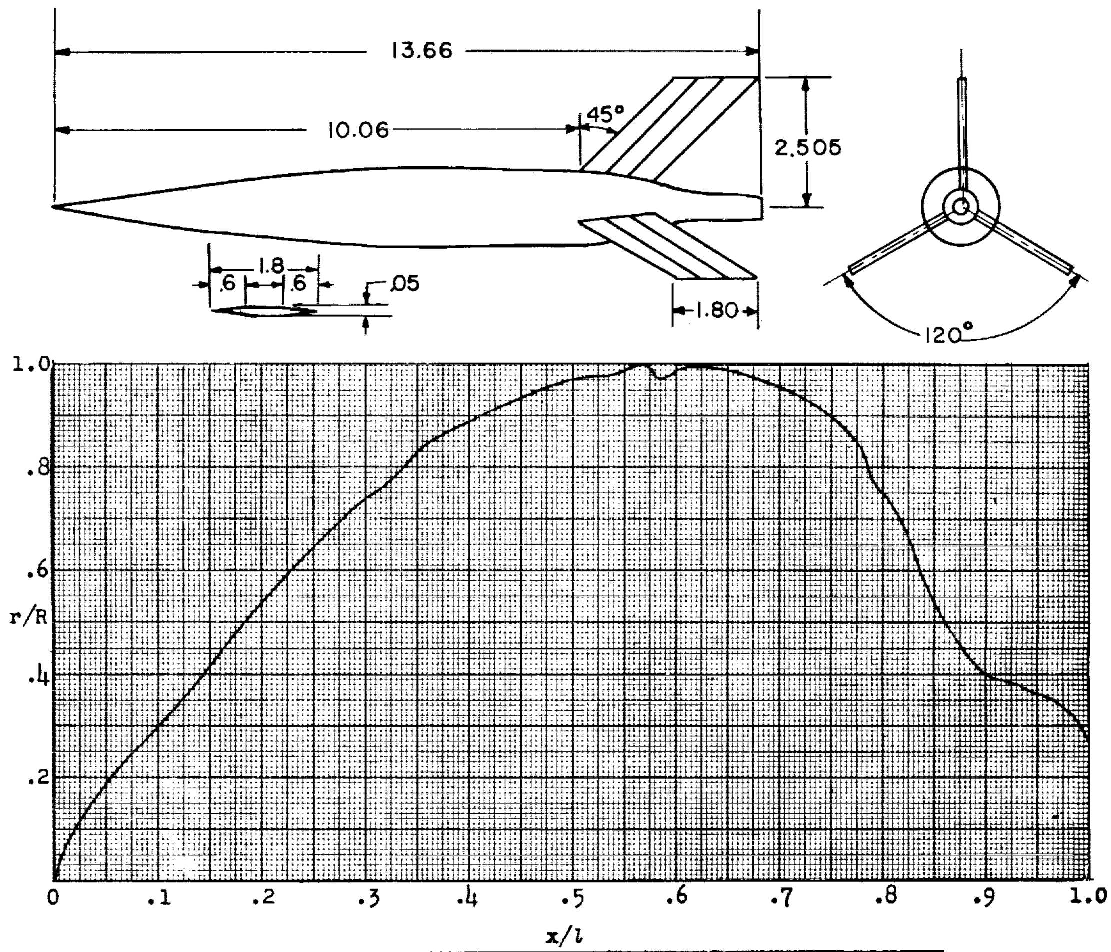

l/d_{Total}	8.92	l/d_{Nose}		S_b/A	24.1	A_b/A	.07
l/d_{N+A}	8.92	l/d_{Aft}		S_f/A	11.5	θ_b	12.6°

Designation: 161

Test: Helium Gun

Figure 167.

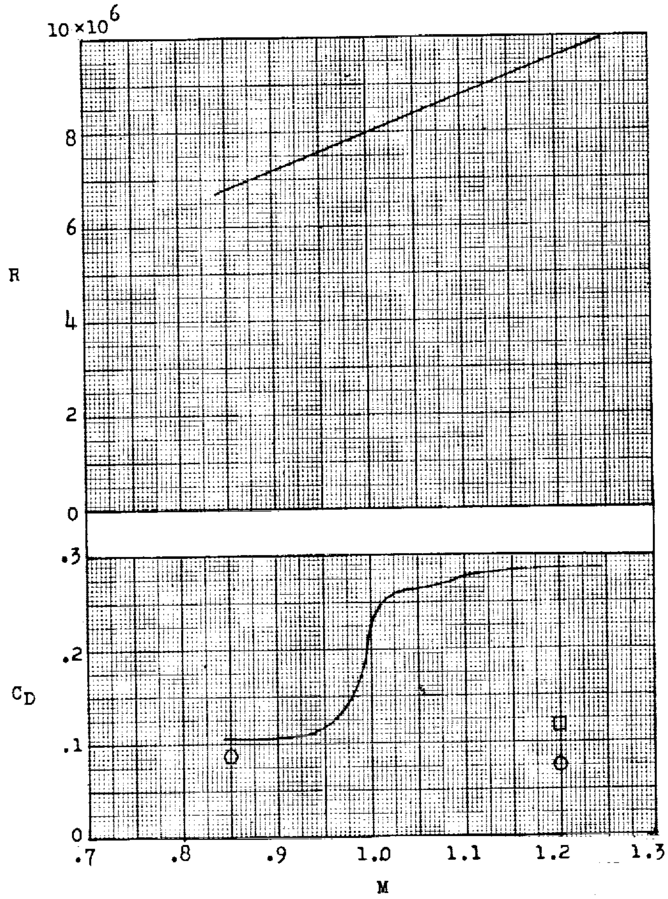

Figure 167.- Concluded.

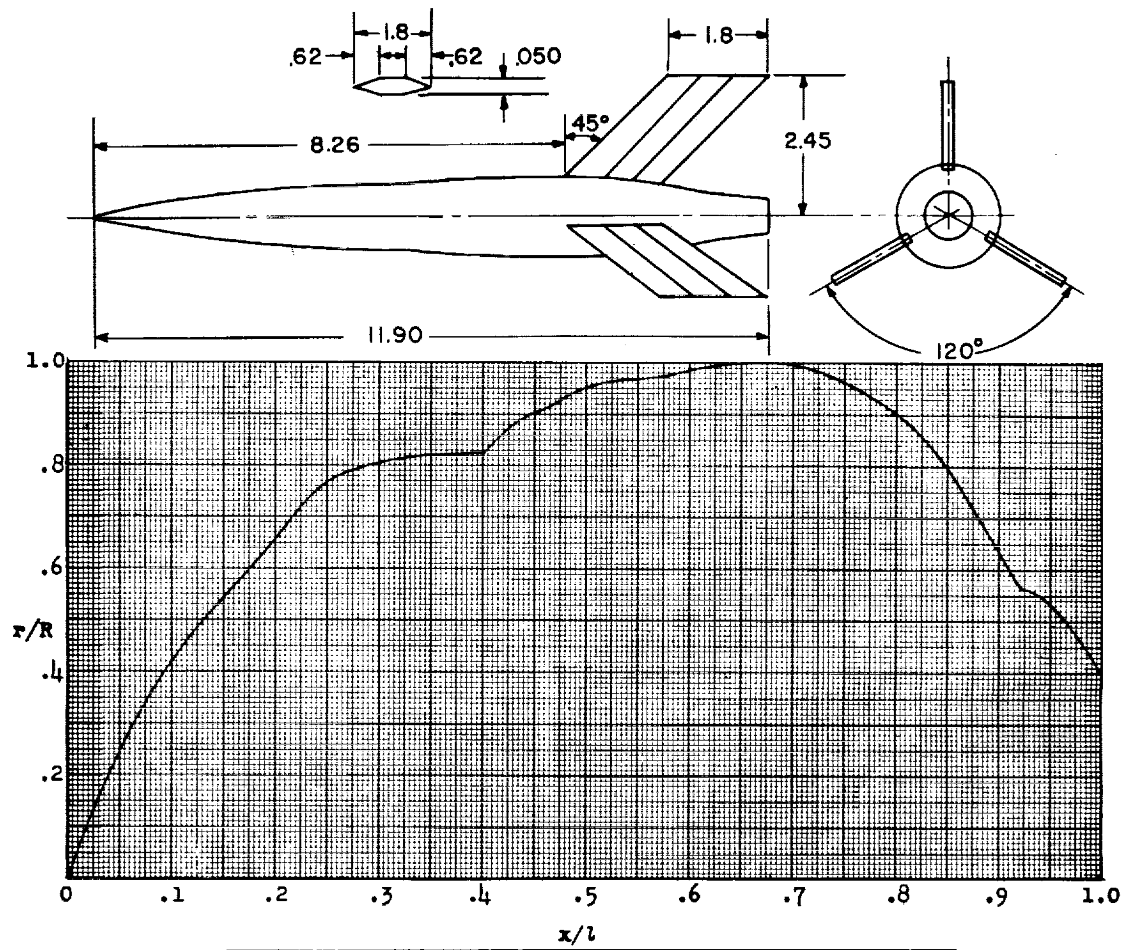

l/d_{Total}	9.08	l/d_{Nose}		S_b/A	26.26	A_b/A	.16
l/d_{N+A}	9.08	l/d_{Aft}		S_f/A	14.4	θ_b	9.1°

Designation: 162

Test: Helium Gun

Figure 168.

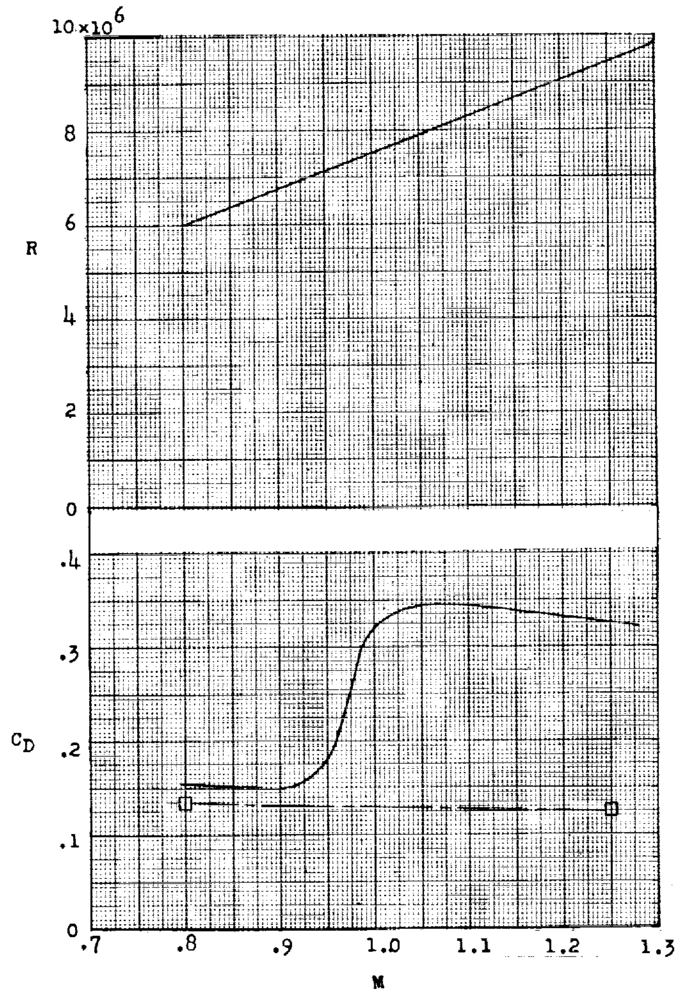

Figure 168.- Concluded.

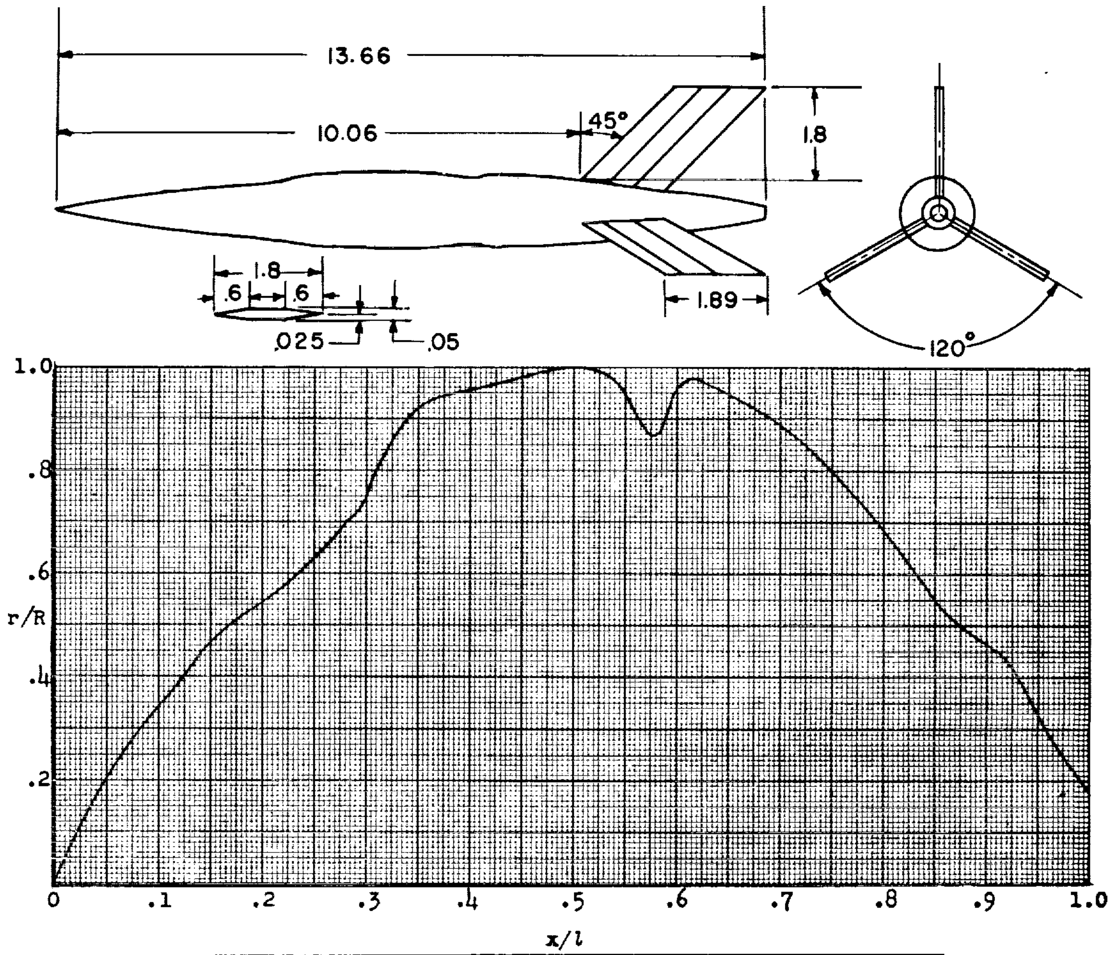

l/d_{Total}	9.09	l/d_{Nose}		S_b/A	24.4	A_b/A	.03
l/d_{N+A}	9.09	l/d_{Aft}		S_f/A	11.6	θ_b	8.5°

Designation: 163

Test: **Helium Gun**

Figure 169.

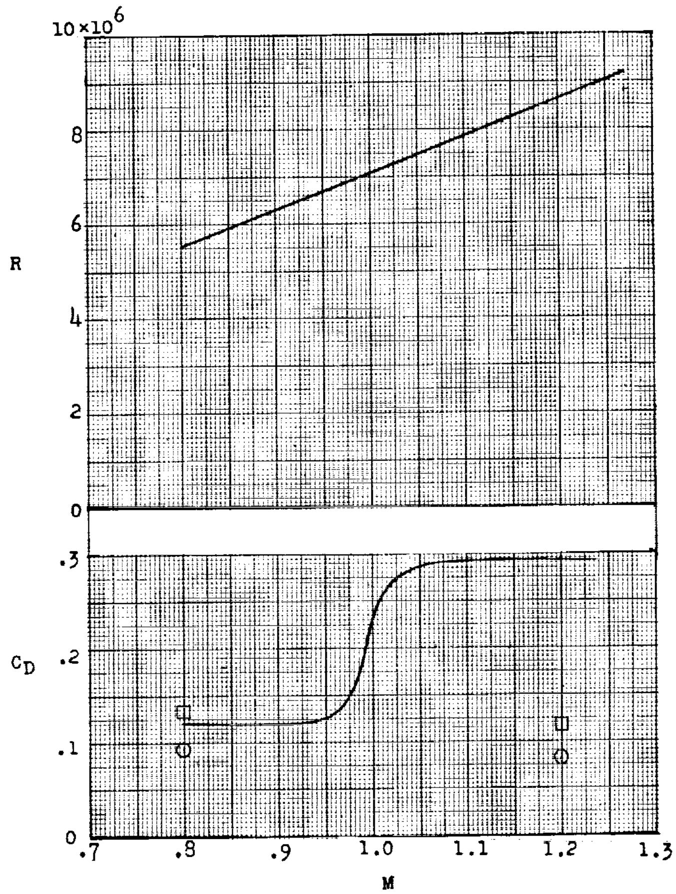

Figure 169.- Concluded.

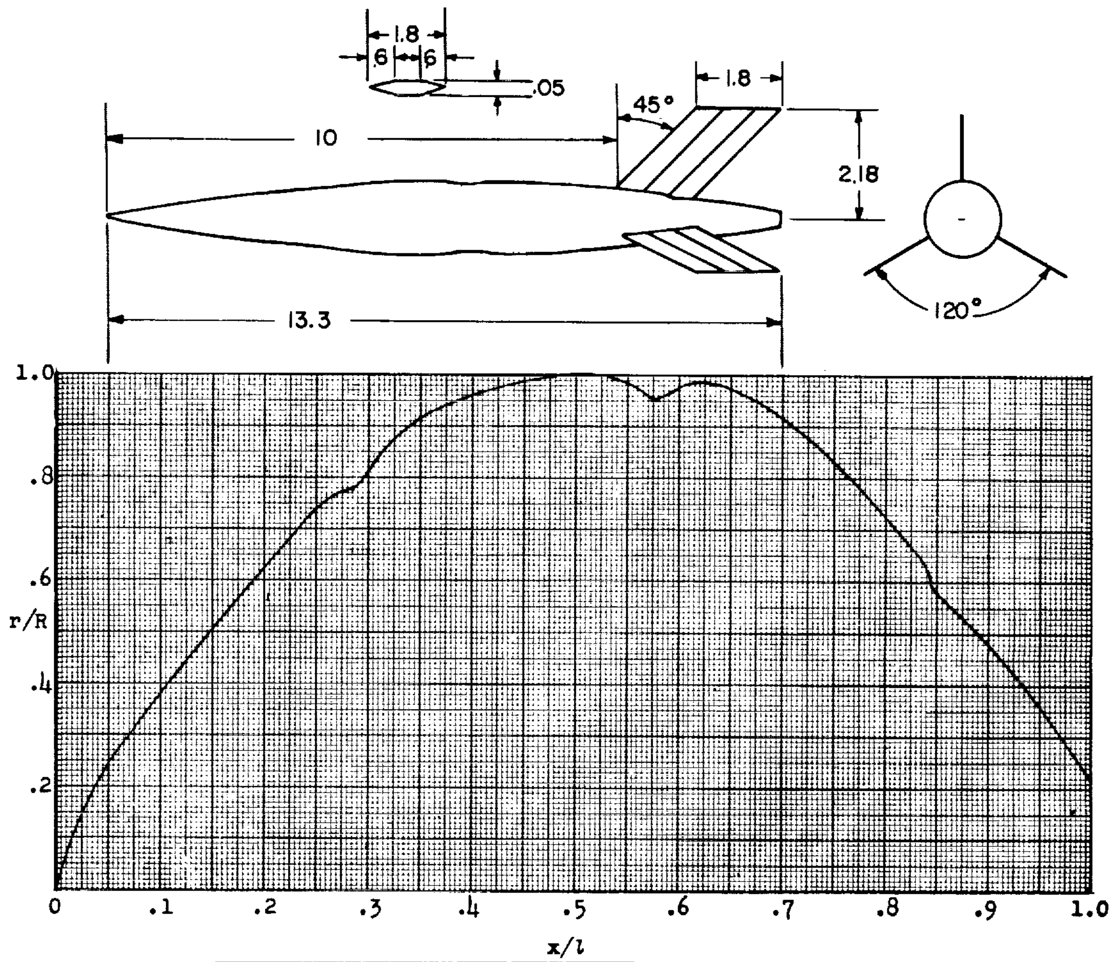

l/d_{Total}	9.1	l/d_{Nose}		S_b/A	25.55	A_b/A	.04
l/d_{N+A}	9.1	l/d_{Aft}		S_f/A	11.64	θ_b	10.0°

Designation: 164

Test: Helium Gun

Figure 170.

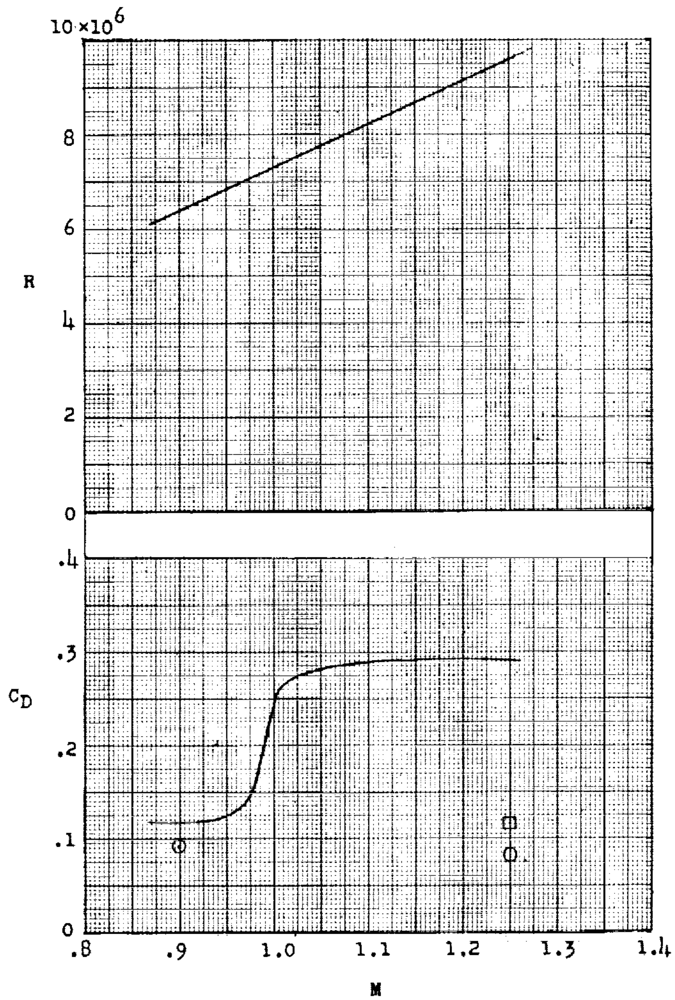

Figure 170.- Concluded.

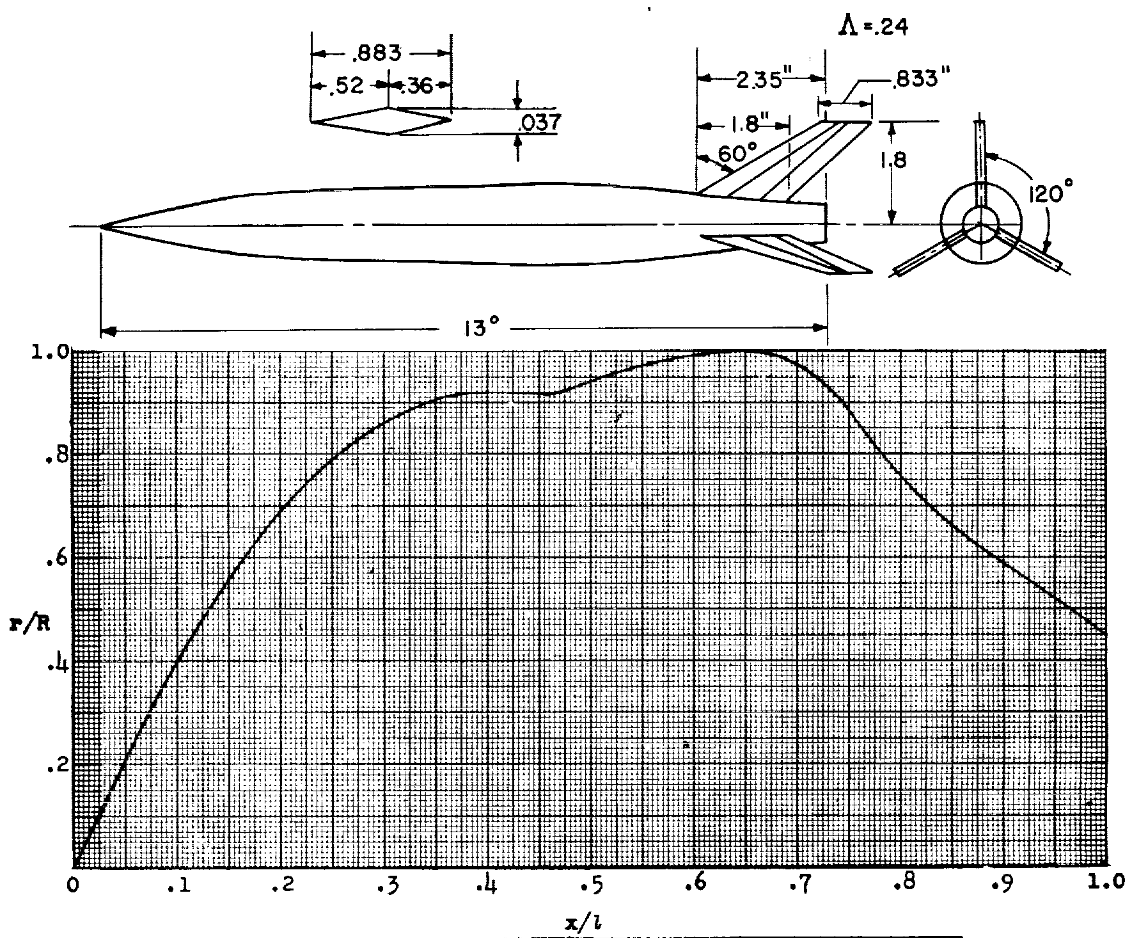

l/d_{Total}	9.22	l/d_{Nose}		S_b/A	26.17	A_b/A	.20
l/d_{N+A}	9.22	l/d_{Aft}		S_f/A	7.14	θ_b	4.35°

Designation: 165

Test: Helium Gun

Figure 171.

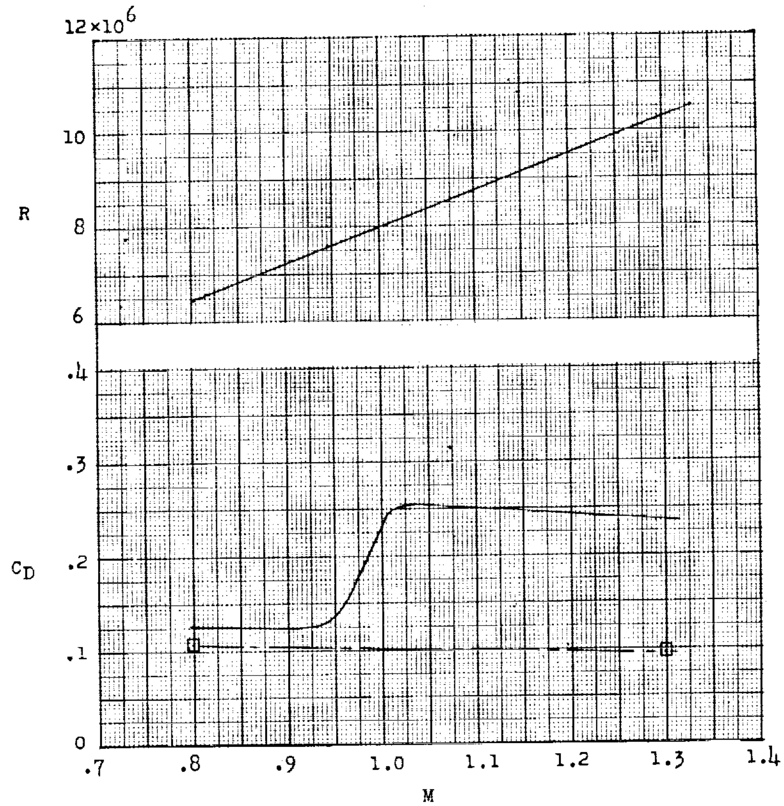

Figure 171.- Concluded.

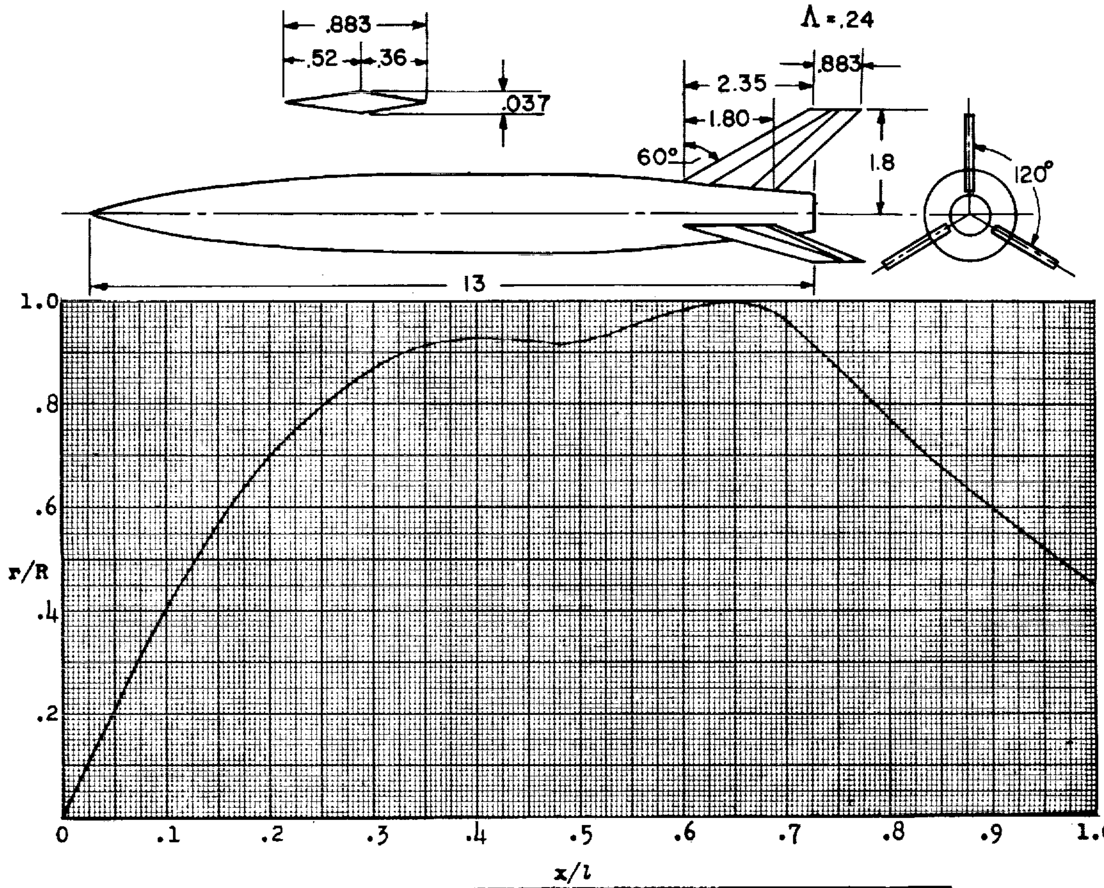

l/d_{Total}	9.28	l/d_{Nose}		S_b/A	26.91	A_b/A	.20
l/d_{N+A}	9.28	l/d_{Aft}		S_f/A	7.28	θ_b	4.06°

Designation: 166

Test: Helium Gun

Figure 172.

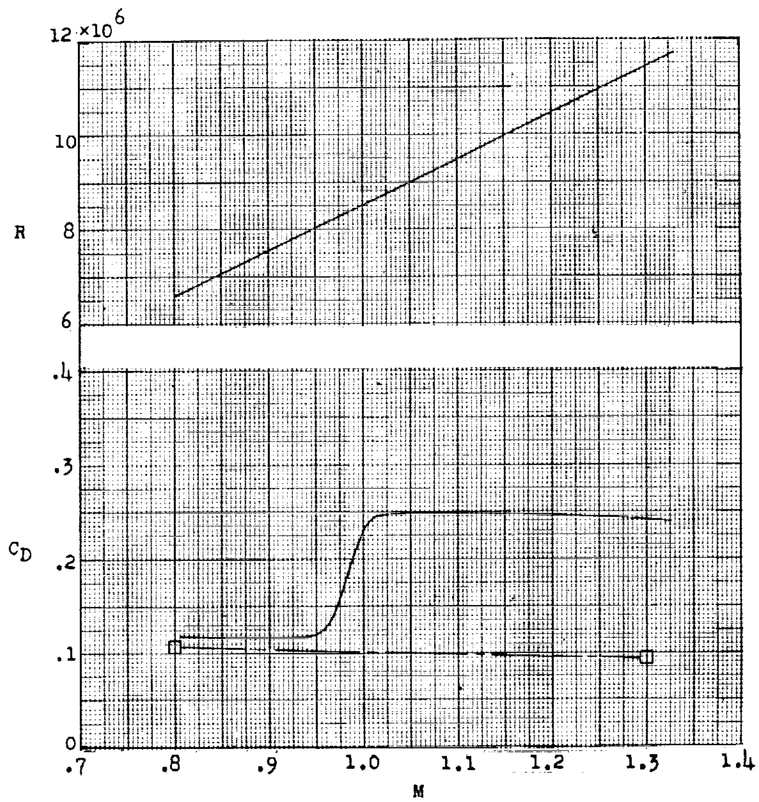

Figure 172.- Concluded.

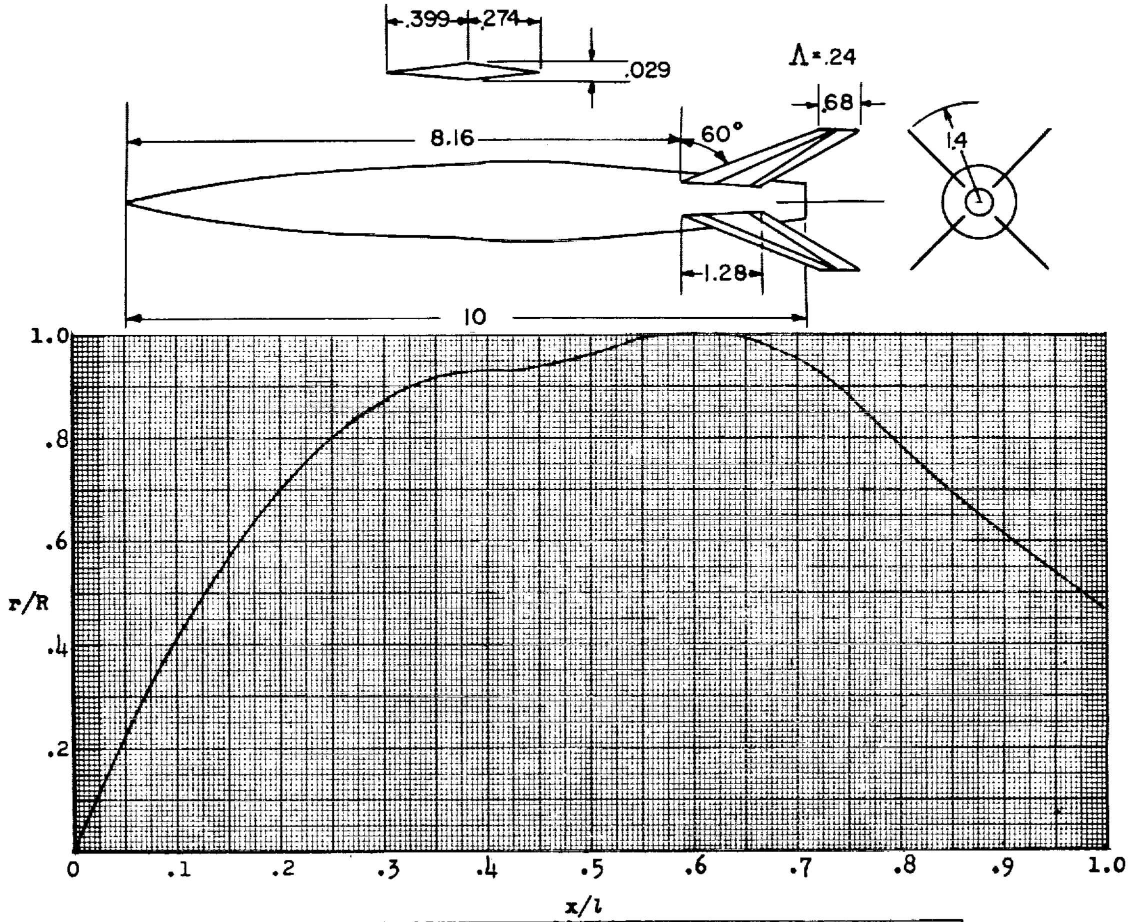

l/d_{Total}	9.31	l/d_{Nose}		S_b/A	28.19	A_b/A	.21
l/d_{N+A}	9.31	l/d_{Aft}		S_f/A	10.00	θ_b	4.6°

Designation: 167

Test: Helium Gun

Figure 173.

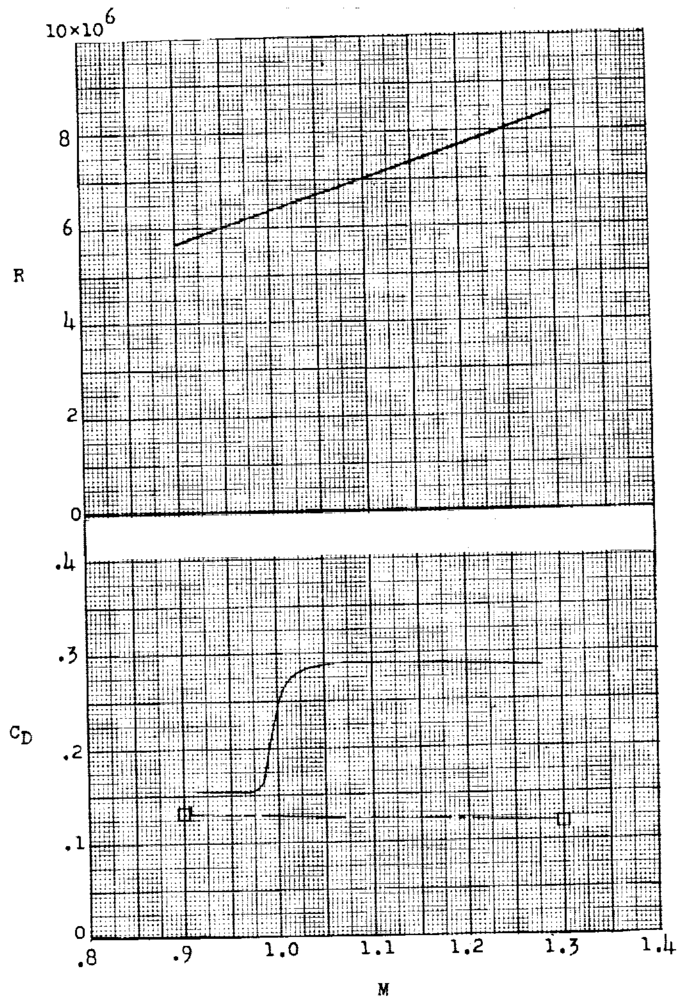

Figure 173.- Concluded.

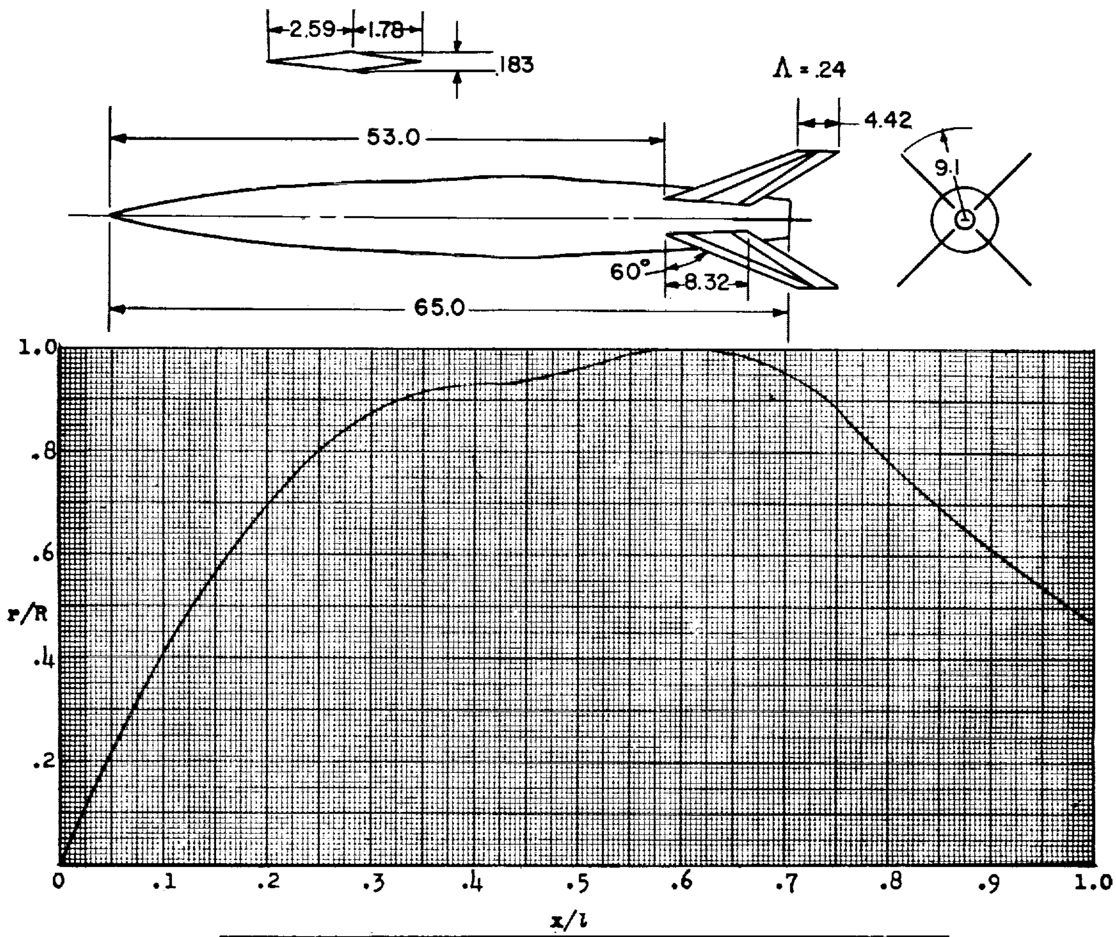

l/d_{Total}	9.31	l/d_{Nose}		S_b/A	28.19	A_b/A	.21
l/d_{N+A}	9.31	l/d_{Aft}		S_f/A	10.00	θ_b	4.6°

Designation: 168

Test: Rocket

Figure 174.

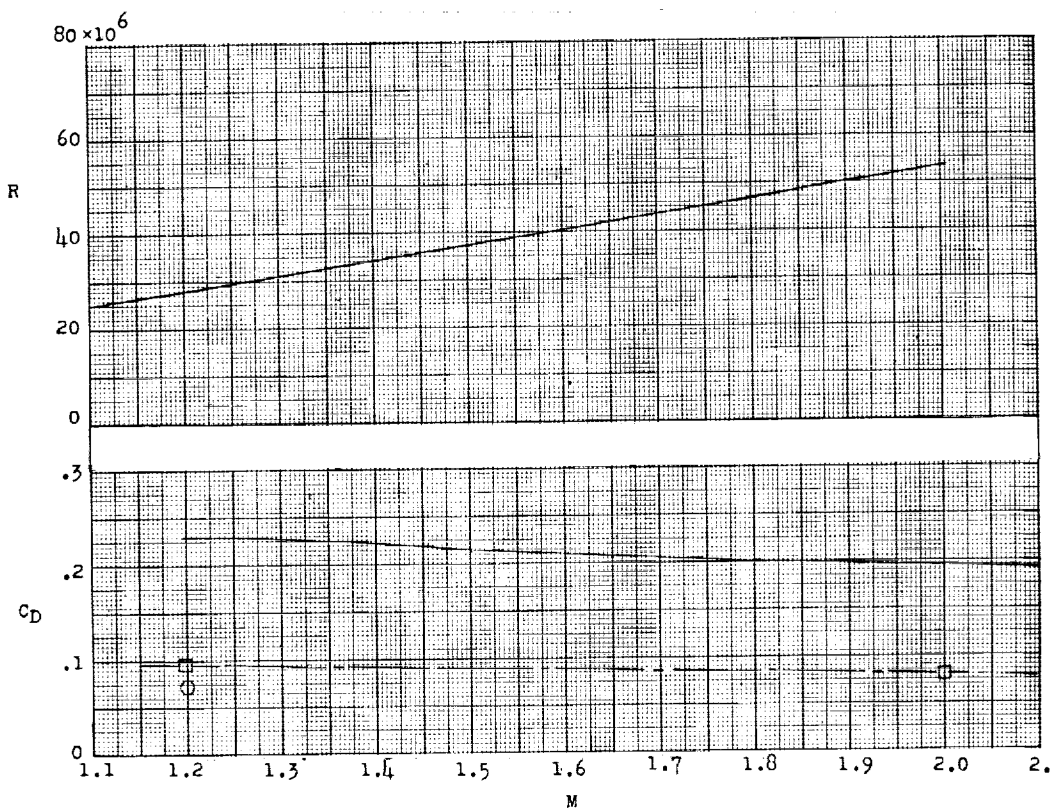

Figure 174.- Concluded.

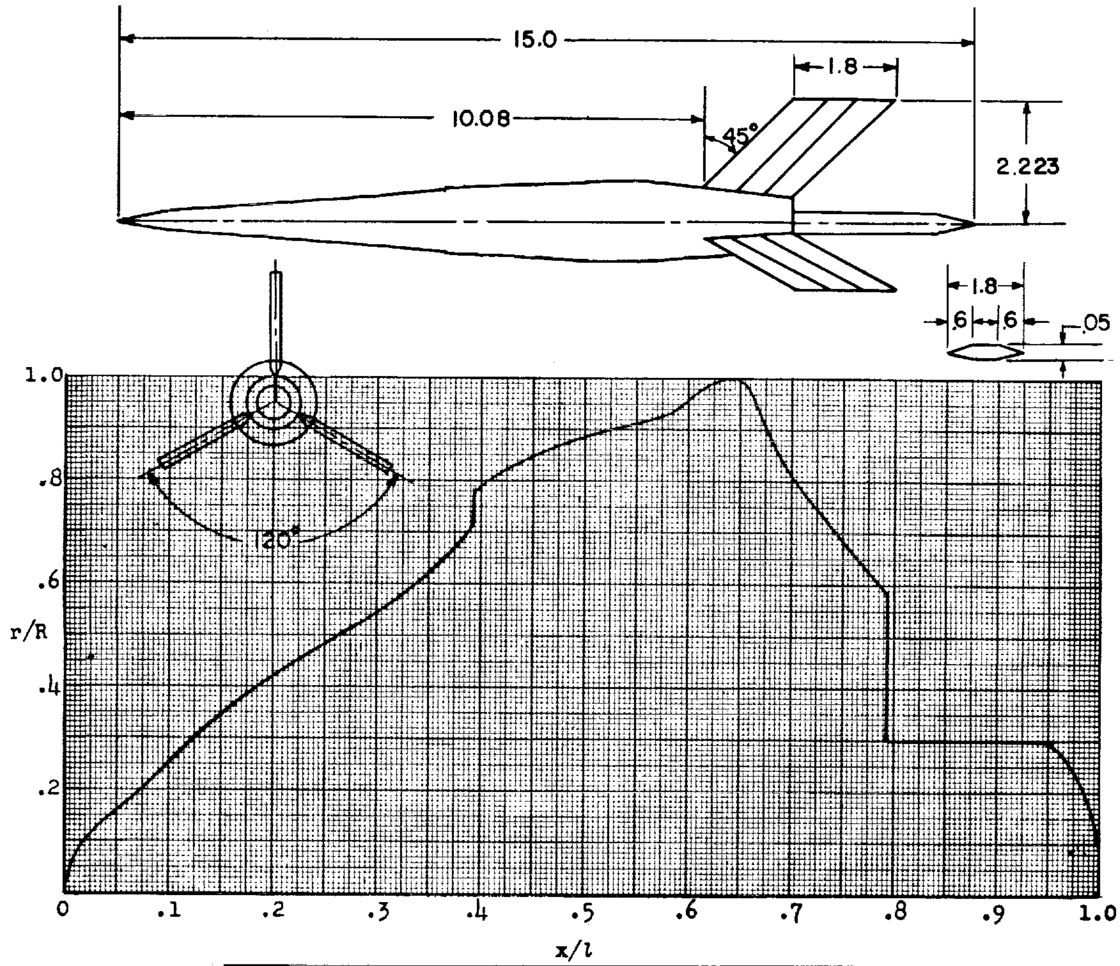

l/d_{Total}	10.0	l/d_{Nose}		S_b/A	20.35	A_b/A	0.0
l/d_{N+A}	10.0	l/d_{Aft}		S_f/A	11.5	θ_b	90°

Designation: 169

Test: **Helium Gun**

Figure 175.

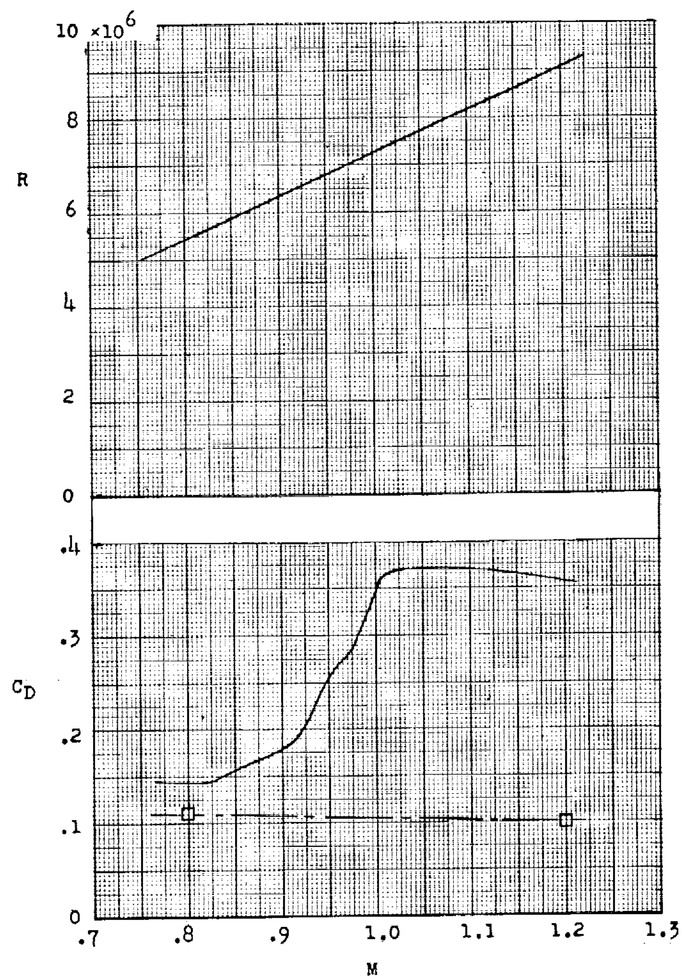

Figure 175.- Concluded.

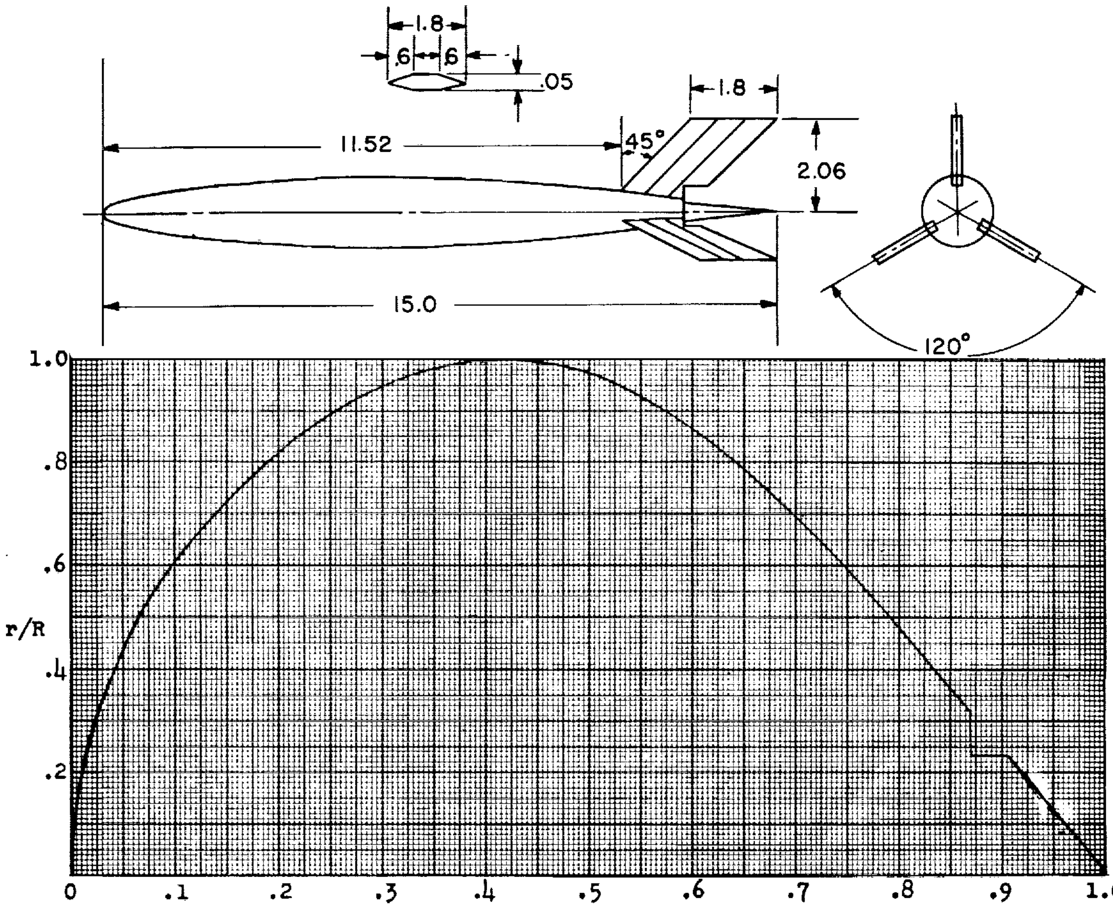

l/d_{Total}	10.00	l/d_{Nose}		S_b/A	27.40	A_b/A	0.0
l/d_{N+A}	10.00	l/d_{Aft}		S_f/A	11.0	θ_b	6.80°

Designation: 170

Test: Helium Gun

Remarks: Apparently there was an appreciable length of laminar flow on the body of this model.

Figure 176.

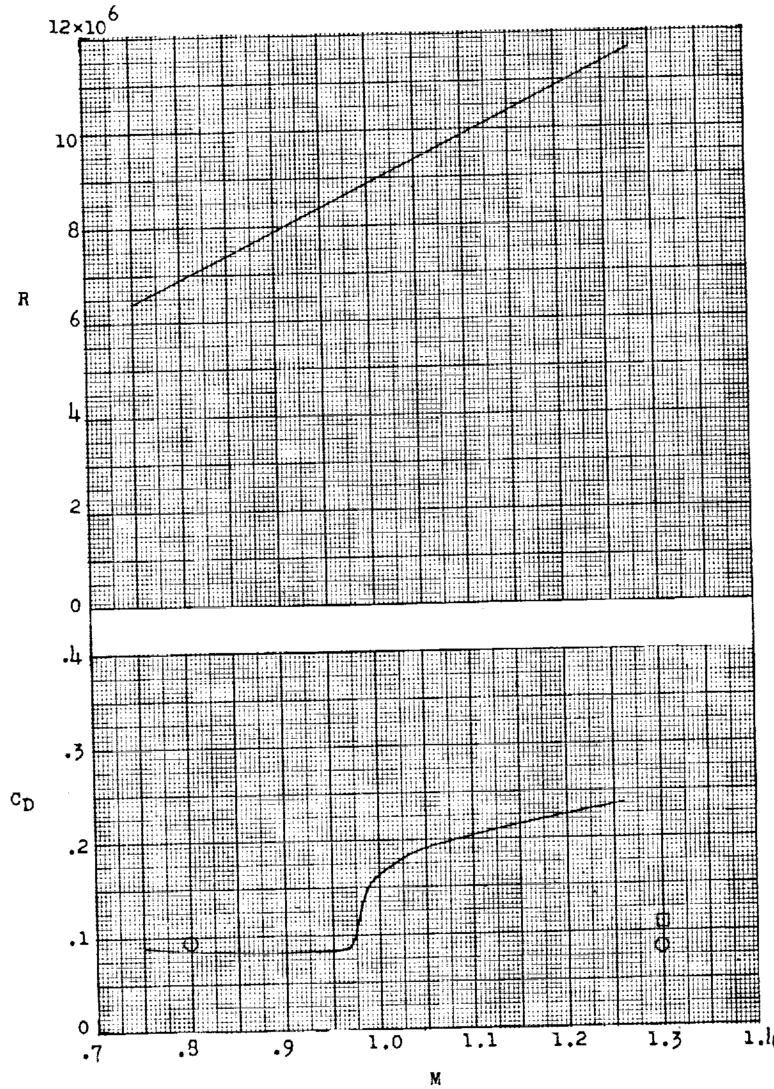

Figure 176.- Concluded.

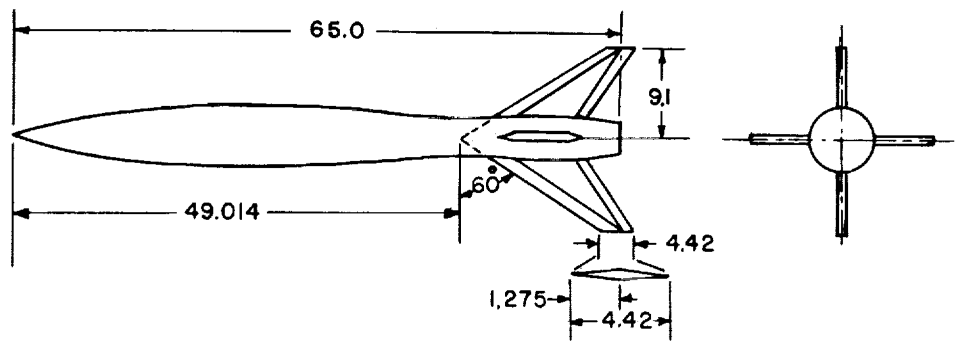

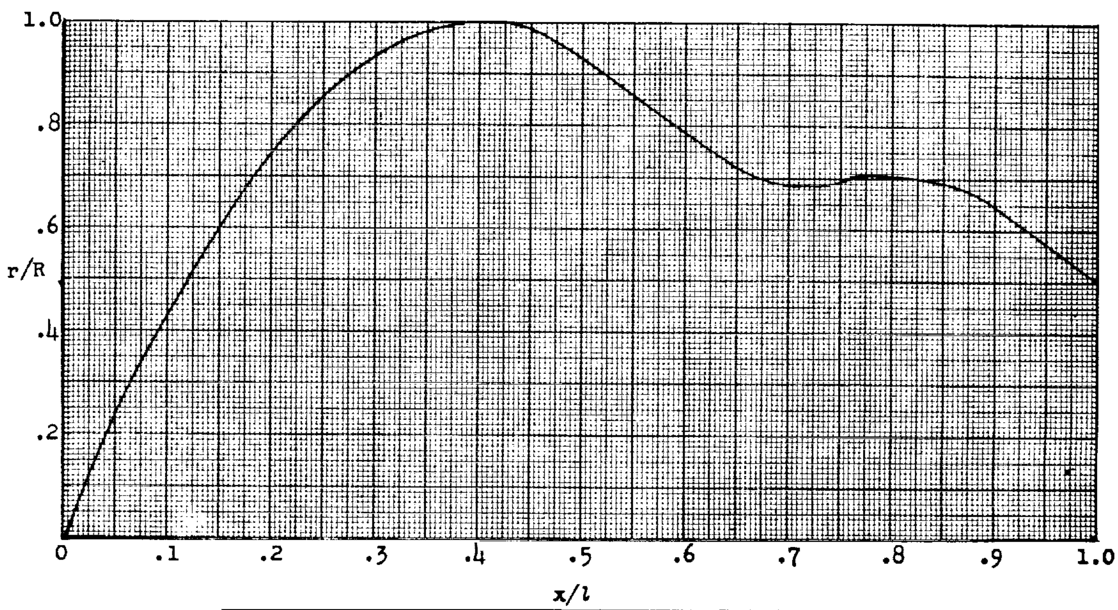

l/d_{Total}	10.0	l/d_{Nose}		S_b/A	28.4	A_b/A	.25
l/d_{N+A}	10.0	l/d_{Aft}		S_f/A	16.5	θ_b	4.15°

Designation: 171

Test: Rocket

Figure 177.

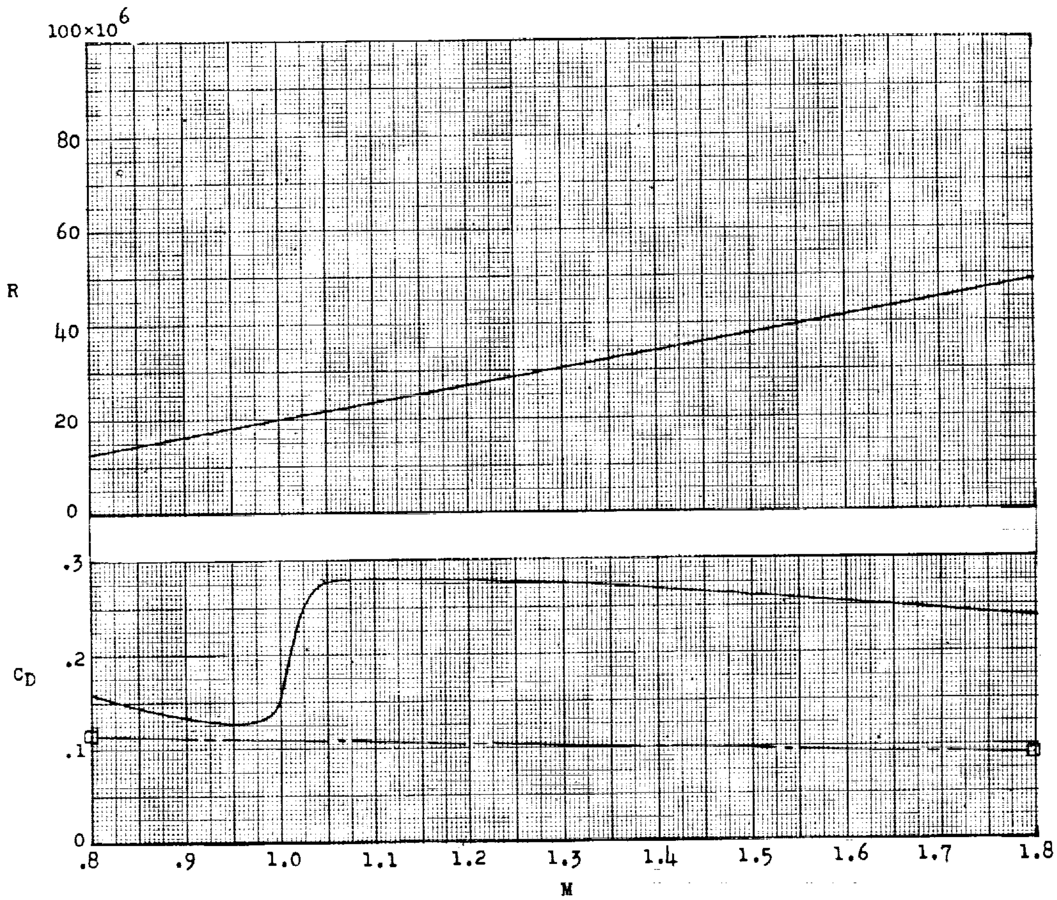

Figure 177.- Concluded.

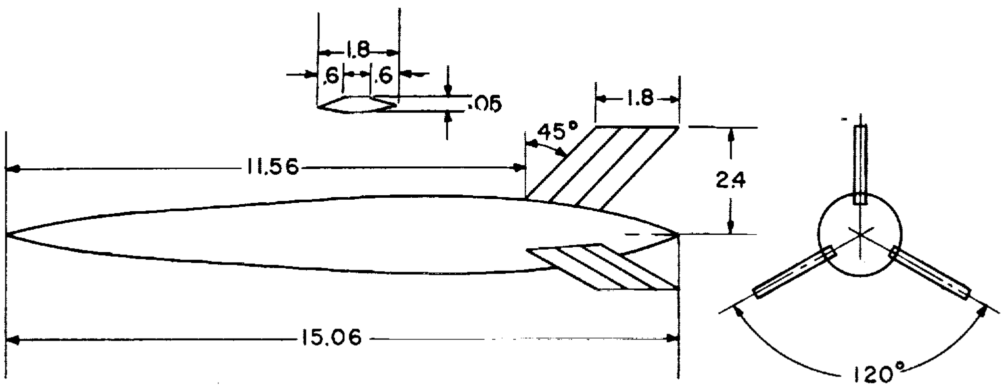

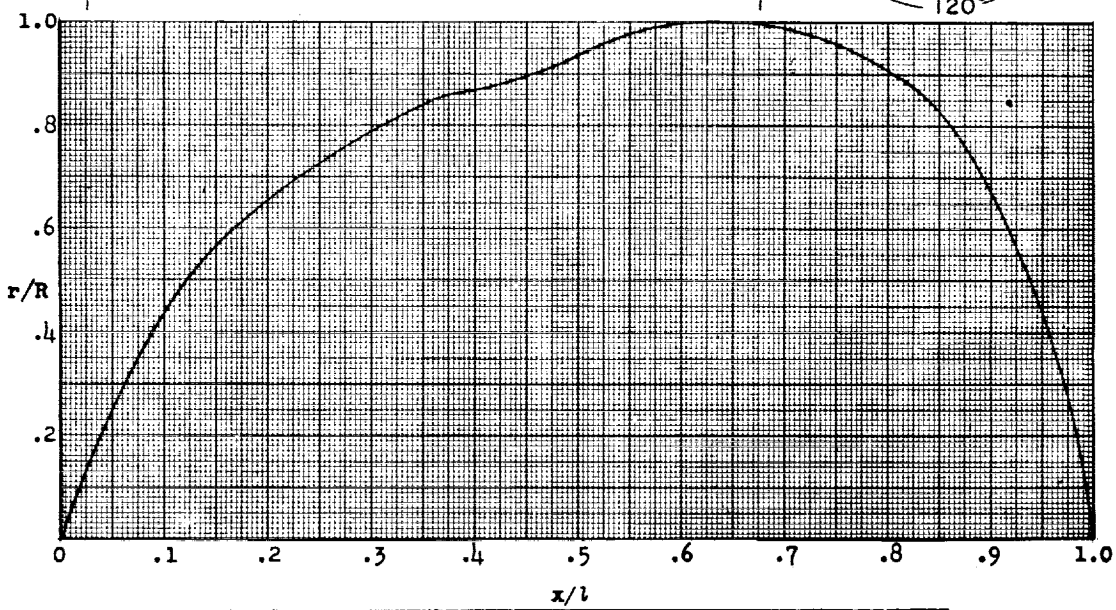

l/d_{Total}	10.04	l/d_{Nose}		S_b/A	30.40	A_b/A	0.0
l/d_{N+A}	10.04	l/d_{Aft}		S_f/A	11.00	θ_b	90°

Designation: 172

Test: Helium Gun

Figure 178.

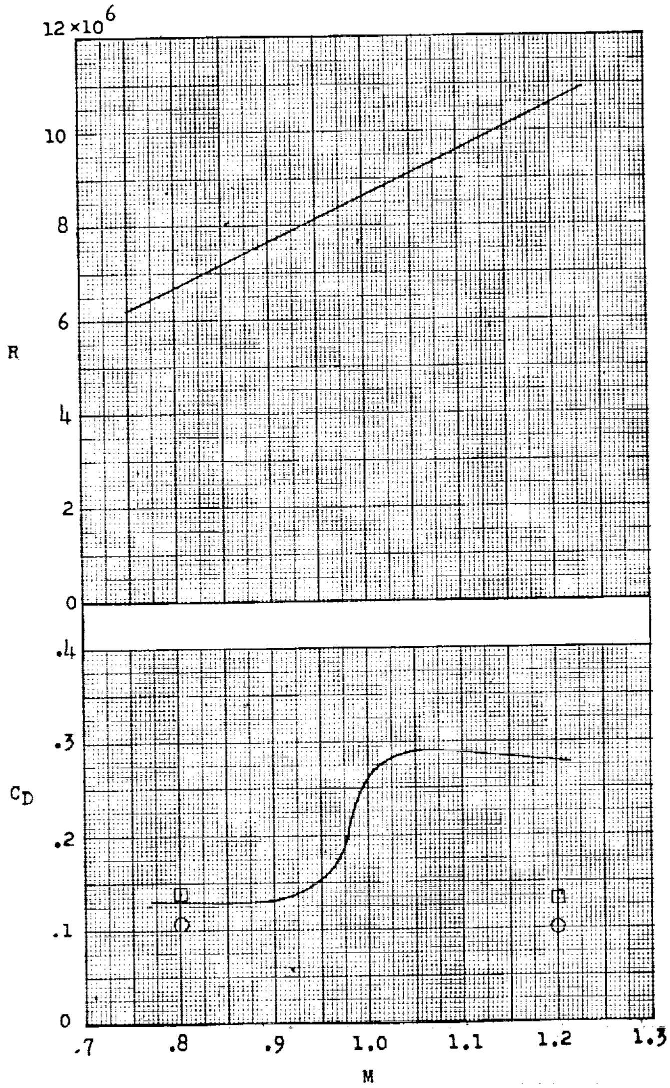

Figure 178.- Concluded.

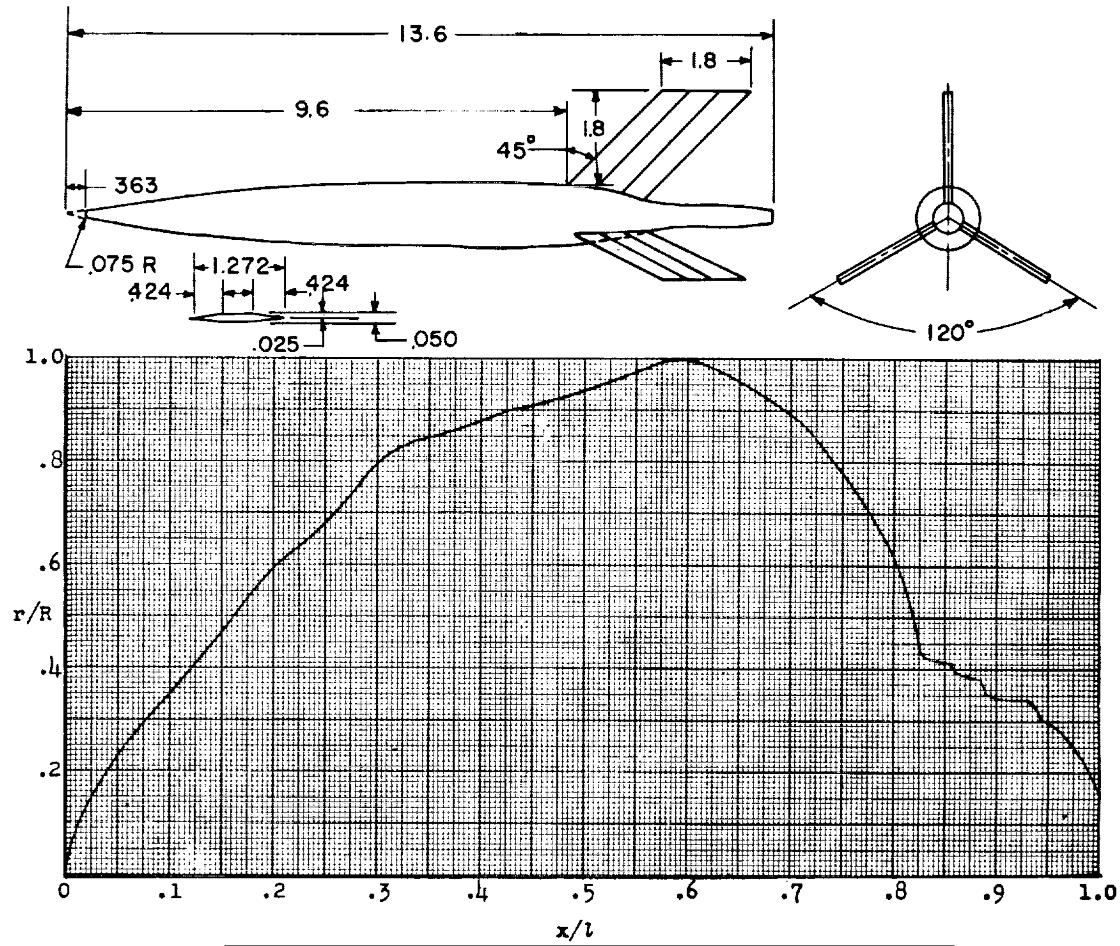

l/d_{Total}	10.4	l/d_{Nose}		S_b/A	27.4	A_b/A	.02
l/d_{N+A}	10.4	l/d_{Aft}		S_f/A	15.35	θ_b	4.0°

Designation: 173

Test: Helium Gun

Figure 179.

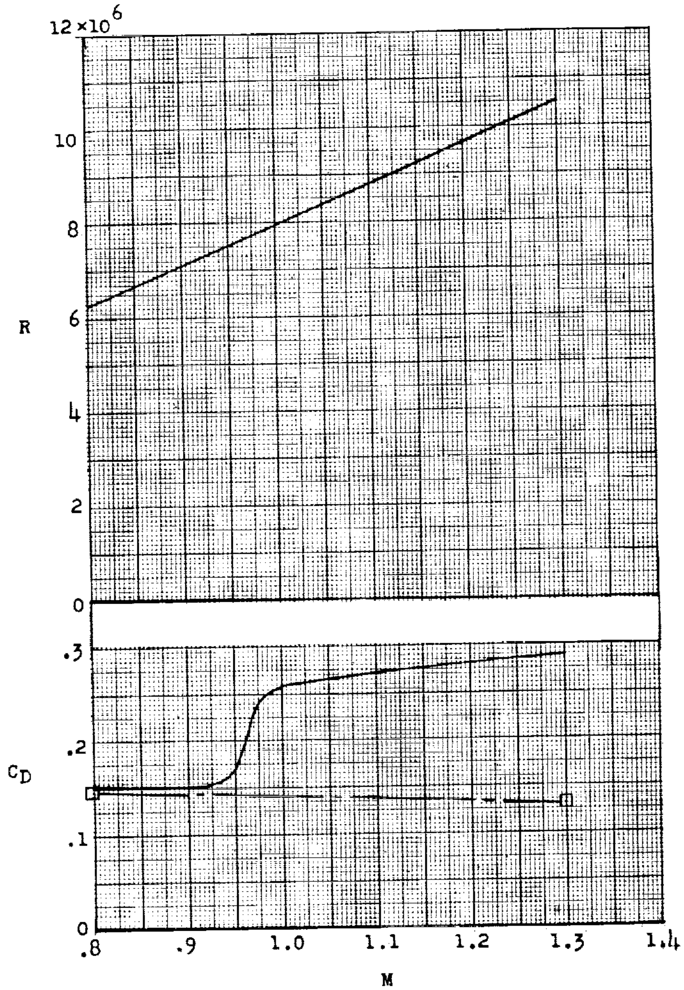

Figure 179.- Concluded.

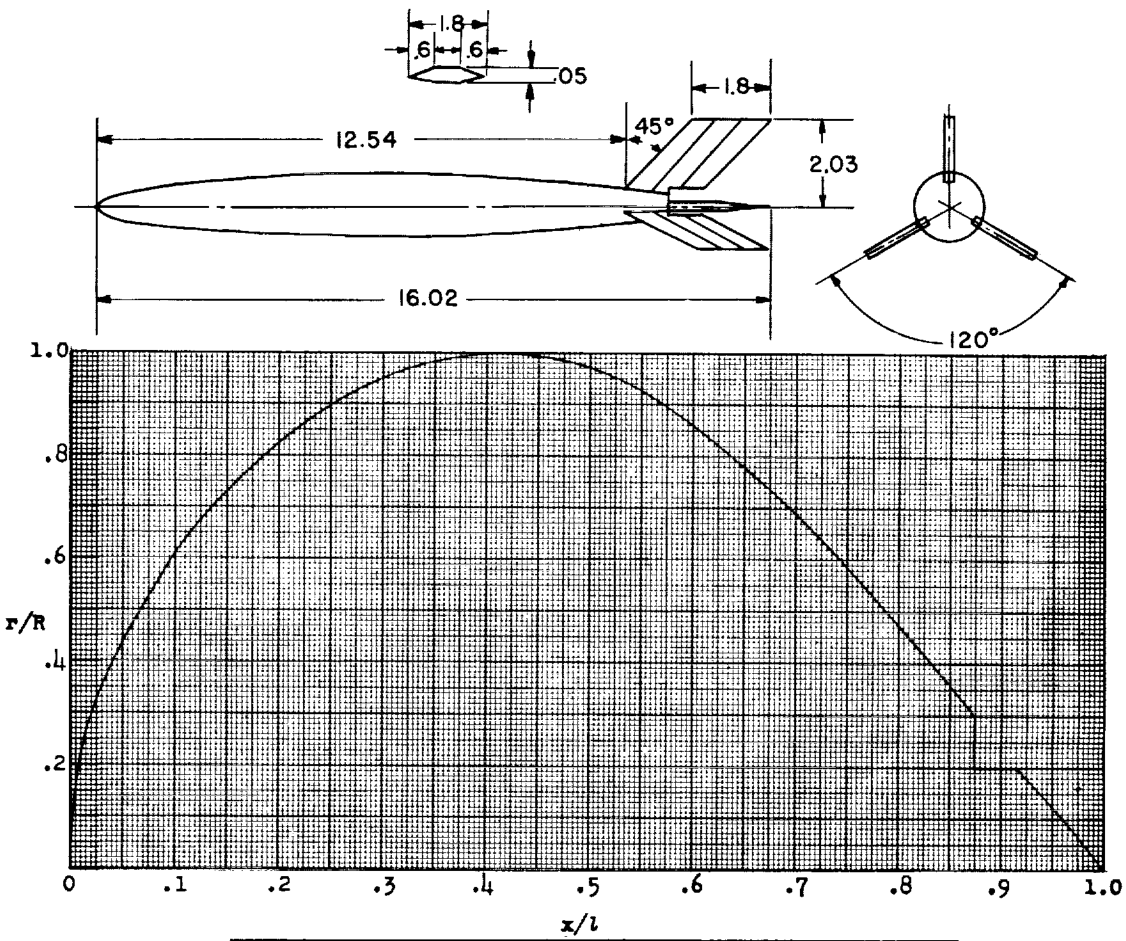

l/d_{Total}	10.70	l/d_{Nose}		S_b/A	29.80	A_b/A	0.0
l/d_{N+A}	10.70	l/d_{Aft}		S_f/A	11.0	θ_b	6.8°

Designation: 174

Test: Helium Gun

Figure 180.

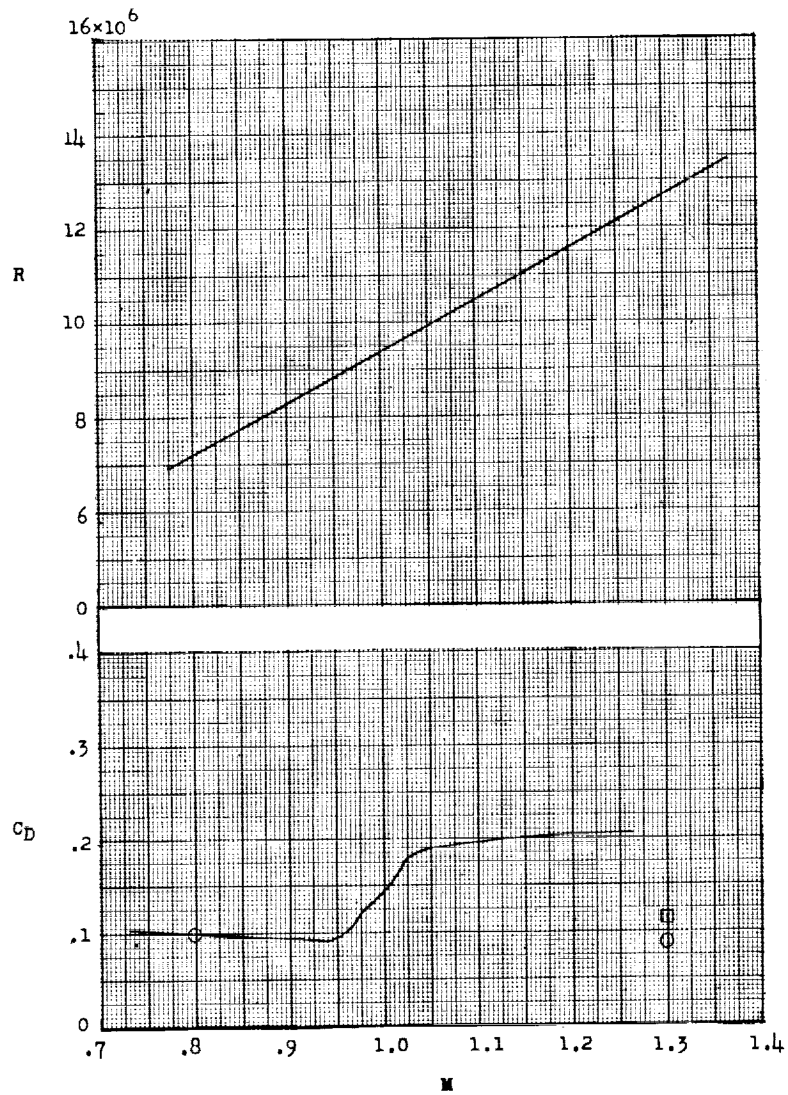

Figure 180.- Concluded.

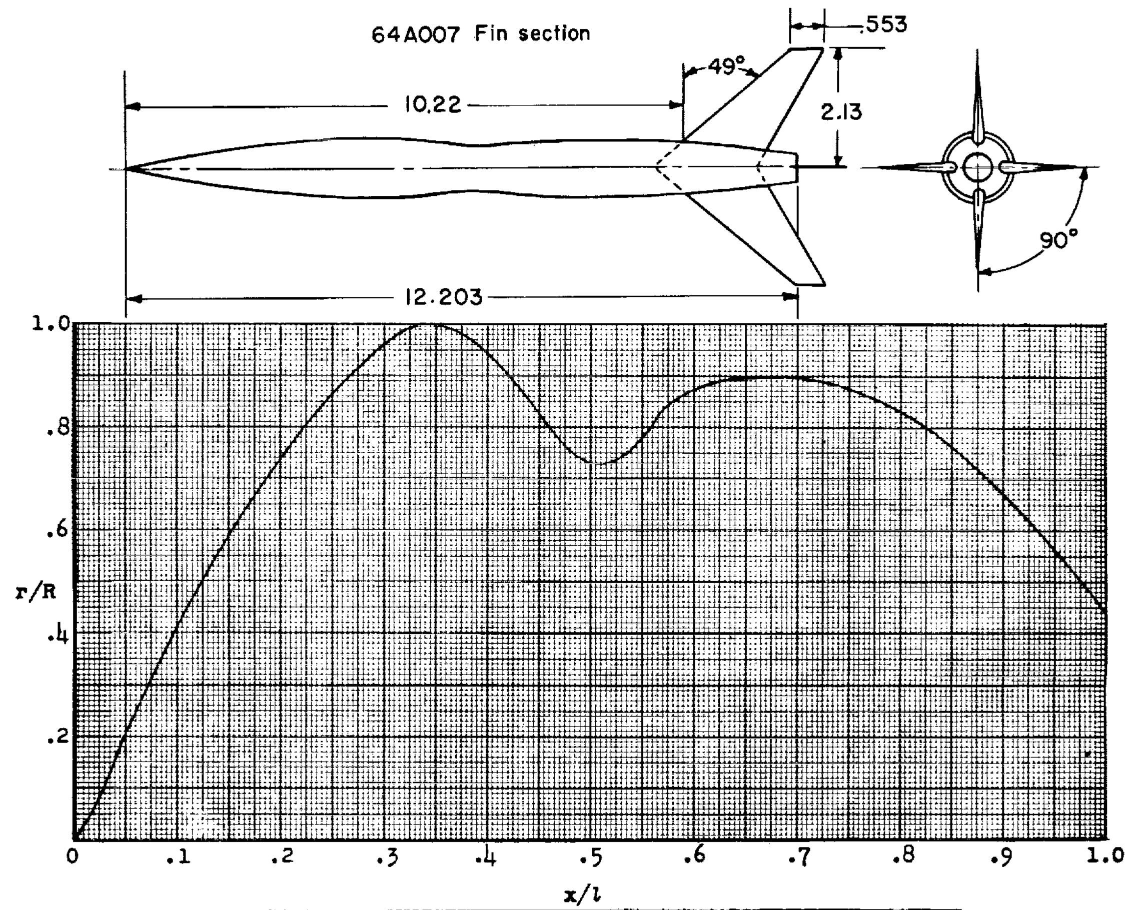

l/d_{Total}	11.02	l/d_{Nose}		S_b/A	32.4	A_b/A	.19
l/d_{N+A}	11.02	l/d_{Aft}		S_f/A	17.04	θ_b	7.05°

Designation: 175

Test: **Helium Gun**

Figure 181.

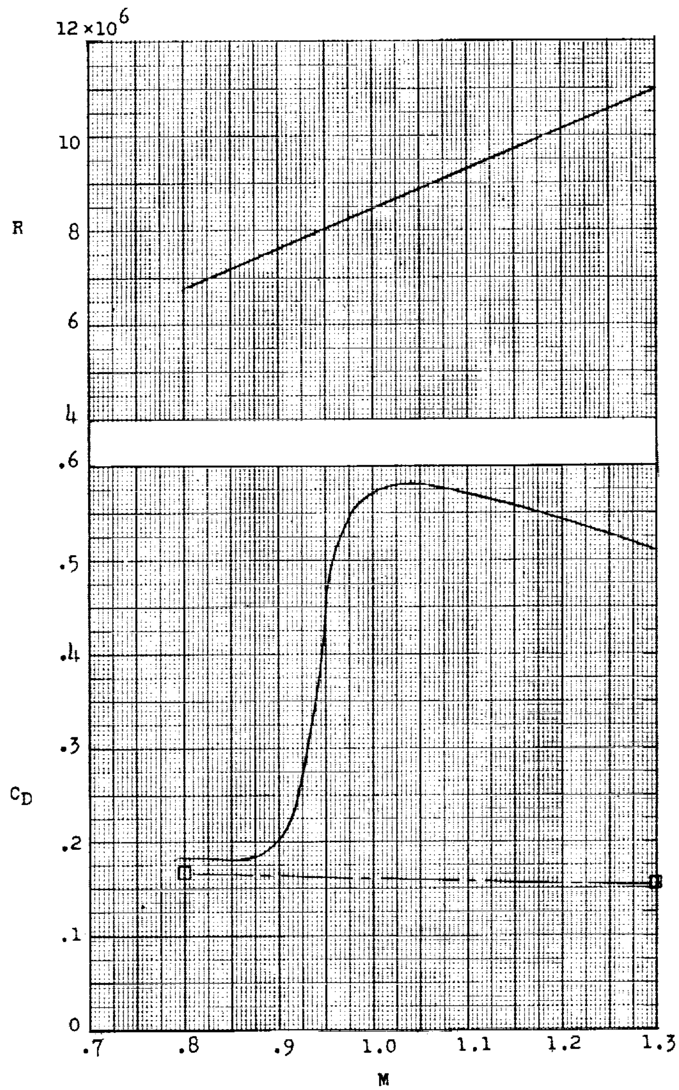

Figure 181.- Concluded.

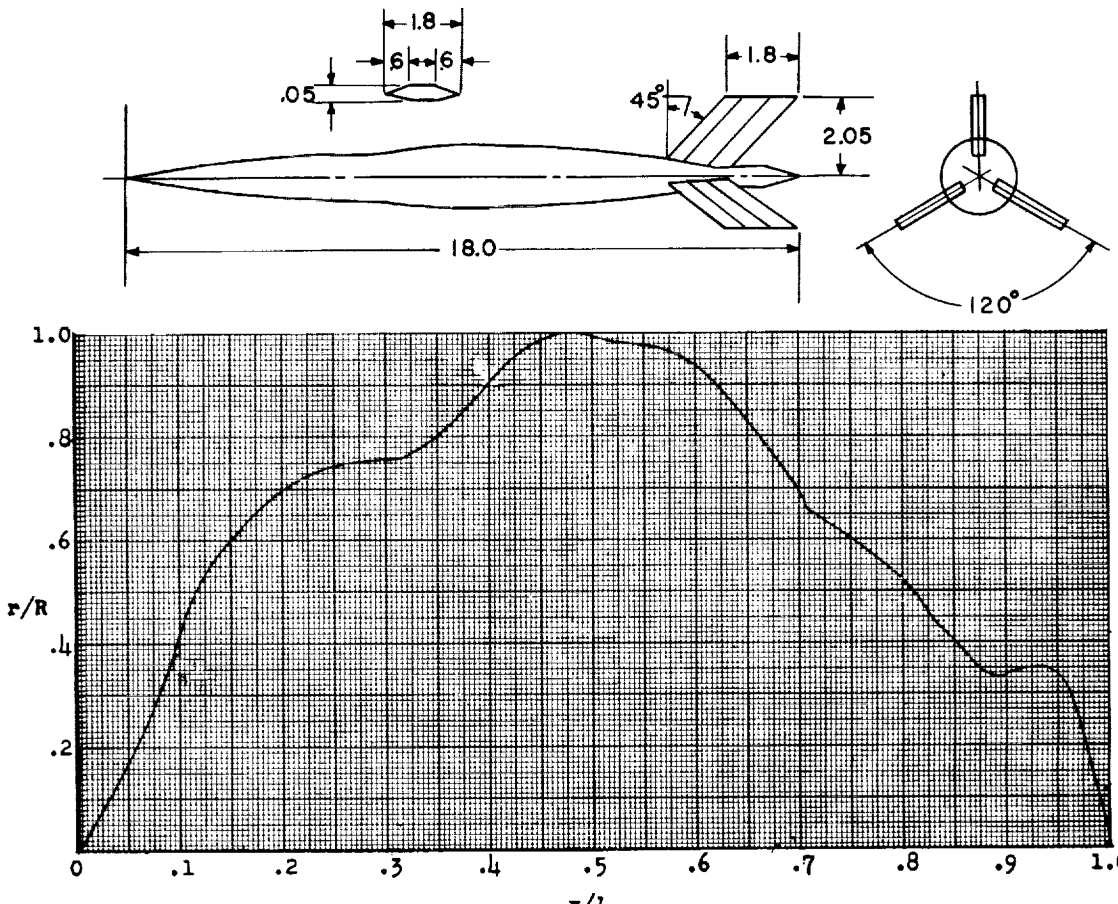

l/d_{Total}	11.39	l/d_{Nose}		S_b/A	29.20	A_b/A	0.0
l/d_{N+A}	11.39	l/d_{Aft}		S_f/A	11.0	θ_b	18.9°

Designation: 176

Test: **Helium Gun**

Figure 182.

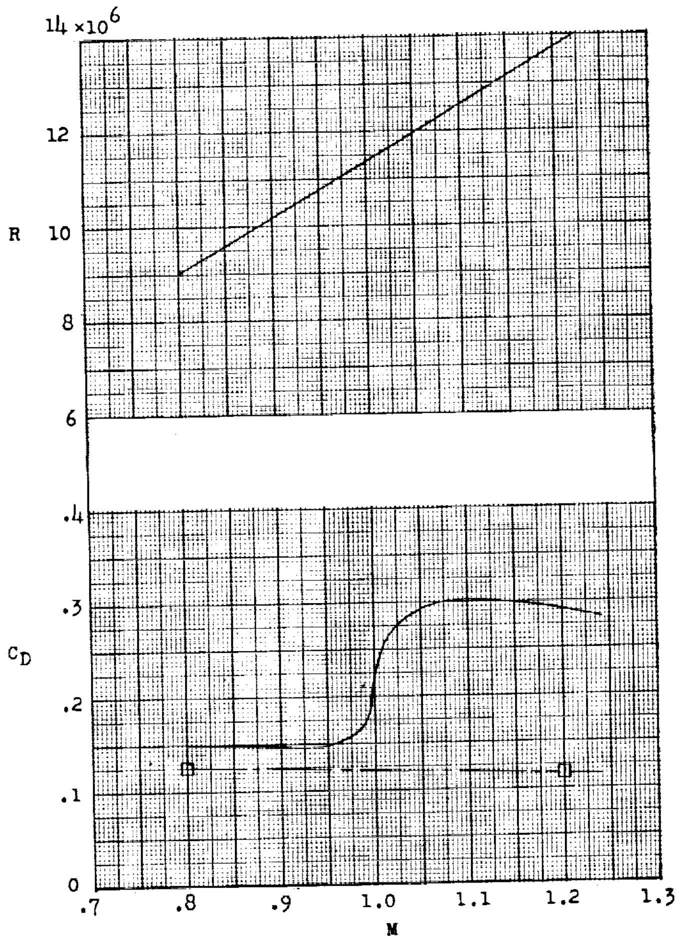

Figure 182.- Concluded.

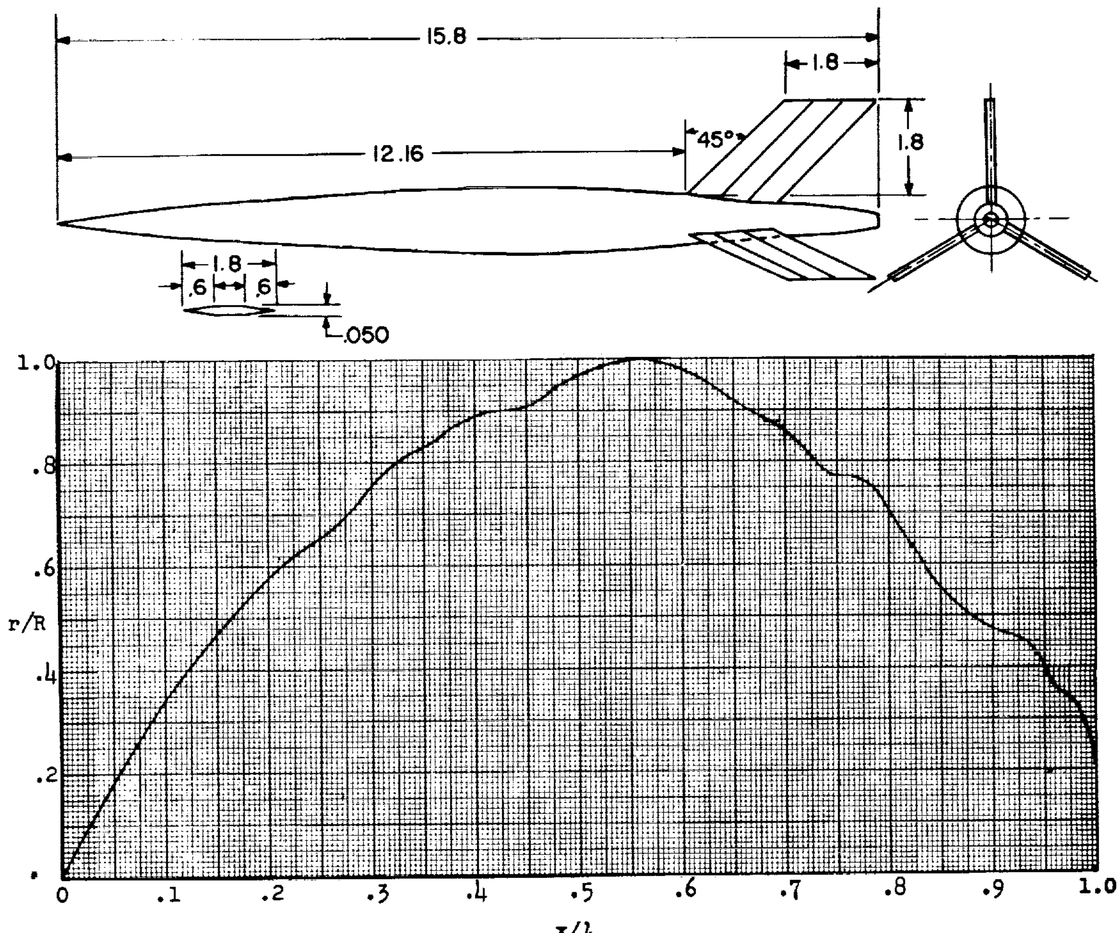

l/d_{Total}	12.05	l/d_{Nose}		S_b/A	31.9	A_b/A	.04
l/d_{N+A}	12.05	l/d_{Aft}		S_f/A	15.0	θ_b	5.0°

Designation: 177

Test: Helium Gun

Figure 183.

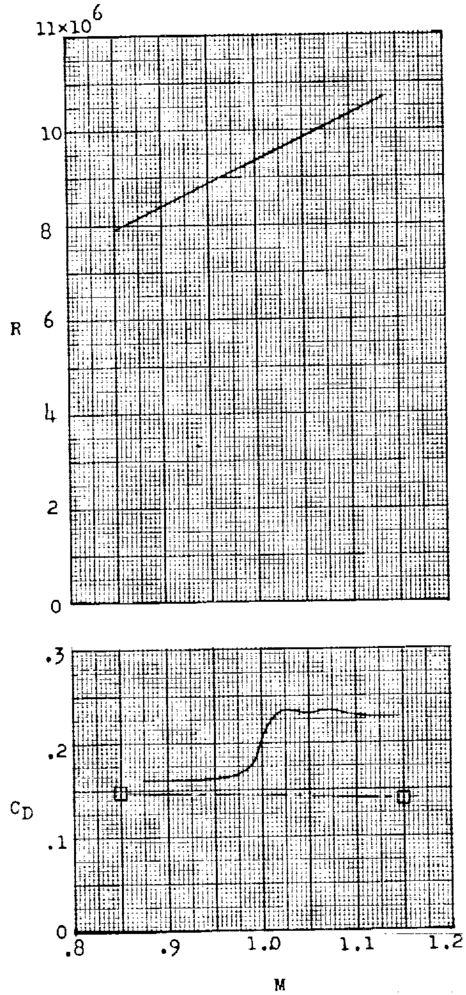

Figure 183.- Concluded.